The lysine demethylase LSD1 regulates nuclear envelope formation at the end of mitosis

Dissertation

der Mathematisch-Naturwissenschaftlichen Fakultät

der Eberhard Karls Universität Tübingen

zur Erlangung des Grades eines

Doktors der Naturwissenschaften

(Dr. rer. nat.)

vorgelegt von

Allana Schooley

aus Toronto (Canada)

Tübingen

2015

Tag der mündlichen Qualifikation:	28.07.2015
Dekan:	Prof. Dr. Wolfgang Rosenstiel
1. Berichterstatter:	PD Dr. Wolfram Antonin
2. Berichterstatter:	Prof Dr. Gabriele Dodt

Acknowledgements

I am truly grateful to my PhD advisor Wolfram Antonin for the opportunity to work in a lab surrounded by new and open-minded approaches towards understanding nuclear architecture. Thank you for challenging me, for your patience and honesty, and above all for your unwavering commitment to scientific questions and well executed experiments.

I would also like to thank the members of my thesis advisory Committee: My university supervisor Prof. Dr. Gabriele Dodt, as well as Dr. Elisa Izaurralde and Dr. Gaspar Jekeley.

I could not imagine my time in the lab without the help and support of my past and current labmates: Susanne Astrinidis, Mona Bodenhöfer, Nathanael Cottam, Paola De Magistris, Nathalie Eisenhardt, Mario Graeve, Cathrin Gramminger, Franziska Hoppe, Michael Lorenz, Jan Overbeck, Adriana Magalska, Daniel Moreno, Ruchika Sachdev, Anna Katharina Schellhaus, Karin Schiller, Cornelia Sieverding, Gandhi Theerthagiri, Benjamin Vollmer, Marion Weberruss, and Hideki Yokoyama. It is a pleasure to work with so many interesting people so willing to share ideas and practical advice. I am especially grateful to Ada for getting me started on the decondensation project, for calling me at 2 a.m. the first time you isolated single chromosomes, for pierogi, critical discussions, and above all friendship. To Ben for sharing scientific ideas, your amazing graphics and 3D point of view, and your surprisingly ironic sense of humour! To Dani for taking an interest in the LSD1 project and helping me get started with live-cell imaging, for your support and perspective, and for many enlightening debates about life and science. To Micha for your balanced advice and to Katharina and Paola for our tea breaks and fun discussions, and of course endless theories regarding frog psychology.

The Friedrich Miescher Laboratory and the Max Planck Institute for Developmental Biology provided a collaborative work environment and I greatly benefited from the expertise of numerous people throughout my PhD. I am grateful to Christian Liebig and Virgilio Falla for supporting light microscopy experiments and Matthias Flötenmeyer for help with TEM. I also want to thank Nadine Weiss for her tireless care of the rabbits and frogs.

Anyone interested in truth knows that kindness is its highest form and I am fortunate to have been surrounded by many other wonderful people in Tübingen. I

am especially grateful to Anthony, Catherine, Berit, Irina, Andrey, Anna-Lena, André, Julia, Diana, Sara, Masa, Nelson, Frederike, Maria, Brock, Alex, Robin, Anna, Maggie and Katharina.

Finally, I am deeply indebted to my parents Rona and David and my sisters Alexis, Caitlin, and Brittany who have always supported me and have never made me question the importance or beauty of an adventure.

Table of Contents

1.1 Summary

The eukaryotic genome is compartmentalized and organized within the two membranes of the nuclear envelope. Integrated at pores spanning the envelope are nuclear pore complexes, which mediate the regulated exchange of macromolecules between the nuclear compartment and the cell cytoplasm. During mitosis, the metazoan nucleus is disassembled so that the mitotic spindle can access the highly condensed chromosomes and mediate their faithful segregation. The nuclear envelope and nuclear pore complexes must therefore be rebuilt on the de-condensing chromatin at the end of every mitotic cell division.

In recent years, advances have been made towards elucidating the molecular composition and structural features of the nuclear envelope and nuclear pore complexes. Additionally, the importance and several determinants of three dimensional chromatin organisation within the boundaries of the nuclear envelope have begun to come to light. However, although many essential factors have been identified, the molecular mechanisms governing the establishment of nuclear architecture at the end of mitosis remain poorly defined. It is particularly unclear how the assembly of the nuclear envelope and pore complexes is coordinated with the changing chromatin landscape at the end of mitosis.

The work presented in this thesis aimed to identify regulatory landmarks of nuclear envelope formation. A cell-free nuclear reconstitution system based on *Xenopus laevis* extracts was employed to screen various chemical inhibitors for nuclear assembly defects. A group of inhibitors targeting Lysine (K) Specific Demethylase 1 (A) (LSD1/KDM1A) blocked the formation of a closed nuclear envelope and nuclear pore complex assembly *in vitro*. LSD1 catalyzes the demethylation of mono- and di-methylated lysines of histone H3 tails. Immunodepletion of LSD1 and rescue experiments using recombinant proteins confirmed that LSD1-dependent demethylation is specifically required for cell-free nuclear assembly. Accordingly RNAi-mediated depletion of LSD1 in human cells significantly extended the length of telophase, during which the nuclear envelope is formed, based on live cell imaging experiments and the automated tracking and annotation of chromatin features during cell division.

A modified version of the cell-free nuclear reconstitution assay that employs mitotic chromatin clusters was developed and used to specifically assay the role of

LSD1 in post-mitotic chromatin decondensation. Although the nuclear and chromatin-occupied volume was consistently smaller both *in vitro* and in cultured cells in the absence of LSD1 activity, LSD1 did not seem to be required for the initial steps of chromatin decondensation. Nonetheless, additional biochemical experiments indicated that LSD1 activity was essential for the recruitment of early-associating nuclear envelope and nuclear pore complex proteins to chromatin.

The data presented here demonstrate that LSD1 regulates the recruitment and assembly of a functional nuclear envelope on post-mitotic chromatin. Although non-histone protein targets cannot be excluded, the identification of the histone demethylase LSD1 as an essential regulator of nuclear assembly represents one of the first descriptions of a factor linking nuclear envelope formation with the changing chromatin landscape at the end of mitosis.

1.2 Zusammenfassung

Die zwei Membranen der Kernhülle trennen das kompakt organisierte Genom vom Rest der Zelle. Eingebettet in die Kernhülle sind Kernporenkomplexe, die den regulierten Transport von Makromolekülen zwischen Zytoplasma und Nukleoplasma vermitteln. In tierischen Zellen wird die Kernhülle während der Mitose aufgelöst, sodass der Spindelapparat Zugang zum stark kondensierten Chromatin erhält und so dessen präzise Aufteilung auf die Tochterzellen vermitteln kann. Am Ende jeder mitotischen Zellteilung müssen sich sowohl die Kernhülle als auch Kernporenkomplexe wieder an dem sich dekondensierenden Chromatin ausbilden.

In den letzten Jahren wurden wichtige Fortschritte bei der Aufklärung der molekularen Zusammensetzung und Struktur von Kernmembran und Kernporenkomplexen gemacht. Des Weiteren wurde die Bedeutung der dreidimensionalen Organisation des Chromatins innerhalb der Begrenzung der Kernhülle offensichtlich. Obwohl viele kritische Faktoren für die Ausbildung der Zellkernarchitektur identifiziert wurden, bleiben die molekularen Mechanismen nur unzureichend definiert. Insbesondere ist unklar, wie der Aufbau der Kernhülle und der Kernporenkomplexe mit der sich verändernden Chromatinarchitektur am Ende der Mitose koordiniert ist.

Ziel dieser Dissertation war es, die Regulation des Kernhüllenaufbaus zu erforschen. Ein zellfreies Zellkernrekonstitutionssystem, welches auf Eiextrakten von *Xenopus laevis* basiert, wurde verwendet, um chemische Inhibitoren des Zellkernaufbaus zu identifizieren. Eine Gruppe dieser Inhibitoren, die die Funktion der Lysindemethylase LSD1/KDM1A blockieren, verhinderte die Ausbildung einer geschlossenen Kernhülle und von Kernporenkomplexen *in vitro*. LSD1 katalysiert die Demethylierung von mono- und dimethylierten Lysinen im endständigen Arm des Histons H3. Eine Immundepletion von LSD1 mit anschließender Zugabe von rekombinantem LSD1 bestätigte, dass die Demethylierungsaktivität von LSD1 für den Wiederaufbau von Zellkernen am Ende der Mitose benötigt wird. Entsprechend konnte durch Live-Cell-Imaging und automatische Bildanalyse der Chromatinarchitektur während der Zellteilung gezeigt werden, dass die Herunterregulierung des LSD-Spiegels durch RNAi in menschlichen Zellen die Dauer der Telophase, während der sich die Kernhülle ausbildet, deutlich verlängerte.

Eine modifizierte Version des Zellkernrekonsitutionssystems, die mitotische Chromatincluster nutzt, wurde entwickelt, um spezifisch die Funktion von LSD1 in der Chromatindekondensierung am Ende der Mitose zu untersuchen. Obwohl die Volumina von Zellkern und Chromatin sowohl *in vitro* als auch in Zellkulturzellen in Abwesenheit von LSD1 kleiner waren, scheint LSD1 nicht für die ersten Schritte der Chromatindekondensierung erforderlich zu sein. Dennoch zeigten weitere biochemische Experimente, dass LSD1 für die Bindung von Kernmembran- und Kernporenproteinen notwendig ist, die früh an das Chromatin rekrutiert werden.

Die hier vorgestellten Ergebnisse zeigen, dass die Histondemethylase LSD1 die Anlagerung und Ausbildung einer funktionellen Kernhülle an Chromatin am Ende der Mitose reguliert. Auch wenn Nicht-Histon-Proteine als potentielle Substrate der LSD1 Aktivität nicht ausgeschlossen werden können, stellt die Identifizierung von LSD1 als notwendigen Regulator des Zellkernwiederaufbaus die erste Beschreibung eines Faktors dar, der die Ausbildung einer Kernhülle mit der sich verändernden Chromatinstruktur am Ende der Mitose funktionell verbindet.

2. Abbreviations

LSD1/KDM1A	Lysine (K) specific demethylase 1(A)
NPC	nuclear pore complex
Nup	nucleoporin
FG	phenylalanine glycine
NE	nuclear envelope
INM	inner nuclear membrane
ONM	outer nuclear membrane
LBR	lamin B receptor
LEM	lamina-associated polypeptide-emerin-MAN1
ER	endoplasmic reticulum
DNA	deoxyribonucleic acid
RNA	ribonucleic acid
RNAi	RNA interference
RNP	ribonucleoprotein
HP1	heterochromatin protein 1
BAF	barrier to auto-integration factor
LAD	lamina-associated domain
LINC	linker of nucleoskeleton and cytoskeleton
NLS	nuclear localisation signal
NES	nuclear export signal
CDK1	cyclin-dependent kinase 1
PP1/PP2	protein phosphatase 1/protein phosphatase 2
FAD	flavin adenine dinucleotide
GFP	green fluorescent protein
µm	micrometer
kDa	kilodalton
DAPI	4‘,6-Diamidin-2-phenylindol
DiIC18	1,1'-Dioctadecyl-3,3,3',3'- Tetramethylindocarbocyanine Perchlorate

3.1 The nucleus

The nucleus is the defining morphological and functional feature of eukaryotes. Compartmentalization of the nuclear genome affords the eukaryotic cell an unprecedented degree of regulatory complexity, which in many ways is only starting to be uncovered. Remarkably, nearly all eukaryotes share the same defined set of ultra-structural nuclear features; the nuclear genome, lamina, envelope, and pore complexes (Fig. 1). The high degree of conservation in nuclear compartmentalization strategies has been proposed to arise because nuclear pore complexes (NPCs) and nuclear envelope membranes co-evolved with both the endomembrane system and the need to segregate and re-partition the genome during mitosis (Reviewed in (Osorio and Gomes 2013, Wilson and Dawson 2011, Field et al. 2014)).

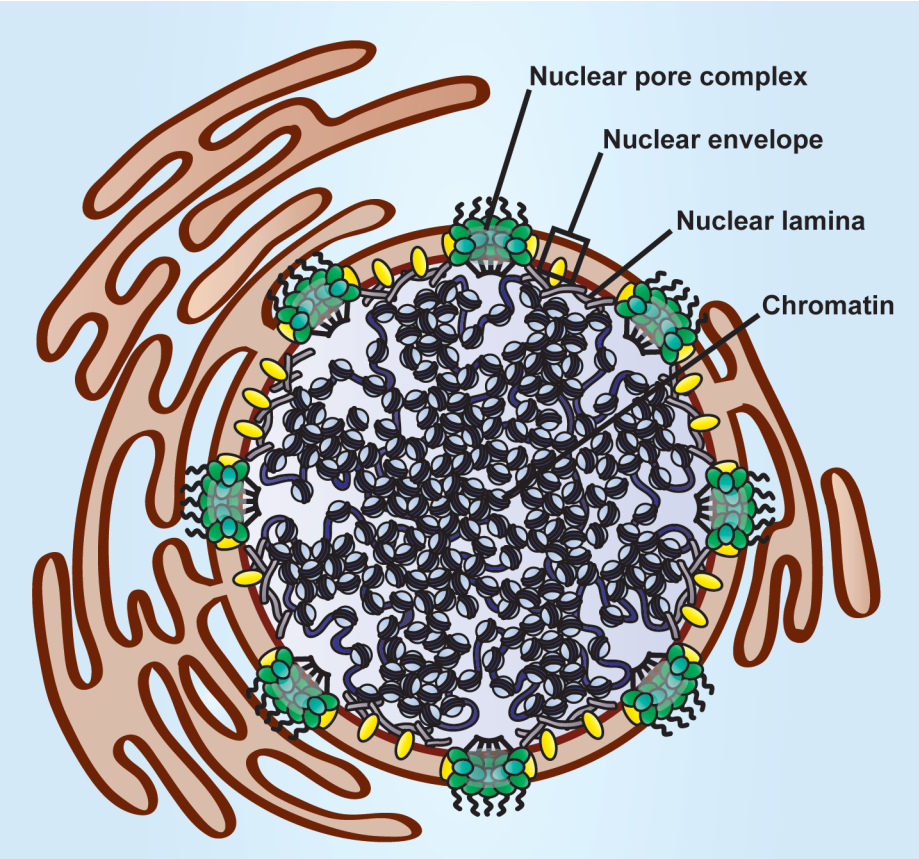

Figure 1. Schematic: The nucleus. The eukaryotic genome is organized within the two membrane bilayers of the nuclear envelope and the underlying nuclear lamina. Nuclear pore complexes span the nuclear envelope at points of fusion between the inner and outer membranes and mediate the bidirectional exchange of proteins, ribonucleic acids, and ribonucleoprotein particles between the nucleoplasm and the cytoplasm.

3.1.1 The nuclear envelope

3.1.1.1 Nuclear membranes

The nuclear envelope provides the hydrophobic barrier separating the nucleoplasm from the cytoplasm. It consists of two membrane bilayers that are juxtaposed in characteristically close proximity, separated by the perinuclear space. The inner and outer nuclear membranes are considered a compartment of the endoplasmic reticulum with which they are contiguous (reviewed in (Voeltz et al. 2002)). However, the inner nuclear membrane is additionally characterized by a distinct protein composition owing to multiple interactions with chromatin factors and proteins of the nuclear lamina (Reviewed in (Schirmer and Gerace 2005)). In vertebrates, the most prominent of these interactions include the lamin B receptor (LBR), which aptly interacts with lamin B as well as with histones and heterochromatin protein 1 (HP1) (Reviewed in (Olins et al. 2010)), and the LEM-domain-containing proteins; lamina-associated polypeptide 2β (LAP2β), Emerin, and Man1, which also interact with lamins and with the chromatin-associated protein, barrier to autointegration factor (BAF) (Reviewed in (Brachner and Foisner 2011, Gruenbaum et al. 2005, Wagner and Krohne 2007)) (Fig. 2). Despite the large number of nuclear membrane-specific proteins identified, relatively few have been characterized in detail.

The nuclear lamina is a polymer of type V intermediate filaments that lines the inner nuclear membrane at the chromatin surface (Fig. 2). The number of lamin genes varies among metazoans and ranges from 3-5 in vertebrates, giving rise to a larger number of distinct lamin proteins (Reviewed in (Dittmer and Misteli 2011)). The vertebrate lamina is composed of cell-type specific ratios of the different lamin proteins, which are regulated during development and cell differentiation. This composition can confer different levels of mechanical support to the nucleus and contributes to chromatin organization and transcriptional regulation (Reviewed in (Butin-Israeli et al. 2012, Dittmer and Misteli 2011, Shimi et al. 2010)).

Mechanical forces from the cytoplasm are transmitted to the nucleus via linker of nucleoskeleton and cytoskeleton (LINC) complexes in the nuclear envelope (Reviewed in (Starr and Fridolfsson 2010)). LINC complexes consist of SUN domain-containing proteins at the inner nuclear membrane, which interact with the underlying lamina, and

KASH domain-containing proteins at the outer nuclear membrane, which interact with cytoplasmic microtubules and the actin cytoskeleton. SUN and KASH proteins form bridges across the perinuclear space where they interact (Reviewed in (Burke 2012, Sosa et al. 2012)).

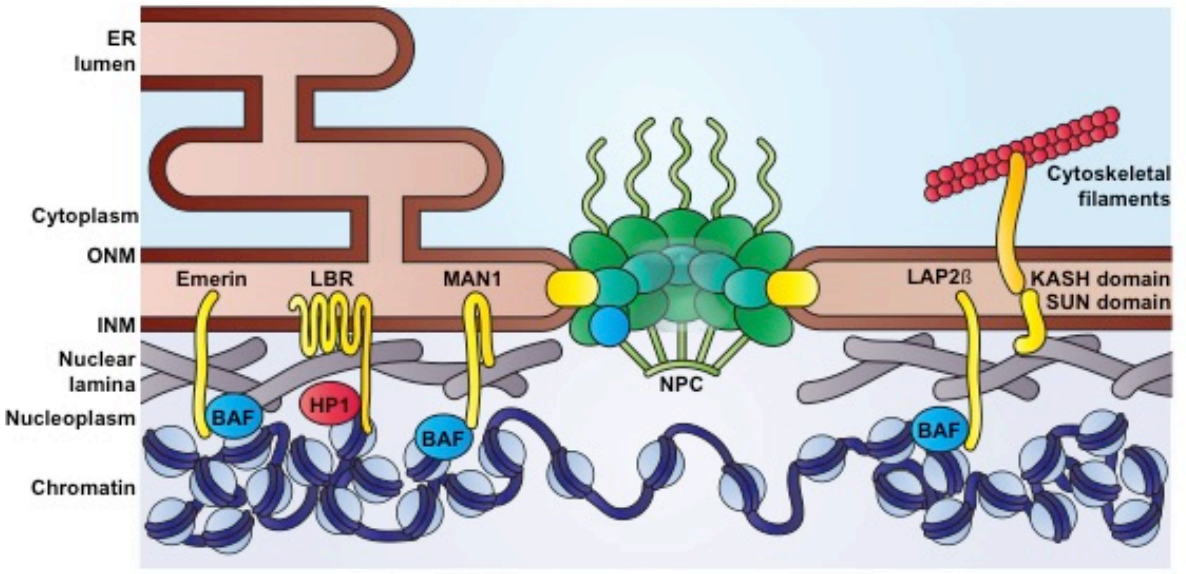

Figure 2. Schematic: The nuclear envelope is a compartment of the endoplasmic reticulum (ER). The outer nuclear membrane (ONM) is continuous with the ER but the inner nuclear membrane (INM) possess a distinct protein composition due to interactions between inner nuclear membrane proteins, such as the lamin B receptor (LBR) and the LEM-domain-containing proteins Lap2b, emerin and Man1, with lamins, histones, or chromatin associated proteins such as heterochromatin protein-1 (HP1) and barrier to auto-integration factor (BAF). The nucleoskeleton is connected to the cytoskeleton by LINC complexes that span the nuclear envelope lumen. These complexes are composed of KASH-domain-containing proteins at the ONM, which interact with intermediate filaments and microtubules in the cytoplasm and SUN-domain containing proteins at the INM, which are anchored to the underlying nuclear lamina.

3.1.1.2 Vertebrate nuclear pore complexes

Integrated at points of fusion between the two bilayers of the envelope are nuclear pore complexes. With the exception of vesicle-mediated nuclear egress employed by herpes viruses (Reviewed in (Johnson and Baines 2011)) and some ribonucleoprotein (RNP) particles in drosophila larvae (Speese et al. 2012), NPCs are

the exclusive gateway through the nuclear envelope for proteins, ribonucleic acids (RNAs) and ribonucleoprotein (RNP) particles (Mohr et al. 2009). They are among the largest multi-protein assemblies in a eukaryotic cell. A single vertebrate NPC has an approximate mass of 120 MDa and is roughly 100 nm in diameter ((Akey and Radermacher 1993, Beck et al. 2007, Fahrenkrog et al. 2000, Hinshaw and Milligan 2003, Ori et al. 2013, Reichelt et al. 1990). Each NPC is composed of multiple copies of 30 distinct nucleoporins arranged in a highly conserved eight-fold rotational symmetry in the nuclear envelope (Reviewed in (Bilokapic and Schwartz 2012, Schwartz 2013, Brohawn et al. 2009, Rout et al. 2000).

Nucleoporins are found in biochemically discrete subcomplexes that act as molecular building blocks of the NPC (Matsuoka et al. 1999, Dultz et al. 2008). The core scaffold of the NPC stabilizes the unusual topology of the highly curved pore membrane and anchors the remaining nucleoporins ((Bui et al. 2013) also reviewed in (Antonin and Mattaj 2005, Schwartz 2013). It consists of three rings and two absolutely essential and highly conserved structural subcomplexes, the Nup107-160 complex (Boehmer et al. 2003, Harel et al. 2003b, Walther et al. 2003a) and the Nup93 complex (Franz et al. 2005, Grandi et al. 1997, Hawryluk-Gara et al. 2008). The outer cytoplasmic and nucleoplasmic rings are each composed of 16 copies of the Y-shaped decameric Nup107-160 complex, which anchor the cytoplasmic filaments and nuclear basket, respectively (Alber et al. 2007, Bui et al. 2013, Lutzmann et al. 2002, Szymborska et al. 2013). The heteromeric Nup93 complex occupies the central ring (Alber et al. 2007, Krull et al. 2004) and is closely associated with the pore membrane, where it is anchored due to interactions of one of its constituent nucleoporins, Nup53, both directly with membranes (Marelli et al. 2001, Vollmer et al. 2012) and via the conserved transmembrane nucleoporin Ndc1 (Eisenhardt et al. 2014a, Mansfeld et al. 2006, Onischenko et al. 2009). Both the Nup93 and Nup107-160 complexes are also linked to the pore membrane by a second transmembrane nucleoporin POM121 (Mitchell et al. 2010, Rasala et al. 2008). A third transmembrane nucleoporin, GP210, has also been identified in vertebrates but its function at the NPC is not essential and it may play a tissue-specific role (Antonin et al. 2005, Cohen et al. 2003, D'Angelo et al. 2012, Eriksson et al. 2004, Gomez-Cavazos and Hetzer 2015, Olsson et al. 2004, Stavru et al. 2006). The central channel of the NPC consists of a meshwork of intrinsically disordered phenylalanine-glycine (FG) repeat-containing nucleoporins (Bayliss et al. 2002, Fribourg

et al. 2001, Grant et al. 2003, Liu and Stewart 2005) that interact with the Nup93 complex (Alber et al. 2007, Grandi et al. 1997, Sachdev et al. 2012, Schlaich et al. 1997). Although the exact nature of this meshwork is not fully understood, the FG-nucleoporins collectively give rise to the diffusion barrier function of the NPC (Reviewed in (Peleg and Lim 2010)) (Fig. 3).

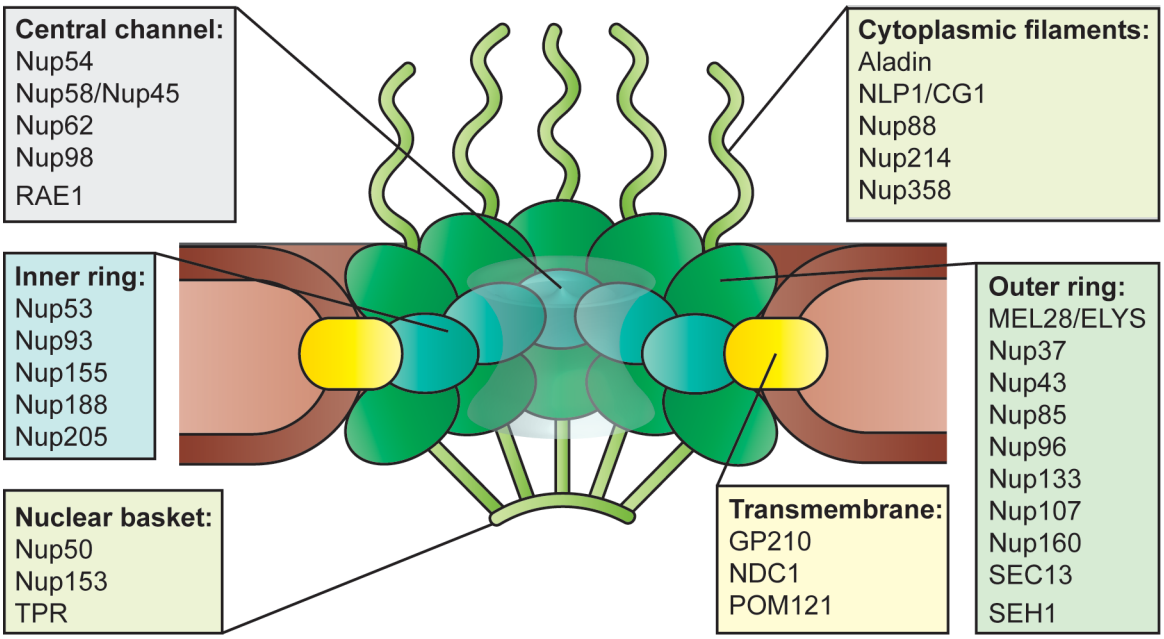

Figure 3. Schematic: The vertebrate nuclear pore complex spans the outer and inner nuclear membranes and is composed of multiple copies of approximately 30 nucleoporins arranged in eight-fold rotational symmetry. The outer rings are primarily composed of the Nup107-160 complex, which connects to the nuclear basket and cytoplasmic filaments on either side of the nuclear envelope, and the inner ring consists of the Nup93 complex. The outer and inner rings comprise the nuclear pore complex (NPC) scaffold and are anchored in the pore membrane due to interactions with transmembrane nucleoporins. The permeability barrier and transport functions of the NPC are conferred by the FG-repeat-containing nucleoporins of the central channel.

3.1.1.3 Nucleocytoplasmic transport

The NPC enables the regulated bidirectional exchange of 40-100 KDa macromolecules, which are beyond the limit of diffusion, between the cytoplasm and the nucleoplasm. Nucleocytoplasmic transport of soluble proteins is facilitated by a large

family of transport receptors collectively termed karyopherins, which recognize cargoes by the presence of nuclear localization (NLS) and nuclear export (NES) signal sequences (Reviewed in (Pemberton and Paschal 2005)). Interactions between these import and export receptors and the FG-repeat nucleoporins are required for translocation through the central channel of the pore (Bayliss et al. 1999, Strasser and Hurt 2000, Strawn et al. 2004, Strawn et al. 2001, Terry et al. 2007), however the precise mechanism by which the receptor-cargo complexes move through the FG-protein rich pore is still the subject of much debate (Frey and Gorlich 2007, Lim et al. 2007, Melcak et al. 2007, Peters 2005, Ribbeck and Gorlich 2002). Nucleoporins localized at both the cytoplasmic and nucleoplasmic sides of the NPC also contribute to the docking and unloading of receptor cargo complexes ((Hamada et al. 2011, Ogawa et al. 2012, Roloff et al. 2013, Waldmann et al. 2012, Walther et al. 2001, Walde et al. 2012), also reviewed in(Walde and Kehlenbach 2010)).The directionality of transport is provided by the asymmetric distribution of the nucleotide-bound state of the small GTPase Ran and the distinct requirements of the import and export receptors for cargo complex formation and dissociation (Reviewed in (Fried and Kutay 2003, Mattaj and Englmeier 1998)). High levels of RanGTP are found in the nucleus due to the local concentration of its guanine exchange factor regulator of chromosome condensation 1 (RCC1) on chromatin. In the nucleus, RanGTP promotes the dissociation of importin-bound cargoes that were imported through the NPC from the cytoplasm and the formation of exportin-cargo complexes, which are then ready for export. In the cytoplasm, exportin-bound cargos are released due to the GTPase activating protein-dependent hydrolysis of RanGTP. The relatively low concentration of RanGTP in the cytoplasm supports the formation of importin-cargo complexes.

Transmembrane proteins of the inner nuclear membrane are transported into the nucleus from the endoplasmic reticulum. Integral membrane proteins harbouring negligibly small extra-lumenal domains can freely diffuse through the NPC in the plane of the membrane. In what is called the diffusion-retention model, these proteins are thought to accumulate in the nuclear membranes due their interactions with specific nuclear proteins such as those associated with chromatin or the lamina (Ohba et al. 2004, Wu et al. 2002). Transmembrane proteins with larger extra-lumenal domains can be transported by karyopherin-mediated import, however it is not clear whether they traverse the NPC through its central FG-protein meshwork or rather through peripheral

NPC channels (Reviewed by (Antonin et al. 2011)).

3.1.2 The nuclear genome

3.1.2.1 Chromatin folding

The total nuclear DNA content of a normal human diploid cell is approximately $6X10^9$ base pairs and if arranged linearly would be close to 2 meters in length. In order to accommodate an average nuclear volume of 100 um^3, it is predicted that DNA must be condensed by a factor of 3×10^5 (Reviewed in (Bloom and Joglekar 2010)). This condensation is accomplished by the hierarchical packaging of DNA into chromatin fibers and subsequent higher order folding. The basic repeating unit of chromatin is the eukaryotic nucleosome. Core nucleosomes are octamers of histones H2A, H2B, H3 and H4 wrapped by 146-147 bp of DNA (Luger et al. 1997). This first level of chromatin organization gives rise to the 10 nm fiber, also known as “beads on a string” (Olins and Olins 1974, Woodcock et al. 1976a, Woodcock et al. 1976b), which is the template for active transcription.

Folding or coiling of 10 nm fibers was traditionally thought to give rise to 30 nm fibers that were then further folded into higher order chromatin assemblies (Belmont and Bruce 1994, Widom and Klug 1985, Finch and Klug 1976, Horowitz et al. 1994, Rattner and Lin 1985, Song et al. 2014, Williams and Langmore 1991, Woodcock et al. 1984, Zentgraf and Franke 1984). However, the combined use of improved sample preparation methods and new high resolution imaging techniques aimed at visualizing these fibers *in situ* have failed to detect 30 nm fibers during interphase or mitosis and even indicated the presence of 10 nm fibers in densely packed chromatin regions of interphase cells (Efroni et al. 2008, Eltsov et al. 2008, Fussner et al. 2012, Joti et al. 2012, Nishino et al. 2012). Although the existence of localized 30 nm fibers cannot be excluded, the higher organization of 10 nm fibers is sufficient to explain the compaction and regulation of the nuclear genome (Reviewed in (Fussner et al. 2011, Maeshima et al. 2010)). Regardless of the exact conformation, higher order chromatin folding during interphase generates less accessible and in turn transcriptionally inactive chromatin (Levy and Noll 1981, Hu et al. 2009, Muller et al. 2001). Accordingly, pluripotent cells characterized by widespread low-level transcription possess a large proportion of open

and uniformly distributed chromatin compared to more differentiated cell types with far less promiscuous transcriptional programs (Efroni et al. 2008, Ahmed et al. 2010, Fussner et al. 2010, Ricci et al. 2015). Open and closed chromatin conformations are thought to be modulated by post-translational modifications to histone tails, including phosphorylation, acetylation, and methylation, which can act directly on higher order chromatin structure or by via the recruitment of non-histone chromatin proteins (Reviewed in (Tessarz and Kouzarides 2014)).

3.1.2.2 Three-dimensional chromatin organization

During interphase, chromatin occupies at most half of the nuclear volume (Fussner et al. 2010) and is organized non-randomly in the three-dimensional space of the nucleus. It is becoming increasingly clear that this 3D organization plays an important role in gene regulation and cell phenotypes. Individual chromosomes have been found to occupy distinct nuclear territories that are maintained throughout cell division cycles (Reviewed in (Cremer and Cremer 2006, Misteli 2007). These territories are often cell type-specific and maintain a relative radial position with respect to the nuclear periphery. In most cases, gene dense chromosomes are preferentially found in the nuclear interior while gene poor chromosomes localize to more peripheral positions (Bolzer et al. 2005, Bridger et al. 2000, Cremer et al. 2003). Within chromosomes, transcriptionally active and inactive chromatin segregates into distinct domains with similar preferences for relative interior and peripheral positioning with respect to the nuclear space (Reviewed in (Bickmore and van Steensel 2013)). These regions can be further partitioned in topological domains that include long-range interactions between regulatory elements and distal promoters as well as clusters of co-regulated genes, which have been proposed to arise by the formation of large chromatin loops (Reviewed in (Dekker 2014, Hofmann and Heermann 2015)).

In recent years, numerous studies have indicated that the nuclear envelope functions not only as a structural barrier in the compartmentalization of the genome but is also an active participant in its 3D organization and in turn regulation. In most cell types, the peripheral chromatin localized adjacent to the nuclear envelope largely consists of conformationally closed, transcriptionally silent heterochromatin (Reviewed in (Akhtar and Gasser 2007, Francastel et al. 2000)). This peripheral heterochromatin

directly contacts the envelope in lamina-associated domains (LADs), an interaction that depends on lamins and transmembrane proteins of the inner nuclear membrane, including LBR (Reviewed in (Talamas and Capelson 2015, Zuleger et al. 2011)). The formation of LADs is thought to contribute to gene silencing in a cell lineage-specific manner and it has been suggested that the tissue-specific expression of lamins and nuclear envelope transmembrane proteins impacts not only the degree of peripheral heterochromatin but also the localization of specific gene loci (Reviewed in (Talamas and Capelson 2015)). Nuclear envelope and lamina proteins are required to maintain peripheral heterochromatin, however, the mechanism that targets chromatin to these domains is less clear. Several chromatin associated factors, including HP1 and BAF, as well as specific histone modifications, including methylation of Histone H3 at lysine 9, have been implicated and it is likely that more than one molecular strategy is employed (Reviewed in (Amendola and van Steensel 2014)).

Proteins of the NPC have also been found to play a role in gene expression and the spatial distribution of chromatin in the nucleus. In contrast to the nuclear lamina, NPCs are generally associated with open transcriptionally active euchromatin (Reviewed in (Capelson et al. 2010)). It has been proposed that this organisation is adopted to facilitate co-regulated transcription and mRNA export (Blobel 1985). The NPC plays an essential active role in the formation of heterochromatin exclusive zones via the nuclear basket protein Tpr (Krull et al. 2010) and possibly other nucleoporins that have been found to bind at boundary elements in drosophila (Kalverda and Fornerod 2010). Furthermore, much like the lamin associated domains, nucleoporin associated chromatin domains have also been identified and various nucleoporins have been implicated in the regulation of tissue-specific gene expression, although the interpretation of these results is often confounded by the presence of nucleoplasmic nucleoporin pools (Reviewed in (Capelson et al. 2010, Talamas and Capelson 2015).

3.2 Nuclear dynamics during open mitosis

The enclosure of chromatin inside the nucleus necessitates the physical segregation of the duplicated genome during eukaryotic cell division. The mitotic spindle, a microtubule-based structure assembled from predominantly cytoplasmic components, facilitates chromosome segregation in all eukaryotes. However, distinct

strategies have evolved to accomplish this task (Reviewed in (De Souza and Osmani 2009, Smoyer and Jaspersen 2014)). Many eukaryotes employ closed or semi-closed mitosis, which involve the assembly of the mitotic spindle inside the nucleus with either no loss or a partial loss of nuclear envelope integrity, respectively. In contrast, metazoan cells divide by open mitosis. The spindle assembles in the cytoplasm and the nuclear envelope is disassembled to facilitate access to the mitotic chromosomes (Fig. 4). This disassembly means that the nucleus must be reconstructed each time an animal cell divides (Fig. 5).

3.2.1 Nuclear disassembly

The cyclin dependent kinase CDK1 and its activating factor cyclin B drives the eukaryotic cell cycle ((Santamaria et al. 2007), also reviewed in (Domingo-Sananes et al. 2011)). The activity of CDK1 and numerous downstream kinases (Lens et al. 2010, Malumbres 2011) gives rise to the remarkable structural changes that characterize nuclear organisation during mitosis and global phosphoproteomic studies have identified thousands of mitotic phosphorylation events (Daub et al. 2008, Olsen et al. 2010, Pagliuca et al. 2011). The recent identification of Greatwall kinase as an essential inhibitor of the protein phosphatase PP2A during mitosis (Alvarez-Fernandez et al. 2013) suggests that mitotic phosphorylation marks are not only conferred but also actively maintained in order to regulate the key events surrounding chromosome segregation during mitosis, including chromosome condensation and nuclear envelope breakdown.

3.2.1.1 Chromosome condensation

The activation CDK1 in the cytoplasm at the onset of mitosis initiates global changes to the nuclear import pathway, which ensure the rapid accumulation of CDK1/cyclin B in the nucleus (Gavet and Pines 2010). This accumulation triggers the reorganization and compaction of interphasic chromatin that gives rise to the characteristic X-shaped mitotic chromosomes. Efforts to quantify to quantify chromosome compaction have produced conflicting results and suggest that, compared to interphase chromatin, mitotic chromosome condensation in animal cells ranges from

2- to 50-fold (Reviewed in (Vagnarelli 2012, Belmont 2006)). Furthermore, mitotic chromosome structure is not random, evidenced by reproducible banding patterns for each chromosome that are transmitted through successive cell division cycles ((Terrenoire et al. 2010), also reviewed in (Craig and Bickmore 1993)). Chromatin condensation is mediated by proteins of the chromatin scaffold particularly Condensins I and II, which are phosphorylated by CDK1, as well as Topoisomerase II, and the chromokinesin KIF4A (Reviewed in (Vagnarelli 2012)). The involvement of other mitotic kinase substrates is likely, however to date they have not been identified. Several histone modifications accompany the transformation of interphasic chromatin to mitotic chromosomes. Given the capacity of phosphorylation, acetylation, and methylation of histone tails to impact nucleosome interactions and higher order chromatin packing, it seems likely that they would contribute to mitotic chromosome condensation. The most prominent cell cycle dependent modification is the phosphorylation of Histone H3 at serine 10 by Aurora B kinase ((Gurley et al. 1974), also reviewed in (Prigent and Dimitrov 2003)), however this mark does not play an active role in the establishment or maintenance of mitotic chromosome condensation *in vivo* (Hsu et al. 2000, MacCallum et al. 2002, Vagnarelli et al. 2006). Instead, it has been proposed that phosphorylation of Histone H3 initiates a cascade of histone modifications events, such as the de-acetylation of Histone H4, to promote chromosome condensation (Wilkins et al. 2014). Other histone modifications that have been implicated in mitotic chromosome condensation include the sequential de-acetylation and methylation of Histone H3 K9 (Park et al. 2011) and a combinatorial mark consisting of Histone H3 T3p, K4me3, and R8me2 ((Markaki et al. 2009), also reviewed in (Georgatos et al. 2009)). It remains to be seen whether histone modifications are directly involved in mitotic chromosome condensation or rather act to recruit and position relevant non-histone chromatin associated proteins.

3.2.1.2 Nuclear envelope breakdown

Following the onset chromosome condensation, nuclear envelope breakdown is initiated by the loss of NPC barrier function, the disassembly of the nuclear lamina, and in some organisms the physical rupturing of the nuclear envelope mediated by microtubules. Hyperphosphorylation of the central channel nucleoporin Nup98 by CDK1

and NIMA-related kinases disrupts its interaction with NPCs and initiates their disassembly and the loss of the nuclear envelope permeability barrier (Laurell et al. 2011). Several other nucleoporins, including Nup107-160 and Nup53 are phosphorylated by mitotic kinases (Favreau et al. 1996, Glavy et al. 2007, Macaulay et al. 1995, Onischenko et al. 2005) and it is likely that the phosphorylation-dependent dissociation of nucleoporin interactions is a general mechanistic feature of NPC disassembly during mitosis. Phosphorylated nucleoporins, many of which nonetheless remain associated in distinct subcomplexes (Matsuoka et al. 1999), are distributed in the cytoplasm during mitosis where they have been found to contribute to various mitotic processes, including spindle assembly and chromosome segregation (Reviewed in (Chatel and Fahrenkrog 2011)). The transmembrane nucleoporin GP210 is also phosphorylated during mitosis (Favreau et al. 1996), a modification that has been found to disrupt its interaction with the NPC (Onischenko et al. 2007). Although GP210 is not strictly required for NPC assembly or integrity it was found to be essential for NPC disassembly during mitosis (Audhya et al. 2007, Galy et al. 2008). The association of inner nuclear membrane proteins with the nuclear lamina and chromatin is similarly regulated by phosphorylation. The mitotic phosphorylation of LAP2α, LAP2β and LBR as well as a chromatin associated interaction binding partner, BAF, promotes the dissociation of the inner nuclear membrane proteins from the lamina and chromatin and supports the release of the nuclear envelope (Collas et al. 1996, Foisner and Gerace 1993, Gorjanacz et al. 2007, Ito et al. 2007, Nichols et al. 2006, Pyrpasopoulou et al. 1996, Tseng and Chen 2011). In mammals, microtubules also contribute to nuclear envelope breakdown by creating the tension that eventually ruptures the nuclear envelope membranes (Beaudouin et al. 2002, Salina et al. 2002, Muhlhausser and Kutay 2007) and by facilitating the transport of membrane remnants away from chromatin (Muhlhausser and Kutay 2007). Only after nuclear envelope rupture (Beaudouin et al. 2002, Lenart et al. 2003) does the nuclear lamina depolymerize due to the cdk1 and PKC dependent phosphorylation of lamins (Collas 1999, Gerace and Blobel 1980, Heald and McKeon 1990, Peter et al. 1990).

Once it is released from chromatin and disassembled, the nuclear envelope is absorbed by the mitotic ER. It has been proposed that the nuclear envelope membranes maintain their identity as a sub-compartment of the ER during mitosis in order to facilitate efficient nuclear assembly upon mitotic exit (Mattaj 2004). This

hypothesis is supported by a number of *in vitro* experiments that indicate distinct vesicle populations with unique biochemical compositions and different capacities to support nuclear envelope assembly can be isolated from mitotic ER preparations (Antonin et al. 2005, Buendia and Courvalin 1997, Chaudhary and Courvalin 1993, Collas et al. 1996, Ulbert et al. 2006, Vigers and Lohka 1991, Vollmar et al. 2009). The mitotic ER has been visualized as both a network of tubules (Puhka et al. 2007) or cisternal sheets (Lu et al. 2009) and it is not clear whether this difference reflects experimental procedures or the possibility that, like the interphase ER (Voeltz et al. 2002, Puhka et al. 2012), the morphology of the mitotic ER is cell type specific. Regardless of whether it is composed mainly of sheets or tubules, these observations suggest that the vesiculation of nuclear envelope membranes in mitotic ER preparations is likely an artifact of their isolation and fractionation. Nonetheless, membrane micro-domains have been found to segregate into distinct vesicles (Simons and Toomre 2000) and it is possible that the potential to isolate nuclear envelope-specific membrane vesicles reflects micro-domain formation in the intact mitotic ER.

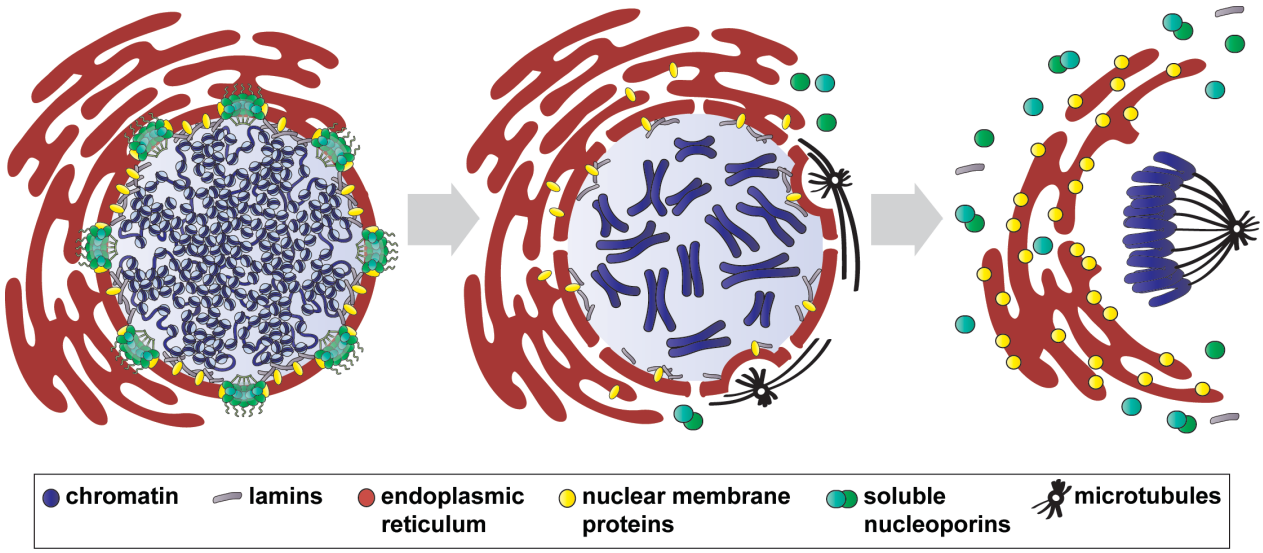

Figure 4. Schematic: Nuclear disassembly during open mitosis. The metazoan nuclear envelope is disassembled during mitosis to facilitate the capture of highly condensed replicated chromosomes by the mitotic spindle. Disassembly is initiated by the dissociation of FG repeat-containing nucleoporins from nuclear pore complexes at the beginning of mitosis. The nuclear membranes and resident integral membrane proteins are released from chromatin and absorbed by the endoplasmic reticulum. Soluble nucleoporins, some of which remain associated in subcomplexes, as well as lamins of the disassembled lamina are dispersed in the common cytoplasm as sister chromatids are pulled apart to give rise to two new daughter cells.

3.2.2 Nuclear reassembly

Mitotic chromosomes achieve maximal compaction during anaphase (Mora-Bermudez et al. 2007, Ohsugi et al. 2008). Following segregation, chromosome decondensation and reorganization is required to give rise to a functional interphase nucleus yet there are very few details regarding the molecular mechanisms that mediate this process. The extraction of the mitotic kinase Aurora B by the AAA+-ATPase p97 (Ramadan et al. 2007) and the activity of the protein phosphatase PP1 (Landsverk et al. 2005, Lee et al. 2010) are thought to be required for post-mitotic chromatin decondensation, however the downstream molecular events that modulate the necessary changes to chromatin structure are unknown. The recent development of a *Xenopus* egg extract-based assay that reconstitutes mitotic chromatin decondensation *in vitro* has overcome some of the inherent difficulties in studying an essential mitotic process (Magalska et al. 2014). The decondensation of mitotic chromatin isolated from cultured mammalian cells was found to be an active process requiring both ATP and GTP hydrolysis. Furthermore, the helicase activity of the RuvB-like ATPases RuvBl1 and RuvBl2 was found to be essential, albeit not sufficient, for *in vitro* chromatin decondensation. Importantly, the activity of either RuvBl1 or RuvBl2 activity was not required for the removal of condensin I from mitotic chromosomes, suggesting that these ATPases modulate chromatin decondensation by an independent mechanism. As the maintenance of Condensin I on mitotic chromosomes depends on the sustained activity of Aurora B (Lipp et al. 2007, Nakazawa et al. 2011, Ono et al. 2004, Tada et al. 2011), the loss of kinase activity could be sufficient to explain the dissociation of condensin I from chromatin during anaphase. Post-mitotic chromosome decondensation is thus likely a multi-step process.

Although the morphophological nature of the mitotic ER is still a matter of debate, it is clear that nuclear envelope formation is initiated by the recruitment and reorganization of cisternal membrane sheets on the decondensing chromatin (Anderson and Hetzer 2007, Anderson and Hetzer 2008, Lu et al. 2011) (See Fig. 2 (Schooley et al. 2012)). Several inner nuclear membrane proteins, including LBR and the LEM domain-containing proteins, and transmembrane proteins of the NPC, including NDC1 and POM121 (Ulbert et al. 2006), have the capacity to bind chromatin or DNA and their recruitment is required to rapidly establish the nuclear envelope sub-compartment at the

end of mitosis (Anderson et al. 2009, Collas et al. 1996, Newport and Dunphy 1992, Wilson and Newport 1988). The existence of nuclear envelope-specific microdomains within the mitotic ER could accelerate the segregation of the nuclear membrane compartment but the extent to which this actually occurs *in vivo* remains to be seen. The final enclosure of chromatin by the nuclear envelope sheets is thought to require cytoplasmic membrane fusion mediated by the ER fusion machinery (Reviewed in (Antonin et al. 2008, Chen et al. 2013) (see Fig.3 (Schooley et al. 2012)).

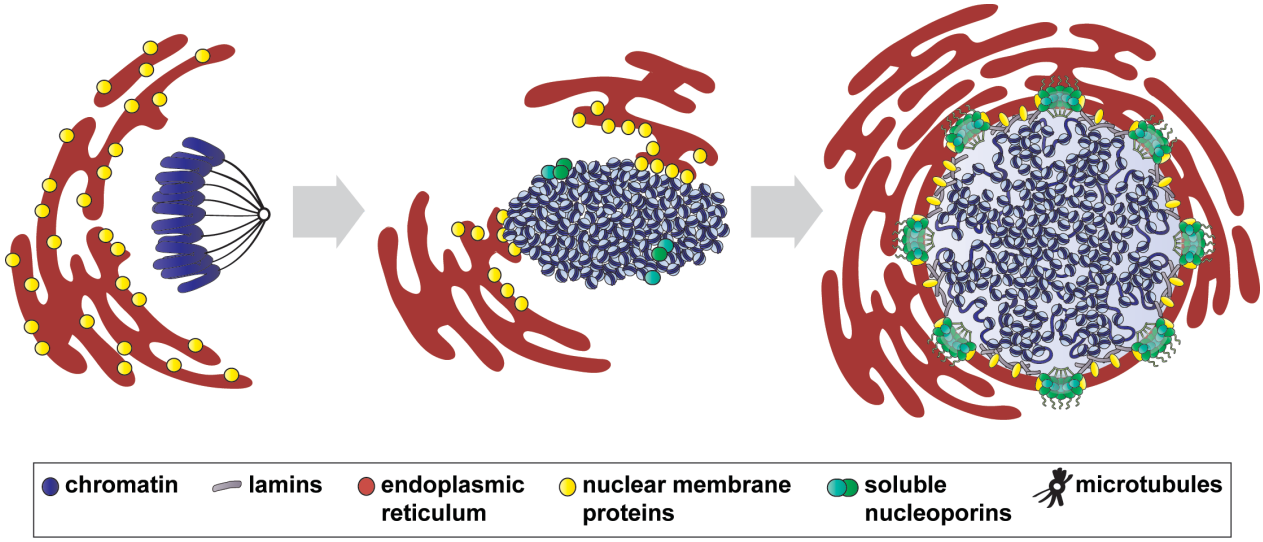

Figure 5. Schematic: Post-mitotic nuclear assembly. At the end of mitosis integral nuclear envelope proteins are sorted from the endoplasmic reticulum on each set of decondensing post-mitotic chromosomes. At the same time, soluble nucleoporins are recruited to chromatin to initiate the step-wise assembly of nuclear pore complexes (NPCs). As chromatin continues to decondense and reorganize, the nuclear lamina polymerizes and a closed nuclear envelope containing functional NPCs is formed.

NPCs are assembled on the chromatin concomitant with the recruitment and organisation of nuclear envelope membranes. Two modes for NPC assembly have been proposed based on detailed *in vitro* an *in vivo* experiments (Reviewed in (Schooley et al. 2012)). NPC insertion is the assembly and integration of NPCs in the two juxtaposed membrane bilayers of the nuclear envelope. Alternatively, NPC assembly can also be initiated on the chromatin and concurrently enclosed by nascent nuclear envelope sheets. Importantly, NPCs are assembled in two distinct stages of the cell cycle. During interphase, particularly in actively dividing cells (D'Angelo et al. 2006,

Maul et al. 1973), NPCs are assembled in the intact nuclear envelope. Recent studies have indicated that although the final composition of NPCs formed during interphase and at the end of mitosis is the same, interphasic NPC assembly is initiated on the membranes rather than on the chromatin and requires distinct membrane deformation activities (Doucet and Hetzer 2010, Doucet et al. 2010, Vollmer et al. 2012). Although interphasic NPC assembly must proceed entirely by insertion into the intact nuclear envelope, post-mitotic NPC assembly could occur either by insertion in partially formed sections of nuclear envelope membranes or enclosure of assembling NPCs as the nuclear membranes envelop the chromatin (Reviewed in (Schooley et al. 2012), see Fig. 4). The relatively rapid kinetics of post-mitotic NPC assembly (Dultz and Ellenberg 2010, Doucet et al. 2010) and the recent findings indicating that post-mitotic and interphasic NPC assembly have different molecular requirements (Doucet et al. 2010, Vollmer et al. 2012, Vollmer et al. in press) imply the use of a distinct assembly modes and suggest that NPC assembly by the enclosure model is employed at the end of mitosis.

Unlike interphasic NPC assembly, which begins at the nuclear envelope membranes, post-mitotic NPC assembly is initiated on the chromatin by the recruitment of MEL28/ELYS, a DNA and chromatin binding protein that is sometimes considered a tenth member of the Nup107-160 complex. A number of immunofluorescence and live cell imaging experiments performed in mammalian cell culture systems as well as detailed biochemical studies based on *Xenopus* egg extract nuclear reconstitution have elucidated the sequence and interdependence of the key molecular steps in NPC assembly. Binding of MEL28/ ELYS to chromatin seeds NPC assembly by recruiting the Nup107-160 complex (Franz et al. 2007, Gillespie et al. 2007, Harel et al. 2003b, Rasala et al. 2008, Rotem et al. 2009, Walther et al. 2003a). These first NPC assembly steps on chromatin can be reconstituted *in vitro* in the absence of membranes. Seeding of the Nup107-160 complex provides the first link to the pore membrane by interacting with POM121 (Antonin et al. 2005, Mitchell et al. 2010, Yavuz et al. 2010). NDC1 is also recruited to the NPC at that time (Dultz et al. 2008) but its early interaction partner has not been identified. The next steps of NPC assembly proceed from inner ring at the pore membrane building laterally towards the centre of the pore. The Nup93 complex is not recruited as a pre-assembled complex but is rather built at the NPC from individual components and smaller subcomplexes (Sachdev et al. 2012, Vollmer et al. 2012, Theerthagiri et al. 2010). Nup53 is the first Nup93 complex member recruited to the

nascent pore where it interacts with the membrane (Vollmer et al. 2012). Nup53 and another Nup93 complex member Nup155 interact with NDC1 and POM121 at the pore membrane (Mansfeld et al. 2006, Mitchell et al. 2010, Yavuz et al. 2010). Via its interaction with Nup53, Nup93 is recruited to the assembling NPC in complex with two independent binding partners Nup188 and Nup205, completing the assembly of the structural scaffold of the NPC. Nup93 recruits the FG repeat-containing nucleoporins of the Nup62 complex to the central channel, which in turn gives rise to the hydrophobic meshwork that confers the functional properties of the NPC (Ribbeck and Gorlich 2001). The formation of the cytoplasmic filaments and nuclear basket at the cytoplasmic and nucleoplasmic faces, respectively, are the final steps of NPC assembly (Dultz et al. 2008) (see Fig. 5 (Schooley et al. 2012)).

3.3 Regulation of post-mitotic nuclear assembly

3.3.1 Chromatin decondensation

The regulation of chromatin decondensation and nuclear envelope assembly at the end of mitosis relies on both the inactivation of mitotic kinases and the active removal of phosphorylation marks by protein phosphatases (Reviewed in (Wurzenberger and Gerlich 2011)). The Aurora B kinase is a member of the chromosome passenger complex and has been implicated in chromosome condensation at various stages of the cell cycle (Reviewed in (Carmena et al. 2012)). It has been found to maintain the phosphorylation of Condensins I and II and the chromatin bound localization of Condensin I until telophase (Lipp et al. 2007, Nakazawa et al. 2011, Ono et al. 2004, Tada et al. 2011, Takemoto et al. 2007). However, conflicting studies have reported that Aurora B is dispensable for normal Condensin loading during mitosis (Losada et al. 2002, MacCallum et al. 2002) and it is possible that other Aurora B substrates contribute to chromosome condensation. Upon mitotic exit, the extraction of polyubiquitinated Aurora B from chromatin by the AAA+-ATPase Cdc28/p97 and its adaptor Ufd-Np14 is required for chromatin decondensation (Ramadan et al. 2007, Dobrynin et al. 2011, Meyer et al. 2010). Two protein phosphatases, PP1 and PP2A are essential for mitotic exit (Reviewed in (De Wulf et al. 2009)) and PP1 and its nuclear targeting unit PNUTS have been implicated in chromatin

decondensation (Landsverk et al. 2005, Lee et al. 2010, Wu et al. 2009). Because condensins are phosphorylated during mitosis (Lipp et al. 2007, Nakazawa et al. 2011, Ono et al. 2004, Tada et al. 2011), it has been proposed that the relevant PP1 substrate is condensin I and/or II. However, other substrates of PP1 and possibly PP2A are also likely to be important given that post-mitotic chromosome decondensation involves multiple pathways, including a currently unidentified GTP-dependent step (Magalska et al. 2014).

3.3.2 Nuclear envelope assembly

The association of nuclear membranes with chromatin *in vitro* is regulated by the counteracting activities of cdk1-cyclin B (Newport and Dunphy 1992, Pfaller et al. 1991, Vigers and Lohka 1992), which blocks membrane binding, and protein phosphatases, such as PP1 (Ito et al. 2007, Pfaller et al. 1991), which promote membrane recruitment. The phosphorylation of multiple integral nuclear envelope proteins, including LBR, Lap2, emerin, MAN1, NDC1, POM121, and GP210, during mitosis prevents their association with chromatin and contributes to the disassembly of the nuclear envelope. At the end of mitosis, inner nuclear membrane proteins recruitment is therefore likely to depend on the reversal of these mitotic phosphorylation events. The best-characterized example of this regulatory mechanism is the recruitment of the lamin B receptor to post-mitotic chromatin. Phosphorylation of a specific serine residue prevents LBR binding to chromatin *in vitro* (Ito et al. 2007, Nikolakaki et al. 1997, Takano et al. 2004) and its de-phosphorylation controls the timing of ER membrane recruitment to anaphase chromosomes in human cells (Tseng and Chen 2011). In addition to de-phosphorylation in its arginine-serine repeat domain, phosphorylation of LBR by the serine/arginine-rich protein-specific kinase 1 (Nikolakaki et al. 1997, Takano et al. 2004, Dreger et al. 1999) is also required for its association with chromatin *in vitro*. Taken together with the observed redundancy of nuclear membrane protein recruitment (Anderson et al. 2009), these findings suggest that the precise timing of nuclear envelope recruitment to post-mitotic chromatin is, at least in part, mediated by a combination of site-specific post-translational modifications to multiple integral nuclear envelope proteins. Many soluble nucleoporins are also phosphorylated during mitosis and it is likely that NPC assembly is similarly regulated by de-phosphorylation upon mitotic exit, however direct evidence for

such a regulatory mechanism is currently lacking.

Cell cycle dependent waves of phosphorylation and de-phosphorylation can account for the temporal co-regulation of mitotic chromosome decondensation, NPC assembly and nuclear envelope formation. However, nuclear envelope assembly must also be directed spatially to the post-mitotic chromatin. This level of regulation is provided by the small GTPase Ran, which ensures the directionality of nuclear transport in the interphase cell. Chromatin is demarcated throughout the cell cycle by a high localized concentration of the GTP-bound form of Ran due to the presence of its exchange factor RCC1 (Kalab et al. 2002). *In vitro,* Ran is essential to ensure that nuclear envelope assembly occurs on the chromatin substrate (Hetzer et al. 2000, Zhang and Clarke 2000) and artificially disturbing the RanGTP gradient results in the aberrant formation of NPCs in ER membrane stacks away from the nuclear envelope (Walther et al. 2003b). A large number of soluble nucleoporins are bound by transport receptors of the importin family during mitosis and it has been proposed that this binding blocks interactions between NPC components (Harel et al. 2003a, Walther et al. 2003b). The inhibition of NPC assembly is reversed in the vicinity of chromatin due to the RanGTP-dependent dissociation of importin-nucleoporin complexes. As integral membrane proteins are targeted to the nuclear envelope during interphase by importins (Doucet et al. 2010, Turgay et al. 2010), the Ran-importin system might similarly regulate their recruitment to post-mitotic chromatin (Reviewed in (Antonin et al. 2011)). In fact, LBR was found to interact with importin β during mitosis (Ma et al. 2007, Lu et al. 2010) and this inhibitory complex could be dissociated in the presence of ranGTP (Ma et al. 2007). The overlap of the importin β and chromatin binding sites on LBR suggests that transport receptor binding could also function to prevent unwanted interactions with mitotic chromosomes during mitosis. It is possible that a similar mechanism is employed by MEL28/ELYS in order to ensure that NPC assembly is not prematurely seeded on mitotic chromatin. Because RanGTP is associated with chromatin throughout mitosis, an additional level of regulation, such as mitotic phosphorylation, is nonetheless required to specify that nuclear assembly only occur on chromatin at the end of mitosis.

3.3.3 Coordination of nuclear envelope assembly and chromatin reorganization

Chromatin organisation is crucial for both chromosome segregation and for the function of the interphase nucleus. As the transitions between these chromatin states are not well defined it is difficult to predict whether the three dimensional organisation of the interphase nucleus depends on the precise conformation or unfolding of the mitotic chromosomes. Given the importance of the nuclear envelope in modulating interphasic chromatin architecture, it is tempting to speculate that the coordination of chromatin decondensation and nuclear envelope assembly at the end of mitosis plays an active role in establishing functional interphase chromatin organisation. However, large scale chromatin mapping techniques, such as chromosome conformation capture and DamID, indicate that higher order chromatin folding is highly stochastic and newly established each time the cell divides and is thus not specified by the mitotic chromosomes (Reviewed in (Dekker 2014, Kind and van Steensel 2014)). Nonetheless, epigenetic bookmarking is likely to occur at the level of DNA methylation, histone modifications, and chromatin associated factors, which are transmitted through successive cell cycles in order to maintain cell type-specific transcriptional programs (Reviewed in (Dekker 2014, Zaidi et al. 2010, Wang and Higgins 2013)) and it remains possible that these types of modifications could serve as landmarks to coordinate chromatin decondensation and nuclear envelope assembly.

Two chromatin-associated proteins, HP1 and BAF, link decondensing chromosomes and nuclear envelope formation. The recruitment of HP1 to post-mitotic chromatin requires the dephosphorylation of Histone H3 at S10 and is promoted by H3K9 methylation, a hallmark of heterochromatin (Fischle et al. 2005, Bannister et al. 2001, Hirota et al. 2005, Lachner et al. 2001). Although LBR can interact directly with histones and other chromatin-associated proteins, the cell cycle-dependent localization of HP1 could regulate its association with post-mitotic chromatin. During anaphase HP1 also interacts with Proline Rich 14, which tethers peripheral heterochromatin to the assembling nuclear lamina via lamins A/C (Poleshko et al. 2013) The recruitment of BAF to post-mitotic chromatin during early anaphase is essential for post-mitotic nuclear envelope assembly (Gorjanacz et al. 2007, Margalit et al. 2005, Segura-Totten et al. 2002, Furukawa et al. 2003). BAF recruits LEM domain-containing proteins to post-

mitotic chromatin, and the LEM proteins reciprocally modulate the distribution of BAF during interphase (Haraguchi et al. 2008, Margalit et al. 2007, Ulbert et al. 2006). The inner nuclear membrane protein LEM4 was found to regulate BAF recruitment to chromatin by promoting vrk1 dependent phosphorylation and PP2A-mediated dephosphorylation at the different cell cycle stages (Asencio et al. 2012).

The presence of Aurora B on mitotic chromosomes is inversely correlated with the recruitment of nuclear membranes (Ramadan et al. 2007) and ensures that nuclear envelope assembly does not proceed before chromosome segregation has occurred (Reviewed in (Carmena et al. 2012)). Indeed, a recent study found that the sustained presence of Aurora B on chromatin in response to lagging chromosomes delayed localized nuclear envelope formation (Karg et al. 2015). In addition to HP1 recruitment, the reversal of Aurora B-dependent phosphorylation is also coordinated with nuclear envelope formation by the PP1 targeting subunit Repo-Man. Targeting of Repo-Man/PP1 to anaphase chromosomes via the C-terminus of Repo-Man mediates Histone H3 dephosphorylation at T3, S10, and S28 while the N-terminus mediates the localization of Repo-Man to peripheral chromatin, where it overlaps with a newly identified interaction partner importin β (Vagnarelli et al. 2011). Loss of Repo-Man/PP1 impaired the reversal of H3 mitotic phosphorylation upon mitotic exit and caused major nuclear envelope defects.

The recruitment of soluble and membrane proteins to the post-mitotic chromatin mass is specifically non-homogeneous and spatially organized with respect to the mitotic spindle. The central or core region at surfaces both proximal and distal to the spindle is enriched in A-type lamins, as well as LAP2β and emerin due to the local accumulation of BAF (Dabauvalle et al. 1999, Haraguchi et al. 2008). Conversely, lamin B, LBR, and nucleoporins preferentially accumulate at peripheral noncore chromatin (Chaudhary and Courvalin 1993, Haraguchi et al. 2008, Haraguchi et al. 2000). The establishment of these subdomains is controlled by the DNA-binding nucleoporin MEL28/ELYS and recruitment of the Nup107-160 complex (Clever et al. 2012), suggesting that the initial stages of NPC formation on chromatin are linked to the establishment of distinct chromatin regions. It is currently unclear whether specific features of post-mitotic chromatin render it competent for MEL28-ELYS binding and subsequent NPC assembly. The dependence of MEL28/ELYS recruitment to chromatin on replication licensing (Gillespie et al. 2007) provides an interesting link between the

functional establishment of post-mitotic chromatin and nuclear envelope assembly. First, because the replication licensing factors are excluded from the interphase nucleus, this regulation of MEL28/ELYS seeding ensures that licensing occurs before the formation of a closed nuclear envelope. A second more speculative link stems from the fact that mitotic chromosomes are organized in linear bands of early and late-replicating chromosome segments that are characterized by differences in gene density, histone modifications, and transcriptional activity during interphase (Reviewed in (Bickmore and van Steensel 2013, Craig and Bickmore 1993)). These domains could modulate the post-mitotic recruitment of MEL28/ELYS, which would in turn coordinate the chromatin state with nuclear envelope assembly.

3.4 Lysine (K) specific demethylase 1(A)

It was the discovery of Lysine (K) specific demethylase 1(A) (LSD1/KDM1A) that first put to rest the debate about the reversible nature of histone methylation (Shi et al. 2004). LSD1 is a nuclear amine oxidase consisting of an N-terminal SWIRM domain, a common structural feature of chromatin binding factors, a central protruding tower domain, which mediates provides a platform for interacting proteins, and a C-terminal amine oxidase domain that mediates its enzymatic activity (Baron and Vellore 2012, Shi et al. 2004, Stavropoulos et al. 2006, Tochio et al. 2006). It is conserved from yeast to humans but in contrast to *S. pombe*, *S. cerevisiae* lack an LSD1 homolog (Shi et al. 2004). LSD1 catalyzes the FAD-dependent demethylation of mono- and di- methylated Histone H3 at lysines 4 and 9 (Shi et al. 2004, Shi et al. 2005, Stavropoulos et al. 2006). Based on structural information and *in vitro* binding assays, the specificity towards mono- and di-methylated lysines is not steric but rather chemical in nature (Forneris et al. 2005, Stavropoulos et al. 2006). LSD1 co-purifies with several corepressor complexes, including CoREST (You et al. 2001, Lee et al. 2005, Shi et al. 2005), CtBP (Shi et al. 2003), NuRD (Wang et al. 2009b), RCOR (Yang et al. 2011) and HDAC1/2 complexes (Humphrey et al. 2001) and demethylation of nucleosomes by LSD1 requires at least one of these cofactors (Shi et al. 2005). Unsurprisingly given the list of interaction partners, LSD1 acts mainly as a transcriptional repressor (Shi et al. 2004, Shi et al. 2005, Lee et al. 2005) by demethylating H3K4me2, a mark of active transcription (Reviewed in (Black et al. 2012)). However, it has also been found to demethylate

repressive H3K9me2 marks and activate the ligand dependent transcription of androgen receptor-responsive genes (Metzger et al. 2005). Importantly, demethylation of histone H3 by LSD1 is locus specific, although the mechanistic details governing this level of specificity are currently unknown.

Since its discovery, LSD1 has been called a gatekeeper of pluripotency and its aberrant activity has been implicated in a plethora of cancers (Reviewed in (Amente et al. 2013)). LSD1 plays a dual role in pluripotent cells, maintaining both the undifferentiated state and the proliferative capacity (Adamo et al. 2011, Nair et al. 2012, Sun et al. 2010, Wang et al. 2007, Wang et al. 2009b, Whyte et al. 2012, Yin et al. 2014, Zhu et al. 2014). Pluripotency is associated with particularly high levels of LSD1 expression. LSD1 is also overexpressed in a number of cancer cell lines and high levels of LSD1 expression have been linked to poor prognosis in patients (Reviewed in (Amente et al. 2013)). These observations combined with importance of the cancer stem cell population during disease progression have made LSD1 an attractive target for the design of novel therapeutics in recent years. However, the function of LSD1 during mitotic progression is far from understood.

4. Thesis objectives

The interphase nucleus consists of a highly organized genome, an intact nuclear envelope barrier and nuclear pore complexes that are competent for the regulated exchange of macromolecules between the nuclear compartment and the cytoplasm. Nuclear architecture undergoes dramatic morphological rearrangements during mitosis. In animal cells the nuclear envelope is disassembled in order to facilitate the capture of highly condensed mitotic chromosomes by the spindle apparatus. Exit from mitosis and the reestablishment of a functional interphase nucleus thus requires the coordinated reassembly of the nuclear envelope and nuclear pore complexes on the de-condensing chromatin. Although many of the essential molecular building blocks have been identified, the regulatory mechanisms coordinating nuclear envelope assembly and the establishment of interphase chromatin architecture are essentially unknown.

The work presented in this thesis aimed to identify novel regulatory landmarks of nuclear envelope formation. A cell-free nuclear reconstitution system based on *Xenopus laevis* extracts was employed to screen various chemical inhibitors for nuclear assembly defects. A group of inhibitors targeting the Histone H3 demethylase Lysine Specific Demethylase-1 (LSD1/KDM1A) blocked the formation of a closed nuclear envelope and nuclear pore complex assembly *in vitro*. This observation is the first report of a histone demethylase regulating post-mitotic nuclear formation and one of only a few studies implicating a chromatin remodeling event as a determinant of nuclear envelope assembly.

The specific role of LSD1 in nuclear assembly was investigated in cell-free nuclear reconstitution assays by immunodepletion and re-addition of recombinant proteins. In order to test the physiological relevance of the *in vitro* findings, LSD1 was depleted by RNAi in HeLa cells and mitotic events were tracked using time lapse fluorescence microscopy. The development of a modified cell-free assay that specifically recapitulates chromatin decondensation in the absence of nuclear envelope assembly made it possible to further dissect the role of LSD1 in post-mitotic nuclear formation. Finally, the recruitment of nuclear envelope and pore complex proteins to chromatin was assayed biochemically using immobilized DNA beads in an effort to gain mechanistic insight regarding the role of LSD1 in linking nuclear envelope assembly to the chromatin state at the end of mitosis.

5. List of publications included in the thesis

Accepted papers

I. Dimerization and direct membrane interaction of Nup53 contribute to nuclear pore complex assembly
Vollmer B, **Schooley A**, Sachdev R, Eisenhardt N, Schneider A, Sieverding C, Madlung J, Gerken U, Macek B, Antonin W
The EMBO Journal (2012) 31, 4072-4084

II. Building a nuclear envelope at the end of mitosis: Coordinating membrane reorganization, nuclear pore complex assembly, and chromatin de-condensation
Schooley A, Vollmer B, Antonin W
Chromosoma (2012) 121, 539-554 (Review)

III. RuvB-like ATPases function in chromatin decondensation at the end of mitosis
Magalska A, Schellhaus AK, Moreno-Andrés D, Zanini F, **Schooley A**, Sachdev R, Schwarz H, Madlung J, Antonin W
Developmental Cell (2014) 31, 1-14

IV. *Xenopus in vitro* assays to analyze the function of transmembrane nucleoporins and targeting of inner nuclear membrane proteins
Eisenhardt N, **Schooley A**, Antonin W
Methods in Cell Biology (2014) 122, 193-218 (Review)

V. Nup153 recruits the Nup107-160 complex to the inner nuclear membrane for interphasic nuclear pore complex assembly
Vollmer B, Lorenz M, Moreno-Andrés D, Bodenhöfer M, De Magistris P, Astrinidis SA, **Schooley A**, Flötenmeyer, Leptihn S, Antonin W
Developmental Cell (2015) 33, 717-728

VI. A cell free assay to study chromatin decondensation at the end of mitosis

Schellhaus KA, Magalska A, **Schooley A**, Antonin W

JoVe (2015) *in press* (Review)

VII. The lysine demethylase LSD1 is required for nuclear envelope formation at the end of mitosis

Schooley A, Moreno-Andrés D, De Magistris P, Vollmer B, Antonin W

Journal of Cell Science (2015), July 29 (Epub ahead of print)

6. Personal contributions to collaborative publications

I. Dimerization and direct membrane interaction of Nup53 contribute to nuclear pore complex assembly

Vollmer B, **Schooley A**, Sachdev R, Eisenhardt N, Schneider A, Sieverding C, Madlung J, Gerken U, Macek B, Antonin W

The EMBO Journal (2012) 31, 4072-4084

As second author of this publication, I quantified nuclear pore complexes for nuclei assembled *in vitro* in mock or Nup53-depleted extracts and supplemented with recombinant Nup53 protein fragments. To this end, nuclei were fixed and NPCs were immuno-labelled with mAB414. Confocal z-stacks were acquired and NPCs were counted using Imaris Bitplane software (Figure 5B). I also prepared the floated membranes and contributed *Xenopus laevis* egg cytosolic extracts used in *in vitro* nuclear assemblies and participated in editing the manuscript. BV and WA designed the experiments and prepared the manuscript. BV optimized and performed Nup53 protein purification and liposome flotation and tubulation experiments. BV and WA performed nuclear assembly experiments. RS performed GST-pulldown experiments for Nup93 and Nup205 (Fig. S1A) and verified the phosphorylation of Nup53 during mitosis (Fig. S3A). NE contributed to the development of liposome preparation techniques and performed GST-pulldown experiments to analyse the interaction between Nup53, Ndc1, and Nup155 (Fig. S1B). AMS performed the analytical size exclusion chromatography for the Nup53-RRM domain and mutant (Fig. 2A). CS cloned all protein expression constructs and helped to prepare *Xenopus* egg extracts. JM and BM performed mass spectra analyses for mitotic Nup53 phosphorylation (Fig. S3B) and UG performed light scattering measurements of liposome radii (Fig. S4). WA supervised this study.

II. Building a nuclear envelope at the end of mitosis: Coordinating membrane reorganization, nuclear pore complex assembly, and chromatin de-condensation
Schooley A, Vollmer B, Antonin W
Chromosoma (2012) 121, 539-554 (Review)

I wrote this review article collaboratively with WA. Together we developed the scope and co-wrote the manuscript. I contributed to the design of the figures with WA and BV. All figures were prepared by BV. The preparation of the manuscript was supervised by WA.

III. RuvB-like ATPases function in chromatin decondensation at the end of mitosis
Magalska A, Schellhaus AK, Moreno-Andrés D, Zanini F, **Schooley A**, Sachdev R, Schwarz H, Madlung J, Antonin W
Developmental Cell (2014) 31, 1-14

As a co-author of this publication I contributed to the development of the cell-free chromatin decondensation and mitotic chromatin cluster isolation protocols. I also prepared *Xenopus laevis* egg extracts and mitotic clusters employed in the decondensation reactions and edited the manuscript. AM and WA designed experiments and prepared the manuscript. AM, AKS, and WA performed chromatin decondensation experiments. AM and DM-A performed live-cell imaging experiments. FZ designed and wrote the image analysis software for the quantification of chromatin decondensation. RS purified recombinant RuvBL1/2 complexes, HS performed electron microscopy, and JM performed mass spectrometry. The study was supervised by WA.

IV. *Xenopus in vitro* assays to analyze the function of transmembrane nucleoporins and targeting of inner nuclear membrane proteins
Eisenhardt N, **Schooley A**, Antonin W
Methods in Cell Biology (2014) 122, 193-218 (Methods review)

As a co-author of this methods paper I contributed to the description of methods related to the preparation of *Xenopus laevis* egg extract cytosol and floated membranes as well as the protocol for the analysis of reconstituted nuclei by immunofluorescence.

WA described methods for the preparation of egg extract and membranes as well as protocols for the immuno-depletion of transmembrane nucleoporins and the assay to measure the transport of integral membrane proteins to the INM. NE described the *in vitro* assays she developed to analyse the role of recombinant integral membrane proteins in NPC assembly or transport to the INM and assembled and edited the manuscript. The preparation of the manuscript was supervised by WA.

V. Nup153 recruits the Nup107-160 complex to the inner nuclear membrane for interphasic nuclear pore complex assembly

Vollmer B, Lorenz M, Moreno-Andrés D, Bodenhöfer M, De Magistris P, Astrinidis SA, **Schooley A**, Flötenmeyer, Leptihn S, Antonin W

Developmental Cell (2015) 33, 717-728

As a co-author of this study I contributed to the design of the NPC quantification strategy employed for *in vitro* assembled nuclei (Fig. 3B, 4C), which was performed by ML. I also prepared the floated membranes and contributed *Xenopus laevis* egg cytosolic extracts used in *in vitro* nuclear assemblies and helped edit the manuscript. BV and WA designed the experiments and prepared the manuscript. BV performed liposome flotation experiments and BV and MB purified recombinant proteins. Live-cell imaging and WGA-based NPC labelling experiments were performed by ML and DM-A. PDM prepared *Xenopus* egg extracts and SAA contributed to nuclear assembly experiments, which were performed by WA. MF performed electron microscopy and SL measured the light scattering of liposomes. WA supervised the study and wrote the manuscript.

VI. A cell free assay to study chromatin decondensation at the end of mitosis

Schellhaus AK, Magalska A, **Schooley A**, Antonin W

JoVe (2015) *in press* (Methods review)

As a co-author of this methods paper I contributed to the development of the protocol used for the preparation of mitotic chromatin clusters from HeLa cells. I also helped refine our understanding of the chromatin decondensation assay. For example, the independence of chromatin decondensation from membranes and nuclear envelope

assembly. AM developed the protocol for the preparation of mitotic clusters and the chromatin decondensation assay under the supervision of WA. AKS and WA wrote the manuscript.

VII. The lysine demethylase LSD1 is required for nuclear envelope formation at the end of mitosis

Schooley A, Moreno-Andrés D, De Magistris P, Vollmer B, Antonin W
Journal of Cell Science (2015), July 29 (Epub ahead of print)

As first author of this study I designed all experiments under the supervision of WA. I performed the cell free nuclear assembly and chromatin decondensation experiments as well as the RNAi experiments in HeLa cells. The live-cell imaging experiments were designed in collaboration with DM-A, who also established the imaging and CellCognition analysis pipeline in the lab. I optimized the protocol for the preparation and use of chromatinized DNA beads to assay protein recruitment. WA performed nuclear assembly and DNA bead binding experiments. BV purified the recombinant LSD1-wt and LSD-K643A proteins used to generate antibodies and employed in nuclear assembly rescue experiments. PDM contributed to the preparation of *Xenopus laevis* egg extracts. I prepared and wrote the manuscript with WA, who also supervised the study.

7.1 Deregulation of mitotic kinases or chromatin modifying enzymes inhibits cell-free nuclear assembly

The numerous remodeling events that characterize mitotic cell division occur almost simultaneously and rely on the fine-tuned activity of a plethora of essential molecular factors, many of which contribute to more than one crucial process. For these reasons, cell-free assay systems in which individual mitotic processes can be faithfully reconstituted and biochemically manipulated have proven instrumental in delineating the relevant molecular pathways. In the 1980s, extracts derived from the cytoplasm of frog eggs were found to induce nuclear envelope formation on sperm chromatin, giving rise to functional nuclei with the capacity for DNA replication and nuclear import (Lohka and Masui 1983, Newmeyer et al. 1986). Since then, *Xenopus laevis* egg extracts have been widely employed to study a variety of mitotic and nuclear processes *in vitro* including chromatin condensation (de la Barre et al. 1999), spindle assembly (Maresca and Heald 2006), nuclear envelope breakdown (Galy et al. 2008), nuclear envelope assembly (Lohka 1998), chromatin decondensation (Magalska et al. 2014), nucleo-cytoplasmic transport (Chan and Forbes 2006), and DNA replication (Gillespie et al. 2012).

The cytoplasm of a frog egg contains all the components necessary for the formation of an embryonic nucleus (Forbes et al. 1983) and represents a particularly rich source of these materials due to the need for rapid cell division during early development. Frog eggs are arrested in Meiosis II and are activated to proceed through the cell cycle upon fertilization. This progression can be induced artificially by various means, including the addition of a calcium ionophore (Steinhardt et al. 1974). The resulting cytoplasmic extracts are competent for the *in vitro* reconstitution of post-mitotic processes such as chromatin decondensation and nuclear assembly although protein turnover and transcription do not occur (Laskey et al. 1978). For simplicity, these extracts will be referred to as interphasic throughout this thesis. The preparation of cytoplasmic extracts from activated *Xenopus laevis* eggs is described in detail in ((Eisenhardt et al. 2014b), (Appendix)) and summarized in Figure 6. Briefly, eggs are crushed and fractionated in a sucrose-containing buffer by several high-speed centrifugation steps. The resulting cytosolic and crude membrane fractions (Fig. 6A) are each essential for *in vitro* nuclear assembly on sperm chromatin (Sheehan et al. 1988, Vigers and Lohka 1991, Wilson and Newport 1988). For the *in vitro* decondensation of mitotic chromatin, discussed in

section 7.4, high-speed interphasic egg cytosol is obtained using a modified centrifugation procedure (Fig. 6B). Crude membranes can be further purified to minimize cytosolic contamination by floatation to through a 6-step sucrose gradient and isolation of the top three phases (Fig. 6C). The use of purified membranes and membrane-free cytosol facilitates the biochemical dissection of the *in vitro* nuclear envelope assembly assay. This advantage is particularly evident in immunodepletion experiments where a protein of interest is generally only removed from either the egg cytosol or membranes.

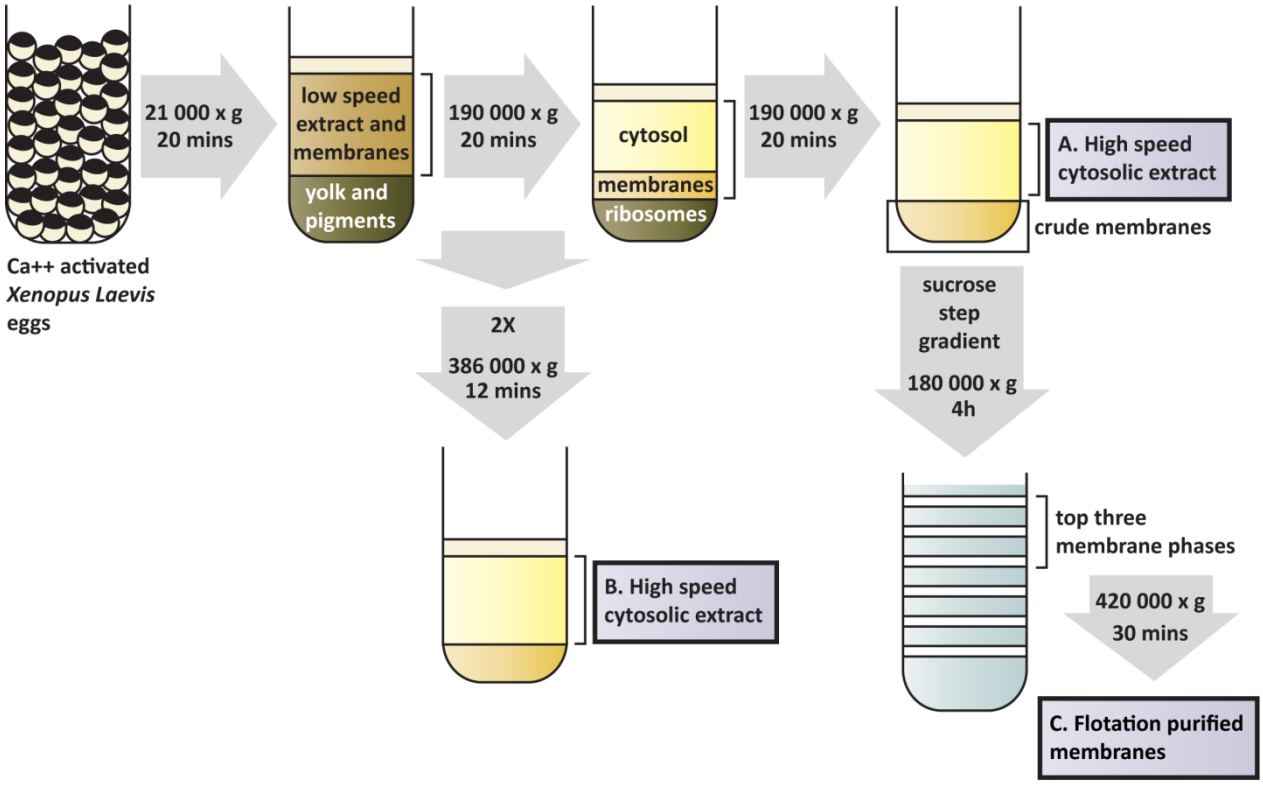

Figure 6. Schematic: Preparation of post-mitotic *Xenopus Laevis* egg cytosol and membranes. Meiosis II-arrested *Xenopus Laevis* eggs are collected and artificially activated with a calcium ionophore. Eggs are crushed and fractionated in a sucrose-containing buffer by several centrifugation steps to obtain high-speed cytosolic extracts. The high speed extracts used in nuclear envelope assembly assays on sperm chromatin **(A)** and mitotic chromatin clusters isolated from HeLa cells **(B)** are prepared using slightly different centrifugation protocols as indicated. Membranes are further purified by floatation through a sucrose step gradient and a final pelleting step in sucrose buffer **(C)**. For a detailed protocol see (Eisenhardt et al. 2014).

Cell-free nuclear envelope formation recapitulates the stepwise recruitment and assembly of soluble and membrane factors on chromatin at the end of mitosis. However, compared to post-mitotic nuclear reassembly in intact cells, the cell-free assay bears two important distinctions (Fig. 7). First, *in vitro* nuclear assembly employs *Xenopus laevis* sperm chromatin as a template. Sperm DNA is wrapped by a unique nucleosome variant consisting of histone H3, histone H4, and two sperm-specific basic proteins. Upon incubation in activated egg cytosol, these sperm protamines are rapidly exchanged for maternal H2A and H2B in a process that relies on a single additional protein expressed in the oocyte, nucleoplasmin (Philpott and Leno 1992, Philpott et al. 1991). This histone exchange results in the first stage of sperm chromatin decondensation (Fig. 7A). The subsequent addition of membranes and an energy regenerating system gives rise to nuclear envelope formation. *In vivo*, nuclear envelope membranes are sorted from the mitotic ER on post-mitotic chromatin. Conversely, the membranes employed *in vitro* are vesiculated during purification (Wilson and Newport 1988), marking a second major divergence from nuclear assembly in the cellular context. In the cell-free assay membrane vesicles, labeled with the fluorescent lipophilic membrane dye DiIC18 (1,1'-Dioctadecyl-3,3,3',3'- Tetramethylindocarbocyanine Perchlorate), are rapidly recruited to the partially decondensed sperm chromatin upon addition (Fig. 7B), where they fuse to form a closed nuclear envelope (Fig. 7C). The concomitant assembly of NPCs, visualized by immuno-labelling with an antibody (mAB414) that recognizes a subset of FG-containing nucleoporins (Davis and Blobel 1986), results in a nucleus with the capacity for nuclear import, facilitating secondary chromatin decondensation and nuclear swelling with prolonged incubation (Fig. 7D).

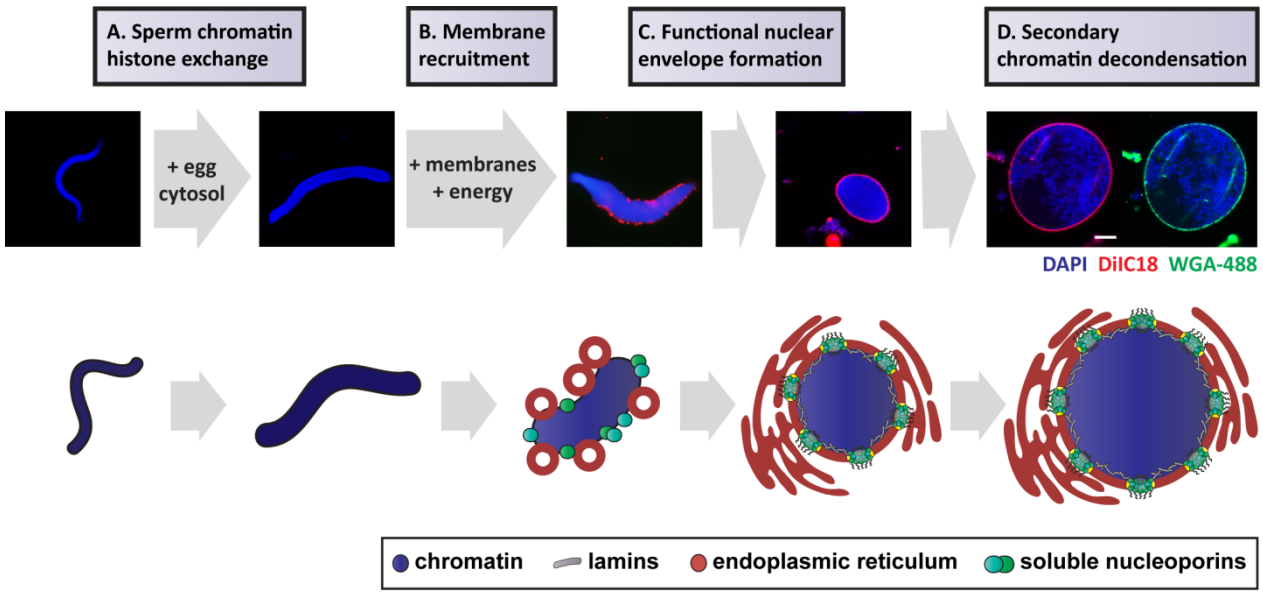

Figure 7. Schematic: Cell free nuclear assembly in *Xenopus Laevis* egg extracts. **(A)** Sperm chromatin isolated from *Xenopus Laevis* testis is incubated in egg cytosol in the absence of exogenous energy or membranes to enable the exchange of sperm specific protamines for maternal histones, resulting in a first stage of chromatin decondensation. **(B)** The addition of membranes and an energy regenerating system initiates nuclear membrane and nuclear pore complex (NPC) protein recruitment to the decondensing chromatin. In the cell-free assay membranes are not sorted from the ER but are rather recruited as distinct populations of membrane vesicles, which are generated during purification. **(C)** NPC assembly and membrane fusion results in the formation of a closed nuclear envelope that is competent for nuclear import and enables nuclear swelling and secondary chromatin decondensation **(D)**. Confocal images of nuclei assembled using DiIC18-labelled membranes (red) are shown in the upper panel. NPCs were labeled with WGA-488 (green) for 15 minutes prior to fixation and chromatin was stained with DAPI (blue) after fixation. Scale bar: 5μm.

Much of what is known regarding the early events of post-mitotic nuclear reassembly, including the recruitment of soluble and membrane components to chromatin and the sequential assembly of NPCs, was characterized using cell-free nuclear reconstitution (reviewed in (Schooley et al. 2012)). Cell-free assays were also instrumental in elucidating the role of the small GTPase ran as a spatial regulator of nuclear envelope assembly directing the release of NPC proteins on chromatin (Hetzer et al. 2000, Zhang and Clarke 2000). Temporally, post-mitotic nuclear formation is thought to be regulated by a widespread inhibition and reversal of mitotic phosphorylation (reviewed in (Schooley et al. 2012, Wurzenberger and Gerlich 2011)). However, the precise regulatory mechanisms that coordinate nuclear envelope and NPC assembly on decondensing chromatin remain largely unknown. In an effort to identify

novel regulatory landmarks of post-mitotic nuclear formation, a variety of chemical inhibitors were screened for their ability to block nuclear assembly *in vitro*.

Nuclei were assembled for two hours in high speed interphasic extract containing DiIC18-labeled membranes. After fixation they were reisolated on coverslips through a sucrose cushion by centrifugation, stained with DAPI, and visualized using fluorescence microscopy. Although the extracts employed were activated and thus in an interphasic state, the addition of Okadaic acid (O.A.), a phosphatase inhibitor targeting PP1 and PP2, blocked cell-free nuclear envelope assembly (Fig. 8A). This observation suggests that active dephosphorylation supports nuclear envelope assembly after mitotic exit. Addition of the broad specificity cyclin-dependent kinase inhibitors, 6-Dimethylaminopurine (6-DMAP) or Roscovitine, to the egg extract also blocked the formation of a closed nuclear envelope (Fig. 8A). Membranes were recruited and could be found in flattened patches on the chromatin, which overlapped with WGA-labelled NPCs (Fig 8B and C). Chromatin was partially decondensed but possessed a distinctive kidney bean-like appearance that did not resemble any of the intermediate steps of *in vitro* nuclear assembly.

Given that mitotic exit is characterized by the loss of largely Cdk1-dependent phosphorylation, the finding that some cyclin-dependent kinase activity is required for nuclear assembly was surprising. Indeed, cyclohexamide is added to the interphasic egg cytosol specifically to inhibit cyclin B synthesis and in turn Cdk1 activity. High levels of Cdk1 activity inititate and maintain the disassembled state of the nuclear envelope during mitosis (reviewed in (Guttinger et al. 2009)) and the reversal of mitotic phosphorylation by protein phosphatases is required for chromatin decondensation (Landsverk et al. 2005, Vagnarelli et al. 2006), membrane recruitment (Ito et al. 2007, Pfaller et al. 1991), and NPC assembly (Onischenko et al. 2005). However, tight spatiotemporal control of these events is important for proper post-mitotic nuclear assembly. The premature inhibition of CDK1 in early metaphase cells, for example, was found to drive mitotic progression but resulted in significant chromosomal bridges, a defect attributed to the ectopic recruitment of LBR (Tseng and Chen 2011). The tight temporal control of dephosphorylation events at mitotic exit might be particularly relevant to coordinating chromatin organisation and nuclear assembly. RepoMan-targeted PP1gamma was recently found to link these processes by regulating the dephosphorylation histones and the recruitment of importin β and Nup153, thereby

promoting NPC assembly on chromatin (Vagnarelli et al. 2011). As NPC assembly occurs relatively late in anaphase, the importance of PP1 in this process could at least partially explain the inhibitory effect of Okadaic acid on *in vitro* nuclear assembly.

Inhibition of a second mitotic kinase, Aurora B, using the competitive inhibitor ZM447439 also blocked nuclear envelope formation *in vitro* (Fig. 8A). Part of the chromosomal passenger complex, Aurora B regulates various mitotic events including spindle attachment to kinetochores, chromosome segregation and cytokinesis (Reviewed in (Carmena et al. 2012)). Upon mitotic exit, the ubiquitination and extraction of Aurora B from chromatin is required for chromatin decondensation and nuclear envelope formation (Ramadan et al. 2007) and localised delays in nuclear envelope assembly have been found to be regulated by Aurora B in response to lagging chromosomes in drosophila cells (Karg et al. 2015). Decreased, albeit detectable, levels of Aurora B in this cellular context resulted in a lost checkpoint and expedient nuclear envelope assembly. However it is possible that, as for CDK1, strict temporal control of Aurora B activity is required for faithful nuclear formation at the end of mitosis.

Post-translational histone modifications comprise a powerful and complex epigenetic code that controls localized chromatin structure and gene expression as well as 3-dimensional chromatin organization in the nucleus. The specific distribution of histone acetylation and methylation marks on chromatin has been proposed to memorize its transcriptional state during cell division and promote the timely reactivation of transcriptional programs upon mitotic exit (reviewed in (Zaidi et al. 2010)). Changes to chromatin compaction are seemingly coordinated with nuclear envelope formation, however presently there is little mechanistic insight regarding the molecular players on chromatin that link these processes. Chemical inhibitors targeting different chromatin modifying enzymes were therefore tested for their impact on *in vitro* nuclear assembly.

Acetylation dynamics mediated by histone acetyltransferases (HATs) and histone deacetylases (HDACs) contribute to the regulation hyperacetylated transcriptionally active euchromatin and hypoacetylated heterochromatin, respectively, in the interphase nucleus (reviewed in (Shahbazian and Grunstein 2007). Deacetylation of histone H3 is required for Aurora B recruitment to mitotic chromosomes and is thus important for progression through mitosis (Li et al. 2006). However, histone acetyltransferases and deacetylases are excluded from mitotic chromatin, which remains globally hypoacetylated until the end of mitosis (Kruhlak et al. 2001). The recruitment of the INM

proteins LBR and LAP2β via HP1 to mitotic chromatin has been linked to histone deacetylation (Kourmouli et al. 2000, Polioudaki et al. 2001). However, inhibition of HDACs using Trichostatin-A (TSA) (Yoshida et al. 1990) did not block *in vitro* nuclear envelope formation (Fig. 8A). Several reciprocal interactions between HDACs and proteins of the lamina and INM of interphasic nuclei have been reported (Demmerle et al. 2012, Montes de Oca et al. 2011, Somech et al. 2005) and it seems likely that histone acetylation dynamics regulate chromatin positioning relative to the nuclear periphery during interphase rather than the establishment of the nuclear envelope at the end of mitosis.

Histone methylation is determined by a large number of methyltransferases and demethylases and the impact of these marks on chromatin structure and transcription is dependent on the specific residue modified as well as the presence of other chromatin modifications in the immediate vicinity (Reviewed in (Jenuwein and Allis 2001)). Many of these methylation marks are dynamic during mitosis and numerous histone methyltransferases and demethylases have been implicated in cell cycle regulation (Reviewed in (Black et al. 2012, Di Lorenzo and Bedford 2011). Two inhibitors of protein arginine methylation; 5'-methylthioadenosine (MTA) and 2′,4′,5′,7′-Tetrabromofluorescein disodium salt (AMI-5), blocked nuclear assembly *in vitro* (Fig. 8A). Although it is certainly possible that histone arginine methylation is important for nuclear envelope assembly, the broad specificity of these competitive inhibitors as well as the large number of potentially methylated non-histone targets made the design of further mechanistic studies relatively complicated.

A second class of inhibitors provided a more specific target. *N*-Methyl-*N*-propargylbenzylamine (pargyline), *trans*-2- Phenylcyclopropylamine (2-PCPA), trans-2-(2-benzyloxy-3,5- difluorophenyl)cyclopropylamine hydrochloride (S2101), and Methyl-3-(4-(4-carbamimidoylbenzoyl)piperazine-1-carbonyl)-5-((4-carbamimidoylpiperazin-1-yl)methyl)benzoate (CBB1007) were found to block nuclear assembly in the cell free assay (Fig. 8A). Membranes were recruited to chromatin but a closed envelope containing uniformly distributed NPCs did not form and the condensed chromatin was reminiscent of the very early stages of *in vitro* assembly ((Schooley et al. in revision, Schooley et al. 2015), Fig.1 and Fig. 2B, 2C (Appendix)). With various levels of efficiency and specificity, these compounds all target the histone demethylase LSD1/KDM1A. LSD1 belongs to the superfamily flavin-dependent amine oxidases.

Pargyline and 2-PCPA were first identified as irreversible inhibitors of Monoamine oxidases (MAOs), enzymes that catalyse the oxidative deamination of neurotransmitters (Reviewed in (Shih et al. 1999)), by binding to the active site and covalently modifying the FAD cofactor (Binda et al. 2003). At comparatively higher concentrations, these compounds were found to inhibit the demethylase activity of LSD1 (Lee et al. 2006b, Schmidt and McCafferty 2007, Yang et al. 2007), prompting the development of more potent and specific LSD1 inhibitors including the 2-PCPA derivative S2101 (Mimasu et al. 2010) and the amidino-guanidinium compound CBB1007 (Wang et al. 2011). LSD1 mediates the demethylation of mono- and di-methylated Histone H3 lysines 4 and 9. Although it has been implicated in the demethylation of non-histone proteins, including the transcription factor p53 (Huang et al. 2007), the DNA methyltransferase Dmnt1 (Wang et al. 2009a), and the E2F transcription factor E2f1 (Kontaki and Talianidis 2010), it has only been found to demethylate proteins localized to chromatin. Thus, LSD1 represented an attractive candidate for further investigation into mechanisms regulating nuclear envelope formation on a rapidly changing chromatin landscape at the end of mitosis.

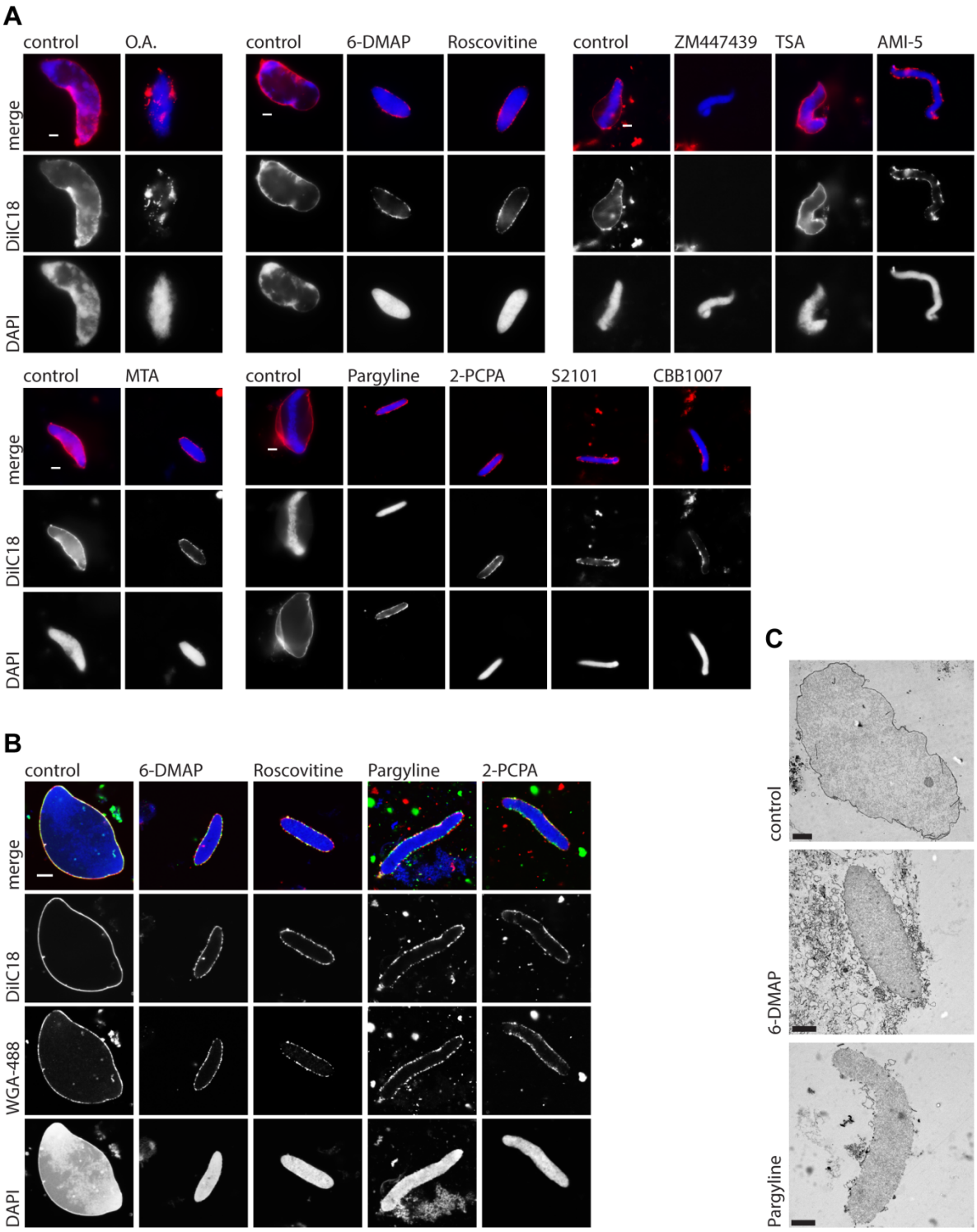

Figure 8. Chemical inhibitor screen for *in vitro* nuclear assembly defects. Nuclei assembled on sperm chromatin in *Xenopus* egg extracts for 120 min were fixed and analysed by fluorescence wide-field (**A**) or confocal microscopy (**B**). Where indicated the following inhibitors were added to assembly reactions at t=05uM Okadaic acid (O.A.), 5mM 6-DMAP, 1.5mM Roscovitine, 5uM, 1mM ZM227239, 200nM Trichostatin A (TSA), 1mM AMI-5, 1mM MTA, 5mM Pargyline, 2.5 mM 2PCPA, 250 uM S2101, CBB1007. Membranes were pre-labelled with DiIC18 (red in overlay) and chromatin was stained

with DAPI (blue in overlays). NPCs were labelled with WGA-488 (green in overlays) for 15 minutes prior to fixation. (**C**) Transmission electron micrographs were acquired of nuclear assemblies fixed with 2.5% gluteraldehyde/4% paraformaldehyde and stained with Uranyl Acetate. All scale bars: 5 µm

7.2 The lysine-specific demethylase LSD1 is required for cell-free nuclear assembly

In order to assess the specific requirement for LSD1 in nuclear assembly, two polyclonal antibodies against the full length *Xenopus laevis* protein were raised in rabbits. The antisera from both rabbits recognized recombinant *Xenopus* LSD1 migrating at approximately 100 KDa in immunoblots of affinity-purified protein preparations subjected to SDS-PAGE ((Schooley et al. in revision, Schooley et al. 2015) Fig. 2A (Appendix)). In interphasic *Xenopus* egg extracts, LSD1 could be detected as two closely migrating bands, implying that two pools with distinct post-translational modifications might be present ((Schooley et al. 2015) Fig. 2A, S1A). Importantly, LSD1 was not detected in the floated membrane fraction from *Xenopus* eggs ((Schooley et al. 2015) Fig. 6A (Appendix)) Although the antibodies were directed against the *Xenopus* protein, they could also detect a single 100 KDa band in immunoblots of whole cell lysates from HeLa cells that was almost completely depleted upon transfection with LSD1-targeting siRNA oligonucleotides ((Schooley et al. 2015) Fig. 3A, S1B (Appendix)).

Immuno-depletion experiments were performed using affinity-purified LSD1 antibodies (for a detailed protocol outlining the preparation of antibody beads see (Eisenhardt et al. 2014b) (Appendix)). As the antibodies from the two antisera pools were equally efficient at removing LSD1 from egg extracts (data not shown), the depletion experiments were routinely performed using a 1:1 ratio of antibodies purified from the antserum of each rabbit. LSD1 was specifically and efficiently immunodepleted from the interphasic egg cytosol by a single round of incubation with antibody-coupled beads ((Schooley et al. 2015) Fig. 2A (Appendix)). Under these conditions, extracts incubated with an equivalent concentration of IgG-coupled beads (mock extracts) maintained a level of activity sufficient to support *in vitro* nuclear assembly ((Schooley et al. 2015) Fig. 2B, left panel (Appendix)). Depletion of LSD1 rendered extracts

incompetent for the formation of a closed nuclear envelope and the assembly of NPCs on sperm chromatin. These defects could be rescued by the addition of purified recombinant *Xenopus* LSD1-wt to roughly endogenous levels ((Schooley et al. 2015) Fig. 2 (Appendix)) validating the specificity of the depletion phenotype and confirming the requirement for LSD1 in nuclear assembly.

The catalytic activity of LSD1 has been well characterised due to the availability of structural data and the meticulous use of *in vitro* demethylase assays combined with mutational analyses. In order to assay whether LSD1-dependent demethylation is essential for nuclear assembly, a catalytically inactive mutant was designed. As LSD1 is a flavin-dependent oxidase, the most straightforward approach was to mutate a positively charged residue in the FAD-binding pocket of the active site. In the human LSD1 protein, a lysine at position 661 fulfils the function of stabilizing FAD (Fig. 9A) and its mutation to an alanine residue completely abrogates the demethylation of a dimethylated histone H3K4 peptide *in vitro* (Stavropoulos et al. 2006). Mutation of the corresponding residue in the *Xenopus* protein (Fig. 9B) resulted in increased dimethylation of histone H3K4 on chromatinized DNA beads compared to either mock treated extracts or recombinant LSD1-wt ((Schooley et al. 2015) Fig. 6A (Appendix)) suggesting that the catalytic activity was indeed abrogated. Although LSD1-K643A was recruited chromatin, it failed to rescue *in vitro* nuclear envelope and NPC formation when added to LSD1-depleted extracts ((Schooley et al. 2015) Fig. 2B, 2C (Appendix)), indicating that it is the demethylase activity of LSD1 that accounts for its requirement in cell-free nuclear assembly.

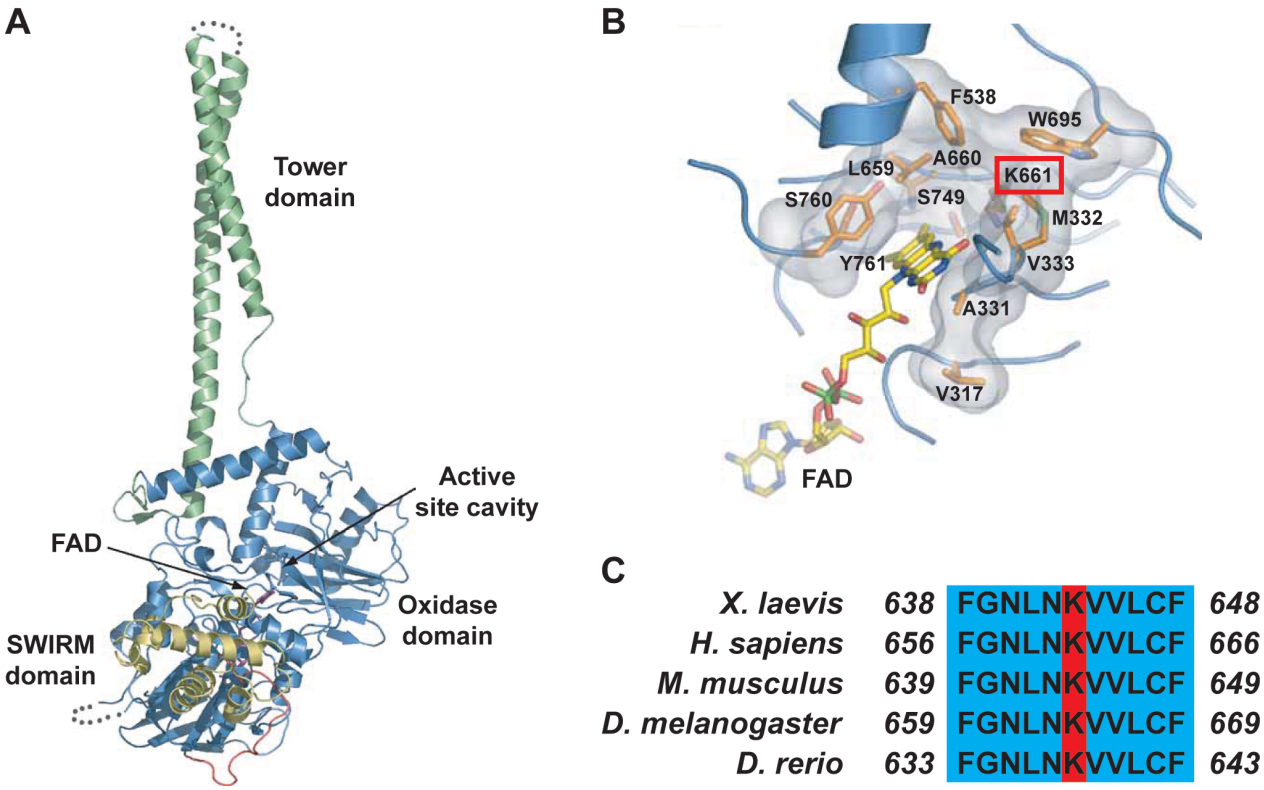

Figure 9. Structure of human LSD1 and design of a catalytically inactive mutant in the *Xenopus* protein. The ribbon representations of the human LSD1 protein (**A**) and its catalytic chamber (**B**) are taken from (Stavropoulos et al. 2006). Based on sequence conservation and alignment, K643 of the *Xenopus* protein corresponds to the human K661 residue (**C**), which is predicted to stabilize FAD and was found to be essential for de-methylation.

LSD1 co-purifies with several co-repressor complexes, including CoREST (You et al. 2001, Lee et al. 2005, Shi et al. 2005), CtBP (Shi et al. 2003), NuRD (Wang et al. 2009b), RCOR (Yang et al. 2011) and HDAC1/2 complexes (Humphrey et al. 2001). Importantly, although recombinant LSD1 is sufficient to demethylate histone H3 peptides, demethylation of nucleosomes by LSD1 requires at least one cofactor (Shi et al. 2005). As the addition of recombinant LSD1 to depleted egg extracts was sufficient to rescue all nuclear assembly defects ((Schooley et al. 2015) Fig. 2, (Appendix)) it can be assumed that any relevant cofactors remained active in the depleted extract. One possible cofactor that was not co-depleted is CoREST ((Schooley et al. 2015) Fig. 2A (Appendix)). A minimal system in which recombinant LSD1 and CoREST demethylate nucleosome substrates can be reconstituted *in vitro* (Shi et al. 2005). Although the

presence of CoREST significantly enhances LSD1 recruitment to chromatin, binding is not strictly required for LSD1-dependent demethylation. Instead, LSD1/CoREST form an allosteric clamp that regulates the catalytic activity of LSD1 in a substrate dependent way (Baron and Vellore 2012, Yang et al. 2006, Pilotto et al. 2015). As the crystal structure of LSD1/CoREST has been solved and a number of interaction surfaces relevant to catalytic activity have been mapped (Yang et al. 2006, Shi et al. 2005), it would be interesting to assay the importance of this complex in nuclear envelope assembly. Of course, the possibility that other cofactors similarly support LSD1-mediated demethylation in the regulation of post-mitotic nuclear assembly should not be excluded.

7.3 Loss of LSD1 in human cells extends telophase and promotes the formation of annulate lamellae

The cell cycle specific localization of LSD1 was determined by immunofluorescence in unsynchronized HeLa cells. A nuclear protein during interphase, LSD1 was excluded from mitotic chromatin starting at prometaphase. It could first be seen re-associating with the decondensing chromatin during telophase, concomitant with NPC assembly ((Schooley et al. 2015) Fig. S2, (Appendix)). A similar dissociation of LSD1 from mitotic chromatin has also been observed in mouse embryonic stem cells (Nair et al. 2012). LSD1 was found to be hyperphosphorylated in nocodazole-arrested HeLa cells (Lv et al. 2010) as well as being a target of the protein kinase CK2 (Costa et al. 2014) and it is possible that this phosphorylation prevents its association with chromatin during mitosis. Alternatively, mitotic phosphorylation of chromatin-associated proteins or histones might account for the cell cycle-dependent localization of LSD1. For example, phosphorylation of histone H3 at serine 10 was found to inhibit the binding of recombinant LSD1 to a synthetic H3 peptide *in vitro* (Forneris et al. 2005). Although it is not clear whether LSD1 recruitment precedes nuclear envelope formation upon mitotic exit, its cell cycle-dependent localization is consistent with the notion that it could play a role in envelope and NPC assembly on the chromatin.

7.3.1 LSD1 is required for timely mitotic exit

Given the requirement for LSD1 in the assembly of cell-free nuclei, a live cell imaging approach was employed to examine the role of LSD1 during mitotic exit in human cells. Time-lapse microscopy has proven invaluable in the identification cell division genes, which might otherwise be missed in endpoint-based assays due to the frequently transient nature of aberrant cell division phenotypes as well as downstream cell viability defects ((Neumann et al. 2010), www.mitocheck.org). In order to address whether LSD1 plays a role in mitotic exit, it was depleted by RNAi in HeLa cells stably expressing H2B fused to a mCherry reporter. Reduction of LSD1 protein levels was efficient from 24-72h ((Schooley et al. 2015) Fig. 3A, S3A (Appendix)). Beginning 30h post-transfection, cells were mounted in a thermal CO_2 chamber and fluorescence images were acquired every 3 minutes over a time period of approximately 20h. Chromatin features were annotated and tracked using the machine learning-based image analysis software, CellCognition (Schmitz and Gerlich 2009, Held et al. 2010). Chromatin was annotated based on morphological characteristics such as size, shape, and fluorescence intensity (Fig. 10A). For each experiment, a new classifier was trained by manually annotating at least 1000 cells in various stages of the cell cycle. The software could then track mitotic events and determine the time (number of 3 minute frames) spent in each cell cycle stage.

Based on chromatin morphology, LSD1 knockdown significantly extended telophase in HeLa cells. While control cells spent an average of 18 minutes in telophase before being considered interphasic, siRNA-mediated depletion of LSD1 using two different oligonucleotides resulted in cells maintaining telophasic chromatin for an average of 28 and 35 minutes (Fig. 10B, (Schooley et al. 2015) Fig. 3B, 3C, S3B (Appendix)). This extended duration of condensed telophasic chromatin following chromosome segregation can easily be visualized in individual mitotic tracks ((Schooley et al. 2015) Fig. 3D (Appendix)). Notably, many cells did not exit telophase in the time frame of the experiment and therefore the duration of telophase reported here could be an underestimate. Indeed, visual inspection of the mitotic tracks suggests that a failure to exit telophase was more frequent in siLSD1-depleted cells (Fig. 10B), however due to the small statistical sample this tendency was not quantified.

In addition to delaying exit from telophase, one LSD1-targeting siRNA oligonucleotide significantly extended metaphase ((Schooley et al. 2015), Fig. S3B (Appendix)). Early mitotic delay is a frequent characteristic of cells with impaired spindle assembly and consequently defects in chromosome segregation (Neumann et al. 2010). LSD1 has been found to localize to the mitotic spindle and has been proposed to play an essential role in chromosome segregation in dividing HeLa cells (Lv et al. 2010). However, LSD1 knockdown using the siRNA oligonucleotides and transfection protocol described in ((Schooley et al. 2015) (Appendix)) did not significantly impact the proportion of defective chromosome segregation events, based on manual scoring of lagging chromosomes and chromosomal bridges in live dividing cells (Fig. 10C). As the timing of all other cell cycle stages was not affected and the telophase extension could be observed independently of extended metaphase (Fig. 10B, (Schooley et al. 2015) Fig. 3D (Appendix)), it is likely that the role of LSD1 during mitosis is specific to the events occurring in telophase.

The extended duration of telophase in LSD1-depleted cells that was determined by CellCognition is based on morphological features of the chromatin. The characteristic changes in chromatin compaction that occur as cells transition from telophase to interphase provide a convenient read-out in screening for possible defects in mitotic exit. However, an assay that measures a functional change during this transition would prove advantageous. To this end, mitotic exit was assayed in live cells by measuring the time from anaphase to the onset of nuclear import, an indicator of nuclear envelope formation (Schmitz et al. 2010). In order to assess the impact of LSD1 knockdown on the timing of nuclear import, HeLa cells stably expressing H2B-mCherry and a nuclear import substrate consisting of the importin β binding domain of importin α fused to eGFP (IBB-GFP) were transfected and imaged live by time-lapse microscopy as described in ((Schooley et al. 2015) (Appendix)). The number of 3 minute frames starting from the last observed metaphase plate until the first frame in which IBB-GFP is visibly accumulated on the chromatin was scored manually. Surprisingly, despite the clear extension in telophasic chromatin features when LSD1 levels were reduced, IBB-GFP import was not delayed in siRNA treated cells compared to controls (Fig. 10C). The accumulation of IBB-GFP on chromatin has been found to precede the formation of a closed nuclear envelope (Lu et al. 2011). Thus the initial presence of IBB-GFP on chromatin is likely due to localised import by NPCs assembled in the partially formed

nuclear membrane sheets and not the presence of a closed nuclear envelope. Nonetheless, the timing of IBB-GFP import in LSD1-depleted cells suggests that NPC assembly proceeds somewhat normally. Furthermore, based on chromatin morphology cells deficient for LSD1 typically exited mitosis, indicating a clear divergence from the phenotype observed in the cell-free assay.

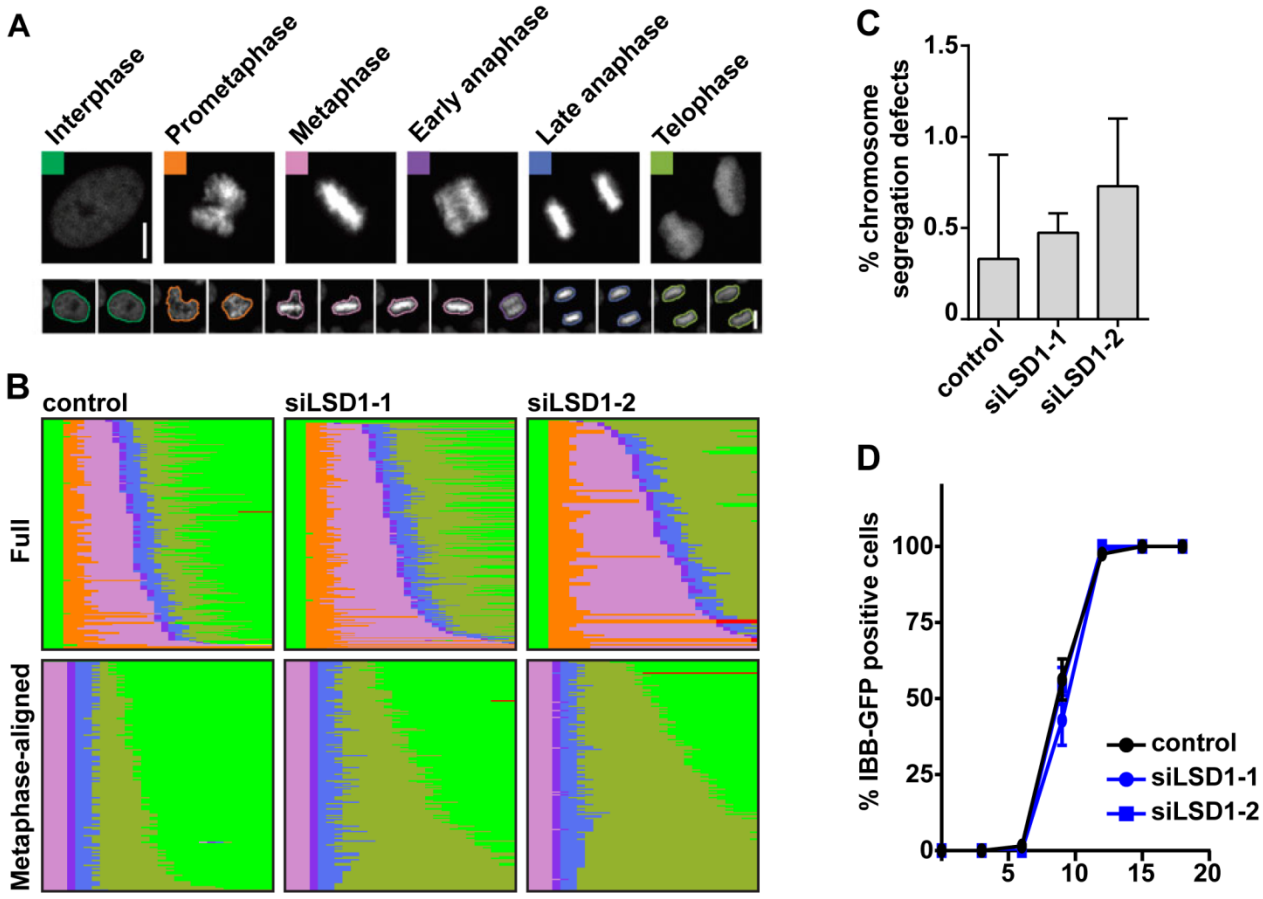

Figure 10. RNAi-mediated depletion of LSD1 in HeLa cells extends the duration of telophase but does not delay the onset of nuclear import or lead to chromosome segregation defects (Supplement to (Schooley et al. in revision) Fig 3). (**A**) An example illustrating the classification of chromatin morphology by CellCognition is shown (taken from (Held et al. 2010)). HeLa cells stably expressing H2B-mcherry and transfected with 20 nM siRNA as indicated were subjected to time-lapse microscopy starting 30h after transfection. Mitotic events were analysed using the machine-learning based program CellCognition . (**B**) Representative colour-coded plots indicating the length of each cell cycle stage for complete mitotic tracks (upper panel) or tracks aligned based on the last metaphase frame (lower panel) were generated. (**C**) Mitotic tracks were manually scored for the presence of lagging chromosomes and chromosome bridges, collectively referred to as “chromosome segregation defects”. The mean percentage of segregation defects is plotted for more than 100 mitotic events per condition in each of three independent experiments. Error bars represent s.d. (**D**) HeLa cells stably expressing H2B-mcherry and IBB-GFP were transfected with 20 nM siRNA and subjected to time-lapse microscopy starting 30h after transfection. Starting from the last observed metaphase frame, cells were scored manually for the presence of IBB-GFP on the chromatin. The percentage of IBB-GFP positive cells over time is plotted for two independent experiments. Bars represent the range.

7.3.2 RNAi-mediated reduction of LSD1 promotes the formation of annulate lamellae but does not impair nuclear envelope and pore complex formation

In agreement with the extension of telophasic chromatin features, the average nuclear volume in unsynchronized HeLa cell populations was significantly reduced when LSD1 was depleted by RNAi ((Schooley et al. 2015) Fig. 4A (Appendix)). Knockdown of LSD1 also narrowed the distribution of nuclear volumes, which were highly variable in untreated HeLa cell populations ((Schooley et al. 2015) Fig. S3C (Appendix)). Taken together with the live cell imaging data, these observations suggest that the events delaying mitotic exit in LSD1-depleted cells result in lasting changes to nuclear architecture and chromatin compaction beyond telophase.

Immunofluorescent labelling of NPCs using mAB414 indicated the presence of significant cytoplasmic aggregates the LSD1-depleted cells ((Schooley et al. 2015) Fig. 4B (Appendix)). This cytoplasmic staining is a signature of annulate lamellae (AL), arrays of NPCs that form ectopically in endoplasmic reticulum-derived membrane stacks (Kessel 1992)(Kessel, 1992). Annulate lamellae formation has been linked to impaired post-mitotic NPC assembly (Franz et al. 2007, Walther et al. 2003a), and suggests that LSD1 could be important for the assembly NPCs on chromatin at the end of mitosis. Despite AL formation, NPCs were distributed throughout the nuclear rim in LSD1-depleted cells. Based on mAB414 staining, LSD1 knockdown significantly reduced the average number of NPCs per nucleus compared to control cells ((Schooley et al. 2015) Fig. 4C (Appendix)). However, NPC density was not affected by the decreased levels of LSD1 and thus the difference in NPC number can be accounted for by the decrease in nuclear size ((Schooley et al. 2015), Fig S4D (Appendix)). Nuclear growth requires both membrane sheet expansion (Anderson and Hetzer 2007, Anderson and Hetzer 2008, Kiseleva et al. 2007) and NPC assembly (D'Angelo et al. 2006, Newport et al. 1990) but their interdependence is not understood and it has been suggested that they are regulated autonomously (Maeshima et al. 2011). Because NPC density was not impacted by LSD1 knockdown, it is not clear whether it is NPC assembly or rather nuclear envelope expansion that is specifically impaired in the smaller LSD1-depleted nuclei. Furthermore, while post-mitoitc NPC and nuclear envelope formation is initiated on chromatin, NPC assembly in the intact nuclear envelope during interphase has different molecular requirements and was recently reported to be initiated at the nuclear

membranes (Vollmer et al. in press). As LSD1 resides on chromatin, it seems unlikely that it would regulate interphasic NPC assembly. Instead, the block in nuclear growth in LSD1 knockdown cells might rather reflect an incompetence that is established during post-mitotic nuclear assembly.

In an effort to dissect potential nuclear assembly defects in greater detail, immunofluorescent labelling of various nuclear envelope and pore complex proteins was performed in fixed HeLa cells. Despite defects in nuclear expansion and NPC assembly, LSD1 knockdown did not impede the assembly of A and B-type lamins into an apparently continuous nuclear lamina ((Schooley et al. 2015) Fig. 4E (Appendix)). The lamin B receptor and Emerin, transmembrane proteins of the inner nuclear membrane, and the transmembrane nucleoporin POM121, were also detected at the nuclear envelope in LSD1-depleted cells. LBR associates with early post-mitotic chromatin and has been strongly implicated in nuclear envelope membrane recruitment and assembly (Reviewed in (Schooley et al. 2012). POM121 also possesses an intrinsic DNA-binding capacity (Ulbert et al. 2006, Shaulov et al. 2011) and is recruited to post-mitotic chromatin slightly later during anaphase (Dultz et al. 2008). Although exact recruitment kinetics would be best analysed using time-lapse imaging of live cells (Dultz et al. 2008, Ellenberg et al. 1997, Lu et al. 2011), both LBR and POM121 could be detected on anaphase chromatin in fixed control and LSD1-deficient cells (Fig. 11), suggesting that LSD1 knockdown did not substantially impair the post-mitotic recruitment of nuclear envelope membranes. Mel28/ELYS, a nucleoporin that mediates the initial seeding of NPC assembly on post-mitoitc chromatin, to anaphase chromosomes was also unaffected by the siRNA-mediated depletion of LSD1 and was found at the nuclear rim in interphasic cells ((Schooley et al. 2015) Fig. 4E (Appendix)). Soluble nucleoporins that are subsequently recruited to the assembling NPC including Nup62, of the central channel; Nup153, from the nucleoplasmic NPC face; and Nup88, from the cytoplasmic face of the NPC, were also all found at the nuclear envelope in LSD1-depleted cells.

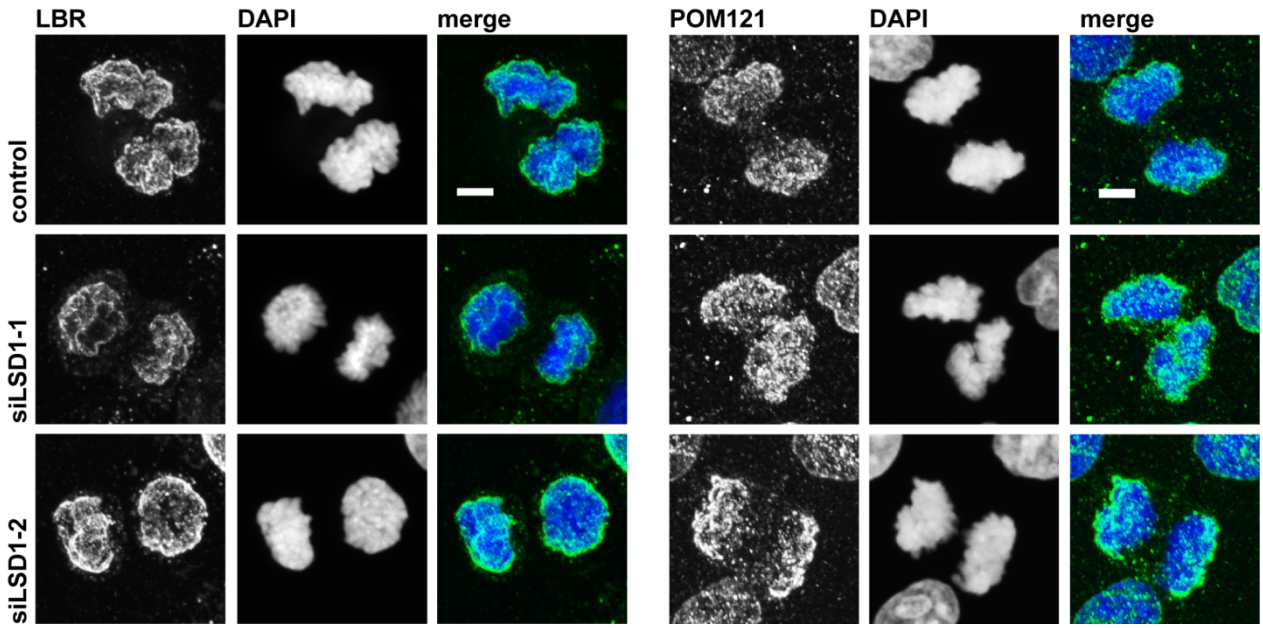

Figure 11. Recruitment of the Lamin B Receptor (LBR) and the transmembrane nucleoporin POM121 to anaphase chromatin is not impaired in LSD1-depleted HeLa cells. HeLa cells transfected with 20 nM control, LSD1-1 or LSD1-2 siRNA oligos were fixed 48h post-transfection and processed for immunofluorescence. POM121 and LBR were immuno-labelled (green in overlays) and DNA was stained with DAPI (blue). Representative maximum intensity projections from 0.25um-spaced optical z-sections traversing the chromatin are shown. Scale bars: 5μm.

The impact of reducing LSD1 protein levels in HeLa cells was relatively modest compared to the complete block in nuclear assembly observed in the cell-free nuclear assembly assay. One reason for this discrepancy could be a reduction in the depletion efficiency of siRNA *in vivo* compared to immunodepletion *in vitro*. It is also possible that the most affected cells failed to divide or died, although the fact that substantial differences in cell density or cell death were not observed 72h post-transfection (data not shown) despite the significant reduction in LSD1 levels argues against this prospect. Alternatively, LSD1-dependent demethylation may not be essential for post-mitotic nuclear assembly in all cell types. LSD1 has been nicknamed a guardian of pluripotency for its role in regulating the expression of Oct4 and Sox2 and promoting cell division in pluripotent cells (Adamo et al. 2011, Nair et al. 2012, Wang et al. 2011, Yin et al. 2014) as well as ensuring proper transcriptional reprogramming in differentiating cells (Whyte et al. 2012). Chemical inhibition of LSD1 was found to block the growth of ES cells and cancer cells that exhibit puripotent properties but had a minimal impact on the

growth of normal somatic cells and non-pluripotent cancer cell types, including HeLa (Wang et al. 2011). As *Xenopus* eggs contain all the factors necessary for totipotency (Gurdon et al. 1958), the discrepancy observed in the absolute requirement for LSD1 during NE assembly *in vitro* and in cells might reflect a redundancy that depends on the differentiation state. Finally, *in vitro* nuclear assembly may be more sensitive to the loss particular aspects of nuclear envelope assembly that are more rhobust in cells. This possibility could be particularly relevant in the context of post-mitotic membrane recruitment and remodeling, which have different starting points in the cell-free and live cell assay systems. For example, LBR was found to be essential for nuclear membrane recruitment *in vitro* (Collas et al. 1996, Pyrpasopoulou et al. 1996, Ye and Worman 1994) in a phosphorylation-dependent way (Ito et al. 2007, Nikolakaki et al. 1997, Takano et al. 2004) but its depletion or misregulation only delayed envelope formation *in vivo* (Anderson et al. 2009, Tseng and Chen 2011).

7.4 LSD1 is not required for cell-free chromatin decondensation in the absence of nuclear membranes

The formation of a functional interphase nucleus involves the assembly of a closed NPC-containing nuclear envelope on decondensing chromatin. In the cellular context these events occur almost simultaneously and are difficult to functionally discern. However, mitotic chromatin decondensation and nuclear envelope formation can functionally uncoupled *in vitro* in order to facilitate the biochemical dissection these distinct processes. As an apparent increase in chromatin compaction was a general feature of LSD1 inhibition or depletion both in cell-free nuclear assemblies and in HeLa cells, the role of LSD1 in post-mitotic chromatin decondensation was specifically examined.

7.4.1 Primary *in vitro* decondensation of sperm chromatin proceeds in the absence of LSD1

Sperm chromatin decondensation, due to the exchange of sperm protamines for maternal histones, occurs upon fertilization and is recapitulated in *Xenopus* egg extracts prior to nuclear assembly. Although nucleoplasmin is sufficient to support the histone exchange, it is possible that LSD1-mediated demethylation might also play a role in the presence of the additional factors in the extract. In order to determine whether this specialized decondensation event requires LSD1, sperm chromatin was incubated in egg extracts lacking membranes and an energy regenerating system for 10 minutes. Depletion of LSD1 did not impact sperm chromatin decondensation ((Schooley et al. 2015) Fig. 5A (Appendix)), indicating that the block in cell free nuclear assembly observed in the absence of LSD1 activity is not due to a defect in the initial decompaction of the sperm chromatin template. Although chromatin is progressively reorganized during *in vitro* nuclear assembly reactions, secondary decondensation or nuclear swelling (Philpott et al. 1991, Wright 1999) depends on the formation of a transport-competent nuclear envelope. The loss of LSD1 activity, either by immuno-depletion or chemical inhibition, impaired NPC and nuclear envelope assembly on the decondensed sperm chromatin template and therefore the initiation of nuclear import. The condensed appearance of chromatin in the LSD1-deficient nuclei can therefore likely due to the absence of nuclear import and consequent secondary chromatin decondensation.

7.4.2 Decondensation of mitotic chromatin clusters is independent of LSD1 activity in the absence of nuclear membranes

Sperm chromatin decondensation is mechanistically very different from the decompaction of mitotic chromosomes that occurs at the end of mitosis in dividing cells. This distinction prompted the development of a cell free assay that reconstitutes the decondensation of mitotic chromosomes in *Xenopus* egg extracts (Magalska et al. 2014). Mitotic chromosome clusters can be isolated from metaphase-arrested HeLa cells by detergent-mediated extraction and purification on a Percoll gradient ((Gasser and Laemmli 1987, Magalska et al. 2014, Schellhaus et al. in press) (Appendix)). Upon

incubation in interphasic egg extracts (see Fig. 6B in section 7.1) in the presence of an energy regenerating system and the mitotic kinase inhibitor 6-DMAP, the chromatin clusters undergo progressive morphological changes that can be visualized by DAPI staining and fluorescence microscopy or uranyl acetate staining and electron microscopy, and which mimic the decondensation of post-mitotic chromatin in living cells ((Magalska et al. 2014) Fig. 1A, 2C (Appendix)). The requirement for 6-DMAP, an inhibitor of the cell-free nuclear assembly assay (see Fig. 8 in section 7.2), can be explained by the need to reverse the mitotic state of the chromatin clusters. For example, they are highly phosphorylated on histone H3 S10 and this mark is rapidly removed in interphasic extracts (Fig. 12). The topological changes to chromatin can be quantified based on the smoothness of the chromatin boundary, the relationship between the perimeter and surface area, and the homogeneity of internal DAPI staining, the relative internal area occupied by prominent (condensed) structures. The increase these parameters over time correlates with the progressive decondensation of mitotic chromatin clusters in egg extracts, particularly during the initial stages of when chromatin structure appears to undergo the most dramatic structural rearrangements ((Magalska et al. 2014) Fig. 1A (Appendix)).

Figure 12. Histone H3 phosphorylation at Serine 10 is rapidly lost on mitotic chromatin clusters incubated with post-mitotic *Xenopus* egg extract. Mitotic chromatin clusters from HeLa cells were incubated with *Xenopus* egg extracts in the absence of added membranes. At the indicated time-points samples were fixed and processed for immunofluorescence. Phosphorylated Histone H3S10 was immuno-labelled (green in overlays) and DNA was stained with DAPI. Representative wide-field fluorescence images are shown. Scale bar: 5μm.

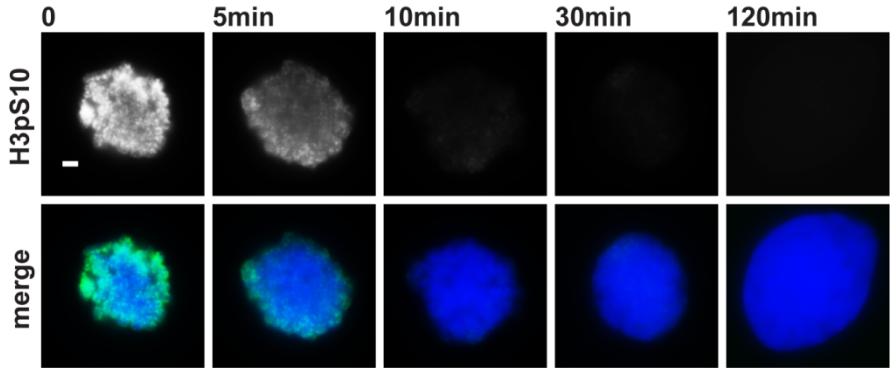

In order to determine whether LSD1 has a direct impact on post-mitotic chromatin decondensation, mitotic chromatin clusters were incubated in mock treated or LSD1-depleted extracts for 2h and visualized using DAPI staining and fluorescence microscopy. Based on the decondensation parameters of boundary smoothness and internal homogeneity, LSD1 depletion did not significantly impact chromatin decondensation *in vitro* ((Schooley et al. 2015) Fig. 5B (Appendix)). Similarly, chemical inhibition of LSD1 by pargyline or 2-PCPA did not noticeably affect cell-free chromatin decondensation in the absence of membranes ((Schooley et al. 2015) Fig. S4D top panel (Appendix)). Because the parameters used to measure decondensation plateau at around 40 minutes ((Magalska et al. 2014) Fig. 1A (Appendix), it is still possible that LSD1 plays a role in the later stages of *in vitro* chromatin decondensation. Indeed, LSD1 depletion consistently resulted in smaller chromatin masses at endpoint indicating a higher degree of compaction.

The addition of membranes to cell-free chromatin decondensation reactions results in the formation of closed nuclear envelopes containing NPCs ((Magalska et al. 2014) Fig. 2A, B (Appendix)). Much like the cell-free nuclear assembly assay, the formation of a functional nuclear envelope allows for nuclear import ((Magalska et al. 2014) Fig. 2D (Appendix)) and results in secondary chromatin decondensation and nuclear expansion ((Schooley et al. 2015) compare mock in Fig. 5B and 5C (Appendix)). In contrast to the relevant control extracts, the presence of membranes in LSD1 depleted or inhibited extracts did not lead to the formation of a closed nuclear envelope or mediate any further chromatin decondensation ((Schooley et al. 2015) Fig. 5C and S4D (Appendix)). This experiment confirms that the requirement for LSD1 in nuclear envelope formation is not specific to sperm chromatin and, considering the minimal effect of LSD1 depletion or inhibition on membrane-free chromatin decondensation, suggests that the main impact of LSD1 on chromatin decondensation is likely to be downstream of its role in envelope assemby. These *in vitro* observations also appear correspond to the chromatin phenotype in LSD1-depleted HeLa cells, despite the fact that the impact on NPC and NE assembly was significantly less pronounced compared to cell-free nuclear assembly. Nonetheless, as LSD1 activity is spatially restricted to chromatin, its impact on the assembly of nuclear membranes and NPCs into a functional envelope *in vitro* implies a causal link between the events occurring on post-mitotic chromatin and nuclear assembly. These data therefore underline an important

conceptual distinction regarding post-mitotic chromatin states, namely the difference between chromatin decondensation and the state of post-mitotic chromatin organization that is competent for NE assembly.

7. 5 LSD1 renders post-mitotic chromatin competent for nuclear envelope assembly *in vitro*

In Hela cells, the siRNA-mediated depletion of LSD1 extended the length of telophase and resulted in smaller interphase nuclei as well as apparent annulate lamellae formation (See section 7.3). Despite this phenotype, no defect in the recruitment or assembly of any nuclear membrane or NPC components was observed. The possible reasons for this discrepancy have already been discussed and indicated that further insight into the mechanistic details regarding the role of LSD1 in nuclear assembly would require the use of cell-free nuclear reconstitution assays. Thus in order to test the hypothesis that LSD1 regulates the competence of post-mitotic chromatin for nuclear envelope formation, the recruitment and assembly of nuclear membrane and NPC components was assayed *in vitro.*

7.5.1 LSD1 activity regulates the recruitment of MEL28 and POM121/NDC1-containing membrane vesicles to chromatin.

The LSD1 activity-dependent recruitment of nuclear envelope proteins to chromatin was quantitatively assayed *in vitro* using magnetic DNA-coated beads (Heald et al. 1996). The beads were generated by coupling a biotinylated linearized plasmid containing a genomic DNA to magnetic streptavidin beads. DNA beads were then chromatinized by incubation with mock or LSD1-depleted interphasic *Xenopus* egg cytosol under constant but gentle shaking. Incubation of immobilized DNA with interphasic egg extracts was previously found to result in the incorporation of evenly spaced nucleosomes (Kimura and Hirano 2000). As LSD1-depletion did not adversely impact histone exchange on the sperm chromatin template, it was assumed that nucleosomes were assembled in its absence. Following chromatinization, the recruitment of cytosolic and membrane proteins was assayed by the addition of fresh egg cytosol and concentrated floated membranes in the presence or absence of recombinant LSD-wt or LSD1-K643A (Summarized in Fig. 13).

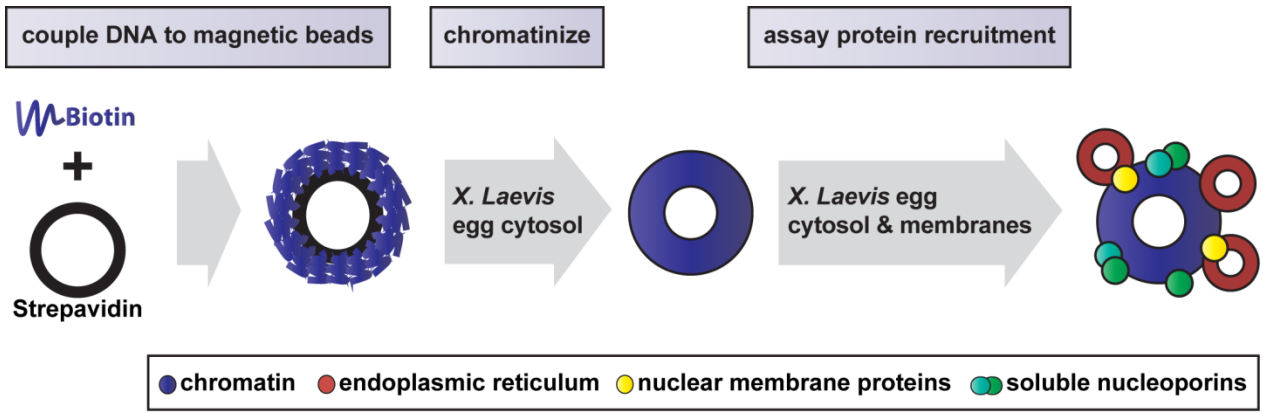

Figure 13. Schematic: Preparation of DNA beads and application in assaying protein recruitment to chromatin. Genomic DNA-containing plasmids are linearized, biotinylated, and coupled to magnetic streptavidin beads. DNA-coupled magnetic beads are then chromatinized by incubation with *Xenopus laevis* egg cytosol. At this stage chemical inhibitors can be added or extracts depleted of a specific protein can be employed. Chromatin beads are further incubated with egg cytosol and membranes, reisolated and washed, eluted in boiling SDS, and finally subjected to SDS-PAGE and western blotting in order to quantify protein recruitment.

Depletion of LSD1 did not impact the incorporation of histone H3 or recruitment of Fig. 6A (Appendix)). Conversely, the absence of LSD1 activity on the beads, in the case of LSD1 depleted extracts alone or supplemented with the demethylase deficient mutant LSD1-K643A, resulted in increased di-methylation of histone H3 at lysine 4 and confirmed that LSD1-dependent demethylation was occurring under the experimental conditions employed. The recruitment of MEL28/ELYS was also dependent on LSD1 activity. In depleted extracts, MEL28/ELYS recruitment was significantly reduced, an effect that was rescued by the addtion of LSD1-wt but not the catalytically inactive LSD1-K643A. Accordingly, MEL28/ELYS was absent from the chromatin of nuclei assembled *in vitro* in the absence of endogenous or wild type recombinant LSD1 ((Schooley et al. 2015) Fig. 6B (Appendix)). MEL28/ELYS is essential for NPC assembly (Franz et al. 2007). It is localized at kinetochores during mitosis (Rasala et al. 2006) and redistributes on the chromatin surface during anaphase, where it acts as the essential seeding point for NPC assembly (Franz et al. 2007, Gillespie et al. 2007). Immunofluorescence of *in vitro* nuclear assemblies performed on sperm chromatin and HeLa chromatin clusters fixed at various timepoints indicates the rapid recruitment of MEL28/ELYS to chromatin followed by progressive nuclear rim localisation (Fig. 14A,B).

Although the mechanism governing its efficient spreading on post-mitotic chromatin is currently unknown, these data suggest that the initial recruitment or seeding of MEL28/ELYS is downstream of LSD1-dependent changes to the chromatin landscape.

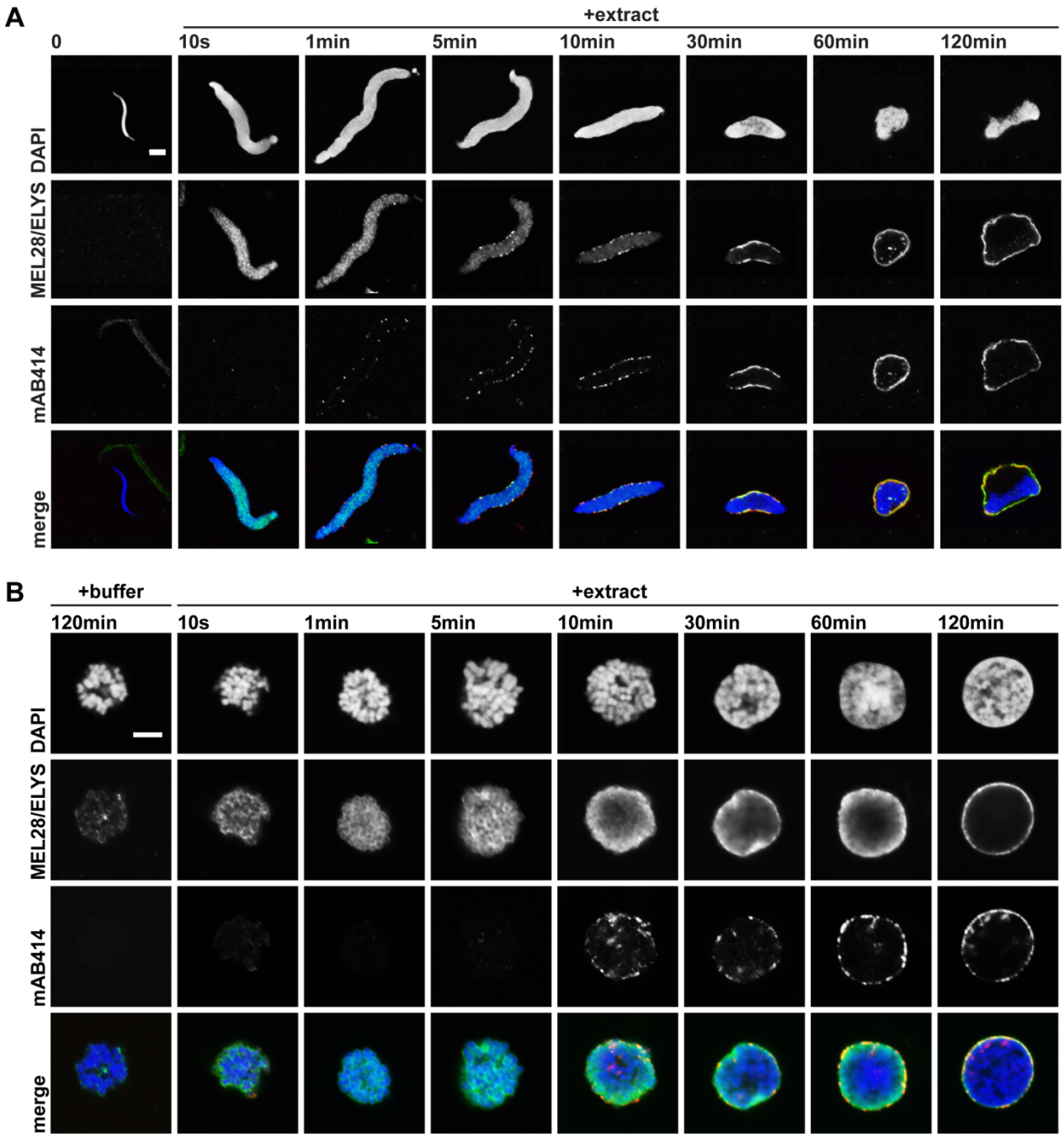

Figure 14. MEL28/ELYS recruitment to chromatin during cell-free nuclear assembly on sperm chromatin or mitotic chromatin clusters isolated from HeLa cells. Nuclei were assembled on either sperm chromatin (**A**) or mitotic chromatin clusters from HeLa cells (**B**). At the indicated times samples were fixed and processed for immunofluorescence. MEL28/ELYS was specifically immuno-labelled (green in overlays), NPCs were immuno-labelled with mAB414 (red in overlays) and DNA was stained with DAPI. Representative confocal images are shown. Scale bars: 5μm.

The recruitment of membrane proteins to chromatinized DNA beads was assayed using the floated membrane fractions that are typically employed in cell-free nuclear assembly. These membranes are vesiculated during their isolation giving rise to a mixed population of membrane vesicles with different capacities to support nuclear envelope formation (Antonin et al. 2005, Buendia and Courvalin 1997, Mansfeld et al. 2006, Ulbert et al. 2006, Vigers and Lohka 1991). The existence of these distinct membrane vesicle pools supports the notion that nuclear envelope microdomains are maintained in the ER during mitosis in order to facilitate efficient reassembly upon mitotic exit (Mattaj 2004). Functionally distinct pools of membrane vesicles can be distinguished biochemically based on the presence of specific marker proteins. These membrane pools include: The vesicles first recruited to post-mitotic chromatin that are enriched for the transmembrane nucleoporins POM121 and NDC1 (Antonin et al. 2005, Mansfeld et al. 2006), a second membrane pool recruited relatively late during nuclear assembly and enriched for the transmembrane nucleoporin GP210 (Antonin et al. 2005, Buendia and Courvalin 1997, Chaudhary and Courvalin 1993), and a third pool of bulk ER membrane vesicles that are not strictly required for nuclear envelope assembly and contain the ER proteins Rtn4 and Calnexin. In mock-treated extracts, each of these distinct membrane vesicle populations was recruited to chromatinized DNA ((Schooley et al. 2015) Fig. 6A (Appendix)). Conversely, chromatin assembled in LSD1-depleted extracts no longer supported the recruitment of POM121 and NDC1-containing membrane vesicles. The addition of recombinant LSD1-wt, but not LSD1-K643A, rescued POM121 and NDC1 recruitment to chromatin. Nuclei assembled in LSD1-depleted extracts were similarly deficient for the presence of POM121 and NDC1, a phenotype that was rescued by the addition of catalytically active LSD1-wt but not LSD1-K643A ((Schooley et al. 2015) Fig. 6B (Appendix)). Importantly, LSD1 depletion did not impact the recruitment of GP210-containing NE vesicles or bulk ER vesicles to chromatinized DNA ((Schooley et al. 2015) Fig. 6A (Appendix)) and membranes were consistently found on chromatin when nuclei were assembled in the absence of LSD1 activity ((Schooley et al. 2015) Fig. 1, 2B, 5C, S4D (Appendix)), suggesting that LSD1-dependent demethylation regulates the recruitment of a specific subpopulation of essential nuclear envelope membranes to post-mitotic chromatin.

POM121 and NDC1 are both essential for NPC assembly (Antonin et al. 2005, Mansfeld et al. 2006). As their early recruitment to chromatin at the end of mitosis (Dultz

et al. 2008) depends on the MEL28/ELYS-dependent recruitment of the Nup107-160 complex (Antonin et al. 2005, Rasala et al. 2008), it is likely that the loss of POM121 and NDC1 on chromatin in the absence of LSD1 activity is at least partially due to the reduced presence of MEL28/ELYS. However, depletion of Mel28 from *Xenopus* egg extracts gives rise to nuclei with closed nuclear envelopes lacking NPCs (Rasala et al. 2008). This phenotype is not mimicked in LSD1-depleted extracts, suggesting that LSD1 activity regulates more than one molecular player during nuclear envelope and NPC assembly. Nuclear envelope precursor vesicles, including POM121-containing vesicles, can bind DNA independently of cytosolic proteins (Ulbert et al. 2006). Furthermore, a soluble fragment of POM121 was found to competitively inhibit cell-free nuclear assembly without disrupting MEL28/ELYS and Nup107-160 complex recruitment (Shaulov et al. 2011). A combination field emission scanning electron microscopy and biochemical experiments revealed the existence of distinct binding sites for POM121 and MEL28/ELYS and suggested that their initial localization on chromatin might be independent. Taken together, it is likely that LSD1 activity regulates the autonomous recruitment of multiple factors to post-mitotic chromatin during the early stages of nuclear envelope and NPC assembly.

7.5.2 Proposed mechanisms of LSD1-dependent nuclear assembly

The *in vitro* data presented in this thesis implicate LSD1-dependent de-methylation in the regulation of NPC and nuclear envelope assembly on post-mitotic chromatin. Although the impact of reduced LSD1 levels on nuclear assembly was significantly less pronounced in living cells, the prolonged maintenance of compact chromatin following cell division and the formation of annulate lamellae suggest that LSD1 plays a physiologically relevant role in nuclear reorganization during telophase. The importance of LSD1 activity for the recruitment of early-associating soluble and transmembrane NPC proteins to chromatin in *Xenopus* egg extracts indicates that LSD1 function likely contributes to the competence of the chromatin landscape for nuclear assembly at the end of mitosis. However, the open question that remains is the exact nature of this chromatin competence. In other words, what are the LSD1-dependent chromatin features that promote nuclear envelope and NPC assembly?

Histone lysine methyltransferases and demethylases have been found to impact mitotsis by modulating the expression of important cell cycle genes (Reviewed in (Black et al. 2012). LSD1 itself has been implicated in cell-cycle regulation upstream of p53-dependent transcription (Scoumanne and Chen 2007) as well as the expression of the spindle assembly checkpoint proteins Mad2 and Bub1 (Lv et al. 2010). However, as frog eggs are not transcriptionally active (Newport and Kirschner 1982) the role of LSD1 in nuclear assembly must also be independent of transcription. Although multiple soluble and transmembrane nucleoporins have the capacity to bind DNA, nuclear envelope and NPC assembly do not occur in the absence of nucleosomes (Inoue and Zhang 2014, Zierhut et al. 2014). This requirement can be been attributed to the nucleosome-dependent recruitment of both MEL28/ELYS and the guanine exchange factor RCC1. In the absence of nucleosomes or DNA, a localized concentration of RanGTP, generated by RCC1, was found to be sufficient for the assembly of import competent pseudo nuclear envelopes in *Xenopus* egg extracts (Zhang and Clarke 2000). Similarly, tethering RCC1 to nucleosome-depleted DNA beads could promote NPC assembly *in vitro.* However, artificial tethering of MEL28/ELYS to DNA beads or to the nuclear rim of paternal pronulclei from mouse zygotes in the absence of nucleosome assembly was also found to enable NPC and nuclear envelope assembly (Inoue and Zhang 2014, Zierhut et al. 2014), suggesting that more than one factor directs NPC and nuclear envelope assembly to chromatin at the end of mitosis. Indeed, tethering both Mel28/ELYS and RCC1 to DNA synergistically rescued NPC assembly when nucleosomes were depleted from *Xenopus* egg extracts (Zierhut et al. 2014). These findings implicate the chromatin-dependent recruitment of MEL28/ELYS and RCC1 as critical determinants of post-mitotic nuclear envelope assembly. However, very little is known regarding the changes to chromatin that facilitates their binding at the end of mitosis. LSD1 demethylase activity was required for the recruitment of MEL28/ELYS to chromatinized DNA beads or to nuclear assemblies on sperm chromatin in *Xenopus* egg extracts ((Schooley et al. 2015) Fig 6 (Appendix)). Thus it is likely that LSD1 plays a role in modulating the post-mitotic chromatin landscape in order to promote the nucleosome-dependent recruitment of MEL28/ELYS.

Histone modifications, particularly methylation and acetylation, have been proposed to memorize the transcriptional state of chromatin throughout cell divisions (Reviewed in (Wang et al. 2013, Moazed 2011)). Nonetheless, several of these

modifications are also dynamic during mitosis. LSD1 demethylates mono- and di-methylated histone H3 at lysine 4 and 9. Levels of H3K4me1, H3K4m2, H3K9me1, and H3K9me2 have been found to globally increase during mitosis (Black et al. 2012), a time when LSD1 is absent from chromatin ((Schooley et al. 2015) Fig. S2 (Appendix)). However, while target promoters were affected in the absence of LSD1 activity, global changes in methylation were not reported (Lv et al. 2010, Nair et al. 2012, Shi et al. 2004), suggesting that LSD1 regulates locus specific demethylation.

Current information regarding the dynamics of histone lysine methylation is primarily derived from chromatin immunoprecipitation experiments and sequencing data and therefore does not indicate the 3-dimensional positions of these marks on chromatin. In order to determine the localization pattern of potential LSD1-targeted histone methylation marks during mitosis, immunofluorescence was performed on fixed unsynchronized HeLa cells. Confocal z-stacks were acquired using constant acquisition settings to capture the relative levels and distribution of the histone marks at different stages of the cell cycle. In agreement with published biochemical data, H3K4me3 levels were somewhat constant throughout the cell cycle and H3K9me3 was reduced from prophase to early anaphase (Fig. 15). Unmethylated H3K4 (H3K4me0), H3K4me1, and H3K4me2, appeared to preferentially occupy more peripheral chromatin regions during mitosis, when levels were also at least slightly elevated, particularly for H3K4me0 and H3K4me1. The return to an interphasic chromatin state correlated with a reduction in H3K4me0 and H3K4me1 and a more even, less peripheral, distribution of H3K4me2. In contrast to previous reports, H3K9me1 was dramatically reduced starting at prophase and seemed to return to chromatin during early anaphase.

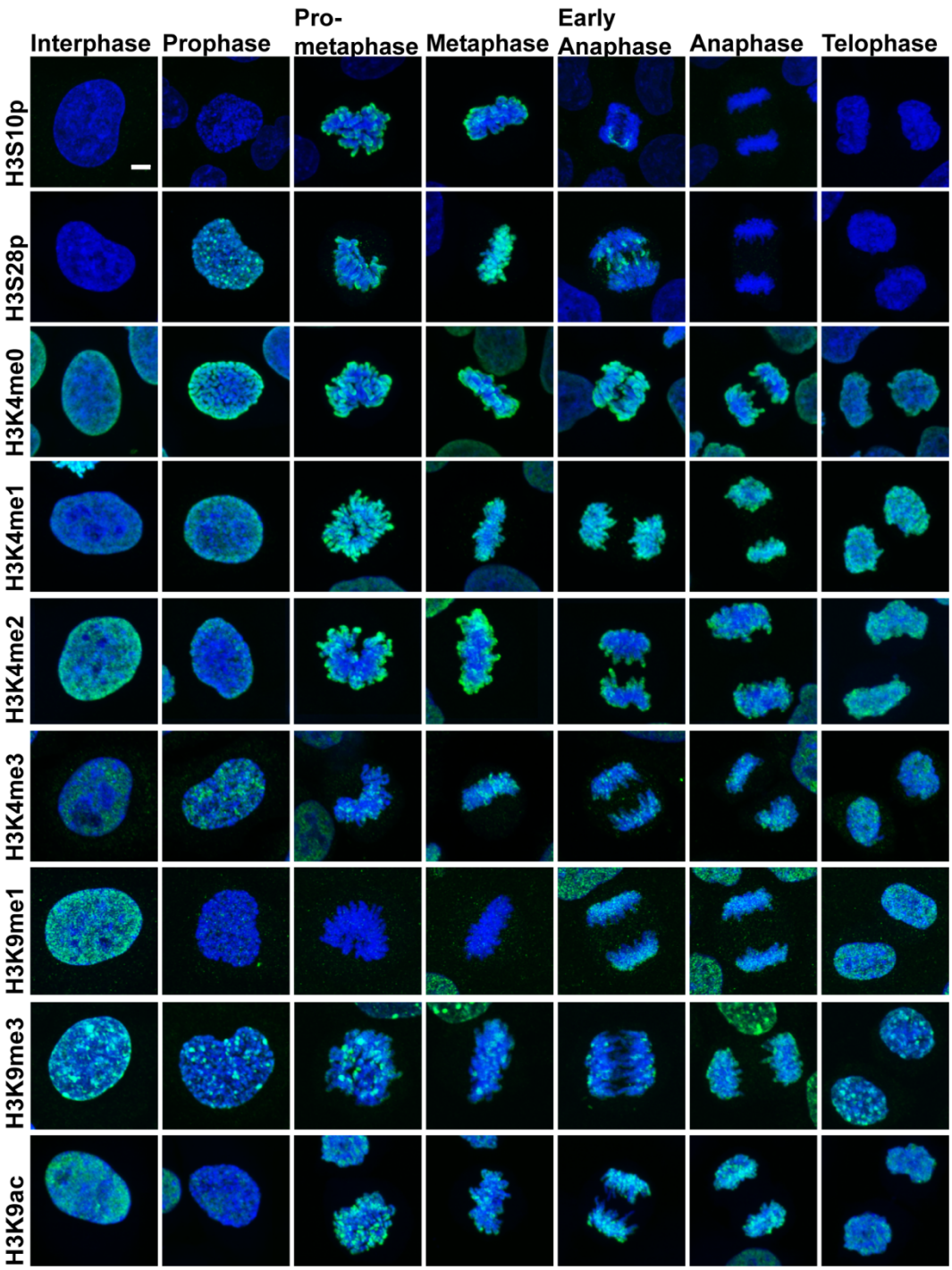

Figure 15. Dynamic localisation of histone modifications during the cell cycle in fixed HeLa cells. HeLa cells were fixed and processed for immunofluorescence. A variety of post-translational modifications to histone H3 were immuno-labelled as indicated (green) and DNA was stained with DAPI (blue). Representative maximum intensity projections from 0.25um-spaced optical z-sections traversing the chromatin are shown. Scale bar: 5μm.

As some cell cycle dependent signatures could be found for several of the methylation marks targeted by LSD1, they were examined by immunofluorescence in LSD1 knockdown HeLa cells (Fig. 16) and nuclei assembled on mitotic chromatin clusters in LSD1-depleted egg extracts (Fig.17). Although an increase in H3K4me2 was detected on chromatin beads in LSD1-depleted extracts, no obvious difference in the levels or distribution of H3K4me1, H3K4me2, or H3K9me1 were observed in either experimental context. Thus any differences in the levels or distribution of LSD1-targeted methylation marks are beyond the resolution of the methods employed, either because of the technical limitations associated with regular confocal light microscopy or due to the fact that, as previously suggested, the LSD1-dependent changes are locus specific.

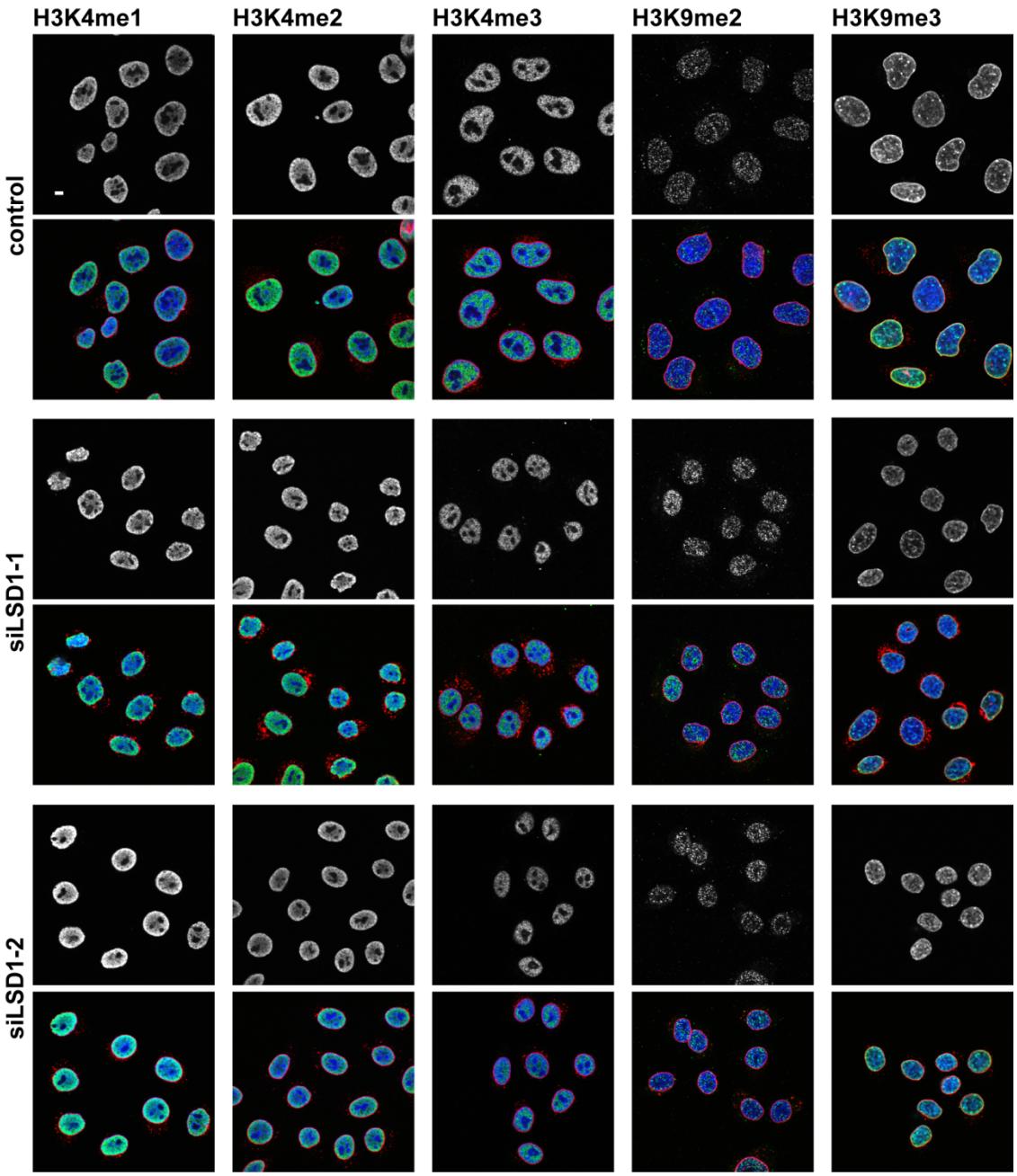

Figure 16. The distribution and global levels of histone methylation marks are not consistently impacted by the RNAi-mediated depletion of LSD1 in HeLa cells. HeLa cells transfected with 20 nM control, LSD1-1 or LSD1-2 siRNA oligos were fixed 48h post-transfection and processed for immunofluorescence. Specific methylation states of histone H3 at K4 and K9 were immuno-labelled as indicated (upper panels, green in overlay) and DNA was stained with DAPI (blue in overlays). Representative confocal images are shown. Scale bar: 5μm.

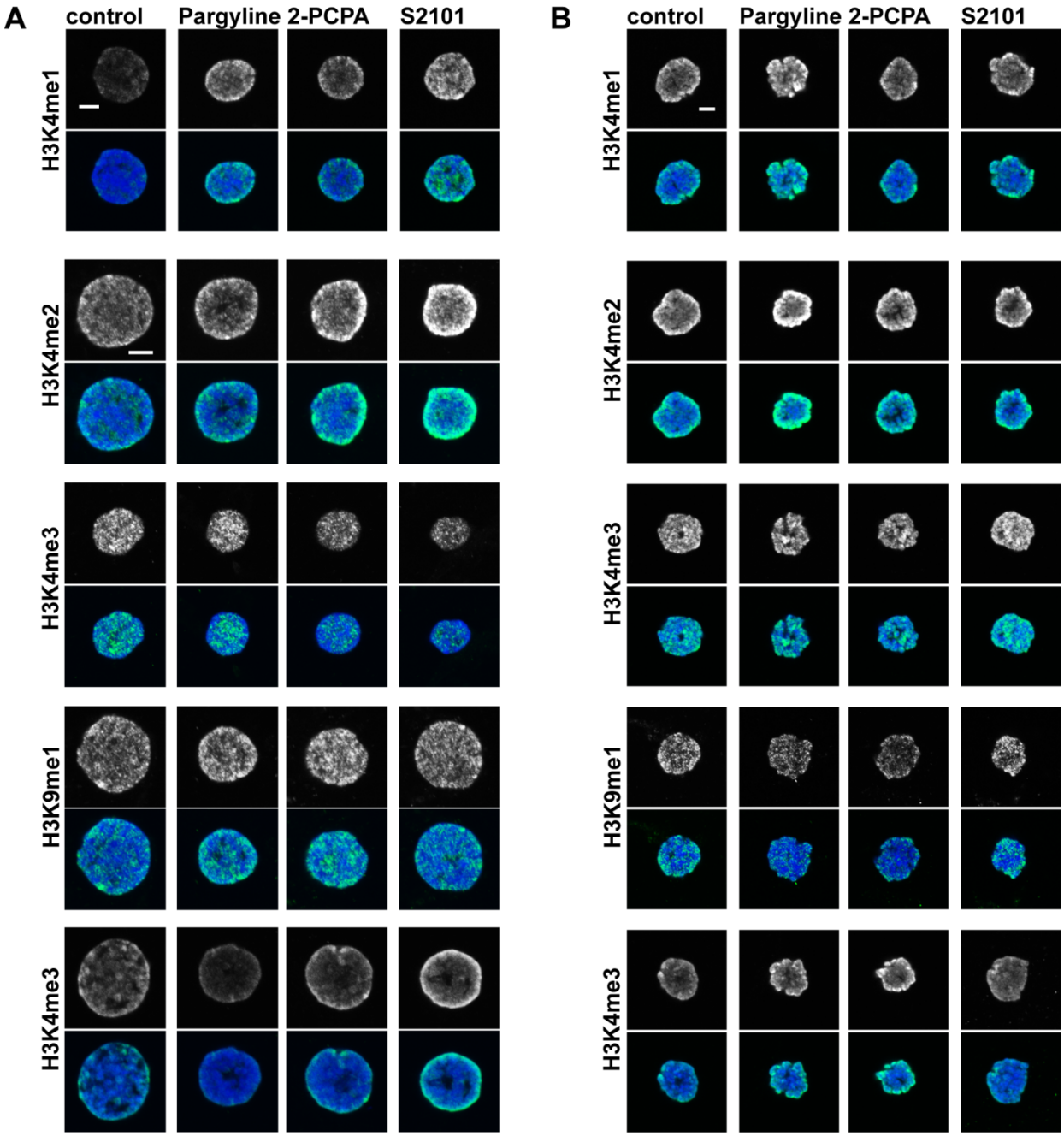

Figure 17. The distribution and global levels of histone methylation marks found on decondensing mitotic chromatin clusters are not consistently impacted by LSD1 inhibition. Nuclei were assembled on mitotic chromatin clusters from HeLa cells in the presence or absence of 5mM Pargyline, 2.5 mM 2PCPA, or 250 uM S2101 for (**A**) 120 min or (**B**) 10 min. Following fixation, specific methylation states of histone H3 at K4 and K9 were immuno-labelled as indicated (upper panels, green in overlay) and DNA was stained with DAPI (blue in overlays). Representative confocal images are shown. Scale bar: 5μm.

Locus-specific demethylation does not preclude the possibility that histone H3 demethylation is the relevant LSD1 target in the regulation of nuclear envelope assembly. In this case, demethylation at specific loci could provide specific initiation points for nuclear envelope or NPC formation and might even help to establish interphase chromatin organisation with respect to the nuclear periphery. Alternatively, locus-specific LSD1-dependent demethylation might also initiate more global changes to the chromatin landscape. In both scenarios, the accumulation or loss of a specific H3K4 or H3K9 methyl mark by LSD1 might directly mediate the recruitment of NPC and nuclear envelope components. To date, the only example of a specific methylation mark directing the recruitent of nuclear envelope factors is H3K9me3, which acts via HP1 (Bannister et al. 2001, Fischle et al. 2005, Hirota et al. 2005, Lachner et al. 2001). Alternatively nuclear components could also be recruited due to other histone modifications that occur downstream of LSD1. For example, LSD1-mediated demethylase activity has been implicated upstream of HDAC1/2 (Lee et al. 2006a). In this regard, LSD1 demethylation might be a crucial step in a cascade of modifications or part of an epigenetic code that modulates nuclear envelope recruitment and assembly. Histone demethylation is the best characterized function of LSD1 and the idea that this chromatin modification regulates nuclear assembly is an exciting one. However, several non-histone targets of LSD1 have already been identified (reviewed in (Nicholson and Chen 2009)) and the possibility that LSD1 promotes nuclear envelope assembly via one of these or a yet unidentified target cannot be excluded.

The accumulation of a specific histone modification, a combination of histone modifications, or the presence of a specific protein with a demethylation-dependent function could mediate LSD1-dependent nuclear envelope and NPC formation on chromatin at the end of mitosis. Alternatively, it is possible that LSD1-dependent demethylation regulates nuclear assembly by modulating the conformation of post-mitotic chromatin. Although the loss of LSD1 activity did not inhibit cell-free chromosome decondensation *per se*, both mitotic chromatin clusters incubated with LSD1-depleted extracts and the nuclei of HeLa cells treated with LSD1-targeting siRNAs were visibly smaller and chromatin was more compacted compared to the relevant controls ((Schooley et al. 2015) Fig. 4A and B, S3A (Appendix)). These observations suggest that LSD1 plays a role in chromatin organization at the end of mitosis, although mechanistically it could effect the relevant conformation in any number of ways. For

example, LSD1 has been implicated in heterochromatin formation in Drosophila (Rudolph et al. 2007) and S. pombe (Lan et al. 2007). H3K9me3, a characteristic heterochromatin modification, regulates the recruitment of HP1 and in turn nuclear envelope membranes to chromatin at the end of mitosis (Ye et al. 1997, Haraguchi et al. 2000, Fischle et al. 2005). It is thus conceiveable that LSD1-dependent heterochromatin formation could contribute nuclear envelope assembly.

Demethylation by LSD1 represents a novel addition to a very short list of events that link post-mitotic chromatin reorganization with nuclear envelope assembly. The most prominent among these is the recruitment of the protein phosphatase PP1 to anaphase chromatin via RepoMan/CDCA2 (Trinkle-Mulcahy et al. 2006), which coordinates the removal of mitotic histone marks with the deposition of importin beta-bound nucleoporins (Vagnarelli et al. 2011). An interesting layer of complexity was recently added with the indentification of Ki-67, a nucleolar protein that localizes to the perichromosomal compartment during mitosis, as an additional regulator of both PP1 recruitment and the reestablishment of interphase chromatin architecture (Booth et al. 2014, Takagi et al. 2014). Although the mechanistic details remain an interesting puzzle for future experimentation, the data presented here identify LSD1 as an important regulator of post-mitotic nuclear reassembly. The recruitment of LSD1 at the end of mitosis initiates demethylation activity-dependent changes to either the composition or the conformation of chromatin that promote the recruitment of MEL28/ELYS and nuclear membranes and thus link the post-mitotic chromatin state to NPC and nuclear envelope formation (Fig. 18).

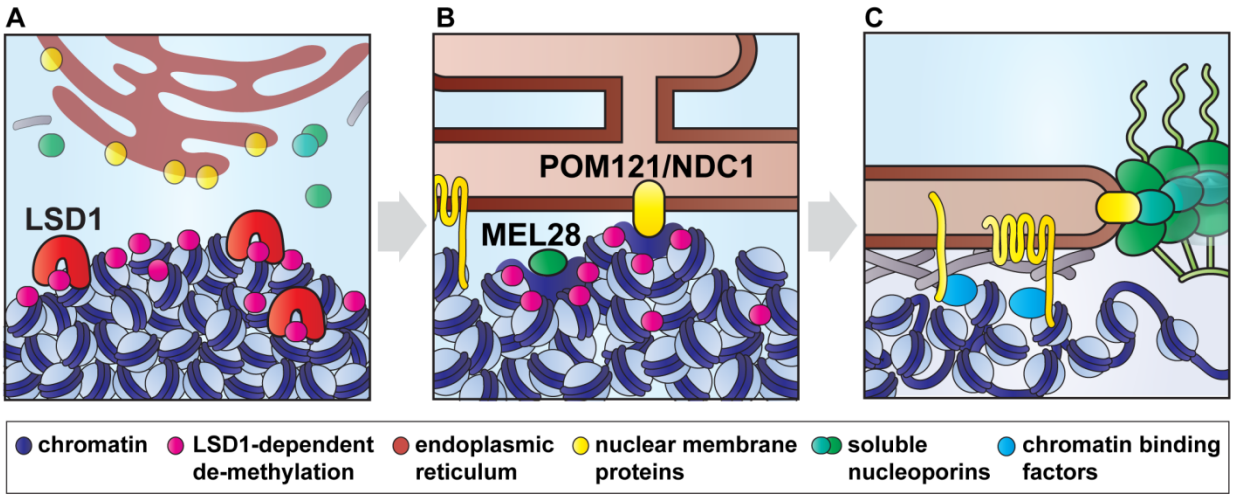

Figure 18. Schematic: Proposed model for the role of LSD1 in post-mitotic nuclear reassembly. Upon mitotic exit, LSD1 re-localizes to chromatin and mediates histone H3 tail de-methylation (**A**). The resultant changes to the chromatin landscape modulate the recruitment of the soluble nucleoporin MEL28/ELYS, which is required to seed post-mitotic NPC assembly, and the nuclear envelope-specific membranes, which are enriched for the transmembrane nucleoporins POM121 and NDC1 (**B**). The relevant histone mark(s) and potential downstream events that precede the recruitment of nucleoporins are unknown. The formation of a continuous functional nuclear envelope and the reestablishment of interphase chromatin architecture (**C**) thus require the activity of LSD1 at the end of mitosis.

8. References

ADAMO A, SESE B, BOUE S, CASTANO J, PARAMONOV I, BARRERO MJ AND IZPISUA BELMONTE JC. 2011. LSD1 regulates the balance between self-renewal and differentiation in human embryonic stem cells. Nature cell biology 13: 652-659.

AHMED K, DEHGHANI H, RUGG-GUNN P, FUSSNER E, ROSSANT J AND BAZETT-JONES DP. 2010. Global chromatin architecture reflects pluripotency and lineage commitment in the early mouse embryo. PloS one 5: e10531.

AKEY CW AND RADERMACHER M. 1993. Architecture of the Xenopus nuclear pore complex revealed by three-dimensional cryo-electron microscopy. The Journal of cell biology 122: 1-19.

AKHTAR A AND GASSER SM. 2007. The nuclear envelope and transcriptional control. Nature reviews Genetics 8: 507-517.

ALBER F ET AL. 2007. The molecular architecture of the nuclear pore complex. Nature 450: 695-701.

ALVAREZ-FERNANDEZ M, SANCHEZ-MARTINEZ R, SANZ-CASTILLO B, GAN PP, SANZ-FLORES M, TRAKALA M, RUIZ-TORRES M, LORCA T, CASTRO A AND MALUMBRES M. 2013. Greatwall is essential to prevent mitotic collapse after nuclear envelope breakdown in mammals. Proc Natl Acad Sci U S A 110: 17374-17379.

AMENDOLA M AND VAN STEENSEL B. 2014. Mechanisms and dynamics of nuclear lamina-genome interactions. Curr Opin Cell Biol 28: 61-68.

AMENTE S, LANIA L AND MAJELLO B. 2013. The histone LSD1 demethylase in stemness and cancer transcription programs. Biochimica et biophysica acta 1829: 981-986.

ANDERSON DJ AND HETZER MW. 2007. Nuclear envelope formation by chromatin-mediated reorganization of the endoplasmic reticulum. Nat Cell Biol 9: 1160-1166.

ANDERSON DJ AND HETZER MW. 2008. Reshaping of the endoplasmic reticulum limits the rate for nuclear envelope formation. The Journal of cell biology 182: 911-924.

ANDERSON DJ, VARGAS JD, HSIAO JP AND HETZER MW. 2009. Recruitment of functionally distinct membrane proteins to chromatin mediates nuclear envelope formation in vivo. The Journal of cell biology 186: 183-191.

ANTONIN W, ELLENBERG J AND DULTZ E. 2008. Nuclear pore complex assembly through the cell cycle: Regulation and membrane organization. FEBS Lett 582: 2004-2016.

ANTONIN W, FRANZ C, HASELMANN U, ANTONY C AND MATTAJ IW. 2005. The integral membrane nucleoporin pom121 functionally links nuclear pore complex assembly and nuclear envelope formation. Mol Cell 17: 83-92.

ANTONIN W AND MATTAJ IW. 2005. Nuclear pore complexes: round the bend? Nat Cell Biol 7: 10-12.

ANTONIN W, UNGRICHT R AND KUTAY U. 2011. Traversing the NPC along the pore membrane: Targeting of membrane proteins to the INM. Nucleus 2: 87-91.

ASENCIO C, DAVIDSON IF, SANTARELLA-MELLWIG R, LY-HARTIG TB, MALL M, WALLENFANG MR, MATTAJ IW AND GORJANACZ M. 2012. Coordination of Kinase and Phosphatase Activities by Lem4 Enables Nuclear Envelope Reassembly during Mitosis. Cell 150: 122-135.

AUDHYA A, DESAI A AND OEGEMA K. 2007. A role for Rab5 in structuring the endoplasmic reticulum. The Journal of cell biology 178: 43-56.

BANNISTER AJ, ZEGERMAN P, PARTRIDGE JF, MISKA EA, THOMAS JO, ALLSHIRE RC AND KOUZARIDES T. 2001. Selective recognition of methylated lysine 9 on histone H3 by the HP1 chromo domain. Nature 410: 120-124.
BARON R AND VELLORE NA. 2012. LSD1/CoREST is an allosteric nanoscale clamp regulated by H3-histone-tail molecular recognition. Proc Natl Acad Sci U S A 109: 12509-12514.
BAYLISS R, LEUNG SW, BAKER RP, QUIMBY BB, CORBETT AH AND STEWART M. 2002. Structural basis for the interaction between NTF2 and nucleoporin FxFG repeats. Embo J 21: 2843-2853.
BAYLISS R, RIBBECK K, AKIN D, KENT HM, FELDHERR CM, GORLICH D AND STEWART M. 1999. Interaction between NTF2 and xFxFG-containing nucleoporins is required to mediate nuclear import of RanGDP. J Mol Biol 293: 579-593.
BEAUDOUIN J, GERLICH D, DAIGLE N, EILS R AND ELLENBERG J. 2002. Nuclear envelope breakdown proceeds by microtubule-induced tearing of the lamina. Cell 108: 83-96.
BECK M, LUCIC V, FORSTER F, BAUMEISTER W AND MEDALIA O. 2007. Snapshots of nuclear pore complexes in action captured by cryo-electron tomography. Nature 449: 611-615.
BELMONT AS. 2006. Mitotic chromosome structure and condensation. Curr Opin Cell Biol 18: 632-638.
BELMONT AS AND BRUCE K. 1994. Visualization of G1 chromosomes: a folded, twisted, supercoiled chromonema model of interphase chromatid structure. The Journal of cell biology 127: 287-302.
BICKMORE WA AND VAN STEENSEL B. 2013. Genome architecture: domain organization of interphase chromosomes. Cell 152: 1270-1284.
BILOKAPIC S AND SCHWARTZ TU. 2012. 3D ultrastructure of the nuclear pore complex. Curr Opin Cell Biol.
BINDA C, LI M, HUBALEK F, RESTELLI N, EDMONDSON DE AND MATTEVI A. 2003. Insights into the mode of inhibition of human mitochondrial monoamine oxidase B from high-resolution crystal structures. Proc Natl Acad Sci U S A 100: 9750-9755.
BLACK JC, VAN RECHEM C AND WHETSTINE JR. 2012. Histone lysine methylation dynamics: establishment, regulation, and biological impact. Mol Cell 48: 491-507.
BLOBEL G. 1985. Gene gating: a hypothesis. Proc Natl Acad Sci U S A 82: 8527-8529.
BLOOM K AND JOGLEKAR A. 2010. Towards building a chromosome segregation machine. Nature 463: 446-456.
BOEHMER T, ENNINGA J, DALES S, BLOBEL G AND ZHONG H. 2003. Depletion of a single nucleoporin, Nup107, prevents the assembly of a subset of nucleoporins into the nuclear pore complex. Proc Natl Acad Sci U S A 100: 981-985.
BOLZER A ET AL. 2005. Three-dimensional maps of all chromosomes in human male fibroblast nuclei and prometaphase rosettes. PLoS biology 3: e157.
BOOTH DG ET AL. 2014. Ki-67 is a PP1-interacting protein that organises the mitotic chromosome periphery. eLife 3: e01641.
BRACHNER A AND FOISNER R. 2011. Evolvement of LEM proteins as chromatin tethers at the nuclear periphery. Biochem Soc Trans 39: 1735-1741.
BRIDGER JM, BOYLE S, KILL IR AND BICKMORE WA. 2000. Re-modelling of nuclear architecture in quiescent and senescent human fibroblasts. Current biology : CB 10: 149-152.
BROHAWN SG, PARTRIDGE JR, WHITTLE JR AND SCHWARTZ TU. 2009. The nuclear pore complex has entered the atomic age. Structure 17: 1156-1168.

BUENDIA B AND COURVALIN JC. 1997. Domain-specific disassembly and reassembly of nuclear membranes during mitosis. Exp Cell Res 230: 133-144.
BUI KH ET AL. 2013. Integrated structural analysis of the human nuclear pore complex scaffold. Cell 155: 1233-1243.
BURKE B. 2012. It takes KASH to hitch to the SUN. Cell 149: 961-963.
BUTIN-ISRAELI V, ADAM SA, GOLDMAN AE AND GOLDMAN RD. 2012. Nuclear lamin functions and disease. Trends in genetics : TIG 28: 464-471.
CAPELSON M, DOUCET C AND HETZER MW. 2010. Nuclear pore complexes: guardians of the nuclear genome. Cold Spring Harbor symposia on quantitative biology 75: 585-597.
CARMENA M, WHEELOCK M, FUNABIKI H AND EARNSHAW WC. 2012. The chromosomal passenger complex (CPC): from easy rider to the godfather of mitosis. Nat Rev Mol Cell Biol 13: 789-803.
CHAN RC AND FORBES DI. 2006. In vitro study of nuclear assembly and nuclear import using Xenopus egg extracts. Methods in molecular biology 322: 289-300.
CHATEL G AND FAHRENKROG B. 2011. Nucleoporins: leaving the nuclear pore complex for a successful mitosis. Cell Signal 23: 1555-1562.
CHAUDHARY N AND COURVALIN JC. 1993. Stepwise reassembly of the nuclear envelope at the end of mitosis. The Journal of cell biology 122: 295-306.
CHEN S, NOVICK P AND FERRO-NOVICK S. 2013. ER structure and function. Curr Opin Cell Biol 25: 428-433.
CLEVER M, FUNAKOSHI T, MIMURA Y, TAKAGI M AND IMAMOTO N. 2012. The nucleoporin ELYS/Mel28 regulates nuclear envelope subdomain formation in HeLa cells. Nucleus 3: 187-199.
COHEN M, FEINSTEIN N, WILSON KL AND GRUENBAUM Y. 2003. Nuclear pore protein gp210 is essential for viability in HeLa cells and Caenorhabditis elegans. Mol Biol Cell 14: 4230-4237. Epub 2003 Jul 4211.
COLLAS P. 1999. Sequential PKC- and Cdc2-mediated phosphorylation events elicit zebrafish nuclear envelope disassembly. Journal of cell science 112 (Pt 6): 977-987.
COLLAS P, COURVALIN JC AND POCCIA D. 1996. Targeting of membranes to sea urchin sperm chromatin is mediated by a lamin B receptor-like integral membrane protein. The Journal of cell biology 135: 1715-1725.
COSTA R, ARRIGONI G, COZZA G, LOLLI G, BATTISTUTTA R, IZPISUA BELMONTE JC, PINNA LA AND SARNO S. 2014. The lysine-specific demethylase 1 is a novel substrate of protein kinase CK2. Biochimica et biophysica acta 1844: 722-729.
CRAIG JM AND BICKMORE WA. 1993. Chromosome bands--flavours to savour. BioEssays : news and reviews in molecular, cellular and developmental biology 15: 349-354.
CREMER M, KUPPER K, WAGLER B, WIZELMAN L, VON HASE J, WEILAND Y, KREJA L, DIEBOLD J, SPEICHER MR AND CREMER T. 2003. Inheritance of gene density-related higher order chromatin arrangements in normal and tumor cell nuclei. The Journal of cell biology 162: 809-820.
CREMER T AND CREMER C. 2006. Rise, fall and resurrection of chromosome territories: a historical perspective. Part I. The rise of chromosome territories. European journal of histochemistry : EJH 50: 161-176.
D'ANGELO MA, ANDERSON DJ, RICHARD E AND HETZER MW. 2006. Nuclear pores form de novo from both sides of the nuclear envelope. Science 312: 440-443.

D'ANGELO MA, GOMEZ-CAVAZOS JS, MEI A, LACKNER DH AND HETZER MW. 2012. A change in nuclear pore complex composition regulates cell differentiation. Dev Cell 22: 446-458.
DABAUVALLE MC, MULLER E, EWALD A, KRESS W, KROHNE G AND MULLER CR. 1999. Distribution of emerin during the cell cycle. Eur J Cell Biol 78: 749-756.
DAUB H, OLSEN JV, BAIRLEIN M, GNAD F, OPPERMANN FS, KORNER R, GREFF Z, KERI G, STEMMANN O AND MANN M. 2008. Kinase-selective enrichment enables quantitative phosphoproteomics of the kinome across the cell cycle. Mol Cell 31: 438-448.
DAVIS LI AND BLOBEL G. 1986. Identification and characterization of a nuclear pore complex protein. Cell 45: 699-709.
DE LA BARRE AE, ROBERT-NICOUD M AND DIMITROV S. 1999. Assembly of mitotic chromosomes in Xenopus egg extract. Methods in molecular biology 119: 219-229.
DE SOUZA CP AND OSMANI SA. 2009. Double duty for nuclear proteins--the price of more open forms of mitosis. Trends in genetics : TIG 25: 545-554.
DE WULF P, MONTANI F AND VISINTIN R. 2009. Protein phosphatases take the mitotic stage. Curr Opin Cell Biol 21: 806-815.
DEKKER J. 2014. Two ways to fold the genome during the cell cycle: insights obtained with chromosome conformation capture. Epigenetics & chromatin 7: 25.
DEMMERLE J, KOCH AJ AND HOLASKA JM. 2012. The nuclear envelope protein emerin binds directly to histone deacetylase 3 (HDAC3) and activates HDAC3 activity. The Journal of biological chemistry 287: 22080-22088.
DI LORENZO A AND BEDFORD MT. 2011. Histone arginine methylation. FEBS Lett 585: 2024-2031.
DITTMER TA AND MISTELI T. 2011. The lamin protein family. Genome biology 12: 222.
DOBRYNIN G, POPP O, ROMER T, BREMER S, SCHMITZ MH, GERLICH DW AND MEYER H. 2011. Cdc48/p97-Ufd1-Npl4 antagonizes Aurora B during chromosome segregation in HeLa cells. Journal of cell science 124: 1571-1580.
DOMINGO-SANANES MR, KAPUY O, HUNT T AND NOVAK B. 2011. Switches and latches: a biochemical tug-of-war between the kinases and phosphatases that control mitosis. Philosophical transactions of the Royal Society of London Series B, Biological sciences 366: 3584-3594.
DOUCET CM AND HETZER MW. 2010. Nuclear pore biogenesis into an intact nuclear envelope. Chromosoma 119: 469-477.
DOUCET CM, TALAMAS JA AND HETZER MW. 2010. Cell cycle-dependent differences in nuclear pore complex assembly in metazoa. Cell 141: 1030-1041.
DREGER M, OTTO H, NEUBAUER G, MANN M AND HUCHO F. 1999. Identification of phosphorylation sites in native lamina-associated polypeptide 2 beta. Biochemistry 38: 9426-9434.
DULTZ E AND ELLENBERG J. 2010. Live imaging of single nuclear pores reveals unique assembly kinetics and mechanism in interphase. The Journal of cell biology 191: 15-22.
DULTZ E, ZANIN E, WURZENBERGER C, BRAUN M, RABUT G, SIRONI L AND ELLENBERG J. 2008. Systematic kinetic analysis of mitotic dis- and reassembly of the nuclear pore in living cells. The Journal of cell biology 180: 857-865.
EFRONI S ET AL. 2008. Global transcription in pluripotent embryonic stem cells. Cell stem cell 2: 437-447.

EISENHARDT N, REDOLFI J AND ANTONIN W. 2014a. Interaction of Nup53 with Ndc1 and Nup155 is required for nuclear pore complex assembly. Journal of cell science 127: 908-921.
EISENHARDT N, SCHOOLEY A AND ANTONIN W. 2014b. Xenopus in vitro assays to analyze the function of transmembrane nucleoporins and targeting of inner nuclear membrane proteins. Methods in cell biology 122: 193-218.
ELLENBERG J, SIGGIA ED, MOREIRA JE, SMITH CL, PRESLEY JF, WORMAN HJ AND LIPPINCOTT-SCHWARTZ J. 1997. Nuclear membrane dynamics and reassembly in living cells: targeting of an inner nuclear membrane protein in interphase and mitosis. The Journal of cell biology 138: 1193-1206.
ELTSOV M, MACLELLAN KM, MAESHIMA K, FRANGAKIS AS AND DUBOCHET J. 2008. Analysis of cryo-electron microscopy images does not support the existence of 30-nm chromatin fibers in mitotic chromosomes in situ. Proc Natl Acad Sci U S A 105: 19732-19737.
ERIKSSON C, RUSTUM C AND HALLBERG E. 2004. Dynamic properties of nuclear pore complex proteins in gp210 deficient cells. FEBS Lett 572: 261-265.
FAHRENKROG B, ARIS JP, HURT EC, PANTE N AND AEBI U. 2000. Comparative spatial localization of protein-A-tagged and authentic yeast nuclear pore complex proteins by immunogold electron microscopy. J Struct Biol 129: 295-305.
FAVREAU C, WORMAN HJ, WOZNIAK RW, FRAPPIER T AND COURVALIN JC. 1996. Cell cycle-dependent phosphorylation of nucleoporins and nuclear pore membrane protein Gp210. Biochemistry 35: 8035-8044.
FIELD MC, KORENY L AND ROUT MP. 2014. Enriching the pore: splendid complexity from humble origins. Traffic (Copenhagen, Denmark) 15: 141-156.
FINCH JT AND KLUG A. 1976. Solenoidal model for superstructure in chromatin. Proc Natl Acad Sci U S A 73: 1897-1901.
FISCHLE W, TSENG BS, DORMANN HL, UEBERHEIDE BM, GARCIA BA, SHABANOWITZ J, HUNT DF, FUNABIKI H AND ALLIS CD. 2005. Regulation of HP1-chromatin binding by histone H3 methylation and phosphorylation. Nature 438: 1116-1122.
FOISNER R AND GERACE L. 1993. Integral membrane proteins of the nuclear envelope interact with lamins and chromosomes, and binding is modulated by mitotic phosphorylation. Cell 73: 1267-1279.
FORBES DJ, KIRSCHNER MW AND NEWPORT JW. 1983. Spontaneous formation of nucleus-like structures around bacteriophage DNA microinjected into Xenopus eggs. Cell 34: 13-23.
FORNERIS F, BINDA C, VANONI MA, MATTEVI A AND BATTAGLIOLI E. 2005. Histone demethylation catalysed by LSD1 is a flavin-dependent oxidative process. FEBS Lett 579: 2203-2207.
FRANCASTEL C, SCHUBELER D, MARTIN DI AND GROUDINE M. 2000. Nuclear compartmentalization and gene activity. Nat Rev Mol Cell Biol 1: 137-143.
FRANZ C, ASKJAER P, ANTONIN W, IGLESIAS CL, HASELMANN U, SCHELDER M, DE MARCO A, WILM M, ANTONY C AND MATTAJ IW. 2005. Nup155 regulates nuclear envelope and nuclear pore complex formation in nematodes and vertebrates. Embo J 24: 3519-3531.
FRANZ C, WALCZAK R, YAVUZ S, SANTARELLA R, GENTZEL M, ASKJAER P, GALY V, HETZER M, MATTAJ IW AND ANTONIN W. 2007. MEL-28/ELYS is required for the recruitment of nucleoporins to chromatin and postmitotic nuclear pore complex assembly. EMBO Rep 8: 165-172.

FREY S AND GORLICH D. 2007. A saturated FG-repeat hydrogel can reproduce the permeability properties of nuclear pore complexes. Cell 130: 512-523.
FRIBOURG S, BRAUN IC, IZAURRALDE E AND CONTI E. 2001. Structural basis for the recognition of a nucleoporin FG repeat by the NTF2-like domain of the TAP/p15 mRNA nuclear export factor. Mol Cell 8: 645-656.
FRIED H AND KUTAY U. 2003. Nucleocytoplasmic transport: taking an inventory. Cellular and molecular life sciences : CMLS 60: 1659-1688.
FURUKAWA K, SUGIYAMA S, OSOUDA S, GOTO H, INAGAKI M, HORIGOME T, OMATA S, MCCONNELL M, FISHER PA AND NISHIDA Y. 2003. Barrier-to-autointegration factor plays crucial roles in cell cycle progression and nuclear organization in Drosophila. Journal of cell science 116: 3811-3823.
FUSSNER E, AHMED K, DEHGHANI H, STRAUSS M AND BAZETT-JONES DP. 2010. Changes in chromatin fiber density as a marker for pluripotency. Cold Spring Harbor symposia on quantitative biology 75: 245-249.
FUSSNER E, CHING RW AND BAZETT-JONES DP. 2011. Living without 30nm chromatin fibers. Trends in biochemical sciences 36: 1-6.
FUSSNER E, STRAUSS M, DJURIC U, LI R, AHMED K, HART M, ELLIS J AND BAZETT-JONES DP. 2012. Open and closed domains in the mouse genome are configured as 10-nm chromatin fibres. EMBO Rep 13: 992-996.
GALY V, ANTONIN W, JAEDICKE A, SACHSE M, SANTARELLA R, HASELMANN U AND MATTAJ I. 2008. A role for gp210 in mitotic nuclear-envelope breakdown. Journal of cell science 121: 317-328.
GASSER SM AND LAEMMLI UK. 1987. Improved methods for the isolation of individual and clustered mitotic chromosomes. Exp Cell Res 173: 85-98.
GAVET O AND PINES J. 2010. Activation of cyclin B1-Cdk1 synchronizes events in the nucleus and the cytoplasm at mitosis. The Journal of cell biology 189: 247-259.
GEORGATOS SD, MARKAKI Y, CHRISTOGIANNI A AND POLITOU AS. 2009. Chromatin remodeling during mitosis: a structure-based code? Frontiers in bioscience (Landmark edition) 14: 2017-2027.
GERACE L AND BLOBEL G. 1980. The nuclear envelope lamina is reversibly depolymerized during mitosis. Cell 19: 277-287.
GILLESPIE PJ, GAMBUS A AND BLOW JJ. 2012. Preparation and use of Xenopus egg extracts to study DNA replication and chromatin associated proteins. Methods 57: 203-213.
GILLESPIE PJ, KHOUDOLI GA, STEWART G, SWEDLOW JR AND BLOW JJ. 2007. ELYS/MEL-28 chromatin association coordinates nuclear pore complex assembly and replication licensing. Current biology : CB 17: 1657-1662.
GLAVY JS, KRUTCHINSKY AN, CRISTEA IM, BERKE IC, BOEHMER T, BLOBEL G AND CHAIT BT. 2007. Cell-cycle-dependent phosphorylation of the nuclear pore Nup107-160 subcomplex. Proc Natl Acad Sci U S A 104: 3811-3816.
GOMEZ-CAVAZOS JS AND HETZER MW. 2015. The nucleoporin gp210/Nup210 controls muscle differentiation by regulating nuclear envelope/ER homeostasis. The Journal of cell biology 208: 671-681.
GORJANACZ M, KLERKX EP, GALY V, SANTARELLA R, LOPEZ-IGLESIAS C, ASKJAER P AND MATTAJ IW. 2007. Caenorhabditis elegans BAF-1 and its kinase VRK-1 participate directly in post-mitotic nuclear envelope assembly. Embo J 26: 132-143.
GRANDI P, DANG T, PANE N, SHEVCHENKO A, MANN M, FORBES D AND HURT E. 1997. Nup93, a vertebrate homologue of yeast Nic96p, forms a complex with a novel 205-

kDa protein and is required for correct nuclear pore assembly. Mol Biol Cell 8: 2017-2038.
GRANT RP, NEUHAUS D AND STEWART M. 2003. Structural basis for the interaction between the Tap/NXF1 UBA domain and FG nucleoporins at 1A resolution. J Mol Biol 326: 849-858.
GRUENBAUM Y, MARGALIT A, GOLDMAN RD, SHUMAKER DK AND WILSON KL. 2005. The nuclear lamina comes of age. Nat Rev Mol Cell Biol 6: 21-31.
GURDON JB, ELSDALE TR AND FISCHBERG M. 1958. Sexually mature individuals of Xenopus laevis from the transplantation of single somatic nuclei. Nature 182: 64-65.
GURLEY LR, WALTERS RA AND TOBEY RA. 1974. Cell cycle-specific changes in histone phosphorylation associated with cell proliferation and chromosome condensation. The Journal of cell biology 60: 356-364.
GUTTINGER S, LAURELL E AND KUTAY U. 2009. Orchestrating nuclear envelope disassembly and reassembly during mitosis. Nat Rev Mol Cell Biol 10: 178-191.
HAMADA M, HAEGER A, JEGANATHAN KB, VAN REE JH, MALUREANU L, WALDE S, JOSEPH J, KEHLENBACH RH AND VAN DEURSEN JM. 2011. Ran-dependent docking of importin-beta to RanBP2/Nup358 filaments is essential for protein import and cell viability. The Journal of cell biology 194: 597-612.
HARAGUCHI T, KOJIDANI T, KOUJIN T, SHIMI T, OSAKADA H, MORI C, YAMAMOTO A AND HIRAOKA Y. 2008. Live cell imaging and electron microscopy reveal dynamic processes of BAF-directed nuclear envelope assembly. Journal of cell science 121: 2540-2554.
HARAGUCHI T, KOUJIN T, HAYAKAWA T, KANEDA T, TSUTSUMI C, IMAMOTO N, AKAZAWA C, SUKEGAWA J, YONEDA Y AND HIRAOKA Y. 2000. Live fluorescence imaging reveals early recruitment of emerin, LBR, RanBP2, and Nup153 to reforming functional nuclear envelopes. Journal of cell science 113 (Pt 5): 779-794.
HAREL A, CHAN RC, LACHISH-ZALAIT A, ZIMMERMAN E, ELBAUM M AND FORBES DJ. 2003a. Importin beta negatively regulates nuclear membrane fusion and nuclear pore complex assembly. Mol Biol Cell 14: 4387-4396.
HAREL A, ORJALO AV, VINCENT T, LACHISH-ZALAIT A, VASU S, SHAH S, ZIMMERMAN E, ELBAUM M AND FORBES DJ. 2003b. Removal of a single pore subcomplex results in vertebrate nuclei devoid of nuclear pores. Mol Cell 11: 853-864.
HAWRYLUK-GARA LA, PLATANI M, SANTARELLA R, WOZNIAK RW AND MATTAJ IW. 2008. Nup53 is required for nuclear envelope and nuclear pore complex assembly. Mol Biol Cell 19: 1753-1762.
HEALD R AND MCKEON F. 1990. Mutations of phosphorylation sites in lamin A that prevent nuclear lamina disassembly in mitosis. Cell 61: 579-589.
HEALD R, TOURNEBIZE R, BLANK T, SANDALTZOPOULOS R, BECKER P, HYMAN A AND KARSENTI E. 1996. Self-organization of microtubules into bipolar spindles around artificial chromosomes in Xenopus egg extracts. Nature 382: 420-425.
HELD M, SCHMITZ MH, FISCHER B, WALTER T, NEUMANN B, OLMA MH, PETER M, ELLENBERG J AND GERLICH DW. 2010. CellCognition: time-resolved phenotype annotation in high-throughput live cell imaging. Nature methods 7: 747-754.
HETZER M, BILBAO-CORTES D, WALTHER TC, GRUSS OJ AND MATTAJ IW. 2000. GTP hydrolysis by Ran is required for nuclear envelope assembly. Mol Cell 5: 1013-1024.
HINSHAW JE AND MILLIGAN RA. 2003. Nuclear pore complexes exceeding eightfold rotational symmetry. J Struct Biol 141: 259-268.

HIROTA T, LIPP JJ, TOH BH AND PETERS JM. 2005. Histone H3 serine 10 phosphorylation by Aurora B causes HP1 dissociation from heterochromatin. Nature 438: 1176-1180.
HOFMANN A AND HEERMANN DW. 2015. The role of loops on the order of eukaryotes and prokaryotes. FEBS Lett.
HOROWITZ RA, AGARD DA, SEDAT JW AND WOODCOCK CL. 1994. The three-dimensional architecture of chromatin in situ: electron tomography reveals fibers composed of a continuously variable zig-zag nucleosomal ribbon. The Journal of cell biology 125: 1-10.
HSU JY ET AL. 2000. Mitotic phosphorylation of histone H3 is governed by Ipl1/aurora kinase and Glc7/PP1 phosphatase in budding yeast and nematodes. Cell 102: 279-291.
HU Y, KIREEV I, PLUTZ M, ASHOURIAN N AND BELMONT AS. 2009. Large-scale chromatin structure of inducible genes: transcription on a condensed, linear template. The Journal of cell biology 185: 87-100.
HUANG J ET AL. 2007. p53 is regulated by the lysine demethylase LSD1. Nature 449: 105-108.
HUMPHREY GW, WANG Y, RUSSANOVA VR, HIRAI T, QIN J, NAKATANI Y AND HOWARD BH. 2001. Stable histone deacetylase complexes distinguished by the presence of SANT domain proteins CoREST/kiaa0071 and Mta-L1. The Journal of biological chemistry 276: 6817-6824.
INOUE A AND ZHANG Y. 2014. Nucleosome assembly is required for nuclear pore complex assembly in mouse zygotes. Nature structural & molecular biology 21: 609-616.
ITO H, KOYAMA Y, TAKANO M, ISHII K, MAENO M, FURUKAWA K AND HORIGOME T. 2007. Nuclear envelope precursor vesicle targeting to chromatin is stimulated by protein phosphatase 1 in Xenopus egg extracts. Experimental cell research 313: 1897-1910.
JENUWEIN T AND ALLIS CD. 2001. Translating the histone code. Science 293: 1074-1080.
JOHNSON DC AND BAINES JD. 2011. Herpesviruses remodel host membranes for virus egress. Nature reviews Microbiology 9: 382-394.
JOTI Y, HIKIMA T, NISHINO Y, KAMADA F, HIHARA S, TAKATA H, ISHIKAWA T AND MAESHIMA K. 2012. Chromosomes without a 30-nm chromatin fiber. Nucleus 3: 404-410.
KALAB P, WEIS K AND HEALD R. 2002. Visualization of a Ran-GTP gradient in interphase and mitotic Xenopus egg extracts. Science 295: 2452-2456.
KALVERDA B AND FORNEROD M. 2010. Characterization of genome-nucleoporin interactions in Drosophila links chromatin insulators to the nuclear pore complex. Cell cycle (Georgetown, Tex) 9: 4812-4817.
KARG T, WARECKI B AND SULLIVAN W. 2015. Aurora B mediated localized delays in nuclear envelope formation facilitates inclusion of late segregating chromosome fragments. Mol Biol Cell.
KESSEL RG. 1992. Annulate lamellae: a last frontier in cellular organelles. International review of cytology 133: 43-120.
KIMURA K AND HIRANO T. 2000. Dual roles of the 11S regulatory subcomplex in condensin functions. Proc Natl Acad Sci U S A 97: 11972-11977.
KIND J AND VAN STEENSEL B. 2014. Stochastic genome-nuclear lamina interactions: modulating roles of Lamin A and BAF. Nucleus 5: 124-130.
KISELEVA E, MOROZOVA KN, VOELTZ GK, ALLEN TD AND GOLDBERG MW. 2007. Reticulon 4a/NogoA locates to regions of high membrane curvature and may have a role in nuclear envelope growth. J Struct Biol 160: 224-235.

KONTAKI H AND TALIANIDIS I. 2010. Lysine methylation regulates E2F1-induced cell death. Mol Cell 39: 152-160.
KOURMOULI N, THEODOROPOULOS PA, DIALYNAS G, BAKOU A, POLITOU AS, COWELL IG, SINGH PB AND GEORGATOS SD. 2000. Dynamic associations of heterochromatin protein 1 with the nuclear envelope. Embo J 19: 6558-6568.
KRUHLAK MJ, HENDZEL MJ, FISCHLE W, BERTOS NR, HAMEED S, YANG XJ, VERDIN E AND BAZETT-JONES DP. 2001. Regulation of global acetylation in mitosis through loss of histone acetyltransferases and deacetylases from chromatin. The Journal of biological chemistry 276: 38307-38319.
KRULL S, DORRIES J, BOYSEN B, REIDENBACH S, MAGNIUS L, NORDER H, THYBERG J AND CORDES VC. 2010. Protein Tpr is required for establishing nuclear pore-associated zones of heterochromatin exclusion. Embo J 29: 1659-1673.
KRULL S, THYBERG J, BJORKROTH B, RACKWITZ HR AND CORDES VC. 2004. Nucleoporins as components of the nuclear pore complex core structure and Tpr as the architectural element of the nuclear basket. Molecular biology of the cell 15: 4261-4277.
LACHNER M, O'CARROLL D, REA S, MECHTLER K AND JENUWEIN T. 2001. Methylation of histone H3 lysine 9 creates a binding site for HP1 proteins. Nature 410: 116-120.
LAN F, COLLINS RE, DE CEGLI R, ALPATOV R, HORTON JR, SHI X, GOZANI O, CHENG X AND SHI Y. 2007. Recognition of unmethylated histone H3 lysine 4 links BHC80 to LSD1-mediated gene repression. Nature 448: 718-722.
LANDSVERK HB, KIRKHUS M, BOLLEN M, KUNTZIGER T AND COLLAS P. 2005. PNUTS enhances in vitro chromosome decondensation in a PP1-dependent manner. Biochem J 390: 709-717.
LASKEY RA, HONDA BM, MILLS AD, MORRIS NR, WYLLIE AH, MERTZ JE, DE ROBERTS EM AND GURDON JB. 1978. Chromatin assembly and transcription in eggs and oocytes of Xenopus laevis. Cold Spring Harbor symposia on quantitative biology 42 Pt 1: 171-178.
LAURELL E, BECK K, KRUPINA K, THEERTHAGIRI G, BODENMILLER B, HORVATH P, AEBERSOLD R, ANTONIN W AND KUTAY U. 2011. Phosphorylation of Nup98 by multiple kinases is crucial for NPC disassembly during mitotic entry. Cell 144: 539-550.
LEE JH, YOU J, DOBROTA E AND SKALNIK DG. 2010. Identification and characterization of a novel human PP1 phosphatase complex. The Journal of biological chemistry 285: 24466-24476.
LEE MG, WYNDER C, BOCHAR DA, HAKIMI MA, COOCH N AND SHIEKHATTAR R. 2006a. Functional interplay between histone demethylase and deacetylase enzymes. Mol Cell Biol 26: 6395-6402.
LEE MG, WYNDER C, COOCH N AND SHIEKHATTAR R. 2005. An essential role for CoREST in nucleosomal histone 3 lysine 4 demethylation. Nature 437: 432-435.
LEE MG, WYNDER C, SCHMIDT DM, MCCAFFERTY DG AND SHIEKHATTAR R. 2006b. Histone H3 lysine 4 demethylation is a target of nonselective antidepressive medications. Chemistry & biology 13: 563-567.
LENART P, RABUT G, DAIGLE N, HAND AR, TERASAKI M AND ELLENBERG J. 2003. Nuclear envelope breakdown in starfish oocytes proceeds by partial NPC disassembly followed by a rapidly spreading fenestration of nuclear membranes. The Journal of cell biology 160: 1055-1068.

LENS SM, VOEST EE AND MEDEMA RH. 2010. Shared and separate functions of polo-like kinases and aurora kinases in cancer. Nature reviews Cancer 10: 825-841.
LEVY A AND NOLL M. 1981. Chromatin fine structure of active and repressed genes. Nature 289: 198-203.
LI Y, KAO GD, GARCIA BA, SHABANOWITZ J, HUNT DF, QIN J, PHELAN C AND LAZAR MA. 2006. A novel histone deacetylase pathway regulates mitosis by modulating Aurora B kinase activity. Genes & development 20: 2566-2579.
LIM RY, FAHRENKROG B, KOSER J, SCHWARZ-HERION K, DENG J AND AEBI U. 2007. Nanomechanical basis of selective gating by the nuclear pore complex. Science 318: 640-643.
LIPP JJ, HIROTA T, POSER I AND PETERS JM. 2007. Aurora B controls the association of condensin I but not condensin II with mitotic chromosomes. Journal of cell science 120: 1245-1255.
LIU SM AND STEWART M. 2005. Structural basis for the high-affinity binding of nucleoporin Nup1p to the Saccharomyces cerevisiae importin-beta homologue, Kap95p. Journal of molecular biology 349: 515-525.
LOHKA MJ. 1998. Analysis of nuclear envelope assembly using extracts of Xenopus eggs. Methods Cell Biol 53: 367-395.
LOHKA MJ AND MASUI Y. 1983. Formation in vitro of sperm pronuclei and mitotic chromosomes induced by amphibian ooplasmic components. Science 220: 719-721.
LOSADA A, HIRANO M AND HIRANO T. 2002. Cohesin release is required for sister chromatid resolution, but not for condensin-mediated compaction, at the onset of mitosis. Genes & development 16: 3004-3016.
LU L, LADINSKY MS AND KIRCHHAUSEN T. 2009. Cisternal organization of the endoplasmic reticulum during mitosis. Molecular biology of the cell 20: 3471-3480.
LU L, LADINSKY MS AND KIRCHHAUSEN T. 2011. Formation of the postmitotic nuclear envelope from extended ER cisternae precedes nuclear pore assembly. The Journal of cell biology 194: 425-440.
LU X, SHI Y, LU Q, MA Y, LUO J, WANG Q, JI J, JIANG Q AND ZHANG C. 2010. Requirement for lamin B receptor and its regulation by importin {beta} and phosphorylation in nuclear envelope assembly during mitotic exit. The Journal of biological chemistry 285: 33281-33293.
LUGER K, MADER AW, RICHMOND RK, SARGENT DF AND RICHMOND TJ. 1997. Crystal structure of the nucleosome core particle at 2.8 A resolution. Nature 389: 251-260.
LUTZMANN M, KUNZE R, BUERER A, AEBI U AND HURT E. 2002. Modular self-assembly of a Y-shaped multiprotein complex from seven nucleoporins. Embo J 21: 387-397.
LV S, BU W, JIAO H, LIU B, ZHU L, ZHAO H, LIAO J, LI J AND XU X. 2010. LSD1 is required for chromosome segregation during mitosis. Eur J Cell Biol 89: 557-563.
MA Y, CAI S, LV Q, JIANG Q, ZHANG Q, SODMERGEN, ZHAI Z AND ZHANG C. 2007. Lamin B receptor plays a role in stimulating nuclear envelope production and targeting membrane vesicles to chromatin during nuclear envelope assembly through direct interaction with importin beta. Journal of cell science 120: 520-530.
MACAULAY C, MEIER E AND FORBES DJ. 1995. Differential mitotic phosphorylation of proteins of the nuclear pore complex. The Journal of biological chemistry 270: 254-262.
MACCALLUM DE, LOSADA A, KOBAYASHI R AND HIRANO T. 2002. ISWI remodeling complexes in Xenopus egg extracts: identification as major chromosomal components that are regulated by INCENP-aurora B. Mol Biol Cell 13: 25-39.

MAESHIMA K, HIHARA S AND TAKATA H. 2010. New insight into the mitotic chromosome structure: irregular folding of nucleosome fibers without 30-nm chromatin structure. Cold Spring Harbor symposia on quantitative biology 75: 439-444.
MAESHIMA K, IINO H, HIHARA S AND IMAMOTO N. 2011. Nuclear size, nuclear pore number and cell cycle. Nucleus 2: 113-118.
MAGALSKA A, SCHELLHAUS AK, MORENO-ANDRES D, ZANINI F, SCHOOLEY A, SACHDEV R, SCHWARZ H, MADLUNG J AND ANTONIN W. 2014. RuvB-like ATPases function in chromatin decondensation at the end of mitosis. Dev Cell 31: 305-318.
MALUMBRES M. 2011. Physiological relevance of cell cycle kinases. Physiological reviews 91: 973-1007.
MANSFELD J ET AL. 2006. The conserved transmembrane nucleoporin NDC1 is required for nuclear pore complex assembly in vertebrate cells. Mol Cell 22: 93-103.
MARELLI M, LUSK CP, CHAN H, AITCHISON JD AND WOZNIAK RW. 2001. A link between the synthesis of nucleoporins and the biogenesis of the nuclear envelope. The Journal of cell biology 153: 709-724.
MARESCA TJ AND HEALD R. 2006. Methods for studying spindle assembly and chromosome condensation in Xenopus egg extracts. Methods in molecular biology 322: 459-474.
MARGALIT A, NEUFELD E, FEINSTEIN N, WILSON KL, PODBILEWICZ B AND GRUENBAUM Y. 2007. Barrier to autointegration factor blocks premature cell fusion and maintains adult muscle integrity in C. elegans. The Journal of cell biology 178: 661-673.
MARGALIT A, SEGURA-TOTTEN M, GRUENBAUM Y AND WILSON KL. 2005. Barrier-to-autointegration factor is required to segregate and enclose chromosomes within the nuclear envelope and assemble the nuclear lamina. Proc Natl Acad Sci U S A 102: 3290-3295.
MARKAKI Y, CHRISTOGIANNI A, POLITOU AS AND GEORGATOS SD. 2009. Phosphorylation of histone H3 at Thr3 is part of a combinatorial pattern that marks and configures mitotic chromatin. Journal of cell science 122: 2809-2819.
MATSUOKA Y, TAKAGI M, BAN T, MIYAZAKI M, YAMAMOTO T, KONDO Y AND YONEDA Y. 1999. Identification and characterization of nuclear pore subcomplexes in mitotic extract of human somatic cells. Biochemical and biophysical research communications 254: 417-423.
MATTAJ IW. 2004. Sorting out the nuclear envelope from the endoplasmic reticulum. Nat Rev Mol Cell Biol 5: 65-69.
MATTAJ IW AND ENGLMEIER L. 1998. Nucleocytoplasmic transport: the soluble phase. Annu Rev Biochem 67: 265-306.
MAUL HM, HSU BY, BORUN TM AND MAUL GG. 1973. Effect of metabolic inhibitors on nuclear pore formation during the HeLa S3 cell cycle. The Journal of cell biology 59: 669-676.
MELCAK I, HOELZ A AND BLOBEL G. 2007. Structure of Nup58/45 suggests flexible nuclear pore diameter by intermolecular sliding. Science 315: 1729-1732.
METZGER E, WISSMANN M, YIN N, MULLER JM, SCHNEIDER R, PETERS AH, GUNTHER T, BUETTNER R AND SCHULE R. 2005. LSD1 demethylates repressive histone marks to promote androgen-receptor-dependent transcription. Nature 437: 436-439.
MEYER H, DROZDOWSKA A AND DOBRYNIN G. 2010. A role for Cdc48/p97 and Aurora B in controlling chromatin condensation during exit from mitosis. Biochemistry and cell biology = Biochimie et biologie cellulaire 88: 23-28.

MIMASU S, UMEZAWA N, SATO S, HIGUCHI T, UMEHARA T AND YOKOYAMA S. 2010. Structurally designed trans-2-phenylcyclopropylamine derivatives potently inhibit histone demethylase LSD1/KDM1. Biochemistry 49: 6494-6503.
MISTELI T. 2007. Beyond the sequence: cellular organization of genome function. Cell 128: 787-800.
MITCHELL JM, MANSFELD J, CAPITANIO J, KUTAY U AND WOZNIAK RW. 2010. Pom121 links two essential subcomplexes of the nuclear pore complex core to the membrane. The Journal of cell biology 191: 505-521.
MOAZED D. 2011. Mechanisms for the inheritance of chromatin states. Cell 146: 510-518.
MOHR D, FREY S, FISCHER T, GUTTLER T AND GORLICH D. 2009. Characterisation of the passive permeability barrier of nuclear pore complexes. Embo J 28: 2541-2553.
MONTES DE OCA R, ANDREASSEN PR AND WILSON KL. 2011. Barrier-to-Autointegration Factor influences specific histone modifications. Nucleus 2: 580-590.
MORA-BERMUDEZ F, GERLICH D AND ELLENBERG J. 2007. Maximal chromosome compaction occurs by axial shortening in anaphase and depends on Aurora kinase. Nat Cell Biol 9: 822-831.
MUHLHAUSSER P AND KUTAY U. 2007. An in vitro nuclear disassembly system reveals a role for the RanGTPase system and microtubule-dependent steps in nuclear envelope breakdown. The Journal of cell biology 178: 595-610.
MULLER WG, WALKER D, HAGER GL AND MCNALLY JG. 2001. Large-scale chromatin decondensation and recondensation regulated by transcription from a natural promoter. The Journal of cell biology 154: 33-48.
NAIR VD, GE Y, BALASUBRAMANIYAN N, KIM J, OKAWA Y, CHIKINA M, TROYANSKAYA O AND SEALFON SC. 2012. Involvement of histone demethylase LSD1 in short-time-scale gene expression changes during cell cycle progression in embryonic stem cells. Molecular and cellular biology 32: 4861-4876.
NAKAZAWA N, MEHROTRA R, EBE M AND YANAGIDA M. 2011. Condensin phosphorylated by the Aurora-B-like kinase Ark1 is continuously required until telophase in a mode distinct from Top2. Journal of cell science 124: 1795-1807.
NEUMANN B ET AL. 2010. Phenotypic profiling of the human genome by time-lapse microscopy reveals cell division genes. Nature 464: 721-727.
NEWMEYER DD, FINLAY DR AND FORBES DJ. 1986. In vitro transport of a fluorescent nuclear protein and exclusion of non-nuclear proteins. The Journal of cell biology 103: 2091-2102.
NEWPORT J AND DUNPHY W. 1992. Characterization of the membrane binding and fusion events during nuclear envelope assembly using purified components. The Journal of cell biology 116: 295-306.
NEWPORT J AND KIRSCHNER M. 1982. A major developmental transition in early Xenopus embryos: II. Control of the onset of transcription. Cell 30: 687-696.
NEWPORT JW, WILSON KL AND DUNPHY WG. 1990. A lamin-independent pathway for nuclear envelope assembly. The Journal of cell biology 111: 2247-2259.
NICHOLS RJ, WIEBE MS AND TRAKTMAN P. 2006. The vaccinia-related kinases phosphorylate the N' terminus of BAF, regulating its interaction with DNA and its retention in the nucleus. Molecular biology of the cell 17: 2451-2464.
NICHOLSON TB AND CHEN T. 2009. LSD1 demethylates histone and non-histone proteins. Epigenetics : official journal of the DNA Methylation Society 4: 129-132.

NIKOLAKAKI E, MEIER J, SIMOS G, GEORGATOS SD AND GIANNAKOUROS T. 1997. Mitotic phosphorylation of the lamin B receptor by a serine/arginine kinase and p34(cdc2). The Journal of biological chemistry 272: 6208-6213.
NISHINO Y ET AL. 2012. Human mitotic chromosomes consist predominantly of irregularly folded nucleosome fibres without a 30-nm chromatin structure. Embo J 31: 1644-1653.
OGAWA Y, MIYAMOTO Y, OKA M AND YONEDA Y. 2012. The interaction between importin-alpha and Nup153 promotes importin-alpha/beta-mediated nuclear import. Traffic (Copenhagen, Denmark) 13: 934-946.
OHBA T, SCHIRMER EC, NISHIMOTO T AND GERACE L. 2004. Energy- and temperature-dependent transport of integral proteins to the inner nuclear membrane via the nuclear pore. The Journal of cell biology 167: 1051-1062.
OHSUGI M, ADACHI K, HORAI R, KAKUTA S, SUDO K, KOTAKI H, TOKAI-NISHIZUMI N, SAGARA H, IWAKURA Y AND YAMAMOTO T. 2008. Kid-mediated chromosome compaction ensures proper nuclear envelope formation. Cell 132: 771-782.
OLINS AL AND OLINS DE. 1974. Spheroid chromatin units (v bodies). Science 183: 330-332.
OLINS AL, RHODES G, WELCH DB, ZWERGER M AND OLINS DE. 2010. Lamin B receptor: multi-tasking at the nuclear envelope. Nucleus 1: 53-70.
OLSEN JV ET AL. 2010. Quantitative phosphoproteomics reveals widespread full phosphorylation site occupancy during mitosis. Science signaling 3: ra3.
OLSSON M, SCHEELE S AND EKBLOM P. 2004. Limited expression of nuclear pore membrane glycoprotein 210 in cell lines and tissues suggests cell-type specific nuclear pores in metazoans. Exp Cell Res 292: 359-370.
ONISCHENKO E, STANTON LH, MADRID AS, KIESELBACH T AND WEIS K. 2009. Role of the Ndc1 interaction network in yeast nuclear pore complex assembly and maintenance. The Journal of cell biology 185: 475-491.
ONISCHENKO EA, CRAFOORD E AND HALLBERG E. 2007. Phosphomimetic mutation of the mitotically phosphorylated serine 1880 compromises the interaction of the transmembrane nucleoporin gp210 with the nuclear pore complex. Exp Cell Res 313: 2744-2751.
ONISCHENKO EA, GUBANOVA NV, KISELEVA EV AND HALLBERG E. 2005. Cdk1 and okadaic acid-sensitive phosphatases control assembly of nuclear pore complexes in Drosophila embryos. Molecular biology of the cell 16: 5152-5162.
ONO T, FANG Y, SPECTOR DL AND HIRANO T. 2004. Spatial and temporal regulation of Condensins I and II in mitotic chromosome assembly in human cells. Mol Biol Cell 15: 3296-3308.
ORI A ET AL. 2013. Cell type-specific nuclear pores: a case in point for context-dependent stoichiometry of molecular machines. Molecular systems biology 9: 648.
OSORIO DS AND GOMES ER. 2013. The contemporary nucleus: a trip down memory lane. Biology of the cell / under the auspices of the European Cell Biology Organization 105: 430-441.
PAGLIUCA FW, COLLINS MO, LICHAWSKA A, ZEGERMAN P, CHOUDHARY JS AND PINES J. 2011. Quantitative proteomics reveals the basis for the biochemical specificity of the cell-cycle machinery. Mol Cell 43: 406-417.
PARK JA, KIM AJ, KANG Y, JUNG YJ, KIM HK AND KIM KC. 2011. Deacetylation and methylation at histone H3 lysine 9 (H3K9) coordinate chromosome condensation during cell cycle progression. Molecules and cells 31: 343-349.

PELEG O AND LIM RY. 2010. Converging on the function of intrinsically disordered nucleoporins in the nuclear pore complex. Biological chemistry 391: 719-730.
PEMBERTON LF AND PASCHAL BM. 2005. Mechanisms of receptor-mediated nuclear import and nuclear export. Traffic (Copenhagen, Denmark) 6: 187-198.
PETER M, NAKAGAWA J, DOREE M, LABBE JC AND NIGG EA. 1990. In vitro disassembly of the nuclear lamina and M phase-specific phosphorylation of lamins by cdc2 kinase. Cell 61: 591-602.
PETERS R. 2005. Translocation through the nuclear pore complex: selectivity and speed by reduction-of-dimensionality. Traffic (Copenhagen, Denmark) 6: 421-427.
PFALLER R, SMYTHE C AND NEWPORT JW. 1991. Assembly/disassembly of the nuclear envelope membrane: cell cycle-dependent binding of nuclear membrane vesicles to chromatin in vitro. Cell 65: 209-217.
PHILPOTT A AND LENO GH. 1992. Nucleoplasmin remodels sperm chromatin in Xenopus egg extracts. Cell 69: 759-767.
PHILPOTT A, LENO GH AND LASKEY RA. 1991. Sperm decondensation in Xenopus egg cytoplasm is mediated by nucleoplasmin. Cell 65: 569-578.
PILOTTO S, SPERANZINI V, TORTORICI M, DURAND D, FISH A, VALENTE S AND FORNERIS F. 2015. Interplay among nucleosomal DNA, histone tails, and corepressor CoREST underlies LSD1-mediated H3 demethylation. 112: 2752-2757.
POLESHKO A, MANSFIELD KM, BURLINGAME CC, ANDRAKE MD, SHAH NR AND KATZ RA. 2013. The human protein PRR14 tethers heterochromatin to the nuclear lamina during interphase and mitotic exit. Cell reports 5: 292-301.
POLIOUDAKI H, KOURMOULI N, DROSOU V, BAKOU A, THEODOROPOULOS PA, SINGH PB, GIANNAKOUROS T AND GEORGATOS SD. 2001. Histones H3/H4 form a tight complex with the inner nuclear membrane protein LBR and heterochromatin protein 1. EMBO Rep 2: 920-925.
PRIGENT C AND DIMITROV S. 2003. Phosphorylation of serine 10 in histone H3, what for? Journal of cell science 116: 3677-3685.
PUHKA M, JOENSUU M, VIHINEN H, BELEVICH I AND JOKITALO E. 2012. Progressive sheet-to-tubule transformation is a general mechanism for endoplasmic reticulum partitioning in dividing mammalian cells. Molecular biology of the cell 23: 2424-2432.
PUHKA M, VIHINEN H, JOENSUU M AND JOKITALO E. 2007. Endoplasmic reticulum remains continuous and undergoes sheet-to-tubule transformation during cell division in mammalian cells. The Journal of cell biology 179: 895-909.
PYRPASOPOULOU A, MEIER J, MAISON C, SIMOS G AND GEORGATOS SD. 1996. The lamin B receptor (LBR) provides essential chromatin docking sites at the nuclear envelope. Embo J 15: 7108-7119.
RAMADAN K, BRUDERER R, SPIGA FM, POPP O, BAUR T, GOTTA M AND MEYER HH. 2007. Cdc48/p97 promotes reformation of the nucleus by extracting the kinase Aurora B from chromatin. Nature 450: 1258-1262.
RASALA BA, ORJALO AV, SHEN Z, BRIGGS S AND FORBES DJ. 2006. ELYS is a dual nucleoporin/kinetochore protein required for nuclear pore assembly and proper cell division. Proc Natl Acad Sci U S A 103: 17801-17806.
RASALA BA, RAMOS C, HAREL A AND FORBES DJ. 2008. Capture of AT-rich chromatin by ELYS recruits POM121 and NDC1 to initiate nuclear pore assembly. Mol Biol Cell 19: 3982-3996.

RATTNER JB AND LIN CC. 1985. Radial loops and helical coils coexist in metaphase chromosomes. Cell 42: 291-296.
REICHELT R, HOLZENBURG A, BUHLE EL, JR., JARNIK M, ENGEL A AND AEBI U. 1990. Correlation between structure and mass distribution of the nuclear pore complex and of distinct pore complex components. The Journal of cell biology 110: 883-894.
RIBBECK K AND GORLICH D. 2001. Kinetic analysis of translocation through nuclear pore complexes. Embo J 20: 1320-1330.
RIBBECK K AND GORLICH D. 2002. The permeability barrier of nuclear pore complexes appears to operate via hydrophobic exclusion. Embo J 21: 2664-2671.
RICCI MA, MANZO C, GARCIA-PARAJO MF, LAKADAMYALI M AND COSMA MP. 2015. Chromatin fibers are formed by heterogeneous groups of nucleosomes in vivo. Cell 160: 1145-1158.
ROLOFF S, SPILLNER C AND KEHLENBACH RH. 2013. Several phenylalanine-glycine motives in the nucleoporin Nup214 are essential for binding of the nuclear export receptor CRM1. The Journal of biological chemistry 288: 3952-3963.
ROTEM A, GRUBER R, SHORER H, SHAULOV L, KLEIN E AND HAREL A. 2009. Importin beta regulates the seeding of chromatin with initiation sites for nuclear pore assembly. Mol Biol Cell 20: 4031-4042.
ROUT MP, AITCHISON JD, SUPRAPTO A, HJERTAAS K, ZHAO Y AND CHAIT BT. 2000. The yeast nuclear pore complex: composition, architecture, and transport mechanism. The Journal of cell biology 148: 635-651.
RUDOLPH T ET AL. 2007. Heterochromatin formation in Drosophila is initiated through active removal of H3K4 methylation by the LSD1 homolog SU(VAR)3-3. Mol Cell 26: 103-115.
SACHDEV R, SIEVERDING C, FLOTENMEYER M AND ANTONIN W. 2012. The C-terminal domain of Nup93 is essential for assembly of the structural backbone of nuclear pore complexes. Mol Biol Cell 23: 740-749.
SALINA D, BODOOR K, ECKLEY DM, SCHROER TA, RATTNER JB AND BURKE B. 2002. Cytoplasmic dynein as a facilitator of nuclear envelope breakdown. Cell 108: 97-107.
SANTAMARIA D, BARRIERE C, CERQUEIRA A, HUNT S, TARDY C, NEWTON K, CACERES JF, DUBUS P, MALUMBRES M AND BARBACID M. 2007. Cdk1 is sufficient to drive the mammalian cell cycle. Nature 448: 811-815.
SCHELLHAUS AK, MAGALSKA A, SCHOOLEY A AND ANTONIN W. in press. A cell free assay to study chromatin decondensation at the end of mitosis. Journal of Visualized Experiments.
SCHIRMER EC AND GERACE L. 2005. The nuclear membrane proteome: extending the envelope. Trends in biochemical sciences 30: 551-558.
SCHLAICH NL, HANER M, LUSTIG A, AEBI U AND HURT EC. 1997. In vitro reconstitution of a heterotrimeric nucleoporin complex consisting of recombinant Nsp1p, Nup49p, and Nup57p. Mol Biol Cell 8: 33-46.
SCHMIDT DM AND MCCAFFERTY DG. 2007. trans-2-Phenylcyclopropylamine is a mechanism-based inactivator of the histone demethylase LSD1. Biochemistry 46: 4408-4416.
SCHMITZ MH AND GERLICH DW. 2009. Automated live microscopy to study mitotic gene function in fluorescent reporter cell lines. Methods in molecular biology (Clifton, NJ) 545: 113-134.

SCHMITZ MH ET AL. 2010. Live-cell imaging RNAi screen identifies PP2A-B55alpha and importin-beta1 as key mitotic exit regulators in human cells. Nature cell biology 12: 886-893.
SCHOOLEY A, MORENO-ANDRES D, DE MAGISTRIS P, VOLLMER B AND ANTONIN W. 2015. The lysine demethylase LSD1 is required for nuclear envelope formation at the end of mitosis. Journal of cell science 128: 3466-3477.
SCHOOLEY A, VOLLMER B AND ANTONIN W. 2012. Building a nuclear envelope at the end of mitosis: coordinating membrane reorganization, nuclear pore complex assembly, and chromatin de-condensation. Chromosoma 121: 539-554.
SCHWARTZ T. 2013. Functional insights from studies on the structure of the nuclear pore and coat protein complexes. Cold Spring Harbor perspectives in biology 5.
SCOUMANNE A AND CHEN X. 2007. The lysine-specific demethylase 1 is required for cell proliferation in both p53-dependent and -independent manners. The Journal of biological chemistry 282: 15471-15475.
SEGURA-TOTTEN M, KOWALSKI AK, CRAIGIE R AND WILSON KL. 2002. Barrier-to-autointegration factor: major roles in chromatin decondensation and nuclear assembly. The Journal of cell biology 158: 475-485.
SHAHBAZIAN MD AND GRUNSTEIN M. 2007. Functions of site-specific histone acetylation and deacetylation. Annu Rev Biochem 76: 75-100.
SHAULOV L, GRUBER R, COHEN I AND HAREL A. 2011. A dominant-negative form of POM121 binds chromatin and disrupts the two separate modes of nuclear pore assembly. Journal of cell science 124: 3822-3834.
SHEEHAN MA, MILLS AD, SLEEMAN AM, LASKEY RA AND BLOW JJ. 1988. Steps in the assembly of replication-competent nuclei in a cell-free system from Xenopus eggs. The Journal of cell biology 106: 1-12.
SHI Y, LAN F, MATSON C, MULLIGAN P, WHETSTINE JR, COLE PA AND CASERO RA. 2004. Histone demethylation mediated by the nuclear amine oxidase homolog LSD1. Cell 119: 941-953.
SHI Y, SAWADA J, SUI G, AFFAR EL B, WHETSTINE JR, LAN F, OGAWA H, LUKE MP, NAKATANI Y AND SHI Y. 2003. Coordinated histone modifications mediated by a CtBP co-repressor complex. Nature 422: 735-738.
SHI YJ, MATSON C, LAN F, IWASE S, BABA T AND SHI Y. 2005. Regulation of LSD1 histone demethylase activity by its associated factors. Molecular cell 19: 857-864.
SHIH JC, CHEN K AND RIDD MJ. 1999. Monoamine oxidase: from genes to behavior. Annual review of neuroscience 22: 197-217.
SHIMI T, BUTIN-ISRAELI V, ADAM SA AND GOLDMAN RD. 2010. Nuclear lamins in cell regulation and disease. Cold Spring Harbor symposia on quantitative biology 75: 525-531.
SIMONS K AND TOOMRE D. 2000. Lipid rafts and signal transduction. Nat Rev Mol Cell Biol 1: 31-39.
SMOYER CJ AND JASPERSEN SL. 2014. Breaking down the wall: the nuclear envelope during mitosis. Curr Opin Cell Biol 26: 1-9.
SOMECH R, SHAKLAI S, GELLER O, AMARIGLIO N, SIMON AJ, RECHAVI G AND GAL-YAM EN. 2005. The nuclear-envelope protein and transcriptional repressor LAP2beta interacts with HDAC3 at the nuclear periphery, and induces histone H4 deacetylation. Journal of cell science 118: 4017-4025.

SONG F, CHEN P, SUN D, WANG M, DONG L, LIANG D, XU RM, ZHU P AND LI G. 2014. Cryo-EM study of the chromatin fiber reveals a double helix twisted by tetranucleosomal units. Science 344: 376-380.
SOSA BA, ROTHBALLER A, KUTAY U AND SCHWARTZ TU. 2012. LINC complexes form by binding of three KASH peptides to domain interfaces of trimeric SUN proteins. Cell 149: 1035-1047.
SPEESE SD ET AL. 2012. Nuclear envelope budding enables large ribonucleoprotein particle export during synaptic Wnt signaling. Cell 149: 832-846.
STARR DA AND FRIDOLFSSON HN. 2010. Interactions between nuclei and the cytoskeleton are mediated by SUN-KASH nuclear-envelope bridges. Annu Rev Cell Dev Biol 26: 421-444.
STAVROPOULOS P, BLOBEL G AND HOELZ A. 2006. Crystal structure and mechanism of human lysine-specific demethylase-1. Nature structural & molecular biology 13: 626-632.
STAVRU F, NAUTRUP-PEDERSEN G, CORDES VC AND GORLICH D. 2006. Nuclear pore complex assembly and maintenance in POM121- and gp210-deficient cells. The Journal of cell biology 173: 477-483.
STEINHARDT RA, EPEL D, CARROLL EJ, JR. AND YANAGIMACHI R. 1974. Is calcium ionophore a universal activator for unfertilised eggs? Nature 252: 41-43.
STRASSER K AND HURT E. 2000. Yra1p, a conserved nuclear RNA-binding protein, interacts directly with Mex67p and is required for mRNA export. Embo J 19: 410-420.
STRAWN LA, SHEN T, SHULGA N, GOLDFARB DS AND WENTE SR. 2004. Minimal nuclear pore complexes define FG repeat domains essential for transport. Nature cell biology 6: 197-206.
STRAWN LA, SHEN T AND WENTE SR. 2001. The GLFG regions of Nup116p and Nup100p serve as binding sites for both Kap95p and Mex67p at the nuclear pore complex. The Journal of biological chemistry 276: 6445-6452.
SUN G, ALZAYADY K, STEWART R, YE P, YANG S, LI W AND SHI Y. 2010. Histone demethylase LSD1 regulates neural stem cell proliferation. Molecular and cellular biology 30: 1997-2005.
SZYMBORSKA A, DE MARCO A, DAIGLE N, CORDES VC, BRIGGS JA AND ELLENBERG J. 2013. Nuclear pore scaffold structure analyzed by super-resolution microscopy and particle averaging. Science 341: 655-658.
TADA K, SUSUMU H, SAKUNO T AND WATANABE Y. 2011. Condensin association with histone H2A shapes mitotic chromosomes. Nature 474: 477-483.
TAKAGI M, NISHIYAMA Y, TAGUCHI A AND IMAMOTO N. 2014. Ki67 antigen contributes to the timely accumulation of protein phosphatase 1gamma on anaphase chromosomes. The Journal of biological chemistry 289: 22877-22887.
TAKANO M, KOYAMA Y, ITO H, HOSHINO S, ONOGI H, HAGIWARA M, FURUKAWA K AND HORIGOME T. 2004. Regulation of binding of lamin B receptor to chromatin by SR protein kinase and cdc2 kinase in Xenopus egg extracts. The Journal of biological chemistry 279: 13265-13271.
TAKEMOTO A, MURAYAMA A, KATANO M, URANO T, FURUKAWA K, YOKOYAMA S, YANAGISAWA J, HANAOKA F AND KIMURA K. 2007. Analysis of the role of Aurora B on the chromosomal targeting of condensin I. Nucleic acids research 35: 2403-2412.
TALAMAS JA AND CAPELSON M. 2015. Nuclear envelope and genome interactions in cell fate. Frontiers in genetics 6: 95.

TERRENOIRE E, MCRONALD F, HALSALL JA, PAGE P, ILLINGWORTH RS, TAYLOR AM, DAVISON V, O'NEILL LP AND TURNER BM. 2010. Immunostaining of modified histones defines high-level features of the human metaphase epigenome. Genome biology 11: R110.
TERRY LJ, SHOWS EB AND WENTE SR. 2007. Crossing the nuclear envelope: hierarchical regulation of nucleocytoplasmic transport. Science 318: 1412-1416.
TESSARZ P AND KOUZARIDES T. 2014. Histone core modifications regulating nucleosome structure and dynamics. Nat Rev Mol Cell Biol 15: 703-708.
THEERTHAGIRI G, EISENHARDT N, SCHWARZ H AND ANTONIN W. 2010. The nucleoporin Nup188 controls passage of membrane proteins across the nuclear pore complex. The Journal of cell biology 189: 1129-1142.
TOCHIO N ET AL. 2006. Solution structure of the SWIRM domain of human histone demethylase LSD1. Structure 14: 457-468.
TRINKLE-MULCAHY L, ANDERSEN J, LAM YW, MOORHEAD G, MANN M AND LAMOND AI. 2006. Repo-Man recruits PP1 gamma to chromatin and is essential for cell viability. The Journal of cell biology 172: 679-692.
TSENG LC AND CHEN RH. 2011. Temporal control of nuclear envelope assembly by phosphorylation of lamin B receptor. Molecular biology of the cell 22: 3306-3317.
TURGAY Y, UNGRICHT R, ROTHBALLER A, KISS A, CSUCS G, HORVATH P AND KUTAY U. 2010. A classical NLS and the SUN domain contribute to the targeting of SUN2 to the inner nuclear membrane. Embo J 29: 2262-2275.
ULBERT S, PLATANI M, BOUE S AND MATTAJ IW. 2006. Direct membrane protein-DNA interactions required early in nuclear envelope assembly. The Journal of cell biology 173: 469-476.
VAGNARELLI P. 2012. Mitotic chromosome condensation in vertebrates. Exp Cell Res 318: 1435-1441.
VAGNARELLI P, HUDSON DF, RIBEIRO SA, TRINKLE-MULCAHY L, SPENCE JM, LAI F, FARR CJ, LAMOND AI AND EARNSHAW WC. 2006. Condensin and Repo-Man-PP1 co-operate in the regulation of chromosome architecture during mitosis. Nat Cell Biol 8: 1133-1142.
VAGNARELLI P, RIBEIRO S, SENNELS L, SANCHEZ-PULIDO L, DE LIMA ALVES F, VERHEYEN T, KELLY DA, PONTING CP, RAPPSILBER J AND EARNSHAW WC. 2011. Repo-Man coordinates chromosomal reorganization with nuclear envelope reassembly during mitotic exit. Dev Cell 21: 328-342.
VIGERS GP AND LOHKA MJ. 1991. A distinct vesicle population targets membranes and pore complexes to the nuclear envelope in Xenopus eggs. The Journal of cell biology 112: 545-556.
VIGERS GP AND LOHKA MJ. 1992. Regulation of nuclear envelope precursor functions during cell division. Journal of cell science 102 (Pt 2): 273-284.
VOELTZ GK, ROLLS MM AND RAPOPORT TA. 2002. Structural organization of the endoplasmic reticulum. EMBO Rep 3: 944-950.
VOLLMAR F, HACKER C, ZAHEDI RP, SICKMANN A, EWALD A, SCHEER U AND DABAUVALLE MC. 2009. Assembly of nuclear pore complexes mediated by major vault protein. Journal of cell science 122: 780-786.
VOLLMER B, LORENZ M, MORENO-ANDRES D, BODENHOEFER M, DEMAGISTIS P, SCHOOLEY A, ASTRINIDIS S, FLOETENMEYER M, LEPTIHN S AND ANTONIN W. in press. Nup153 recruits the Nup107-160 complex to the inner nuclear membrane for interphasic nuclear pore complex assembly. Dev Cell.

VOLLMER B, SCHOOLEY A, SACHDEV R, EISENHARDT N, SCHNEIDER AM, SIEVERDING C, MADLUNG J, GERKEN U, MACEK B AND ANTONIN W. 2012. Dimerization and direct membrane interaction of Nup53 contribute to nuclear pore complex assembly. Embo J 31: 4072-4084.
WAGNER N AND KROHNE G. 2007. LEM-Domain proteins: new insights into lamin-interacting proteins. International review of cytology 261: 1-46.
WALDE S AND KEHLENBACH RH. 2010. The Part and the Whole: functions of nucleoporins in nucleocytoplasmic transport. Trends in cell biology 20: 461-469.
WALDE S, THAKAR K, HUTTEN S, SPILLNER C, NATH A, ROTHBAUER U, WIEMANN S AND KEHLENBACH RH. 2012. The nucleoporin Nup358/RanBP2 promotes nuclear import in a cargo- and transport receptor-specific manner. Traffic (Copenhagen, Denmark) 13: 218-233.
WALDMANN I, SPILLNER C AND KEHLENBACH RH. 2012. The nucleoporin-like protein NLP1 (hCG1) promotes CRM1-dependent nuclear protein export. Journal of cell science 125: 144-154.
WALTHER TC ET AL. 2003a. The conserved Nup107-160 complex is critical for nuclear pore complex assembly. Cell 113: 195-206.
WALTHER TC, ASKJAER P, GENTZEL M, HABERMANN A, GRIFFITHS G, WILM M, MATTAJ IW AND HETZER M. 2003b. RanGTP mediates nuclear pore complex assembly. Nature 424: 689-694.
WALTHER TC, FORNEROD M, PICKERSGILL H, GOLDBERG M, ALLEN TD AND MATTAJ IW. 2001. The nucleoporin Nup153 is required for nuclear pore basket formation, nuclear pore complex anchoring and import of a subset of nuclear proteins. Embo J 20: 5703-5714.
WANG F AND HIGGINS JM. 2013. Histone modifications and mitosis: countermarks, landmarks, and bookmarks. Trends in cell biology 23: 175-184.
WANG J ET AL. 2009a. The lysine demethylase LSD1 (KDM1) is required for maintenance of global DNA methylation. Nature genetics 41: 125-129.
WANG J ET AL. 2011. Novel histone demethylase LSD1 inhibitors selectively target cancer cells with pluripotent stem cell properties. Cancer research 71: 7238-7249.
WANG J ET AL. 2007. Opposing LSD1 complexes function in developmental gene activation and repression programmes. Nature 446: 882-887.
WANG S, ROMANO FB, FIELD CM, MITCHISON TJ AND RAPOPORT TA. 2013. Multiple mechanisms determine ER network morphology during the cell cycle in Xenopus egg extracts. J Cell Biol 203: 801-814.
WANG Y ET AL. 2009b. LSD1 is a subunit of the NuRD complex and targets the metastasis programs in breast cancer. Cell 138: 660-672.
WHYTE WA, BILODEAU S, ORLANDO DA, HOKE HA, FRAMPTON GM, FOSTER CT, COWLEY SM AND YOUNG RA. 2012. Enhancer decommissioning by LSD1 during embryonic stem cell differentiation. Nature 482: 221-225.
WIDOM J AND KLUG A. 1985. Structure of the 300A chromatin filament: X-ray diffraction from oriented samples. Cell 43: 207-213.
WILKINS BJ, RALL NA, OSTWAL Y, KRUITWAGEN T, HIRAGAMI-HAMADA K, WINKLER M, BARRAL Y, FISCHLE W AND NEUMANN H. 2014. A cascade of histone modifications induces chromatin condensation in mitosis. Science 343: 77-80.
WILLIAMS SP AND LANGMORE JP. 1991. Small angle x-ray scattering of chromatin. Radius and mass per unit length depend on linker length. Biophysical journal 59: 606-618.

WILSON KL AND DAWSON SC. 2011. Evolution: functional evolution of nuclear structure. The Journal of cell biology 195: 171-181.
WILSON KL AND NEWPORT J. 1988. A trypsin-sensitive receptor on membrane vesicles is required for nuclear envelope formation in vitro. The Journal of cell biology 107: 57-68.
WOODCOCK CL, FRADO LL AND RATTNER JB. 1984. The higher-order structure of chromatin: evidence for a helical ribbon arrangement. The Journal of cell biology 99: 42-52.
WOODCOCK CL, SAFER JP AND STANCHFIELD JE. 1976a. Structural repeating units in chromatin. I. Evidence for their general occurrence. Exp Cell Res 97: 101-110.
WOODCOCK CL, SWEETMAN HE AND FRADO LL. 1976b. Structural repeating units in chromatin. II. Their isolation and partial characterization. Exp Cell Res 97: 111-119.
WRIGHT SJ. 1999. Sperm nuclear activation during fertilization. Current topics in developmental biology 46: 133-178.
WU JQ, GUO JY, TANG W, YANG CS, FREEL CD, CHEN C, NAIRN AC AND KORNBLUTH S. 2009. PP1-mediated dephosphorylation of phosphoproteins at mitotic exit is controlled by inhibitor-1 and PP1 phosphorylation. Nat Cell Biol 11: 644-651.
WU W, LIN F AND WORMAN HJ. 2002. Intracellular trafficking of MAN1, an integral protein of the nuclear envelope inner membrane. Journal of cell science 115: 1361-1371.
WURZENBERGER C AND GERLICH DW. 2011. Phosphatases: providing safe passage through mitotic exit. Nat Rev Mol Cell Biol 12: 469-482.
YANG M, CULHANE JC, SZEWCZUK LM, JALILI P, BALL HL, MACHIUS M, COLE PA AND YU H. 2007. Structural basis for the inhibition of the LSD1 histone demethylase by the antidepressant trans-2-phenylcyclopropylamine. Biochemistry 46: 8058-8065.
YANG M, GOCKE CB, LUO X, BOREK D, TOMCHICK DR, MACHIUS M, OTWINOWSKI Z AND YU H. 2006. Structural basis for CoREST-dependent demethylation of nucleosomes by the human LSD1 histone demethylase. Mol Cell 23: 377-387.
YANG P, WANG Y, CHEN J, LI H, KANG L, ZHANG Y, CHEN S, ZHU B AND GAO S. 2011. RCOR2 is a subunit of the LSD1 complex that regulates ESC property and substitutes for SOX2 in reprogramming somatic cells to pluripotency. Stem Cells 29: 791-801.
YAVUZ S, SANTARELLA-MELLWIG R, KOCH B, JAEDICKE A, MATTAJ IW AND ANTONIN W. 2010. NLS-mediated NPC functions of the nucleoporin Pom121. FEBS Lett 584: 3292-3298.
YE Q, CALLEBAUT I, PEZHMAN A, COURVALIN JC AND WORMAN HJ. 1997. Domain-specific interactions of human HP1-type chromodomain proteins and inner nuclear membrane protein LBR. The Journal of biological chemistry 272: 14983-14989.
YE Q AND WORMAN HJ. 1994. Primary structure analysis and lamin B and DNA binding of human LBR, an integral protein of the nuclear envelope inner membrane. The Journal of biological chemistry 269: 11306-11311.
YIN F ET AL. 2014. LSD1 regulates pluripotency of embryonic stem/carcinoma cells through histone deacetylase 1-mediated deacetylation of histone H4 at lysine 16. Mol Cell Biol 34: 158-179.
YOSHIDA M, KIJIMA M, AKITA M AND BEPPU T. 1990. Potent and specific inhibition of mammalian histone deacetylase both in vivo and in vitro by trichostatin A. The Journal of biological chemistry 265: 17174-17179.
YOU A, TONG JK, GROZINGER CM AND SCHREIBER SL. 2001. CoREST is an integral component of the CoREST- human histone deacetylase complex. Proc Natl Acad Sci U S A 98: 1454-1458.

ZAIDI SK, YOUNG DW, MONTECINO MA, LIAN JB, VAN WIJNEN AJ, STEIN JL AND STEIN GS. 2010. Mitotic bookmarking of genes: a novel dimension to epigenetic control. Nature reviews Genetics 11: 583-589.
ZENTGRAF H AND FRANKE WW. 1984. Differences of supranucleosomal organization in different kinds of chromatin: cell type-specific globular subunits containing different numbers of nucleosomes. The Journal of cell biology 99: 272-286.
ZHANG C AND CLARKE PR. 2000. Chromatin-independent nuclear envelope assembly induced by Ran GTPase in Xenopus egg extracts. Science 288: 1429-1432.
ZHU D ET AL. 2014. Lysine-specific demethylase 1 regulates differentiation onset and migration of trophoblast stem cells. Nature communications 5: 3174.
ZIERHUT C, JENNESS C, KIMURA H AND FUNABIKI H. 2014. Nucleosomal regulation of chromatin composition and nuclear assembly revealed by histone depletion. Nature structural & molecular biology 21: 617-625.
ZULEGER N, ROBSON MI AND SCHIRMER EC. 2011. The nuclear envelope as a chromatin organizer. Nucleus 2: 339-349.

9. Appendix

Original published articles included in this thesis

The EMBO Journal (2012) 31, 4072–4084 | © 2012 European Molecular Biology Organization | Some Rights Reserved 0261-4189/12
www.embojournal.org

THE EMBO JOURNAL

EMBO open

Dimerization and direct membrane interaction of Nup53 contribute to nuclear pore complex assembly

Benjamin Vollmer[1], Allana Schooley[1], Ruchika Sachdev[1], Nathalie Eisenhardt[1], Anna M Schneider[2], Cornelia Sieverding[1], Johannes Madlung[3], Uwe Gerken[4,5], Boris Macek[3] and Wolfram Antonin[1,*]

[1]Friedrich Miescher Laboratory of the Max Planck Society, Tübingen, Germany, [2]Max Planck Institute for Developmental Biology, Department of Biochemistry, Tübingen, Germany, [3]Proteome Center Tübingen, University of Tübingen, Tübingen, Germany and [4]Institute of Microbiology, University of Hohenheim, Stuttgart, Germany

Nuclear pore complexes (NPCs) fuse the two membranes of the nuclear envelope (NE) to a pore, connecting cytoplasm and nucleoplasm and allowing exchange of macromolecules between these compartments. Most NPC proteins do not contain integral membrane domains and thus it is largely unclear how NPCs are embedded and anchored in the NE. Here, we show that the evolutionary conserved nuclear pore protein Nup53 binds independently of other proteins to membranes, a property that is crucial for NPC assembly and conserved between yeast and vertebrates. The vertebrate protein comprises two membrane binding sites, of which the C-terminal domain has membrane deforming capabilities, and is specifically required for *de novo* NPC assembly and insertion into the intact NE during interphase. Dimerization of Nup53 contributes to its membrane interaction and is crucial for its function in NPC assembly.

The EMBO Journal (2012) **31,** 4072–4084. doi:10.1038/emboj.2012.256; Published online 7 September 2012
Subject Categories: membranes & transport; cell & tissue architecture
Keywords: nuclear envelope formation; nuclear pore complex assembly; nuclear membrane; Nup35; Nup53

Introduction

The defining feature of the eukaryotic cell is the compartmentalization of genetic material inside the nucleus. The spatial and temporal separation of transcription and translation has enabled eukaryotes to achieve a level of regulatory complexity that is unprecedented in prokaryotes. This is accomplished by the nuclear envelope (NE), which serves as the physical barrier between the cytoplasm and the nucleoplasm. Nuclear pore complexes (NPCs) are the exclusive gateways in the NE allowing diffusion of small substances and regulated trafficking of macromolecules up to a size of 15 nm for ribosomal subunits or even 50 nm for Balbiani ring particles (for review, see Wente and Rout, 2010; Hoelz *et al*, 2011; Bilokapic and Schwartz, 2012). NPCs form large pores in the NE, having a diameter of ~130 nm. Unlike other transport channels, NPCs span two lipid bilayers, at sites where the outer and inner membranes of the NE are fused. Therefore, NPCs are assumed to play an important role in deforming these membranes to form a pore as well as in stabilizing this highly curved pore membrane (Antonin *et al*, 2008).

Given the structural complexity and extraordinary transport capabilities of NPCs, it is quite surprising that these huge macromolecular assemblies of 40–60 MDa are only composed of ~30 different proteins. These nucleoporins (Nups) can be roughly categorized into those forming the structure of the pore and those mediating transport through the NPC. The latter class is characterized by a high number of FG repeats. Two evolutionary conserved subcomplexes form the major part of the structural scaffold. The Nup107–160 complex in metazoa, or the corresponding Nup84 complex in yeast, is the best characterized of these owing to an extensive set of genetic, biochemical and structural data. Computational and structural analyses suggest that this complex is related to vesicle coats (Devos *et al*, 2004; Mans *et al*, 2004; Brohawn *et al*, 2008). It is possible that these proteins form a coat-like assembly stabilizing the curved pore membrane of the NPC, which is analogous to clathrin or COPI and II during vesicle formation (Field *et al*, 2011; Onischenko and Weis, 2011). Notably, neither clathrin nor COP coats interact directly with the lipid bilayers. They are rather linked to the deformed membrane via adaptor and integral proteins (McMahon and Mills, 2004). Although three integral membrane proteins are known in the vertebrate NPC, it is unclear how a possible link between the Nup107–160 complex and the membrane is established.

The second major structural and evolutionarily conserved subcomplex of the NPC is the metazoan Nup93 complex, Nic96 in yeast, which might serve as a link to the pore membrane. In vertebrates, it is composed of five nucleoporins: Nup205, Nup188, Nup155, Nup93 and Nup53. Nup53, also referred to as Nup35 (Cronshaw *et al*, 2002), interacts with Nup93 and Nup155 (Hawryluk-Gara *et al*, 2005), corresponding to Nup170 and Nic96 in yeast (Marelli *et al*, 1998; Fahrenkrog *et al*, 2000). Nup155, Nup93 and Nup53 are each indispensable for NPC formation in vertebrates (Franz *et al*, 2005; Hawryluk-Gara *et al*, 2008; Mitchell *et al*, 2010; Sachdev *et al*, 2012). Interestingly, Nup53 and its corresponding yeast homologues Nup53p and Nup59p interact with the transmembrane nucleoporin NDC1, thereby potentially linking the NPC to the pore membrane (Mansfeld *et al*, 2006; Onischenko *et al*, 2009). Although NDC1 is essential in both vertebrates and yeast (Winey *et al*, 1993; West *et al*, 1998; Mansfeld *et al*, 2006; Stavru *et al*, 2006) it is not found in all eukaryotes (Mans *et al*, 2004; DeGrasse *et al*, 2009; Neumann *et al*, 2010), suggesting that in

*Corresponding author. Friedrich Miescher Laboratory of the Max Planck Society, Spemannstraße 39, Tübingen 72076, Germany.
Tel.: +49 70 7160 1836; Fax: +49 70 7160 1801;
E-mail: wolfram.antonin@tuebingen.mpg.de
[5]Present address: Lehrstuhl für Experimentalphysik IV, University of Bayreuth, Universitätsstrasse 30, 95447 Bayreuth, Germany

Received: 16 April 2012; accepted: 21 August 2012; published online: 7 September 2012

some organisms NPCs can form in the absence of a Nup53–NDC1 interaction. Indeed, *Aspergillus nidulans* is viable in the absence of all three known transmembrane nucleoporins (Liu *et al*, 2009). This suggests that there are alternative modes of interaction between the nucleoporins and the pore membrane.

Here, we show that Nup53 binds membranes directly and independently of other proteins. It possesses two membrane interaction regions, which are important for NPC assembly. Although either site is sufficient for NPC assembly at the end of mitosis, the C-terminal membrane binding site of Nup53 is specifically required for NPC assembly during interphase, probably because of its membrane deforming capabilities.

Results

Nup53 is a membrane binding protein

Overexpression of Nup53 in yeast causes expansion of the NE (Marelli *et al*, 2001). Similar membrane proliferation phenotypes have been observed upon overexpression of nuclear membrane binding proteins, such as lamin B (Prufert *et al*, 2004). Yeast Nup53 contains a C-terminal region predicted to form an amphipathic helix (Marelli *et al*, 2001; Patel and Rexach, 2008), which could serve as a membrane binding module. However, Nup53 interacts with the integral pore membrane protein NDC1 in both yeast and metazoa (Mansfeld *et al*, 2006; Onischenko *et al*, 2009) and thus might be linked to the membrane via this interaction. We therefore tested whether Nup53 is able to interact with membranes independently of other proteins.

To assay for membrane binding, we generated liposomes with an average radius of ~150 nm. These liposomes were incubated with different, recombinantly expressed nucleoporins and floated through sucrose cushions. Liposome binding proteins were recovered after centrifugation from the top fraction (Figure 1A). A Nup133 membrane binding fragment (Drin *et al*, 2007) was used as a positive control and found in the liposome containing top fraction (Figure 1A). Similarly, Xenopus Nup53 was found in the top fraction, indicating membrane interaction. In contrast, a fragment of the FG repeat-containing nucleoporin Nup98 did not bind liposomes. Thus, Xenopus Nup53 binds directly to

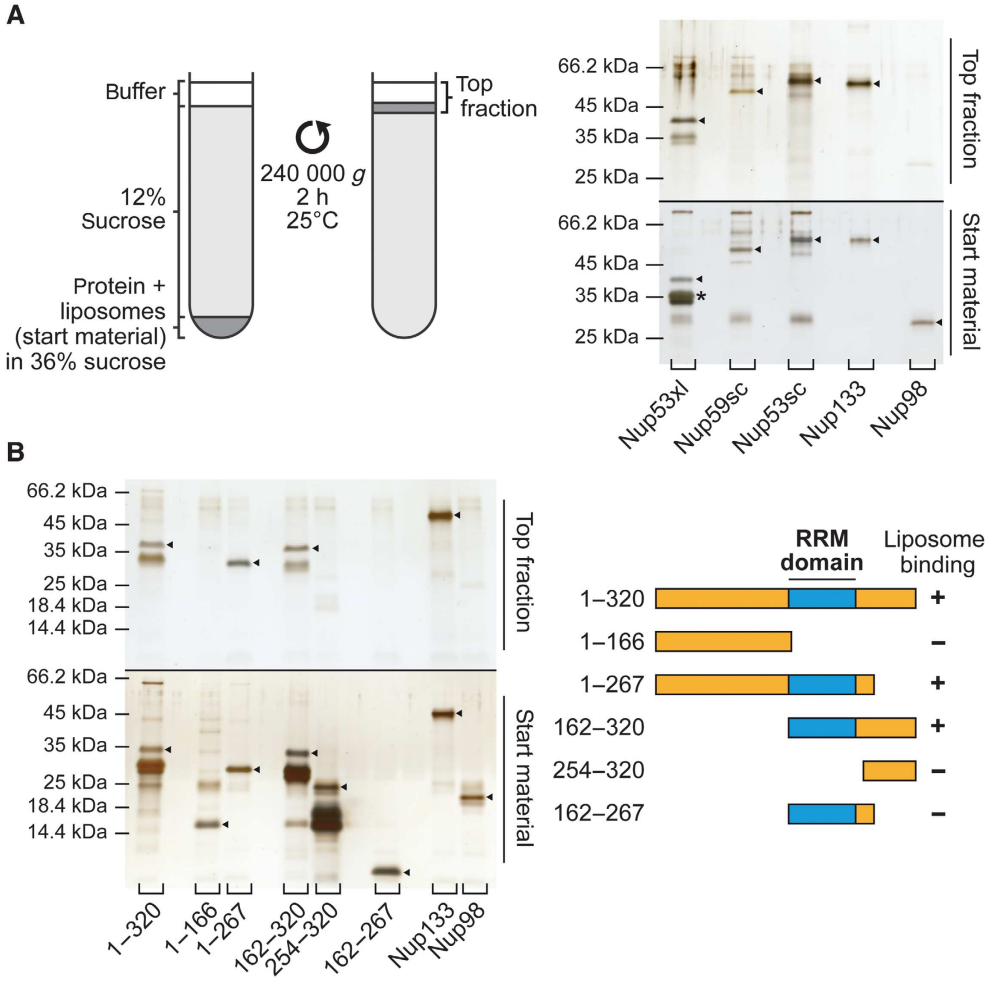

Figure 1 Nup53 directly binds membranes. (**A**) 3 μM recombinant Xenopus Nup53 (Nup53xl), the two yeast orthologues Nup59sc and Nup53sc as well as fragments of Nup133 and Nup98 as positive and negative controls, respectively, were incubated with 6 mg/ml fluorescently labelled liposomes prepared from *E. coli* polar lipids and floated through a sucrose gradient as indicated on the left. Top fractions of the gradient, as well as 3% of the starting material, were analysed by SDS–PAGE and silver staining. Please note that Nup53 is sensitive to C-terminal degradation (*) and that the full-length protein significantly enriched in the liposome bound fraction. (**B**) Full-length (1–320) and different fragments of Xenopus Nup53 as well as fragments of Nup133 and Nup98 were analysed for liposome binding as in (**A**). Only fragments comprising the RRM domain (indicated in blue in the schematic representation) bound liposomes.

membranes independently of other interacting proteins. To determine whether this feature is conserved during evolution, we tested the two yeast homologues Nup53p and Nup59p, which both bound liposomes (Figure 1A).

We next sought to define the regions of Xenopus Nup53 important for its membrane interaction. Nup53 can be roughly divided into three parts: the N-terminus (amino acid (aa) 1–166), a middle region (aa 166–267) comprising a conserved RNA recognition motif (RRM) domain and the C-terminus (aa 267–320) (Figure 1B). We generated different N- and C-terminal truncations of Nup53 and tested them for liposome binding (Figure 1B). While full-length Nup53 (aa 1–320) bound to liposomes, the N-terminal region of the protein (aa 1–166) showed no binding. Extending this fragment by 100 aa to include the RRM domain rendered the protein capable of membrane binding (aa 1–267). The C-terminal half of Nup53 (aa 162–320), which included the RRM domain, also interacted with liposomes. However, a fragment consisting of only the C-terminal region of Nup53 but lacking the RRM domain (aa 254–320) could not bind liposomes. Surprisingly, a fragment comprising only the RRM domain (aa 162–267) did not bind liposomes showing that the RRM domain is necessary but not sufficient for Nup53 membrane binding.

Nup53 dimerization is necessary for membrane binding and NPC formation

As the RRM domain is crucial for Nup53 membrane interaction we investigated the function of this domain. The crystal structure of the mouse domain suggests that it acts as a dimerization rather than an RNA binding module (Handa *et al*, 2006). We designed a mutant of this domain by exchanging two amino acids (F172E/W203E) in the dimerization surface. Size exclusion chromatography in combination with multi-angle laser light scattering revealed that the resulting fragment was monomeric (Figure 2A).

To confirm that the dimerization occurs also *in vivo*, we performed co-transfection experiments in HeLa cells using HA- and myc-tagged Xenopus Nup53. Either α-HA or α-myc antibodies immunoprecipitated both HA- and myc-tagged wild-type Nup53 indicating that the proteins formed a complex (Figure 2B, lanes 5 and 10). If cells were transfected with either construct separately before they were mixed for protein extraction, then no co-immunoprecipitation was observed (Figure 2B, lanes 9 and 14) demonstrating that complex formation cannot occur under the conditions of the immunoprecipitation. Co-transfections of RRM mutants as well as RRM mutants and wild-type protein did not result in complex formation (Figure 2B, lanes 6–8 and 11–13) indicating that the F172E/W203E exchange inhibited dimerization/oligomerization.

Next, we tested the effect of these mutations on membrane binding. In the context of the full-length protein, these mutations decreased liposome binding by 70% (Figure 2C) suggesting that the dimerization of Nup53 is important for its membrane interaction.

As Nup53 is essential for postmitotic NPC formation (Hawryluk-Gara *et al*, 2008) we examined the relevance of Nup53 membrane binding for this. We employed *Xenopus laevis* egg extracts to study nuclear reformation *in vitro* (Lohka, 1998). With antibodies against Nup53 we depleted the endogenous protein without co-depletion of other nucleoporins including the other members of the Nup93 complex: Nup93, Nup155, Nup205 and Nup188 (Figure 2D). These depleted extracts were incubated with sperm heads serving as chromatin template. In the absence of Nup53, NPC formation was blocked (Figure 2E) as reported (Hawryluk-Gara *et al*, 2008). This was indicated by the absence of immunofluorescent signal on the chromatin surface for mab414, an antibody recognizing several nucleoporins that represent a major subfraction of the NPC. Addition of recombinantly expressed wild-type Nup53 to the depleted extracts at levels similar to the endogenous protein (Figure 2D) restored NPC formation. The recombinant protein was integrated into NPCs as indicated by immunostaining with a Nup53 antibody. In contrast, the dimerization and membrane binding defective Nup53 mutant (1–320 F172E/W203E) was unable to substitute for the endogenous protein in NPC formation (Figure 2E).

Individual depletion of several nucleoporins essential for NPC assembly from Xenopus egg extracts also blocks formation of a closed NE. These nucleoporins include POM121, NDC1, Nup155, Nup93 (Antonin *et al*, 2005; Franz *et al*, 2005; Mansfeld *et al*, 2006; Sachdev *et al*, 2012) and Nup53 (Hawryluk-Gara *et al*, 2008). Upon Nup53 depletion, membrane vesicles bound to the chromatin surface but did not fuse to form a closed NE (Figure 2F; Hawryluk-Gara *et al*, 2008). This phenotype was rescued by the wild-type Nup53 protein, but not by the dimerization defective mutant. Together with the liposome-binding assay, this suggests that Nup53 membrane binding could be important for NPC assembly and formation of a closed NE. However, we cannot exclude that the RRM mutant also affects interaction of Nup53 with other nucleoporins. Indeed, in GST pull-down assays we observed a slight reduction of Nup93, Nup205 and Nup155 binding to Nup53 in the context of the RRM mutant as compared to the wild-type protein (Supplementary Figure S1A). In contrast, NDC1 binding to Nup53 was unaffected by the dimerization mutant (Supplementary Figure S1B).

Nup53 possesses two membrane binding regions

These results reveal a crucial role for Nup53 dimerization via its RRM domain in NE reformation. However, the RRM domain alone did not bind to membranes. We tested different Nup53 truncations for liposome binding to map the membrane interaction sites (Figure 3A; Supplementary Figure S2 shows the purity of all recombinant proteins used in the different liposome experiments). An N-terminal fragment of Nup53 including the RRM domain (aa 1–267) bound to liposomes with only a slightly decreased binding efficiency, 83% of the levels of the full-length protein. Further truncations from the N-terminus revealed a minimal membrane binding region between aa 93 and 107 as indicated by a four-fold decrease in liposome binding upon removal of these 15 amino acids. This region comprises a patch of basic residues, which as in other membrane binding proteins might be important for the interaction with negatively charged lipids. Indeed, changing two residues to negatively charged residues (R105E/K106E) abolished membrane binding (Figure 3A, 83% reduction as compared to the 93–267 fragment).

Interestingly, the N-terminal membrane binding region of Nup53 contains one of two regions that were differentially phosphorylated depending on the cell-cycle stage (Supplementary Figure S3; Supplementary Table S1). Two

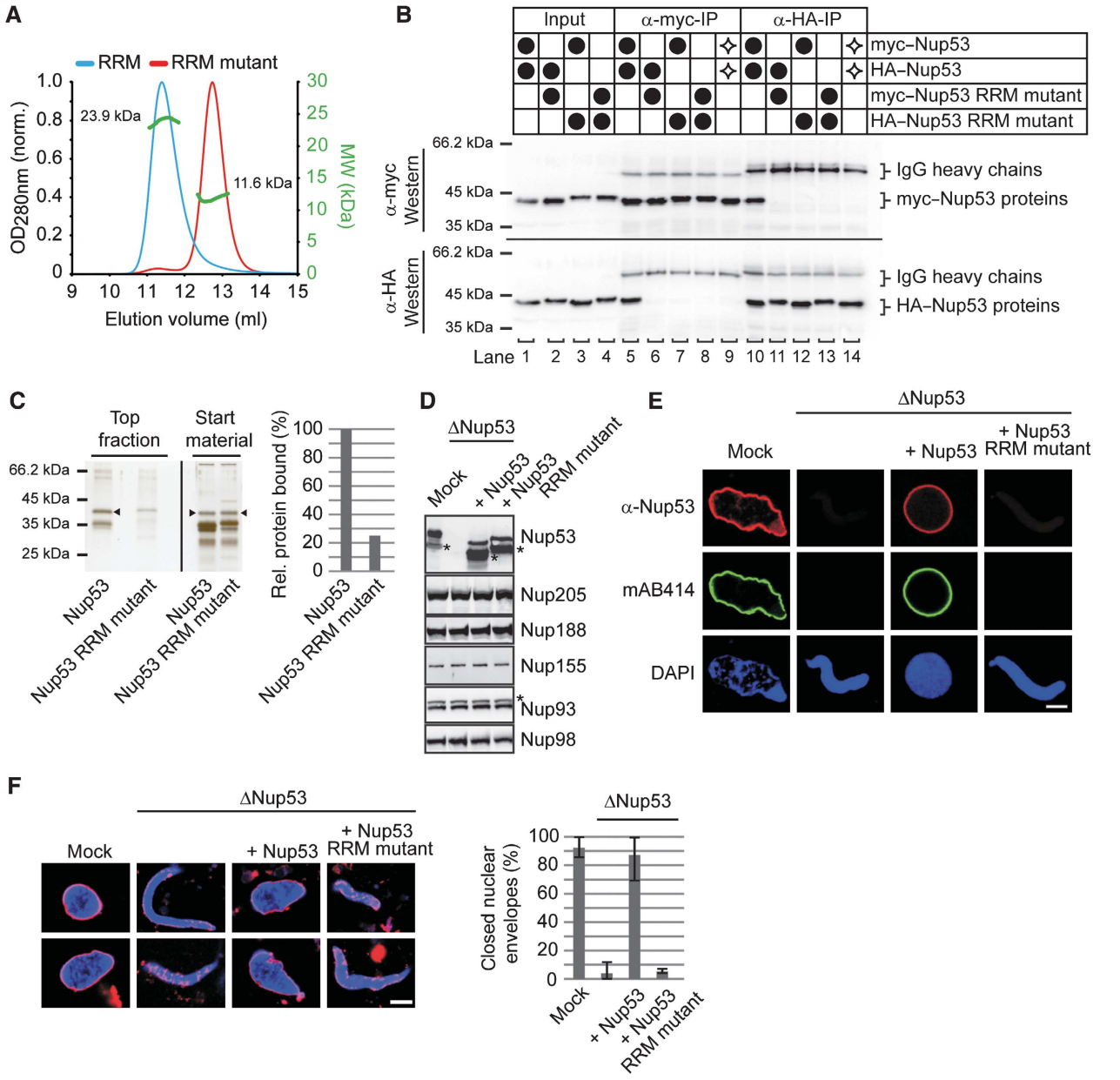

Figure 2 Dimerization of the RRM domain is essential for Nup53 membrane binding and nuclear pore complex formation. (**A**) Size exclusion chromatography on a Superdex75 10/300 GL column followed by multi-angle static laser light scattering of the Xenopus Nup53 RRM domain and the F172E/W203E mutant, which rendered the domain monomeric. The green dots relate to the secondary axis and show the molecular weight of the eluting particles. (**B**) HeLa cells were co-transfected with myc- and HA-tagged Xenopus Nup53 wild-type protein and/or dimerization mutant as indicated (●). Proteins were immunoprecipitated from cell lysates with α-myc or α-HA antibodies, and analysed by western blotting. Ten per cent of the start materials are loaded as input. To exclude complex formation after cell lysis, extracts from single transfected myc–Nup53 and HA–Nup53 cell batches were mixed and processed for immunoprecipitation (✧). Under these conditions, no co-precipitation was observed. (**C**) Full-length Xenopus Nup53 and the respective F172E/W203E mutant (RRM mutant) were analysed for liposome binding as in Figure 1. The right panel shows the quantitation of liposome binding analysed by western blotting and normalized to the levels of the wild-type protein (one out of two independent experiments). (**D**) Western blot analysis of mock, Nup53-depleted (ΔNup53) and Nup53-depleted extracts supplemented with recombinant wild-type protein (Nup53) or the dimerization mutant (Nup53 RRM mutant), respectively. Recombinant proteins were added to approximate endogenous Nup53 levels (judged by the full-length protein, please note for both endogenous and recombinant Nup53 proteins C-terminal degradation products (*)). The recombinant Nup53 migrated slightly faster than the endogenous protein due to absence of eukaryotic post-translational modifications. The Nup93 antibody recognizes a slightly slower migrating cross-reactivity by western blotting (*). (**E**) Nuclei were assembled in mock, Nup53-depleted extracts or Nup53-depleted extracts supplemented with wild-type protein (Nup53) or the dimerization mutant for 120 min, fixed with 4% PFA and analysed with Nup53 antibodies (red) and mAb414 (green). Chromatin was stained with DAPI. Bar: 10 μm. (**F**) Nuclei were assembled as in (**E**), fixed with 2% PFA and 0.5% glutaraldehyde and analysed for chromatin (blue: DAPI) and membrane staining (red: DiIC18, bar: 10 μm). Right panel shows the quantitation of chromatin substrates with a closed nuclear envelope (averages of three independent experiments with >300 randomly chosen chromatin substrates per sample, error bars represent the range).

amino acids identified, Serine 94 and Threonine 100, are phosphorylated during mitosis, most likely by cdk 1 as they possess a consensus site for this kinase (Blethrow *et al*, 2008). To investigate the impact of this modification on membrane binding, we generated mutants mimicking the phosphorylated (S94E/T100E) and the unphosphorylated

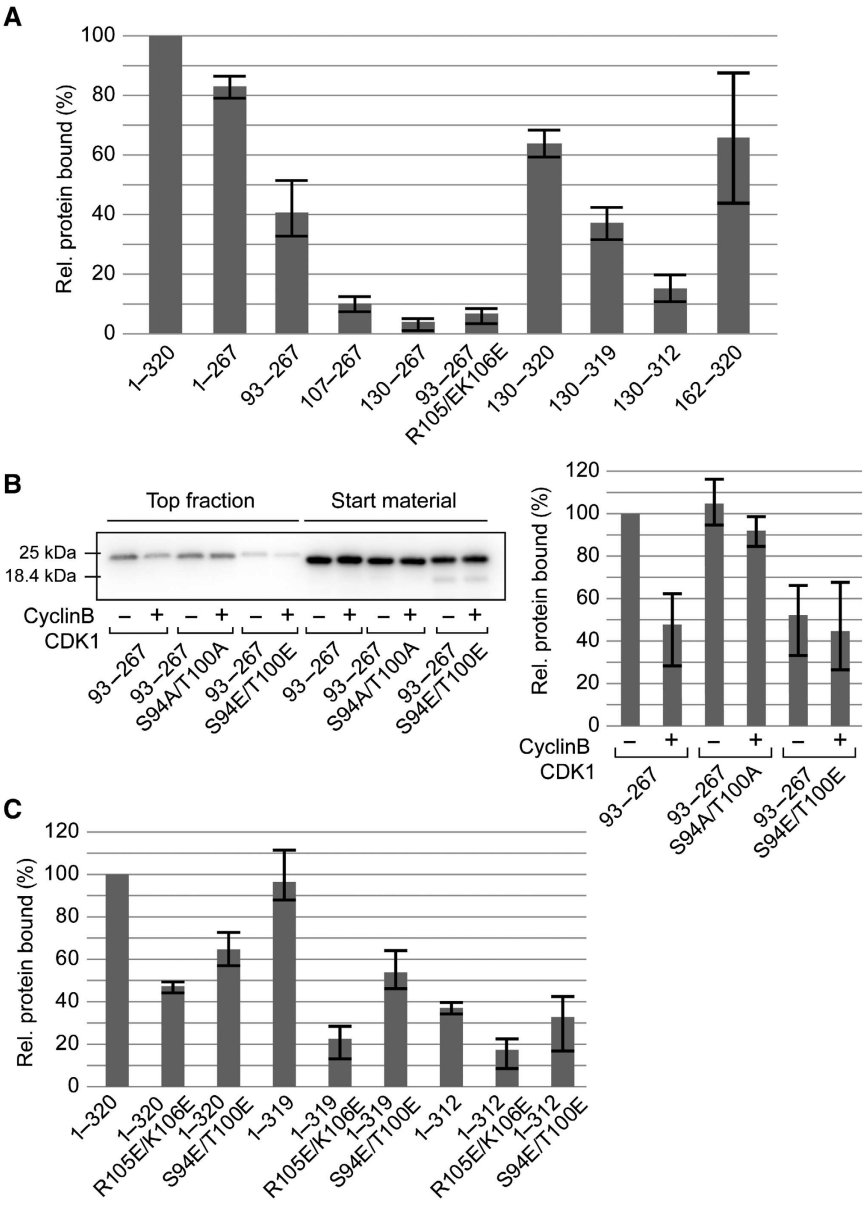

Figure 3 Nup53 possesses two independent membrane binding regions. (**A**) Full-length protein (1–320) and different fragments of Xenopus Nup53 were quantitatively analysed for liposome binding as in Figure 2B (normalized to the full-length protein, three independent experiments). (**B**) A fragment comprising the first membrane binding region and the RRM domain (93–267) as well as a phosphomimetic (93–267 S94E/T100E) and a non-phosphorylatable mutant (93–267 S94A/T100A) was treated with CyclinB/CDK1. Samples were tested for liposome binding as in Figure 1A and analysed by western blotting (left panel) and quantified (right panel: two independent experiments, normalized to liposome binding of wild-type fragment without CDK1 pretreatment). (**C**) Mutants/truncations affecting the N- (1–320 R105E/K106E, 1–320 S94E/T100E), the C-terminal (1–319, 1–312) as well as both (1–319 R105E/K106E, 1–319 S94E/T100E, 1–312 R105E/K106E, 1–312 S94E/T100E) membrane binding sites of Nup53 were quantitatively assayed for liposome binding in the context of full-length protein (normalized to wild-type protein (1–320), average of three independent experiments, error bars represent the range).

(S94A/T100A) state of the protein. The phosphomimetic mutant was impaired in liposome binding (Figure 3B, reduced by 50% compared to the 93–267 fragment) while the S94A/T100A control bound to liposomes with efficiency comparable to the wild type. Furthermore, *in vitro* phosphorylation by CyclinB/CDK1 reduced liposome binding of the wild-type protein by 50%, levels similar to the phosphomimetic mutant (S94E/T100E), but did not affect the S94A/T100A mutant, suggesting that mitotic phosphorylation regulates the membrane binding of Nup53.

The C-terminal part of Nup53 also interacts with membranes, an activity that requires the presence of the RRM domain (Figure 1B). Fragments comprising both regions showed efficient binding to liposomes (aa 130–320 and 162–320) (Figure 3A). The second membrane binding region was mapped to the absolute C-terminus of Nup53 as deletion of the last amino acid reduced liposome binding by 42% (aa 130–319) and removal of the last eight amino acids abolished liposome binding (aa 130–312).

These data suggest that Nup53 possesses two independent membrane binding sites. Consistently, in the context of the full-length protein mutations in the N-terminal site (R105E/K106E as well as S94E/T100E) reduced liposome binding by 50 and 40% (Figure 3C). Deletion of the

C-terminal amino acid had a less prominent effect, but removal of the last eight amino acids reduced liposome binding by 60%. The combination of mutations and truncations affecting both binding sites showed an additive effect supporting the view that each site is individually capable of membrane binding. Our data also suggest that the N-terminal membrane interaction is mediated via a pair of basic amino acids. The N-terminal binding site is additionally dependent on membrane curvature, the fragment binding less efficiently to more highly curved membranes (Supplementary Figure S4). Conversely, the C-terminal membrane binding site is less sensitive to membrane curvature and seems to largely depend on the last amino acid, a hydrophobic tryptophan. This could indicate that the two membrane interaction sites operate via different binding mechanisms. In both cases, the dimerization of Nup53 via the RRM domain is important: mutations in the individual membrane binding fragments (93–267 F172E/W203E and 130–320 F172E/W203E) rendering the RRM domain monomeric reduced their membrane interaction (Supplementary Figure S5).

Nup53 membrane binding is necessary for NPC formation

The Nup53 mutant defective in RRM dimerization, which showed reduced membrane binding, was unable to substitute for the endogenous protein in nuclear assembly (Figure 2). We therefore analysed the contribution of each of the membrane interaction sites to NPC assembly by substituting endogenous Nup53 with constructs defective in the N-terminal membrane interaction site, lacking the C-terminal membrane interaction site, or comprising a combination of both deficient sites (Figure 4A). Surprisingly, mutants of the N-terminal membrane binding site (1–320 R105E/K106E and 1–320 S94E/T100E) supported NPC formation as indicated by mAB414 staining (Figure 4A). They also supported formation of a closed NE (Figure 4A and B). Correspondingly, mutations in the N-terminal binding region did not alter the NE localization of any other nucleoporins (Figure 4D). These nucleoporins include members of the Nup93 complex (Nup93, Nup188, Nup205 and Nup155) as well as the transmembrane nucleoporins NDC1 and POM121. Accordingly, interactions of these mutants with Nup93 and Nup205, which bind the N-terminal part of Nup53 (Fahrenkrog *et al*, 2000; Hawryluk-Gara *et al*, 2008), were unaffected as shown by GST pull downs (Supplementary Figure S1A).

The fragment lacking the C-terminal tryptophan (1–319) also supported NPC assembly and formation of a closed NE. Deletion of this tryptophan did not interfere with Nup53 binding to NDC1 or Nup155 (Supplementary Figure S1B), two binding partners interacting with the C-terminal region. The truncation lacking the last eight C-terminal amino acids (1–312) also allowed for NPC assembly and formation of a closed NE. All tested nucleoporins were located at the NE in these nuclei (Figure 4D). Notably, this truncation did not bind to NDC1 (Supplementary Figure S1B), supporting the view that the Nup53–NDC1 interaction is not required for postmitotic NPC formation (Hawryluk-Gara *et al*, 2008). These observations suggest that a single Nup53 membrane binding region is sufficient for NPC assembly at the end of mitosis.

In contrast to the Nup53 mutants and truncations that abrogate one membrane binding region, mutants affecting both membrane binding sites (1–319 R105E/K106E, 1–319 S94E/T100E, 1–312 R105E/K106E and 1–312 S94E/T100E) did not support NPC assembly and NE reformation (Figure 4A). Under these conditions, MEL28 (also referred to as ELYS) as well as Nup107, which both bind early to chromatin during the NPC assembly process (Galy *et al*, 2006; Rasala *et al*, 2006; Franz *et al*, 2007), as well as the transmembrane nucleoporins, NDC1 and POM121, were detected on the chromatin (Figure 4D). In contrast, Nup205, Nup188, Nup155 and Nup93 were not recruited. However, this lack of recruitment as well as the block in NPC assembly is unlikely to be caused by disrupting Nup53 binding to these interaction partners as the mutations introduced did not affect binding to Nup93, Nup205 and Nup155 in GST pull downs (Supplementary Figure S1A). It is also unlikely that the loss of the Nup53–NDC1 interaction caused this phenotype as the Nup53 fragment 1–312 still allowed for postmitotic NPC assembly but was not able to bind NDC1 (Supplementary Figure S1B). Nup58 representing an FG-containing nucleoporin of the central channel as well as the peripheral nucleoporin Nup88 was also absent on chromatin in the presence of a Nup53 construct that lacked both membrane binding regions (1–312 R105E/K106E) (Figure 4D). These data support the conclusion that the direct Nup53 membrane interaction is important for postmitotic NPC formation.

Interphasic NPC assembly requires the C-terminal membrane binding site of Nup53

Metazoan NPC assembly occurs in two different stages of the cell cycle: at the end of mitosis when NPCs assemble concomitantly with the reforming NE and during interphase when new NPCs are assembled and integrated into the intact NE (Antonin *et al*, 2008; Doucet and Hetzer, 2010). Recent data suggest that there are different requirements for these two possible modes of NPC assembly (Doucet *et al*, 2010). The *in vitro* nuclear assemblies described up to now reflect the situation at the end of mitosis. We therefore assayed whether the mutants that support postmitotic NPC assembly also support NPC formation during interphase. In an experimental set-up developed by the Hetzer laboratory (Dawson *et al*, 2009), nuclei with newly integrated NPCs can be visualized by an influx of dextrans when nucleoporins forming the permeability barrier of newly formed NPCs are depleted. Under these conditions, mutants defective in the N-terminal membrane binding site of Nup53 (1–320 R105E/K106E and 1–320 S94E/T100E) supported interphasic NPC formation (Figure 5A). Conversely, Nup53 truncations affecting the C-terminal membrane binding site did not substitute for the wild-type protein in this mode of NPC assembly. This indicates that, in contrast to postmitotic NPC assembly where both membrane binding regions individually support NPC formation, only the C-terminal membrane binding site of Nup53 is required for interphasic NPC formation.

Interestingly, the Nup53 truncation lacking the C-terminal tryptophan (1–319) did not support interphasic NPC assembly in the dextran influx assay despite the fact that membrane interaction is only slightly reduced (Figure 3C). We confirmed these findings in an independent assay directly counting NPCs identified by mAB414 immunostaining (D'Angelo *et al*, 2006; Theerthagiri *et al*, 2010). NPC numbers were determined on nuclei where NPCs assembled in the postmitotic and interphasic mode and nuclei where interphasic

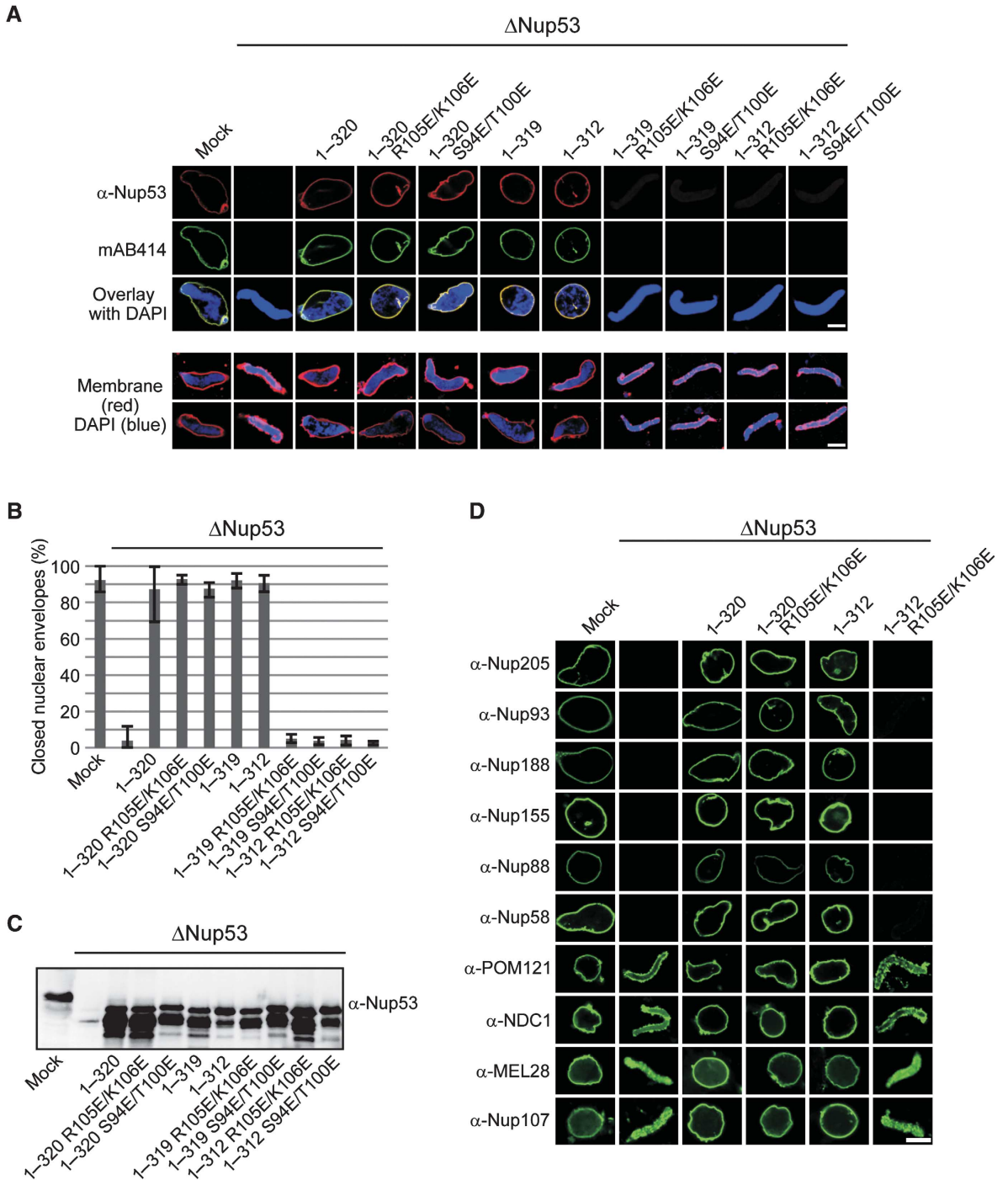

Figure 4 Either of the two membrane binding regions of Nup53 is sufficient for postmitotic NPC assembly. (**A**) Nuclei were assembled in mock, Nup53-depleted extracts or Nup53-depleted extracts supplemented with wild-type Nup53 (1–320), constructs featuring mutations in the N-terminal membrane binding site (1–320 R105E/K106E, 1–320 S94E/T100E), constructs lacking the C-terminal membrane binding site (1–319, 1–312) or both (1–319 R105E/K106E, 1–319 S94E/T100E, 1–312 R105E/K106E, 1–312 S94E/T100E), respectively. Samples were fixed after 120 min with 4% PFA and analysed with Nup53 antibodies (red) and mAb414 (green, upper panel) or with 2% PFA and 0.5% glutaraldehyde and analysed for chromatin (blue: DAPI) and membrane staining (red: DiIC18, lower panel). Bars: 10 μm. (**B**) Quantitation of chromatin substrates with a closed NE was done as in Figure 2F. (**C**) Western blot analysis of extracts used in (**A**) showing the re-addition of the recombinant proteins to approximately endogenous Nup53 levels. (**D**) Nuclei were assembled as in (**A**), fixed with 4% PFA and analysed with respective antibodies. Bar: 10 μm.

NPC formation was specifically blocked by addition of 2 μM importin β (D'Angelo *et al*, 2006; Theerthagiri *et al*, 2010). The NPC numbers of nuclei assembled for 120 min in the presence of recombinant wild-type Nup53 as well as the Nup53 mutant defective in the N-terminal membrane binding site (1–320 R105E/K106E) were reduced by importin β addition after 50 min, i.e., when a closed NE with intact NPC was formed (Figure 5B). In contrast, the Nup53 truncation lacking the C-terminal tryptophan showed after 120 min a lower number of NPCs, which was not sensitive to importin β addition, indicating that in this condition interphasic NPC assembly did not occur.

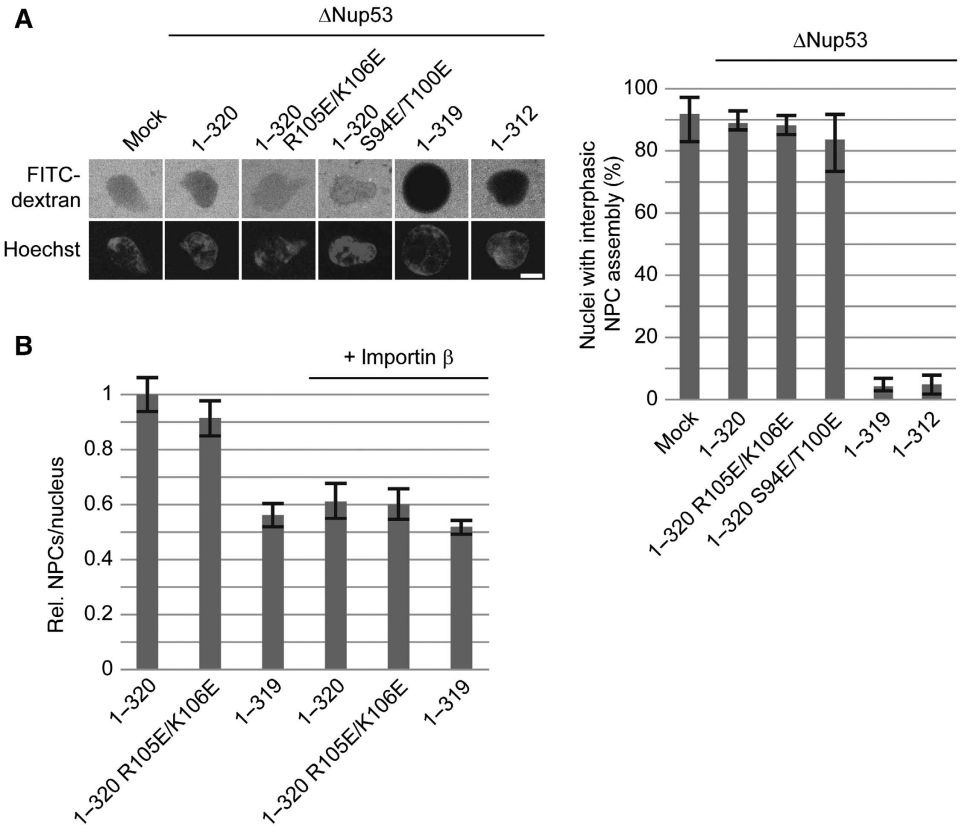

Figure 5 The C-terminal Nup53 membrane binding site is essential for interphasic nuclear pore complex (NPC) formation. (**A**) Nuclei were preassembled in mock or Nup53-depleted extracts supplemented with wild-type full-length protein (1–320), constructs with a mutated N-terminal membrane binding site (1–320 R105E/K106E, 1–320 S94E/T100E), or constructs lacking the C-terminal membrane interaction site (1–319, 1–312), respectively. After 90 min, the samples were supplemented with cytosol depleted of Nup53 and FG-containing nucleoporins. After 60 min, FITC-labelled 70-kDa dextran and Hoechst was added. Bar: 10 μm. The right panel shows the quantitation of three independent experiments with >300 randomly chosen chromatin substrates per sample. Error bars represent the range. (**B**) Nuclei were assembled in Nup53-depleted extracts supplemented with wild-type full-length protein (1–320), a construct with a mutated N-terminal membrane binding site (1–320 R105E/K106E), or a construct lacking the last C-terminal amino acid (1–319), respectively, for 120 min. Where indicated, *de novo* NPC assembly was blocked by the addition of 2 μM importin β after 50 min and nuclei were further incubated for 70 min. For each construct, total NPC numbers per nucleus identified by mAB414 immunofluorescence were quantified from 20 nuclei in 2 independent experiments and normalized to the wild-type full-length protein. Error bars represent the s.e. of the mean.

Nup53 can deform membranes

Many membrane binding proteins induce membrane deformation. Such a function is of special interest in the context of NPC formation as NPCs are integrated in the NE at sites where both nuclear membranes are deformed and fused to a pore. We therefore analysed the morphology of Nup53-bound liposomes using electron microcopy. As reported (Daumke *et al*, 2007), tubulation of liposomes is induced by the EH domain-containing protein EHD2 (Figure 6A). Interestingly, a Nup53 fragment containing both membrane binding sites (93–320) strongly induced liposome tubulation indicating a membrane deformation capability. A shorter fragment containing only the N-terminal membrane binding site and including the RRM domain (93–267) did not induce membrane tubulation, despite the fact that it was able to bind liposomes (Figure 3A). In contrast, a fragment comprising the RRM domain and the full C-terminus of Nup53 (130–320) strongly induced membrane tubulation indicating that the second, C-terminal membrane binding domain deforms membranes. Accordingly, fragments lacking the last eight residues (130–312), and therefore the second membrane binding site or only the last C-terminal tryptophan (130–319) did not cause membrane tubulation. Consistently, fragments mutated in the first, or N-terminal, membrane binding region of Nup53 (93–320 R105E/K106E and 93–320 S94E/T100E) induced membrane deformation. Efficient membrane binding of Nup53 depends not only on the individual membrane binding domains but also on dimerization (Figure 2C; Supplementary Figure S5). To determine the importance of the dimerization of Nup53 for membrane tubulation the RRM mutants of fragments that contained either both (93–320 RRM mutant) or only the C-terminal binding site (130–320 RRM mutant) were tested. Neither of the two fragments induced membrane tubulation emphasizing that membrane interaction is indeed required for this phenotype. The membrane binding fragment of Nup133 did not induce detectable tubulation, emphasizing that membrane binding alone does not account for membrane deformation.

Similar to Xenopus Nup53 both yeast isoforms—Nup53p and Nup59p—induced membrane tubulation (Figure 6B). This indicates that, in addition to membrane binding (Figure 1A), the membrane bending activity of Nup53 is conserved during evolution which suggests an important role for Nup53-induced membrane deformation in NPC formation and/or function.

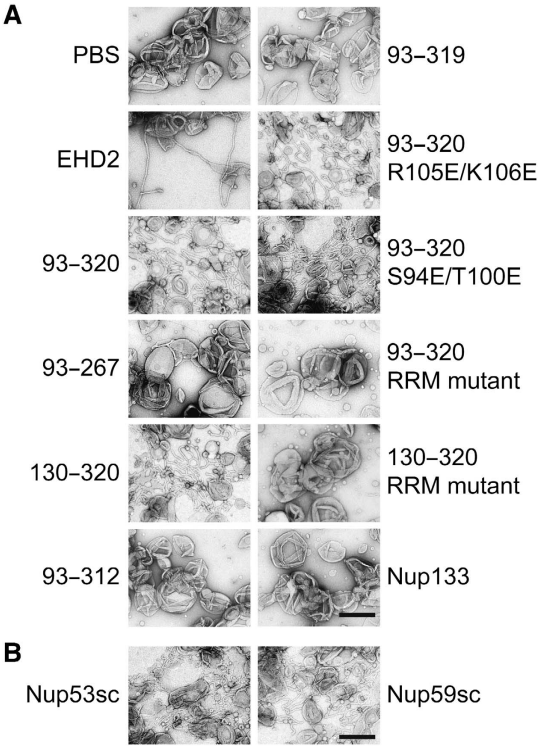

Figure 6 The C-terminus of Nup53 binds and deforms membranes. (**A**) Folch fraction I liposomes were incubated where indicated with 3 μM recombinant Nup53 fragments containing both (93–320), the N-terminal (93–267) or C-terminal (130–320) membrane binding sites including the RRM domain as well as fragments and mutants where the C-terminal (93–312, 93–319), the N-terminal (93–320 R105E/K106E, 93–320 S94E/T100E) membrane interaction site or the dimerization (93–320 RRM mutant and 130–320 RRM mutant) is compromised. The liposome deforming protein EHD2 (aa 1–543) and a fragment of Nup133 were used as positive and negative control, respectively. (**B**) 3 μM recombinant yeast Nup53 and Nup59 protein was incubated with liposomes and analysed. Bars: 400 nm.

Discussion

Here, we show that Nup53 binds membranes directly and independently of other proteins. We demonstrate that dimerization of the protein via its RRM domain is necessary for membrane interaction and identify two separate membrane binding regions within the protein. Binding of Nup53 to membranes is important for NPC assembly. Although either of the two membrane interaction regions is sufficient for postmitotic NPC formation, NPC assembly in interphase specifically requires the C-terminal membrane binding site, probably because of its capacity to induce membrane deformation.

Our results support the view that Nup53 is crucial for postmitotic NPC assembly in Xenopus egg extracts (Hawryluk-Gara *et al*, 2008). Depletion of Nup53 blocks NPC assembly and the formation of a closed NE. This phenotype is rescued by the addition of recombinant Nup53, confirming the specificity of the depletion (Hawryluk-Gara *et al*, 2008; Figures 2 and 4). In agreement with the cell-free data, RNAi-mediated depletion of Nup53 in HeLa cells results in severe nuclear morphology defects and reduced levels of Nup93, Nup205 and Nup155 at the nuclear rim, suggestive of defects in NPC assembly (Hawryluk-Gara *et al*, 2005). In *C. elegans*, RNAi knockdown of Nup53 as well as a deletion within the protein blocks postmitotic nuclear reformation and results in embryonic lethality (Galy *et al*, 2003; Rodenas *et al*, 2009), suggesting that Nup53 function is conserved in metazoa. Notably, Nup53 is found in all eukaryotic supergroups indicating that it is part of the NPC in the last common ancestor of eukaryotes (Neumann *et al*, 2010). However, its absence in some eukaryotic organisms shows that its loss can be compensated (DeGrasse *et al*, 2009; Neumann *et al*, 2010). Double deletion of both *S. cerevisiae* orthologues, Nup53p and Nup59p, is viable (Marelli *et al*, 1998; Onischenko *et al*, 2009). However, these strains exhibit growth defects and Nup53 becomes essential when interacting nucleoporins, including integral membrane proteins, are deleted (Marelli *et al*, 1998; Miao *et al*, 2006; Onischenko *et al*, 2009).

NPC assembly is a highly ordered process. In metazoa the NE and NPCs break down and reform during each round of mitosis. Postmitotic reassembly occurs on the decondensing chromatin. The earliest step involves the recruitment of the Nup107–160 subcomplex to the chromatin surface by MEL28/ELYS (Galy *et al*, 2006; Rasala *et al*, 2006; Franz *et al*, 2007), a DNA-binding protein that acts as a seeding point for NPC assembly. Membranes are subsequently recruited to chromatin causing an enrichment of NE/NPC-specific membrane proteins, including the transmembrane nucleoporins POM121 and NDC1 (Antonin *et al*, 2005; Mansfeld *et al*, 2006; Anderson *et al*, 2009). The order of these initial steps has been defined using both *in vitro* experiments and live-cell imaging (Dultz *et al*, 2008); however, less is known about the order of nucleoporin assembly following these events. MEL28 and Nup107 as well as POM121 and NDC1 containing membranes are detectable on the chromatin in Nup53-depleted nuclear assemblies (Figure 4D). The same pattern was seen in Nup93-depleted extracts (Sachdev *et al*, 2012). Our results suggest that Nup53, which is part of the Nup93 complex, is a key determinant for the recruitment of the other members of this complex. In the absence of Nup53, the chromatin recruitment of Nup155, Nup205, Nup188 and Nup93 was impaired (Figure 4D). Similarly, *C. elegans* Nup53 is necessary for the efficient accumulation of Nup155 and Nup58 but not Nup107 at the NE (Rodenas *et al*, 2009). This is also supported by live-cell imaging experiments in HeLa cells, which capture the recruitment of Nup58 slightly after Nup93 (Dultz *et al*, 2008). Accordingly, we have found that upon depletion of the two Nup93 containing subcomplexes, Nup93–Nup188 and Nup93–205, the two other members of the complex, Nup155 and Nup53, are still detectable, albeit at reduced levels on the assembling NPCs (Sachdev *et al*, 2012). Recruitment of the Nup62 complex to the chromatin template is prevented in the absence of both Nup53 (see lack of a Nup58 immunostaining, which is a constituent of the Nup62 complex, in Figure 4D) and Nup93 (Sachdev *et al*, 2012) consistent with the notion that Nup93 is a key determinant in recruiting the Nup62 complex during vertebrate NPC assembly at the end of mitosis (Sachdev *et al*, 2012). Taken together, these data suggest that after the binding of the Nup107–160 complex and nuclear membranes to the chromatin surface, Nup53 recruitment is the next decisive step in NPC assembly. Nup93 (Nup93–Nup188/Nup93–Nup205) binding and the subsequent recruitment of the Nup62 complex follow.

Nup53 interacts with a number of other nucleoporins, including NDC1, Nup155 and Nup93 (Lusk *et al*, 2002;

Hawryluk-Gara *et al*, 2005, 2008; Mansfeld *et al*, 2006; Sachdev *et al*, 2012) a feature that is conserved in yeast (Fahrenkrog *et al*, 2000; Onischenko *et al*, 2009; Amlacher *et al*, 2011). As previously reported (Hawryluk-Gara *et al*, 2008), the interaction of Nup53 with NDC1 is not necessary for postmitotic NPC assembly in Xenopus egg extracts (Figure 4A). A possible explanation might be that Nup53 can interact directly with membranes and that one of its two membrane binding regions is sufficient for postmitotic NPC formation. In addition, Nup53 interaction with other nucleoporins such as Nup155, which in turn binds POM121 (Mitchell *et al*, 2010; Yavuz *et al*, 2010) could be a possible mechanism linking Nup53 to the pore membrane which might compensate for the loss of the direct Nup53–NDC1 interaction.

The interaction of Nup53 with Nup155 is thought to be important for NPC assembly. A previous study found that after depleting Nup53 from Xenopus egg extracts, only fragments capable of binding to Nup155 allow for NPC formation (Hawryluk-Gara *et al*, 2008). However, in this case all fragments that rescued the NE/NPC assembly defect included the RRM domain and all fragments defective in NPC assembly and the Nup155 interaction lacked the intact RRM domain. Similarly, a deletion in *C. elegans* Nup53 blocked NE assembly also impaired the RRM domain (Rodenas *et al*, 2009). We demonstrate here that the RRM domain is important for Nup53 dimerization and in turn for membrane binding. Therefore, we currently cannot rule out that the primary cause for the previously described defects was a loss of the Nup53 membrane interaction.

Nup93 binds directly Nup53 (Hawryluk-Gara *et al*, 2005; Sachdev *et al*, 2012) and the interaction domain resides in the N-terminal half of Nup53 (Hawryluk-Gara *et al*, 2008). This interaction was previously considered to be dispensable for NPC assembly as a fragment lacking the N-terminal region as well as the C-terminal 26 amino acids replaced endogenous Nup53 in nuclear assemblies in Xenopus egg extracts (Hawryluk-Gara *et al*, 2008). This is quite surprising in the light of the results presented here, as this fragment also lacked both membrane binding regions identified in this study and does not allow for Nup93 recruitment which is an essential factor for postmitotic NPC assembly (Sachdev *et al*, 2012). Using a number of different Nup53 fragments that lacked the Nup93 binding region we were not able to replace endogenous Nup53 in NPC assembly (Supplementary Figure S6). Currently, we cannot rule out that this discrepancy is due to different Nup53 depletion efficiencies. In fact, we found that a small percentage of floated membrane preparations used in the nuclear assembly reactions contained minor amounts of Nup53, and we were careful to exclude these from our experiments.

Nup53 is also known as mitotic phosphoprotein of 44 kDa (Stukenberg *et al*, 1997). Indeed, Nup53 from mitotic extracts migrates significantly slower in SDS–PAGE compared to Nup53 from interphasic extracts (Supplementary Figure S3A). We identified a number of mitosis-specific phosphorylation sites on Nup53, of which a subset were consensus sites for CDK1. These findings are consistent with the fact that Nup53 has been identified as a CDK1 target in both yeast and humans (Lusk *et al*, 2007; Blethrow *et al*, 2008). The N-terminal membrane binding region of Nup53 is phosphorylated during mitosis. Phosphomimetic mutations and *in vitro* phosphorylation experiments suggest that CDK1-mediated phosphorylation renders this region incompetent for membrane interaction (Figure 3B). It is therefore possible that this mitotic phosphorylation weakens the interaction of Nup53 with the pore membrane to facilitate NPC disassembly during prophase.

Proteins without integral membrane regions can associate with cellular membranes by a variety of mechanisms (Cho and Stahelin, 2005). First, they can be covalently attached to a lipid moiety. However, we have no indication that Nup53 is modified in such a way. Second, peripheral membrane proteins are recruited to the lipid bilayer by specific protein–lipid interactions that involve binding to particular lipid head groups. In this regard, lipid arrays performed to date have not demonstrated an affinity of Nup53 for any specific lipid (unpublished observation). Furthermore, recombinant Nup53 binds to liposomes prepared from different lipid sources like pure DOPC (1,2-dioleoyl-*sn*-glycero-3-phosphocholine), a lipid mixture mimicking the ER/NE lipid composition (Franke *et al*, 1970; Supplementary Figure S7) or folch fraction I (unpublished observation). Third, some proteins are recruited to membranes via electrostatic interactions. As a fraction of the lipid head groups are negatively charged this involves positively charged clusters on the protein surface. Indeed, we found that the first membrane binding region of Nup53 contains such a cluster. Replacing these positive with negative residues as well as introducing negative charge by phosphorylation rendered this site incapable of membrane interaction (Figure 3A and B). Finally, peripheral membrane proteins can associate with lipid bilayers via hydrophobic regions. It has been suggested that the C-terminal region of Nup53 contains an amphipathic helix, which could serve as a hydrophobic module (Marelli *et al*, 2001; Patel and Rexach, 2008). In fact, the C-terminus of Nup53 contains a membrane binding region and deleting the last eight amino acids abolished its membrane interaction. Deletion of the C-terminal tryptophan only slightly reduced membrane binding of Nup53 in the full-length protein (Figure 3C), but inhibited interphasic NPC assembly (Figure 5) suggesting that this residue fulfills an important additional function. Indeed, the insertion of hydrophobic parts of a protein into a membrane is one of several mechanisms by which proteins can deform membranes (McMahon and Gallop, 2005). Our data suggest that the C-terminal membrane binding region and especially the last tryptophan of Nup53 fulfills this task (Figure 6A). Interestingly, *in vivo* intranuclear tubular membranes are induced upon overexpression of yeast Nup53p which is dependent on its C-terminus (Marelli *et al*, 2001). Thus, Nup53 might not only have an important function in binding to the pore membrane in turn promoting the recruitment of other nucleoporins, especially members of the Nup93 complex, but may additionally function to deform the NE membrane into a pore. In the latter instance, the insertion of the Nup53 C-terminus into the hydrophobic phase of the membrane would result in displacement of lipid head groups and reorientation of the hydrophobic lipid side chains, bending the lipid bilayer into a convex shape and inducing membrane curvature necessary to form and stabilize the pore (Antonin *et al*, 2008). The doughnut-like shape of the pore requires likewise stabilization of a concave curvature in the plane of the pore in addition to the convex curved membrane

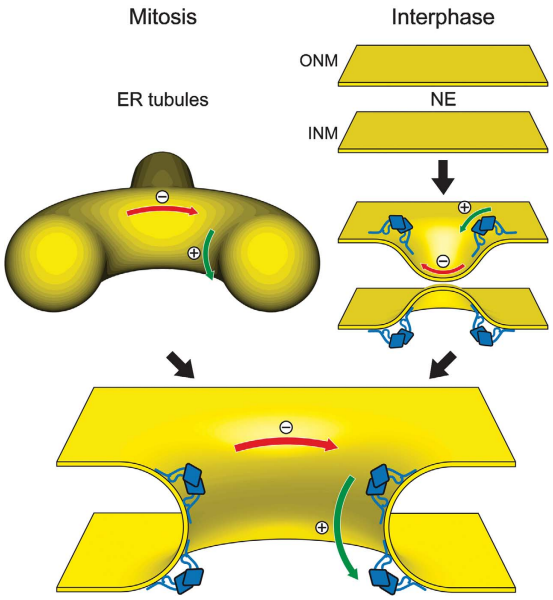

Figure 7 The role of Nup53 in NPC assembly. Schematic drawing of the postmitotic and interphasic modes of nuclear pore assembly focused on the membrane interacting function of Nup53. For the sake of clarity other membrane associated and integral proteins, including nucleoporins, participating in this process are omitted. Left pathway: after mitosis, outgrowing ER tubules (yellow) surround assembling NPCs providing negative/concave (red) and positive/convex (green) curvature which is stabilized by membrane binding Nup53 dimers (blue) for pore formation. Right pathway: in interphase, the intact nuclear envelope membranes (yellow) are deformed by the C-terminal membrane binding site of Nup53 introducing a convex membrane curvature for the approximation and following fusion of the two membranes leading to pore formation.

connection between outer and inner nuclear membrane (see Figure 7). This curvature might be induced and stabilized by a number of at least partially redundant mechanisms, such as formation of a coat-like structure by the Nup107–160 complex (Devos *et al*, 2004; Mans *et al*, 2004; Brohawn *et al*, 2008) or oligomerization of pore membrane proteins, although it is not clear how the different proteins contribute to the different modes of membrane bending. Similarly, in the context of the protein interaction network of an assembled NPC the N-terminal membrane binding region of Nup53, in addition to membrane interaction, might induce and/or stabilize curved membranes. Indeed, Nup53 is only functional when it dimerizes probably because this increases the avidity of the Nup53 membrane interaction. In addition, all the factors might also impose geometrical constrains to the membranes supporting a pore structure.

Although either one of the two membrane binding regions of Nup53 is sufficient for postmitotic NPC assembly and stability, the C-terminal site is specifically required for NPC assembly during interphase. It is a matter of debate whether NPC assembly during these different cell-cycle phases occurs by distinct mechanisms (Doucet *et al*, 2010; Dultz and Ellenberg, 2010; Lu *et al*, 2011). At the end of mitosis, NPC assembly occurs concomitantly with formation of a closed NE. It is possible that this mode of NPC formation does not require fusion between the outer and inner nuclear membrane to form a nuclear pore, in contrast to interphasic NPC assembly. Postmitotic pore assembly could rather arise by the enclosement of the assembling NPCs on the chromatin surface by an outgrowing ER network. In this scenario, Nup53 would stabilize the membrane curvature provided by the ER tubules rather than induce membrane deformation (see Figure 7, left pathway). The different requirements for Nup53 membrane binding regions in postmitotic and interphasic NPC assembly support the view of two different mechanistic pathways. A loss of the membrane deforming capability of Nup53 in postmitotic NPC assembly and NPC stability might be compensated by other factors such as the Nup107–160 complex or integral membrane proteins. However, during metazoan interphasic NPC assembly Nup53-mediated membrane deformation might be crucial for the initial approximation and/or fusion of both membrane layers (see Figure 7, right pathway). Interestingly, ER bending proteins of the reticulon family that induce convex membrane curvature (Hu *et al*, 2008) were shown to be important for NPC assembly into the intact NE both in yeast and in vertebrates (Dawson *et al*, 2009). Currently, it is unknown whether these proteins do also contribute to postmitotic NPC assembly. As their effect on ER membrane reorganization at the end of mitosis is a prerequisite for NE reformation (Anderson and Hetzer, 2008) it is difficult to separate these two functions. Finally, how the fusion of outer and inner nuclear membranes is achieved is largely unclear but our results suggest that Nup53, importantly its C-terminal membrane binding region, is critical for this process.

Materials and methods

Antibodies against POM121 and GP210 (Antonin *et al*, 2005), NDC1 (Mansfeld *et al*, 2006), Nup155 (Franz *et al*, 2005), MEL28/ELYS (Franz *et al*, 2007), Nup107 (Walther *et al*, 2003), Nup53 and Nup58 (Sachdev *et al*, 2012) as well as Nup188, Nup205, Nup98 and Nup53 (Theerthagiri *et al*, 2010) have been described. mAB414 and Nup88 antibodies were from Babco or BD Bioscience, respectively. For quantitation of Nup53 liposomes binding the antibody was affinity purified with a fragment comprising the RRM domain as this domain is included in all tested fragments (please see Supplementary Table S2 for list of all DNA constructs used in this study).

Nuclear assemblies

Nuclear assemblies and immunofluorescence (Theerthagiri *et al*, 2010), generation of affinity resins, sperm heads and floated membranes (Franz *et al*, 2005) as well as prelabelled membranes (Antonin *et al*, 2005) were done as described. Interphasic NPC assembly using dextran influx was monitored as described (Dawson *et al*, 2009) except that mock or Nup53-depleted extracts were incubated with 1.5 vol WGA-Agarose (Sigma) for 40 min. Counting of NPCs was performed on mAB414-labelled nuclei as described (Theerthagiri *et al*, 2010).

Protein expression and purification

Constructs for full-length Xenopus Nup53 and fragments, *S. cerevisiae* Nup53 and Nup59 were generated from a synthetic DNA optimized for codon usage in *E. coli* (Geneart, see Supplementary data) and cloned into a modified pET28a vector with a yeast SUMO solubility tag followed by a TEV site upstream of the Nup53 fragments. Proteins were expressed in *E. coli*, purified using Ni-agarose, His_6 and SUMO tags were cleaved by TEV protease, concentrated using VIVASPIN columns (Sartorius) and purified by gel filtration (Superdex200 10/300 GL or Superdex200 PC 3.2/30, GE Healthcare) either in PBS for liposome binding experiments or in sucrose buffer (Theerthagiri *et al*, 2010) for nuclear assemblies, respectively. Nup53 fragments aa 162–320 and aa 254–320 were purified by size exclusion chromatography without removal of the tags to retain stability. Fragments of Xenopus Nup98 (aa 676-863) as well as human Nup133 (aa 67–514) (Berke *et al*, 2004) were expressed from modified pET28a vectors with a His_6-NusA or

His_6 tag, which was cleaved of by thrombin or precision protease, respectively.

Liposome generation and flotation

E. coli polar lipid extract with 0.2 mol% 18:1–12:0 NBD-PE (1-oleoyl-2-{12-[(7-nitro-2-1,3-benzoxadiazol-4-yl)amino]dodecanoyl}-sn-glycero-3-phosphoethanolamine) (Avanti polar lipids) were dissolved in ethanol at 45°C. To form liposomes, the mixture was diluted 10-fold into PBS resulting in a final lipid concentration of 6.7 mg/ml while gently agitating. Liposomes were passed 21 × through Nuclepore Track-Etched Membranes (Whatman) with defined pore sizes (50, 100, 200, 400, 800 nm) at 45°C using the Avanti Mini-Extruder. To remove ethanol, liposomes were dialysed against PBS using Spectra/Por 2 dialysis tubing (MWCO 12-14 kDa). Liposome sizes were determined by light scattering using the AvidNano W130i. For quantitation of liposome binding, fluorescence intensity of the protein/liposome mixture and the top fraction was determined using a Molecular Imager VersaDoc MP 4000 Imaging System and ImageJ.

Folch fraction I lipids (Sigma) dissolved in chloroform were dried on a rotary evaporator and overnight under vacuum. PBS buffer was gently added to result in a final lipid concentration of 10 mg/ml. After 2 h of incubation at 37°C to allow spontaneous liposome formation the flask was agitated to dissolve residual lipids. After 10 cycles of freeze/thawing, liposomes were diluted 10-fold in PBS and extruded as described before.

Immunoprecipitation

Xenopus Nup53 as well as the RRM dimerization mutant (F172E/W203E) was cloned with N-terminal myc or HA tag, respectively, into a pSI vector (Promega). HeLa cells were transfected using Fugene 6 (Roche) following manufacturer's instructions, harvested 24 h post transfection and solubilized in 1% Triton X-100 in PBS supplemented with protease inhibitors (2 μg/ml leupeptin, 1 μg/ml pepstatin, 2 μg/ml aprotinin, 0.1 mg/ml AEBSF final concentration) for 10 min at 4°C. After centrifugation for 10 min at 15 000 *g* samples were diluted five-fold in PBS and employed for immunoprecipitation using α-myc or α-HA antibodies (Roche).

Miscellaneous

For *in vitro* phosphorylation, 3 μM proteins were incubated with 0.33 U/μl CDK1-CyclinB (NEB), 1 mM ATP, 10 mM $MgCl_2$ and 1 mM EDTA in PBS for 1 h at 30°C.

For liposome tubulation copper grids filmed with pioloform and carbon-coated were glow discharged before usage. Proteins were incubated with 1 mg/ml folch fraction I liposomes for 7 min on grids, washed with buffer (10 mM Hepes, 150 mM NaCl, 4.5 mM KCl) and stained with 2% UAc for 2 min and examined on a FEI Technai spirit 120 kV microscope.

Supplementary data

Supplementary data are available at *The EMBO Journal* Online (http://www.embojournal.org).

Acknowledgements

We thank M Flötenmeyer and S Würtenberger for help with the tubulation assay, B Uluvar for support in protein purification and M Lorenz for critical reading of the manuscript.

Author contributions: BV and WA designed and performed experiments and wrote the manuscript. AS quantified interphasic NPC assembly, RS and NE performed pull-down experiments, AMS performed the size determinations of the RRM domains. CS cloned constructs and prepared *Xenopus laevis* extracts. JM and BM performed mass spec analysis, UG performed measurements of different liposome sizes.

Conflict of interest

The authors declare that they have no conflict of interest.

References

Amlacher S, Sarges P, Flemming D, van Noort V, Kunze R, Devos DP, Arumugam M, Bork P, Hurt E (2011) Insight into structure and assembly of the nuclear pore complex by utilizing the genome of a eukaryotic thermophile. *Cell* **146:** 277–289

Anderson DJ, Hetzer MW (2008) Reshaping of the endoplasmic reticulum limits the rate for nuclear envelope formation. *J Cell Biol* **182:** 911–924

Anderson DJ, Vargas JD, Hsiao JP, Hetzer MW (2009) Recruitment of functionally distinct membrane proteins to chromatin mediates nuclear envelope formation *in vivo*. *J Cell Biol* **186:** 183–191

Antonin W, Ellenberg J, Dultz E (2008) Nuclear pore complex assembly through the cell cycle: regulation and membrane organization. *FEBS Lett* **582:** 2004–2016

Antonin W, Franz C, Haselmann U, Antony C, Mattaj IW (2005) The integral membrane nucleoporin pom121 functionally links nuclear pore complex assembly and nuclear envelope formation. *Mol Cell* **17:** 83–92

Berke IC, Boehmer T, Blobel G, Schwartz TU (2004) Structural and functional analysis of Nup133 domains reveals modular building blocks of the nuclear pore complex. *J Cell Biol* **167:** 591–597

Bilokapic S, Schwartz TU (2012) 3D ultrastructure of the nuclear pore complex. *Curr Opin Cell Biol* **24:** 86–91

Blethrow JD, Glavy JS, Morgan DO, Shokat KM (2008) Covalent capture of kinase-specific phosphopeptides reveals Cdk1-cyclin B substrates. *Proc Natl Acad Sci USA* **105:** 1442–1447

Brohawn SG, Leksa NC, Spear ED, Rajashankar KR, Schwartz TU (2008) Structural evidence for common ancestry of the nuclear pore complex and vesicle coats. *Science* **322:** 1369–1373

Cho W, Stahelin RV (2005) Membrane-protein interactions in cell signaling and membrane trafficking. *Annu Rev Biophys Biomol Struct* **34:** 119–151

Cronshaw JM, Krutchinsky AN, Zhang W, Chait BT, Matunis MJ (2002) Proteomic analysis of the mammalian nuclear pore complex. *J Cell Biol* **158:** 915–927

D'Angelo MA, Anderson DJ, Richard E, Hetzer MW (2006) Nuclear pores form de novo from both sides of the nuclear envelope. *Science* **312:** 440–443

Daumke O, Lundmark R, Vallis Y, Martens S, Butler PJ, McMahon HT (2007) Architectural and mechanistic insights into an EHD ATPase involved in membrane remodelling. *Nature* **449:** 923–927

Dawson TR, Lazarus MD, Hetzer MW, Wente SR (2009) ER membrane-bending proteins are necessary for de novo nuclear pore formation. *J Cell Biol* **184:** 659–675

DeGrasse JA, DuBois KN, Devos D, Siegel TN, Sali A, Field MC, Rout MP, Chait BT (2009) Evidence for a shared nuclear pore complex architecture that is conserved from the last common eukaryotic ancestor. *Mol Cell Proteomics* **8:** 2119–2130

Devos D, Dokudovskaya S, Alber F, Williams R, Chait BT, Sali A, Rout MP (2004) Components of coated vesicles and nuclear pore complexes share a common molecular architecture. *PLoS Biol* **2:** e380

Doucet CM, Hetzer MW (2010) Nuclear pore biogenesis into an intact nuclear envelope. *Chromosoma* **119:** 469–477

Doucet CM, Talamas JA, Hetzer MW (2010) Cell cycle-dependent differences in nuclear pore complex assembly in metazoa. *Cell* **141:** 1030–1041

Drin G, Casella JF, Gautier R, Boehmer T, Schwartz TU, Antonny B (2007) A general amphipathic alpha-helical motif for sensing membrane curvature. *Nat Struct Mol Biol* **14:** 138–146

Dultz E, Ellenberg J (2010) Live imaging of single nuclear pores reveals unique assembly kinetics and mechanism in interphase. *J Cell Biol* **191:** 15–22

Dultz E, Zanin E, Wurzenberger C, Braun M, Rabut G, Sironi L, Ellenberg J (2008) Systematic kinetic analysis of mitotic dis- and reassembly of the nuclear pore in living cells. *J Cell Biol* **180:** 857–865

Fahrenkrog B, Hubner W, Mandinova A, Pante N, Keller W, Aebi U (2000) The yeast nucleoporin Nup53p specifically interacts with

Nic96p and is directly involved in nuclear protein import. *Mol Biol Cell* **11:** 3885–3896

Field MC, Sali A, Rout MP (2011) Evolution: on a bender–BARs, ESCRTs, COPs, and finally getting your coat. *J Cell Biol* **193:** 963–972

Franke WW, Deumling B, Baerbelermen, Jarasch ED, Kleinig H (1970) Nuclear membranes from mammalian liver. I. Isolation procedure and general characterization. *J Cell Biol* **46:** 379–395

Franz C, Askjaer P, Antonin W, Iglesias CL, Haselmann U, Schelder M, de Marco A, Wilm M, Antony C, Mattaj IW (2005) Nup155 regulates nuclear envelope and nuclear pore complex formation in nematodes and vertebrates. *EMBO J* **24:** 3519–3531

Franz C, Walczak R, Yavuz S, Santarella R, Gentzel M, Askjaer P, Galy V, Hetzer M, Mattaj IW, Antonin W (2007) MEL-28/ELYS is required for the recruitment of nucleoporins to chromatin and postmitotic nuclear pore complex assembly. *EMBO Rep* **8:** 165–172

Galy V, Askjaer P, Franz C, López-Iglesias C, Mattaj IW (2006) MEL-28, a novel nuclear envelope and kinetochore protein essential for zygotic nuclear envelope assembly in C. elegans. *Curr Biol* **16:** 1748–1756

Galy V, Mattaj IW, Askjaer P (2003) Caenorhabditis elegans nucleoporins Nup93 and Nup205 determine the limit of nuclear pore complex size exclusion *in vivo*. *Mol Biol Cell* **14:** 5104–5115

Handa N, Kukimoto-Niino M, Akasaka R, Kishishita S, Murayama K, Terada T, Inoue M, Kigawa T, Kose S, Imamoto N, Tanaka A, Hayashizaki Y, Shirouzu M, Yokoyama S (2006) The crystal structure of mouse Nup35 reveals atypical RNP motifs and novel homodimerization of the RRM domain. *J Mol Biol* **363:** 114–124

Hawryluk-Gara LA, Platani M, Santarella R, Wozniak RW, Mattaj IW (2008) Nup53 is required for nuclear envelope and nuclear pore complex assembly. *Mol Biol Cell* **19:** 1753–1762

Hawryluk-Gara LA, Shibuya EK, Wozniak RW (2005) Vertebrate Nup53 interacts with the nuclear lamina and is required for the assembly of a Nup93-containing complex. *Mol Biol Cell* **16:** 2382–2394

Hoelz A, Debler EW, Blobel G (2011) The structure of the nuclear pore complex. *Annu Rev Biochem* **80:** 613–643

Hu J, Shibata Y, Voss C, Shemesh T, Li Z, Coughlin M, Kozlov MM, Rapoport TA, Prinz WA (2008) Membrane proteins of the endoplasmic reticulum induce high-curvature tubules. *Science* **319:** 1247–1250

Liu HL, De Souza CP, Osmani AH, Osmani SA (2009) The three fungal transmembrane nuclear pore complex proteins of Aspergillus nidulans are dispensable in the presence of an intact An-Nup84-120 complex. *Mol Biol Cell* **20:** 616–630

Lohka MJ (1998) Analysis of nuclear envelope assembly using extracts of Xenopus eggs. *Methods Cell Biol* **53:** 367–395

Lu L, Ladinsky MS, Kirchhausen T (2011) Formation of the postmitotic nuclear envelope from extended ER cisternae precedes nuclear pore assembly. *J Cell Biol* **194:** 425–440

Lusk CP, Makhnevych T, Marelli M, Aitchison JD, Wozniak RW (2002) Karyopherins in nuclear pore biogenesis: a role for Kap121p in the assembly of Nup53p into nuclear pore complexes. *J Cell Biol* **159:** 267–278

Lusk CP, Waller DD, Makhnevych T, Dienemann A, Whiteway M, Thomas DY, Wozniak RW (2007) Nup53p is a target of two mitotic kinases, Cdk1p and Hrr25p. *Traffic* **8:** 647–660

Mans BJ, Anantharaman V, Aravind L, Koonin EV (2004) Comparative genomics, evolution and origins of the nuclear envelope and nuclear pore complex. *Cell Cycle* **3:** 1612–1637

Mansfeld J, Guttinger S, Hawryluk-Gara LA, Pante N, Mall M, Galy V, Haselmann U, Muhlhausser P, Wozniak RW, Mattaj IW, Kutay U, Antonin W (2006) The conserved transmembrane nucleoporin NDC1 is required for nuclear pore complex assembly in vertebrate cells. *Mol Cell* **22:** 93–103

Marelli M, Aitchison JD, Wozniak RW (1998) Specific binding of the karyopherin Kap121p to a subunit of the nuclear pore complex containing Nup53p, Nup59p, and Nup170p. *J Cell Biol* **143:** 1813–1830

Marelli M, Lusk CP, Chan H, Aitchison JD, Wozniak RW (2001) A link between the synthesis of nucleoporins and the biogenesis of the nuclear envelope. *J Cell Biol* **153:** 709–724

McMahon HT, Gallop JL (2005) Membrane curvature and mechanisms of dynamic cell membrane remodelling. *Nature* **438:** 590–596

McMahon HT, Mills IG (2004) COP and clathrin-coated vesicle budding: different pathways, common approaches. *Curr Opin Cell Biol* **16:** 379–391

Miao M, Ryan KJ, Wente SR (2006) The integral membrane protein Pom34p functionally links nucleoporin subcomplexes. *Genetics* **172:** 1441–1457

Mitchell JM, Mansfeld J, Capitanio J, Kutay U, Wozniak RW (2010) Pom121 links two essential subcomplexes of the nuclear pore complex core to the membrane. *J Cell Biol* **191:** 505–521

Neumann N, Lundin D, Poole AM (2010) Comparative genomic evidence for a complete nuclear pore complex in the last eukaryotic common ancestor. *PLoS ONE* **5:** e13241

Onischenko E, Stanton LH, Madrid AS, Kieselbach T, Weis K (2009) Role of the Ndc1 interaction network in yeast nuclear pore complex assembly and maintenance. *J Cell Biol* **185:** 475–491

Onischenko E, Weis K (2011) Nuclear pore complex-a coat specifically tailored for the nuclear envelope. *Curr Opin Cell Biol* **23:** 293–301

Patel SS, Rexach MF (2008) Discovering novel interactions at the nuclear pore complex using bead halo: a rapid method for detecting molecular interactions of high and low affinity at equilibrium. *Mol Cell Proteomics* **7:** 121–131

Prufert K, Vogel A, Krohne G (2004) The lamin CxxM motif promotes nuclear membrane growth. *J Cell Sci* **117:** 6105–6116

Rasala BA, Orjalo AV, Shen Z, Briggs S, Forbes DJ (2006) ELYS is a dual nucleoporin/kinetochore protein required for nuclear pore assembly and proper cell division. *Proc Natl Acad Sci USA* **103:** 17801–17806

Rodenas E, Klerkx EP, Ayuso C, Audhya A, Askjaer P (2009) Early embryonic requirement for nucleoporin Nup35/NPP-19 in nuclear assembly. *Dev Biol* **327:** 399–409

Sachdev R, Sieverding C, Flotenmeyer M, Antonin W (2012) The C-terminal domain of Nup93 is essential for assembly of the structural backbone of nuclear pore complexes. *Mol Biol Cell* **23:** 740–749

Stavru F, Hulsmann BB, Spang A, Hartmann E, Cordes VC, Gorlich D (2006) NDC1: a crucial membrane-integral nucleoporin of metazoan nuclear pore complexes. *J Cell Biol* **173:** 509–519

Stukenberg PT, Lustig KD, McGarry TJ, King RW, Kuang J, Kirschner MW (1997) Systematic identification of mitotic phosphoproteins. *Curr Biol* **7:** 338–348

Theerthagiri G, Eisenhardt N, Schwarz H, Antonin W (2010) The nucleoporin Nup188 controls passage of membrane proteins across the nuclear pore complex. *J Cell Biol* **189:** 1129–1142

Walther TC, Alves A, Pickersgill H, Loiodice I, Hetzer M, Galy V, Hulsmann BB, Kocher T, Wilm M, Allen T, Mattaj IW, Doye V (2003) The conserved Nup107-160 complex is critical for nuclear pore complex assembly. *Cell* **113:** 195–206

Wente SR, Rout MP (2010) The nuclear pore complex and nuclear transport. *Cold Spring Harb Perspect Biol* **2:** a000562

West RR, Vaisberg EV, Ding R, Nurse P, McIntosh JR (1998) cut11(+): A gene required for cell cycle-dependent spindle pole body anchoring in the nuclear envelope and bipolar spindle formation in Schizosaccharomyces pombe. *Mol Biol Cell* **9:** 2839–2855

Winey M, Hoyt MA, Chan C, Goetsch L, Botstein D, Byers B (1993) NDC1: a nuclear periphery component required for yeast spindle pole body duplication. *J Cell Biol* **122:** 743–751

Yavuz S, Santarella-Mellwig R, Koch B, Jaedicke A, Mattaj IW, Antonin W (2010) NLS-mediated NPC functions of the nucleoporin Pom121. *FEBS Lett* **584:** 3292–3298

Supplementary Information

Dimerization and direct membrane interaction of Nup53 contribute to nuclear pore complex assembly

Benjamin Vollmer[1], Allana Schooley[1], Ruchika Sachdev[1], Nathalie Eisenhardt[1], Anna Schneider[2], Cornelia Sieverding[1], Johannes Madlung[3], Uwe Gerken[4,5], Boris Macek[3], Wolfram Antonin[1,6]

[1] Friedrich Miescher Laboratory of the Max Planck Society, Spemannstraße 39, 72076 Tübingen, Germany

[2] Max Planck Institute for Developmental Biology, Spemannstraße 35, 72076 Tübingen, Germany

[3] Proteome Center Tübingen, University of Tübingen, 72076 Tübingen, Germany

[4] Institute of Microbiology, University of Hohenheim, Garbenstrasse 30, 70599 Stuttgart, Germany

[5] Present address: Lehrstuhl für Experimentalphysik IV, University of Bayreuth, Universitätsstrasse 30, 95447 Bayreuth

[6] author for correspondence: wolfram.antonin@tuebingen.mpg.de

Supplementary information contains:

Supplementary Figures S1–S7 & Table S1–S2

Supplementary Methods

Supplementary References

Supplementary Figure S1

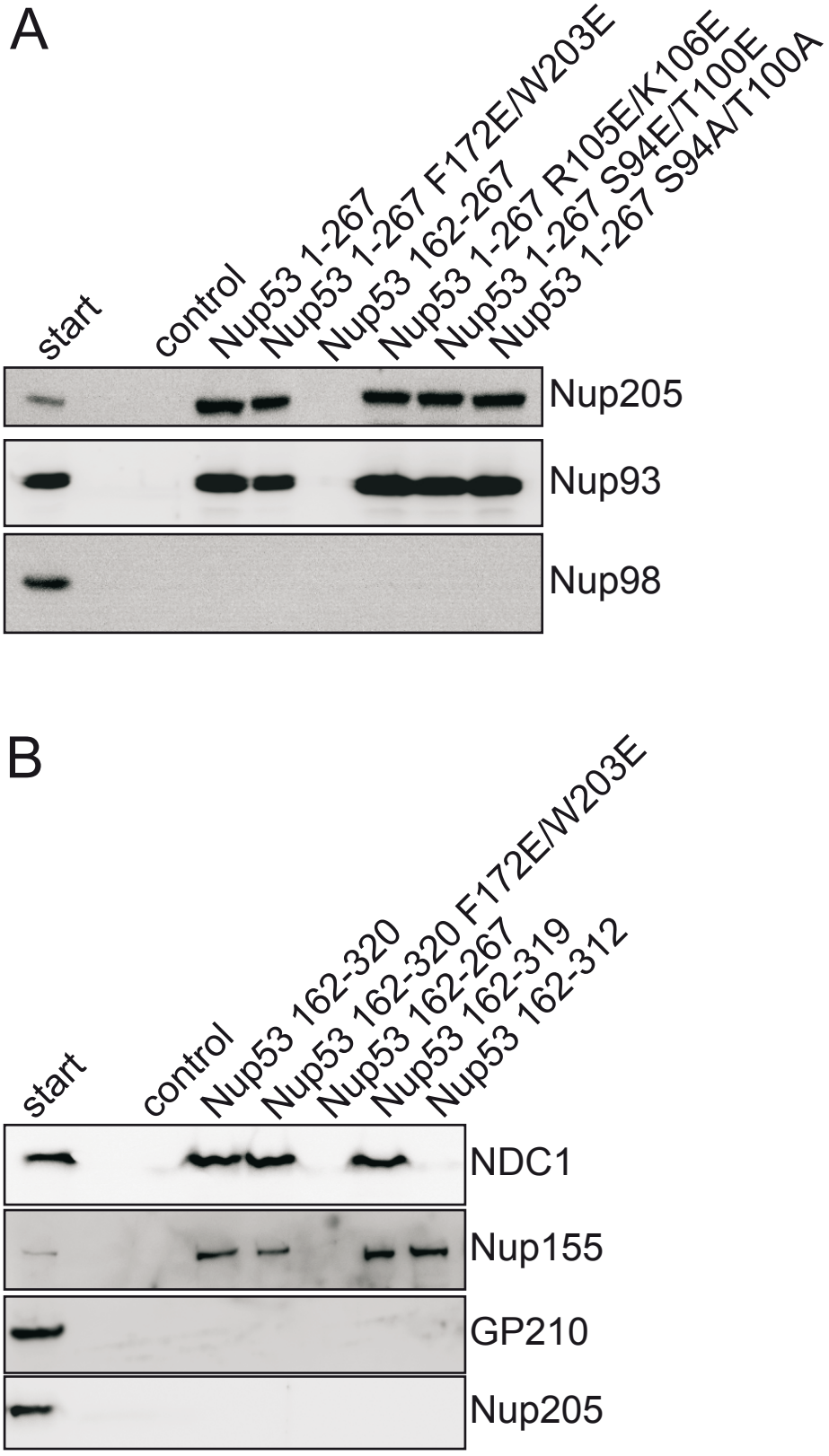

Figure S1

Nup53 has different binding sites for membrane and protein interaction.

(A) GST fusions of an N-terminal fragment of Xenopus Nup53 as well as Xenopus Nup98 (aa 487-634) (control) were incubated with cytosol from Xenopus egg extracts. Eluates were analyzed by western blotting with antibodies against the nucleoporins Nup205 and Nup93, known to bind this region, as well as Nup98 as a negative control. Please note that introducing amino acid changes causing the monomerization of Nup53 (F172E/W203E) also negatively influenced the interaction with Nup205 and Nup93. In contrast, mutations that inactivate the N-terminal membrane binding region (R105E/K106E and S94E/T100E) as well as the S94A/T100A control mutation did not interfere with Nup205 and Nup93 binding.

(B) GST fusions Xenopus Nup98 (aa 487-634) (control), the C-terminal fragment of Xenopus Nup53 (162-320), the RRM mutant (F172E/W203E) and C-terminal truncations were incubated with cytosol (for detection of Nup155 and Nup205) or Triton X-100 solubilized membranes (for NDC1 and GP210 detection) from Xenopus egg extracts. Eluates were analyzed by western blotting with antibodies against the nucleoporins Nup155 and NDC1, known to bind this region as well as Nup205 and GP210 as negative controls. Please note that mutation of the RRM domain (F172E/W203E) did not influence the interaction with NDC1 but results in a decreased binding to Nup155. The C-terminal truncations weakening the C-terminal membrane binding region (162-319 and 162-312) did not interfere with Nup155 binding and the 162-319 fragment was still able to interact with NDC1.

Supplementary Figure S2

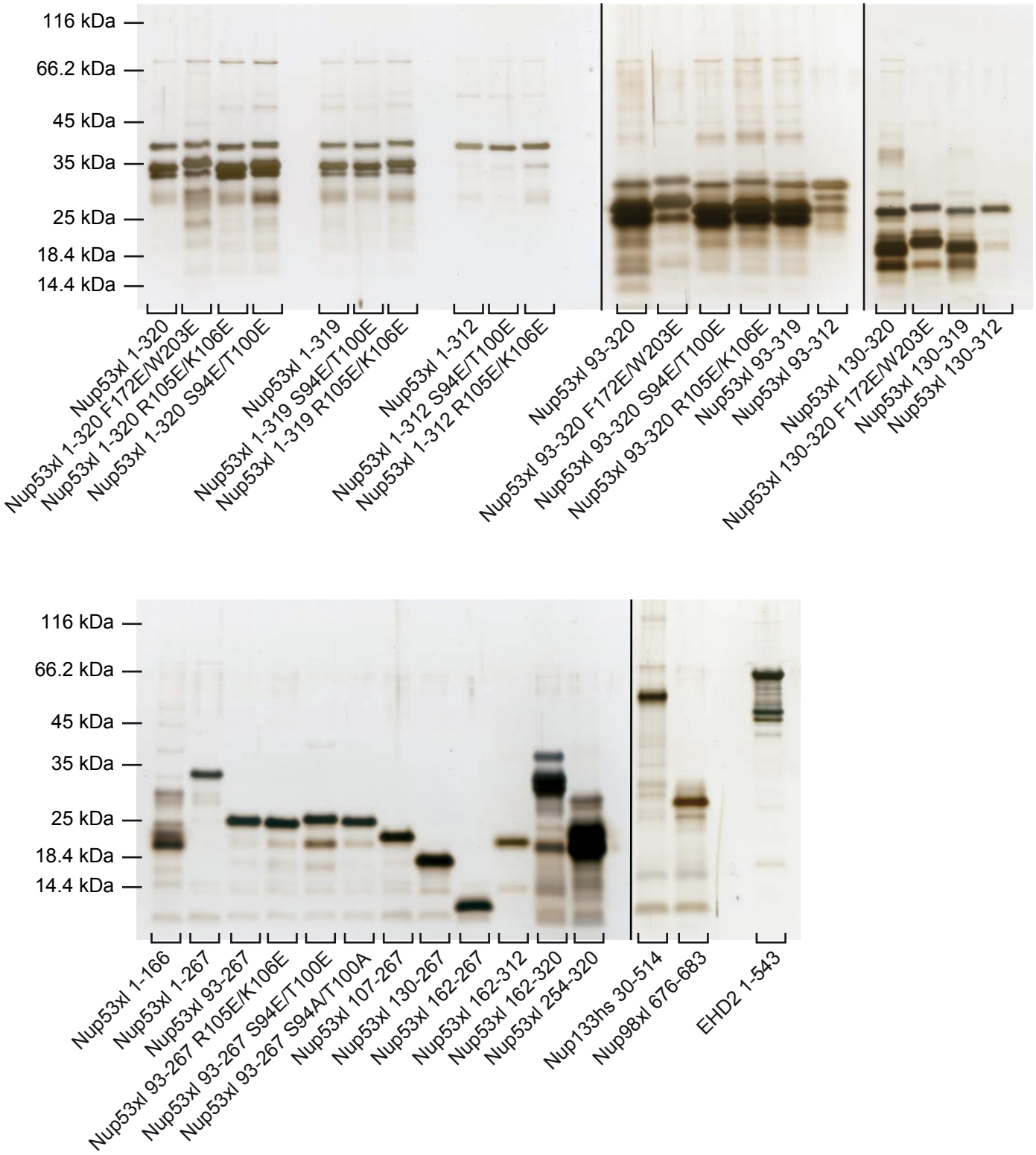

Figure S2

Proteins were separated on Tricine-SDS-PAGE Schägger gels (Schagger & von Jagow, 1987) followed by silver staining.

Supplementary Figure S3

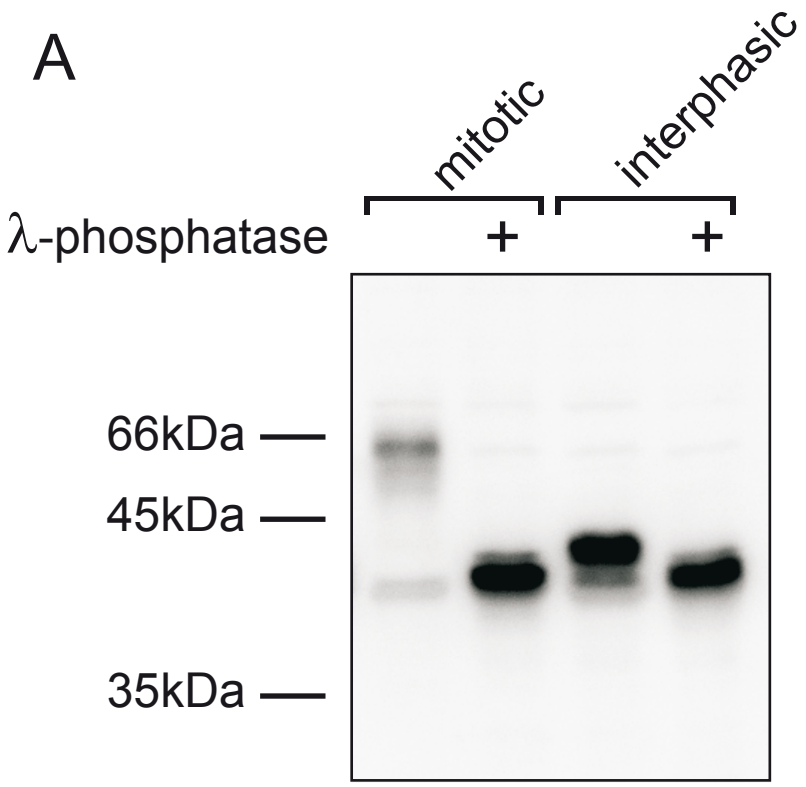

B

Protein IDs: gi_4584796;gi_148232142;gi_15987768;gi_nup53a;gi_nup53b;gi_32450351
Scannumber 8537
Source: 20101220_JM_CO_0221_R7_mitotic_01
Method: CID; ITMS

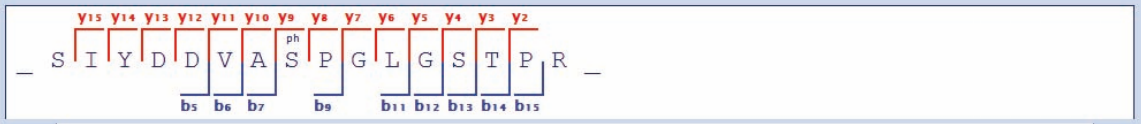

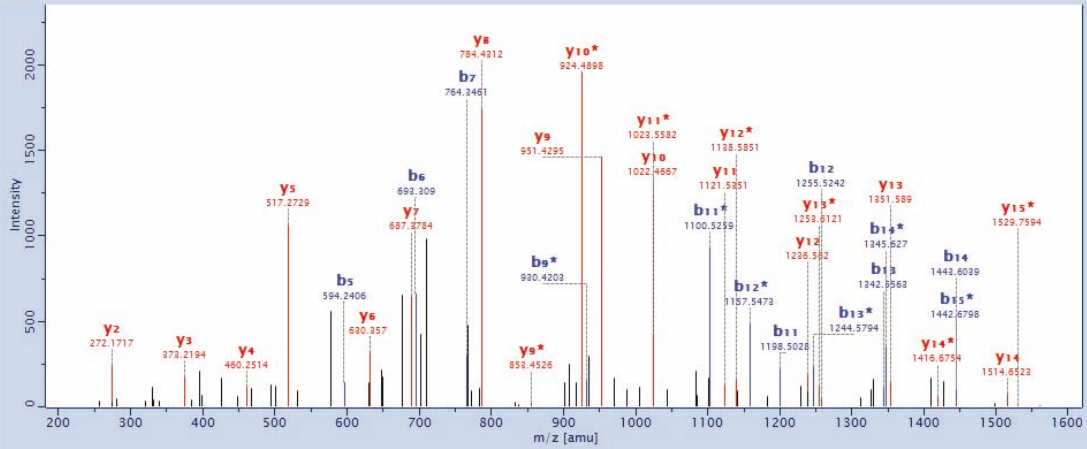

parent information

Mass:	1713.7611
m/z:	857.89
Charge:	2+
Mass Error [ppm]:	0.030899
PTM Score:	250.7
PEP:	7.5085E-41
Mascot Score:	100.54
Intensity:	13664197

general information

Annotation:	14 of 16 => 88 %
Intensity Coverage:	63 %
Protein Localisation:	89 ... 104

B-Ion					Y-Ion	
Δ Da	mass		seq		mass	Δ Da
NaN	88.0393049	1	S	16	NaN	NaN
NaN	201.1233689	2	I	15	1529.7594479	0.1181156
NaN	364.1866974	3	Y	14	1416.6753839	0.0124823
NaN	479.2136404	4	D	13	1253.6120554	0.0177054
0.310625	594.2405835	5	D	12	1138.5851123	0.0339649
0.1467521	693.3089974	6	V	11	1023.5581693	0.2597628
0.0844919	764.3461112	7	A	10	924.4897554	0.0853789
NaN	931.3444706	8	S	9	853.4526416	0.0651807
0.1978867	930.4203384	9	P	8	784.4311782	0.1097764
NaN	1085.4186981	10	G	7	687.3784143	0.0730627
0.1684698	1100.5258661	11	L	6	630.3569506	0.1070997
0.0851164	1157.5473299	12	G	5	517.2728866	0.1069351
0.0762814	1244.5793583	13	S	4	460.2514229	0.0053902
0.1205219	1345.6270367	14	T	3	373.2193945	0.0125464
0.1888518	1442.6798006	15	P	2	272.171716	0.0410398
NaN	NaN	16	R	1	175.1189522	NaN

Protein IDs: gi_4584796;gi_148232142;gi_15987768;gi_nup53a;gi_nup53b;gi_32450351
Scannumber 8673
Source: 20101126_CO_JM_0221WoAn_R5_IP_mitotic_01
Method: CID; ITMS

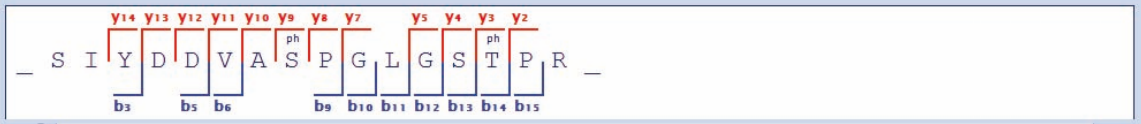

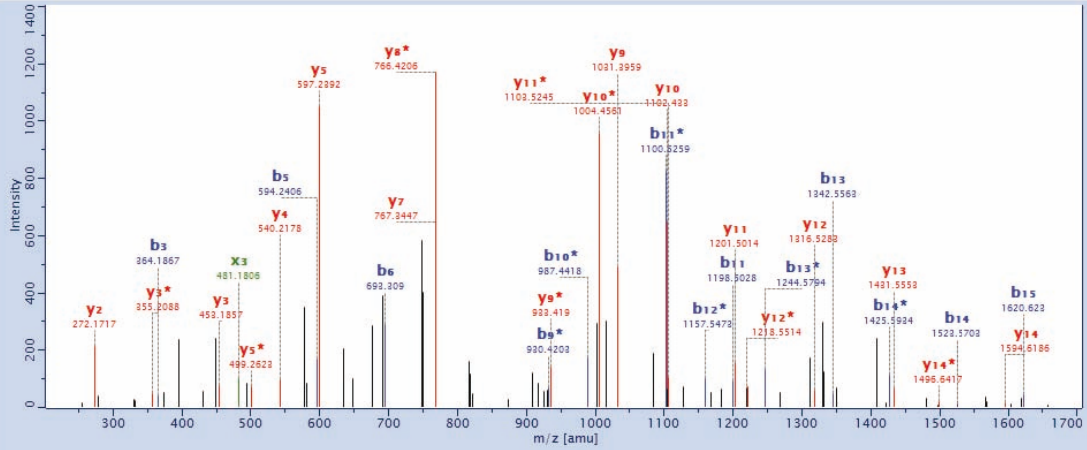

parent information

Mass:	1793.7274
m/z:	897.87
Charge:	2+
Mass Error [ppm]:	0.13197
PTM Score:	238.2
PEP:	8.3029E-53
Mascot Score:	51.05
Intensity:	18521420

general information

Annotation:	13 of 16 => 81 %
Intensity Coverage:	55 %
Protein Localisation:	89 ... 104

B-Ion					X-Ion		Y-Ion	
Δ Da	mass		seq		mass	Δ Da	mass	Δ Da
NaN	88.0393049	1	S	16	NaN	NaN	NaN	NaN
NaN	201.1233689	2	I	15	1733.6819395	NaN	1707.7026749	NaN
0.1353668	364.186697	3	Y	14	1620.5978755	NaN	1496.64171	0.2575771
NaN	479.2136404	4	D	13	1457.5345469	NaN	1431.55528	0.0981291
0.0384082	594.240583	5	D	12	1342.5076039	NaN	1218.55144	0.3596895
0.0780403	693.308997	6	V	11	1227.4806609	NaN	1103.5245	0.2493034
NaN	764.3461112	7	A	10	1128.412247	NaN	1004.45609	0.0672901
NaN	931.3444706	8	S	9	1057.3751332	NaN	933.418973	0.1262544
0.0214951	930.420338	9	P	8	890.3767738	NaN	766.420613	0.0788163
0.2336739	987.441802	10	G	7	793.3240099	NaN	767.344745	0.0776179
0.0236689	1100.52587	11	L	6	736.3025462	NaN	710.3232816	NaN
0.1385832	1157.54733	12	G	5	623.2184822	NaN	499.262322	0.0559618
0.0184452	1244.57936	13	S	4	566.1970185	NaN	540.217754	0.1073804
0.0542153	1425.59337	14	T	3	481.18064	0.1698237	355.20883	0.0389732
0.0871775	1620.62303	15	P	2	298.1509806	NaN	272.171716	0.0123227
NaN	NaN	16	R	1	201.0982167	NaN	175.1189522	NaN

Protein IDs: gi_4584796;gi_148232142;gi_15987768;gi_nup53a;gi_nup53b
Scannumber 5067
Source: 20101126_CO_JM_0221WoAn_R5_IP_mitotic_01
Method: CID; ITMS

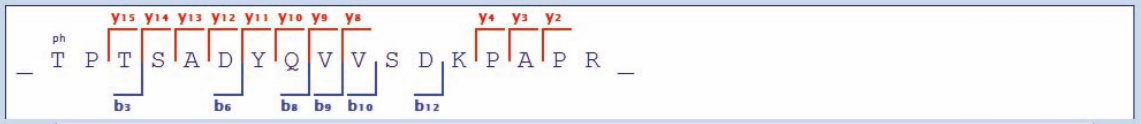

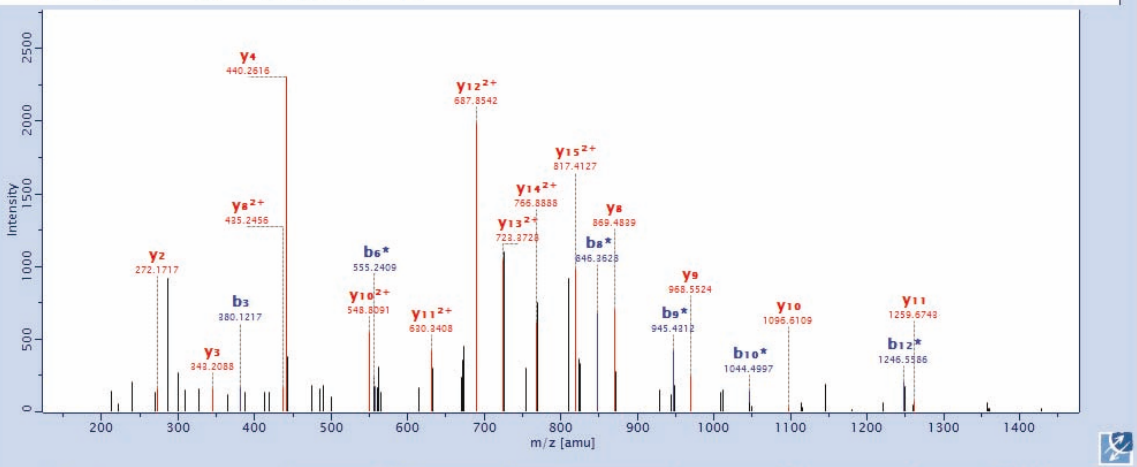

parent information

Mass:	1910.8775
m/z:	638.3
Charge:	3+
Mass Error [ppm]:	0.1223
PTM Score:	110.8
PEP:	5.3158E-06
Mascot Score:	37.4
Intensity:	1839497.9

general information

Annotation:	12 of 17 => 71 %
Intensity Coverage:	49 %
Protein Localisation:	288 ... 304

B-Ion					Y-Ion		Y-Ion²⁺	
Δ Da	mass		seq		mass	Δ Da	mass	Δ Da
NaN	182.0212859	1	T	17	NaN	NaN	NaN	NaN
NaN	279.0740498	2	P	16	1730.8707896	NaN	1730.8707896	NaN
0.0860354	**380.121728**	3	T	15	1633.8180257	NaN	**817.412651**	**0.3084793**
NaN	467.1537567	4	S	14	1532.7703472	NaN	**766.888812**	**0.0390804**
NaN	538.1908705	5	A	13	1445.7383188	NaN	**723.372798**	**0.0150096**
0.1898076	**555.240917**	6	D	12	1374.701205	NaN	**687.854241**	**0.315559**
NaN	816.281142	7	Y	11	**1259.67426**	**0.1249323**	**630.340769**	**0.0778099**
0.1566467	**846.362824**	8	Q	10	**1096.61093**	**0.0732137**	**548.809105**	**0.0020371**
0.0182254	**945.431237**	9	V	9	**968.552356**	**0.1522949**	968.552356	NaN
0.1110664	**1044.49965**	10	V	8	**869.483942**	**0.0255184**	**435.245609**	**0.0565758**
NaN	1229.5085758	11	S	7	770.4155281	NaN	770.4155281	NaN
0.2735886	**1246.55862**	12	D	6	683.3834997	NaN	683.3834997	NaN
NaN	1472.6304818	13	K	5	568.3565567	NaN	568.3565567	NaN
NaN	1569.6832457	14	P	4	**440.261594**	**0.0740997**	440.2615937	NaN
NaN	1640.7203595	15	A	3	**343.20883**	**0.0171794**	343.2088298	NaN
NaN	1737.7731233	16	P	2	**272.171716**	**0.1399295**	272.171716	NaN
NaN	NaN	17	R	1	175.1189522	NaN	175.1189522	NaN

Protein IDs: gi_4584796;gi_148232142;gi_15987768;gi_nup53a;gi_nup53b
Scannumber 5827
Source: 20101126_CO_JM_0221WoAn_R5_IP_mitotic_01
Method: CID; ITMS

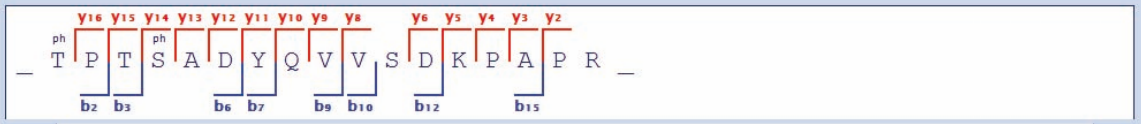

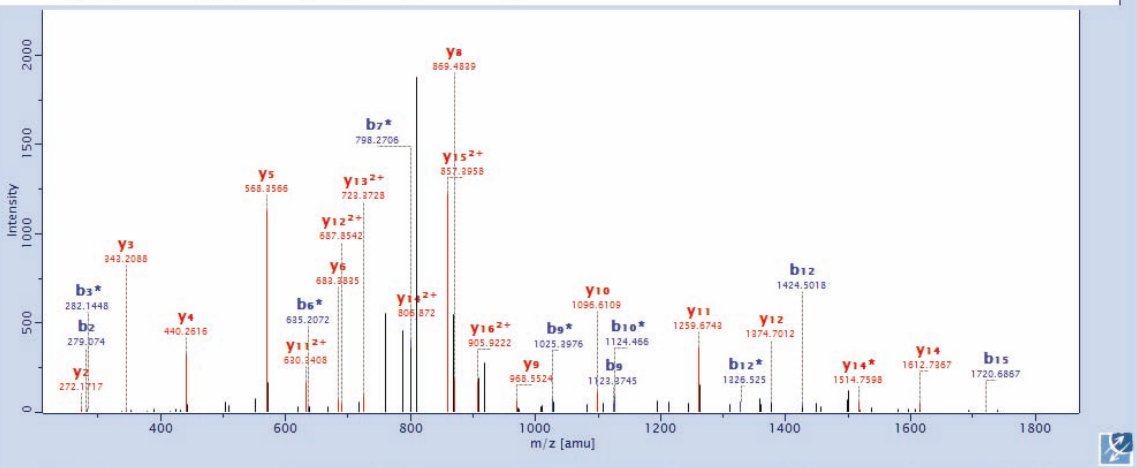

parent information

Mass:	1990.8439
m/z:	996.93
Charge:	2+
Mass Error [ppm]:	0.12316
PTM Score:	173.19
PEP:	3.1561E-23
Mascot Score:	52.53
Intensity:	723052.1

general information

Annotation:	14 of 17 => 82 %
Intensity Coverage:	46 %
Protein Localisation:	288 ... 304

B-Ion					Y-Ion		Y-Ion²⁺	
Δ Da	mass		seq		mass	Δ Da	mass	Δ Da
NaN	182.0212859	1	T	17	NaN	NaN	NaN	NaN
0.280595	**279.07405**	2	P	16	1810.8371206	NaN	**905.922199**	**0.03349**
0.2120625	**282.144832**	3	T	15	1713.7843567	NaN	**857.395817**	**0.1478846**
NaN	547.1200877	4	S	14	**1514.75978**	**0.204207**	**806.871977**	**0.2981887**
NaN	618.1572015	5	A	13	1445.7383188	NaN	**723.372798**	**0.4335988**
0.0729639	**635.207248**	6	D	12	**1374.70121**	**0.0788243**	**687.854241**	**0.1524731**
0.03962	**798.270577**	7	Y	11	**1259.67426**	**0.0252142**	**630.340769**	**0.1820579**
NaN	1024.3060505	8	Q	10	**1096.61093**	**0.1455363**	1096.6109335	NaN
0.0783546	**1025.39757**	9	V	9	**968.552356**	**0.0307739**	968.552356	NaN
0.1582852	**1124.46598**	10	V	8	**869.483942**	**0.1000423**	869.483942	NaN
NaN	1309.4749068	11	S	7	770.4155281	NaN	770.4155281	NaN
0.0591335	**1326.52495**	12	D	6	**683.3835**	**0.0513464**	683.3834997	NaN
NaN	1552.5968128	13	K	5	**568.356557**	**0.0124619**	568.3565567	NaN
NaN	1649.6495767	14	P	4	**440.261594**	**0.0915863**	440.2615937	NaN
0.2862099	**1720.68669**	15	A	3	**343.20883**	**0.1309529**	343.2088298	NaN
NaN	1817.7394543	16	P	2	**272.171716**	**0.0334842**	272.171716	NaN
NaN	NaN	17	R	1	175.1189522	NaN	175.1189522	NaN

Figure S3

(A) Nup53 is phosphorylated in interphase and mitosis

4 µl of mitotic (CSF arrested) or interphasic Xenopus egg extracts were diluted in 100 µl of phosphatase buffer (NEB) and incubated where indicated with 400 U λ-phosphatase for 30 min at 30°C. Samples were analyzed by 12% SDS-PAGE and Western blotting using the Xenopus Nup53 antibody. Please note the different shifting of mitotic and interphasic Nup53 after phosphatase treatment indicating that Nup53 is a phosphoprotein throughout the cell cycle but hyperphosphorylated during mitosis.

(B) Fragmentation mass spectra of Xenopus Nup53 peptides carrying mitotic specific phosphorylations

Supplementary Figure S4

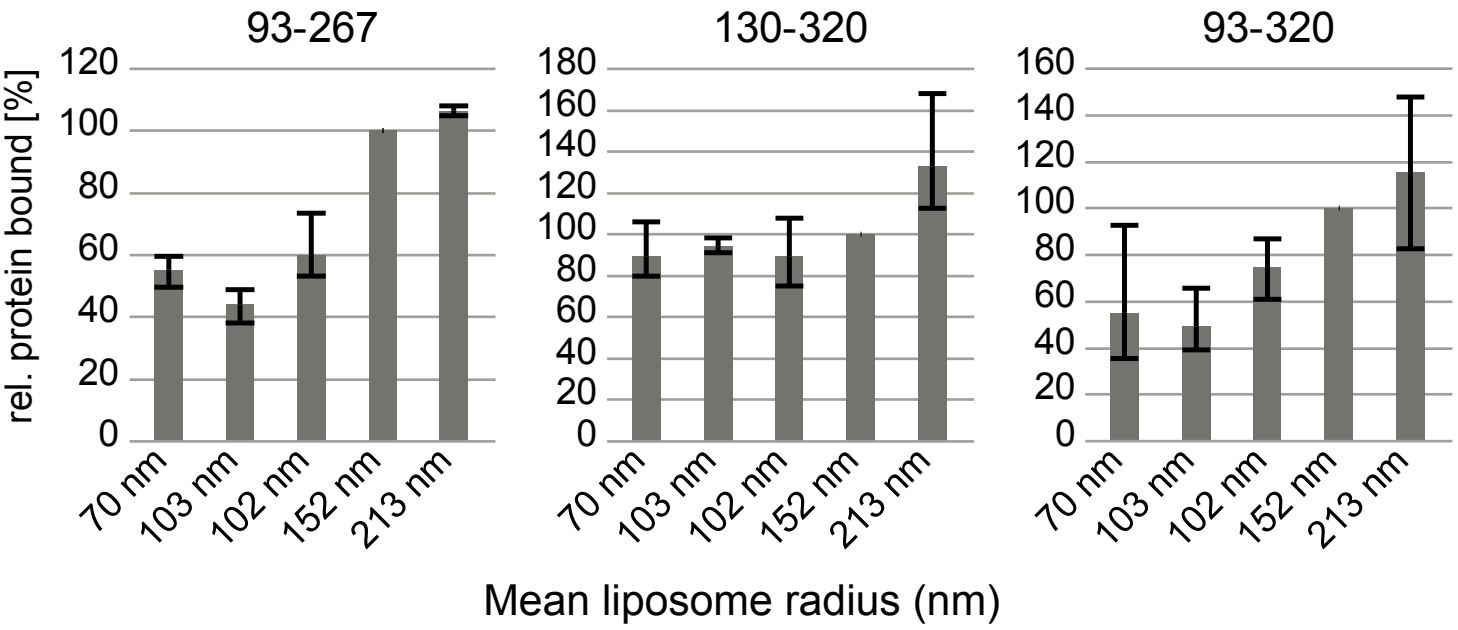

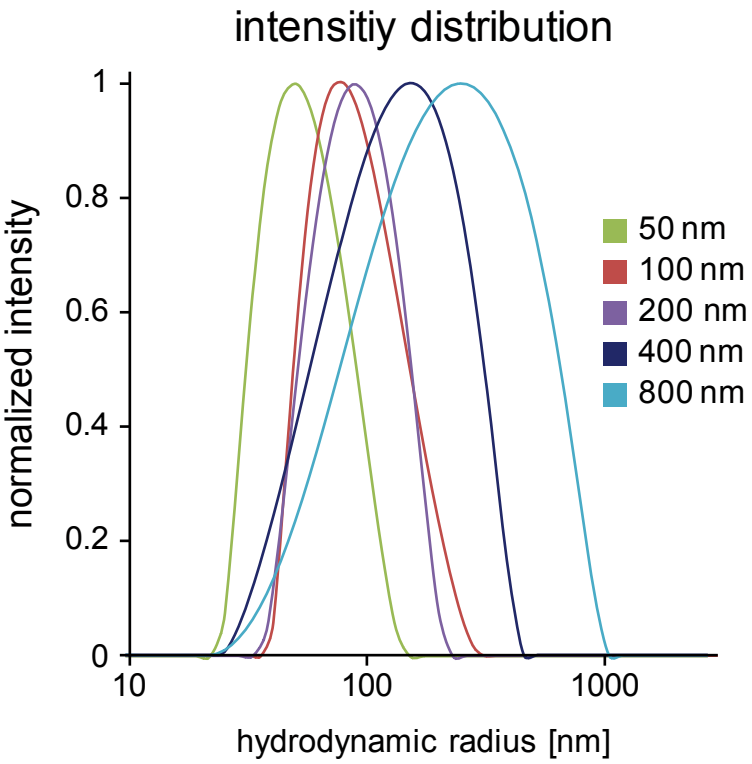

Figure S4

The two Nup53 membrane binding regions show different sensitivity to membrane curvature. Fragments comprising the N-terminal (93-267), C-terminal (130-320) or both (93-320) membrane binding sites, respectively, including the RRM domains were incubated with differently sized liposomes as indicated by the determined mean radii. Liposome binding was quantified as in Figure 2C. Whereas fragments which include the N-terminal membrane binding site (93-267 and 93-320) showed a significantly reduced binding to smaller liposome diameters and thus to higher membrane curvature this effect was not seen for the C-terminal membrane binding site (130-320). The averages of three independent experiments, normalized to the binding of the respective fragments to 150 nm liposomes, are shown. Error bars represent the range. Liposome radii were determined by light scattering after extrusion through membranes of different pore size as indicated for the different measurements. The lower panel shows one exemplary measurement done to determine the average radius of the respective preparation. Please note the rather similar average radii of liposomes prepared using 100 nm and 200 nm membranes.

Supplementary Figure S5

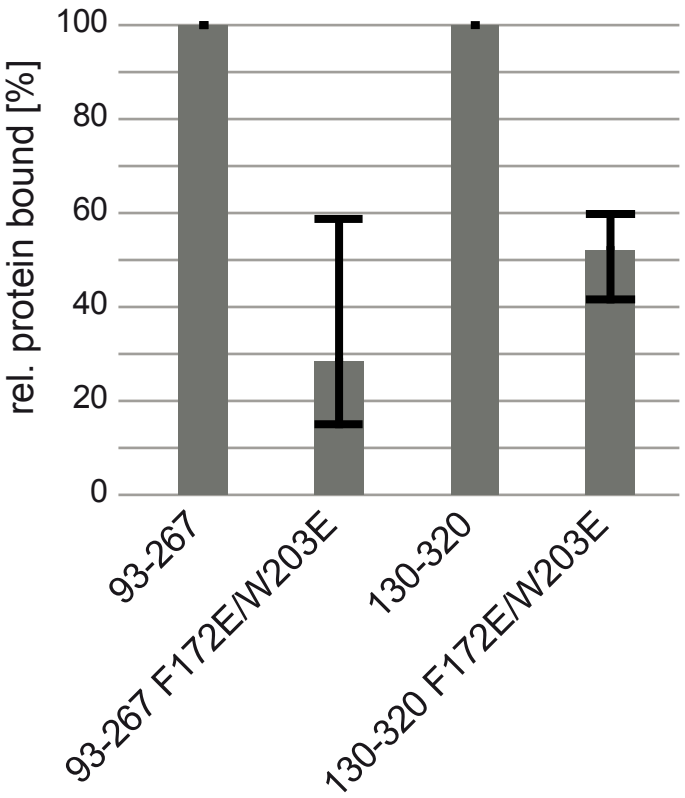

Figure S5

Both Nup53 membrane binding regions require dimerization by the RRM domain.

Nup53 fragments containing the first (93-267) or second (130-320) membrane binding region including the RRM domain were quantitatively assayed for liposome binding as in Figure 2C. Whereas fragments containing the wild type RRM domain bound to liposomes, introduction of two amino acid changes (F172E/W203E), which render the RRM domain incapable of dimerization, reduced liposome binding for both fragments. The averages of three independent experiments, normalized to liposome binding of the wild type protein, are shown. Error bars represent the range.

Supplementary Figure S6

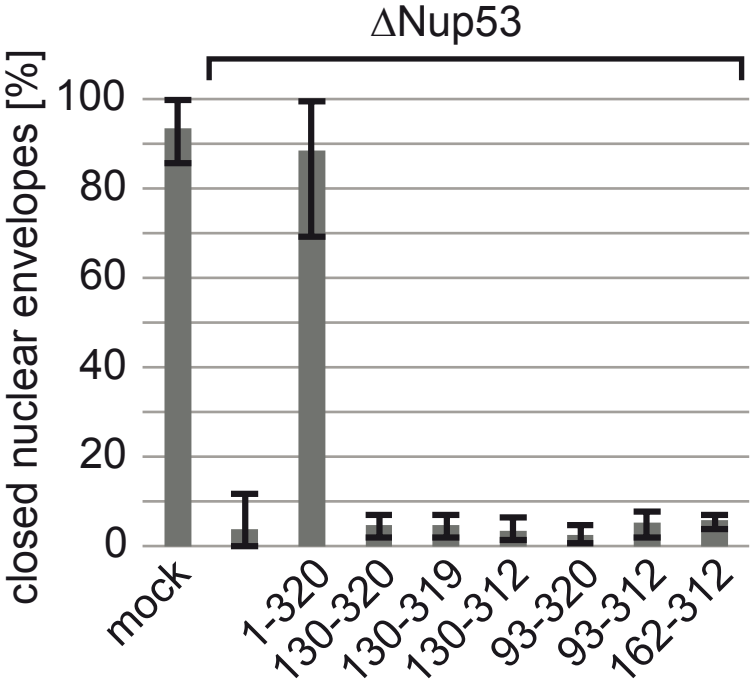

Figure S6

The interaction of Nup53 to Nup93 is necessary for nuclear envelope formation.

Nuclei were assembled in mock, Nup53 depleted extracts or Nup53 depleted extracts supplemented with wild type protein (1-320) or various fragments of Nup53 for 120 min, fixed with 2% PFA and 0.5% glutaraldehyde and analyzed for chromatin and membrane staining. Shown is the quantitation of chromatin substrates with a closed nuclear envelope as done in Figure 2F. Please note that all fragments lacking the N-terminal region of Nup53 necessary for Nup93 interaction (Figure S1A) and especially fragment 162-312 which has the ability to interact with Nup155 (Figure S1B) did not support nuclear envelope formation.

Supplementary Figure S7

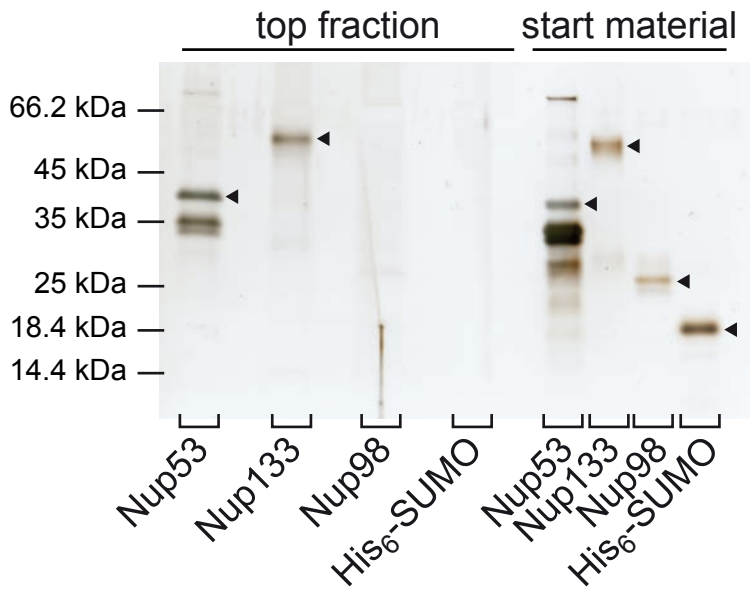

Figure S7

Recombinant Nup53 binds to liposomes mimicking the ER / nuclear envelope lipid composition

3 µM recombinant Xenopus Nup53 (Nup53) a fragment of Nup133 (aa 67-514) as positive control and Nup98 (aa 676-863) and His_6-tagged SUMO as negative controls, were incubated with 6 mg/ml fluorescently labeled liposomes prepared from a lipid mixture mimicking the ER/nuclear envelope lipid composition (see materials and methods). Flotation was done as described in Figure 1A.

Table S1: Peptides and phosphorylation sites identified in Xenopus Nup53 by mass spectrometric analysis

phosphopeptide	amino acid
PSAGAQFLPGFLLGDIPTPV**T**PQPR	T46
SPLH**S**GG**S**PPQPVLPTHK	S60, S64, S67
SPLHSGG**S**PPQPVLPTHK	S67
SIYDDVA**S**PGLGSTPR	S94
SIYDDVA**S**PGLGS**T**PR	S94, T100
MASFSVLHTPLSGAIPS**S**PAVFSPATIGQSR	S124
MASFSVLHTPLSGAIPSSPAVF**S**PATIGQSR	S131
V**S**TPSVSSVFTPPVK	S249
VS**T**PSVSSVFTPPVK	T250
VSTP**S**VSSVFTPPVK	S252
VSTP**S**VSSVF**T**PPVK	S252, T258
VSTPSVSSVF**T**PPVK	T258
SIRTPTQSVGTPR	S263
SIR**T**PTQSVGTPR	T266
SIRTPTQ**S**VGTPR	S270
TPTQSVG**T**PR	T273
TPTSADYQVVSDKPAPR	T288
TPT**S**ADYQVVSDKPAPR	T288, S291

Phosphorylation sites mapped in XenopusNup53 (genebank accession JQ747515) after immunoprecipitation from mitotic or interphase Xenopus egg extracts. Phosphorylation sites are indicated in red. Position T100, T288 and S291 were phosphorylated on Nup53 isolated from mitotic, but not interphasic extracts.

Table S2: DNA constructs used in this study

Constructs
pET28a SUMO Nup53xl 1-166
pET28a SUMO Nup53xl 1-267
pET28a SUMO Nup53xl 1-312
pET28a SUMO Nup53xl 1-312 S94E/T100E
pET28a SUMO Nup53xl 1-312 R105E/K106E
pET28a SUMO Nup53xl 1-319
pET28a SUMO Nup53xl 1-319 S94E/T100E
pET28a SUMO Nup53xl 1-319 R105E/K106E
pET28a SUMO Nup53xl 1-320
pET28a SUMO Nup53xl 1-320 S94E/T100E
pET28a SUMO Nup53xl 1-320 R105E/K106E
pET28a SUMO Nup53xl 1-320 F172E/W203E
pET28a SUMO Nup53xl 93-267
pET28a SUMO Nup53xl 93-267 S94A/T100A
pET28a SUMO Nup53xl 93-267 S94E/T100E
pET28a SUMO Nup53xl 93-267 R105E/K106E
pET28a SUMO Nup53xl 93-267 F172E/W203E
pET28a SUMO Nup53xl 93-312
pET28a SUMO Nup53xl 93-319
pET28a SUMO Nup53xl 93-320
pET28a SUMO Nup53xl 93-320 S94E/T100E
pET28a SUMO Nup53xl 93-320 R105E/K106E
pET28a SUMO Nup53xl 93-320 F172E/W203E
pET28a SUMO Nup53xl 107-267
pET28a SUMO Nup53xl 130-267
pET28a SUMO Nup53xl 130-312
pET28a SUMO Nup53xl 130-319
pET28a SUMO Nup53xl 130-320
pET28a SUMO Nup53xl 130-320 F172E/W203E
pET28a SUMO Nup53xl 162-267
pET28a SUMO Nup53xl 162-267 F172E/W203E
pET28a SUMO Nup53xl 162-312
pET28a SUMO Nup53xl 162-320
pET28a SUMO Nup53xl 254-320
pET28a SUMO Nup59sc 1-528
pET28a SUMO Nup53sc 1-475
pET28a PP Nup133hs 30-514
pET28a NusA Nup98xl 676-863
pET28a GST Nup53xl 1-267
pET28a GST Nup53xl 1-267 S94A/T100A
pET28a GST Nup53xl 1-267 S94E/T100E
pET28a GST Nup53xl 1-267 R105E/K106E
pET28a GST Nup53xl 1-267 F172E/W203E
pET28a GST Nup53xl 162-267
pET28a GST Nup53xl 162-312
pET28a GST Nup53xl 162-319
pET28a GST Nup53xl 162-320
pET28a GST Nup53xl 162-320 F172E/W203E
pET28a GST Nup98xl 487-634

Constructs
pSI HA Nup53xl
pSI HA Nup53xl F172E/W203E
pSI myc Nup53xl
pSI myc Nup53xl F172E/W203E

Supplementary Methods

Pulldown experiments

Fragments used for the GST pulldown experiments were cloned into a modified pET28a vector with GST tag followed by a recognition site for TEV protease and purified via the N-terminal His_6 tag. 60 µl GSH–Sepharose (GE Healthcare) were incubated with 300 µg of the respective bait proteins, washed and blocked with 5% BSA in PBS. Beads were incubated with cytosol from Xenopus egg extracts (diluted 1:1 with PBS, and cleared by centrifugation for 30 min at 100,000 rpm in a TLA110 rotor (Beckman Coulter) for 2 h and washed six times with PBS. Bound proteins were eluted by cleavage with TEV protease (0.5 mg/ml) for 1 h at RT and analyzed by SDS-PAGE and Western blotting. For detection of NDC1 and GP210, 5 mg of membranes from Xenopus egg extracts (Antonin et al, 2005) were solubilized in 5 ml 50 mM Phosphate buffer pH 7.4, 500 mM NaCl, 1% Triton X-100 and protease inhibitors (Roche), instead of cytosol and the first four washes with PBS were in the presence of 0.1% Triton X-100.

Mass Spectrometry

2 ml interphasic (Hartl et al, 1994) or (CSF arrested) mitotic (Murray, 1991) Xenopus egg extracts were diluted with 1.2 ml wash buffer (10 mM HEPES, 50 mM KCl, 2.5 mM $MgCl_2$ pH 7.4), cleared by centrifugation for 10 min at 100,000 rpm in a TLA110 rotor and incubated with 50 µl Protein A Sepharose (GE Healthcare), to which affinity purified Nup53 antibodies were bound and crosslinked with 10 mM dimethylpimelimidate (Pierce). After 1h incubation the sepharose was washed 10 times with wash buffer. Proteins were eluted with SDS sample buffer (without DTT) and separated by SDS-PAGE. Gel sections from 30-45 kDa were excised and proteins were in-gel digested by trypsin. The resulting peptide mixtures were measured on an LTQ-Orbitrap XL and processed by MaxQuant software as described (Borchert et al, 2010). Multistage activation was enabled in all MS measurements.

Generation of liposomes

A mixture of lipids resembling the ER/nuclear envelope composition (Franke et al, 1970) (60 mol % phosphatidylcholine, 19.8 mol % phosphatidylethanolamine, 10 mol % phosphatidylinositol, 5 mol % cholesterol, 2.5 mol % sphingomyelin, 2.5 mol % phosphatidylserine 0.2 mol % 18:1-12:0 NBD-PE all Avanti polar lipids) dissolved in chloroform were dried on a rotary evaporator and overnight under vacuum. PBS buffer was gently added to result in a final lipid concentration of 6 mg/ml. After 2 h of incubation at

37°C to allow spontaneous liposome formation the flask was agitated to dissolve residual lipids. After ten cycles of freeze/thawing liposomes were extruded as described before.

DNA sequence of Xenopus laevis Nup53 optimized for expression in E. coli

ATGATGGCAGCAGCATTTAGCATGGAACCGATGGGTGCAGAACCGATGGCACTG
GGTAGCCCGACCAGCCCGAAACCGAGTGCCGGTGCACAGTTTCTGCCTGGTTTTC
TGCTGGGTGATATTCCGACACCGGTTACACCGCAGCCTCGTCCGAGCCTGGGTAT
TATGGAAGTTCGTAGTCCGCTGCATAGCGGTGGTAGTCCTCCGCAGCCGGTTCTG
CCGACCCATAAAGATAAAAGCGGTGCACCTCCGGTTCGTAGCATTTATGATGATG
TTGCAAGTCCGGGTCTGGGTAGCACACCGCGTAATACCCGTAAAATGGCAAGCTT
TAGCGTTCTGCATACACCTCTGAGCGGTGCAATTCCGAGCAGTCCGGCAAGCAAT
GTTTTTAGTCCGGCAACCATTGGTCAGAGCCGTAAAACCACCCTGAGTCCGGCAC
AGATGGACCCGTTTTATACCCAGGGTGATGCACTGACCAGTGATGATCAGCTGGA
TGATACCTGGGTTACCGTTTTTGGTTTTCCGCAGGCAAGCGCAAGCTATATTCTGC
TGCAGTTTGCACAGTATGGCAATATTATTAAACATGTGATGAGCAATAATGGCAA
TTGGATGCATATTCAGTATCAGAGCAAACTGCAGGCACGTAAAGCACTGAGCAA
AGATGGTCGTATTTTTGGTGAAAGCATTATGATTGGTGTGAAACCGTGCATTGAT
AAAAGCGTTATGGAAGCAACCGAAAAAGTTAGCACCCCGAGCGTTAGCAGCGTT
TTTACACCTCCGGTTAAAAGCATTCGTACCCCGACCCAGAGCGTTGGTACACCGC
GTGCAGCAAGCATGCGTCCGCTGGCAGCAACCTATCGCACCCCGACCAGCGCAG
ATTATCAGGTTGTTAGCGATAAACCGGCACCGCGTAAAGATGAAAGCATTGTTAG
CAAAGCCATGGAATATATGTTTGGTTGGTGATAG

DNA sequence of Saccharomyces cerevisiae NUP53 optimized for expression in E. coli

ATGGCAGATCTGCAGAAACAAGAAAATTCAAGCCGTTTTACCAATGTTAGCGTTA
TTGCACCGGAAAGCCAGGGTCAGCATGAACAGCAGAAACAGCAAGAACAACAA
GAACAGCAGAAACAGCCGACAGGTCTGCTGAAAGGTCTGAATGGTTTTCCGAGC
GCACCGCAGCCGCTGTTTATGGAAGATCCTCCGAGCACCGTTAGCGGTGAACTGA
ATGATAATCCGGCATGGTTTAATAATCCGCGTAAACGTGCAATTCCGAATAGCAT
TATTAAACGTAGCAATGGTCAGAGCCTGAGTCCGGTTCGTAGCGATAGCGCAGAT
GTTCCGGCATTTAGCAATAGCAATGGCTTTAATAATGTGACCTTTGGCAGCAAAA
AAGATCCGCGTATTCTGAAAAATGTGAGCCCGAATGATAATAATAGCGCCAATA
ATAATGCCCATAGCAGCGATCTGGGCACCGTTGTTTTTGATAGCAATGAAGCACC
TCCGAAAACCAGCCTGGCAGATTGGCAGAAAGAAGATGGTATTTTTAGCAGCAA
AACCGATAATATTGAAGATCCGAATCTGAGCAGCAATATTACCTTTGATGGTAAA
CCGACCGCAACCCCGAGCCCGTTTCGTCCGCTGGAAAAAACCAGCCGTATTCTGA
ATTTTTTTGATAAAAATACCAAAACCACCCCGAATACCGCAAGCAGCGAAGCAA
GCGCAGGTAGCAAAGAAGGTGCAAGCACCAATTGGGATGATCATGCCATTATTA
TTTTTGGCTATCCGGAAACCATTGCCAATAGTATTATTTTTCATTTTGCCAATTTTG
GCGAAATTCTGGAAGATTTTCGCGTGATTAAAGATTTTAAAAAGCTGAACAGCAA
AAATAAAAGCAAAAGCCCGAGCCTGACCGCACAGAAATATCCGATTTATACCGG
TGATGGTTGGGTTAAACTGACCTATAAAAGCGAACTGAGCAAAAGCCGTGCACT
GCAAGAAAATGGCATTATTATGAATGGCACCCTGATTGGTTGCGTTAGCTATAGT
CCGGCAGCACTGAAACAGCTGGCAAGCCTGAAAAAAAGCGAAGAAATTATTAAT
AATAAAACCAGCAGCCAGACCAGCCTGAGCAGCAAAGATCTGAGCAATTATCGT
AAAACCGAAGGCATTTTTGAAAAAGCCAAAGCAAAAGCGGTGACCAGCAAAGTT
CGTAATGCCGAATTTAAAGTGAGCAAAAATAGCACCAGCTTTAAAAATCCGCGTC
GCCTGGAAATTAAAGATGGTCGTAGCCTGTTTCTGCGTAATCGTGGTAAAATTCA
TAGCGGTGTTCTGAGCAGCATTGAAAGCGATCTGAAAAAACGTGAACAGGCAAG
CAAAAGCAAAAAAAGCTGGCTGAATCGCCTGAATAATTGGCTGTTTGGTTGGAAT
GATCTGTAGTGA

DNA sequence of Saccharomyces cerevisiae NUP59 optimized for expression in E. coli

ATGTTTGGTATTCGCAGCGGCAATAATAATGGTGGTTTTACCAATCTGACCAGCC
AGGCACCGCAGACCACCCAGATGTTTCAGAGCCAGAGCCAGCTGCAGCCGCAGC
CGCAGCCTCAACCGCAGCAGCAGCAACAGCATCTGCAGTTTAATGGTAGCAGTG
ATGCAAGCAGCCTGCGTTTTGGTAATAGCCTGAGCAATACCGTGAATGCCAATAA
TTATAGCAGCAATATTGGCAATAACAGCATCAACAATAATAACATCAAAAATGG
CACCAATAACATTAGCCAGCATGGTCAGGGCAATAATCCGAGCTGGGTTAATAAT
CCGAAAAAACGTTTTACACCGCATACCGTTATTCGTCGTAAAACCACCAAACAGA
ATAGCAGCAGCGATATTAATCAGAATGATGATAGCAGCAGCATGAATGCAACCA
TGCGTAATTTTAGCAAACAGAATCAGGATAGCAAACATAATGAACGCAATAAAA
GCGCAGCCAATAATGATATTAATAGCCTGCTGAGCAACTTTAATGATATTCCTCC
GAGCGTTACCCTGCAGGATTGGCAGCGTGAAGATGAATTTGGTAGCATTCCGAGC
CTGACCACCCAGTTTGTTACCGATAAATATACCGCCAAAAAAACCAATCGCAGCG
CCTATGATAGCAAAAATACCCCGAATGTGTTTGATAAAGATAGCTATGTGCGCAT
TGCCAATATTGAACAGAATCATCTGGATAATAATTATAATACCGCAGAAACCAAT
AATAAAGTGCATGAAACCAGCAGCAAAAGCAGCAGCCTGAGCGCAATTATTGTT
TTTGGTTATCCGGAAAGCATTAGCAATGAACTGATTGAACATTTTAGCCATTTTGG
CCATATTATGGAAGATTTTCAGGTTCTGCGTCTGGGTCGTGGTATTAATCCGAATA
CCTTTCGCATTTTTCATAATCATGATACCGGCTGTGATGAAAATGATAGCACCGTG
AATAAAAGCATTACCCTGAAAGGTCGCAATAATGAAAGTAATAACAAAAAATAT
CCGATTTTTACAGGCGAAAGCTGGGTTAAACTGACCTATAATAGCCCGAGCAGCG
CACTGCGTGCACTGCAAGAAAATGGTACAATTTTTCGTGGTAGCCTGATTGGTTG
TATTCCGTATAGCAAAAATGCCGTTGAACAGCTGGCAGGTTGCAAAATTGATAAT
GTGGATGATATTGGCGAATTTAATGTGAGCATGTATCAGAATAGCAGTACCAGCA
GCACCAGCAATACCCCGAGTCCTCCGAATGTTATTATTACCGATGGCACCCTGCT
GCGCGAAGATGATAATACACCGGCAGGTCATGCAGGCAATCCGACCAATATTAG
CAGCCCGATTGTTGCAAATAGCCCGAATAAACGTCTGGATGTGATTGATGGTAAA
CTGCCGTTTATGCAGAATGCAGGTCCGAATAGCAATATTCCGAATCTGCTGCGTA
ATCTGGAAAGCAAAATGCGTCAGCAAGAAGCAAAATATCGTAATAATGAACCGG
CAGGCTTTACCCATAAACTGAGCAATTGGCTGTTTGGTTGGAATGATCTGTAGTG
A

Supplementary References

Antonin W, Franz C, Haselmann U, Antony C, Mattaj IW (2005) The integral membrane nucleoporin pom121 functionally links nuclear pore complex assembly and nuclear envelope formation. *Molecular cell* **17:** 83-92

Borchert N, Dieterich C, Krug K, Schutz W, Jung S, Nordheim A, Sommer RJ, Macek B (2010) Proteogenomics of Pristionchus pacificus reveals distinct proteome structure of nematode models. *Genome research* **20:** 837-846

Franke WW, Deumling B, Baerbelermen, Jarasch ED, Kleinig H (1970) Nuclear membranes from mammalian liver. I. Isolation procedure and general characterization. *The Journal of cell biology* **46:** 379-395

Hartl P, Olson E, Dang T, Forbes DJ (1994) Nuclear assembly with lambda DNA in fractionated Xenopus egg extracts: an unexpected role for glycogen in formation of a higher order chromatin intermediate. *The Journal of cell biology* **124:** 235-248

Murray AW (1991) Cell cycle extracts. *Methods in cell biology* **36:** 581-605

Schagger H, von Jagow G (1987) Tricine-sodium dodecyl sulfate-polyacrylamide gel electrophoresis for the separation of proteins in the range from 1 to 100 kDa. *Analytical biochemistry* **166:** 368-379

Chromosoma (2012) 121:539–554
DOI 10.1007/s00412-012-0388-3

REVIEW

Building a nuclear envelope at the end of mitosis: coordinating membrane reorganization, nuclear pore complex assembly, and chromatin de-condensation

Allana Schooley · Benjamin Vollmer · Wolfram Antonin

Received: 31 August 2012 / Revised: 4 October 2012 / Accepted: 4 October 2012 / Published online: 27 October 2012

Abstract The metazoan nucleus is disassembled and re-built at every mitotic cell division. The nuclear envelope, including nuclear pore complexes, breaks down at the beginning of mitosis to accommodate the capture of massively condensed chromosomes by the spindle apparatus. At the end of mitosis, a nuclear envelope is newly formed around each set of segregating and de-condensing chromatin. We review the current understanding of the membrane restructuring events involved in the formation of the nuclear membrane sheets of the envelope, the mechanisms governing nuclear pore complex assembly and integration in the nascent nuclear membranes, and the regulated coordination of these events with chromatin de-condensation.

Keywords Nuclear envelope formation · Nuclear pore complex assembly · Chromatin decondensation · Mitotic exit

Introduction

A functional nucleus relies on the precise structural organization of its genome and the existence of an intact boundary that separates nuclear and cytoplasmic activities, the nuclear envelope (NE). These features are repeatedly established in the mitotically dividing cells of animals. While many lower eukaryotes employ closed or semi-closed mitosis, during which the NE remains at least partially intact (De Souza and Osmani 2009), the onset of mitosis in metazoan cells is marked by dramatic changes to nuclear architecture. Open mitosis requires the complete disassembly of the NE in order to form the mitotic spindle on condensed chromosomes. The consequence of this disassembly is the need to re-build the NE each time the cell divides.

The NE is composed of two concentric bilayers surrounding the chromatin: the outer nuclear membrane (ONM), which is continuous with the endoplasmic reticulum (ER), and the inner nuclear membrane (INM), separated from the ONM by a lumenal space (Fig. 1). These membranes are fused at sites of nuclear pore complex (NPC) integration. NPCs are large protein complexes that contribute to the diffusion barrier of the NE and act as a regulatory gateway for the bidirectional exchange of proteins, RNA, and ribonucleoprotein complexes between the nucleus and the cytoplasm (for review, see Wente and Rout 2010). While the outer membrane is biochemically and functionally similar to the ER, the inner membrane is distinctly characterized by a specific set of integral membrane proteins that establish connections to chromatin and, in metazoan cells, to the overlying nuclear lamina. The lamina is a meshwork of nucleus-specific intermediate filaments called lamins, which maintain the shape and mechanical stability of the nucleus (for review, see Gruenbaum et al. 2005; Shimi et al. 2010). The lamina is also indirectly connected to the cytoplasmic cytoskeleton via linker of nucleoskeleton and cytoskeleton (LINC) complexes that span the NE lumen (for review, see Burke 2012; Starr and Fridolfsson 2010).

Building a nucleus at the end of mitosis involves the complete reconstruction of nuclear membrane sheets and macromolecular NPCs on two sets of de-condensing chromosomes. Here, we review our current understanding of vertebrate NE reassembly as a coordinated process of membrane restructuring, NPC assembly, and chromatin de-condensation.

Re-organizing the mitotic ER

The NE is a distinct domain of the ER, owing to direct and indirect interactions between NE-specific proteins and chromatin. During mitosis, these proteins are released from the

Communicated by Erich Nigg

A. Schooley · B. Vollmer · W. Antonin (✉)
Friedrich Miescher Laboratory of the Max Planck Society, Tübingen, Germany
e-mail: wolfram.antonin@tuebingen.mpg.de

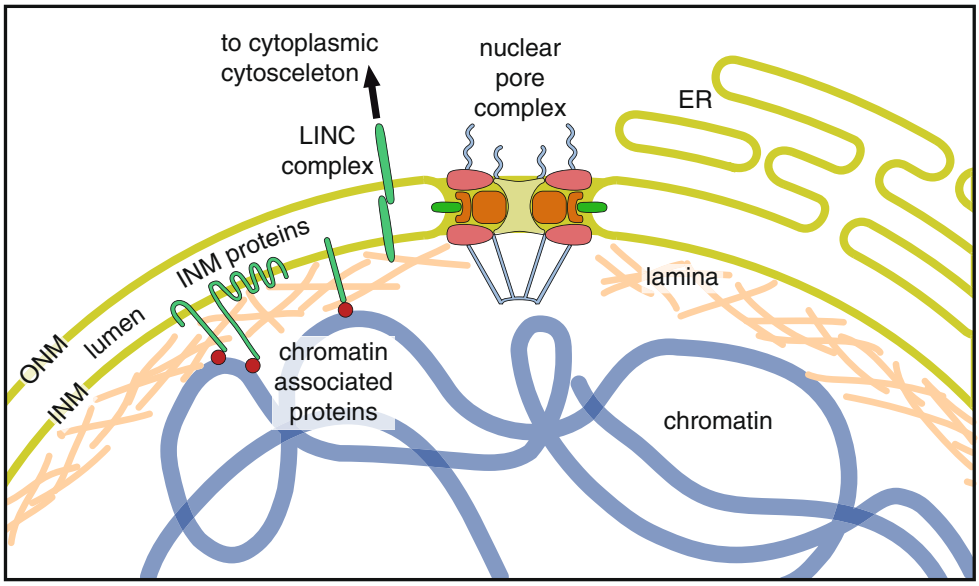

Fig. 1 The vertebrate nuclear envelope. The two-membrane sheets of the nuclear envelope are separated by a lumenal space and are continuous with the bulk endoplasmic reticulum (*ER*) network. The outer nuclear membrane (*ONM*) and the inner nuclear membrane (*INM*) are fused at nuclear pores, where nuclear pore complexes are integrated to regulate bidirectional transport between the cytoplasm and the nucleoplasm. The INM is distinctly characterized by a set of integral membrane proteins that connect the nuclear envelope to chromatin by interacting directly or indirectly via chromatin-associated proteins and the nuclear lamina. The nuclear lamina is additionally connected to the cytoplasmic cytoskeleton by the interaction of LINC complex proteins of the ONM and INM across the NE lumen

disassembled lamina and the underlying chromatin, resulting in their redistribution throughout the ER and thus the absorption of the NE membranes in the ER network (Daigle et al. 2001; Ellenberg et al. 1997; Yang et al. 1997). At the end of mitosis, the dramatic reorganization of the mitotic ER gives rise to a new NE forming around each mass of segregating chromatin. The architectural starting point for this ER re-structuring is, however, a matter of debate. In addition to the NE, the entire ER network undergoes significant morphological changes during mitosis. According to two contradictory models, the interphase system of ER sheets and tubules is transformed into either a tubular ER or sheet-like network during mitosis.

The mitotic ER has been observed as an exclusively tubular network (Puhka et al. 2007) and in vitro experiments suggest that an intact tubular ER is required for post-mitotic NE formation (Anderson and Hetzer 2007). This network is recruited via tubule ends that make first contact to the chromatin substrate and become immobilized (Fig. 2a). Subsequent flattening and lateral expansion of membranes on the chromatin surface is proposed to give rise to inner and ONM sheets. In further support of this model, ER tubules have been found to surround post-mitotic chromatin in vivo (Anderson and Hetzer 2008a). Overexpression of reticulons, proteins that shape the ER into tubules, delays NE formation while the depletion of reticulons by siRNA accelerates the formation of a closed NE. These experiments suggest that ER reshaping events, specifically those promoting membrane sheet formation from tubules, are crucial for NE assembly.

Recent live cell imaging and electron microscope tomography studies have provided evidence that NE re-assembly rather initiates from a cisternal, or sheet-like, mitotic ER (Lu et al. 2011) (Fig. 2b). During mitosis, the ER was found to consist almost entirely of extended cisternae, with the exception a few tubules contacting the mitotic spindle (Lu et al. 2009). Cisternal mitotic ER has also been observed in 3D reconstructions of light microscopy sections from *Caenorhabditis elegans* embryos (Poteryaev et al. 2005). The conservation of this ER structure in different cell types and organisms suggests that a sheet-like network could be a general feature of mitotic cells. NE assembly from extended cisternae is initiated by contact between ER sheets and chromatin (Lu et al. 2011). As membrane sheets enclose the chromatin they are organized into a NE-specific domain.

The organization of the interphase ER network varies between cell types and differentiation states (Voeltz et al. 2002). Similarly, the relative abundance of ER sheets and tubules is not the same in all mitotic cells (Puhka et al. 2012). Observations of entirely tubular or cisternal networks might therefore reflect extreme examples on a spectrum of possible mitotic ER arrangements. Assuming that the predominance of mitotic ER sheets and tubules varies between cell types, the question becomes: What is the morphology of the ER that contacts chromatin and gives rise to the sheets of the NE? The transformation of ER tubules into membrane sheets on the chromatin has not been directly visualized (Anderson and Hetzer 2008a). Reticulon-positive membrane tubules have been recorded around the post-mitotic chromatin mass

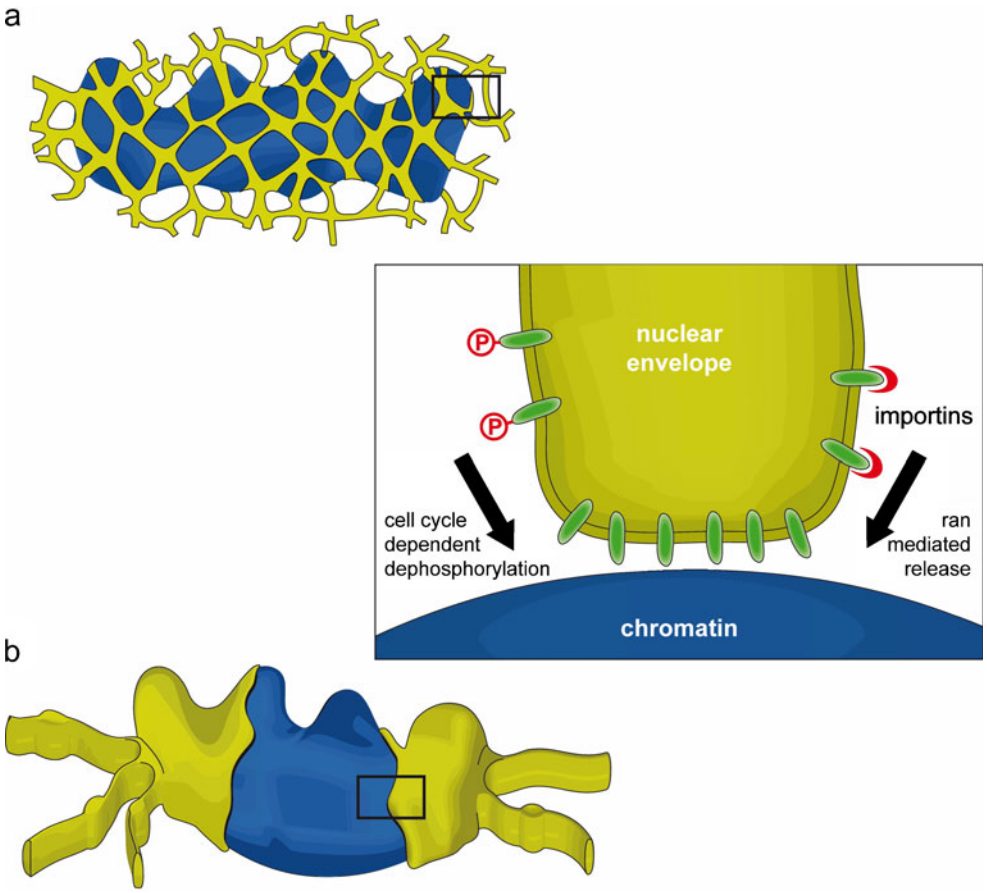

Fig. 2 The nuclear envelope is constructed by the re-organization of the mitotic ER on the chromatin. Two models have been proposed to explain nuclear envelope formation based on the predominant organization of the ER during mitosis. In the first model (**a**), a tubular ER network contacts chromatin via tubule ends, which flatten and expand on the chromatin surface to give rise to nuclear envelope sheets. Alternatively, ER-derived membrane sheets initiate nuclear envelope formation by associating laterally with the chromatin mass and spreading around it (**b**). In both cases, the regulated recruitment of membrane proteins of the INM (*inset*, see "Regulating the recruitment of nuclear envelope membranes to chromatin") mediates the accumulation of nuclear envelope-specific membranes and thus the establishment of this distinct ER subdomain

in live cells but in this case the tubules dynamically contact chromatin and do not directly contribute to the NE (Lu and Kirchhausen 2012). It therefore seems likely that the conversion of tubules to cisternal sheets is a prerequisite for the stable association of future NE membranes with chromatin.

Regardless of whether it is initiated by the outgrowth of ER tubules or from cisternal ER sheets, the complete enclosure of chromatin by the NE requires membrane fusion (Fig. 3a). As a subdomain of the ER, it is plausible that the NE employs the ER membrane fusion machinery to achieve this task. Many of the cellular membrane fusion events are mediated by the assembly of SNARE complexes (fo review Jahn and Scheller 2006). Indeed, NE assembly requires NSF and α-SNAP (Baur et al. 2007), fusion factors that activate SNARE proteins (Jahn and Scheller 2006). Integral membrane GTPases of the ER, called atlastins, were recently found to mediate fusion between ER tubules (Hu et al. 2009; Orso et al. 2009). It will be interesting to see if and when atlastins are involved in fusion events necessary for NE reformation. It is currently unknown whether atlastins and the SNAREs involved in ER fusion, such as syntaxin 18 (Hatsuzawa et al. 2000), act cooperatively to form and maintain the membrane network of the ER or whether they mediate distinct fusion events on different types of membranes. Both machineries mediate the approximation and fusion of ER membranes across a cytoplasmic space (Fig. 3a) and are therefore localized to the cytoplasmic side of the respective membranes or in the cytoplasm. The cytoplasmic membrane fusion events required to re-form the NE should be distinguished from the fusion required for NPC assembly into an intact NE, which occurs during interphase and possibly during post-mitotic nuclear formation (Fig. 3b). The nature and localization of the machinery required for fusion between the inner and ONMs during pore insertion have not been identified but might be non-cytoplasmic.

Establishing a NE membrane domain

The NE is rapidly established by the concentration of specific proteins from the mitotic ER network on the decondensing chromatin. In vitro, the recruitment of NE-forming membranes depends on transmembrane proteins (Collas et al. 1996; Newport and Dunphy 1992; Wilson and Newport 1988). Integral proteins of the INM including LBR (Collas et al. 1996; Pyrpasopoulou et al. 1996; Ye and Worman 1994), and the LEM-domain containing proteins Lap2β (Foisner and Gerace 1993; Furukawa et al. 1997), MAN1/LEMD3 (Liu et al. 2003) and emerin (Hirano et al. 2005) bind chromatin. The nucleoplasmic domain of LBR

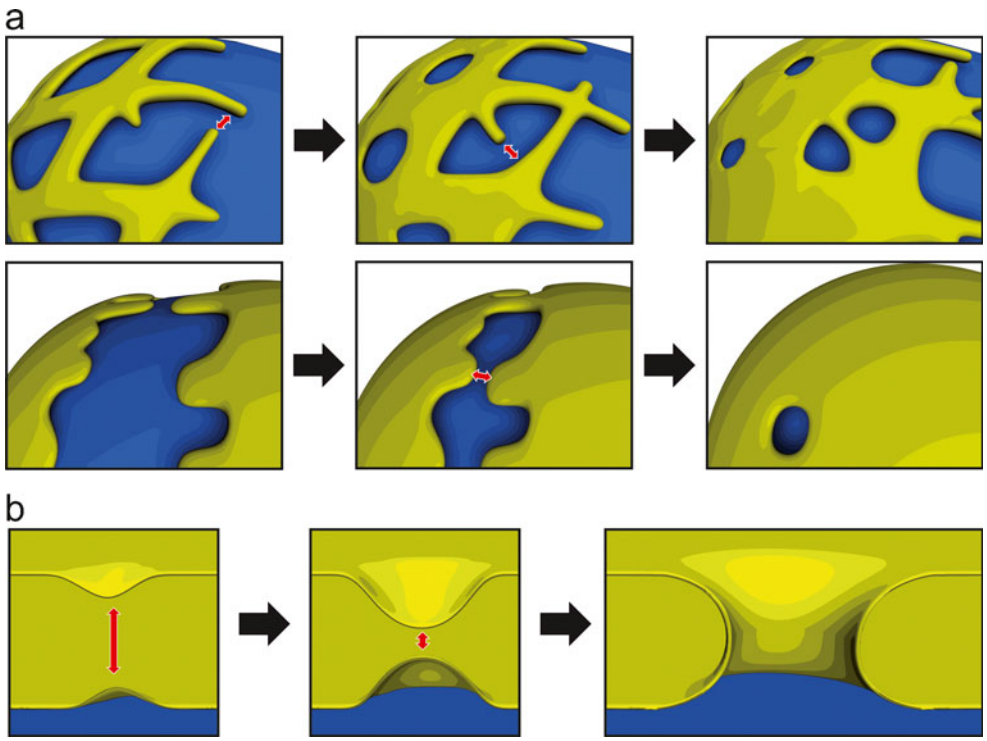

Fig. 3 Membrane fusion is required for nuclear envelope formation. Cytoplasmic fusion between outgrowing ER-derived tubules (**a**, *upper*) or sheets (**a**, *lower*) is required for re-assembly of a nuclear envelope around the chromatin mass at the end of mitosis. A second type of fusion between the outer and INMs across the lumenal space is required to create a pore in the intact nuclear envelope (**b**) for the insertion of NPCs during interphase and possibly post-mitotically

interacts with heterochromatin-binding protein (HP1) (Ye et al. 1997), while the LEM domain-containing proteins interact with the chromatin-associated protein barrier to auto-integration factor (BAF) (see Brachner and Foisner 2011). Several proteins of the INM, as well as the transmembrane nucleoporins NDC1 and POM121, also possess intrinsic DNA-binding capacities based on the presence of basic domains (Ulbert et al. 2006b). The use of multiple chromatin interaction strategies by the INM proteins could at least partially account for the rapid accumulation of membranes on chromatin at the onset of anaphase.

With the exception of LBR, for which contradicting results have been reported (Anderson et al. 2009; Lu et al. 2010), none of the INM proteins are essential for nuclear re-assembly in vivo. The depletion of individual INM proteins delays but does not inhibit NE formation in cultured cells and co-depletion of multiple INM proteins or depletion of the chromatin factor BAF, exacerbates the delay (Anderson et al. 2009), suggesting that the chromatin-binding NE proteins could play a redundant role in NE membrane recruitment. Furthermore, removing one INM protein, Lap2β, does not affect the distribution of another, LBR, despite delaying NE formation, implying that the recruitment of various nuclear membrane proteins is not only redundant but also cooperative towards NE assembly.

In addition to chromatin binding by INM proteins, the formation of membrane micro-domains has been proposed to support the segregation of NE membranes from the bulk ER (Mattaj 2004). A number of in vitro experiments in different experimental systems have revealed specific pools of membrane vesicles with the capacity to bind chromatin and give rise to a NE (Antonin et al. 2005; Buendia and Courvalin 1997; Chaudhary and Courvalin 1993; Collas et al. 1996; Ulbert et al. 2006b; Vigers and Lohka 1991; Vollmar et al. 2009). Although these NE membrane populations are likely to originate during the process of their isolation and fractionation when the mitotic ER vesiculates, membrane micro-domains have been found to segregate into distinct vesicles (Simons and Toomre 2000). It is therefore possible that the identification of NE-specific vesicles reflects the existence of micro-domain organization within the seemingly homogeneous mitotic ER.

The existence of NE-specific lipid rafts within the ER is unlikely given the low relative abundance of cholesterol at these membranes. However, the possibility that distinct lipid compositions contribute to functional partitioning at the NE, in analogy to the mitochondria-associated ER membrane (Fujimoto and Hayashi 2011), cannot be excluded. In support of this notion, NE vesicles isolated from sea urchin egg extracts are specifically enriched in phosphoinositides (Larijani et al. 2000), which confer a unique level of fluidity at the membrane (Zhendre et al. 2011). It should be noted that sea urchin pronucleus formation differs significantly from nuclear assembly in vertebrates (Collas 2000) and distinct lipid compositions have not been detected in vertebrate NE membranes to date.

In addition to lipid-mediated domain organization, membrane coating proteins have been proposed to function in micro-domain formation at different endosome compartments (Zerial and McBride 2001). If an analogous strategy

is employed by the NE, lamins could represent attractive candidates for the coating protein component. Several INM proteins interact with lamin B (see Wilson and Foisner 2010 for a comprehensive review), which can be found on mitotic ER-derived membrane vesicles (Chaudhary and Courvalin 1993; Gerace and Blobel 1980). However, despite recent advances in the study of membrane micro-domains (Simons and Gerl 2010), there is no direct evidence for NE subdomain formation in the ER, nor is it clear that such domain organization would impact NE reformation.

Regulating the recruitment of NE membranes to chromatin

Nuclear membranes first re-associate with chromatin during the late stages of anaphase (Daigle et al. 2001; Ellenberg et al. 1997; Robbins and Gonatas 1964). This recruitment can be artificially accelerated in vivo by overexpressing chromatin-binding membrane proteins, or by depleting reticulons to alter ER organization (Anderson et al. 2009). In both cases, premature NE formation interferes with chromosome segregation underlining the importance of robust temporal coordination between chromatin and nuclear membrane dynamics during the cell cycle.

Phosphorylation of nuclear lamins (Heald and McKeon 1990; Peter et al. 1990) and INM proteins (Foisner and Gerace 1993; Pyrpasopoulou et al. 1996) initiates disassembly of the NE at the onset of mitosis. The major driving force of mitotic phosphorylation, cdk1-cyclin B, has been found to inhibit the association of membranes with post-mitotic chromatin in vitro (Newport and Dunphy 1992; Pfaller et al. 1991), likely via one or several downstream kinases (Newport and Dunphy 1992; Vigers and Lohka 1992). If mitotic phosphorylation prevents the association of membranes with chromatin, the process must be reversed at the end of mitosis (Fig. 2, inset). Indeed, membranes isolated from mitotic *Xenopus* egg extracts, containing active cdk1-cyclin B, can be induced to bind chromatin when they are first incubated with interphase cytosol (Ito et al. 2007). This shift in membrane affinity for chromatin is due to the activity of phosphatases, such as PP1 (Ito et al. 2007; Pfaller et al. 1991).

The target of mitotic phosphorylation events that regulate membrane recruitment is on the membranes and not the chromatin (Pfaller et al. 1991). In vitro experiments using protein-free liposomes imply that lipid recruitment to chromatin could be specifically regulated during the cell cycle (Ramos et al. 2006). However, biological membranes are covered with proteins, largely due to mosaics of transmembrane proteins and their interaction partners, with relatively little area of exposed lipids (Dupuy and Engelman 2008; Takamori et al. 2006). Thus although regulation at the lipid surface may be a contributing factor, it is more likely that the cell cycle-dependent recruitment of membranes to chromatin is mediated by the integral nuclear membrane proteins.

Two INM proteins that are recruited quickly following the onset of anaphase, Lapβ and LBR, are phosphorylated during mitosis, preventing their association with chromatin (Foisner and Gerace 1993; Ito et al. 2007; Courvalin et al. 1992). The precise regulation of LBR by mitotic phosphorylation is particularly well studied. In post-mitotic extracts, an arginine-serine repeat-containing region of LBR mediates its recruitment to chromatin (Takano et al. 2002). Phosphorylation of a specific serine residue within this domain prevents LBR binding to chromatin in vitro (Ito et al. 2007; Nikolakaki et al. 1997; Takano et al. 2004) and its de-phosphorylation controls the timing of ER membrane recruitment to anaphase chromosomes in human cells (Tseng and Chen 2011). Given the redundancy of INM protein recruitment, it is likely that other integral NE proteins are regulated similarly. In fact, the pore membrane proteins NDC1, POM121, and GP210 as well as the INM proteins emerin and MAN1 are also phosphorylated during mitosis (Dephoure et al. 2008; Mansfeld et al. 2006; Ellis et al. 1998; Favreau et al. 1996), but the significance of these events with regard to nuclear membrane recruitment is unclear.

Although exit from mitosis is characterized by an overall decrease in phosphorylation, the in vitro association of LBR with chromatin also requires specific phosphorylation events, which are mediated by serine/arginine-rich protein-specific kinase 1 (Nikolakaki et al. 1997; Takano et al. 2002; Dreger et al. 1999). Similarly, Lap2β is phosphorylated within its chromatin-binding region during interphase (Dreger et al. 1999). These observations suggest that a simple model of mitotic phosphorylation and post-mitotic de-phosphorylation cannot account for the precise timing of membrane recruitment to chromatin but rather that multiple site-specific phosphorylation events tune this process.

In addition to cell cycle-dependent phosphorylation events, transport receptors and the GTPase ran may regulate the association of INM proteins with chromatin. Chromatin is demarcated throughout the cell cycle by a high concentration of the GTP-bound ran (Kalab et al. 2002). Ran is best known for its function in nucleo-cytoplasmic transport across the NPC, where it stimulates the release of importin-bound cargo in the nucleus, but it is also required for nuclear assembly in vitro (Hetzer et al. 2000; Zhang and Clarke 2000), where it provides the positional information necessary to specify that nuclear assembly occurs on the decondensing chromatin (for review, see Hetzer et al. 2002). Integral membrane proteins can be targeted to the interphase NE via importins (Doucet et al. 2010; Turgay et al. 2010), and it is possible that the ran-importin system could similarly regulate the recruitment of INM proteins to post-mitotic chromatin (Turgay et al. 2010; Antonin et al. 2011) (Fig. 2, inset). In agreement with this notion, LBR was found to interact with importin β during mitosis (Ma et al.

2007; Lu et al. 2010) and this inhibitory complex could be dissociated in the presence of ranGTP (Ma et al. 2007). The importin β and chromatin-binding sites of LBR overlap, thus it is conceivable that members of the importin family act as molecular chaperones to prevent undesired interactions between the DNA-binding domains of INM proteins and chromatin during mitosis.

It has also been suggested that importins mediate the recruitment of NE membranes to chromatin by bridging the membrane precursors and either ran (Ma et al. 2007) or NLS-containing chromatin proteins (Lu et al. 2012). This model requires a stable interaction between ran and importins, which is difficult to rectify with the ran-dependent dissociation of importin-cargo complex during nuclear import. Furthermore, it is not clear how a non-canonical importin interaction with two binding partners is established. Nonetheless, the contribution of NLS-containing chromatin proteins could represent an important link between post-mitotic chromatin structure and membrane recruitment and warrants further investigation.

In summary, the timing of nuclear membrane recruitment to chromatin is regulated by the reversal of mitosis-specific phosphorylation events on nuclear membrane proteins. With few exceptions, the relevant target proteins, precise sites of modification, and the phosphatases involved have yet to be identified. Spatial organization by the ran system might contribute to nuclear membrane recruitment by exposing DNA-binding domains of membrane proteins in the vicinity of chromatin but the relevance of such a mechanism has not been determined.

Building NPCs in the NE: post-mitotic assembly modes

As the ER membranes are reorganized to accommodate the distinct composition of the NE and enclose the chromatin, the coordinated assembly of NPCs begins. NPCs form large pores in the NE, having a diameter of approximately 100 nm. Unlike membrane transporters, which give rise to channels within a single lipid bilayer, NPCs span two lipid bilayers at sites where the outer and inner membranes of the NE are fused. As a result, only a small sub-fraction of the roughly thirty NPC proteins (nucleoporins) are integral membrane proteins residing in the pore membrane. Most nucleoporins do not possess membrane-spanning domains and are thus recruited from the cytosol to assemble NPCs at the conclusion of open mitosis in animals.

Post-mitotic NPC assembly has been proposed to proceed via two fundamentally different modes: insertion or enclosure. In an insertion model (Fig. 4a), NPCs assemble and integrate into the two juxtaposed membrane sheets of the intact NE (Fichtman et al. 2010; Lu et al. 2011; Macaulay and Forbes 1996). Formation of the pore requires the fusion of the outer and INMs across the lumen of the NE

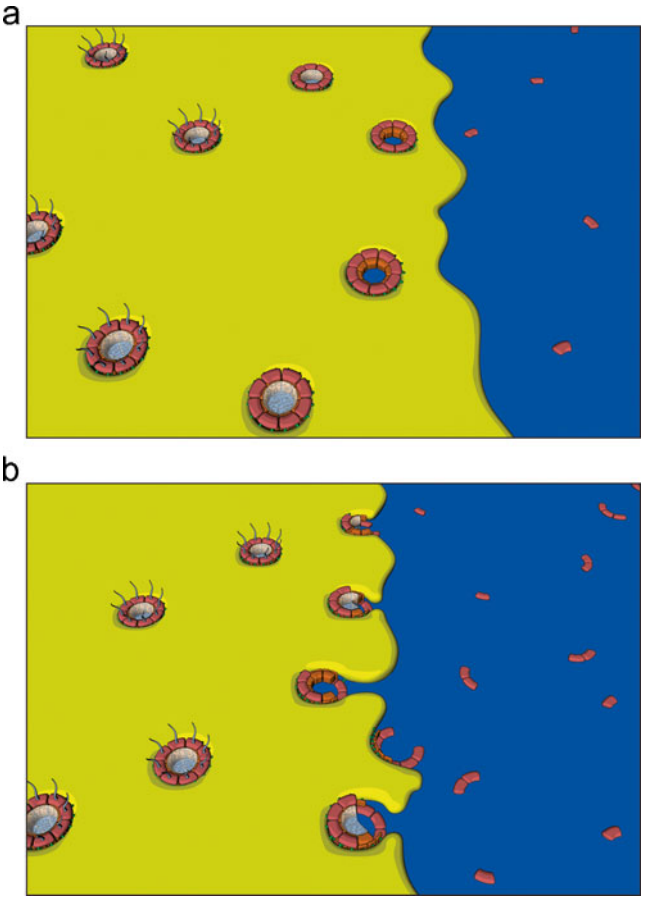

Fig. 4 Post-mitotic NPC assembly as envisioned by the insertion and enclosure models. As the cisternal sheets of the nuclear membrane wrap around chromatin, NPC assembly proceeds by either insertion into the locally intact nuclear envelope (**a**) or by enclosure of NPC assembly intermediates by the outgrowing membranes (**b**). In both cases, NPC assembly is initiated by the Mel-28/ELYS-dependent recruitment of the Nup107-160 complex to chromatin. Following the initial contact between nuclear membranes and the Nup107-160 complex, additional nucleoporins are incorporated in the assembling NPCs (see also Fig. 5 for details)

(see Fig. 3b). In dividing metazoan cells the number of NPCs roughly doubles during interphase (Dultz and Ellenberg 2010; Maul et al. 1972; Doucet and Hetzer 2010), when NPCs must be formed by insertion into the intact NE. Furthermore, organisms that employ closed mitosis for cell division, such as yeast, can only assemble new NPCs by insertion into the intact nuclear membranes (Rexach 2009; Winey et al. 1997). Thus, an insertion model represents a unifying mechanism for NPC assembly across species and in all stages of the cell cycle.

In contrast to interphase NPC assembly, which occurs as a collection of singular and sporadic events, the post-mitotic assembly of thousands of NPCs in metazoan cells proceeds simultaneously and rapidly, on average one order of magnitude faster, in order to quickly re-establish nuclear compartmentalization (Dultz and Ellenberg 2010; D'Angelo et al.

2006; Dultz et al. 2008). The distinct kinetics of post-mitotic NPC formation could be explained by the use of a mechanistically unique assembly mode. Enclosure models suggest (Antonin et al. 2008; Burke and Ellenberg 2002; Walther et al. 2003a) that post-mitotic NPC assembly following open mitosis does not occur by insertion into intact membrane sheets but is rather completed by the envelopment of the assembling NPCs on the chromatin surface by the outgrowing ER-derived membranes (Fig. 4b). In this case, NPC assembly is initiated by the recruitment of the Nup107-160 complex to chromatin, which has been observed in vitro (Walther et al. 2003a) and in vivo (Dultz et al. 2008; Belgareh et al. 2001). Membranes are subsequently recruited, resulting in the enrichment of NE-specific membrane proteins, including the integral membrane nucleoporins POM121 and NDC1 (Antonin et al. 2005; Mansfeld et al. 2006; Rasala et al. 2008). Kinetic analyses of individual NPC proteins suggest that the ordered recruitment of NE components at the end of mitosis is distinct from interphase pore assembly, where POM121 gradually accumulates prior to the recruitment of the Nup107-160 complex (Doucet et al. 2010; Dultz and Ellenberg 2010). This reversal of recruitment events implies that post-mitotic NPC assembly is initiated on the chromatin, as the enclosure model proposes, while interphase insertion of NPCs begins on the nuclear membranes.

The DNA-binding protein Mel-28/ELYS recruits the Nup107-160 complex and acts as a seeding point for post-mitotic NPC assembly (Franz et al. 2007; Gillespie et al. 2007; Rasala et al. 2008). In agreement with the notion of chromatin-directed NPC assembly at the end of mitosis, Mel-28/ELYS is essential for post-mitotic NPC formation but is dispensable to this end during interphase (Doucet et al. 2010). Conversely, the transmembrane nucleoporin POM121 is proposed to be specifically required for interphase NPC assembly, where it initiates pore formation on the membranes. However, it should be noted that the dispensability of POM121 for the formation of NPCs at the end of mitosis (Doucet et al. 2010) is not a consistent observation in the field (Antonin et al. 2005; Shaulov et al. 2011) and could be attributed to an incomplete depletion, resulting in a small pool of residual POM121 that was sufficient for post-mitotic assembly but completely consumed when nuclei reached interphase.

The existence of membrane intermediates specific to post-mitotic and interphase pore formation can be inferred from differences in the requirement of membrane bending and curvature-sensing proteins. Our recent work demonstrates distinct functions of the membrane-associated nucleoporin Nup53, which are essential for pore formation post-mitotically or during interphase (Vollmer et al. 2012). While either of the two Nup53 membrane-binding sites is sufficient for post-mitotic NPC assembly, interphase assembly specifically requires the second binding site at the C terminus. As the C-terminal-binding site was also found to induce membrane curvature, this could indicate that a unique membrane deformation activity is required for interphase pore assembly. Similarly, ER-bending proteins of the reticulon family that induce convex membrane curvature (Hu et al. 2008) were found to be important for NPC assembly into the intact NE both in yeast and vertebrates (Dawson et al. 2009). It is difficult to ascertain whether reticulons also contribute to post-mitotic NPC assembly because their role in ER membrane reorganization at the end of mitosis is a prerequisite for NE reformation (Anderson and Hetzer 2008a). Interestingly, a membrane curvature sensing domain of the Nup107-160 complex member Nup133 was found to be required for interphase but not post-mitotic assembly (Doucet and Hetzer 2010). It is possible that specific membrane curvature events are required during the insertion of interphase NPCs when the two nuclear membranes approximate and fuse (Fig. 3b). Other modes of pore membrane stabilization might be sufficient at the end of mitosis, when NPCs on the chromatin are enclosed by the outgrowing ER.

The existence of cell cycle-dependent differences in the molecular requirements of NPC formation does not unambiguously prove the use of distinct assembly mechanisms. The specific requirement for Mel-28/ELYS during post-mitotic assembly, for example, could rather reflect a need for the efficient recruitment of NPC components during open mitosis when they cannot be enriched in the nucleus by active NPC-dependent import. Assembly of NPCs into an intact envelope requires the Nup107-160 complex on the nucleoplasmic site of the NE (D'Angelo et al. 2006; Walther et al. 2003a). Thus, regardless of the assembly mode employed, NPC components will need to be enriched on the chromatin at the end of mitosis. Similarly, the unique requirement for proteins inducing membrane curvature during interphase NPC formation does not prove the use of dissimilar assembly mechanisms at different points in the cell cycle although it strongly implies distinct modes.

Nuclear formation can be decelerated in *Xenopus* extracts, which are commonly used to recapitulate post-mitotic NPC assembly, by reducing the temperature of the reaction (Fichtman et al. 2010). Under these conditions, a NE intermediate that possesses a closed NE but no pores or NPCs can be observed, suggesting that post-mitotic NPC assembly proceeds by insertion and requires the fusion of outer and INMs. However, the lower temperature might specifically inhibit or delay the post-mitotic mode of assembly, resulting in an artificial bias towards interphase NPC assembly. Recent live cell imaging experiments suggest that the local generation of NE membranes on chromatin from ER cisternae precedes NPC assembly, which would also implicate an insertion mode for post-mitotic NPC assembly (Lu et al. 2011). However, the precise order of recruitment,

particularly with regard to the small number of nucleoporins that might be sufficient to seed NPC assembly is difficult to ascertain. In order to ultimately resolve this issue, it will be crucial to determine whether the hitherto unknown factors mediating fusion of the outer and INM are equally required for interphase and post-mitotic NPC assembly.

Importantly, while the tubular or cisternal organization of the post-mitotic ER recruited to chromatin would appear to favor enclosure or insertion of NPCs, respectively, these structures are in principle compatible with both assembly modes. Although it is easy to imagine how intermediates of NPC assembly are seeded in the gaps of a tubular ER network and enclosed by the flattening and expansion of those membrane areas (Anderson and Hetzer 2008b; Antonin et al. 2008), an ER network on the chromatin surface might first close the gaps to form a closed NE into which NPCs are assembled according to the insertion model. Similarly, outgrowth of flat ER cisternae could first form a closed NE, at least locally, into which NPCs are inserted (Lu et al. 2011) (Fig. 4a). However, it is also possible that the growing sheets of the cisternae enclose assembling NPC intermediates similar to waves flowing around wooden posts on a beach (Fig. 4b).

Assembling NPCs at the end of mitosis: ordered recruitment of nucleoporins

A single vertebrate NPC has a mass of roughly 60MDa, an approximate diameter of 100 nm and consists of multiple copies of 30 unique nucleoporins, which are arranged to give rise to a cylindrical pore with eightfold rotational symmetry (Brohawn et al. 2009). Nucleoporins can be categorized based on their contribution to either the structural scaffold or the transport properties of the NPC. The latter group consists of nucleoporins with phenylalanine-glycine (FG) repeat sequences that mostly occupy the central channel of the pore and contribute to the diffusion barrier and regulated transport capacity of the NPC (Weis 2007). The construction of this macromolecular structure is accomplished by the sequential recruitment of nucleoporins (Bodoor et al. 1999; Dultz et al. 2008; Haraguchi et al. 2000). Immunofluorescence and live cell imaging in cultured mammalian cells, as well as depletion experiments in *Xenopus* egg extracts, have elucidated the order and interdependence of the important recruitment steps (Fig. 5).

Post-mitotic NPC assembly starts on chromatin, where the DNA-binding nucleoporin Mel-28/ELYS recruits the Nup107-160 complex (Franz et al. 2007; Walther et al. 2003a; Rotem et al. 2009; Rasala et al. 2008; Harel et al. 2003). In vitro, these events can occur in the absence of membranes. The subsequent association of the transmembrane nucleoporin POM121 at the newly forming pores (Antonin et al. 2005) is thought to be mediated by direct binding of POM121 to the Nup107-160 complex (Mitchell et al. 2010; Yavuz et al. 2010) and constitutes the first connection between the assembling NPC and nuclear membranes. The transmembrane nucleoporin NDC1 is also

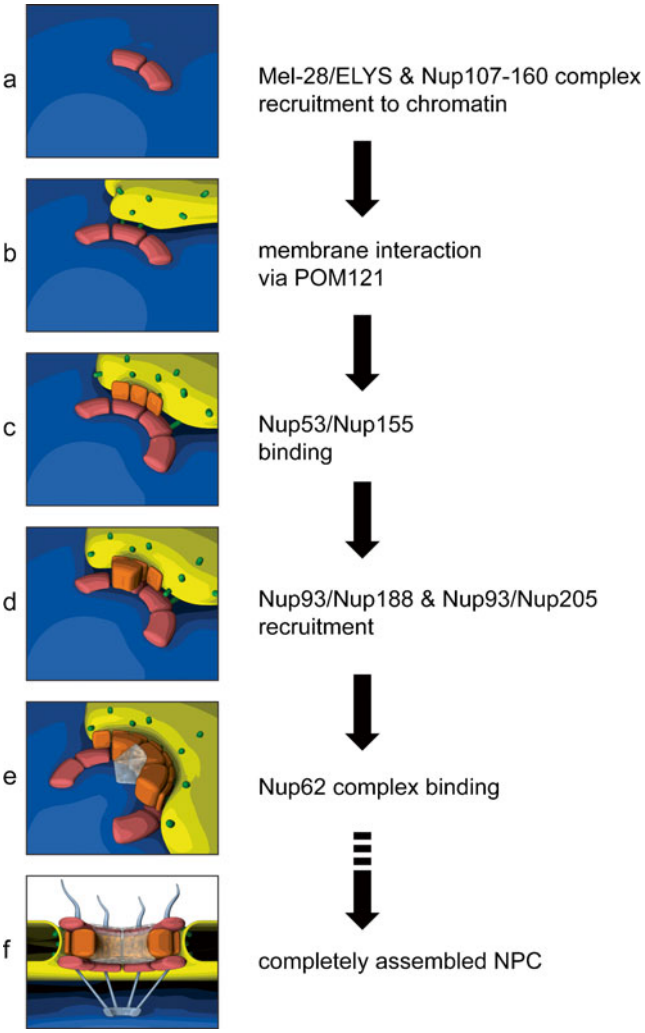

Fig. 5 Model for the ordered assembly of NPCs at the end of mitosis (see text for details and alternative models). The DNA-binding nucleoporin Mel-28/ELYS initiates NPC assembly on the chromatin by recruiting the Nup107-160 complex (**a**), which in turn associates with the nuclear envelope membranes via the transmembrane nucleoporin POM121 (**b**). The recruitment of the Nup93 complex is mediated by its membrane-associated nucleoporins, Nup53 and Nup155, which interact with integral membrane proteins at the nascent pore membrane (**c**) and promote the incorporation of Nup93, Nup188, and Nup205 to complete the structural backbone of the NPC (**d**). The subsequent recruitment of FG-repeat containing nucleoporins of the Nup62 complex (**e**) combined with the previous association Nup98 (not shown) establishes the central channel, a hydrophobic meshwork that confers the transport properties of the NPC. The fully assembled NPC (**f**) consists of multiple copies of the component nucleoporins, which are arranged in octagonal symmetry to create a cylindrical channel. Peripheral structures include the cytoplasmic filaments and the nuclear basket, protruding from opposite faces of the NPC. Initial membrane contact (**b**) is depicted according to the enclosure model. It should be noted that the order of events is the same for both the enclosure and insertion modes of NPC assembly

found at the NE around this time. The steps following membrane recruitment can be ordered in space starting from the membrane and building laterally towards the center of the pore, as was suggested by the protein-protein interaction network of yeast (Rexach 2009). First, the Nup93 complex joins the assembling pore (Dultz et al. 2008). Recent experiments in *Xenopus* egg extracts suggest that the recruitment of the Nup93 complex proceeds by assembly of the individual components rather than by recruitment of the pre-assembled complex (Sachdev et al. 2012; Theerthagiri et al. 2010; Vollmer et al. 2012). Of these components, Nup53 is the first to associate with the nascent pore, probably followed by Nup155. Both proteins interact with the transmembrane nucleoporins NDC1 and POM121 (Mansfeld et al. 2006; Mitchell et al. 2010; Yavuz et al. 2010) and thus provide a second link between the NPC and membranes at the pore. The capacity for Nup53 to interact directly with membranes may further contribute to the formation or stability of the growing NPC (Vollmer et al. 2012). Nup93 interacts with Nup53 and is consequently incorporated, along with its binding partners Nup188 and Nup205 to complete the structural backbone of the pore. Nup93 subsequently recruits the FG repeat-containing nucleoporins of the Nup62 complex. The FG-containing nucleoporin Nup98 is recruited concomitantly with Nup93 (Dultz et al. 2008) and has recently been found to be key to the establishment of the transport and exclusion properties of the pore (Hulsmann et al. 2012; Laurell et al. 2011). Together, these FG nucleoporins form a substantial part of the hydrophobic meshwork in the center of the pore (Ribbeck and Gorlich 2001).

Open questions remain regarding the construction of a fully assembled NPC. Many nucleoporins, including the Nup107-160 complex, are symmetrically distributed on both the nucleoplasmic and cytoplasmic side of the NPC (Brohawn et al. 2009; Rout et al. 2000; Belgareh et al. 2001) but the timing and mechanistic details regarding assembly of the cytoplasmic portion of the NPC are largely unknown. Similarly, the formation of peripheral NPC structures, such as the nuclear basket and the cytoplasmic filaments, follows the establishment of the structural pore and central channel but the precise order of events is not well defined. Finally, although the complete pore possesses octagonal symmetry, it is not clear whether the numerous copies of each subcomplex are recruited simultaneously. This question is beyond the resolution of current experimental techniques.

Regulating NPC assembly on chromatin at the end of mitosis

Nucleoporins play diverse roles during mitosis (for review, see Chatel and Fahrenkrog 2011) but they do not assemble NPCs until mitotic exit. Multiple nucleoporins, including members of the Nup107-160 complex, Nup98, and Nup53, are phosphorylated by mitotic kinases (Favreau et al. 1996; Glavy et al. 2007; Laurell et al. 2011; Macaulay et al. 1995; Mansfeld et al. 2006; Onischenko et al. 2005), and it is tempting to speculate that mitotic phosphorylation acts as a general mechanism to keep nucleoporins in a dissociated state. Indeed, hyperphosphorylation of Nup98 interferes with its associations at the pore and initiates the disassembly of the NPC at the start of mitosis (Laurell et al. 2011). Conversely, dephosphorylation at the end of mitosis should promote interactions between nucleoporins and thus NPC assembly. In most instances direct evidence for such a mechanism is lacking because the kinases and phosphatases responsible perform a plethora of functions that are essential to mitotic entry, progression, and exit. Furthermore, the identification of decisive phosphorylation events is complicated by a high degree of redundancy. For example, Nup98 is phosphorylated at 13 different sites by cdk1 and members of the NIMA-related kinase family during mitosis (Laurell et al. 2011).

Spatial regulation of NPC assembly on chromatin is provided by the localized concentration of ranGTP (Kalab et al. 2002). The importance of this spatial information is underlined by the aberrant formation of NPCs in ER membrane stacks apart from NE when the ranGTP gradient is disturbed (Walther et al. 2003b). Transport receptors of the importin family bind a large proportion of nucleoporins and have been proposed to regulate the post-mitotic formation of NPCs by blocking the relevant interactions between NPC components (Harel et al. 2003; Walther et al. 2003b). This inhibition is reversed by the ranGTP-dependent release of importin-bound nucleoporins in the vicinity of chromatin, which is required for NPC formation at the NE. MEL-28/ELYS and the Nup107-160 complex represent attractive candidates for such a mode of regulation because they bind transport receptors and associate with chromatin in the early stages of NPC assembly (Walther et al. 2003b; Rasala et al. 2008; Rotem et al. 2009; Franz et al. 2007). However, the functional outcome of transport receptor binding is generally difficult to dissect due to the existence of multiple distinct interaction-dependent activities. Interactions between FG nucleoporins and transportins or importins are required to facilitate transport of cargoes through the NPC, a function that may also extend to other NPC components, such as Nup50 (Lindsay et al. 2002). Several nucleoporins also bind transport receptors in order to be imported to the nucleoplasmic side of the pore, where they contribute to interphase NPC assembly. The integral membrane nucleoporin POM121 is transported in this way (Doucet et al. 2010; Funakoshi et al. 2011) and it is likely that the Nup107-160 complex employs a similar mechanism. Thus, as for the temporal regulation of NPC assembly, challenges still lie ahead in deciphering the molecular mechanisms that control NPC assembly on post-mitotic chromatin.

Unpacking chromatin during mitotic exit

In metazoans, the establishment of an interphase nucleus that is competent for regulated transcription and replication depends on the coordination of chromatin de-condensation and NE formation during mitotic exit. Whereas the molecular mechanisms involved in NE and NPC assembly are beginning to emerge, much less is known about the contemporaneous changes that occur on chromatin at the end of mitosis.

We are only starting to understand the molecular and structural dynamics that determine chromatin organization. This reflects the inherent complications in investigating the complexity of protein-DNA interactions involved in packing DNA molecules into chromatin (Maeshima et al. 2010). As a result, the structural rearrangements and relevant effector molecules that enable the 50-fold compaction of mammalian mitotic chromosomes are far from understood (for review, see Belmont 2006; Ohta et al. 2011).

Chromosomes achieve maximal compaction during anaphase, a feat that requires the chromokinesin KID (Ohsugi et al. 2008) and the mitotic kinase Aurora B at the chromatin (Mora-Bermudez et al. 2007). The de-condensation of mitotic chromosomes during late anaphase of mitosis requires the extraction of polyubiquitinylated Aurora B by the AAA ATPase p97 (Ramadan et al. 2007). The precise consequences of Aurora B inhibition, including the relevant targets of this kinase, and of other p97-dependent activities are not currently understood. In addition to p97, the protein phosphatase PP1 and its nuclear targeting unit PNUTS have been implicated in post-mitotic chromatin de-condensation (Landsverk et al. 2005; Lee et al. 2010). Mitotic exit is generally promoted by the activities of PP1 and PP2A (Wurzenberger and Gerlich 2011) but the molecular targets regulated by these phosphatases, particularly with regard to post-mitotic changes to chromatin structure, are largely unknown.

Coordinating the establishment of the NE and interphase chromatin architecture

Interphase chromatin architecture is not random. Individual chromosomes occupy distinct territories within the 3D organization of the nucleus, which are maintained throughout a lifetime of cell divisions (reviewed in Cremer et al. 2006; Misteli 2007). Furthermore, highly condensed chromatin regions, known as heterochromatin, are predominantly found at the nuclear periphery and have been observed in close proximity to the NE (reviewed in Akhtar and Gasser 2007; Francastel et al. 2000). Proteins of the nuclear lamina, INM, and NPC interact with chromatin during interphase and have been implicated in chromatin organization at the envelope. Our current understanding of how these interactions impact chromatin structure and transcriptional activity are beyond the scope of this review and are discussed thoroughly by others (Capelson et al. 2010; Zuleger et al. 2011; Kubben et al. 2010).

Although many of the interactions between chromatin and proteins at the nuclear periphery are either transient or established following the formation of a closed NE, the broad organization of chromatin in the nucleus must be established as the chromosomes de-condense and could be coupled to NE formation. In support of this hypothesis, common focal points for chromatin condensation and de-condensation have been observed at the nuclear periphery (Hiraoka et al. 1989). Multiple transmembrane proteins of the NE have been found to impact chromatin de-condensation (Korfali et al. 2010; Chi et al. 2007). However, the molecular mechanisms that account for the involvement of NE proteins in chromatin de-condensation have yet to be elucidated.

We are therefore still confronted with the question of how chromatin organization is established at the end of mitosis. A recent study suggests that the peripheral identity of chromatin is maintained throughout the cell cycle (Olins et al. 2011). Peripheral chromatin of both interphase nuclei and mitotic chromosomes, termed epichromatin, can be characterized by presence of a specific nucleosome-based and conformation-dependent epitope. Although the functional significance of epichromatin is currently unclear, it is tempting to speculate that the continuity of peripheral chromatin architecture contributes to the establishment of nuclear organization at the end of mitosis. In this context, epichromatin could provide a scaffold for components of the NE. Phosphatidylserine is associated with histones specifically localized to epichromatin and it might provide a seeding point for nuclear membranes at these defined chromatin regions (Prudovsky et al. 2012). During mitosis, a layer of largely nucleoplasmic proteins and ribonucleoproteins, collectively referred to as perichromatin, associates with non-repetitive DNA sequences at the chromatin periphery (for review, see Hernandez-Verdun and Gautier 1994; Van Hooser et al. 2005), and it is possible that epichromatin also mediates this localization. Importantly, perichromosomal components have been proposed to contribute to the early events of post-mitotic nuclear assembly (Hernandez-Verdun and Gautier 1994).

Structural features of chromatin are often correlated with post-translational modifications to histones. As specific histone phosphorylation and methylation events are reportedly coordinated with the cell cycle (Oki et al. 2007; Markaki et al. 2009), they might contribute to the changes in chromatin structure observed during the cell cycle. However, there is no evidence that histone modifications actually mediate the dramatically altered compaction of chromatin during mitosis. For example, histone H3 phosphorylation at serine 10 is perhaps the most prominent mitotic histone modification but

it is not essential for chromatin condensation in yeast or vertebrates (Hsu et al. 2000; MacCallum et al. 2002). Nonetheless, cell cycle-specific histone modifications could regulate the association of non-histone factors with chromatin.

Two chromatin-binding proteins, HP1 and BAF, provide a link between the de-condensing chromosomes and NE assembly by binding to LBR and LEM domain containing INM proteins, respectively. Interestingly, HP1 binding to chromatin is inhibited by H3 phosphorylation at serine 10 and promoted by methylation at lysine 9 (Fischle et al. 2005; Bannister et al. 2001; Lachner et al. 2001; Hirota et al. 2005). Although LBR can interact directly with histones and with other chromatin-associated proteins (reviewed in Olins et al. 2010), the regulation of HP1 binding by cell cycle-dependent modifications of histone H3 could regulate the post-mitotic association of the INM protein with chromatin. BAF binds to both histone H3 and histone H1 in vitro, which might mediate its interaction with chromatin, but this interaction is not dependent on post-translational histone modifications (Montes de Oca et al. 2005). Instead, BAF has been found to promote the accumulation of interphase histone H3 marks at the end of mitosis (Montes de Oca et al. 2011).

The recruitment of BAF to chromatin occurs in early anaphase and is required for post-mitotic NE assembly (Gorjanacz et al. 2007; Margalit et al. 2005; Segura-Totten et al. 2002; Furukawa et al. 2003). BAF directs the post-mitotic incorporation and interphase distribution of LEM-domain containing proteins, which reciprocally modulate the distribution of BAF during interphase (Haraguchi et al. 2008; Margalit et al. 2007; Ulbert et al. 2006a; Brachner and Foisner 2011). The INM protein LEM4 was recently found to act at the convergence of NE assembly and chromatin structure (Asencio et al. 2012). During mitosis, the association of BAF with chromatin is negatively regulated by vrk1-dependent phosphorylation (Gorjanacz et al. 2007; Nichols et al. 2006), which is reversed by PP2A upon mitotic exit (Asencio et al. 2012). These counteracting events require LEM4 and its interaction with both the kinase and the phosphatase to control BAF-dependent NE assembly on the chromatin. It is currently unclear how the interaction of LEM4 with vrk1 and PP2A is controlled to ensure this regulation. As LEM2 was found to interact with PP1, it will be interesting to determine whether a similar regulatory mechanism is employed and to identify the downstream targets. PP1 has been implicated as a link between chromatin re-organization during mitotic exit and NE reassembly with its regulatory subunit RepoMan (Vagnarelli et al. 2011).

Fluorescence imaging data from human cells indicates that DNA-binding and INM proteins are not recruited uniformly to chromatin at the end of mitosis. From late anaphase until the establishment of an import competent nucleus, the chromatin mass can be divided into two distinct territories. When telophase chromatin is viewed in the axis of the mitotic spindle, the “core” refers the central region at surfaces both proximal and distal to the spindle. Along the same axis, the more peripheral chromatin domain corresponds to “noncore” chromatin. The core region is enriched in A-type lamins and is established by the local accumulation of BAF (Haraguchi et al. 2008). Accordingly, Lap2β and emerin are found at core chromatin in late anaphase before being distributed rather homogeneously at the rim of the completed nucleus (Dabauvalle et al. 1999; Haraguchi et al. 2000). Conversely, LBR is recruited to the noncore region, where nucleoporins and lamin B also accumulate (Chaudhary and Courvalin 1993; Haraguchi et al. 2000, 2008). The DNA-binding nucleoporin MEL-28/ELYS was recently found to control the establishment of these subdomains (Clever et al. 2012), an event that requires the Nup107-160 complex. Thus, the initial stages of NPC formation on chromatin are linked to the establishment of distinct chromatin regions. The importance of these transient chromatin domains in the establishment of a functional nucleus has yet to be determined.

Conclusions

Re-establishing the vertebrate nuclear compartment after mitosis invokes remarkable changes to chromatin structure and ER membrane organization. As chromatin de-condenses, NPCs are assembled and incorporated in the re-forming nuclear membranes to ensure that regulated exchange can occur across the otherwise impermeable nuclear boundary. The construction of a functional nucleus thus requires seamless coordination and multifaceted interactions between membrane, NPC, and chromatin components. Nuclear membranes are segregated from the mitotic ER in anaphase due to interactions between transmembrane proteins destined for the NE with chromatin-associated factors. Assembly of copious NPCs is also initiated on chromatin, but whether NPCs assemble and are inserted into intact NE sheets or are rather enclosed by the re-forming NE remains controversial. Mitotic kinases and phosphatases, along with the activity of the ran system, provide the temporal and spatial cues that control nuclear membrane and NPC protein recruitment and assembly on de-condensing chromatin. The molecular mechanisms underlying the transition of nuclear membranes and NPC components to a post-mitotic state with the capacity to form a NE are beginning to emerge. Comparatively, little is known about the series of structural changes that occur on chromatin during de-condensation and render it competent for the initial recruitment of nuclear membranes and NPC components. The faithful completion of post-mitotic nuclear assembly relies on the coordination

of major NE and chromatin restructuring events as well as the construction of functional NPCs, and it is likely that several mitotic signaling nodes link these processes.

Acknowledgments We thank Nathalie Eisenhardt, Michael Lorenz, and Ruchika Sachdev for critical discussions and helpful comments.

References

Akhtar A, Gasser SM (2007) The nuclear envelope and transcriptional control. Nat Rev Genet 8(7):507–517. doi:10.1038/nrg2122

Anderson DJ, Hetzer MW (2007) Nuclear envelope formation by chromatin-mediated reorganization of the endoplasmic reticulum. Nat Cell Biol 9(10):1160–1166

Anderson DJ, Hetzer MW (2008a) Reshaping of the endoplasmic reticulum limits the rate for nuclear envelope formation. J Cell Biol 182(5):911–924. doi:10.1083/jcb.200805140

Anderson DJ, Hetzer MW (2008b) Shaping the endoplasmic reticulum into the nuclear envelope. J Cell Sci 121(Pt 2):137–142. doi:10.1242/jcs.005777

Anderson DJ, Vargas JD, Hsiao JP, Hetzer MW (2009) Recruitment of functionally distinct membrane proteins to chromatin mediates nuclear envelope formation in vivo. J Cell Biol 186(2):183–191. doi:10.1083/jcb.200901106

Antonin W, Franz C, Haselmann U, Antony C, Mattaj IW (2005) The integral membrane nucleoporin pom121 functionally links nuclear pore complex assembly and nuclear envelope formation. Mol Cell 17(1):83–92

Antonin W, Ellenberg J, Dultz E (2008) Nuclear pore complex assembly through the cell cycle: regulation and membrane organization. FEBS Lett 582(14):2004–2016

Antonin W, Ungricht R, Kutay U (2011) Traversing the NPC along the pore membrane: targeting of membrane proteins to the INM. Nucleus 2(2):87–91. doi:10.4161/nucl.2.2.14637

Asencio C, Davidson IF, Santarella-Mellwig R, Ly-Hartig TB, Mall M, Wallenfang MR, Mattaj IW, Gorjanacz M (2012) Coordination of kinase and phosphatase activities by Lem4 enables nuclear envelope reassembly during mitosis. Cell 150(1):122–135. doi:10.1016/j.cell.2012.04.043

Bannister AJ, Zegerman P, Partridge JF, Miska EA, Thomas JO, Allshire RC, Kouzarides T (2001) Selective recognition of methylated lysine 9 on histone H3 by the HP1 chromo domain. Nature 410(6824):120–124. doi:10.1038/35065138

Baur T, Ramadan K, Schlundt A, Kartenbeck J, Meyer HH (2007) NSF- and SNARE-mediated membrane fusion is required for nuclear envelope formation and completion of nuclear pore complex assembly in *Xenopus laevis* egg extracts. J Cell Sci 120(Pt 16):2895–2903

Belgareh N, Rabut G, Bai SW, van Overbeek M, Beaudouin J, Daigle N, Zatsepina OV, Pasteau F, Labas V, Fromont-Racine M, Ellenberg J, Doye V (2001) An evolutionarily conserved NPC subcomplex, which redistributes in part to kinetochores in mammalian cells. J Cell Biol 154(6):1147–1160. doi:10.1083/jcb.200101081

Belmont AS (2006) Mitotic chromosome structure and condensation. Curr Opin Cell Biol 18(6):632–638

Bodoor K, Shaikh S, Salina D, Raharjo WH, Bastos R, Lohka M, Burke B (1999) Sequential recruitment of NPC proteins to the nuclear periphery at the end of mitosis. J Cell Sci 112(Pt 13):2253–2264

Brachner A, Foisner R (2011) Evolvement of LEM proteins as chromatin tethers at the nuclear periphery. Biochem Soc Trans 39 (6):1735–1741. doi:10.1042/BST20110724

Brohawn SG, Partridge JR, Whittle JR, Schwartz TU (2009) The nuclear pore complex has entered the atomic age. Structure 17 (9):1156–1168. doi:10.1016/j.str.2009.07.014

Buendia B, Courvalin JC (1997) Domain-specific disassembly and reassembly of nuclear membranes during mitosis. Exp Cell Res 230(1):133–144

Burke B (2012) It takes KASH to hitch to the SUN. Cell 149(5):961–963. doi:10.1016/j.cell.2012.05.004

Burke B, Ellenberg J (2002) Remodelling the walls of the nucleus. Nat Rev Mol Cell Biol 3(7):487–497

Capelson M, Doucet C, Hetzer MW (2010) Nuclear pore complexes: guardians of the nuclear genome. Cold Spring Harb Symp Quant Biol 75:585–597. doi:10.1101/sqb.2010.75.059

Chatel G, Fahrenkrog B (2011) Nucleoporins: leaving the nuclear pore complex for a successful mitosis. Cell Signal 23(10):1555–1562. doi:10.1016/j.cellsig.2011.05.023

Chaudhary N, Courvalin JC (1993) Stepwise reassembly of the nuclear envelope at the end of mitosis. J Cell Biol 122(2):295–306

Chi YH, Haller K, Peloponese JM Jr, Jeang KT (2007) Histone acetyltransferase hALP and nuclear membrane protein hsSUN1 function in de-condensation of mitotic chromosomes. J Biol Chem 282(37):27447–27458

Clever M, Funakoshi T, Mimura Y, Takagi M, Imamoto N (2012) The nucleoporin ELYS/Mel28 regulates nuclear envelope subdomain formation in HeLa cells. Nucleus 3(2):187–199. doi:10.4161/nucl.19595

Collas P (2000) Formation of the sea urchin male pronucleus in cell-free extracts. Mol Reprod Dev 56 (2Suppl):265-270. doi:10.1002/(SICI)1098-2795(200006)56:2+<265::AID-MRD11>3.0.CO;2-P

Collas P, Courvalin JC, Poccia D (1996) Targeting of membranes to sea urchin sperm chromatin is mediated by a lamin B receptor-like integral membrane protein. J Cell Biol 135(6 Pt 2):1715–1725

Courvalin JC, Segil N, Blobel G, Worman HJ (1992) The lamin B receptor of the inner nuclear membrane undergoes mitosis-specific phosphorylation and is a substrate for p34cdc2-type protein kinase. J Biol Chem 267(27):19035–19038

Cremer T, Cremer M, Dietzel S, Muller S, Solovei I, Fakan S (2006) Chromosome territories—a functional nuclear landscape. Curr Opin Cell Biol 18(3):307–316. doi:10.1016/j.ceb.2006.04.007

D'Angelo MA, Anderson DJ, Richard E, Hetzer MW (2006) Nuclear pores form de novo from both sides of the nuclear envelope. Science 312(5772):440–443

Dabauvalle MC, Muller E, Ewald A, Kress W, Krohne G, Muller CR (1999) Distribution of emerin during the cell cycle. Eur J Cell Biol 78(10):749–756

Daigle N, Beaudouin J, Hartnell L, Imreh G, Hallberg E, Lippincott-Schwartz J, Ellenberg J (2001) Nuclear pore complexes form immobile networks and have a very low turnover in live mammalian cells. J Cell Biol 154(1):71–84

Dawson TR, Lazarus MD, Hetzer MW, Wente SR (2009) ER membrane-bending proteins are necessary for de novo nuclear pore formation. J Cell Biol 184(5):659–675. doi:10.1083/jcb.200806174

De Souza CP, Osmani SA (2009) Double duty for nuclear proteins–the price of more open forms of mitosis. Trends Genet 25 (12):545–554. doi:10.1016/j.tig.2009.10.005

Dephoure N, Zhou C, Villen J, Beausoleil SA, Bakalarski CE, Elledge SJ, Gygi SP (2008) A quantitative atlas of mitotic phosphorylation. Proc Natl Acad Sci U S A 105(31):10762–10767. doi:10.1073/pnas.0805139105

Doucet CM, Hetzer MW (2010) Nuclear pore biogenesis into an intact nuclear envelope. Chromosoma 119(5):469–477. doi:10.1007/s00412-010-0289-2

Doucet CM, Talamas JA, Hetzer MW (2010) Cell cycle-dependent differences in nuclear pore complex assembly in metazoa. Cell 141(6):1030–1041. doi:10.1016/j.cell.2010.04.036

Dreger M, Otto H, Neubauer G, Mann M, Hucho F (1999) Identification of phosphorylation sites in native lamina-associated polypeptide 2 beta. Biochemistry 38(29):9426–9434. doi:10.1021/bi990645f

Dultz E, Ellenberg J (2010) Live imaging of single nuclear pores reveals unique assembly kinetics and mechanism in interphase. J Cell Biol 191(1):15–22. doi:10.1083/jcb.201007076

Dultz E, Zanin E, Wurzenberger C, Braun M, Rabut G, Sironi L, Ellenberg J (2008) Systematic kinetic analysis of mitotic dis- and reassembly of the nuclear pore in living cells. J Cell Biol 180(5):857–865

Dupuy AD, Engelman DM (2008) Protein area occupancy at the center of the red blood cell membrane. Proc Natl Acad Sci U S A 105 (8):2848–2852. doi:10.1073/pnas.0712379105

Ellenberg J, Siggia ED, Moreira JE, Smith CL, Presley JF, Worman HJ, Lippincott-Schwartz J (1997) Nuclear membrane dynamics and reassembly in living cells: targeting of an inner nuclear membrane protein in interphase and mitosis. J Cell Biol 138(6):1193–1206

Ellis JA, Craxton M, Yates JR, Kendrick-Jones J (1998) Aberrant intracellular targeting and cell cycle-dependent phosphorylation of emerin contribute to the Emery–Dreifuss muscular dystrophy phenotype. J Cell Sci 111(Pt 6):781–792

Favreau C, Worman HJ, Wozniak RW, Frappier T, Courvalin JC (1996) Cell cycle-dependent phosphorylation of nucleoporins and nuclear pore membrane protein Gp210. Biochemistry 35(24):8035–8044

Fichtman B, Ramos C, Rasala B, Harel A, Forbes DJ (2010) Inner/outer nuclear membrane fusion in nuclear pore assembly: biochemical demonstration and molecular analysis. Mol Biol Cell. doi:10.1091/mbc.E10-04-0309

Fischle W, Tseng BS, Dormann HL, Ueberheide BM, Garcia BA, Shabanowitz J, Hunt DF, Funabiki H, Allis CD (2005) Regulation of HP1-chromatin binding by histone H3 methylation and phosphorylation. Nature 438(7071):1116–1122. doi:10.1038/nature04219

Foisner R, Gerace L (1993) Integral membrane proteins of the nuclear envelope interact with lamins and chromosomes, and binding is modulated by mitotic phosphorylation. Cell 73 (7):1267–1279

Francastel C, Schubeler D, Martin DI, Groudine M (2000) Nuclear compartmentalization and gene activity. Nat Rev Mol Cell Biol 1 (2):137–143. doi:10.1038/35040083

Franz C, Walczak R, Yavuz S, Santarella R, Gentzel M, Askjaer P, Galy V, Hetzer M, Mattaj IW, Antonin W (2007) MEL-28/ELYS is required for the recruitment of nucleoporins to chromatin and postmitotic nuclear pore complex assembly. EMBO Rep 8(2):165–172

Fujimoto M, Hayashi T (2011) New insights into the role of mitochondria-associated endoplasmic reticulum membrane. Int Rev Cell Mol Biol 292:73–117. doi:10.1016/B978-0-12-386033-0.00002-5

Funakoshi T, Clever M, Watanabe A, Imamoto N (2011) Localization of Pom121 to the inner nuclear membrane is required for an early step of interphase nuclear pore complex assembly. Mol Biol Cell 22(7):1058–1069. doi:10.1091/mbc.E10-07-0641

Furukawa K, Glass C, Kondo T (1997) Characterization of the chromatin binding activity of lamina-associated polypeptide (LAP) 2. Biochem Biophys Res Commun 238(1):240–246. doi:10.1006/bbrc.1997.7235

Furukawa K, Sugiyama S, Osouda S, Goto H, Inagaki M, Horigome T, Omata S, McConnell M, Fisher PA, Nishida Y (2003) Barrier-to-autointegration factor plays crucial roles in cell cycle progression and nuclear organization in *Drosophila*. J Cell Sci 116(Pt 18):3811–3823. doi:10.1242/jcs.00682

Gerace L, Blobel G (1980) The nuclear envelope lamina is reversibly depolymerized during mitosis. Cell 19(1):277–287

Gillespie PJ, Khoudoli GA, Stewart G, Swedlow JR, Blow JJ (2007) ELYS/MEL-28 chromatin association coordinates nuclear pore complex assembly and replication licensing. Curr Biol 17 (19):1657–1662

Glavy JS, Krutchinsky AN, Cristea IM, Berke IC, Boehmer T, Blobel G, Chait BT (2007) Cell-cycle-dependent phosphorylation of the nuclear pore Nup107-160 subcomplex. Proc Natl Acad Sci U S A 104(10):3811–3816

Gorjanacz M, Klerkx EP, Galy V, Santarella R, Lopez-Iglesias C, Askjaer P, Mattaj IW (2007) *Caenorhabditis elegans* BAF-1 and its kinase VRK-1 participate directly in post-mitotic nuclear envelope assembly. EMBO J 26(1):132–143. doi:10.1038/sj.emboj.7601470

Gruenbaum Y, Margalit A, Goldman RD, Shumaker DK, Wilson KL (2005) The nuclear lamina comes of age. Nat Rev Mol Cell Biol 6 (1):21–31. doi:10.1038/nrm1550

Haraguchi T, Koujin T, Hayakawa T, Kaneda T, Tsutsumi C, Imamoto N, Akazawa C, Sukegawa J, Yoneda Y, Hiraoka Y (2000) Live fluorescence imaging reveals early recruitment of emerin, LBR, RanBP2, and Nup153 to reforming functional nuclear envelopes. J Cell Sci 113(Pt 5):779–794

Haraguchi T, Kojidani T, Koujin T, Shimi T, Osakada H, Mori C, Yamamoto A, Hiraoka Y (2008) Live cell imaging and electron microscopy reveal dynamic processes of BAF-directed nuclear envelope assembly. J Cell Sci 121(Pt 15):2540–2554. doi:10.1242/jcs.033597

Harel A, Chan RC, Lachish-Zalait A, Zimmerman E, Elbaum M, Forbes DJ (2003) Importin beta negatively regulates nuclear membrane fusion and nuclear pore complex assembly. Mol Biol Cell 14(11):4387–4396

Hatsuzawa K, Hirose H, Tani K, Yamamoto A, Scheller RH, Tagaya M (2000) Syntaxin 18, a SNAP receptor that functions in the endoplasmic reticulum, intermediate compartment, and cis-Golgi vesicle trafficking. J Biol Chem 275(18):13713–13720

Heald R, McKeon F (1990) Mutations of phosphorylation sites in lamin A that prevent nuclear lamina disassembly in mitosis. Cell 61(4):579–589

Hernandez-Verdun D, Gautier T (1994) The chromosome periphery during mitosis. Bioessays 16(3):179–185. doi:10.1002/bies.950160308

Hetzer M, Bilbao-Cortes D, Walther TC, Gruss OJ, Mattaj IW (2000) GTP hydrolysis by Ran is required for nuclear envelope assembly. Mol Cell 5(6):1013–1024

Hetzer M, Gruss OJ, Mattaj IW (2002) The Ran GTPase as a marker of chromosome position in spindle formation and nuclear envelope assembly. Nat Cell Biol 4(7):E177–E184

Hirano Y, Segawa M, Ouchi FS, Yamakawa Y, Furukawa K, Takeyasu K, Horigome T (2005) Dissociation of emerin from barrier-to-autointegration factor is regulated through mitotic phosphorylation of emerin in a xenopus egg cell-free system. J Biol Chem 280 (48):39925–39933. doi:10.1074/jbc.M503214200

Hiraoka Y, Minden JS, Swedlow JR, Sedat JW, Agard DA (1989) Focal points for chromosome condensation and decondensation revealed by three-dimensional in vivo time-lapse microscopy. Nature 342(6247):293–296. doi:10.1038/342293a0

Hirota T, Lipp JJ, Toh BH, Peters JM (2005) Histone H3 serine 10 phosphorylation by Aurora B causes HP1 dissociation from heterochromatin. Nature 438(7071):1176–1180. doi:10.1038/nature04254

Hsu JY, Sun ZW, Li X, Reuben M, Tatchell K, Bishop DK, Grushcow JM, Brame CJ, Caldwell JA, Hunt DF, Lin R, Smith MM, Allis CD (2000) Mitotic phosphorylation of histone H3 is governed by Ipl1/Aurora kinase and Glc7/PP1 phosphatase in budding yeast and nematodes. Cell 102(3):279–291

Hu J, Shibata Y, Voss C, Shemesh T, Li Z, Coughlin M, Kozlov MM, Rapoport TA, Prinz WA (2008) Membrane proteins of the endoplasmic reticulum induce high-curvature tubules. Science 319 (5867):1247–1250. doi:10.1126/science.1153634

Hu J, Shibata Y, Zhu PP, Voss C, Rismanchi N, Prinz WA, Rapoport TA, Blackstone C (2009) A class of dynamin-like GTPases involved in the generation of the tubular ER network. Cell 138 (3):549–561. doi:10.1016/j.cell.2009.05.025

Hulsmann BB, Labokha AA, Gorlich D (2012) The permeability of reconstituted nuclear pores provides direct evidence for the selective phase model. Cell 150(4):738–751. doi:10.1016/j.cell.2012.07.019

Ito H, Koyama Y, Takano M, Ishii K, Maeno M, Furukawa K, Horigome T (2007) Nuclear envelope precursor vesicle targeting to chromatin is stimulated by protein phosphatase 1 in *Xenopus* egg extracts. Exp Cell Res 313(9):1897–1910. doi:10.1016/j.yexcr.2007.03.015

Jahn R, Scheller RH (2006) SNAREs—engines for membrane fusion. Nat Rev Mol Cell Biol 7(9):631–643. doi:10.1038/nrm2002

Kalab P, Weis K, Heald R (2002) Visualization of a Ran-GTP gradient in interphase and mitotic *Xenopus* egg extracts. Science 295 (5564):2452–2456. doi:10.1126/science.1068798

Korfali N, Wilkie GS, Swanson SK, Srsen V, Batrakou DG, Fairley EA, Malik P, Zuleger N, Goncharevich A, de Las HJ, Kelly DA, Kerr AR, Florens L, Schirmer EC (2010) The leukocyte nuclear envelope proteome varies with cell activation and contains novel transmembrane proteins that affect genome architecture. Mol Cell Proteomics 9(12):2571–2585. doi:10.1074/mcp.M110.002915

Kubben N, Voncken JW, Misteli T (2010) Mapping of protein- and chromatin-interactions at the nuclear lamina. Nucleus 1(6):460–471. doi:10.4161/nucl.1.6.13513

Lachner M, O'Carroll D, Rea S, Mechtler K, Jenuwein T (2001) Methylation of histone H3 lysine 9 creates a binding site for HP1 proteins. Nature 410(6824):116–120. doi:10.1038/35065132

Landsverk HB, Kirkhus M, Bollen M, Kuntziger T, Collas P (2005) PNUTS enhances in vitro chromosome decondensation in a PP1-dependent manner. Biochem J 390(Pt 3):709–717

Larijani B, Poccia DL, Dickinson LC (2000) Phospholipid identification and quantification of membrane vesicle subfractions by 31P-1H two-dimensional nuclear magnetic resonance. Lipids 35 (11):1289–1297

Laurell E, Beck K, Krupina K, Theerthagiri G, Bodenmiller B, Horvath P, Aebersold R, Antonin W, Kutay U (2011) Phosphorylation of Nup98 by multiple kinases is crucial for NPC disassembly during mitotic entry. Cell 144(4):539–550. doi:10.1016/j.cell.2011.01.012

Lee JH, You J, Dobrota E, Skalnik DG (2010) Identification and characterization of a novel human PP1 phosphatase complex. J Biol Chem 285(32):24466–24476. doi:10.1074/jbc.M110.109801

Lindsay ME, Plafker K, Smith AE, Clurman BE, Macara IG (2002) Npap60/Nup50 is a tri-stable switch that stimulates importin-alpha:beta-mediated nuclear protein import. Cell 110 (3):349–360

Liu J, Lee KK, Segura-Totten M, Neufeld E, Wilson KL, Gruenbaum Y (2003) MAN1 and emerin have overlapping function(s) essential for chromosome segregation and cell division in *Caenorhabditis elegans*. Proc Natl Acad Sci U S A 100(8):4598–4603. doi:10.1073/pnas.0730821100

Lu L, Kirchhausen T (2012) Visualizing the high curvature regions of post-mitotic nascent nuclear envelope membrane. Commun Integr Biol 5(1):16–18

Lu L, Ladinsky MS, Kirchhausen T (2009) Cisternal organization of the endoplasmic reticulum during mitosis. Mol Biol Cell 20 (15):3471–3480. doi:10.1091/mbc.E09-04-0327

Lu X, Shi Y, Lu Q, Ma Y, Luo J, Wang Q, Ji J, Jiang Q, Zhang C (2010) Requirement for lamin B receptor and its regulation by importin beta and phosphorylation in nuclear envelope assembly during mitotic exit. J Biol Chem 285(43):33281–33293. doi:10.1074/jbc.M110.102368

Lu L, Ladinsky MS, Kirchhausen T (2011) Formation of the postmitotic nuclear envelope from extended ER cisternae precedes nuclear pore assembly. J Cell Biol 194(3):425–440. doi:10.1083/jcb.201012063

Lu Q, Lu Z, Liu Q, Guo L, Ren H, Fu J, Jiang Q, Clarke PR, Zhang C (2012) Chromatin-bound NLS proteins recruit membrane vesicles and nucleoporins for nuclear envelope assembly via importin-alpha/beta. Cell Res. doi:10.1038/cr.2012.113

Ma Y, Cai S, Lv Q, Jiang Q, Zhang Q, Sodmergen ZZ, Zhang C (2007) Lamin B receptor plays a role in stimulating nuclear envelope production and targeting membrane vesicles to chromatin during nuclear envelope assembly through direct interaction with importin beta. J Cell Sci 120(Pt 3):520–530. doi:10.1242/jcs.03355

Macaulay C, Forbes DJ (1996) Assembly of the nuclear pore: biochemically distinct steps revealed with NEM, GTP gamma S, and BAPTA. J Cell Biol 132(1–2):5–20

Macaulay C, Meier E, Forbes DJ (1995) Differential mitotic phosphorylation of proteins of the nuclear pore complex. J Biol Chem 270 (1):254–262

MacCallum DE, Losada A, Kobayashi R, Hirano T (2002) ISWI remodeling complexes in *Xenopus* egg extracts: identification as major chromosomal components that are regulated by INCENP-Aurora B. Mol Biol Cell 13(1):25–39

Maeshima K, Hihara S, Eltsov M (2010) Chromatin structure: does the 30-nm fibre exist in vivo? Curr Opin Cell Biol 22(3):291–297. doi:10.1016/j.ceb.2010.03.001

Mansfeld J, Guttinger S, Hawryluk-Gara LA, Pante N, Mall M, Galy V, Haselmann U, Muhlhausser P, Wozniak RW, Mattaj IW, Kutay U, Antonin W (2006) The conserved transmembrane nucleoporin NDC1 is required for nuclear pore complex assembly in vertebrate cells. Mol Cell 22(1):93–103

Margalit A, Segura-Totten M, Gruenbaum Y, Wilson KL (2005) Barrier-to-autointegration factor is required to segregate and enclose chromosomes within the nuclear envelope and assemble the nuclear lamina. Proc Natl Acad Sci U S A 102(9):3290–3295. doi:10.1073/pnas.0408364102

Margalit A, Neufeld E, Feinstein N, Wilson KL, Podbilewicz B, Gruenbaum Y (2007) Barrier to autointegration factor blocks premature cell fusion and maintains adult muscle integrity in *C. elegans*. J Cell Biol 178(4):661–673. doi:10.1083/jcb.200704049

Markaki Y, Christogianni A, Politou AS, Georgatos SD (2009) Phosphorylation of histone H3 at Thr3 is part of a combinatorial pattern that marks and configures mitotic chromatin. J Cell Sci 122(Pt 16):2809–2819. doi:10.1242/jcs.043810

Mattaj IW (2004) Sorting out the nuclear envelope from the endoplasmic reticulum. Nat Rev Mol Cell Biol 5(1):65–69

Maul GG, Maul HM, Scogna JE, Lieberman MW, Stein GS, Hsu BY, Borun TW (1972) Time sequence of nuclear pore formation in phytohemagglutinin-stimulated lymphocytes and in HeLa cells during the cell cycle. J Cell Biol 55(2):433–447

Misteli T (2007) Beyond the sequence: cellular organization of genome function. Cell 128(4):787–800. doi:10.1016/j.cell.2007.01.028

Mitchell JM, Mansfeld J, Capitanio J, Kutay U, Wozniak RW (2010) Pom121 links two essential subcomplexes of the nuclear pore complex core to the membrane. J Cell Biol 191(3):505–521. doi:10.1083/jcb.201007098

Montes de Oca R, Lee KK, Wilson KL (2005) Binding of barrier to autointegration factor (BAF) to histone H3 and selected linker histones including H1.1. J Biol Chem 280(51):42252–42262. doi:10.1074/jbc.M509917200

Montes de Oca R, Andreassen PR, Wilson KL (2011) Barrier-to-autointegration factor influences specific histone modifications. Nucleus 2(6):580–590. doi:10.4161/nucl.2.6.17960

Mora-Bermudez F, Gerlich D, Ellenberg J (2007) Maximal chromosome compaction occurs by axial shortening in anaphase and depends on Aurora kinase. Nat Cell Biol 9(7):822–831

Newport J, Dunphy W (1992) Characterization of the membrane binding and fusion events during nuclear envelope assembly using purified components. J Cell Biol 116(2):295–306

Nichols RJ, Wiebe MS, Traktman P (2006) The vaccinia-related kinases phosphorylate the N′ terminus of BAF, regulating its interaction with DNA and its retention in the nucleus. Mol Biol Cell 17(5):2451–2464. doi:10.1091/mbc.E05-12-1179

Nikolakaki E, Meier J, Simos G, Georgatos SD, Giannakouros T (1997) Mitotic phosphorylation of the lamin B receptor by a serine/arginine kinase and p34(cdc2). J Biol Chem 272(10):6208–6213

Ohsugi M, Adachi K, Horai R, Kakuta S, Sudo K, Kotaki H, Tokai-Nishizumi N, Sagara H, Iwakura Y, Yamamoto T (2008) Kid-mediated chromosome compaction ensures proper nuclear envelope formation. Cell 132(5):771–782. doi:10.1016/j.cell.2008.01.029

Ohta S, Wood L, Bukowski-Wills JC, Rappsilber J, Earnshaw WC (2011) Building mitotic chromosomes. Curr Opin Cell Biol 23 (1):114–121. doi:10.1016/j.ceb.2010.09.009

Oki M, Aihara H, Ito T (2007) Role of histone phosphorylation in chromatin dynamics and its implications in diseases. Subcell Biochem 41:319–336

Olins AL, Rhodes G, Welch DB, Zwerger M, Olins DE (2010) Lamin B receptor: multi-tasking at the nuclear envelope. Nucleus 1 (1):53–70. doi:10.4161/nucl.1.1.10515

Olins AL, Langhans M, Monestier M, Schlotterer A, Robinson DG, Viotti C, Zentgraf H, Zwerger M, Olins DE (2011) An epichromatin epitope: persistence in the cell cycle and conservation in evolution. Nucleus 2(1):47–60. doi:10.4161/nucl.1.6.13271

Onischenko EA, Gubanova NV, Kiseleva EV, Hallberg E (2005) Cdk1 and okadaic acid-sensitive phosphatases control assembly of nuclear pore complexes in *Drosophila* embryos. Mol Biol Cell 16 (11):5152–5162. doi:10.1091/mbc.E05-07-0642

Orso G, Pendin D, Liu S, Tosetto J, Moss TJ, Faust JE, Micaroni M, Egorova A, Martinuzzi A, McNew JA, Daga A (2009) Homotypic fusion of ER membranes requires the dynamin-like GTPase atlastin. Nature 460(7258):978–983. doi:10.1038/nature08280

Peter M, Nakagawa J, Doree M, Labbe JC, Nigg EA (1990) In vitro disassembly of the nuclear lamina and M phase-specific phosphorylation of lamins by cdc2 kinase. Cell 61(4):591–602

Pfaller R, Smythe C, Newport JW (1991) Assembly/disassembly of the nuclear envelope membrane: cell cycle-dependent binding of nuclear membrane vesicles to chromatin in vitro. Cell 65(2):209–217

Poteryaev D, Squirrell JM, Campbell JM, White JG, Spang A (2005) Involvement of the actin cytoskeleton and homotypic membrane fusion in ER dynamics in *Caenorhabditis elegans*. Mol Biol Cell 16(5):2139–2153. doi:10.1091/mbc.E04-08-0726

Prudovsky I, Vary CP, Markaki Y, Olins AL, Olins DE (2012) Phosphatidylserine colocalizes with epichromatin in interphase nuclei and mitotic chromosomes. Nucleus 3(2):200–210. doi:10.4161/nucl.19662

Puhka M, Vihinen H, Joensuu M, Jokitalo E (2007) Endoplasmic reticulum remains continuous and undergoes sheet-to-tubule transformation during cell division in mammalian cells. J Cell Biol 179(5):895–909

Puhka M, Joensuu M, Vihinen H, Belevich I, Jokitalo E (2012) Progressive sheet-to-tubule transformation is a general mechanism for endoplasmic reticulum partitioning in dividing mammalian cells. Mol Biol Cell 23(13):2424–2432. doi:10.1091/mbc.E10-12-0950

Pyrpasopoulou A, Meier J, Maison C, Simos G, Georgatos SD (1996) The lamin B receptor (LBR) provides essential chromatin docking sites at the nuclear envelope. EMBO J 15(24):7108–7119

Ramadan K, Bruderer R, Spiga FM, Popp O, Baur T, Gotta M, Meyer HH (2007) Cdc48/p97 promotes reformation of the nucleus by extracting the kinase Aurora B from chromatin. Nature 450 (7173):1258–1262

Ramos C, Rafikova ER, Melikov K, Chernomordik LV (2006) Transmembrane proteins are not required for early stages of nuclear envelope assembly. Biochem J 400(3):393–400. doi:10.1042/BJ20061218

Rasala BA, Ramos C, Harel A, Forbes DJ (2008) Capture of AT-rich chromatin by ELYS recruits POM121 and NDC1 to initiate nuclear pore assembly. Mol Biol Cell 19(9):3982–3996. doi:10.1091/mbc.E08-01-0012

Rexach M (2009) Piecing together nuclear pore complex assembly during interphase. J Cell Biol 185(3):377–379. doi:10.1083/jcb.200904022

Ribbeck K, Gorlich D (2001) Kinetic analysis of translocation through nuclear pore complexes. EMBO J 20(6):1320–1330. doi:10.1093/emboj/20.6.1320

Robbins E, Gonatas NK (1964) The ultrastructure of a mammalian cell during the mitotic cycle. J Cell Biol 21:429–463

Rotem A, Gruber R, Shorer H, Shaulov L, Klein E, Harel A (2009) Importin beta regulates the seeding of chromatin with initiation sites for nuclear pore assembly. Mol Biol Cell 20(18):4031–4042. doi:10.1091/mbc.E09-02-0150

Rout MP, Aitchison JD, Suprapto A, Hjertaas K, Zhao Y, Chait BT (2000) The yeast nuclear pore complex: composition, architecture, and transport mechanism. J Cell Biol 148(4):635–651

Sachdev R, Sieverding C, Flotenmeyer M, Antonin W (2012) The C-terminal domain of Nup93 is essential for assembly of the structural backbone of nuclear pore complexes. Mol Biol Cell 23 (4):740–749. doi:10.1091/mbc.E11-09-0761

Segura-Totten M, Kowalski AK, Craigie R, Wilson KL (2002) Barrier-to-autointegration factor: major roles in chromatin decondensation and nuclear assembly. J Cell Biol 158(3):475–485. doi:10.1083/jcb.200202019

Shaulov L, Gruber R, Cohen I, Harel A (2011) A dominant-negative form of POM121 binds chromatin and disrupts the two separate modes of nuclear pore assembly. J Cell Sci 124(Pt 22):3822–3834. doi:10.1242/jcs.086660

Shimi T, Butin-Israeli V, Adam SA, Goldman RD (2010) Nuclear lamins in cell regulation and disease. Cold Spring Harb Symp Quant Biol 75:525–531. doi:10.1101/sqb.2010.75.045

Simons K, Gerl MJ (2010) Revitalizing membrane rafts: new tools and insights. Nat Rev Mol Cell Biol 11(10):688–699. doi:10.1038/nrm2977

Simons K, Toomre D (2000) Lipid rafts and signal transduction. Nat Rev Mol Cell Biol 1(1):31–39. doi:10.1038/35036052

Starr DA, Fridolfsson HN (2010) Interactions between nuclei and the cytoskeleton are mediated by SUN-KASH nuclear-envelope bridges. Annu Rev Cell Dev Biol 26:421–444. doi:10.1146/annurev-cellbio-100109-104037

Takamori S, Holt M, Stenius K, Lemke EA, Gronborg M, Riedel D, Urlaub H, Schenck S, Brugger B, Ringler P, Muller SA, Rammner B, Grater F, Hub JS, De Groot BL, Mieskes G, Moriyama Y, Klingauf J, Grubmuller H, Heuser J, Wieland F, Jahn R (2006) Molecular anatomy of a trafficking organelle. Cell 127(4):831–846. doi:10.1016/j.cell.2006.10.030

Takano M, Takeuchi M, Ito H, Furukawa K, Sugimoto K, Omata S, Horigome T (2002) The binding of lamin B receptor to chromatin is regulated by phosphorylation in the RS region. Eur J Biochem 269(3):943–953

Takano M, Koyama Y, Ito H, Hoshino S, Onogi H, Hagiwara M, Furukawa K, Horigome T (2004) Regulation of binding of lamin B receptor to chromatin by SR protein kinase and cdc2 kinase in *Xenopus* egg extracts. J Biol Chem 279(13):13265–13271. doi:10.1074/jbc.M308854200

Theerthagiri G, Eisenhardt N, Schwarz H, Antonin W (2010) The nucleoporin Nup188 controls passage of membrane proteins across the nuclear pore complex. J Cell Biol 189(7):1129–1142. doi:10.1083/jcb.200912045

Tseng LC, Chen RH (2011) Temporal control of nuclear envelope assembly by phosphorylation of lamin B receptor. Mol Biol Cell 22(18):3306–3317. doi:10.1091/mbc.E11-03-0199

Turgay Y, Ungricht R, Rothballer A, Kiss A, Csucs G, Horvath P, Kutay U (2010) A classical NLS and the SUN domain contribute to the targeting of SUN2 to the inner nuclear membrane. EMBO J 29(14):2262–2275. doi:10.1038/emboj.2010.119

Ulbert S, Antonin W, Platani M, Mattaj IW (2006a) The inner nuclear membrane protein Lem2 is critical for normal nuclear envelope morphology. FEBS Lett 580(27):6435–6441. doi:10.1016/j.febslet.2006.10.060

Ulbert S, Platani M, Boue S, Mattaj IW (2006b) Direct membrane protein–DNA interactions required early in nuclear envelope assembly. J Cell Biol 173(4):469–476

Vagnarelli P, Ribeiro S, Sennels L, Sanchez-Pulido L, de Lima AF, Verheyen T, Kelly DA, Ponting CP, Rappsilber J, Earnshaw WC (2011) Repo-Man coordinates chromosomal reorganization with nuclear envelope reassembly during mitotic exit. Dev Cell 21 (2):328–342. doi:10.1016/j.devcel.2011.06.020

Van Hooser AA, Yuh P, Heald R (2005) The perichromosomal layer. Chromosoma 114(6):377–388. doi:10.1007/s00412-005-0021-9

Vigers GP, Lohka MJ (1991) A distinct vesicle population targets membranes and pore complexes to the nuclear envelope in *Xenopus* eggs. J Cell Biol 112(4):545–556

Vigers GP, Lohka MJ (1992) Regulation of nuclear envelope precursor functions during cell division. J Cell Sci 102(Pt 2):273–284

Voeltz GK, Rolls MM, Rapoport TA (2002) Structural organization of the endoplasmic reticulum. EMBO Rep 3(10):944–950. doi:10.1093/embo-reports/kvf202

Vollmar F, Hacker C, Zahedi RP, Sickmann A, Ewald A, Scheer U, Dabauvalle MC (2009) Assembly of nuclear pore complexes mediated by major vault protein. J Cell Sci 122(Pt 6):780–786. doi:10.1242/jcs.039529

Vollmer B, Schooley A, Sachdev R, Eisenhardt N, Sieverding C, Schneider A, Madlung J, Gerken U, Macek B, Antonin W (2012) Dimerization and the direct membrane interaction of Nup53 contribute to nuclear pore complex assembly. EMBO J (in press)

Walther TC, Alves A, Pickersgill H, Loiodice I, Hetzer M, Galy V, Hulsmann BB, Kocher T, Wilm M, Allen T, Mattaj IW, Doye V (2003a) The conserved Nup107-160 complex is critical for nuclear pore complex assembly. Cell 113(2):195–206

Walther TC, Askjaer P, Gentzel M, Habermann A, Griffiths G, Wilm M, Mattaj IW, Hetzer M (2003b) RanGTP mediates nuclear pore complex assembly. Nature 424(6949):689–694

Weis K (2007) The nuclear pore complex: oily spaghetti or gummy bear? Cell 130(3):405–407

Wente SR, Rout MP (2010) The nuclear pore complex and nuclear transport. Cold Spring Harb Perspect Biol 2(10):a000562. doi:10.1101/cshperspect.a000562

Wilson KL, Foisner R (2010) Lamin-binding proteins. Cold Spring Harb Perspect Biol 2(4):a000554. doi:10.1101/cshperspect.a000554

Wilson KL, Newport J (1988) A trypsin-sensitive receptor on membrane vesicles is required for nuclear envelope formation in vitro. J Cell Biol 107(1):57–68

Winey M, Yarar D, Giddings TH Jr, Mastronarde DN (1997) Nuclear pore complex number and distribution throughout the *Saccharomyces cerevisiae* cell cycle by three-dimensional reconstruction from electron micrographs of nuclear envelopes. Mol Biol Cell 8(11):2119–2132

Wurzenberger C, Gerlich DW (2011) Phosphatases: providing safe passage through mitotic exit. Nat Rev Mol Cell Biol 12(8):469–482. doi:10.1038/nrm3149

Yang L, Guan T, Gerace L (1997) Integral membrane proteins of the nuclear envelope are dispersed throughout the endoplasmic reticulum during mitosis. J Cell Biol 137(6):1199–1210

Yavuz S, Santarella-Mellwig R, Koch B, Jaedicke A, Mattaj IW, Antonin W (2010) NLS-mediated NPC functions of the nucleoporin Pom121. FEBS Lett 584(15):3292–3298. doi:10.1016/j.febslet.2010.07.008

Ye Q, Worman HJ (1994) Primary structure analysis and lamin B and DNA binding of human LBR, an integral protein of the nuclear envelope inner membrane. J Biol Chem 269(15):11306–11311

Ye Q, Callebaut I, Pezhman A, Courvalin JC, Worman HJ (1997) Domain-specific interactions of human HP1-type chromodomain proteins and inner nuclear membrane protein LBR. J Biol Chem 272(23):14983–14989

Zerial M, McBride H (2001) Rab proteins as membrane organizers. Nat Rev Mol Cell Biol 2(2):107–117. doi:10.1038/35052055

Zhang C, Clarke PR (2000) Chromatin-independent nuclear envelope assembly induced by Ran GTPase in *Xenopus* egg extracts. Science 288(5470):1429–1432

Zhendre V, Grelard A, Garnier-Lhomme M, Buchoux S, Larijani B, Dufourc EJ (2011) Key role of polyphosphoinositides in dynamics of fusogenic nuclear membrane vesicles. PLoS One 6(9): e23859. doi:10.1371/journal.pone.0023859

Zuleger N, Robson MI, Schirmer EC (2011) The nuclear envelope as a chromatin organizer. Nucleus 2(5):339–349. doi:10.4161/nucl.2.5.17846

Developmental Cell
Article

RuvB-like ATPases Function in Chromatin Decondensation at the End of Mitosis

Adriana Magalska,[1,4] Anna Katharina Schellhaus,[1] Daniel Moreno-Andrés,[1] Fabio Zanini,[2] Allana Schooley,[1] Ruchika Sachdev,[1] Heinz Schwarz,[2] Johannes Madlung,[3] and Wolfram Antonin[1,*]
[1]Friedrich Miescher Laboratory of the Max Planck Society, Spemannstrasse 39, 72076 Tübingen, Germany
[2]Max Planck Institute for Developmental Biology, Spemannstrasse 35, 72076 Tübingen, Germany
[3]Proteome Center Tübingen, University of Tübingen, 72076 Tübingen, Germany
[4]Present address: Nencki Institute of Experimental Biology, Polish Academy of Sciences, 3 Pasteur Street, 02-093 Warsaw, Poland
*Correspondence: wolfram.antonin@tuebingen.mpg.de
http://dx.doi.org/10.1016/j.devcel.2014.09.001

SUMMARY

Chromatin undergoes extensive structural changes during the cell cycle. Upon mitotic entry, metazoan chromatin undergoes tremendous condensation, creating mitotic chromosomes with 50-fold greater compaction relative to interphase chromosomes. At the end of mitosis, chromosomes reestablish functional interphase chromatin competent for replication and transcription through a decondensation process that is cytologically well described. However, the underlying molecular events and factors remain unidentified. We describe a cell-free system that recapitulates chromatin decondensation based on purified mitotic chromatin and *Xenopus* egg extracts. Using biochemical fractionation, we identify RuvB-like ATPases as chromatin decondensation factors and demonstrate that their ATPase activity is essential for decondensation. Our results show that decompaction of metaphase chromosomes is not merely an inactivation of known chromatin condensation factors but rather an active process requiring specific molecular machinery. Our cell-free system provides an important tool for further molecular characterization of chromatin decondensation and its coordination with concomitant processes.

INTRODUCTION

Cells have evolved highly elaborate mechanisms to transmit genetic information accurately to their offspring. These mechanisms often involve major cellular reorganization. In metazoa, the nucleus entirely disintegrates during each round of cell division (for a review, see Kutay and Hetzer, 2008). At the beginning of mitosis, the nuclear envelope breaks down and the chromatin condenses to rod-shaped chromosomes, which are captured by the mitotic spindle and segregated to the emerging daughter cells. The two resulting cells and their nuclei must therefore reestablish the functional interphase state. This reestablishment during mitotic exit requires the complete reversal of events that occurred at the onset of mitosis. The chromosomes decondense, and the nuclear envelope and other nuclear structures reform.

Whereas mitotic entry and the processes leading to successful spindle formation and chromatin segregation are comparatively well studied (Walczak et al., 2010; Walczak and Heald, 2008) much less is known about the important processes at the end of mitosis. In animal cells, mitotic exit is driven by the inactivation of mitotic kinases (Peters, 2006), the extraction of ubiquitinylated Aurora B from chromosomes by the AAA+ (ATPases associated with diverse cellular activities) ATPase p97 (Ramadan et al., 2007), and the activation of several protein phosphatases, most prominently, PP1 (Landsverk et al., 2005; Steen et al., 2000; Thompson et al., 1997) and PP2A (Schmitz et al., 2010). These events collectively result in the reversal of mitotic phosphorylation on a broad range of substrates (Dephoure et al., 2008; Olsen et al., 2010), yet little is known about the actual machineries that mediate specific mitotic exit events (Wurzenberger and Gerlich, 2011). This is especially evident for chromatin decondensation, a prerequisite for the formation of interphase nuclear structures. Metaphase chromosomes are highly condensed—DNA compaction is up to 50-fold higher than in interphase (Belmont, 2006)—but how this condensation is achieved is still ill defined (for a review, see Hansen, 2012; Ohta et al., 2011). However, the process that reorganizes the genome into a structure competent for transcription and replication is largely unchartered territory. We are ignorant about the proteins that mediate chromatin decondensation, the distinct steps in this most likely multistep procedure, and its regulation.

To date, chromatin decondensation has mainly been examined in the context of sperm chromatin remodeling after fertilization. Highly compacted sperm DNA undergoes reorganization due to the presence of nucleoplasmin (NPM2) stored in oocyte cytoplasm (Philpott et al., 1991). This process has been intensively studied using *Xenopus laevis* egg extracts. *Xenopus* sperm chromatin consists of a complex mixture of sperm-specific basic proteins and histones H3 and H4. NPM2 replaces these basic proteins from the male pronucleus with histones H2A and H2B stored in the egg, relaxing the tightly wound sperm chromatin structure (Philpott and Leno, 1992). However, as mitotic chromatin is already structured around H2A and H2B and does not contain these sperm-specific proteins, chromatin decondensation at the end of mitosis is likely to proceed by another yet-unknown mechanism.

Here, we describe a cell-free assay that faithfully recapitulates decondensation of mitotic chromatin. Using this assay, we show that chromatin decondensation requires ATP and GTP hydrolysis and is, thus, an active process. We identify RuvB-like

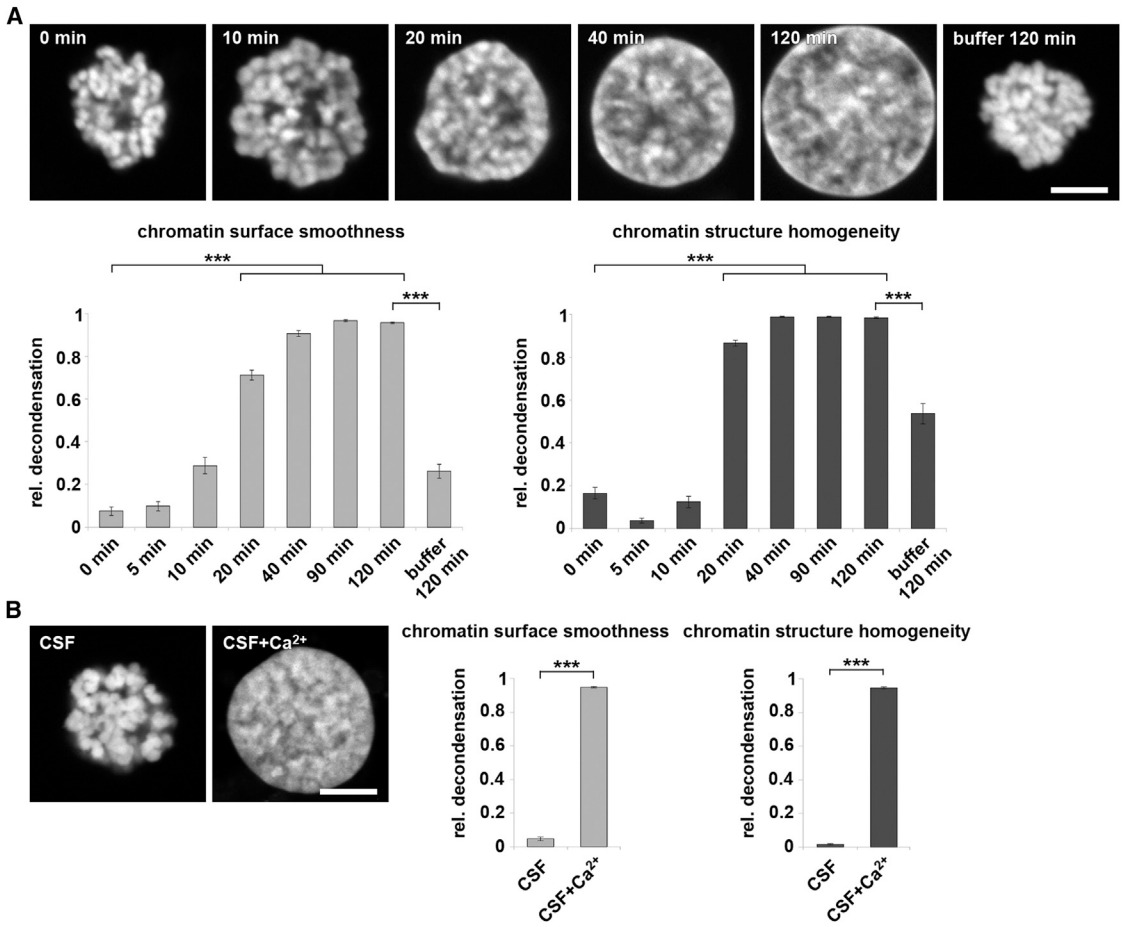

Figure 1. Reconstitution of Chromatin Decondensation in *Xenopus* Egg Extracts

(A) Time course of the in vitro decondensation reaction. Mitotic chromatin clusters from HeLa cells were incubated with postmitotic *Xenopus* egg extracts for the indicated time. Samples were fixed with 4% PFA and 0.5% glutaraldehyde, stained with DAPI, and analyzed by confocal microscopy. For quantification of the decondensation reaction, the smoothness of the boundary of the chromatin (light gray) and the homogeneity of DAPI staining (dark gray) were analyzed. The means (± SEM) of three independent experiments are shown, each including at least ten chromatin substrates for each time point, ***$p < 0.001$ by one-way ANOVA, Dunnett's C post hoc test. rel, relative.

(B) Mitotic chromatin clusters from HeLa cells were incubated for 120 min with CSF-arrested *Xenopus* egg extracts in the absence or presence of 1 mM $CaCl_2$, which induces mitotic exit. Samples were fixed, and the decondensation reaction was quantified as in (A). The means (±SEM) of three independent experiments are shown, each including at least ten chromatin substrates, ***$p < 0.001$ by Mann-Whitney test.

Scale bars, 5 μm. See also Figure S1.

ATPases as crucial chromatin decondensation factors and show that their ATPase activity is essential for decondensation. Intriguingly, both metazoan RuvB-like proteins, RuvBL1 and RuvBL2 can function alone in chromatin decondensation in contrast to many other RuvBL1/RuvBL2-mediated processes, which require both components.

RESULTS

A Cell-free Assay to Monitor Mitotic Chromatin Decondensation

Chromatin decondensation at the end of mitosis is underinvestigated due to a lack of appropriate assays to monitor the process. To overcome this limitation, we have developed a cell-free assay that recapitulates chromatin decondensation in vitro. We incubated highly condensed chromosome clusters isolated from mitotic HeLa cells with cytosol and purified membranes derived from *Xenopus* egg extracts mimicking the postmitotic state. Using DAPI staining and confocal microscopy, we observed sequential morphological changes of chromatin structure (Figure 1A) that resembled chromosome decondensation in cells exiting mitosis (see Figure S1A available online). Highly compacted distinguishable metazoan chromosomes decondensed in a time-dependent manner. After 10–20 min, the individual chromosomes merged to an apparently single corpus, which became progressively spherical and finally adopted an interphasic nuclear appearance. Chromatin decondensation was not induced by the incubation of chromatin substrates with buffer alone, indicating the presence of an essential decondensation activity in egg extracts. Mitotic (cytostatic factor [CSF]-arrested) egg extracts did not support the decondensation of the chromatin substrate (Figure 1B). However, addition of 1 mM Ca^{2+} ions to

mitotic extracts, which causes mitotic exit (Murray, 1991), did induce chromatin decondensation, indicating that postmitotic conditions are required for the process. An equal progressive decondensation was observed when, instead of HeLa cell chromatin, mitotic chromatin generated from *Xenopus* sperm DNA was used (Figure S1B) demonstrating the universality of the process.

We quantified mitotic HeLa chromatin decondensation based on the homogeneity of DAPI staining and the smoothness of the chromatin boundary (Figure 1A; see Experimental Procedures for details). These features were chosen with the following rationale: when chromatin is completely decondensed, the nuclear shape is spherical and bulk chromatin appears to be distributed rather homogenously; when chromatin is condensed, the surface appears rough and bulk chromatin is clustered in distinct chromosomes. Both parameters increased over the time course of HeLa chromosome decondensation and reliably built up the process, indicating a highly reproducible progression of chromatin decondensation in our assay system.

In addition to chromatin decondensation, our in vitro system recapitulates several other mitotic exit events. Histone H3 phosphorylation at serine 10, a marker of the mitotic state of chromatin (Hendzel et al., 1997), was rapidly diminished on incubation with postmitotic *Xenopus* egg extract (Figure 2A, upper panel). Dephosphorylation of this site also occurred when mitotic chromatin was incubated with buffer alone, indicating that the relevant phosphatase activity is present on mitotic chromatin. However, mitotic chromatin incubated with buffer remained condensed (Figures 1A and 2A), consistent with previous findings that this modification is not essential for the establishment or maintenance of condensed mitotic chromatin in yeast or vertebrates (Hsu et al., 2000; MacCallum et al., 2002).

The decondensing chromatin in our assay system was enclosed by membranes, which eventually formed a smooth nuclear envelope (Figures 2B and 2C). The nuclear envelope contained nuclear pore complexes, gatekeepers of the nucleus that mediate nuclear import and export. Nuclear pore complex formation was analyzed by immunofluorescence with mAB414 (Davis and Blobel, 1986), an antibody that recognizes four different nuclear pore complex proteins (Figure 2A, middle panel). Nuclear pore complex proteins labeled by this antibody were first detected approximately 20 min after initiation of decondensation. After a 60–120 min incubation in postmitotic *Xenopus* extracts, the nuclei were capable of nuclear import and export (Figure 2D). Taken together, these results show that our cell-free system recapitulates chromatin decondensation as well as nuclear envelope and pore reformation and is, thus, an invaluable tool for studying mitotic exit events. Notably, in the absence of added membranes, chromatin decondensation similarly occurred, although nuclear envelopes and pore complexes, as expected, did not reform (data not shown). This indicates that chromatin decondensation does not require a reforming nuclear envelope and functional pore complexes, but it is possible that this is a peculiarity of the cell-free assay.

Chromatin Decondensation Requires ATP and GTP Hydrolysis

Having established the versatility of the assay, we first investigated the basic requirements of chromatin decondensation. The removal of endogenous nucleoside triphosphates from the extracts by hexokinase treatment blocked chromatin decondensation (Figure S2A), indicating that some energy-consuming step is required. Nonhydrolyzable ATP or GTP analogs inhibited chromatin decondensation, suggesting that both ATP- and GTP-dependent activities are involved in chromatin decondensation (Figure 3). ATP dependence might be explained by a requirement for the ATPase p97, which removes Aurora kinase B from chromatin during decondensation (Ramadan et al., 2007). However, inhibition of Aurora kinase B by hesperadin, which bypasses the need for p97 in this process (Ramadan et al., 2007), did not restore chromatin decondensation in the presence of nonhydrolyzable ATP analogs, suggesting that at least one other ATPase is involved (data not shown).

Although DNA transcription is thought to be absent in *Xenopus* egg extracts (Newport and Kirschner, 1982), we wanted to exclude that transcriptional activity is required for chromatin decondensation in our assay system. As expected, addition of the transcription inhibitors actinomycin D or 5,6-dichloro-1-β-D-ribofuranosylbenzimidazole did not affect chromatin decondensation (Figure S2B).

RuvBL1 and RuvBL2 Can Function Individually as ATPases in Chromatin Decondensation

To identify essential chromatin decondensation factors, we fractionated the cytosol derived from postmitotic *Xenopus* egg extracts and assayed for chromatin decondensation activity. Differential ammonium sulfate precipitation yielded two fractions that individually had severely reduced decondensation activity but were highly active when combined (Figure 4A; Figure S3A). We further purified the first of these ammonium sulfate fractions by ion exchange and size exclusion chromatography (see Experimental Procedures for detailed information) and assayed the activities of the obtained fractions in combination with the second ammonium sulfate fraction. By mass spectrometry analysis of the gel filtration fractions with highest decondensation activity (G13–G15), we identified several candidate chromatin decondensation factors, including the ATPase RuvBL2. RuvBL2 is known to form a double hexameric ring complex with a second ATPase, RuvBL1 (Jha and Dutta, 2009; Puri et al., 2007). Indeed, western blot analysis confirmed the presence of RuvBL1 and RuvBL2 in the active fractions throughout the purification procedure and enrichment in the most active gel filtration fractions (Figure 4A), which makes these proteins possible candidates for the decondensation activity. RuvBL1/RuvBL2 (also known as RVB1/RVB2, pontin/reptin, and TIP49/TIP48) are two highly conserved members of the AAA+ superfamily. They associate with diverse chromatin remodeling complexes, which are implicated in a variety of nuclear processes, including transcriptional regulation, DNA damage response, and small nuclear ribonucleoprotein particle (snoRNP) assembly (for a review, see Jha and Dutta, 2009; Nano and Houry, 2013; Tosi et al., 2013).

To assess the relevance of RuvBL1 and RuvBL2 for chromatin decondensation, we performed antibody inhibition experiments in the decondensation assay. The addition of purified anti-RuvBL1 or anti-RuvBL2 immunoglobulin G (IgG) to the reactions significantly impaired chromatin decondensation compared to the addition of control IgG (Figures 4B and S3B).

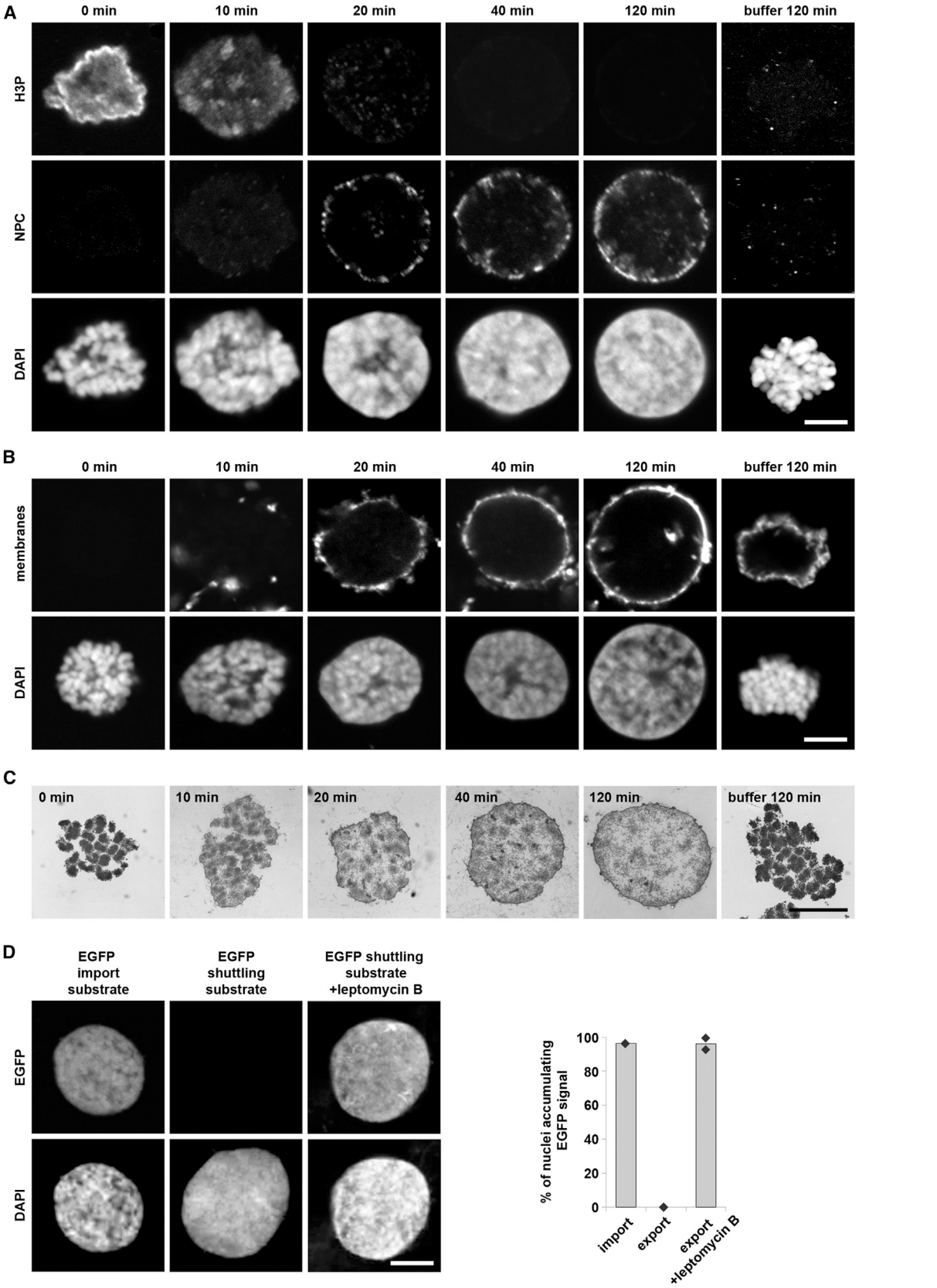

(legend on next page)

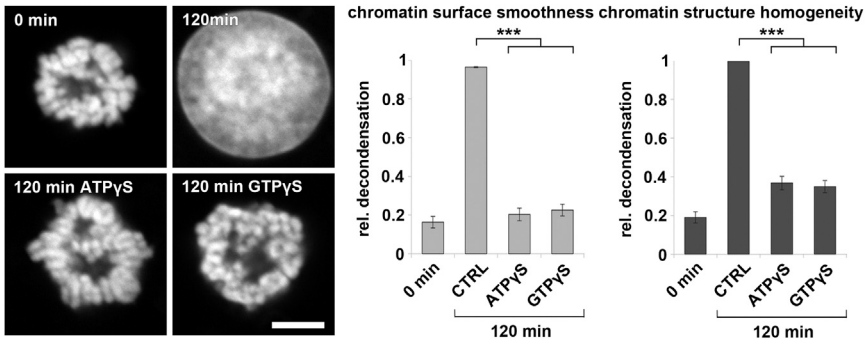

Figure 3. Chromatin Decondensation Requires ATP and GTP Hydrolysis

HeLa mitotic chromatin was decondensed in the presence of 10 mM ATPγS, 10 mM GTPγS, or buffer control (CTRL). Samples were fixed with 4% PFA and 0.5% glutaraldehyde at indicated time points, analyzed, and quantified. The means (±SEM) of three independent experiments are shown, each including at least ten chromatin substrates for each time point, ***$p < 0.001$ by one-way ANOVA, Dunnett's C post hoc test. rel, relative. Scale bar, 5 μm. See also Figure S2.

Immunodepletion using antibodies against either RuvBL1 or RuvBL2, respectively, removed both proteins efficiently from the extracts (Figure 4C), indicating that, in *Xenopus* egg extracts, RuvBL1 and RuvBL2 occur mostly together in heteromeric complexes. Both immunodepletion procedures rendered egg extracts incompetent for chromatin decondensation in contrast to control depletions (Figure 4D). The addition of purified recombinant RuvBL1-RuvBL2 complexes to a final concentration of 0.04 μg/μl, which matches the endogenous concentration (Figure S3C), was sufficient to rescue the depletion phenotype (Figure 4D), indicating on-target specificity of the immunodepletion. These experiments demonstrate that RuvBL1/2 indeed function in chromatin decondensation and are crucial for this process.

RuvBL1 and RuvBL2 Can Function Individually as ATPases in Chromatin Decondensation

In many cellular processes, RuvBL1 and RuvBL2 operate together by forming heteromeric complexes (Jha and Dutta, 2009; Nano and Houry, 2013; Nguyen et al., 2013; Tosi et al., 2013; Venteicher et al., 2008); however, in some instances, these proteins act antagonistically (Bauer et al., 2000; Rottbauer et al., 2002). Surprisingly, the addition of either purified homohexameric RuvBL1 or RuvBL2 complexes to depleted extracts restored decondensation activity as efficiently as the addition of the heteromeric RuvBL1-RuvBL2 complex (Figure 5A). This indicates that both proteins can function redundantly and independently of each other in this process.

The addition of recombinant ATPase-deficient RuvBL1/2 mutants, either individually or in a heteromeric complex (RuvBL1 D302N/RuvBL2 D298N) (Matias et al., 2006; Mézard et al., 1997) (Figure S4C), did not rescue the depletion phenotype, indicating that the ATPase function of either proteins is required for its role in chromatin decondensation (Figure 5B). The addition of excess RuvBL1 D302N, RuvBL2 D298N, or the RuvBL1 D302N/RuvBL2 D298N complex to untreated extracts inhibited chromatin decondensation, while the wild-type proteins and complexes had no effect (Figures 5C and S4A). RuvB-like ATPases perform their different cellular functions in conjunction with a variety of cofactors (for a review, see Jha and Dutta, 2009; Nano and Houry, 2013), and this is most likely also the case for chromatin decondensation (see Discussion). Thus, the dominant-negative effect of ATPase-deficient RuvBL1/2 mutants is likely to be caused by a sequestration of these cofactors. Together, these experiments using ATPase-deficient RuvBL1/2 versions demonstrate that chromatin decondensation depends on ATPase-proficient RuvB-like proteins.

Although RuvB-like proteins are required for chromatin decondensation, they are not sufficient. When purified recombinant RuvBL1, RuvBL2, or the heteromeric RuvBL1/2 complex were added to HeLa mitotic chromatin in buffer in the presence of ATP, no chromatin decondensation was detected (Figure S4B), indicating that other factors are also crucially required (see Discussion).

RuvBL1 and RuvBL2 Localize on the Decondensing Chromatin

We next analyzed the localization of RuvBL1 and RuvBL2 during mitotic exit. Consistent with their role in chromatin decondensation, RuvBL1 and RuvBL2 localize and enrich on postmitotic decondensing chromatin, both in the in vitro assay (Figure 6A) and in HeLa cells (Figure S5A). Both RuvB-like proteins are excluded from chromatin during earlier stages of mitosis, including

Figure 2. Decondensing Chromatin Assembles into Functional Nuclei

(A) Mitotic chromatin clusters from HeLa cells were incubated with *Xenopus* egg extracts for the indicated time and fixed with 4% PFA. Immunofluorescence shows histone H3 serine 10 phosphorylation (H3P, upper panel), nuclear pore complexes (NPC, middle panel), and chromatin (DAPI).

(B) For visualization of nuclear envelope reformation, HeLa mitotic chromatin substrates and DiIC18 (1,1′-dioctadecyl-3,3,3′,3′-tetramethylindocarbocyanine perchlorate)-labeled membranes (upper panel) were added to the egg extracts or the buffer control. Samples were fixed at indicated time points with 4% PFA and 0.5% glutaraldehyde, stained with DAPI (lower panel), and analyzed by confocal microscopy.

(C) Chromatin decondensation using HeLa mitotic chromatin was analyzed by transmission electron microscopy. Samples were fixed at indicated time points with 4% PFA and 2.5% glutaraldehyde, postfixed in 1% OsO_4, and stained with 1% uranyl acetate. After embedding in Epon, ultrathin sections (50–70 nm) were stained with uranyl acetate and lead citrate and viewed with a Philips CM10 microscope.

(D) HeLa mitotic chromatin was decondensed for 120 min. An enhanced green fluorescent protein (EGFP)-fused import substrate (left column) or a shuttling substrate containing a nuclear localization signal and a nuclear export signal (middle and right column) was added. Nuclear export was inhibited by the addition of 300 nM leptomycin B. Samples were stained with DAPI and analyzed by confocal microscopy. The weighted average percentage of two independent experiments, each including at least 100 randomly chosen chromatin substrates, is shown. Diamonds indicate data points of the individual experiments.

Scale bars, 5 μm.

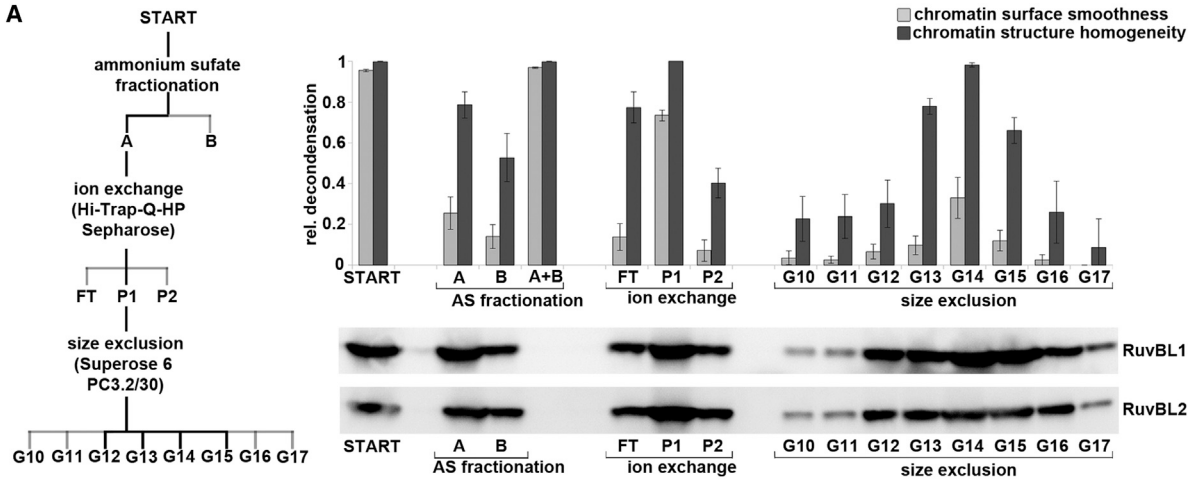

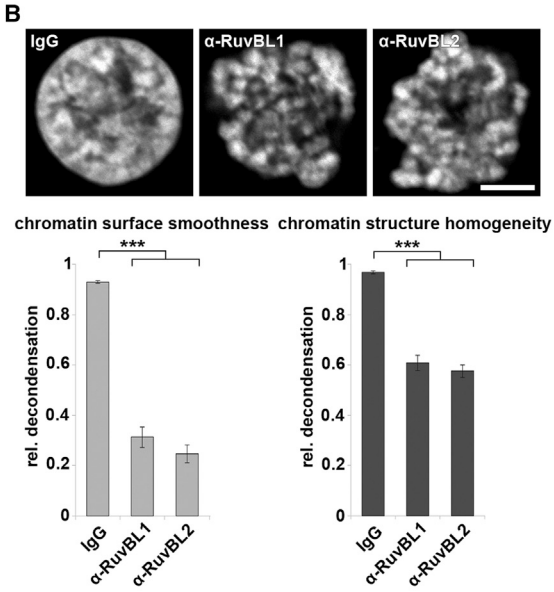

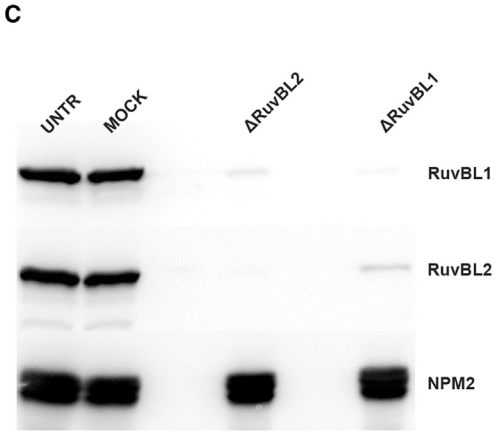

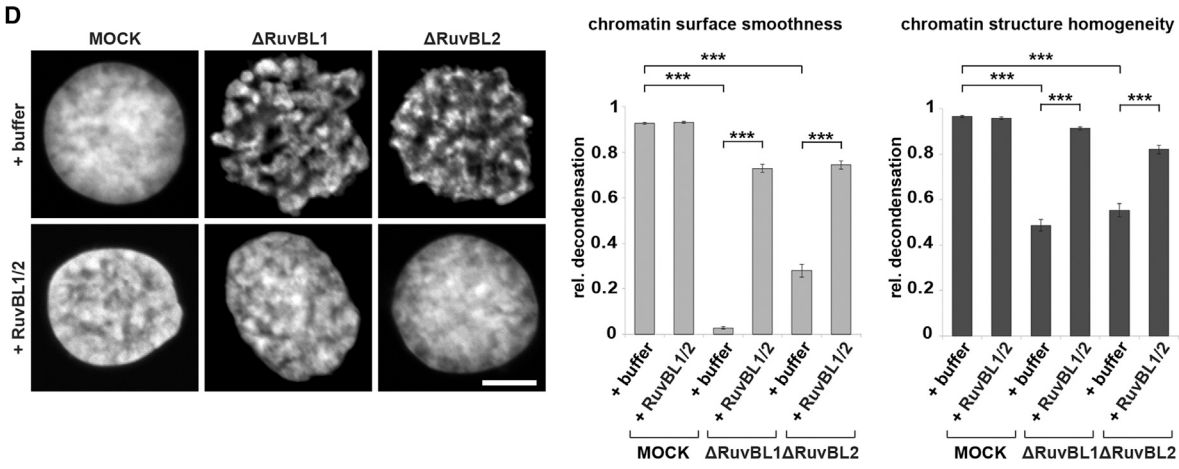

(legend on next page)

metaphase in agreement with previous reports (Gartner et al., 2003; Sigala et al., 2005).

When depleting the endogenous RuvBL1/2 complex, both recombinant RuvBL1 and RuvBL2 could be detected on the chromatin template (Figure 6A), indicating that both proteins can independently localize to chromatin. This observation is consistent with the finding that either homomeric complex can substitute the heteromeric complex to support chromatin decondensation (Figure 5A). The ATPase-deficient mutants similarly localized to chromatin, indicating that the ATPase function is not required for chromatin localization.

Having identified RuvBL1/2 as chromatin decondensation factors, we analyzed the fate of known chromatin condensation factors on the chromatin on depletion of RuvB-like proteins. Topoisomerase II, KIF4A, and the condensin II complex were detected on the chromatin at all stages of the decondensation reaction (Figures 6B and S5B), as expected (Gerlich et al., 2006; Mazumdar et al., 2004; Tavormina et al., 2002). A similar pattern was observed for Repo-Man, also known as CDCA2, which recruits the protein phosphatase PP1 to chromatin during mitotic exit and was shown to coordinate chromatin decondensation and nuclear envelope reformation (Vagnarelli et al., 2011); and for Mel28 (also referred to as ELYS), a chromatin-binding protein that acts as a seeding point for nuclear pore complex formation (Franz et al., 2007). The condensin I complex is lost from the chromatin in the course of decondensation (Gerlich et al., 2006). In all instances, depletion of RuvBL1/2 did not affect the spatiotemporal localization of these proteins on decondensing chromatin, indicating that RuvB-like ATPases act independently of these factors during decondensation.

RuvB-like ATPases Are Not Required for Nuclear Envelope and Pore Complex Formation

Our data show that the RuvB-like ATPases function as key decondensation factors of mitotic chromatin. In organisms undergoing open mitosis, the nuclear envelope and nuclear pore complexes break down at the beginning of mitosis and reform on the decondensing chromatin in telophase (for a review, see (Kutay and Hetzer, 2008; Schooley et al., 2012). On depletion of RuvBL1/2 in the decondensation assay, we did not observe formation of a closed nuclear envelope and nuclear pore complex reassembly (data not shown). This could indicate that RuvB-like ATPases are also involved in these processes. Alternatively, chromatin decondensation might be a prerequisite for nuclear envelope and pore complex assembly. To distinguish these two possibilities, we sought to bypass the need of RuvBL1/2 for chromatin decondensation by using an already decompacted chromatin template. For this, *Xenopus* sperm heads were incubated in postmitotic egg extracts. In this assay, which recapitulates the processes naturally occurring after entry of sperm DNA into an egg, pronuclei with intact nuclear envelopes and pore complexes are formed, and this system has been widely used to study these assembly processes (Gant and Wilson, 1997). Notably, sperm DNA is, in this experimental setup, decompacted by the NPM2-mediated exchange of protamines to histones H2A and H2B (Philpott and Leno, 1992). When sperm heads were incubated with control or RuvBL1/2-depleted postmitotic extracts, pronuclei with closed nuclear envelopes and intact nuclear pore complexes were formed (Figure 7). These experiments demonstrate that, as expected, RuvB-like proteins are not required for sperm DNA decompaction. Notably, they are also not crucial for nuclear envelope and pore complex formation. In this experimental system, the pronuclei undergo nuclear expansion after initial NPM2-dependent sperm DNA decompaction. This process, which is also referred to as nuclear swelling/expansion or secondary decondensation, requires nuclear import and, thus, a functional nuclear envelope including pore complexes (Philpott et al., 1991; Wright, 1999). The DAPI staining of the pronuclei assembled in the absence of RuvBL1/2 indicates that this nuclear swelling does not require RuvB-like ATPases. These data also show that distinct mitotic exit events such as chromatin decondensation and nuclear envelope/pore complex reformation can be uncoupled in vitro.

Mitotic chromatin decondensation does not require NPM2, which, in turn, is needed for sperm DNA decompaction (Figure S6). This supports the view that sperm DNA and mitotic chromatin decondensation are mechanistically fundamentally different.

DISCUSSION

Here, we show that chromatin decondensation can be faithfully reconstituted in a cell-free assay. Using this system, we demonstrate that the process requires ATP and GTP hydrolysis. It is not merely an inactivation of known chromatin condensation factors but an active process involving specific molecular machinery. We identify a defined requirement for the RuvB-like ATPases in chromatin decondensation, but not for nuclear envelope and pore complex formation. Our assay system is, therefore, a valuable tool for the dissection of the cellular processes

Figure 4. Chromatin Decondensation Requires RuvB-like ATPases

(A) *Xenopus* egg extracts were fractionated by differential ammonium sulfate precipitation, ion exchange, and size exclusion chromatography (see fractionation scheme on the left with the fractions showing decondensation activity in black) and were tested for the state of chromatin decondensation on HeLa mitotic chromatin after 120 min. For ion exchange and size exclusion fractions, reactions were performed in the presence of fraction B of the ammonium sulfate precipitation. The lower panels show the distribution of RuvBL1 and RuvBL2 in fractions analyzed by western blotting. Representative quantification and western blot analysis of one fractionation experiment is shown. FT, flowthrough. rel, relative.

(B) Chromatin decondensation on HeLa mitotic chromatin was performed for 120 min in the presence of 4 mg/ml affinity-purified IgG against RuvBL1, RuvBL2, or control IgGs.

(C) Western blot of untreated (UNTR), mock, and RuvBL1/2-depleted extracts, the latter two generated by two passages over control IgG- or anti-RuvBL1 or anti-RuvBL2 IgG-bound beads, respectively. NPM2 serves as a control protein unaffected by this treatment.

(D) Mock or RuvBL1/2-depleted extracts supplemented with buffer or purified recombinant RuvBL1-RuvBL2 complex (0.04 μg/μl to match the endogenous concentration) were tested for chromatin decondensation on HeLa mitotic chromatin (120 min time point).

In (B) and (D), the means (±SEM) of three independent experiments are shown, each including at least 20 chromatin substrates. ***$p < 0.001$ by one-way ANOVA, Dunnett's C post hoc test. Scale bars, 5 μm. See also Figure S3.

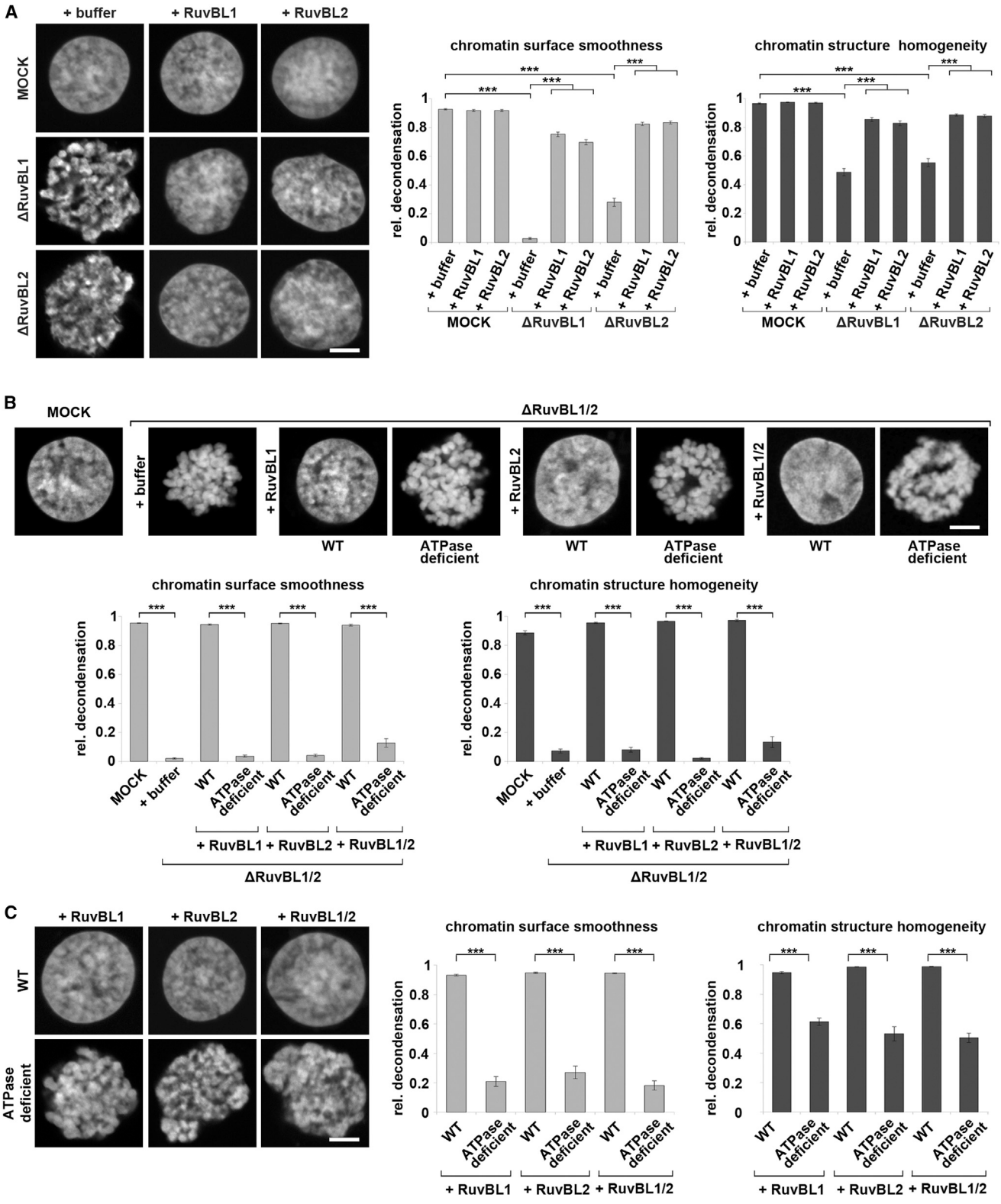

Figure 5. RuvBL1 or RuvBL2 Alone Is Sufficient to Support Chromatin Decondensation and Require ATPase Activity

(A) RuvBL1/2-depleted extracts (generated by two passages over anti-RuvBL1 or anti-RuvBL2 IgG-bound beads, respectively) were supplemented with purified recombinant RuvBL1 or RuvBL2 (0.02 μg/μl to match the endogenous concentration) and tested for chromatin decondensation on HeLa mitotic chromatin. rel, relative.

(legend continued on next page)

that lead to the assembly of functional interphase chromatin after mitosis.

Cell-free extracts derived from frog eggs, especially from *Xenopus laevis*, have been widely used to study cell cycle regulation as well as many mitotic and nuclear processes since their development and first use 30 years ago (Lohka and Masui, 1983). These extracts recapitulate complex cellular reactions such as chromatin condensation, spindle assembly, and nuclear envelope breakdown (Galy et al., 2008; Maresca and Heald, 2006). Nuclear envelope and pore complex formation has been intensively studied in pronucleus formation using sperm DNA as a chromatin template (for a review, see Gant and Wilson, 1997). Here, we use mitotic chromatin to study chromatin decondensation and nuclear reformation during mitotic exit. We show that the nuclei formed on the decondensing chromatin contain a closed nuclear envelope with two membranes and nuclear pore complexes (Figure 2). These nuclei are competent for nuclear import and export and DNA replication (Figure 2D; A.M. and W.A., unpublished data), showing that they represent a functional interphasic status.

So far, chromatin decondensation has been mainly investigated in the context of male pronucleus formation around sperm DNA. However, it is unlikely that this involves the same machinery as chromatin decondensation at the end of mitosis. Indeed, our data show that sperm DNA decompacts in the absence of the RuvB-like ATPases (Figure 7), which are required for mitotic chromatin decondensation. In contrast, sperm DNA decondensation depends on the histone chaperone NPM2 (Philpott and Leno, 1992; Philpott et al., 1991), which conversely is not necessary for mitotic chromatin decondensation (Figure S6), consistent with the fact that NPM2 is absent in somatic cells (Burns et al., 2003).

In contrast to sperm DNA decompaction, which is an energy-independent process (Philpott et al., 1991), mitotic chromatin decondensation requires cellular energy (Figure S2). The inhibition of mitotic chromatin decondensation observed in the presence of nonhydrolyzable ATP (Figure 3) suggests that ATPases are involved in the process. Indeed, we show that RuvB-like ATPases and, specifically, their ATPase functions are compulsory in addition to p97, the only protein previously implicated in the postmitotic decondensation of chromatin (Ramadan et al., 2007).

We envision chromatin decondensation as a multistep procedure involving several activities. Indeed, each fraction of our ammonium sulfate fractionation is largely inactive on its own, and only when they are recombined is decondensation activity restored (Figures 4A and S3A). Consistent with the notion of multiple necessary decondensation factors, RuvB-like ATPases are not sufficient to promote chromatin decondensation if added alone to the mitotic chromatin template (Figure S4B). Most likely, yet-unidentified RuvBL1/2 interacting factors are crucially required for the RuvBL1/2-mediated step in chromatin decondensation as in other processes mediated by these ATPases (for a review, see Jha and Dutta, 2009; Nano and Houry, 2013). In addition, chromatin decondensation most likely involves other RuvBL1/2-independent steps. The inhibition by nonhydrolyzable GTP (Figure 3) suggests that at least one GTPase is involved. The nature of the GTPases is currently unknown but an interesting avenue for future research.

RuvB-like proteins are highly conserved and essential eukaryotic AAA+ ATPases involved in a wide range of cellular reactions as components of large protein complexes (for a review, see Jha and Dutta, 2009; Nano and Houry, 2013). These include many chromatin-related, but also other, processes such as chromatin remodeling, transcriptional regulation, and DNA damage response, as well as snoRNP, telomere, and spindle assembly (Ducat et al., 2008; Ikura et al., 2000; Jónsson et al., 2001; Krogan et al., 2003; Lim et al., 2000; Newman et al., 2000; Shen et al., 2000; Venteicher et al., 2008; Wood et al., 2000; Zhao et al., 2005). RuvB-like ATPases show similarity to prokaryotic RuvB proteins but, because of an insertion into the ATPase domain, lack the helicase activity found in the bacterial proteins (Ikura et al., 2000; Matias et al., 2006). Currently, the precise function of RuvB-like ATPases in the different chromatin remodeling and other complexes is unclear (Jha and Dutta, 2009; Rosenbaum et al., 2013). Here, we add chromatin decondensation, a yet-ill-defined but nevertheless essential process during mitosis, to the list of RuvBL1/2-dependent processes. We show that the ATPase activity of RuvBL1/2 is mandatory for chromatin decondensation (Figure 5), in contrast to other RuvBL1/2-dependent processes such as transcriptional regulation (Jónsson et al., 2001). Because RuvB-like ATPases are part of several chromatin remodeling complexes (for a review, see Jha and Dutta, 2009; Rosenbaum et al., 2013), it is tempting to speculate that chromatin decondensation at the end of mitosis functionally requires histone rearrangements, a hypothesis that needs to be addressed in the future.

Many RuvBL1/2-dependent processes rely on a heterododecameric complex formed by both proteins (Nguyen et al., 2013; Tosi et al., 2013; Venteicher et al., 2008; Zhao et al., 2005), and our results confirm that, also in *Xenopus* eggs, these proteins are found to a large extent in heteromeric complexes. In other processes, such as Polycomb or NF-κB-mediated gene repression and β-catenin signaling, RuvBL1 and RuvBL2 act antagonistically (Baek et al., 2002; Bauer et al., 2000; Diop et al., 2008; Kim et al., 2005; Rottbauer et al., 2002). Our readdition experiments suggest that RuvBL1 or RuvBL2 alone can fulfil the RuvB-like dependent functions in chromatin decondensation and thus, in this context, are redundant (Figure 5). Whether this feature is also seen in other RuvB-like-dependent processes

(B) Chromatin decondensation was analyzed in RuvBL1/2-depleted extracts (generated by consecutive passage over anti-RuvBL1 and anti-RuvBL2 IgG-bound beads) supplemented with ATPase-deficient mutant versions of the RuvBL1, RuvBL2, or the RuvBL1-RuvBL2 complex (RuvBL1 D302N and RuvBL2 D298N) matching the endogenous concentration. WT, wild-type.

(C) Chromatin decondensation in the presence of 40-fold excess compared to endogenous concentrations of recombinant wild-type RuvBL1, RuvBL2, or the RuvBL1-RuvBL2 complex or ATPase-deficient mutants of the respective proteins.

Samples were analyzed after 120 min. The means (±SEM) of three independent experiments are shown, each including at least 20 chromatin substrates. ***$p < 0.001$ by two-way ANOVA, Sidlak post hoc test for (A) and (B) and by one-way ANOVA, Dunnett's C post hoc test for (C). WT, wild-type. Scale bars, 5 μm. See also Figure S4.

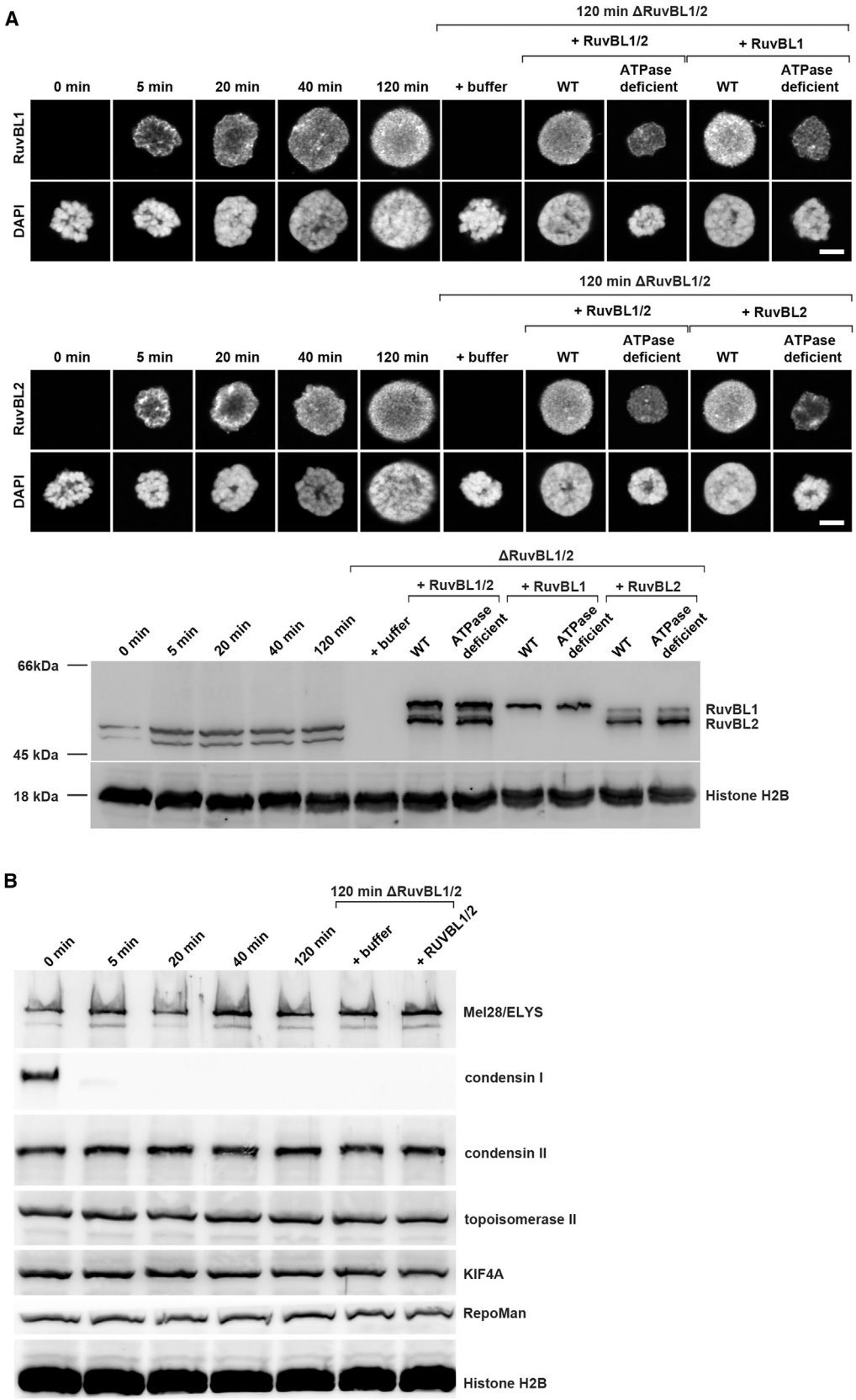

(legend on next page)

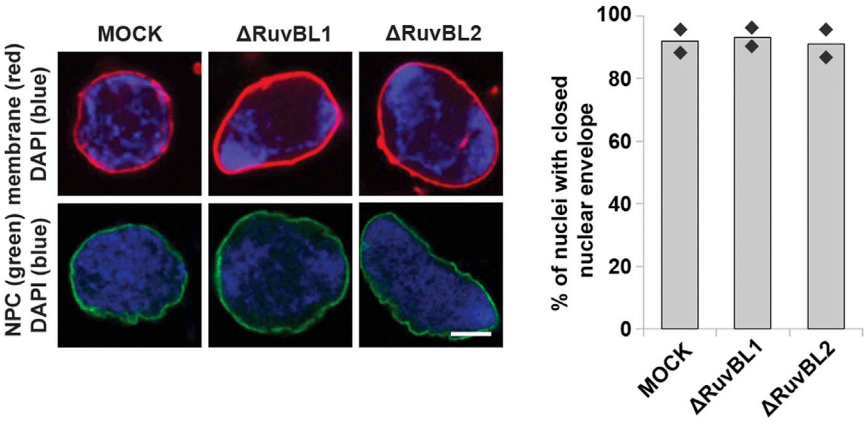

Figure 7. RuvB-like ATPases Are Specifically Required for Chromatin Decondensation during Mitotic Exit

Pronuclei were assembled on *Xenopus* sperm chromatin in mock-treated or RuvBL1/2-depleted extracts (using anti-RuvBL1 or anti-RuvBL2 antibodies). After 120 min, samples were fixed with 4% PFA and 0.5% glutaraldehyde and analyzed for membrane staining (DiIC18, upper panel) or for nuclear pore complexes (NPC, lower panel) by immunofluorescence with the antibody mAB414. Chromatin was stained with DAPI. Right panel shows the quantitation of chromatin substrates with closed nuclear envelopes as weighted average percentage of two independent experiments, each including at least 100 chromatin substrates. Diamonds indicate data points of the individual experiments. Scale bar, 5 μm. See also Figure S6.

remains to be investigated. It is also possible that chromatin decondensation constitutes a unique and probably archetypal process where RuvBL1 and RuvBL2 can substitute for each other.

Interestingly, RuvB-like ATPases have been implicated in various human cancers and have been speculated to be a promising therapeutic target (for a review, see Huber et al., 2008; Nano and Houry, 2013). Often, the precise function of RuvBL1 and RuvBL2 in pathogenesis is not defined. Whether their role in chromatin decondensation is relevant for this will be an exciting and promising avenue for future research.

EXPERIMENTAL PROCEDURES

Cell-free Decondensation of Mitotic Chromatin

Cytosol was prepared by crushing activated *Xenopus laevis* eggs by a low-speed centrifugation (20 min at 21,000 × *g*) to obtain egg extracts, followed by high-speed centrifugations (twice, 12 min at 360,000 × *g*). Activation of the eggs—which are naturally arrested in the second meiotic metaphase—by treatment with a Ca^{2+} ionophore induces meiotic exit. Thus, extracts prepared from these eggs represent a postmitotic/interphasic state and are competent to induce late mitotic/interphasic events such as nuclear reformation or DNA replication. The protocol including the preparation of flotation purified membranes is described in detail in Eisenhardt et al. (2014). Mitotic chromatin was isolated as in Gasser and Laemmli (1987). In vitro chromatin decondensation was induced by incubating approximately 1,000 mitotic chromatin clusters in 18 μl of cytosol from *Xenopus* egg extracts and 2 μl of flotation purified membranes supplemented with 3 μM 6-dimethylaminopurine, 10 mM ATP, 10 mM creatine phosphate, 0.2 mg/ml creatine kinase, and 0.4 mg/ml glycogen at 20°C. As a negative control, sucrose buffer (250 mM sucrose, 50 mM KCl, 2.5 mM $MgCl_2$, and 10 mM HEPES [pH 7.5]) was used instead of cytosol. At the end of the incubation time, samples were fixed in 0.5 ml 4% paraformaldehyde (PFA) and 0.5% glutaraldehyde in 80 mM PIPES [pH 6.8], 1 mM $MgCl_2$, 150 mM sucrose, and 10 μg/ml DAPI for 30 min on ice. Chromatin was reisolated by centrifugation though a 30% sucrose cushion in PBS (15 min at 2,500 × *g*) on poly-L-lysine-coated coverslips and mounted in Vectashield (Vector Laboratories). Samples were analyzed using a confocal microscope (FV1000; Olympus; equipped with a photomultiplier [model R7862; Hamamatsu]) with 405, 488, and 559 nm laser lines and a 60× numerical aperture 1.35 oil immersion objective lens using the FluoView software (Olympus) at room temperature. Immunofluorescence and transmission electron microscopy was performed as in Theerthagiri et al. (2010).

For western blot analysis of reisolated chromatin (modified from Hayashihara et al. (2008), the decondensation reaction was increased by a factor of ten. At the end of the reaction, samples were immediately layered on top of 1 ml wash buffer—10 mM HEPES [pH 7.5], 50 mM KCl, 14% (v/v) Optiprep (Sigma), 1 mM dithiothreitol, 2.5 mM $MgCl_2$, 0.2 mM spermine, 0.5 mM spermidine, 1 mM ATP, 10 μg/ml 4-(2-aminoethyl)-benzenesulfonylfluoride, 0.2 μg/ml leupeptin, 0.1 μg/ml pepstatin, 0.2 μg/ml aprotinin—and the chromatin was pelleted (30 min at 10,000 × *g* in a swing-out rotor) and analyzed.

In depletion experiments, cytosol was incubated twice with antibody-coated beads at a 1.2:1 beads-to-cytosol ratio for 20 min. CSF-arrested extracts were prepared as in Murray (1991) and released into interphase by the addition of 1 mM $CaCl_2$.

Quantification of In Vitro Chromatin Decondensation

Chromatin boundaries were defined by an intensity threshold, and the total chromatin area was calculated. For the smoothness analysis, the perimeter of the boundary was used to estimate the surface roughness as a ratio of the perimeter squared over area. To analyze chromatin homogeneity, chromosomes were defined using an edge-finding algorithm (the largest eigenvalue of the structure tensor; ImageJ plugin FeatureJ, http://www.imagescience.org/meijering/), and the sum of the chromosomes' areas was computed and normalized to the total area within the boundary. To minimize the statistical effects of very irregularly shaped (highly condensed) chromatin, a maximum of 20% (in roughness/relative area) above the fully decondensed state was adopted for both analyses. Surface smoothness and internal homogeneity were defined as the differences from the maximal roughness and maximal relative area, respectively. The fully condensed state was set to zero, and the maximal decondensed state to one and all other values were normalized accordingly.

Figure 6. RuvBL1 and RuvBL2 Localize to the Decondensing Chromatin

(A) HeLa mitotic chromatin was incubated with extracts for the indicated time. RuvBL1/2-depleted extracts (generated by consecutive passage over anti-RuvBL1 and anti-RuvBL2 IgG-bound beads) were supplemented with buffer, recombinant RuvBL1-RuvBL2 complex, RuvBL1, or RuvBL2 or ATPase-deficient versions of the proteins (matching the endogenous concentrations) and used in the decondensation reaction for 120 min. Samples were fixed with 4% PFA and processed for immunofluorescence, or chromatin was reisolated and analyzed by western blot (histone H2B shows equal chromatin loading). Scale bars, 5 μm.

(B) HeLa mitotic chromatin incubated as in (A) was reisolated and probed for the presence of Mel28/ELYS, the condensing I and II complex (CAP-G or CAP-D3 antibodies, respectively), topoisomerase IIα, the chromokinesin KIF4A, and Repo-MAN. Please note that during the reisolation procedure, rapid rebinding of *Xenopus* proteins to chromatin and/or their exchange with the HeLa proteins occurs so that they can be detected already at t = 0.

See also Figure S5.

Fractionation of *Xenopus* Egg Extracts

Xenopus egg cytosol was subjected to sequential fractionation to allow the identification of factors involved in chromatin decondensation. The fractions obtained were then tested in the in vitro assay described earlier for decondensation activity. First, cytosolic egg extract was fractionated by ammonium sulfate precipitation. Proteins that precipitated in 20% ammonium sulfate (fraction A) and those that did not precipitate (fraction B) were separated. Fraction B was then precipitated by increasing the ammonium sulfate concentration to 50%. Both fractions were resuspended in sucrose buffer. Fraction A was then applied to a Hi-Trap-Q-HP-Sepharose column (GE Healthcare) and eluted using a step gradient of 500 mM KCl. The decondensation-active fraction (P1) was further separated on a Superose 6 PC3.2/30 column (GE Healthcare) in sucrose buffer. Fractions were eluted at a 1.5–2.0 ml retention volume. For the decondensation assay, fractions A and B obtained from ammonium sulfate precipitation—as well as the flowthrough, P1, and P2 from the ion exchange—were dialyzed against sucrose buffer. The decondensation assay was always performed in the presence of fraction B in a 1:4 volume ratio. Active fractions eluted from the size exclusion column (G13–G15) were analyzed by mass spectrometry (described in the Supplemental Information).

Pronuclear Assembly Assay

For pronuclear assembly, cytosol from *Xenopus* egg was incubated with 1,000 sperm heads prepared from *Xenopus* testis (Gurdon, 1976) for 10 min at 20°C to allow for sperm chromatin decondensation. To start the reaction, floated DiIC18 (1,1′-dioctadecyl-3,3,3′,3′-tetramethylindocarbocyanine perchlorate)-labeled membranes (Antonin et al., 2005), 10 mM ATP, 10 mM creatine phosphate, 0.2 mg/ml creatine kinase, and 0.4 mg/ml glycogen were added. For depletions, cytosol was incubated twice with antibody-coated beads at a 1.2:1 bead-to-cytosol ratio for 20 min.

Miscellaneous

Statistical analysis was performed with the IBM-SPSS Statistics 21 software. Live cell imaging, nuclear import and ATPase assays, production of recombinant proteins, and a description of the antibodies used can be found in the Supplemental Experimental Procedures.

SUPPLEMENTAL INFORMATION

Supplemental Information includes Supplemental Experimental Procedures and six figures and can be found with this article online at http://dx.doi.org/10.1016/j.devcel.2014.09.001.

AUTHOR CONTRIBUTIONS

A.M. and W.A. designed the experiments. A.M., A.K.S., A.S., and W.A. performed decondensation experiments; A.M. and D.M.-A. performed live-cell imaging; F.Z. designed and wrote the image analysis software for the decondensation measurements; R.S. purified recombinant RuvBL1/2 complexes; H.S. performed electron microscopy; J.M. performed mass spectrometry; and W.A. wrote the manuscript.

ACKNOWLEDGMENTS

This work was supported by the German Research Foundation and the European Research Council (AN377/3-1 and 309528 CHROMDECON to W.A.) and by a PhD Fellowship of the Boehringer Ingelheim Fonds to A.K.S. We are grateful to A. Konopka (Nencki Institute of Experimental Biology) for help with the statistical analysis; K. Feldmeier for advice on the ATPase activity measurements (Max Planck Institute [MPI] for Developmental Biology); C. Liebig (Light Microscopy Facility of the MPI for Developmental Biology) for suggestions on image acquisition and analysis; and I. Poser in the lab of A. Hyman (MPI of Molecular Cell Biology and Genetics) for providing stable HeLa BAC cell lines (funded by the MitoSys project, European Community's Seventh Framework Programme [FP7/2007-2013], grant agreement 241548). A.M. is especially thankful for continuous support by G. Wilczyński (Nencki Institute of Experimental Biology).

Received: May 5, 2014
Revised: July 22, 2014
Accepted: September 3, 2014
Published: October 23, 2014

REFERENCES

Antonin, W., Franz, C., Haselmann, U., Antony, C., and Mattaj, I.W. (2005). The integral membrane nucleoporin pom121 functionally links nuclear pore complex assembly and nuclear envelope formation. Mol. Cell *17*, 83–92.

Baek, S.H., Ohgi, K.A., Rose, D.W., Koo, E.H., Glass, C.K., and Rosenfeld, M.G. (2002). Exchange of N-CoR corepressor and Tip60 coactivator complexes links gene expression by NF-kappaB and beta-amyloid precursor protein. Cell *110*, 55–67.

Bauer, A., Chauvet, S., Huber, O., Usseglio, F., Rothbächer, U., Aragnol, D., Kemler, R., and Pradel, J. (2000). Pontin52 and reptin52 function as antagonistic regulators of beta-catenin signalling activity. EMBO J. *19*, 6121–6130.

Belmont, A.S. (2006). Mitotic chromosome structure and condensation. Curr. Opin. Cell Biol. *18*, 632–638.

Burns, K.H., Viveiros, M.M., Ren, Y., Wang, P., DeMayo, F.J., Frail, D.E., Eppig, J.J., and Matzuk, M.M. (2003). Roles of NPM2 in chromatin and nucleolar organization in oocytes and embryos. Science *300*, 633–636.

Davis, L.I., and Blobel, G. (1986). Identification and characterization of a nuclear pore complex protein. Cell *45*, 699–709.

Dephoure, N., Zhou, C., Villén, J., Beausoleil, S.A., Bakalarski, C.E., Elledge, S.J., and Gygi, S.P. (2008). A quantitative atlas of mitotic phosphorylation. Proc. Natl. Acad. Sci. USA *105*, 10762–10767.

Diop, S.B., Bertaux, K., Vasanthi, D., Sarkeshik, A., Goirand, B., Aragnol, D., Tolwinski, N.S., Cole, M.D., Pradel, J., Yates, J.R., 3rd., et al. (2008). Reptin and Pontin function antagonistically with PcG and TrxG complexes to mediate Hox gene control. EMBO Rep. *9*, 260–266.

Ducat, D., Kawaguchi, S., Liu, H., Yates, J.R., 3rd, and Zheng, Y. (2008). Regulation of microtubule assembly and organization in mitosis by the AAA+ ATPase Pontin. Mol. Biol. Cell *19*, 3097–3110.

Eisenhardt, N., Schooley, A., and Antonin, W. (2014). Xenopus in vitro assays to analyze the function of transmembrane nucleoporins and targeting of inner nuclear membrane proteins. Methods Cell Biol. *122*, 193–218.

Franz, C., Walczak, R., Yavuz, S., Santarella, R., Gentzel, M., Askjaer, P., Galy, V., Hetzer, M., Mattaj, I.W., and Antonin, W. (2007). MEL-28/ELYS is required for the recruitment of nucleoporins to chromatin and postmitotic nuclear pore complex assembly. EMBO Rep. *8*, 165–172.

Galy, V., Antonin, W., Jaedicke, A., Sachse, M., Santarella, R., Haselmann, U., and Mattaj, I. (2008). A role for gp210 in mitotic nuclear-envelope breakdown. J. Cell Sci. *121*, 317–328.

Gant, T.M., and Wilson, K.L. (1997). Nuclear assembly. Annu. Rev. Cell Dev. Biol. *13*, 669–695.

Gartner, W., Rossbacher, J., Zierhut, B., Daneva, T., Base, W., Weissel, M., Waldhäusl, W., Pasternack, M.S., and Wagner, L. (2003). The ATP-dependent helicase RUVBL1/TIP49a associates with tubulin during mitosis. Cell Motil. Cytoskeleton *56*, 79–93.

Gasser, S.M., and Laemmli, U.K. (1987). Improved methods for the isolation of individual and clustered mitotic chromosomes. Exp. Cell Res. *173*, 85–98.

Gerlich, D., Hirota, T., Koch, B., Peters, J.M., and Ellenberg, J. (2006). Condensin I stabilizes chromosomes mechanically through a dynamic interaction in live cells. Curr. Biol. *16*, 333–344.

Gurdon, J.B. (1976). Injected nuclei in frog oocytes: fate, enlargement, and chromatin dispersal. J. Embryol. Exp. Morphol. *36*, 523–540.

Hansen, J.C. (2012). Human mitotic chromosome structure: what happened to the 30-nm fibre? EMBO J. *31*, 1621–1623.

Hayashihara, K., Uchiyama, S., Kobayashi, S., Yanagisawa, M., Matsunaga, S., and Fukui, K. (2008). Isolation method for human metaphase chromosomes. Protocol Exchange. Published online August 13, 2008. http://dx.doi.org/10.1038/nprot.2008.166.

Hendzel, M.J., Wei, Y., Mancini, M.A., Van Hooser, A., Ranalli, T., Brinkley, B.R., Bazett-Jones, D.P., and Allis, C.D. (1997). Mitosis-specific phosphorylation of histone H3 initiates primarily within pericentromeric heterochromatin during G2 and spreads in an ordered fashion coincident with mitotic chromosome condensation. Chromosoma *106*, 348–360.

Hsu, J.Y., Sun, Z.W., Li, X., Reuben, M., Tatchell, K., Bishop, D.K., Grushcow, J.M., Brame, C.J., Caldwell, J.A., Hunt, D.F., et al. (2000). Mitotic phosphorylation of histone H3 is governed by Ipl1/aurora kinase and Glc7/PP1 phosphatase in budding yeast and nematodes. Cell *102*, 279–291.

Huber, O., Ménard, L., Haurie, V., Nicou, A., Taras, D., and Rosenbaum, J. (2008). Pontin and reptin, two related ATPases with multiple roles in cancer. Cancer Res. *68*, 6873–6876.

Ikura, T., Ogryzko, V.V., Grigoriev, M., Groisman, R., Wang, J., Horikoshi, M., Scully, R., Qin, J., and Nakatani, Y. (2000). Involvement of the TIP60 histone acetylase complex in DNA repair and apoptosis. Cell *102*, 463–473.

Jha, S., and Dutta, A. (2009). RVB1/RVB2: running rings around molecular biology. Mol. Cell *34*, 521–533.

Jónsson, Z.O., Dhar, S.K., Narlikar, G.J., Auty, R., Wagle, N., Pellman, D., Pratt, R.E., Kingston, R., and Dutta, A. (2001). Rvb1p and Rvb2p are essential components of a chromatin remodeling complex that regulates transcription of over 5% of yeast genes. J. Biol. Chem. *276*, 16279–16288.

Kim, J.H., Kim, B., Cai, L., Choi, H.J., Ohgi, K.A., Tran, C., Chen, C., Chung, C.H., Huber, O., Rose, D.W., et al. (2005). Transcriptional regulation of a metastasis suppressor gene by Tip60 and beta-catenin complexes. Nature *434*, 921–926.

Krogan, N.J., Keogh, M.C., Datta, N., Sawa, C., Ryan, O.W., Ding, H., Haw, R.A., Pootoolal, J., Tong, A., Canadien, V., et al. (2003). A Snf2 family ATPase complex required for recruitment of the histone H2A variant Htz1. Mol. Cell *12*, 1565–1576.

Kutay, U., and Hetzer, M.W. (2008). Reorganization of the nuclear envelope during open mitosis. Curr. Opin. Cell Biol. *20*, 669–677.

Landsverk, H.B., Kirkhus, M., Bollen, M., Küntziger, T., and Collas, P. (2005). PNUTS enhances in vitro chromosome decondensation in a PP1-dependent manner. Biochem. J. *390*, 709–717.

Lim, C.R., Kimata, Y., Ohdate, H., Kokubo, T., Kikuchi, N., Horigome, T., and Kohno, K. (2000). The Saccharomyces cerevisiae RuvB-like protein, Tih2p, is required for cell cycle progression and RNA polymerase II-directed transcription. J. Biol. Chem. *275*, 22409–22417.

Lohka, M.J., and Masui, Y. (1983). Formation in vitro of sperm pronuclei and mitotic chromosomes induced by amphibian ooplasmic components. Science *220*, 719–721.

MacCallum, D.E., Losada, A., Kobayashi, R., and Hirano, T. (2002). ISWI remodeling complexes in Xenopus egg extracts: identification as major chromosomal components that are regulated by INCENP-aurora B. Mol. Biol. Cell *13*, 25–39.

Maresca, T.J., and Heald, R. (2006). Methods for studying spindle assembly and chromosome condensation in Xenopus egg extracts. Methods Mol. Biol. *322*, 459–474.

Matias, P.M., Gorynia, S., Donner, P., and Carrondo, M.A. (2006). Crystal structure of the human AAA+ protein RuvBL1. J. Biol. Chem. *281*, 38918–38929.

Mazumdar, M., Sundareshan, S., and Misteli, T. (2004). Human chromokinesin KIF4A functions in chromosome condensation and segregation. J. Cell Biol. *166*, 613–620.

Mézard, C., Davies, A.A., Stasiak, A., and West, S.C. (1997). Biochemical properties of RuvBD113N: a mutation in helicase motif II of the RuvB hexamer affects DNA binding and ATPase activities. J. Mol. Biol. *271*, 704–717.

Murray, A.W. (1991). Cell cycle extracts. Methods Cell Biol. *36*, 581–605.

Nano, N., and Houry, W.A. (2013). Chaperone-like activity of the AAA+ proteins Rvb1 and Rvb2 in the assembly of various complexes. Philos. Trans. R. Soc. Lond. B Biol. Sci. *368*, 20110399.

Newman, D.R., Kuhn, J.F., Shanab, G.M., and Maxwell, E.S. (2000). Box C/D snoRNA-associated proteins: two pairs of evolutionarily ancient proteins and possible links to replication and transcription. RNA *6*, 861–879.

Newport, J., and Kirschner, M. (1982). A major developmental transition in early Xenopus embryos: I. characterization and timing of cellular changes at the midblastula stage. Cell *30*, 675–686.

Nguyen, V.Q., Ranjan, A., Stengel, F., Wei, D., Aebersold, R., Wu, C., and Leschziner, A.E. (2013). Molecular architecture of the ATP-dependent chromatin-remodeling complex SWR1. Cell *154*, 1220–1231.

Ohta, S., Wood, L., Bukowski-Wills, J.C., Rappsilber, J., and Earnshaw, W.C. (2011). Building mitotic chromosomes. Curr. Opin. Cell Biol. *23*, 114–121.

Olsen, J.V., Vermeulen, M., Santamaria, A., Kumar, C., Miller, M.L., Jensen, L.J., Gnad, F., Cox, J., Jensen, T.S., Nigg, E.A., et al. (2010). Quantitative phosphoproteomics reveals widespread full phosphorylation site occupancy during mitosis. Sci. Signal. *3*, ra3.

Peters, J.M. (2006). The anaphase promoting complex/cyclosome: a machine designed to destroy. Nat. Rev. Mol. Cell Biol. *7*, 644–656.

Philpott, A., and Leno, G.H. (1992). Nucleoplasmin remodels sperm chromatin in Xenopus egg extracts. Cell *69*, 759–767.

Philpott, A., Leno, G.H., and Laskey, R.A. (1991). Sperm decondensation in Xenopus egg cytoplasm is mediated by nucleoplasmin. Cell *65*, 569–578.

Puri, T., Wendler, P., Sigala, B., Saibil, H., and Tsaneva, I.R. (2007). Dodecameric structure and ATPase activity of the human TIP48/TIP49 complex. J. Mol. Biol. *366*, 179–192.

Ramadan, K., Bruderer, R., Spiga, F.M., Popp, O., Baur, T., Gotta, M., and Meyer, H.H. (2007). Cdc48/p97 promotes reformation of the nucleus by extracting the kinase Aurora B from chromatin. Nature *450*, 1258–1262.

Rosenbaum, J., Baek, S.H., Dutta, A., Houry, W.A., Huber, O., Hupp, T.R., and Matias, P.M. (2013). The emergence of the conserved AAA+ ATPases Pontin and Reptin on the signaling landscape. Sci. Signal. *6*, mr1.

Rottbauer, W., Saurin, A.J., Lickert, H., Shen, X., Burns, C.G., Wo, Z.G., Kemler, R., Kingston, R., Wu, C., and Fishman, M. (2002). Reptin and pontin antagonistically regulate heart growth in zebrafish embryos. Cell *111*, 661–672.

Schmitz, M.H., Held, M., Janssens, V., Hutchins, J.R., Hudecz, O., Ivanova, E., Goris, J., Trinkle-Mulcahy, L., Lamond, A.I., Poser, I., et al. (2010). Live-cell imaging RNAi screen identifies PP2A-B55alpha and importin-beta1 as key mitotic exit regulators in human cells. Nat. Cell Biol. *12*, 886–893.

Schooley, A., Vollmer, B., and Antonin, W. (2012). Building a nuclear envelope at the end of mitosis: coordinating membrane reorganization, nuclear pore complex assembly, and chromatin de-condensation. Chromosoma *121*, 539–554.

Shen, X., Mizuguchi, G., Hamiche, A., and Wu, C. (2000). A chromatin remodelling complex involved in transcription and DNA processing. Nature *406*, 541–544.

Sigala, B., Edwards, M., Puri, T., and Tsaneva, I.R. (2005). Relocalization of human chromatin remodeling cofactor TIP48 in mitosis. Exp. Cell Res. *310*, 357–369.

Steen, R.L., Martins, S.B., Taskén, K., and Collas, P. (2000). Recruitment of protein phosphatase 1 to the nuclear envelope by A-kinase anchoring protein AKAP149 is a prerequisite for nuclear lamina assembly. J. Cell Biol. *150*, 1251–1262.

Tavormina, P.A., Côme, M.G., Hudson, J.R., Mo, Y.Y., Beck, W.T., and Gorbsky, G.J. (2002). Rapid exchange of mammalian topoisomerase II alpha at kinetochores and chromosome arms in mitosis. J. Cell Biol. *158*, 23–29.

Theerthagiri, G., Eisenhardt, N., Schwarz, H., and Antonin, W. (2010). The nucleoporin Nup188 controls passage of membrane proteins across the nuclear pore complex. J. Cell Biol. *189*, 1129–1142.

Thompson, L.J., Bollen, M., and Fields, A.P. (1997). Identification of protein phosphatase 1 as a mitotic lamin phosphatase. J. Biol. Chem. *272*, 29693–29697.

Tosi, A., Haas, C., Herzog, F., Gilmozzi, A., Berninghausen, O., Ungewickell, C., Gerhold, C.B., Lakomek, K., Aebersold, R., Beckmann, R., and Hopfner, K.P. (2013). Structure and subunit topology of the INO80 chromatin remodeler and its nucleosome complex. Cell *154*, 1207–1219.

Vagnarelli, P., Ribeiro, S., Sennels, L., Sanchez-Pulido, L., de Lima Alves, F., Verheyen, T., Kelly, D.A., Ponting, C.P., Rappsilber, J., and Earnshaw, W.C. (2011). Repo-Man coordinates chromosomal reorganization with nuclear envelope reassembly during mitotic exit. Dev. Cell *21*, 328–342.

Venteicher, A.S., Meng, Z., Mason, P.J., Veenstra, T.D., and Artandi, S.E. (2008). Identification of ATPases pontin and reptin as telomerase components essential for holoenzyme assembly. Cell *132*, 945–957.

Walczak, C.E., and Heald, R. (2008). Mechanisms of mitotic spindle assembly and function. Int. Rev. Cytol. *265*, 111–158.

Walczak, C.E., Cai, S., and Khodjakov, A. (2010). Mechanisms of chromosome behaviour during mitosis. Nat. Rev. Mol. Cell Biol. *11*, 91–102.

Wood, M.A., McMahon, S.B., and Cole, M.D. (2000). An ATPase/helicase complex is an essential cofactor for oncogenic transformation by c-Myc. Mol. Cell *5*, 321–330.

Wright, S.J. (1999). Sperm nuclear activation during fertilization. Curr. Top. Dev. Biol. *46*, 133–178.

Wurzenberger, C., and Gerlich, D.W. (2011). Phosphatases: providing safe passage through mitotic exit. Nat. Rev. Mol. Cell Biol. *12*, 469–482.

Zhao, R., Davey, M., Hsu, Y.C., Kaplanek, P., Tong, A., Parsons, A.B., Krogan, N., Cagney, G., Mai, D., Greenblatt, J., et al. (2005). Navigating the chaperone network: an integrative map of physical and genetic interactions mediated by the hsp90 chaperone. Cell *120*, 715–727.

Developmental Cell, Volume *31*

Supplemental Information

RuvB-like ATPases Function in Chromatin Decondensation at the End of Mitosis

Adriana Magalska, Anna Katharina Schellhaus, Daniel Moreno-Andrés, Fabio Zanini, Allana Schooley, Ruchika Sachdev, Heinz Schwarz, Johannes Madlung, and Wolfram Antonin

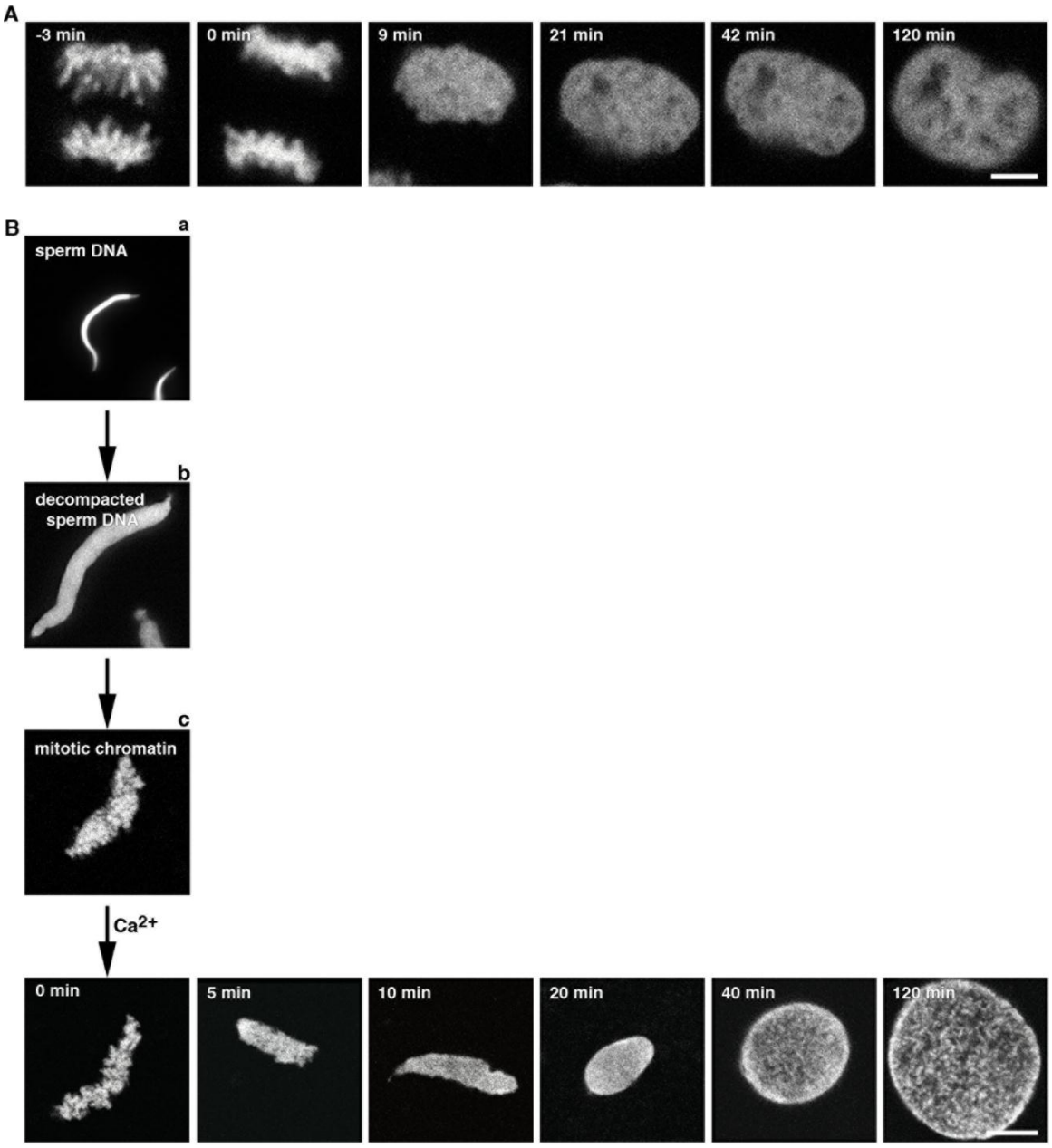

Figure S1, related to Figure 1

A) Time course of chromatin decondensation in HeLa cells recorded with time-lapse confocal microscopy. Chromatin is visualized as mCherry-tagged histone H2B. Time is normalized to telophase onset.

B) *Xenopus* sperm heads were incubated in CSF-arrested *Xenopus* egg extracts for 60 min to generate mitotic chromatin. Please note that during this treatment the highly condensed crescent shaped sperm DNA (a) is de-compacted in CSF extracts in a nucleoplasmin (NPM2) dependent exchange of protamines to histones (b), which is not occurring during post-mitotic chromatin decondensation, and then condensed to mitotic chromatin (c). For a more extensive documentation of these steps see e.g. (de

la Barre et al., 1999). The transition to interphase was induced by addition of 1 mM $CaCl_2$, which initiates post-mitotic chromatin decondensation. Samples were fixed at indicated time points after Ca^{2+} addition with 4% PFA and 0.5% glutaraldehyde, stained with DAPI, and analyzed by confocal microscopy.

Scale bars are 5 μm.

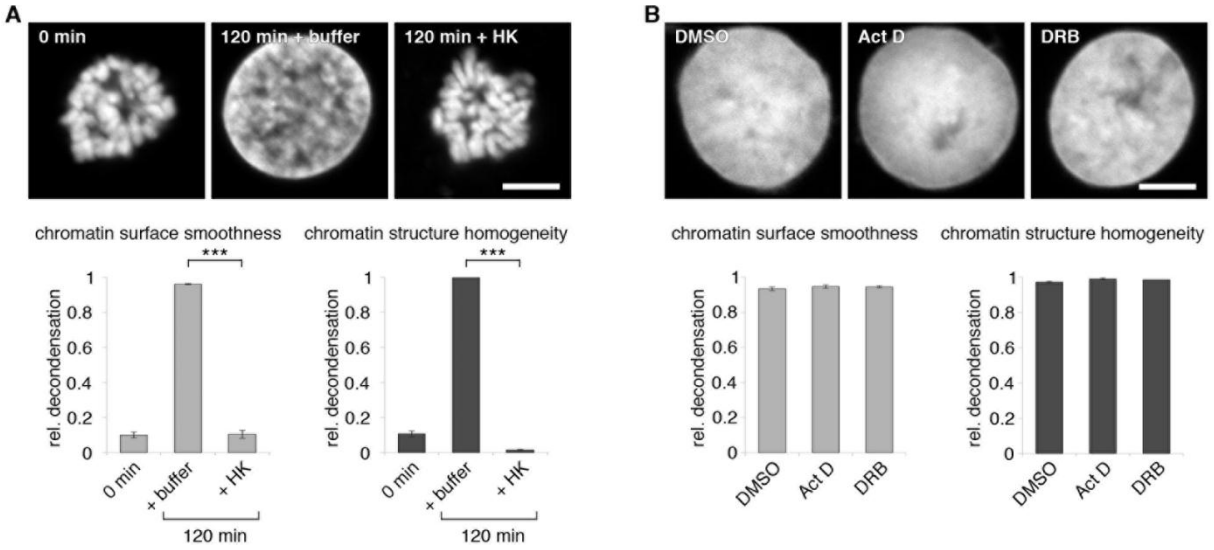

Figure S2, related to Figure 3

A) The decondensation reaction using HeLa mitotic clusters was incubated with 100 U of hexokinase (HK) to eliminate endogenous ATP. Samples were fixed at indicated time points with 4% PFA and 0.5% glutaraldehyde, stained with DAPI, analyzed by confocal microscopy.

B) The decondensation reaction using HeLa mitotic clusters was supplemented with 12 µM actinomycin D (Act D), a concentration sufficient to inhibit class I, II and III gene transcription (Bensaude, 2011), or 1 mM 5,6-dichloro-1-beta-D-ribofuranosylbenzimidazole (DRB, both dissolved in DMSO), which inhibits class II gene transcription, or the same volume of DMSO. Samples were fixed after 120 min with 4% PFA and 0.5% glutaraldehyde, stained with DAPI, analyzed by confocal microscopy.

Decondensation was quantified as in Figure 1A. The mean of three independent experiments each including at least ten chromatin substrates are shown. Error bars represent the SEM, *** represents P <0.001 by Mann Whitney test for A. For B no statistical significant difference (P >0.05) was detected by one-way ANOVA test. Scale bars are 5 µm.

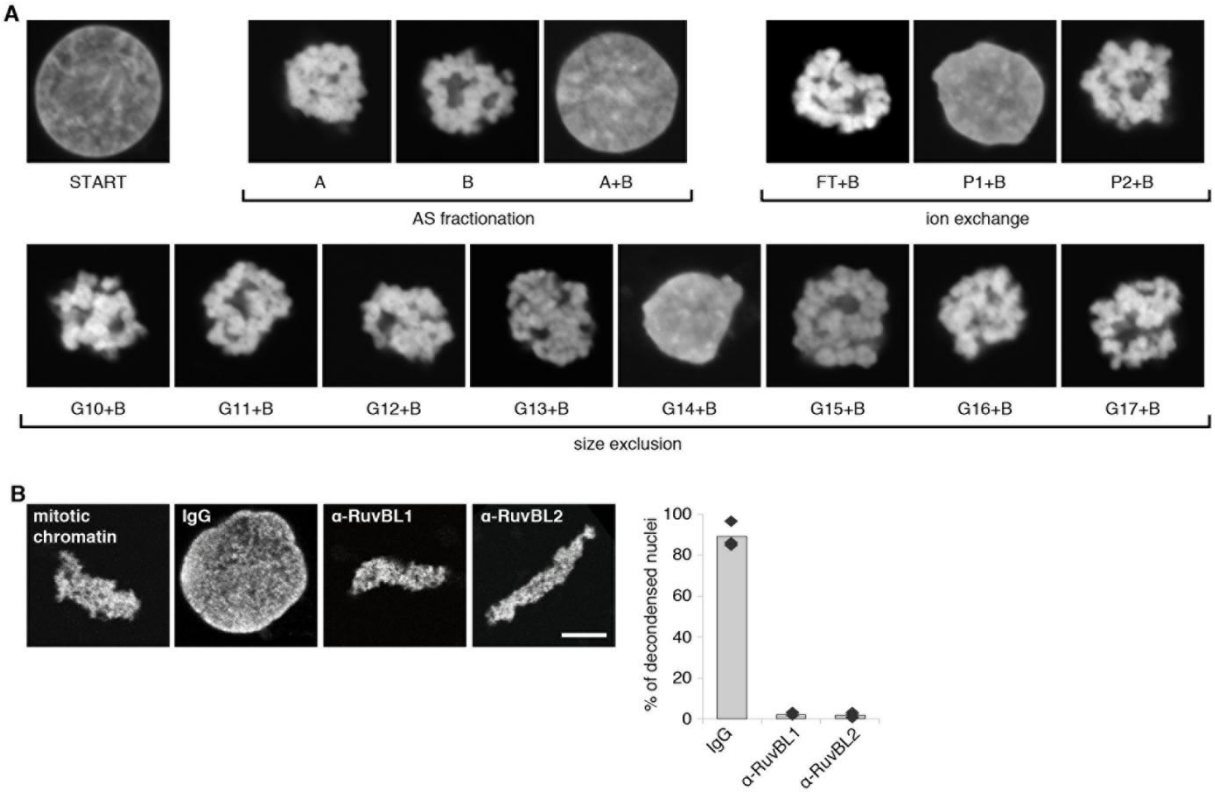

Figure S3, related to Figure 4

A) Representative confocal images of DAPI stained HeLa mitotic chromatin incubated with the different fractions according to the fractionation procedure as presented in Figure 4A. Please note that as in Figure 4A the fractions of the ion exchange and size exclusion chromatography are only shown in combination with fraction B.

B) *Xenopus* sperm heads were incubated in CSF-arrested *Xenopus* egg extracts for 60 min to generated mitotic chromatin and pre-incubated for 5 min with 4 mg/ml affinity purified IgG against RuvBL1, RuvBL2 or control IgGs. Transition to interphase was induced by addition of 1 mM $CaCl_2$. Samples were fixed 120 min after Ca^{2+} addition with 4% PFA and 0.5% glutaraldehyde, stained with DAPI and the fraction of decondensed chromatin templates was quantified. The weighted average percentage of three independent experiments, each including at least 100

randomly chosen chromatin substrates is shown, diamonds indicate individual data points.

C) Dilution series of *Xenopus* egg extracts and purified recombinant RuvBL1 or RuvBL2 were analyzed by western blot and quantified. Based on the quantitation the endogenous RuvBL1 and RuvBL2 concentrations are estimated both to 0.02 µg/µl which corresponds to a 0.4 µM concentration of the monomers. The equal concentration of RuvBL1 and RuvBL2 is in agreement with the notion that these proteins are mostly found in a heteromeric complex in *Xenopus* egg extracts (see Figure 4D).

Scale bars are 5 µm.

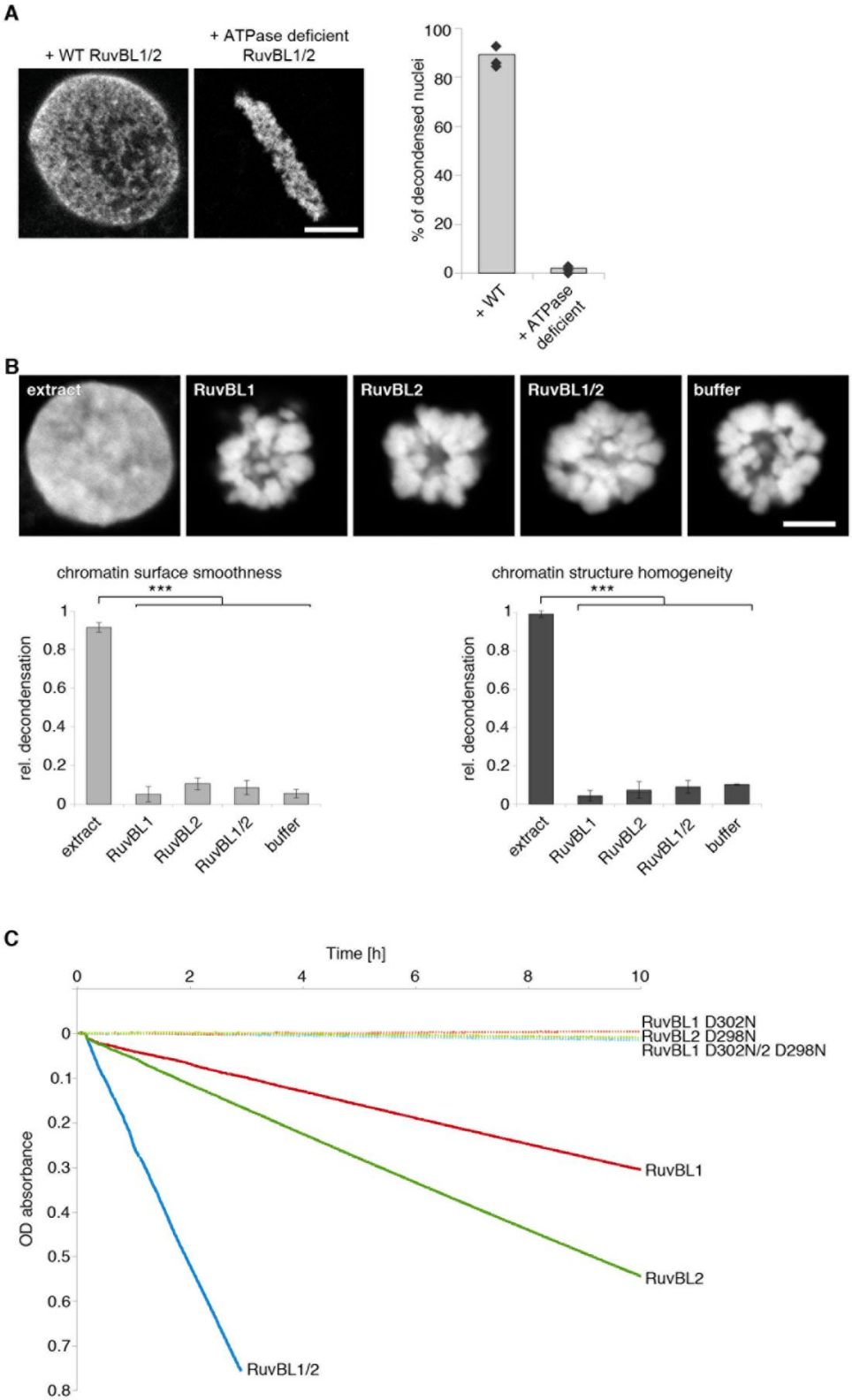

Figure S4, related to Figure 5

A) *Xenopus* sperm heads were incubated in CSF-arrested *Xenopus* egg extracts for 60 min to generate mitotic chromatin and pre-incubated for 5 min with recombinant wild type or ATPase deficient RuvBL1-RuvBL2 complex. The transition to interphase was

induced by addition of 1 mM $CaCl_2$. Samples were fixed 120 min after Ca^{2+} addition with 4% PFA and 0.5% glutaraldehyde, stained with DAPI and the fraction of decondensed chromatin templates quantified. The weighted average percentage of three independent experiments, each including at least 100 randomly chosen chromatin substrates is shown, diamonds indicate individual data points.

B) Mitotic chromatin clusters from HeLa cells were incubated at 20ºC with post-mitotic *Xenopus* egg extracts or 0.4µM recombinant purified RuvBL1, RuvBL1 or the heteromeric RuvBL1/2 complex in sucrose buffer supplemented with 3 µM 6-Dimethylaminopurine, 10 mM ATP, 10 mM creatine phosphate, 0.2 mg/ml creatine kinase, and 0.4 mg/ml glycogen. Samples were fixed after 120 min with 4% PFA and 0.5% glutaraldehyde, stained with DAPI, analyzed by confocal microscopy and decondensation was quantified as in Figure 1A. The mean of three independent experiments each including at least ten chromatin substrates are shown. Error bars represent the SEM, *** represents P <0.001 by one-way ANOVA, Sidlak post-hoc test. No statistical significant difference was detected within the RuvB-like ATPase and buffer samples (P =1). Scale bars are 5 µm.

C) The ATPase activity of the RuvBL1, RuvBL2 and the heteromeric RuvBL1/2 complexes as well as the ATPase deficient versions (RuvBL1 D302N, RuvBL2 D298N or the RuvBL1 D302N/RuvBL2 D298N) was analyzed at a protein concentration of 2 µg/ml for RuvBL1 and RuvBL2 complexes and 4 µg/ml for RuvBL1/2 complexes. The rather low ATPase activity with a generation rate of 18 mol Pi/(min x mol RuvBL1/2), 2 mol Pi/(min x mol RuvBL1) and 3.5 mol Pi/(min x mol RuvBL2) is in agreement with reported values (e.g. (Puri et al., 2007)). Similarly, an elevated ATPase activity for the heteromeric complex has been reported before (e.g. (Puri et al., 2007), see also http://www.gref-bordeaux.fr/en/node/303 for a comprehensive summary of ATPase activity measurements of RuvB-like ATPases). Please note that no ATPase activity can be detected for the ATPase deficient versions.

Scale bars are 5 µm.

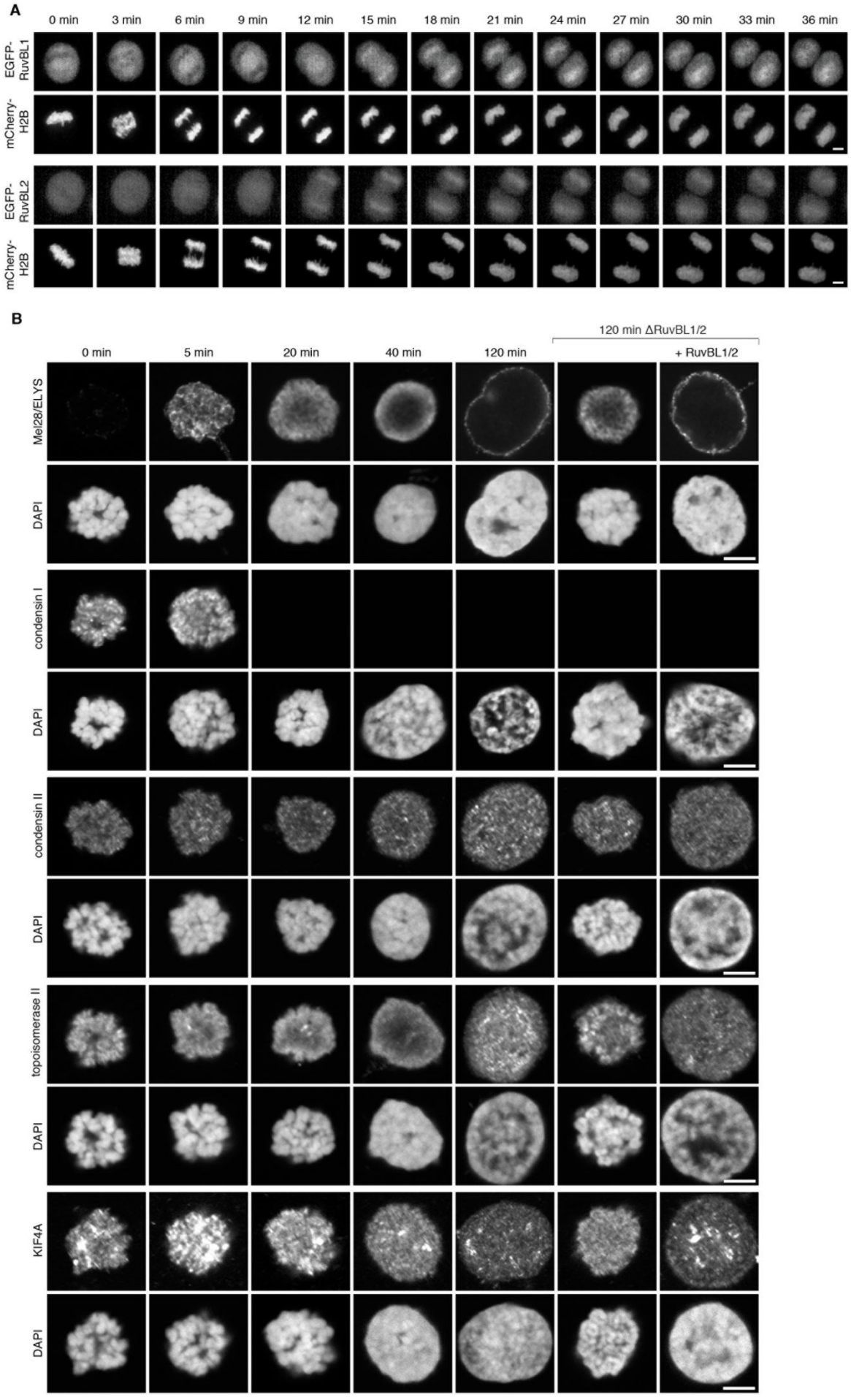
A
0 min
3 min
6 min
9 min
12 min
15 min
18 min
21 min
24 min
27 min
30 min
33 min
36 min
EGFP-RuvBL1
mCherry-H2B
EGFP-RuvBL2
mCherry-H2B
B
120 min ΔRuvBL1/2
+ RuvBL1/2
0 min
5 min
20 min
40 min
120 min
Mel28/ELYS
DAPI
condensin I
DAPI
condensin II
DAPI
topoisomerase II
DAPI
KIF4A
DAPI

Figure S5, related to Figure 6

A) Time course of mitotic exit in HeLa cells stably expressing mCherry-tagged histone H2B and EGFP-RuvBL1 (upper panel) or EGFP-RuvBL2 (lower panel) recorded by time-lapse confocal microscopy. Time is normalized to the last metaphase frame before anaphase onset.

B) Mitotic chromatin clusters from HeLa cells were incubated with post-mitotic *Xenopus* egg extracts for the indicated time to induce chromatin decondensation. RuvBL1/2 depleted extracts (generated by consecutive passage over anti-RuvBL1 and anti-RuvBL2 IgG bound beads) were supplemented with buffer or recombinant RuvBL1-RuvBL2 complex for 120 min. Samples were fixed with 4% PFA and stained using antibodies against the nuclear pore complex protein Mel28/ELYS, the condensin I and II complex (using CAP-G or CAP-D3 antibodies, respectively), topoisomerase IIα and the chromokinesin KIF4A.

Scale bars are 5 µm.

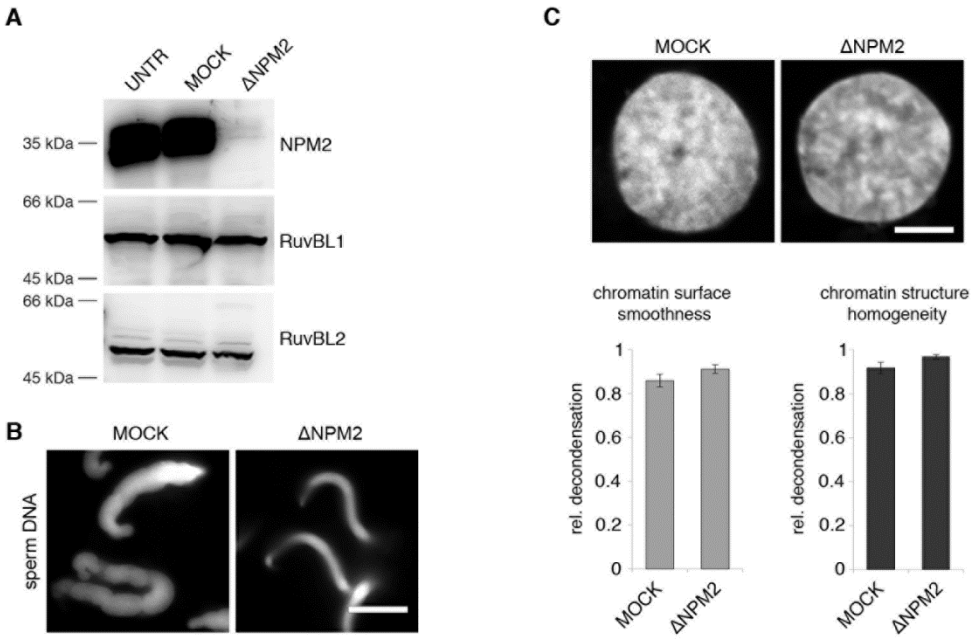

Figure S6, related to Figure 7

A) Western blot of untreated, mock or nucleoplasmin (NPM2) depleted *Xenopus laevis* egg extracts. The quantities of RuvBL1 and RuvBL2 in extracts are not affected by this treatment.

B) *Xenopus laevis* sperm heads were incubated with mock or nucleoplasmin (NPM2) depleted extracts for 10 min, fixed with 4% PFA and 0.5% glutaraldehyde, stained with DAPI and analyzed on a Axiovert 200 M fluorescence wide field microscope (Zeiss). Please note the block in sperm chromatin de-compaction in the absence of nucleoplasmin as previously reported (Philpott et al., 1991).

C) Mock or nucleoplasmin (NPM2) depleted extracts were tested for chromatin decondensation on HeLa mitotic chromatin (120 min time point). The mean (+/- SEM) of three independent experiments each including at least 20 chromatin substrates are shown. Mann-Whitney test showed no statistical significant difference between the samples ($P > 0.05$)

Scale bars are 5 µm.

Supplemental Experimental Procedures

Antibodies and recombinant proteins

Antibodies against Ser10 phosphorylated Histone H3 were from Cell Signaling, mAb414 from Babco, topoisomerase IIa (Ki-S1) from Millipore, RepoMan (R11611) from Sigma and Kif4A (H00024137-B01) from Abnova. Antibodies against Mel28/ELYS were described in (Franz et al., 2007). Antibodies against *Xenopus* CAP-D3 and CAP-G were generated as described (Kimura and Hirano, 2000; Ono et al., 2003). Full-length *Xenopus* nucleoplasmin (NPM2) was expressed from a pET28a construct and used for antibody production in rabbits. *Xenopus* RuvBL1 and RuvBL2 were expressed from pET30a constructs (Ducat et al., 2008), purified in the presence of 1 mM ATP and 0.1 mM $MgCl_2$ by Ni-affinity chromatography and used for antibody production in rabbits. For biochemical experiments RuvBL1 and RuvBL2 were further purified by size exclusion chromatography on a Superose 6 10/300GL column (GE-Healthcare). Purified hexameric RuvBL1 and RuvBL2 complexes were incubated overnight in an equimolar ratio and isolated as hetero-dodecameric complexes by size exclusion chromatography on a Superose 6 10/300GL column. ATPase-dead RuvBL1 and RuvBL2 mutants were generated by *in vitro* mutagenesis and purified as above.

Cell culture and live-cell imaging

HeLa cells stably expressing either EGFP-mouse RuvBL1 or EGFP-mouse RuvBL2 generated from EGFP-tagged BACs (Poser et al., 2008) were transfected with pIRES-puro-mCherryH2B (Steigemann et al., 2009) using FUGENE 6 (Promega) and selected in complete DMEM medium supplemented with 2.5 µg/ml puromycine and 500 µg/ml G418. Positive clones with adequate expression levels of both fluorophores were amplified in complete DMEM medium with 0.5 µg/ml puromycine and 500 µg/ml G418. The cells were seeded 24 hours before live-cell imaging in µ-slide 8 well chamber (Ibidi) with complete DMEM medium. Live-cell confocal microscopy was conducted using an LSM 5 live microscope (Zeiss) equipped with a heating and CO_2 incubation system (Ibidi). Images were acquired under the control of the ZEN software (Zeiss) as time and Z-series. A LD-Apocromant 40x/1.1 W objective was used for image acquisition. EGFP was excited with a 488-nm diode laser and mCherry was excited with a 561-nm diode laser. Images were projected in Z using the maximum intensity projection tool of ZEN software.

Liquid Chromatography-Mass Spectrometry (MS) Analysis

Proteins were subjected to tryptic in-gel digestion (Borchert et al., 2010), and the peptide mixtures were desalted with C18 Stage Tips (Rappsilber et al., 2007). LC-MS analyses were performed on a nanoLC (Easy-nLC, Thermo Fisher Scientific) coupled to a 4000QTrap (Applied Biosystems/MDS Sciex) mass spectrometer equipped with a nanoelectrospray ion source. Chromatographic separation of the peptides was performed on a 15-cm fused silica emitter of 75-mm inner diameter (New Objective), packed in-house with reversed-phase ReproSil-Pur C18-AQ 3-mm resin (Dr. Maisch GmbH). The peptide mixtures were injected onto the column in HPLC solvent A (0.5% acetic acid) at a flow rate of 500 nl/min and subsequently eluted with a 43-min segmented gradient of 5%–80% HPLC solvent B (80% ACN in 0.5% acetic acid) at a flow rate of 200 nl/min. MS data acquisition was conducted in the positive ion mode. The mass spectrometer was operated in data-dependent mode to automatically switch between MS and MS/MS acquisition. One MS was followed by three MS/MS events. MS data were searched using the Mascot search engine (Matrix Science, London, UK) against a target-decoy database (Elias and Gygi, 2007) consisting of the X. laevis database (Xenbase 20100129) plus 262 commonly observed contaminants.

All MS data were combined into a single peak list and processed in a combined database search using the MS Quant software package. In the database search, carbamidomethylation (Cys) was set as fixed modification, whereas oxidation (Met) and acetylation (protein N termini) were set as variable modifications. The mass tolerances for precursor and fragment ions were set to 1.5 Daltons and 0.5 Daltons, respectively. The identified peptides were classified based on their mascot ion scores; protein identification was defined as valid if at least two peptides with mascot scores better than $P < 0.1$ were identified and at least one of them had a score of $P < 0.05$. RuvBL2 was identified with two peptides covering 4.6% of the protein sequence, GLGLDDALEPR (peptide score 55, mass deviation 0.07945Da) and VYSLFLDESR (peptide score 75, mass deviation 0.03565Da). The peptide scores of both peptides correspond to mascot scores better than $P < 0.01$.

In vitro nuclear transport assay

Nuclear import and export were tested using modified Nplc-M9-M10 or Nplc-M9-NES reporters, respectively, from (Englmeier et al., 1999). Reporters were fused to an N-terminal EGFP, cloned into pET28a and purified via an N-terminal Hexa-Histidine tag and size exclusion chromatography on a Superose 6 10/300 GL column (GE-Healthcare). A 0.1 mg/ml aliquot of the purified protein was added to nuclei assembled in the decondensation reaction

and supplemented with an energy regenerating system (10 mM ATP, 10 mM creatine phosphate, 0.2 mg/ml creatine kinase, and 0.4 mg/ml glycogen; final concentrations). Samples were incubated for another 30 min, fixed and processed for microscopy. Leptomycin B (300 nM) was added to block nuclear export.

ATPase assay

ATPase activity was measured in sucrose buffer supplemented with 2 mM phosphoenol-pyruvate, 1mM ATP, 0.2 mM NADH, 0.1 mg/ml BSA 2 µg/ml lactate dehydrogenase (Roche), 2 µg/ml pyruvate kinase (Sigma) at 25ºC on a Cary 50 spectrophotometer (Varian) following the rational described in (Huang and Hackney, 1994). In short, the ADP generated by the RuvB-like ATPases is reconverted by the pyruvate kinase to ATP. The resulting pyruvate is processed to lactate by the lactate dehydrogenase under consumption of NADH, the loss of which is monitored at 340 nm.

Supplemental References

Bensaude, O. (2011). Inhibiting eukaryotic transcription: Which compound to choose? How to evaluate its activity? Transcr *2*, 103-108.

Borchert, N., Dieterich, C., Krug, K., Schutz, W., Jung, S., Nordheim, A., Sommer, R.J., and Macek, B. (2010). Proteogenomics of Pristionchus pacificus reveals distinct proteome structure of nematode models. Genome Res *20*, 837-846.

de la Barre, A.E., Robert-Nicoud, M., and Dimitrov, S. (1999). Assembly of mitotic chromosomes in Xenopus egg extract. Methods Mol Biol *119*, 219-229.

Ducat, D., Kawaguchi, S., Liu, H., Yates, J.R., 3rd, and Zheng, Y. (2008). Regulation of microtubule assembly and organization in mitosis by the AAA+ ATPase Pontin. Molecular biology of the cell *19*, 3097-3110.

Elias, J.E., and Gygi, S.P. (2007). Target-decoy search strategy for increased confidence in large-scale protein identifications by mass spectrometry. Nat Methods *4*, 207-214.

Englmeier, L., Olivo, J.C., and Mattaj, I.W. (1999). Receptor-mediated substrate translocation through the nuclear pore complex without nucleotide triphosphate hydrolysis. Curr Biol *9*, 30-41.

Franz, C., Walczak, R., Yavuz, S., Santarella, R., Gentzel, M., Askjaer, P., Galy, V., Hetzer, M., Mattaj, I.W., and Antonin, W. (2007). MEL-28/ELYS is required for the recruitment of nucleoporins to chromatin and postmitotic nuclear pore complex assembly. EMBO Rep *8*, 165-172.

Huang, T.G., and Hackney, D.D. (1994). Drosophila kinesin minimal motor domain expressed in Escherichia coli. Purification and kinetic characterization. J Biol Chem *269*, 16493-16501.

Kimura, K., and Hirano, T. (2000). Dual roles of the 11S regulatory subcomplex in condensin functions. Proceedings of the National Academy of Sciences of the United States of America *97*, 11972-11977.

Ono, T., Losada, A., Hirano, M., Myers, M.P., Neuwald, A.F., and Hirano, T. (2003). Differential contributions of condensin I and condensin II to mitotic chromosome architecture in vertebrate cells. Cell *115*, 109-121.

Philpott, A., Leno, G.H., and Laskey, R.A. (1991). Sperm decondensation in Xenopus egg cytoplasm is mediated by nucleoplasmin. Cell *65*, 569-578.

Poser, I., Sarov, M., Hutchins, J.R., Heriche, J.K., Toyoda, Y., Pozniakovsky, A., Weigl, D., Nitzsche, A., Hegemann, B., Bird, A.W.*, et al.* (2008). BAC TransgeneOmics: a high-throughput method for exploration of protein function in mammals. Nat Methods *5*, 409-415.

Puri, T., Wendler, P., Sigala, B., Saibil, H., and Tsaneva, I.R. (2007). Dodecameric structure and ATPase activity of the human TIP48/TIP49 complex. J Mol Biol *366*, 179-192.

Rappsilber, J., Mann, M., and Ishihama, Y. (2007). Protocol for micro-purification, enrichment, pre-fractionation and storage of peptides for proteomics using StageTips. Nat Protoc *2*, 1896-1906.

Steigemann, P., Wurzenberger, C., Schmitz, M.H., Held, M., Guizetti, J., Maar, S., and Gerlich, D.W. (2009). Aurora B-mediated abscission checkpoint protects against tetraploidization. Cell *136*, 473-484.

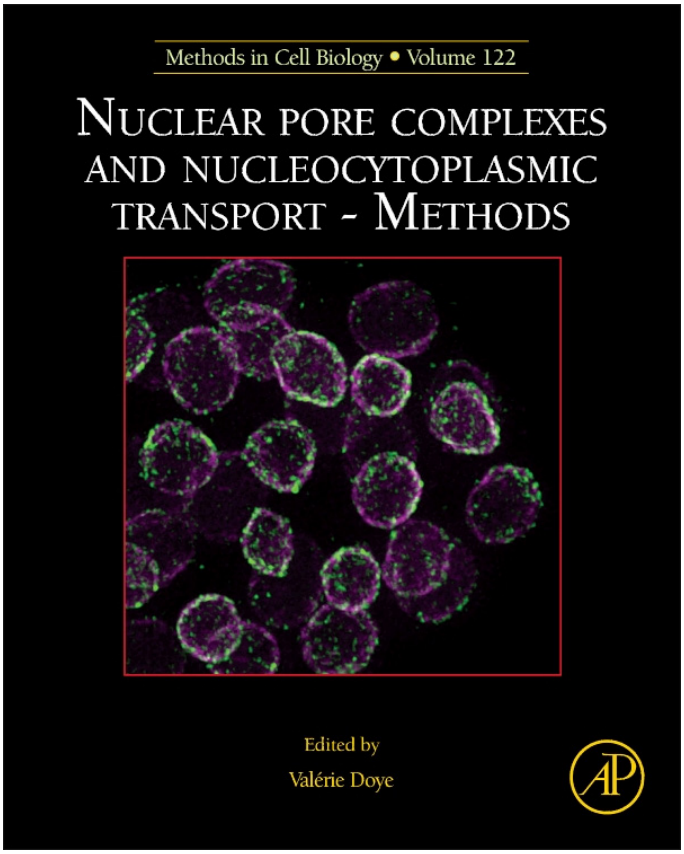

From Nathalie Eisenhardt, Allana Schooley, and Wolfram Antonin. *Xenopus In Vitro* Assays to Analyze the Function of Transmembrane Nucleoporins and Targeting of Inner Nuclear Membrane Proteins. In Valérie Doye, editor: *Methods in Cell Biology,* Vol. 122, Burlington: Academic Press, 2014, pp. 193-218.
ISBN: 978-0-12-417160-2

CHAPTER

9

Xenopus In Vitro Assays to Analyze the Function of Transmembrane Nucleoporins and Targeting of Inner Nuclear Membrane Proteins

Nathalie Eisenhardt, Allana Schooley, and Wolfram Antonin
Friedrich Miescher Laboratory of the Max Planck Society, Tübingen, Germany

CHAPTER OUTLINE

Methods in Cell Biology, Volume 122 **ISSN 0091-679X**

http://dx.doi.org/10.1016/B978-0-12-417160-2.00009-6

Abstract

Xenopus egg extracts have been widely used to study cell cycle regulation and to analyze mitotic or nuclear processes on a biochemical level. Most instrumental, proteins of interest can be immunodepleted by specific antibodies. However, this approach has

been restricted to non-membrane proteins, which limits its versatility especially when studying membrane-dependent processes such as nuclear envelope reformation at the end of mitosis or nuclear pore complex assembly. We describe here the methods developed and used in our laboratory to specifically remove transmembrane proteins from endogenous membranes and to insert recombinant integral membrane proteins into endogenous membranes. The latter procedure is important not only for readdition of a depleted protein in rescue experiments but also for introducing artificial membrane proteins such as reporters to investigate the passage of inner nuclear membrane proteins through nuclear pore complexes.

INTRODUCTION

Cell-free extracts derived from frog eggs (Lohka & Masui, 1983) have widely been used to study cell cycle regulation as well as many mitotic and nuclear processes since their development and first use 30 years ago. Although eggs from other sources such as *Rana pipiens* (Lohka & Masui, 1983) or *Xenopus tropicalis* (Brown et al., 2007) can be employed, the use of *Xenopus laevis* eggs is most popular because these frogs are relatively easily maintained in a laboratory environment and they provide plentiful eggs with little seasonal variation in yield and quality.

In the absence of intact cells, *X. laevis* egg extracts recapitulate complicated cellular reactions in a test tube such as chromatin condensation (de la Barre, Robert-Nicoud, & Dimitrov, 1999), spindle assembly (Maresca & Heald, 2006), nuclear breakdown and reformation (Galy et al., 2008; Lohka, 1998), nucleocytoplasmic transport (Chan & Forbes, 2006), or DNA replication (Gillespie, Gambus, & Blow, 2012). Since these egg extracts can be prepared at different stages of the cell cycle, which are easily interconvertible, cell cycle-dependent processes can also be studied (Murray, 1991). Most importantly, a single defined step in a complex series of processes such as the metazoan cell cycle can be isolated and investigated in molecular detail with this system. To identify key factors involved in various distinct processes of interest, convenient biochemical manipulations of the extracts are possible. In this regard, the opportunity to easily remove proteins of interest from these extracts by specific antibodies is most instrumental. For example, the importance of individual nuclear pore complex (NPC) proteins, nucleoporins, for NPC assembly and function has been defined in this way (see Chapter 8 by Bernis and Forbes in this volume). This "biochemical knockout" strategy is highly efficient to deplete proteins of interest below a detection limit. In contrast to RNAi, gene deletion or morpholino experiments, this method is naturally not limited by the viability of cells and organisms. As assays can be tailored to monitor a single process of interest, this also avoids complications due to secondary effects upon protein depletion, which might occur in other stages of the cell cycle or during development. However, this approach has been majorly restricted to non-membrane proteins, which limits its versatility especially when studying membrane-dependent processes such as nuclear envelope or NPC formation.

In this chapter, we describe the methods developed and employed in our lab to immunodeplete-specific integral membrane proteins of the NPC from *Xenopus*

membranes. Removing integral membrane proteins from *Xenopus* membranes is technically challenging as this procedure includes membrane solubilization and a final reconstitution of the depleted membranes besides the specific immunodepletion (Fig. 9.2A). However, the method is in our eyes superior to antibody (IgG or Fab) inhibition experiments classically used to study the function of integral membrane proteins, which are often ill-defined especially with regard to the precise molecular inhibiting effect of the antibody. Preferably, immunodepletion of a given protein should be followed by an "add-back experiment," in which a recombinant version of the depleted factor is readded to revert the observed depletion phenotype, thereby demonstrating the point specificity of the depletion. Such add-back experiments are also feasible for transmembrane proteins (Fig. 9.2B and C). Here, we outline the procedures of the expression of eukaryotic transmembrane proteins in *Escherichia coli*, their purification and their reconstitution in *Xenopus* membranes. Moreover, recombinant-modified transmembrane proteins can be added to endogenous *Xenopus* membranes to analyze the passage of integral membrane proteins through the NPC *in vitro* (Fig. 9.3). As nuclear transport has mainly been studied for soluble proteins in the past, the mechanisms of NPC passage of transmembrane proteins are only emerging (for review, see Antonin, Ungricht, & Kutay, 2011; Lusk, Blobel, & King, 2007). The assay we describe here provides a powerful tool to study NPC passage of integral membrane proteins in *Xenopus* egg extracts in a quantitative and time-resolved manner. By combining it with immunodepletion approaches, integral membrane protein transport through NPCs can be studied not only under wild-type conditions but also in the absence of specific factors including distinct NPC proteins.

9.1 PREPARATION OF *XENOPUS* EGG EXTRACT CYTOSOL AND MEMBRANES

9.1.1 Preparation of interphasic egg extracts

Xenopus eggs are arrested in the second metaphase of meiosis. Addition of calcium ionophore, which mimics the calcium influx generated during fertilization, activates these unfertilized eggs to enter the first interphase. Cell cycle progression into the first mitosis requires the translation of a single protein, cyclin B (Murray & Kirschner, 1989). To arrest the extracts in interphase, cyclin B synthesis is prevented by the translation inhibitor cycloheximide. We use a protocol for interphasic egg extract preparation adapted from Newmeyer and Wilson (1991).

9.1.1.1 Materials and equipment

- 240-IU/ml pregnant mare serum gonadotropin (PMSG, available as Intergonan, Intervet)
- 1000-IU/ml human chorionic gonadotropin (HCG, available as Ovogest, Intervet)
- Beckman L-60 Ultracentrifuge, SW55 Ti swinging bucket rotor and ultraclear tubes (or equivalents)

- Beckman Optima TLX Ultracentrifuge, TLA120.2 rotor and tubes (or equivalent system)
- Häreus-Multifuge 1-LR-Centrifuge (or equivalent)
- 5 ml syringes, 27G 3/4 in. and 16G 1½ in. needles
- large orifice tip (MBP® 1000G Pipet Tips, Molecular BioProducts)

9.1.1.2 Buffers and solutions

- MMR buffer: 100 mM NaCl, 2 mM KCl, 5 mM Hepes, 0.1 mM EDTA, pH 8.0, 1 mM $MgCl_2$, 2 mM $CaCl_2$. Prepare a 20× stock solution in deionized water and autoclave, adjust pH to 8.0 with 5 M KOH. 1× MMR is freshly prepared before use by dilution in deionized water and readjustment of the pH to 8.0 with 5 M KOH.
- Dejellying buffer: 2% cysteine in 0.25 × MMR buffer, pH 7.8. This buffer should be prepared freshly and kept at 4–8 °C. To save time, precool the water.
- Calcium ionophore A23187: 2 mg/ml in ethanol.
- Protease inhibitor (PI) mix: 10 mg/ml 4-(2-aminoethyl)-benzenesulfonylfluoride, 0.2 mg/ml leupeptin, 0.1 mg/ml pepstatin, 0.2 mg/ml aprotinin in deionized water. Store in aliquots at −20 °C.
- Dithiothreitol (DTT): 1 M in deionized water.
- Cycloheximide: 20 mg/ml in ethanol.
- Cytochalasin B: 10 mg/ml in DMSO.
- Sucrose buffer: 250 mM sucrose, 50 mM KCl, 2.5 mM $MgCl_2$, 10 mM Hepes, pH 7.5, 1 mM DTT (freshly added), 1:100 PI. Keep at 4 °C.
- Dilution buffer: 50 mM KCl, 2.5 mM $MgCl_2$, 10 mM Hepes, pH 7.5, 1 mM DTT (freshly added), 1:100 PI. Keep at 4 °C.

9.1.1.3 Method

Note: For frog maintenance, see Sive, Grainger, and Harland (2000).

1. Prime frogs to ovulate by injecting 60 U PMSG into their dorsal lymph sac 3–10 days before the experiment (5 ml syringes, 27G 3/4 in. needles).
2. On the day before the experiment, inject frogs with 250 U HCG in their dorsal lymph sac (5 ml syringes, 27G 3/4 in. needles) and place them in individual laying tanks containing 2 l of 1 × MMR buffer for 16–18 h at 18 °C.
3. Collect high-quality eggs by pooling the good batches and wash them several times with 1 × MMR buffer. Good eggs will be individually laid, uniform in size, and pigmented with clearly defined animal and vegetal hemispheres. Eggs laid in clumps or strings or white eggs should be excluded. It is important to carefully sort the eggs at this early step and throughout the procedure as the presence of a few "bad eggs" can quickly spoil the rest.
   Note: For detailed description of "good" versus "bad" eggs, see Gillespie et al. (2012).
4. Dejelly eggs in cold dejellying buffer for 10 min. Change buffer once and swirl continuously. Eggs become closely packed during this step.

5. Rinse eggs four times with 1 × MMR buffer. This washing must be done gently, as the eggs are now fragile, and taking care not to expose the eggs to air.
6. Activate eggs in 100 ml 1 × MMR buffer by adding 8 µl of the calcium ionophore A23187 for 10 min or until activation becomes visible (animal cap contraction), whichever comes first.
7. Rinse eggs carefully four times with 1 × MMR buffer and once again carefully to keep them from being exposed to air.
8. Incubate eggs for 20 min at room temperature.
9. Replace the MMR buffer with cold sucrose buffer by washing twice. All subsequent steps must be carried out on ice.
10. Carefully place the eggs in SW55 tubes containing 50 µl sucrose buffer, 50 µl PI, 5 µl 1 M DTT, 12.5 µl cycloheximide, and 2.5 µl cytochalasin B using a wide-mouthed (cut) transfer pipette. Remove excess buffer and refill the tubes until they are completely full.
11. Pack eggs by centrifugation at 400 rpm (approx. $3 \times g_{av}$) for 60 s in Häreus-Multifuge 1-LR-centrifuge. Remove excess liquid along with white eggs that have now floated to the top.
12. Crush the eggs by centrifugation at 15,000 rpm ($21{,}000 \times g_{av}$) for 20 min in a SW55 Ti rotor at 4 °C (Fig. 9.1).

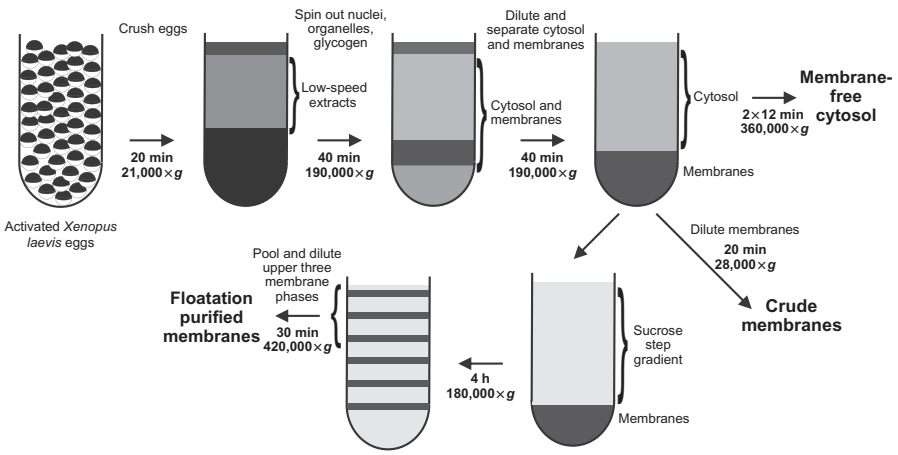

FIGURE 9.1 Schematic Overview of Cytosol and Membrane Preparation from *Xenopus* Eggs

Activated *Xenopus laevis* eggs are crushed by centrifugation to obtain the cellular content as low-speed extracts. These low-speed extracts are further separated into a cytosol and a membrane fraction. After separating both fractions, residual membrane components are removed from the cytosol by two additional high-speed centrifugation steps. The membranes can either be purified in a crude preparation by dilution and centrifugation or further fractionated by floatation through a sucrose step gradient. Floated membrane fractions, for example, fractions 1–3 are pooled and purified by a final dilution and centrifugation step.

13. Remove the (pale yellow) low-speed extracts between the bright yellow yolk on top and dark broken eggs at the bottom using a syringe (16G 1½ in. needle). From one full SW55 tube, expect approximately 2.5 ml of low-speed extract.
14. Add 10 µl PI, 1 µl 1 M DTT, 2.5 µl cycloheximide, and 0.5 µl cytochalasin B per milliliter of low-speed extract. Mix well and load into fresh SW55 tubes. Spin for 40 min at 45,000 rpm (190,000 × g_{av}) in a SW55 Ti rotor at 4 °C.
15. Remove the (pale yellow) cytosolic phase between the white lipids on the top and the dark pellet-containing pigments using a syringe (16G 1½ in. needle). From one full SW55 tube, expect approximately 3–4 ml of extract.
16. Dilute the extract with 0.3 ml of dilution buffer per 1 ml of cytosolic extract, mix well, and load into fresh SW55 tubes for a final round of centrifugation. Spin for 40 min at 45,000 rpm (190,000 × g_{av}) in a SW55 Ti rotor at 4 °C.
17. Carefully remove the cytosol between the white lipids on the top and membranes, mitochondria, and pigments at the bottom using a pipette. It is important to avoid contamination from the white lipids as they can hinder the *in vitro* nuclear assembly reaction. The membranes obtained at this step can be further purified using the protocols described in Section 9.1.2.
18. Cytosol is cleared from residual membranes by two rounds of centrifugation for 12 min each at 100,000 rpm (360,000 × g_{av}) in a TLA120.2 rotor at 4 °C and used directly in the nuclear assembly reactions (Section 9.4).

9.1.2 Preparation of *Xenopus* membranes

Nuclear envelope assembly in high-speed fractionated egg extracts requires the presence of both the cytosolic and membrane fractions (Sheehan, Mills, Sleeman, Laskey, & Blow, 1988; Vigers & Lohka, 1991; Wilson & Newport, 1988). Although it is possible to employ the crude membrane fraction to this end, this fraction contains cytosolic contaminations. At least after depletion of proteins from egg extract cytosol, a purified membrane fraction should be used. Crude membranes are mostly used in biochemical applications, such as membrane protein depletion and reconstitution, due to their high concentration. We describe here the preparation of both the crude membranes, adapted from Pfaller, Smythe, and Newport (1991) and floatation-purified membranes, adapted from Wilson and Newport (1988).

9.1.2.1 Materials and equipment

- Tissue grinders: One 30 ml douncer with loose pestel and one 7 ml douncer with tight pestel (Wheaton, Millville, USA)
- Beckman L-60 Ultracentrifuge, SW40 Ti swinging bucket rotor, and ultraclear tubes (or equivalent system)
- Beckman Optima TLX Ultracentrifuge, TLA100.4 rotor, and tubes (or equivalent system)

9.1.2.2 Buffers and solutions

- PI mix, DTT, and sucrose buffer are described in Section 9.1.1.

- 2.1 M sucrose buffer: 2.1 M sucrose, 50 mM KCl, 2.5 mM $MgCl_2$, 10 mM Hepes, pH 7.5, 1 mM DTT (freshly added), 1:100 PI. Keep at 4 °C.
- Sucrose cushions: 1400, 1300, 1100, 900, and 700 mM sucrose. Prepare sucrose cushions by mixing sucrose buffer from Section 9.1.1 and 2.1 M sucrose buffer in appropriate ratios to obtain the according sucrose concentration.

9.1.2.3 Method

Our protocols for the preparation of crude and floated membranes start with the generation of high-speed interphasic egg extract outlined in Section 9.1.1 (Fig. 9.1).

PREPARATION OF CRUDE MEMBRANES:

1. Membranes are isolated immediately following the final centrifugation step of high-speed extract preparation (step 17 in Section 9.1.1). At this point, they are easily distinguishable as a slightly viscous pale yellow layer located above the darkly colored mitochondria and pigments. Following removal of the egg cytosol, membranes are extracted with a syringe. From a full SW55 tube, expect approximately 1–1.5 ml of membrane suspension. Dilute the pooled membranes in 10 volumes of sucrose buffer and homogenize with two strokes of the loose pestel in a 30-ml glass douncer.
2. Transfer the homogenized membranes to SW40 tubes and spin for 20 min at 15,000 rpm ($28{,}000 \times g_{av}$) in a SW40 Ti rotor at 4 °C.
3. After removing the supernatant, resuspend the membrane pellet in sucrose buffer. Homogenize the membrane suspension with five strokes of the tight pestel in a 7-ml glass douncer.
4. Adjust the final volume of the membrane suspension to 50% of the cytosol volume with sucrose buffer. Aliquot, snap freeze, and store in liquid nitrogen.

PREPARATION OF FLOATATION-PURIFIED MEMBRANES:

1. As for the crude membrane preparation, the yellow membrane layer is extracted immediately following the final centrifugation step of the high-speed extract preparation using a syringe.
2. Mix membranes with four volumes of cold 2.1 M sucrose. Homogenize membranes with two strokes of the loose pestel in a 30-ml douncer.
3. Place 5 ml of homogenized membranes in SW40 tubes and overlay sequentially with 1.4 ml of each of the five sucrose cushions starting from 1400 to 700 mM sucrose. Finish the step gradient with 0.2 ml of sucrose buffer.
4. Membranes are separated by centrifugation for 4 h at 38,000 rpm ($180{,}000 \times g_{av}$) in an SW40 Ti rotor at 4 °C.
5. Following centrifugation, carefully isolate the upper three-membrane phases. Dilute the pooled membrane fractions with three volumes of sucrose buffer and spin for 30 min at 100,000 rpm ($420{,}000 \times g_{av}$) in a TLA100.4 rotor at 4 °C.
6. After removing the supernatant, resuspend the membrane pellet in sucrose buffer. Homogenize the membrane suspension with five strokes of the tight pestel in a 7-ml glass douncer. Take care that the membranes are completely resuspended.

7. Adjust the final volume of the floated membranes to 50% of the volume of the cytosol. Aliquot, snap freeze, and store in liquid nitrogen.

9.2 PROTEIN EXPRESSION

9.2.1 Expression and purification of integral membrane proteins in *E. coli*

For add-back reactions, after depletion of soluble as well as transmembrane proteins natively purified proteins from *Xenopus* membranes (Antonin, Franz, Haselmann, Antony, & Mattaj, 2005) but also recombinant proteins might be employed (Eisenhardt, Redolfi, & Antonin, 2013; Mansfeld et al., 2006). Wherever possible, recombinant proteins are preferable as this obviates the copurification and coaddition of other *Xenopus* proteins.

Expression of eukaryotic transmembrane proteins can be achieved in several systems such as yeast, insect cells, or mammalian cell lines. We have good experience with *E. coli* as expression system when fusing the protein of interest to the Mistic sequence from *Bacillus subtilis* in a pET28a vector for expression in *E. coli* (Eisenhardt et al., 2013; Theerthagiri et al., 2010). The Mistic sequence directs the integral membrane protein to the inner *E. coli* membrane (Roosild et al., 2005) and can be fused either N- or C-terminal of the protein sequence. For most proteins, expression in a BL21de3 strain works well but it might be worth testing other expression strains as expression efficiency in different strains varies for different proteins.

9.2.1.1 Materials and equipment

- 2-l glass flasks (Duran, Roth, Germany)
- Bacterial shaker
- French press (e.g., EmulsiFlex-C3 from Avestin, Germany, or equivalent system)
- Sorvall centrifuge and rotors (or equivalent system)
- Rotating wheel
- Cheese cloth (Ypsifix® 8 cm/4 m, Holthaus Medical, Germany)
- Ni-NTA Agarose (Qiagen, Germany)
- 20-ml plastic chromatography columns (Econo-Pac® disposable chromatography columns, Bio-Rad, Germany)

9.2.1.2 Buffers and solutions

- LB medium: 1% peptone (w/v), 0.5% yeast extract (w/v), and 0.5% NaCl (w/v), adjust pH to 7.0 with 10 N NaOH, autoclave.
- Kanamycin: 25 mg/ml in water.
- 1 M $MgSO_4$: 24.65 g $MgSO_4 \cdot 7H_2O$ in water, autoclave.
- 20 × NPS (NPS = 100 mM PO_4, 25 mM SO_4, 50 mM NH_4, 100 mM Na, 50 mM K): 0.5 M $(NH_4)_2SO_4$, 1 M KH_2PO_4, and 1 M Na_2HPO_4. pH of 20 × NPS in water should be ~6.75, autoclave.

- 50 × 5052: 25% glycerol (v/v), 0.25% glucose (w/v), and 2% alpha-lactose (w/v) in water, autoclave.
- Ni-wash buffer: 20 mM Tris, pH 7.4, 500 mM NaCl, and 30 mM imidazole, autoclave.
- $MgCl_2$: 1 M stock in water, autoclave.
- Phenylmethanesulfonylfluoride (PMSF): 0.2 M in ethanol (Applichem, Germany).
- Deoxyribonuclease I (DNase I): 10 U/µl in phosphate-buffered saline (PBS) (bovine pancreas, ≥60.000 Dornase units/mg dry weight, Merck KGaA, Germany).
- Ni-elution buffer: 20 mM Tris, pH 7.4, 500 mM NaCl, 400 mM imidazole, 10% glycerol (v/v).
- EDTA: 500 mM stock, dissolved in deionized water, pH 8.0, autoclave.
- Sucrose buffer as in Section 9.1.1.
- Cetyltrimethylammonium bromide (CTAB, Calbiochem, Germany).

9.2.1.3 Method

1. Grow primary culture overnight in LB medium with kanamycin 1:1000 at 37 °C in a bacterial shaker.
2. Inoculate large scale expression cultures from overnight culture 1:100. Supplement the LB medium with 1 mM $MgSO_4$, 1 × 5052, 1 × NPS and kanamycin 1:1000 (in this order). Fill at maximum 500 ml culture in 2 l flasks.
3. Grow cultures at 37 °C and 300 rpm until $OD_{600} = 1.5$ in a bacterial shaker.
4. Shift to expression temperature and shake at 300 rpm for 12–20 h (OD_{600} should be at least five before harvesting).

   Notes: Induction in LB medium with IPTG is an alternative. However, as bacteria can be grown in much higher density in autoinduction medium the yield per expression volume is much higher. In our hands, autoinduction works fine for most of the tested proteins.

   Best expression temperature needs to be determined experimentally.
5. Harvest cultures for 15 min at 4500 × *g* and 4 °C in Sorvall centrifuge (or equivalent system).
6. Resuspend bacterial pellet obtained from 1 l culture in 150–200 ml cold Ni-wash buffer and add 1 ml of 0.2 M PMSF. All following steps should be done on ice or in the cold and using cold buffers.
7. Break bacteria by a French press or equivalently.
8. Add 2 mM $MgCl_2$, 450 ml of 10 U/µl DNAse I in PBS, and 2 ml of 0.2 M PMSF per 1 l of expression culture to the lysate and incubate 10 min on ice.
9. Freeze lysate at −20 °C or proceed immediately. Spin lysate for 20 min at 28,000 × *g* and 4 °C in Sorvall centrifuge.
10. Resuspend pellets at room temperature in 10 ml Ni-wash buffer + 1% CTAB and add 2 ml of 0.2 M PMSF per 1 l expression culture. Add Ni-wash buffer + 1% CTAB to a total volume of 320 ml per 1 l expression culture and rotate for 45 min at room temperature on a rotating wheel to solubilize the

bacterial membranes. All following steps, in which CTAB is present, should be done at room temperature as CTAB precipitates in the cold.

11. Spin for 15 min at 20 °C and 15,000 × *g* to remove unsolubilized membranes in Sorvall centrifuge and filter the supernatant through a cheese cloth.
12. Add 500 µl Ni-NTA Agarose beads to the supernatant derived from 1 l expression culture for 2 h at room temperature. Rotate samples on a rotating wheel.

    Note: The amount of Ni-NTA Agarose beads depends on the expression yield and has to be determined for each construct.
13. Collect Ni-NTA Agarose beads in a 20 ml plastic chromatography column. Wash beads two to three times with one-column volume of Ni-wash buffer + 0.1% CTAB.
14. Close column and elute the protein of interest from the beads with 500 µl Ni-elution buffer + 1% CTAB for 5 min at room temperature. Collect eluate and elute beads again with 250 µl Ni-elution buffer + 1% CTAB for 5 min. Pool both eluates.

    Note: The volume of Ni-elution buffer depends on the protein concentration and the Agarose beads volume. Elution works best with 50% slurry of Agarose beads or more diluted. A third elution might be done if a lot of protein remains on the Agarose beads. Analyze beads for elution efficiency if you purify the protein the first time.
15. Dialyze eluates to sucrose buffer + 1 mM EDTA for 1 h at 4 °C and again over night with fresh buffer.

    Note: Dependent on the later use of the protein, the dialysis buffer can be altered. For addback in nuclear assembly assays (Section 9.4.1) sucrose buffer is recommended.
16. Determine protein concentration by SDS-PAGE, aliquot and freeze in liquid nitrogen. Store protein aliquots at −80 °C for later use.

    Note: Traces of CTAB are still present in the protein sample and might interfere with most methods of protein concentration determination. It is best to judge the protein concentration by comparing the band on a protein gel to a known concentration of BSA.

9.2.2 Expression and purification of NusA–tobacco etch virus protease

Tobacco etch virus (TEV) protease for nuclear assembly reactions to measure the transport of inner nuclear membrane proteins through NPCs (Section 9.4.4) is fused to NusA to increase its size above the size exclusion limit of NPCs, cloned into a pET28a expression vector, and transformed into BL21de3 bacteria for expression.

9.2.2.1 Materials and equipment

- Chromatography columns (Econo-Column® Chromatography Column, 5.0 × 20 cm, Bio-Rad, Germany).
- Other material as in Section 9.2.1.

9.2.2.2 Buffers and solutions

- As in Section 9.2.1.

9.2.2.3 Method

1. Inoculate 4 ml of an overnight culture of transformed bacteria (grown in LB medium with 25 µg/ml kanamycin) in 400 ml autoinduction medium (LB supplemented as in Section 9.2.1). Fill in 2 l glass flasks and grow at 37 °C at 300 rpm in bacterial shaker.
2. Shift culture to expression temperature of 25 °C when $OD_{600} = 1.5$.
3. After 14–20 h at 25 °C, OD_{600} should be at least 5. Harvest bacteria by centrifugation for 15 min at $4500 \times g$ in a cold rotor at 4 °C in a Sorvall centrifuge.
4. Resuspend pellet in 10 ml cold Ni-wash buffer, fill up to at least 100 ml and add 1 ml of 0.2 M PMSF. All following steps should be done keeping the proteins on ice or in the cold and using cold buffers.
5. Break bacteria in Emulsiflex, French press, or equivalent system.
6. Add 1 mM $MgCl_2$, 200 µl of 10 U/µl DNAse I in PBS, and 1 ml of 0.2 M PMSF and incubate 10 min on ice.
7. Spin 15 min at $22{,}000 \times g$ in a rotor at 4 °C. Spin again if supernatant is not cleared sufficiently. Filter supernatant through cheese cloth.
8. Apply 1.6 ml of 50% slurry of Ni-NTA Agarose to the supernatant and incubate for 2 h at 4 °C on a rotating wheel.
9. Apply Agarose beads to chromatography column. If all Agarose is collected in the column wash with 100 ml cold Ni-wash buffer.
10. Elute the His_6–NusA–TEV protein with 4 ml Ni-elution buffer.
11. Dialyze eluate to sucrose buffer, determine protein concentration, and store aliquots at −80 °C. We usually obtain 20 mg of protein from 400 ml autoinduction culture.

9.3 BIOCHEMICAL PROCEDURES

9.3.1 Generation of antibody beads

Depletion of soluble or membrane integral proteins from *Xenopus* egg extracts is achieved by passage of the cytosol or solubilized membrane fraction, respectively, over a bead material with crosslinked antibodies. Because of the high abundance of many nucleoporins these antibody beads should provide a high capacity and we therefore prefer Protein A–Sepharose over magnetic Protein A beads.

9.3.1.1 Materials and equipment

- Protein A–Sepharose (GE Healthcare, Sweden)
- Rabbit IgG (Calbiochem, Germany)
- Häreus-Multifuge 1-LR-Centrifuge (or equivalent)

- Dimethylpimelimidate (DMP, store solid and dry at 4 °C; Pierce, Thermo Fisher Scientific, Bonn, Germany)
- Rotating wheel (or equivalent)
- BSA (Fraction V, Calbiochem, Germany)
- Sodium azide (NaN_3)

9.3.1.2 Buffers and solutions

- PBS: 2.7 mM KCl, 137 mM NaCl, 10 mM $Na_2HPO_4 \cdot 2H_2O$, 2 mM KH_2PO_4. Prepare a 10 × stock solution, adjust to pH 7.4 with 10 N NaOH, and autoclave. Dilute to 1 × PBS freshly before use.
- Coupling buffer: 200 mM $NaHCO_3$, 100 mM NaCl, pH 9.3.
- Blocking buffer: 0.1 M ethanolamine, pH 8.2.
- Buffer A: 100 mM sodium acetate, 500 mM NaCl, pH 4.2.
- Buffer B: 100 mM $NaHCO_3$, 500 mM NaCl, pH 8.3.
- PI mix as in Section 9.1.1.

9.3.1.3 Method

1. Incubate 4 mg of affinity-purified antibody with 1 ml Protein A–Sepharose (50% slurry) in PBS for 4–16 h at 4 °C on a rotating wheel. For control beads, use rabbit IgGs at approximately the same concentration.
2. Wash beads twice with coupling buffer by spinning beads down for 2 min at 3000 rpm and 4 °C in a Häreus-Multifuge 1-LR-Centrifuge. Remove supernatant and add fresh buffer.
3. Crosslink antibodies and Protein A–Sepharose beads in 10 mM DMP in coupling buffer for 20 min at room temperature on a rotating wheel.
4. Wash beads once with coupling buffer (spin as in step 2) and crosslink again in 10 mM DMP in coupling buffer for 20 min at room temperature on a rotating wheel.
5. Wash beads once with blocking buffer (spin as in step 2) and rotate for 1 h in blocking buffer at room temperature.
6. Wash beads alternating twice with buffers A and B (spin as in step 2).
7. Block beads in 3% BSA in PBS supplemented with PI (1:1000) for 1 h at 4 °C on a rotating wheel.
8. Store beads as a 50% slurry in 3% BSA in PBS supplemented with PI (1:1000) and 0.05% NaN_3 at 4 °C.

9.3.2 Preparation of G50-chromatography columns

For reconstitution of membranes after depletion (Section 9.3.3) or generation of proteoliposomes (Section 9.3.4), detergent is removed by gel filtration with Sephadex G50-columns. To avoid major protein and lipid loss during column passage, the gel filtration column is preblocked with BSA and a lipid mixture.

9.3.2.1 Materials and equipment

- G50 gel filtration medium (Sephadex G-50 Fine, GE Healthcare, Sweden)
- Glass chromatography column (Econo-Column®, 0.5 × 20 cm, Bio-Rad, Germany)
- Polyethylene tubing (or equivalent)
- BSA
- *n*-Octyl-β-D-glucopyranoside (Calbiochem, Germany) or equivalent detergent

9.3.2.2 Buffers and solutions

- Lipid mix: 3 mg/ml cholesterol (ovine wool, >98), 3 mg/ml L-α-phosphatidylserine (sodium salt, brain, porcine), 3 mg/ml L-α-phosphatidylinositol (sodium salt, liver, bovine), 6 mg/ml L-α-phosphatidylethanolamine (egg, chicken), 15 mg/ml L-α-phosphatidylcholine (egg, chicken; all from Avanti Polar Lipids, USA) in 10% *n*-octyl-β-D-glucopyranoside
- $DiIC_{18}$: 1 mg/ml 1,1′-dioctadecyl-3,3,3′,3′-tetramethylindocarbocyanine perchlorate in DMSO ("DiI," $DiIC_{18}$(3), crystalline; Life Technologies GmbH, Germany)
- Sucrose buffer as in Section 9.1.1 and PBS as in Section 9.3.1

9.3.2.3 Method

1. Swell G50 beads in sucrose buffer for 10 min at room temperature.
2. Remove bottom and top lids from the chromatography column and fill column with swollen G50 beads. Let beads settle by gravity. Add more beads carefully until the glass cylinder of the column is nearly filled (leave about 0.5 cm space at the top). The upper edge of the bead layer should remain visible.
   Note: Avoid air bubbles in the column. Be careful that columns do not run dry.
3. Fill column with sucrose buffer, put top lid on, and connect the lid to a buffer reservoir via tubing.
4. Wash column with sucrose buffer from the reservoir by letting the buffer pass by gravity flow.
5. To block the column, take top lid off, carefully remove excess buffer and add 100 µl of 1 mg/ml BSA in sucrose buffer directly onto the bead layer. Let the solution enter the beads, then fill the column immediately but carefully with buffer, put top lid back on, and wash the column as in step 4.
6. Block column again with 20 µl lipid mix diluted 1:5 with PBS in 100 µl total volume as in step 5.
   Note: Lipid mix can be altered as well as the detergent used to dissolve the lipids. A relatively high-CMC (critical micelle concentration) value of the detergent and small aggregation number is important to ensure its removal by gel filtration.
7. Wash column with sucrose buffer for 30 min as in step 4.
8. Close bottom lid of the column. To store your columns for longer term, add 0.1% NaN_3 to the sucrose buffer.
   Note: For long-term storage of the columns, let some buffer pass from time to time.

9.3.3 Depletion of transmembrane proteins from *Xenopus* membranes

To specifically deplete transmembrane proteins, *Xenopus* membranes are solubilized by detergent and the protein of interest is immunodepleted by passage of the solubilized membrane fraction over an antibody column (Fig. 9.2A). Detergent removal from the solubilized and depleted membrane fraction reconstitutes the membranes. An efficient way for detergent removal is passage of a gel filtration column (Allen, Romans, Kercret, & Segrest, 1980) under the precondition that the detergent has a relative high-CMC value, which defines the concentration of the free detergent in solution in contrast to its micellar form, and a not small aggregation number.

For add-back experiments, the purified integral membrane protein (see Section 9.2.1) is added to the solubilized and depleted membrane fraction and coreconstituted by passage of the gel filtration column.

9.3.3.1 Materials and equipment

- *n*-Octyl-β-D-glucopyranoside or equivalent detergent as in Section 9.3.2
- Beckman Optima TLX Ultracentrifuge, TLA100 rotor and tubes (or equivalent system)
- Mobicol columns (Mobicol "classic" with 1 closed screw cap and plug and 35 µm pore size filters, MoBiTec GmbH, Germany)
- Cooled tabletop microcentrifuge
- Crude membranes, antibody beads, and G50-chromatography columns described in Sections 9.1.2, 9.3.1, and 9.3.2

9.3.3.2 Buffers and solutions

- Sucrose buffer, lipid mix, and $DiIC_{18}$ as in Sections 9.1.1 and 9.3.2.

9.3.3.3 Method

1. Solubilize 20 µl of crude membranes (for preparation, see Section 9.1.2) in sucrose buffer with 1% *n*-octyl-β-D-glucopyranoside for 10 min at 4 °C.

   Notes: Frozen membrane aliquots can be used.

   Ensure proper membrane solubilization with marker proteins by western blotting. If necessary other detergents (with relative high-CMC values and small aggregation numbers to allow for their removal afterwards) might be used such as CHAPS.

   Use high-quality detergent, some batches of *n*-octyl-β-D-glucopyranoside need to be purified before use by passage over a mixed bead resin (e.g., AG501-X8 from Bio-Rad, Germany).
2. Clear by centrifugation for 10 min at 200,000 × *g* and 4 °C in a TLA100 rotor and take supernatant.
3. Equilibrate 40 µl of antibody beads (50% slurry, prepared as described in Section 9.3.1) in a Mobicol column with sucrose buffer immediately before use, spin dry by centrifugation for 30 s at 5000 × *g* and 4 °C in a cooled tabletop

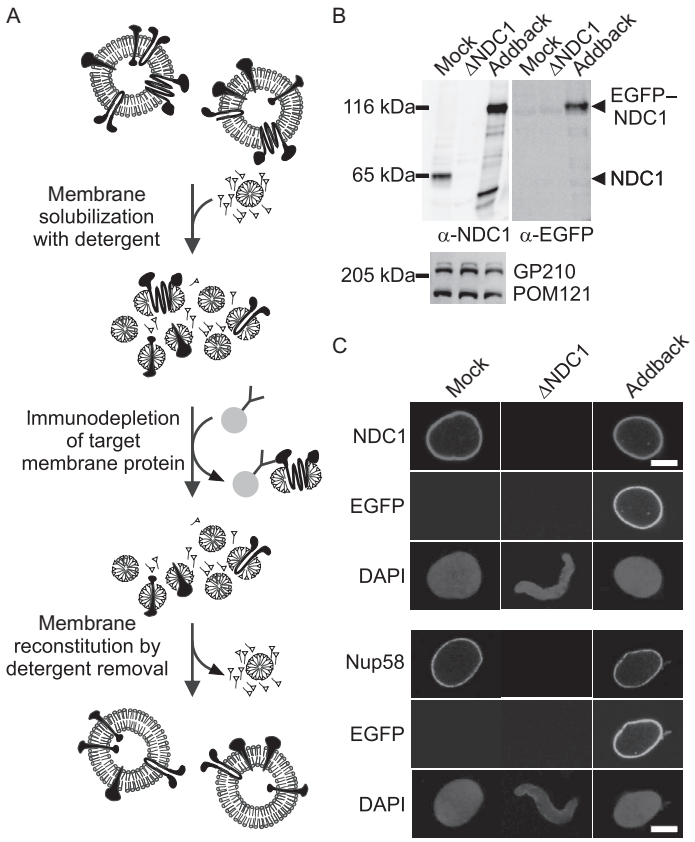

FIGURE 9.2 Depletion and Functional Add-Back of Membrane Proteins.

(A) Schematic illustration of immunodepletion of transmembrane proteins from *Xenopus* membranes. Membranes are solubilized with a detergent and the target membrane protein is depleted from the solubilized membrane fraction by specific antibody beads. Finally, the depleted membranes are reconstituted by detergent removal. (B) Western blot analysis of *Xenopus* membranes, which were mock-depleted, immunodepleted of endogenous NDC1 or NDC1-depleted and substituted with recombinant EGFP–NDC1 expressed in *E. coli* (addback). Endogenous and recombinant NDC1 are detected by NDC1-antibodies, the recombinant protein also by EGFP-antibodies. The NDC1 depletion does not affect levels of other integral membrane proteins including the transmembrane nucleoporins GP210 and POM121. (C) Immunofluorescence of nuclear assembly reactions with *Xenopus* cytosol and membranes from (B). Recombinant EGFP–NDC1 is faithfully integrated into the nuclear membranes as detected by NDC1- and EGFP-antibodies. NDC1 depletion blocks NPC formation (ΔNDC1). This phenotype is rescued by the addition of recombinant EGFP–NDC1 (addback) as indicated by the presence of Nup58, a nucleoporin located in the inner part of the NPC. DNA is stained with DAPI. Bar: 10 μm.

microcentrifuge. Apply supernatant of step 2 to dried beads and incubate for 30 min at 4 °C on a rotating wheel.

Note: Optimal bead to solubilized membranes ratio needs to be determined. However, the given conditions work for most of the proteins we tested.

4. Elute unbound supernatant (spin as in step 3) and incubate a second time as in step 3 with fresh antibody beads.
5. Elute unbound supernatant and add 20 µl lipid mix and 0.2 µl of 1 mg/ml $DiIC_{18}$ in DMSO. For add-back experiments, add your protein of interest in approximately endogenous concentration together with the lipid mix to the eluate.

   Notes: The optimal amount of readded protein needs to be determined. In our hands, for most add-back attempts achieving endogenous protein levels works fine (Fig. 9.2B).

   If necessary one can avoid the use of a fluorescent dye and reconstituted membranes are collected blindly. For this, a test run in which one can follow the reconstituted fraction with a marker (e.g., a fluorescent dye) is performed and the number of drops counted until the reconstituted membrane fraction runs out of the column.
6. Reconstitute membranes by detergent removal by passing the sample over a G50-chromatography column (prepared as described in Section 9.3.2) equilibrated to sucrose buffer. Remove excess of buffer and load the samples directly on the bead layer. Fill the column with buffer as soon as the sample has entered the beads. Collect the membrane-containing fraction (~400 µl or 8–9 drops), which appears pink due to addition of $DiIC_{18}$.
7. Pellet reconstituted membranes by centrifugation for 30 min at 200,000 × *g* in a TLA100 rotor.
8. Resuspend membrane pellet in 20 µl sucrose buffer. Reconstituted membranes are now ready to use in the nuclear assembly reaction (Section 9.4.1).

9.3.4 Reconstitution of recombinant integral membrane proteins in proteoliposomes

For purification, integral membrane proteins are detergent solubilized from membranes. At the end of the purification process, the detergent is removed to maintain the proper functionality of the integral membrane protein by reconstitution in proteoliposomes, which can be used as a tool for functional studies as in Section 9.4.

9.3.4.1 Materials and equipment

- Beckman Optima TLX Ultracentrifuge, TLA120.2 rotor and tubes (or equivalent system)
- G50-chromatography columns described in Section 9.3.2

9.3.4.2 Buffers and solutions

- PBS, lipid mix, $DiIC_{18}$ and sucrose buffer as in Sections 9.1.1, 9.3.1, and 9.3.2

9.3.4.3 Method

1. Prepare preblocked G50-columns as described in Section 9.3.2 but use PBS instead of sucrose buffer.
2. Apply a mix consisting of 20 µl lipid mix, 5 µl purified protein (conc. <1 mg/ml), 50 µl PBS, and 0.5 µl $DiIC_{18}$ (1 mg/ml in DMSO) directly onto the bead layer.
3. Fill column with buffer as soon as the lipid mixture has entered the column. Collect $DiIC_{18}$-labeled fraction (~8–9 drops or 400 µl)-containing reconstituted proteoliposomes.

   Note: Alternatively, another fluorescent membrane dye or fluorescently labeled lipids can be used.
4. Pellet proteoliposomes in PBS in a TLA120.2 rotor for 30 min at 100,000 rpm (360,000 × g_{av}) and 4 °C. Resuspend pellet in 20 µl sucrose buffer.
5. Wash column after use with buffer and store it as described in Section 9.3.2.

   Note: If you do not want to use a fluorescent dye, proteoliposomes can be collected blindly (compare Notes for Section 9.3.3). Column can be reused but upper bead layers (~1 cm) have to be exchanged from time to time. After renewal of the upper bead layer, block column with BSA and lipids before next use as described in Section 9.3.2.

9.4 NUCLEAR ASSEMBLY REACTIONS

9.4.1 Nuclear assembly reactions using depleted and reconstituted membranes

In vitro-assembled nuclei can be reconstituted using cytosol and membranes from egg extracts combined with chromatin of demembranated sperm. Preparation of demembranated sperm is described in Murray (1991), see also Bernis and Forbes, Chapter 8 in this volume. For depletion experiments of transmembrane nucleoporins, endogenous membranes are replaced by a depleted membrane fraction prepared as described in Section 9.3.3.

9.4.1.1 Materials and equipment

- Vectashield 1000 (Vector Laboratories, Burlingame, USA)
- Round glass coverslips (12 mm diameter, Menzel, Braunschweig, Germany)
- 6-ml flat bottom tubes (Greiner, Germany)
- Large orifice tip (MBP® 200G/1000G Pipet Tips, Molecular BioProducts)
- Häreus-Multifuge 1-LR-Centrifuge
- Nail polish/coverslip sealant
- 24-well plates (Greiner, Germany)

9.4.1.2 Buffers and solutions

- Energy mix: 50 mM ATP, 50 mM GTP, 500 mM creatine phosphate, and 10 mg/ml creatine kinase in sucrose buffer. The energy mixture can be prepared and stored as single use aliquots at −80 °C.
- Glycogen: 0.2 g/ml in sucrose buffer (oyster glycogen, USB, Amersham).

- 0.1% Poly-L-lysine solution in water (Sigma-Aldrich, USA).
- Sucrose cushion: 30% sucrose in PBS.
- 4′,6-Diamidino-2-phenylindole (DAPI): 10 mg/ml in water, store in small aliquots in the dark at −20 °C.
- Membrane fixative: 2% paraformaldehyde, 0.5% glutaraldehyde (Sigma-Aldrich, USA) in 80 mM Pipes, pH 6.8, 1 mM $MgCl_2$, 150 mM sucrose. Add 1 µg/ml DAPI prior to use.
- IF fixative: 2% paraformaldehyde in 80 mM Pipes, pH 6.8, 1 mM $MgCl_2$, 150 mM sucrose.
- PBS, sucrose buffer, and $DiIC_{18}$, see Sections 9.1.1, 9.3.1, and 9.3.2.

9.4.1.3 Method

1. Add 0.6 µl of demembranated sperm chromatin (from stock of 3000 sperm heads/µl to reach a final concentration of ~100 sperm heads/µl) to 20 µl of freshly prepared membrane-free cytosol (described in Section 9.1.1) and mix carefully with a large orifice tip. Incubate for 10 min at 20 °C to allow for sperm chromatin decondensation.

   Note: In contrast to most nuclear assembly reactions, for which frozen aliquots of egg extract cytosol are used, this assay is very sensitive to the quality of the cytosol and we only use freshly prepared extracts.
2. Add 0.5 µl energy mix, 0.5 µl glycogen, and 4.4 µl of reconstituted membranes (described in Section 9.3.3) and mix carefully with a large orifice tip. Incubate for 110 min at 20 °C.

   Note: Include control samples, in which membranes are replaced by sucrose buffer, to confirm that cytosol is membrane free.
3. For visualization of membranes: Add 0.2 µl of 0.1 mg/ml $DiIC_{18}$ (dissolved in DMSO) 5 min before the end of incubation and mix carefully.
4. Fix samples for 20 min on ice either in 0.5 ml membrane fixative (for $DiIC_{18}$ membrane staining) or in 0.5 ml IF fixative (for immunofluorescence).
5. Load fixed nuclei onto a 0.8-ml sucrose cushion in the flat-bottomed tubes containing poly-L-lysine coated coverslips. Transfer nuclei onto the coverslips by spinning at 3500 rpm ($250 \times g_{av}$) for 15 min at 4 °C in a Häreus-Multifuge 1-LR-Centrifuge.

   Note: Coverslips are coated by covering them with a 0.1% poly-L-lysine solution for 5 min, washed once with water and dried.
6. For visualization of membranes: Wash coverslips once with deionized water and mount them on a 2 µl drop of Vectashield 1000. Seal coverslips with nail polish. Be careful that the coverslips do not dry out.

   For immunofluorescence staining: Place coverslips in 24-well plates, wash once and store in PBS. Continue with Section 9.4.2.

9.4.2 Immunofluorescence of nuclear assembly reactions

The membrane staining of nuclei prepared in nuclear assembly reactions (Section 9.4.1) visualizes the formation of a closed nuclear envelope around the reconstituted nuclei. The incorporation of NPCs into the nuclear envelope can be

examined by immunofluorescence (Fig. 9.2C). By using specific antibodies against individual nucleoporins, NPC composition can be investigated. This is especially useful after immunodepletion of nucleoporins to assay the impact of these individual NPC components on NPC formation.

9.4.2.1 Materials and equipment

- Fluorescently labeled secondary antibody (e.g., from Life Technologies GmbH, Germany)
- Vectashield 1000, nail polish or coverslip sealant and 24-well plates as in Section 9.4.1.

9.4.2.2 Buffers and solutions

- PBS and DAPI stock solution as in Sections 9.3.1 and 9.4.1.
- 50 mM NH_4Cl in PBS.
- Blocking buffer: 3% BSA in PBS + 0.1% Triton X-100 (Carl Roth GmbH + Co. KG, Karlsruhe, Germany).

9.4.2.3 Method

1. Carefully remove PBS and quench samples for 5 min with 50 mM NH_4Cl in PBS. Although the samples are fixed, the nuclei and particularly the nuclear envelope are very fragile to small breaks. All washes and buffer exchanges should be done carefully. It is also important that the coverslips do not dry out.
2. Incubate coverslips in blocking buffer for 30 min.
3. Incubate coverslips upside down on top of a drop of approximately 70 µl of primary antibody dilution in blocking buffer in a humidity chamber for 2 h. The user should determine optimal antibody dilutions.

   Note: Rabbit sera produced in our lab are generally diluted 1:100, while not only purified antibodies but also the widely used monoclonal antibody mAB414 can often be diluted to 1:1000 or 1:2000.
4. Wash coverslips three times for 2 min with PBS + 0.1% Triton X-100 in the 24-well plate.
5. Incubate coverslips with 250 µl of fluorescently labeled secondary antibodies (usually diluted 1:2000 in blocking buffer) for 1 h in 24-well plates in the dark.
6. Wash coverslips three times for 2 min with PBS + 0.1% Triton X-100. Avoid longer light exposure.
7. Incubate coverslips for 10 min in PBS + DAPI (1:2000) in the dark.
8. Wash coverslips once with water and mount them on a 1 µl drop of Vectashield 1000. Seal coverslips with nail polish. Keep coverslips in the dark and store at 4 °C.

9.4.3 Transmission electron microscopy of nuclear assembly reactions

For ultrastructural analysis of the assembled nuclei, samples are prepared for transmission electron microscopy. Nuclear membranes and NPCs are easily detectable due to the use of osmium tetroxide for contrast enhancement of membranes.

The protocol is adapted from Macaulay and Forbes (1996) including a reisolation of fixed *in vitro*-assembled nuclei on the surface of a coverslip before embedding. In this way, most nuclei are concentrated in a relative small volume and easily identified in a limited number of ultrathin sections.

Note: for field emission scanning electron microscopy of nuclei assembled *in vitro* using *Xenopus* extracts and anchored chromatin, see Chapter 2 by Fichtman et al., in this volume.

9.4.3.1 Materials and equipment

- 24-well plate as in Section 9.4.1.
- Epon/Araldite kit (EMS, Hatfield, USA)
- Dissecting microscope
- Needle
- Jigsaw

9.4.3.2 Buffers and solutions

- Fix buffer: 25 mM Hepes, pH 7.5, 25 mM Pipes, 1 mM EGTA, 50 mM KCl, 2 mM MgAc, 5% sucrose.
- Cacodylate buffer: 100 mM cacodylate dissolved in deionized water, pH 7.2.
- 1% Osmium tetroxide (OsO_4): dissolved in cacodylate buffer (w/v).
- 1.5% Potassium hexacyanidoferrate (II) ($K_4[Fe(CN)_6]\cdot 3H_2O$): dissolved in cacodylate buffer.
- 1% Uranyl acetate: dissolved in deionized water, keep in the dark at 4 °C.
- Epon/araldite mixture: for 26.5 ml of resin use 7.75 g Epon 812 Procure, 5.55 g Araldite 502, and 15.25 g DDSA. After thorough mixing, add 490 µl DMP-30.

9.4.3.3 Method

1. After centrifugation of the assembly reactions on poly-L-lysine coated coverslips (see Section 9.4.1), place coverslips in a 24-well plate.
2. Wash coverslips once with fix buffer.
3. Fix coverslips for 1 h on ice in fix buffer with 1% glutaraldehyde (v/v).
4. Postfix samples for 2 h on ice in fix buffer with 2.5% glutaraldehyde (v/v).
5. Wash once with ice-cold cacodylate buffer.
6. Incubate samples for 40 min on ice in 1% OsO_4 and 1.5% $K_4[Fe_6]$ (Orso et al., 2009).
7. Wash coverslips with deionized water.
8. Incubate for 1 h with 1% uranyl acetate at 4 °C in the dark.
9. Wash coverslips with water.
10. Dehydrate samples in a graded ethanol series of 30%, 50%, 90%, and 2 × 100% ethanol each for 10 min.
11. Resin infiltration: 50% Epon/Araldite in Ethanol, 2 × 100% Epon/Araldite each 30 min.

12. After resin infiltration, remove the coverslips from the 24-well plate and place them on a resin filled lid of a 1.5-ml Eppendorf cup, sample side facing down.
    Note: Avoid capturing any air bubbles.
13. Resin curing at 60 °C for 48 h.
14. Remove the glass coverslips from the cured resin-embedded samples by submerging them in liquid nitrogen.
    Note: This step has to be repeated several times until every bit of glass is removed from the sample surface. More often than not, remaining glass shards have to be carefully pried from the resin surface with a fine tungsten needle under the dissecting microscope. Wear personal protective equipment while working with liquid nitrogen and glass.
15. Find and mark out areas with nuclear assemblies under the dissecting microscope with a fine needle.
16. Cut out the areas of interest with a fine jigsaw.
17. Prepare ultrathin sections parallel to the sample surface.

9.4.4 Nuclear assembly reactions measuring transport of inner nuclear membrane proteins through NPCs

Nuclei assembled *in vitro* in *Xenopus* egg extracts can be used both, to study nuclear import of soluble cargos (for a detailed method description, see Chan & Forbes, 2006) and to analyze transport of inner nuclear membrane proteins through NPCs. For the latter use, integral membrane protein reporters are expressed and purified from *E. coli* (see Section 9.2.1) and reconstituted in proteoliposomes (see Section 9.3.4). These proteoliposomes are added to a nuclear assembly reaction at time points when the nuclear envelope is already closed around the chromatin. Proteoliposomes readily fuse with the endoplasmic reticulum and the reporter is immediately distributed throughout the membranes of the endoplasmic reticulum including the outer nuclear membrane.

NPC passage of the reporter to the inner nuclear membrane is monitored by its protection from a protease added to the cytoplasm (Fig. 9.3). We have best experience with a TEV protease fused to the large bacterial protein NusA, which increases the size of the protease-fusion protein to at least 90 kDa, thereby preventing its diffusion through the NPC (Fig. 9.3B). Consequently, reporter proteins contain a TEV protease recognition site followed by a domain, which is cleaved off upon TEV protease activity (Fig. 9.3A). The latter domain is usually an EGFP-tag in our assay, as this allows to follow cleavage by both light microscopy (Fig. 9.3C) and western blotting (Fig. 9.3D). We have good experience with reporter constructs containing EGFP-tag and TEV cleavage site N-terminally fused to BC08, a INM protein with a single C-terminal transmembrane region (Ulbert, Platani, Boue, & Mattaj, 2006) or the first transmembrane region of LBR (lamin B receptor), which is sufficient for INM targeting (Soullam & Worman, 1995). But also multispanning INM proteins such as full-length LBR or nurim work as reporters.

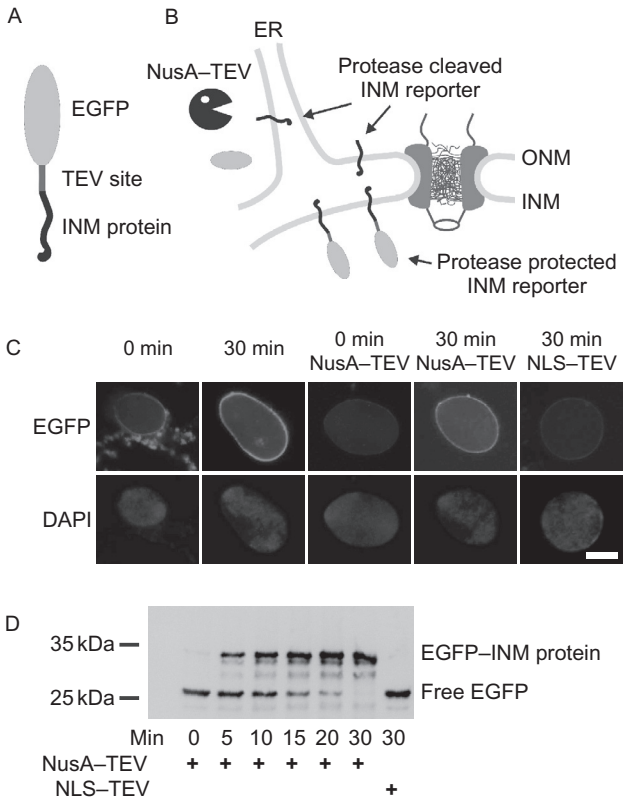

FIGURE 9.3 Analysis of Inner Nuclear Membrane Protein Passage Through Nuclear Pore Complexes

(A) Schematic illustration of an inner nuclear membrane (INM) protein reporter. The reporter protein is fused to an N-terminal EGFP-tag followed by a TEV protease recognition site. (B) The reporter construct reconstituted in proteoliposomes is added to nuclear assembly reactions when the nuclear envelope is already closed. The reporter is immediately distributed throughout the membranes of the endoplasmic reticulum (ER), including the outer nuclear membrane (ONM). To monitor its transport through nuclear pore complexes, a NusA-fused TEV protease is added, which is excluded from NPC passage due to its size. The reporter protein is accessible for cleavage of the EGFP-tag by the TEV protease if present in the membranes of the ER or ONM, whereas in the inner nuclear membrane (INM) the reporter constructs are protease protected. (C) Immunofluorescence of the assay described in (B). The reporter construct is visualized by EGFP-antibodies and can be detected in the ER and ONM at 0 min. Thirty minutes after addition, the reporter construct is enriched in the INM, where it is protease protected from NusA–TEV due to size exclusion of nuclear pore complexes. If the TEV protease construct is actively imported into the nucleus due to a nuclear localization site (NLS), the EGFP-tag of the reported is cleaved off, also when residing in the INM after 30 min. DNA is stained with DAPI. Bar: 10 μm. (D) Western blot analysis of isolated nuclei from the experiment in (C) at different time points using the EGFP-antibody. Cleavage of the reporter by TEV protease results in the appearance of a band of free EGFP (around 25 kDa) which is absent if the reporter is protease protected due to transport to the INM, which occurs approximately 15 min after addition of the reporter construct.

Modified after Theerthagiri, Eisenhardt, Schwarz, and Antonin (2010).

9.4.4.1 Materials and equipment

- EGFP-antibody (cat. no. 11814460001, Roche, Germany)

9.4.4.2 Buffers and solutions

- SDS-sample buffer: 0.19 M Tris, pH 6.8, 30% sucrose (w/v), 0.9% SDS (w/v), 0.1% Bromphenol blue (w/v), 0.1 M DTT.
- Energy mix, glycogen, and IF fixative as in Section 9.4.1.

9.4.4.3 Method

1. Incubate 45 µl of freshly prepared membrane-free cytosol (preparation described in Section 9.1.1) with 2.5 µl sperm heads (3000 sperm heads/µl) for 10 min at 20 °C to allow for sperm decondensation.
2. Add 1 µl energy mix, 1 µl glycogen, and 2.5 µl of floatation-purified membranes (preparation described in Section 9.1.2) and incubate for 50 min at 20 °C.
3. Add 5 µl of resuspended proteoliposomes (prepared as described in Section 9.3.4) and mix carefully, incubate at 20 °C.
4. Take out 10 µl from the sample each after 0, 5, 10, 15, and 30 min after proteoliposome addition and add 1 µl of 5 µg/µl TEV protease for 5 min at 20 °C to each. Stop cleavage reaction by adding 5 µl SDS-sample buffer and immediate heating for 5 min at 95 °C.
5. Analyze time course of cleavage reaction by western blotting with an EGFP-antibody. Alternatively, the loss of EGFP signal can be monitored by immunofluorescence. For this, stop TEV cleavage reaction by fixation in IF fixative and proceed with immunofluorescence as described in Section 9.4.2.

CONCLUSION

Xenopus egg extracts provide a powerful cell-free tool to study nuclear assembly and functions. Since their first use more than 30 years ago (Lohka & Masui, 1983), they have been employed in a variety of assays focusing on different aspects of nuclear organization, dynamics, and functions. Accordingly, slight variations in the protocols for preparing such extracts exist (e.g., see Chapter 8 for a modified egg extract preparation protocol).

Immunodepletion of soluble proteins is a key advantage of the *Xenopus* egg extract system. It facilitates analysis of the function of specific proteins in definite aspects of nuclear dynamics, such as NPC assembly. By employing the methods described here, the technical repertoire is expanded to include integral membrane proteins. These methods have already been applied to analyze the function of transmembrane nucleoporins or the passage of membrane proteins through the pore but they are certainly not limited to these questions. In the future, they could be used to study the functional interaction of transmembrane proteins with chromatin or membrane fusion reactions mediated by transmembrane proteins to name just two examples.

References

Allen, T. M., Romans, A. Y., Kercret, H., & Segrest, J. P. (1980). Detergent removal during membrane reconstitution. *Biochimica et Biophysica Acta*, *601*(2), 328–342.

Antonin, W., Franz, C., Haselmann, U., Antony, C., & Mattaj, I. W. (2005). The integral membrane nucleoporin pom121 functionally links nuclear pore complex assembly and nuclear envelope formation. *Molecular Cell*, *17*(1), 83–92.

Antonin, W., Ungricht, R., & Kutay, U. (2011). Traversing the NPC along the pore membrane: Targeting of membrane proteins to the INM. *Nucleus*, *2*(2), 87–91. http://dx.doi.org/10.4161/nucl.2.2.14637.

Brown, K. S., Blower, M. D., Maresca, T. J., Grammer, T. C., Harland, R. M., & Heald, R. (2007). Xenopus tropicalis egg extracts provide insight into scaling of the mitotic spindle. *Journal of Cell Biology*, *176*(6), 765–770. http://dx.doi.org/10.1083/jcb.200610043.

Chan, R. C., & Forbes, D. I. (2006). In vitro study of nuclear assembly and nuclear import using Xenopus egg extracts. *Methods in Molecular Biology*, *322*, 289–300.

de la Barre, A. E., Robert-Nicoud, M., & Dimitrov, S. (1999). Assembly of mitotic chromosomes in Xenopus egg extract. *Methods in Molecular Biology*, *119*, 219–229. http://dx.doi.org/10.1385/1-59259-681-9:219.

Eisenhardt, N., Redolfi, J., & Antonin, W. (2013). Nup53 interaction with Ndc1 and Nup155 are required for nuclear pore complex assembly. *Journal of Cell Science*, *127*(Pt 4), 908–921. http://dx.doi.org/10.1242/jcs.141739.

Galy, V., Antonin, W., Jaedicke, A., Sachse, M., Santarella, R., & Haselmann, U. (2008). A role for gp210 in mitotic nuclear-envelope breakdown. *Journal of Cell Science*, *121*(Pt 3), 317–328.

Gillespie, P. J., Gambus, A., & Blow, J. J. (2012). Preparation and use of Xenopus egg extracts to study DNA replication and chromatin associated proteins. *Methods*, *57*(2), 203–213. http://dx.doi.org/10.1016/j.ymeth.2012.03.029.

Lohka, M. J. (1998). Analysis of nuclear envelope assembly using extracts of Xenopus eggs. *Methods in Cell Biology*, *53*, 367–395.

Lohka, M. J., & Masui, Y. (1983). Formation in vitro of sperm pronuclei and mitotic chromosomes induced by amphibian ooplasmic components. *Science*, *220*(4598), 719–721.

Lusk, C. P., Blobel, G., & King, M. C. (2007). Highway to the inner nuclear membrane: Rules for the road. *Nature Reviews. Molecular Cell Biology*, *8*(5), 414–420, nrm2165 [pii] 1038/nrm2165.

Macaulay, C., & Forbes, D. J. (1996). Assembly of the nuclear pore: Biochemically distinct steps revealed with NEM, GTP gamma S, and BAPTA. *Journal of Cell Biology*, *132*(1–2), 5–20.

Mansfeld, J., Guttinger, S., Hawryluk-Gara, L. A., Pante, N., Mall, M., & Galy, V. (2006). The conserved transmembrane nucleoporin NDC1 is required for nuclear pore complex assembly in vertebrate cells. *Molecular Cell*, *22*(1), 93–103.

Maresca, T. J., & Heald, R. (2006). Methods for studying spindle assembly and chromosome condensation in Xenopus egg extracts. *Methods in Molecular Biology*, *322*, 459–474.

Murray, A. W. (1991). Cell cycle extracts. *Methods in Cell Biology*, *36*, 581–605.

Murray, A. W., & Kirschner, M. W. (1989). Cyclin synthesis drives the early embryonic cell cycle. *Nature*, *339*(6222), 275–280. http://dx.doi.org/10.1038/339275a0.

Newmeyer, D. D., & Wilson, K. L. (1991). Egg extracts for nuclear import and nuclear assembly reactions. *Methods in Cell Biology*, *36*, 607–634.

Orso, G., Pendin, D., Liu, S., Tosetto, J., Moss, T. J., & Faust, J. E. (2009). Homotypic fusion of ER membranes requires the dynamin-like GTPase atlastin. *Nature*, *460*(7258), 978–983. http://dx.doi.org/10.1038/nature08280.

Pfaller, R., Smythe, C., & Newport, J. W. (1991). Assembly/disassembly of the nuclear envelope membrane: Cell cycle-dependent binding of nuclear membrane vesicles to chromatin in vitro. *Cell*, *65*(2), 209–217.

Roosild, T. P., Greenwald, J., Vega, M., Castronovo, S., Riek, R., & Choe, S. (2005). NMR structure of Mistic, a membrane-integrating protein for membrane protein expression. *Science*, *307*(5713), 1317–1321. http://dx.doi.org/10.1126/science.1106392.

Sheehan, M. A., Mills, A. D., Sleeman, A. M., Laskey, R. A., & Blow, J. J. (1988). Steps in the assembly of replication-competent nuclei in a cell-free system from Xenopus eggs. *Journal of Cell Biology*, *106*(1), 1–12.

Sive, H. L., Grainger, R. M., & Harland, R. M. (2000). *Early development of Xenopus laevis—A laboratory manual*. New York, USA: Cold Spring Harbor Laboratory Press.

Soullam, B., & Worman, H. J. (1995). Signals and structural features involved in integral membrane protein targeting to the inner nuclear membrane. *Journal of Cell Biology*, *130*(1), 15–27.

Theerthagiri, G., Eisenhardt, N., Schwarz, H., & Antonin, W. (2010). The nucleoporin Nup188 controls passage of membrane proteins across the nuclear pore complex. *Journal of Cell Biology*, *189*(7), 1129–1142. http://dx.doi.org/10.1083/jcb.200912045.

Ulbert, S., Platani, M., Boue, S., & Mattaj, I. W. (2006). Direct membrane protein-DNA interactions required early in nuclear envelope assembly. *Journal of Cell Biology*, *173*, 469–476. http://dx.doi.org/10.1083/jcb.200512078.

Vigers, G. P., & Lohka, M. J. (1991). A distinct vesicle population targets membranes and pore complexes to the nuclear envelope in Xenopus eggs. *Journal of Cell Biology*, *112*(4), 545–556.

Wilson, K. L., & Newport, J. (1988). A trypsin-sensitive receptor on membrane vesicles is required for nuclear envelope formation in vitro. *Journal of Cell Biology*, *107*(1), 57–68.

Article

Developmental Cell

Nup153 Recruits the Nup107-160 Complex to the Inner Nuclear Membrane for Interphasic Nuclear Pore Complex Assembly

Graphical Abstract

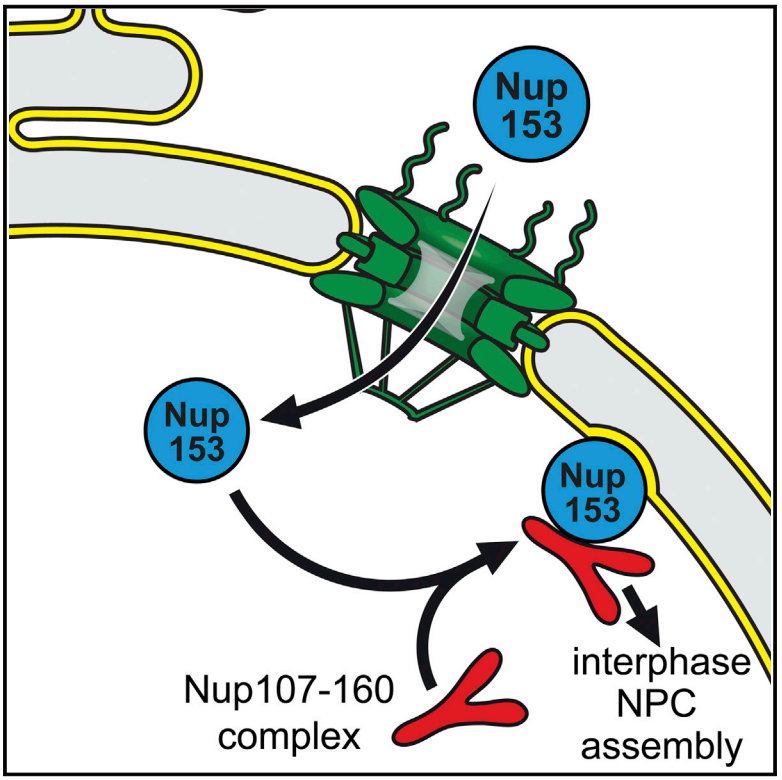

Authors

Benjamin Vollmer, Michael Lorenz, Daniel Moreno-Andrés, ..., Matthias Flötenmeyer, Sebastian Leptihn, Wolfram Antonin

Correspondence

wolfram.antonin@tuebingen.mpg.de

In Brief

Nuclear pore complexes assemble and integrate into the intact nuclear envelope during interphase. Vollmer et al. show that the nucleoporin Nup153 is critical for this process. It binds to the nuclear membrane and recruits the Nup107-160 complex, an essential structural component of nuclear pore complexes, to newly forming pores.

Highlights

- Nup153 binds synthetic membranes via its N terminus
- Transportin binding regulates Nup153 synthetic membrane interaction
- Nup153 membrane binding is required for interphasic nuclear pore complex assembly
- Nup153 recruits the Nup107-160 complex to the inner nuclear membrane

Vollmer et al., 2015, Developmental Cell *33*, 717–728
June 22, 2015
http://dx.doi.org/10.1016/j.devcel.2015.04.027

CellPress

Developmental Cell
Article

Nup153 Recruits the Nup107-160 Complex to the Inner Nuclear Membrane for Interphasic Nuclear Pore Complex Assembly

Benjamin Vollmer,[1,4,5] Michael Lorenz,[1,4] Daniel Moreno-Andrés,[1] Mona Bodenhöfer,[1] Paola De Magistris,[1] Susanne Adina Astrinidis,[1] Allana Schooley,[1] Matthias Flötenmeyer,[2] Sebastian Leptihn,[3] and Wolfram Antonin[1,*]
[1]Friedrich Miescher Laboratory of the Max Planck Society, Spemannstraße 39, 72076 Tübingen, Germany
[2]Max Planck Institute for Developmental Biology, Spemannstraße 37, 72076 Tübingen, Germany
[3]Institute for Microbiology and Molecular Biology, University of Hohenheim, Garbenstraße 30, 70599 Stuttgart, Germany
[4]Co-first author
[5]Present address: Oxford Particle Imaging Centre, Division of Structural Biology, Wellcome Trust Centre for Human Genetics, University of Oxford, Oxford 3 7BN, UK
*Correspondence: wolfram.antonin@tuebingen.mpg.de
http://dx.doi.org/10.1016/j.devcel.2015.04.027

SUMMARY

In metazoa, nuclear pore complexes (NPCs) are assembled from constituent nucleoporins by two distinct mechanisms: in the re-forming nuclear envelope at the end of mitosis and into the intact nuclear envelope during interphase. Here, we show that the nucleoporin Nup153 is required for NPC assembly during interphase but not during mitotic exit. It functions in interphasic NPC formation by binding directly to the inner nuclear membrane via an N-terminal amphipathic helix. This binding facilitates the recruitment of the Nup107-160 complex, a crucial structural component of the NPC, to assembly sites. Our work further suggests that the nuclear transport receptor transportin and the small GTPase Ran regulate the interaction of Nup153 with the membrane and, in this way, direct pore complex assembly to the nuclear envelope during interphase.

INTRODUCTION

Nuclear pore complexes (NPCs) are gatekeepers of the nucleus. They restrict the diffusion of proteins and nucleic acids between the cytosol and nuclear interior and enable tightly controlled transport between these compartments (Wente and Rout, 2010). Nuclear import of soluble proteins is mediated by transport receptors that bind cargo proteins in the cytosol. This interaction massively enhances the passage of otherwise inert cargos through NPCs. In the nucleoplasm, transport receptors are detached from cargos by binding to the small GTPase Ran in its GTP-bound form. The RanGTP-transport receptor complexes then traverse the NPC in the opposite direction. RanGTP hydrolysis at the cytoplasmic side of the NPC frees transport receptors, which are able to act in another round of the cycle.

Despite their enormous size and flexibility with regard to transport substrates, NPCs are composed of only about 30 different proteins, nucleoporins, present in multiple copies (Bui et al., 2013). They can be roughly categorized into structural nucleoporins, which form the scaffold of the pore, and those responsible for the transport and exclusion functions of the NPC. Nucleoporins of the latter class are characterized by a high number of phenylalanine glycine (FG) repeats that form a meshwork within the pore. A stack of three rings forms the NPC scaffold. The middle ring is laterally linked to the pore membrane and connected to the central transport channel formed mostly by the FG nucleoporins. The cytoplasmic and nucleoplasmic rings are connected to cytoplasmic filaments and the nuclear basket structure, respectively.

Most structural nucleoporins are part of one of two evolutionarily conserved subcomplexes within the pore. The Nup93 complex (Nic96 complex in yeast) forms a large part of the inner ring and connects the pore membrane to the central transport channel (Vollmer and Antonin, 2014). The Nup107-160 complex (Nup84 complex in yeast) forms the cytoplasmic and nucleoplasmic rings (Bui et al., 2013) and is, because of its Y shaped structure (Lutzmann et al., 2002), also referred to as Y-complex. This complex is related to vesicle coats and presumably stabilizes the curved pore membrane of the NPC (Brohawn et al., 2008). Connected to the nucleoplasmic ring is the nuclear basket, a fish trap-like structure extending to the nuclear interior. In metazoans, three nucleoporins localize to the basket, Nup153, Nup50, and TPR (Cordes et al., 1997; Guan et al., 2000; Sukegawa and Blobel, 1993), the best characterized being Nup153.

Nup153 possesses a tripartite structure (Ball and Ullman, 2005). The N-terminal region is important for NPC targeting (Bastos et al., 1996; Enarson et al., 1998), most likely because it mediates binding to the Y-complex (Vasu et al., 2001). A central zinc-finger-containing domain interacts with Ran (Nakielny et al., 1999). The C-terminal FG-repeat-containing region provides binding sites for a variety of transport receptors (Moroianu et al., 1997; Nakielny et al., 1999; Shah and Forbes, 1998; Shah et al., 1998). Because of its localization at the nucleoplasmic exit site of NPCs as well as its interactions with transport receptors and Ran, Nup153 is thought to assist in the dissociation of import cargo-transport receptor complexes and thus facilitates nuclear import cycles. Indeed, Nup153 depletion reduces importin α/β mediated import (Ogawa et al., 2012; Walther et al., 2001). Nup153 is also important for mRNA export from

the nucleus (Bastos et al., 1996; Ullman et al., 1999). Although Nup153 is essential in *C. elegans* and HeLa cells (Galy et al., 2003; Harborth et al., 2001), no homologs have been found in yeast species. Nonetheless, yeast nucleoporins (such as Nup1 and Nup60 in *S. cerevisiae*, Nup124 in *S. pombe*) might share functional and sequence features with Nup153 (Cronshaw et al., 2002; Hase and Cordes, 2003; Varadarajan et al., 2005).

While significant progress has been made in understanding how NPCs function in nuclear transport, elucidating the NPC formation pathway remains a formidable task. In metazoa, NPC assembly occurs at two different stages of the cell cycle: at the end of mitosis and during interphase. During mitotic exit, NPC assembly is concomitant with the formation of a closed nuclear envelope (NE). The early steps of postmitotic NPC formation, such as the recruitment of a subset of nucleoporins to the chromatin, are particularly well characterized due to their faithful reconstitution in *Xenopus* egg extracts. Assembly is initiated by MEL28/ELYS, a chromatin binding nucleoporin, which recruits the Y-complex (Franz et al., 2007; Gillespie et al., 2007; Harel et al., 2003; Rasala et al., 2006, 2008; Rotem et al., 2009; Walther et al., 2003a). Interphasic NPC assembly in metazoan is relatively poorly characterized. It takes place under fundamentally different conditions. Whereas large numbers of NPCs form in a short time span during mitotic exit, NPC assembly events in interphase are rare and sporadic (D'Angelo et al., 2006; Dultz and Ellenberg, 2010). Both assembly pathways require the Y-complex as an essential structural component of the NPC (D'Angelo et al., 2006; Doucet et al., 2010; Harel et al., 2003; Walther et al., 2003a). However, while the Y-complex is recruited to the chromatin by MEL28 at the end of mitosis, a feature essential for postmitotic NPC assembly, MEL28 is not required for interphasic NPC assembly (Doucet et al., 2010). It is possible that NPC assembly during interphase is rather initiated at the nuclear membranes (Doucet et al., 2010; Dultz and Ellenberg, 2010; Vollmer et al., 2012), but the precise mechanism by which this occurs has not been defined.

Here, we show that the nuclear basket component Nup153 is required for NPC assembly during interphase but not at the end of mitosis. Nup153 binds the inner nuclear membrane via its N terminus, a feature that is fundamental for its function in interphasic NPC assembly as it recruits the Y-complex to the assembling pores. Transportin regulates the interaction of Nup153 with the membrane and thus might direct interphasic NPC assembly specifically to the NE from inside the nucleus.

RESULTS

Nup153 Interacts via Its N Terminus Directly with Membranes

Nup153 contains a region within its N terminus that directs it to the inner nuclear membrane (Enarson et al., 1998). It is possible that Nup153 is localized to the NE due to interactions with integral inner nuclear membrane proteins or lamins, proteins that underlay and stabilize the NE, but it could also bind directly to the lipid bilayer. To test for a direct membrane interaction we incubated the purified recombinant N-terminal region comprising the first 149 aa of *Xenopus laevis* Nup153 with small unilamellar liposomes with a NE lipid composition (Lorenz et al., 2015). Due to their density, lipid vesicles float up through a sucrose gradient. Membrane binding proteins can be identified in the top fraction together with the liposomes. This is indeed the case for Nup153 (Figure 1A) as well as for a Nup133 fragment previously identified as membrane interacting (Drin et al., 2007). The N-terminal region of Nup153 showed preference for small vesicles with high curvature independent of lipid composition (Figure 1B).

Sequence analysis of the N terminus of Nup153 identified a conserved region among vertebrates that might form an amphipathic helix, as depicted in the helical wheel representation (Figures 1C and 1D). We generated a point mutation (a valine to glutamate exchange in position 50, V50E) that predictably disrupts the hydrophobic surface of the helix. Indeed, the V50E mutation impaired liposome binding in flotation assays (Figures 1A and 1B). To directly visualize the interaction of Nup153 with membranes, we generated giant unilamellar vesicles (GUVs) with sizes up to 50 μm using the NE lipid composition. When the EGFP-tagged N terminus of Nup153 was added to the exterior of these GUVs, it was efficiently recruited to the vesicle membrane indicating a direct membrane interaction (Figure 1E). As a negative control, we employed purified recombinant EGFP, which did not bind the GUV membrane. Importantly, the V50E mutant did not bind to GUVs, confirming that the amphipathic helix is responsible for the membrane binding capacity of Nup153.

The N-terminal fragment of *Xenopus* Nup153 fused to EGFP, when ectopically expressed in HeLa cells, localized to the NE, presumably the inner nuclear membrane (Figures 1F and S1C). Overexpression of this fragment induced NE proliferation (Movie S1), as is typical for nuclear membrane-interacting proteins (Ralle et al., 2004). Membrane proliferation has previously been observed for the overexpression of full-length Nup153 (Bastos et al., 1996). In our experiments, the V50E mutation abolished NE localization and membrane proliferation. Instead, the protein localized to the nucleoplasm, indicating that the mutation is sufficient to prevent the interaction of the N terminus of Nup153 with membranes in cells.

To confirm the direct membrane binding of full-length Nup153, we turned to the human ortholog, due to the low expression yield of the *Xenopus* Nup153. Human Nup153 possesses 42% amino acid identity and 55% similarity with the *Xenopus* protein. The fluorescently labeled human Nup153 efficiently bound GUVs (Figure 1G). The corresponding membrane-binding-deficient mutation (V47E in the human protein) abrogated the membrane interaction.

Nup153 Membrane Binding Is Not Required for NPC Targeting in Mammalian Cells

To understand the functional implication of the direct membrane interaction, we tested whether nuclear membrane targeting of Nup153 is required for its incorporation into NPCs. HeLa cells were transfected with EGFP-tagged full-length human Nup153 as well as the membrane-binding-deficient mutant (V47E). Both proteins localized to the nuclear rim and showed a typical punctate pattern (Daigle et al., 2001) on the NE surface (Figures 2A and S2). The pattern overlaps with mCherry-labeled Nup62 but not lamin B, indicating proper NPC localization. Despite its nuclear rim localization, the V47E mutant exhibited increased nucleoplasmic staining consistent with an abolished direct membrane interaction.

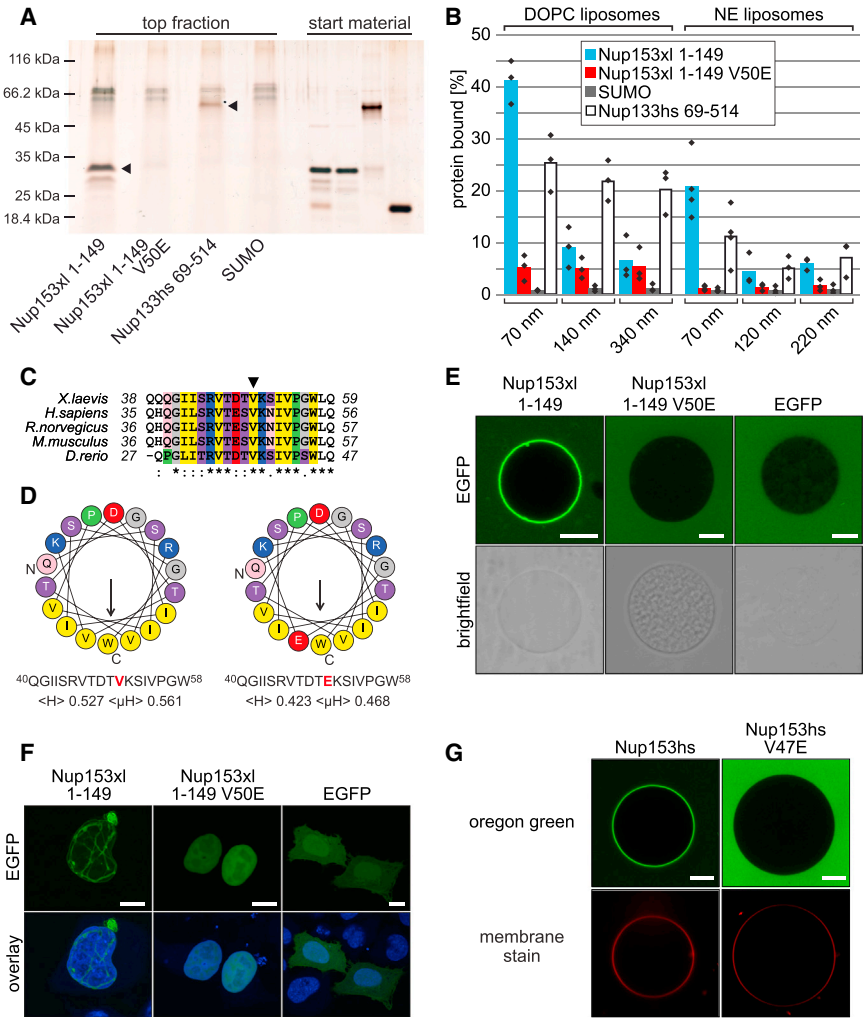

Figure 1. Nup153 Interacts via Its N Terminus Directly with Membranes

(A) 3 μM of the N-terminal domain (aa 1–149) of *Xenopus* Nup153 and the corresponding V50E mutant fragment, as well as a membrane-interacting fragment of Nup133 and SUMO as positive and negative controls, respectively, were incubated with 2.5 mg/ml fluorescently labeled 70 nm NE liposomes and floated through a sucrose gradient. The top gradient fractions and the starting materials were analyzed by SDS-PAGE and silver staining.

(B) Binding of the Nup153 N terminus, the V50E mutant, SUMO, and the Nup133 fragment to DOPC or NE liposomes of different diameters were analyzed by flotation experiments and quantified by western blotting (columns are the average bound quantities of three or four independent experiments; individual data points are indicated).

(C) Sequence alignment of the N-terminal region of vertebrate Nup153.

(D) Amino acid sequence of *Xenopus* Nup153 with the predicted amphipathic helix in a helical wheel representation (generated with HeliQuest (Gautier et al., 2008)). Valine (V) was exchanged to glutamate (E) in the membrane binding mutant, indicated in red. The length of the arrow within the helix is proportional to the mean hydrophobic moment (< μH >), which is also indicated as well as the hydrophobicity (< H >) as calculated by HeliQuest.

(E) NE lipid GUVs were incubated with 500 nM EGFP-tagged Nup153 N terminus, the corresponding V50E mutant, or EGFP alone.

(F) HeLa cells transfected with EGFP-tagged Nup153 N terminus, the V50E mutant, or EGFP. Chromatin is stained with DAPI (blue in overlay).

(G) NE lipid GUVs were incubated with Oregon-green-labeled full-length human Nup153 and the corresponding V47E mutant.

Bars, 10 μm. See also Figure S1 and Movie S1.

Immunoprecipitation from transfected HEK cells demonstrated that the V47E mutation did not impair known interactions, namely, to the Y-complex (Nup160 and Nup107) or other nucleoporins (Nup50 and TPR), to A/C and B-type lamins, or to components of the nuclear import machinery, Ran, importin α and β, and transportin (Figure 2B). Together these results indicate that membrane binding is not required for the assembly of Nup153 into NPCs. Furthermore, the V47E mutation does not disturb the interaction network of Nup153 but rather specifically affects its direct membrane binding.

Nup153 Membrane Interaction Is Not Required for NPC Assembly at the End of Mitosis

We used *Xenopus* egg extracts to assess whether the membrane binding capacity of Nup153 is important for the assembly and function of NPCs. Nup153 can be specifically immuno-depleted from these extracts without affecting the levels of other nucleoporins, including TPR and Nup50 as well as two components of the Y-complex, Nup133, and Nup107, which interact with Nup153 within intact NPCs (Figure 2C). Similarly, the levels of lamin LIII, a *Xenopus* B-type lamin, and components of the nuclear transport machinery (Ran, importin α and β, transportin) were unchanged.

When de-membranated sperm heads are incubated with egg extracts, a NE forms around the decondensing chromatin in a process resembling the reassembly of the nucleus at the end of mitosis (Gant and Wilson, 1997). The NE contains NPCs visualized with the antibody mAB414, which recognizes several FG nucleoporins, as seen in the control (mock) depletion (Figure 2D). When Nup153 was depleted, the protein was absent from the nuclear rim confirming the depletion efficiency. The assembled nuclei contained a closed NE with NPCs that were unevenly distributed. This NPC clustering phenotype upon Nup153 depletion has been previously observed (Walther et al., 2001) and is best visualized by surface rendering of confocal stacks (Figure 2D). Addition of recombinant Nup153 to endogenous levels (see Figure 2C) rescued the NPC clustering phenotype (Figures 2D–2F) demonstrating its specificity. NPC clustering was also rescued by the Nup153 membrane-binding mutant, which indicates that the Nup153 membrane interaction is not required for proper NPC spacing.

Depletion of Nup153 did not affect the localization and regular distribution of lamin B or integral inner nuclear membrane proteins, such as LBR or BC08. Several nucleoporin antibodies including those recognizing the integral pore membrane protein POM121, the Y-complex members Nup133 and Nup107 as well

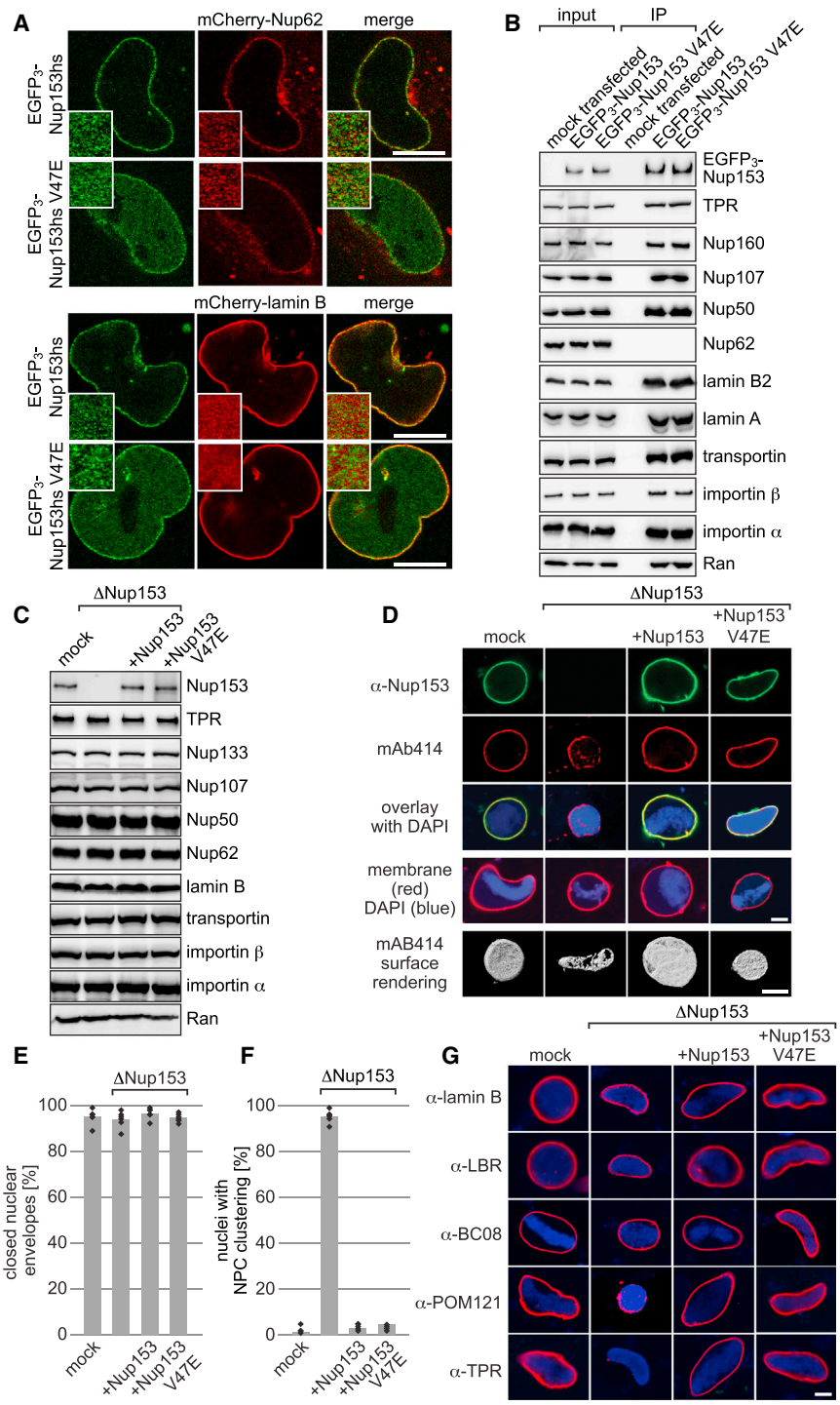

Figure 2. Nup153 Membrane Binding Is Not Required for Its NPC Targeting and NPC Assembly at the End of Mitosis

(A) HeLa cells were co-transfected with triple-EGFP human Nup153 or the corresponding V47E mutant and mCherry-Nup62 or mCherry-lamin B and analyzed by live cell imaging. Insets show the nuclear surface at a 1.5-fold higher magnification.

(B) HEK293 cells were mock transfected, transfected with triple-EGFP human Nup153 or the V47E mutant. Inputs and immunoprecipitates from cell lysates were analyzed by western blotting.

(C) Western blot of mock-depleted, Nup153-depleted (ΔNup153), and Nup153-depleted *Xenopus* egg extracts supplemented with recombinant wild-type Nup153 or the membrane-binding mutant (Nup153 V47E).

(D) Nuclei assembled for 120 min in extracts generated as in (C) were analyzed by immunofluorescence for Nup153 (green) and mAB414 (red). DNA was stained with DAPI (blue) and membranes with DiIC18 (fourth row, red). The fifth row shows the surface rendering of confocal stacks of mAB414-labeled nuclei.

(E) Quantification of chromatin substrates with closed NEs. Columns are the average of six independent experiments with individual data points (each 100 randomly chosen chromatin substrates) indicated.

(F) Quantification of nuclei with NPC clustering identified by mAB414 staining (mean of six independent experiments with individual data points [100 chromatin substrates each] indicated).

(G) Immunofluorescence on nuclei assembled as in (D). Chromatin is stained with DAPI (blue).

Bars, 10 μm. See also Figure S2.

as the Nup93 complex members Nup155 and Nup53 showed a patchy staining (Figures 2G and S2B). These observations demonstrate that the structural backbones of NPCs can assemble in the absence of Nup153. Furthermore, Nup58 as a central transport channel nucleoporin (Figure S2B) is also present at NPCs lacking Nup153. Consistent with previous reports, TPR was not detectable at Nup153-depleted nuclei, as it depends on this interaction for NPC localization (Hase and Cordes, 2003; Walther et al., 2001). Re-addition of recombinant wild-type or membrane-binding-deficient Nup153 rescued not only the NPC clustering phenotype but also TPR recruitment. This is consistent with the notion that the V47E mutation does not interfere with TPR binding (Figure 2B).

Taken together, these results suggest that the membrane binding capability of Nup153 is not crucial for NPC assembly at the end of mitosis. The interaction of Nup153 with membranes is not mandatory for proper NPC spacing, as the V47E mutant also rescues the NPC clustering phenotype. However, we observed that the nuclei assembled in the presence of the V47E mutant were smaller in comparison to the wild-type addback (Figures 2D, 2G, and S2B). Similarly, nuclei lacking Nup153 were smaller than control nuclei.

Nup153 Membrane Interaction Is Not Required for Efficient Nuclear Import

The addition of membranes to sperm DNA decondensed in egg extracts results in a fully closed NE-containing NPCs within

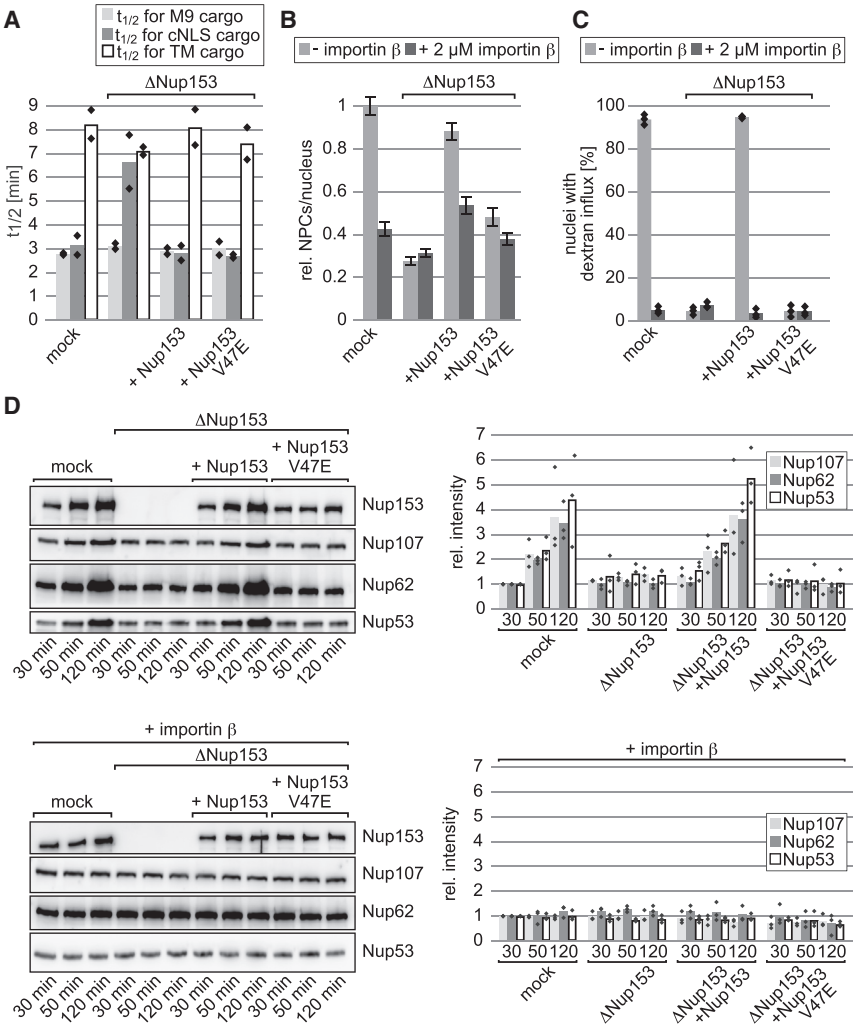

Figure 3. Nup153 Membrane Interaction Is Not Important for Nuclear Import Efficiency, but Rather for Interphasic NPC Assembly

(A) Nuclei were assembled in mock, Nup153-depleted extracts, or Nup153-depleted extracts supplemented with Nup153 or the V47E mutant. After closed NE formation, import rates for soluble M9 and cNLS cargos as well as for a transmembrane (TM) cargo were determined (average of two independent experiments, individual data points are indicated).

(B) Nuclei assembled as in (A) were fixed after 120 min, and NPCs per nucleus were counted based on mAB414 staining. Where indicated, interphasic NPC assembly was blocked by importin β addition after 50 min (average from a total of 50 nuclei in five independent experiments, normalized to the mock control; error bars are SEM).

(C) Nuclei assembled as in (A) for 50 min were supplemented with cytosol depleted of FG nucleoporins in addition to being either mock depleted or Nup153 depleted. After a further 60-min incubation, fluorescein isothiocyanate (FITC)-labeled 70 kDa dextran and Hoechst were added, and the percentage of nuclei with nuclear dextran, i.e., those in which interphasic NPC assembly occurred, was determined (average of three independent experiments, each comprising 100 nuclei; individual data points are indicated).

(D) Nuclei were assembled as in (A) and re-isolated after 30, 50, and 120 min. Nucleoporin levels were determined by quantitative western blotting. Plotted are the averages from three independent experiments, individual data points are indicated. In the lower panel, importin β was added after 30 min to block interphasic NPC assembly.

20 min. After this assembly, which reproduces nuclear reformation at the end of mitosis, the nuclei grow in size—the extent to which depends on the extract quality and an ATP re-generating system—for another 180 min. This nuclear growth requires import of nuclear proteins through NPCs. During this time, new NPCs integrate into the growing NE (D'Angelo et al., 2006) in a process reproducing interphasic NPC assembly, which, in turn, allows for more import and accelerated growth.

Nup153 contributes to the efficiency of nuclear transport cycles (Ogawa et al., 2012; Walther et al., 2001). We therefore tested whether the Nup153 membrane interaction is necessary for its role in nuclear import. We added different nuclear import substrates to nuclei assembled for 30 min in vitro (i.e., 20 min after addition of membranes), which is the time point when a closed NE had formed. Nuclear import rates for soluble cargos can be determined by the time-dependent protection of different import substrates from a cytoplasmic protease as they accumulate in the nucleus (described in Theerthagiri et al., 2010). The translocation of integral membrane proteins from the ER to the inner nuclear membranes can be assessed in a similar way when the reporter is reconstituted into liposomes, which are then added to the assembly reactions and integrated into the ER. Compared to mock reactions, nuclei depleted of Nup153 exhibited reduced import of a soluble import cargo with a classical bipartite nuclear localization signal (cNLS cargo), which is imported in an importin α/β-dependent manner (Figure 3A). In contrast, import of a transportin-dependent cargo (containing an M9 sequence) was not affected by Nup153 depletion. The dependency of the importin α/β import pathway on Nup153 has been previously reported (Walther et al., 2001). Import of the cNLS-containing cargo was rescued by the re-addition of either wild-type or membrane-binding-deficient Nup153. Transport of a transmembrane cargo through NPCs was not affected by Nup153 depletion or the addition of either wild-type or membrane-binding-deficient Nup153. These results demonstrate that the membrane interaction of Nup153 is not important for efficient nuclear import.

Nup153 Is Necessary for Interphasic NPC Assembly

We next tested whether interphasic NPC assembly was affected by Nup153 depletion. Nuclei were assembled for 120 min, and individual NPCs were counted using mAB414 staining (D'Angelo et al., 2006; Vollmer et al., 2012). Addition of 2 μM importin β, which blocks interphasic NPC assembly (D'Angelo et al.,

2006), to nuclei formed under control conditions resulted in a reduction in the number of NPCs per nucleus by approximately 60% when added 50 min after starting the reaction (Figure 3B). Depletion of Nup153 caused a severe reduction in NPC number, which was not further affected by the addition importin β. Re-addition of wild-type Nup153 but not the membrane-binding-deficient V47E mutant rescued the reduced number of NPCs formed to nearly wild-type levels. These data suggest that NPC formation during interphase requires Nup153, specifically in its capacity to bind the NE.

The antibody mAB414 recognizes several FG nucleoporins including Nup153 (Sukegawa and Blobel, 1993). Although we did not employ overall staining intensity as readout for NPC numbers but counted individual NPC-containing spots on the NE, this procedure might be considered as biased due to the loss of a major antigen. Furthermore, counting might also be affected by the NPC clustering observed in Nup153-deficient nuclei. We therefore employed an assay for interphasic NPC assembly that is independent of mAB414 staining. In this setup, interphasic NPC assembly proceeds in the presence of extract depleted of the nucleoporins forming the permeability barrier of the pore. Nuclei with newly integrated NPCs lack this barrier and can be visualized by an influx of fluorescently labeled dextrans (Dawson et al., 2009; Vollmer et al., 2012). It should be noted that each nucleus is counted as either competent or deficient for interphasic NPC assembly. The addition of importin β, for example, completely inhibited interphasic NPC assembly monitored by dextran influx. Dextran influx was blocked in nuclei formed in the absence of Nup153, consistent with a block in interphasic NPC assembly (Figure 3C). Wild-type Nup153 but not the V47E mutant rescued interphasic NPC assembly based on dextran influx (Figure 3C).

As an alternative means to assess the increase in NPCs, we re-isolated the chromatin substrate in the assembly reactions at different time points and quantified the relative abundance of Nup107, Nup62, and Nup53 as members of the Y-complex, Nup62 complex, and Nup93 complex, respectively (Figure 3D). In mock-depleted extracts the levels of these nucleoporins re-isolated with the chromatin increases over time. However, this accumulation is not observed in Nup153-depleted extracts. The addition of wild-type Nup153 but not the V47E mutant rescues the depletion phenotype. Also in this assay, addition of importin β 30 min after initiation of nuclear assembly blocks the time-dependent increase in NPCs on the chromatin indicating that this experimental setup is a valuable readout for NPC assembly in the NE. It thus suggests that the increase in Nup107, Nup62, and Nup53 levels from 50 to 120 min represents interphasic NPC assembly.

Having identified an essential role for Nup153 and specifically its membrane interaction in interphasic NPC assembly, we wondered how Nup153 could function in this process. Two known Nup153 interactors are necessary for interphasic NPC assembly, Ran, and the Y-complex (D'Angelo et al., 2006; Doucet et al., 2010). Ran is most likely required to release import receptors from targets that are crucial for NPC assembly. Meanwhile the Y-complex is a structural component of NPCs. We speculated that Nup153 might localize these crucial components to the inner nuclear membrane.

Nup153 Recruits the Y-Complex to the Inner Nuclear Membrane for Interphasic NPC Assembly

To assess whether Nup153-dependent recruitment of Ran or the Y-complex to the NE is important for interphasic NPC assembly, we generated fusion proteins containing the Nup153 membrane binding domain (MBD, aa 1–149) and either the Y-complex (ycBD, aa 210–338) or the Ran binding domain (RanBD, aa 658–890) of human Nup153 (Figures 4A and S3). When added to Nup153-depleted extracts, the MBD-ycBD fusion resulted in larger nuclei. Conversely, the Nup153 phenotype was not rescued by the addition of either the MBD-RanBD fusion or any construct containing a defective membrane-binding domain (MBD V50E) (Figure 4B). Furthermore, only the MBD-ycBD construct restored interphasic NPC assembly when Nup153 was depleted (Figures 4C–4E). These data suggest that the requirement for Nup153 in interphasic NPC assembly is due to its capacity for directing the Y-complex to the nuclear membranes. To specifically assay interphasic NPC formation and to visualize the Y-complex in this process, we added Y-complex, purified from *Xenopus* egg extracts (see Figure S3) and fluorescently labeled, to pre-assembled nuclei (Figure 4F). The Y-complex foci formed in this way partly overlap with wheat germ agglutinin (WGA) staining, which labels NPCs formed both post-mitotically and after the formation of a closed NE. They can be either newly formed NPCs (overlapping with WGA staining, which recognizes mostly nucleoporins of the central channel) or NPCs that are just emerging (probably lacking a major subfraction of nucleoporins recognized by WGA). The appearance of Y-complex-containing NPCs was blocked by Nup153 depletion, confirming that interphasic Y-complex recruitment depends on Nup153. The addition of importin β also blocked the formation of Y-complex foci, validating the approach as a measure of interphasic NPC assembly. Importantly, addition of Nup153 but not the membrane-binding mutant rescued interphasic NPC assembly in Nup153-depleted nuclei. In agreement with the nuclear assembly data, the MBD-ycBD fusion protein but not the MBD-RanBD construct rescued the formation of Y-complex foci and thus the assembly interphasic NPCs.

Next, we asked whether we could directly recruit the Y-complex to the inner nuclear membrane thereby bypassing the function of Nup153. Nup153 Y-complex binding region or the Ran binding region were each fused N-terminally to EGFP and at the C terminus with the transmembrane protein BC08, yielding EGFP-ycBD-BC08 and EGFP-RanBD-BC08 (Figure 5A). BC08 contains a C-terminal transmembrane region and efficiently targets to the inner nuclear membrane (Theerthagiri et al., 2010). Both constructs were expressed in *E. coli*, purified, and reconstituted into small liposomes. To test the functionality of the fusion proteins, these liposomes were incubated with purified Y-complex or recombinant Ran and floated through a sucrose gradient. Liposomes containing the EGFP-ycBD-BC08 protein efficiently bound the Y-complex but not Ran, and EGFP-RanBD-BC08 liposomes bound Ran but not the Y-complex (Figure 5B). Similarly, when incorporated into GUVs, EGFP-ycBD-BC08 recruited fluorescently labeled Y-complex to the GUV membrane and EGFP-RanBD-BC08 recruited Ran (Figure 5C).

When EGFP-ycBD-BC08 or EGFP-RanBD-BC08-containing liposomes were added to nuclear assembly reactions, they efficiently targeted to the inner nuclear membrane (Figures 5D and

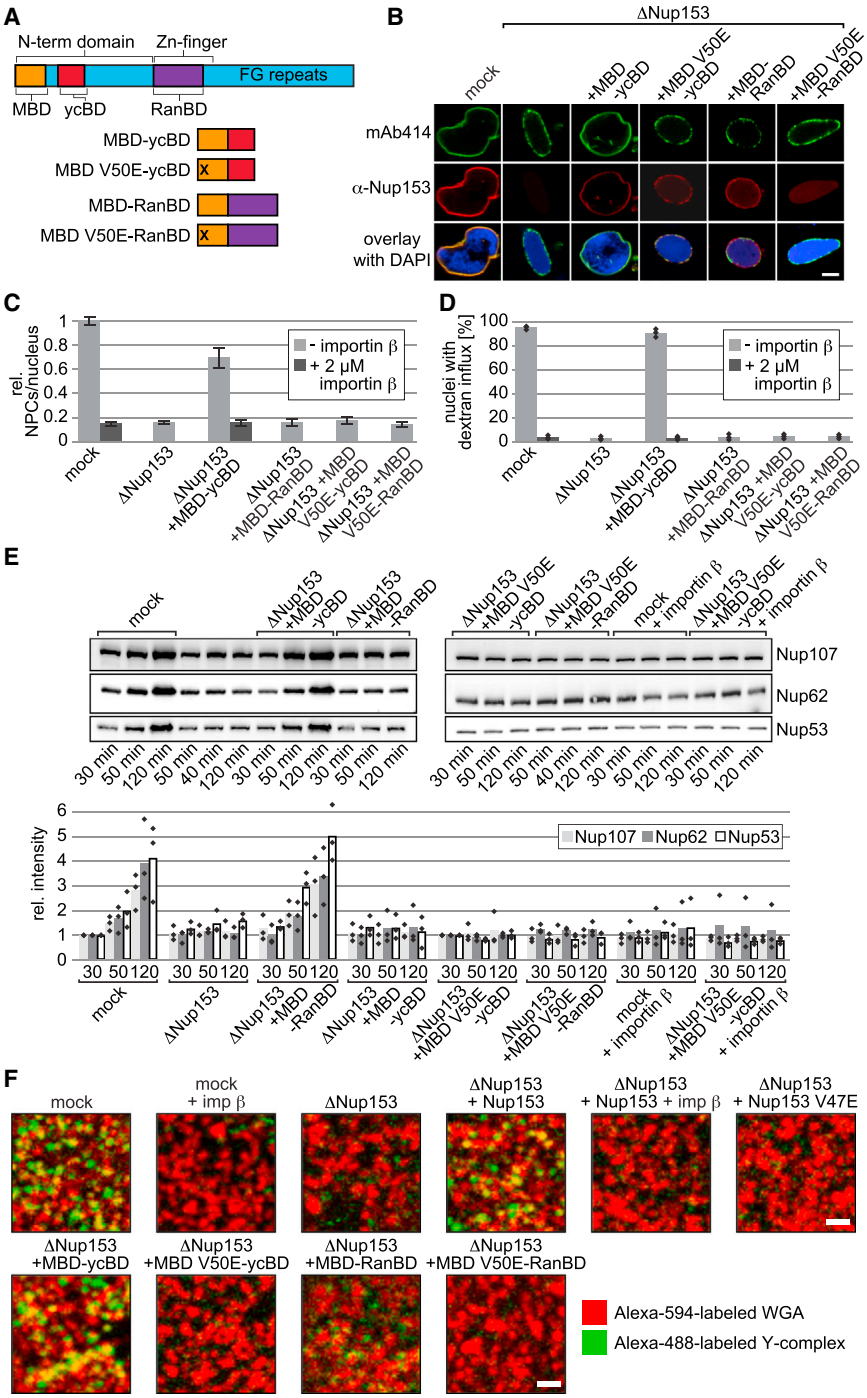

Figure 4. Membrane Recruitment of the Y-Complex Is Important for Interphasic NPC Assembly

(A) Schematic representation of the Nup153 fusion constructs. The Nup153 membrane binding domain (MBD) and the corresponding V50E mutant were fused to the Y-complex (ycBD) and the Ran-interacting region (RanBD).

(B) Nuclei were assembled in mock-depleted, Nup153-depleted, and Nup153-depleted extracts supplemented with the different MBD-fusions. Samples were fixed after 120 min and visualized using mAB414 (red), and Nup153 immunofluorescence. DNA was stained with DAPI (blue in overlay). Please note that the MBD-fusions are detected as the Nup153 antibody is directed against the Nup153 N terminus. Bar, 10 μm.

(C) NPC numbers in nuclei assembled as in (B) were determined using mAB414 staining as in Figure 3B (average from 30 nuclei from three independent experiments).

(D) Nuclei were assembled as in (B) and interphasic NPC assembly was analyzed by dextran influx as in Figure 3C.

(E) Nuclei were assembled as in (B). Chromatin was re-isolated at indicated time points, and nucleoporin levels were determined as in Figure 3D.

(F) Nuclei were assembled in mock-depleted, Nup153-depleted, and Nup153-depleted extracts supplemented with wild-type Nup153, the membrane-binding mutant (Nup153 V47E) or the different MBD fusions. Purified Alexa-488-labeled Y-complex (green) was added after 50 min and after another 60 min Alexa-594-WGA (red) for 10 min. Samples were fixed and the NE analyzed for WGA-positive structures, i.e., NPCs. Where indicated, interphasic NPC assembly was blocked by addition of importin β together with the Y-complex. Bars, 1 μm.

See also Figure S3.

S4C). Interestingly, Nup153 depletion resulted in larger nuclei when EGFP-ycBD-BC08 was incorporated compared to EGFP-RanBD-BC08 nuclei. Most importantly, EGFP-ycBD-BC08 but not EGFP-RanBD-BC08 incorporation into the nuclear membrane restored interphasic NPC assembly when Nup153 was depleted (Figures 5E–5G and S4B). We conclude that recruitment of the Y-complex to the inner nuclear membrane is sufficient to bypass the requirement for full-length Nup153 in interphasic NPC assembly in vitro. Thus, the crucial function of Nup153 in interphasic NPC assembly is to direct the Y-complex to the newly forming NPCs at the NE. This is consistent with the fact that a Nup153 construct lacking the Y-complex binding site cannot substitute Nup153 in interphasic NPC assembly (Figures S4E–S4G).

Annulate Lamellae Formation Depends on Nup153 Membrane Interaction

NPCs can assemble outside the nucleus in the membranes of the ER forming annulate lamellae (AL). AL form in egg extracts in the absence of chromatin, and this process is highly induced upon addition of the constitutively active Ran mutant Q69L, which is blocked in the GTP-bound state (Walther et al., 2003b). We wondered whether this NPC assembly mode also depends on Nup153 and specifically on its membrane targeting capability. Membranes were incubated with control or Nup153-depleted cytosol, re-isolated, and analyzed by western blotting (Figures 6A and 6B). As expected, addition of RanQ69L strongly induced AL formation in control extracts, evidenced by an increased presence of Nup107, Nup62, and Nup53

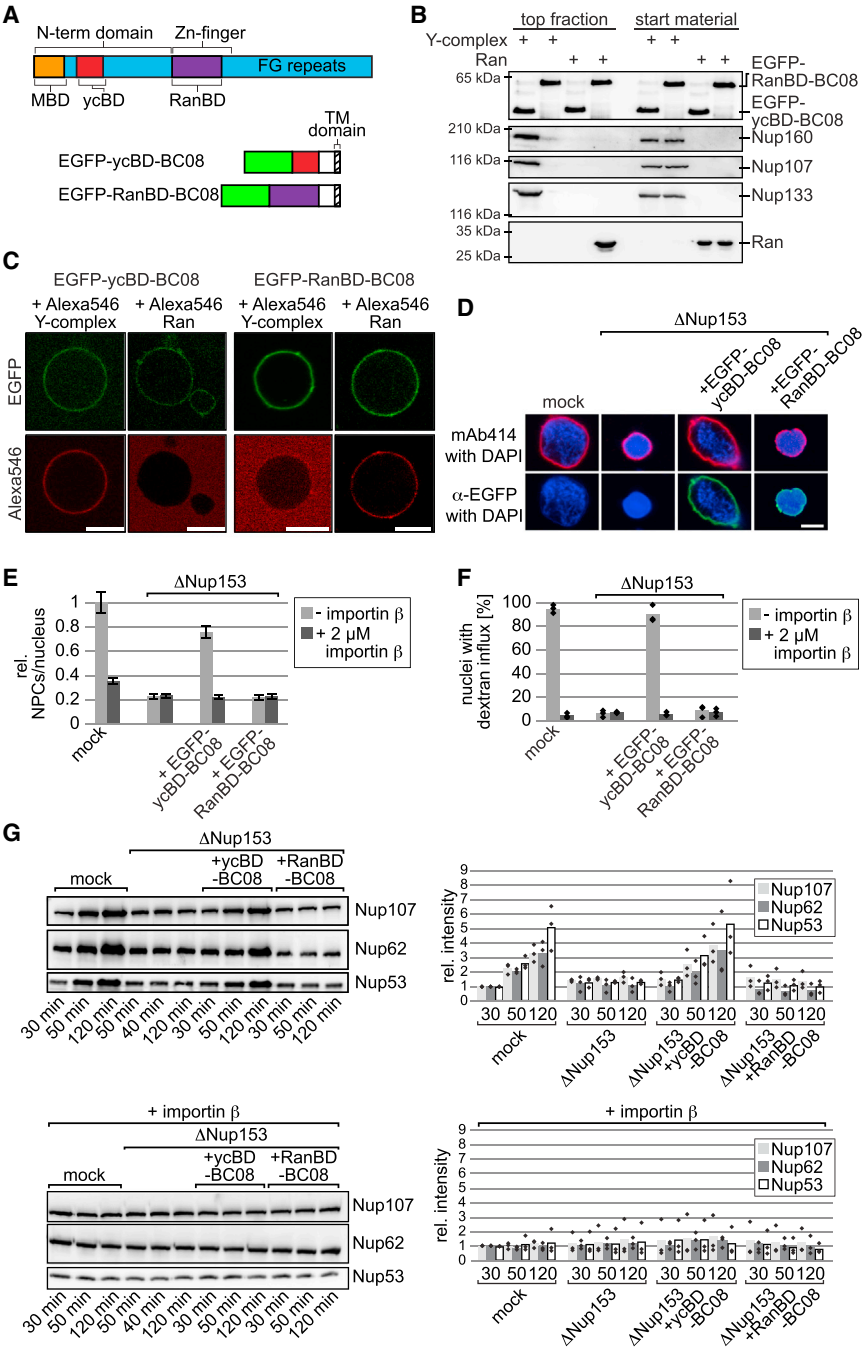

Figure 5. Inner Nuclear Membrane Tethering of the Y-Complex Bypasses the Nup153 Necessity for Interphasic NPC Assembly

(A) Schematic representation of the Nup153 fusion constructs. The Y-complex and the Ran-interacting region, flanked by EGFP (green) and the inner nuclear membrane protein BC08, yield EGFP-ycBD-BC08 or EGFP-RanBD-BC08, respectively.

(B) EGFP-ycBD-BC08 or EGFP-RanBD-BC08 was reconstituted into NE liposomes and incubated with Y-complex or Ran. Start material (50% for the EGFP-ycBD-BC08 or EGFP-RanBD-BC08, 30% for the Y-complex and Ran) and top fractions were analyzed using EGFP, Nup160, Nup133, Nup107, and Ran antibodies.

(C) EGFP-ycBD-BC08 or EGFP-RanBD-BC08 were reconstituted into NE lipid GUVs and membrane recruitment of Alexa-546-labeled Y-complex or Ran was analyzed.

(D) Nuclei were assembled in mock or Nup153-depleted extracts supplemented with empty, EGFP-ycBD-BC08, or EGFP-RanBD-BC08-containing liposomes. Samples were fixed after 120 min and visualized using EGFP (green) and immunofluorescence for mAB414 (red). DNA was stained with DAPI (blue).

(E) NPC numbers in nuclei assembled as in (D) were determined using mAB414 staining as in Figure 3B (average from 30 nuclei from three independent experiments).

(F) Nuclei were assembled as in (D) and interphasic NPC assembly analyzed by dextran influx as in Figure 3C.

(G) Nuclei were assembled as in (D). Chromatin was re-isolated at indicated time points, and nucleoporin levels were determined as in Figure 3D.

Bars, 10 μm. See also Figure S4.

in the re-isolated membrane fraction. The transmembrane pore proteins POM121, GP210, and NDC1 were found in equal quantities, independent of the presence of RanQ69L. Reticulon 4, an ER marker, was used to control for equal membrane re-isolation efficiency. Nup153 depletion severely reduced the quantity of soluble nucleoporins re-isolated with membranes. Furthermore, the addition of RanQ69L did not result in increased re-isolation of the soluble nucleoporins as was seen in mock-depleted extracts, indicating a block in AL formation. Addition of wild-type Nup153, but not the Nup153 mutant defective for direct membrane binding, to depleted extracts rescued AL formation. Analysis of the re-isolated membrane fraction by electron microscopy showed AL in mock and Nup153-depleted extracts supplemented with the wild-type protein but not in depleted extracts supplemented with the V47E mutant (Figure 6C). Thus, these data indicate that Nup153 membrane binding is also required for NPC assembly in the ER.

Transportin Regulates Nup153 Membrane Interaction

Having identified a Nup153 membrane interaction that is crucial for both interphasic NPC assembly and AL formation, we wondered why the protein does not localize to cytoplasmic membranes under normal growth conditions but is rather specifically found at the NE (Figures 1F, S1C, and 2A). The N-terminal region of Nup153 interacts with transportin and mediates its import to the nucleus, a pre-requisite for its incorporation in NPCs (Bastos et al., 1996; Enarson et al., 1998; Nakielny et al., 1999; Shah and Forbes, 1998; Figure S5). Rapid transportin-dependent import of Nup153 might prevent its membrane association outside of the nucleus. We wondered whether transportin interaction could also directly affect Nup153 membrane binding similar to

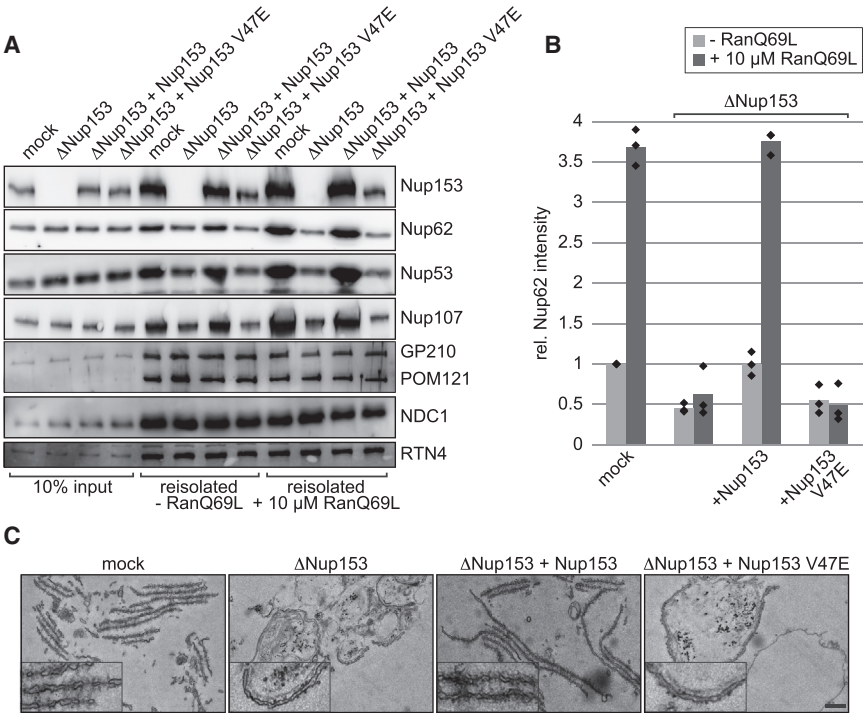

Figure 6. Nup153 Membrane Interaction Is Required for AL Formation

(A) Mock, Nup153-depleted cytosol, or Nup153-depleted cytosol supplemented with Nup153 or the V47E mutant were incubated for 4 hr with membranes and where indicated with RanQ69L. 10% of the start material and the re-isolated membranes were analyzed. Reticulon 4 (RTN4) serves as an ER marker.

(B) Quantification of Nup62 re-isolated with membranes (average intensity value from three independent experiments performed as in A), normalized to mock control in the absence of RanQ69L).

(C) Transmission electron microscopy of re-isolated membranes as in (A) in the presence of 10 μM RanQ69L. Insets show a 3-fold higher magnification. Bar, 500 nm.

Kap123, which regulates membrane interaction of the spindle body component Nbp1p and the C-terminal domain of the transmembrane nucleoporin Pom33p in yeast (Floch et al., 2015; Kupke et al., 2011). To test this, the N terminus of Nup153 was employed in liposome flotation assays after pre-incubation with transportin. The presence of transportin strongly reduced the ability of Nup153 to interact with membranes (Figure 7A). Importin β, a related import receptor that does not bind to this region, had no effect on the membrane binding of Nup153. Addition of RanQ69L, which releases import receptors including transportin from their cargos, reversed the inhibitory effect of transportin. Together, these data indicate that transportin inhibits Nup153 membrane binding and that this block is released by RanGTP. As high RanGTP concentrations are found in the nucleus, it is conceivable that Nup153 can only function as a membrane-interacting protein once it has reached the nucleus.

DISCUSSION

Here, we show that Nup153 can directly interact with membranes via an N-terminal amphipathic helix. This membrane interaction is important for interphasic NPC assembly as well as AL formation. During interphasic NPC assembly, Nup153 recruits the Y-complex, a crucial structural component of newly forming pores, to the inner nuclear membrane. Transportin binding to Nup153 inhibits its membrane interaction presumably by masking the membrane interaction surface of Nup153. Taken together, our results imply a model in which transportin binding to Nup153, following its synthesis in the cytoplasm, would prevent Nup153 from interacting with membranes outside of the nucleus (Figure 7B). After translocation through NPCs, Nup153 is released from transportin due to high nucleoplasmic concentrations of RanGTP. The liberated Nup153 interacts with the inner nuclear membrane and recruits the Y-complex to this locality where it functions in interphasic NPC assembly.

NPC assembly, both at the end of mitosis and in interphase, is regulated by Ran and transport receptors (D'Angelo et al., 2006; Walther et al., 2003b). At the end of mitosis, the chromatin binding nucleoporin MEL28 is a critical Ran-regulated target (Franz et al., 2007; Rotem et al., 2009). Our data suggest that Nup153 acts during interphasic NPC assembly as an important Ran target. In the different assembly modes, MEL28 or Nup153, once liberated from the inhibitory effect of importin β or transportin, could recruit the Y-complex to NPC assembly sites.

The Y-complex as a basic structural component of the NPC is crucial for NPC formation both at the end of mitosis and during interphase (D'Angelo et al., 2006; Doucet et al., 2010; Harel et al., 2003; Walther et al., 2003a). Nup153 is dispensable for NPC assembly at the end of mitosis (Figure 2) as previously observed (Walther et al., 2001). Although NPCs cluster upon Nup153 depletion, the number of NPC assembled by the postmitotic mode are most likely not reduced. Nuclei reisolated after 30 min, at which point most NPCs would have been assembled in the postmitotic mode, do not contain strikingly different quantities of Nup107, Nup62, or Nup53 when Nup153 is depleted (Figure 3D). Furthermore, the fact that nuclear import of both M9 and transmembrane cargoes is not affected at this time point, argues for comparable NPC numbers. At the end of mitosis, NPC assembly is initiated on the decondensing chromatin by MEL28, which recruits the Y-complex (Franz et al., 2007; Gillespie et al., 2007; Rasala et al., 2006; Figure 7B). However, MEL28 has been reported to be dispensable for interphasic NPC assembly (Doucet et al., 2010), most likely because it is initiated at the NE. During interphase, it is Nup153 that acts as the crucial Y-complex recruitment factor at the inner nuclear membrane in a, presumably, chromatin-independent manner. Accordingly, AL formation is Nup153 dependent but does not require MEL28, as it is initiated at the membrane in the absence of chromatin. Loss of MEL28 actually induces AL formation,

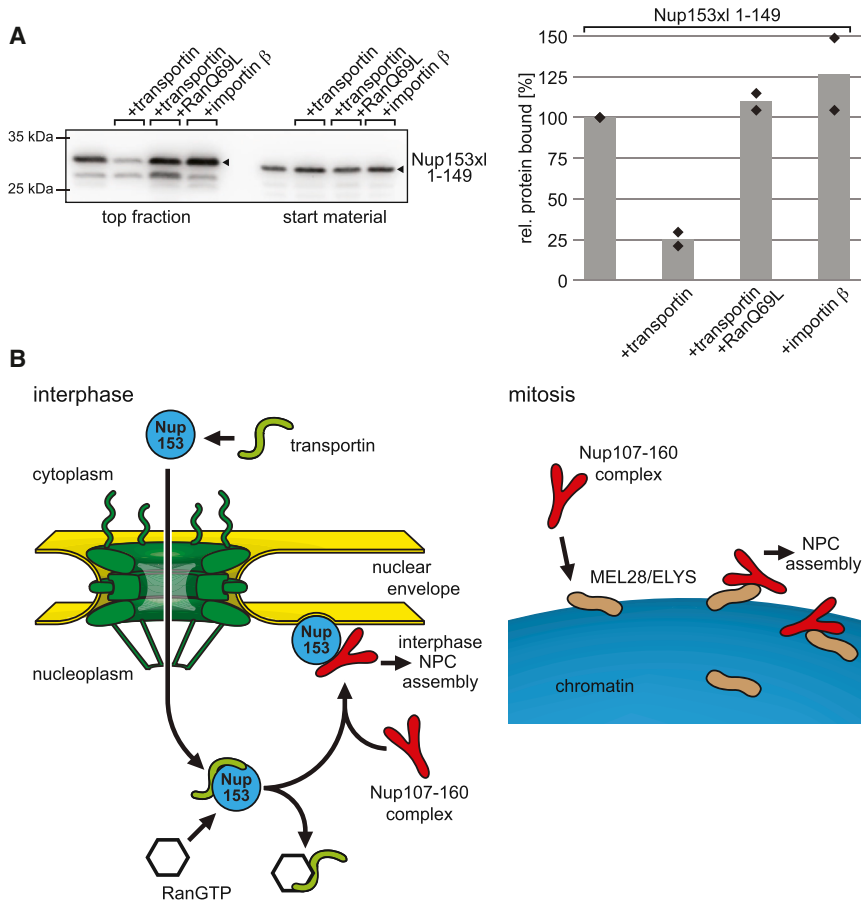

Figure 7. Transportin Regulates Nup153 Membrane Interaction and Might by that Function in Interphasic NPC Assembly

(A) 3 μM of the *Xenopus* Nup153 N terminus was, where indicated, pre-incubated with 5 μM transportin, 5 μM importin β, or 5 μM transportin along with 15 μM RanQ69L. Proteins were incubated with fluorescently labeled NE liposomes and floated through a sucrose gradient. Top gradient fractions and input materials were analyzed by western blot. For quantification from two independent experiments, liposome binding was normalized to the untreated Nup153 N terminus.

(B) Model for transportin and Nup153 function in interphasic NPC assembly (left panel). Transportin binding to Nup153 in the cytoplasm prevents its membrane interaction and mediates its nuclear import. In the nucleus, RanGTP releases transportin from Nup153, which becomes free to interact with the inner nuclear membrane and to recruit the Y-complex for interphasic NPC assembly. In contrast, at the end of mitosis (right panel), MEL28/ELYS recruits the Y-complex to chromatin and NPC assembly sites without an essential contribution from Nup153.

See also Figure S5.

presumably because it prevents postmitotic NPC assembly from being initiated on the chromatin (Franz et al., 2007).

Although Nup133, a component of the Y-complex, possesses an evolutionary conserved amphipathic helix (Drin et al., 2007; Kim et al., 2014), it does not seem to be sufficient to target the Y-complex to the inner nuclear membrane during interphasic NPC assembly. One possible explanation is that the Nup153 and Nup133 membrane interaction motifs need to act together to possess sufficient affinity for the inner nuclear membrane. In addition, other interactions, such as those occurring between the transmembrane nucleoporin POM121 and the Y-complex (Mitchell et al., 2010; Yavuz et al., 2010) might contribute. While a fragment containing this Nup133 motif does bind liposomes (Figure 1A), the assembled Y-complex does not detectably bind liposomes or GUVs (Figures 5B and 5C), which might, however, be explained by the larger vesicle sizes (Figure S4A).

Whether the Nup153 mediated membrane recruitment of the Y-complex is the initial step of interphasic NPC assembly is an open question. Due to the experimental setup of the interphasic NPC formation assay, it is difficult to determine the precise assembly order as it was done for the postmitotic NPC formation pathway (described in Schooley et al., 2012). The amphipathic helix of Nup133 has been proposed to target the Y-complex to the highly curved pore membrane during interphasic NPC assembly (Doucet et al., 2010). The amphipathic helix of Nup153 shows a similar preference for high curvature (Figure 1B) and can induce membrane tubulation in vitro (Figure S1B). However, it is of course difficult to distinguish whether these observations represent a curvature sensing or inducing function. In other words, it is unclear whether Nup153 itself initiates interphasic pore assembly by inducing membrane curvature or whether it binds already curved membranes. If Nup153 only binds highly curved membranes, its recruitment would necessarily be preceded by proteins inducing pore formation, such as Nup53, reticulons, and POM121 (Dawson et al., 2009; Doucet et al., 2010; Dultz and Ellenberg, 2010; Vollmer et al., 2012). Interestingly, the fact that the fusion of Nup153's Y-complex binding region to an inner nuclear membrane protein can replace Nup153 in interphasic NPC assembly suggest that Nup153 induced membrane curving might not be critical for its function in interphasic NPC formation.

In summary, our work identifies a crucial function for Nup153 in interphasic NPC assembly. We provide insight on an interesting mechanistic difference between NPC assembly at the end of mitosis and during interphase. Whereas postmitotic assembly is initiated by the MEL28-mediated recruitment of the Y-complex to chromatin, interphasic NPC formation crucially requires Nup153 to interact with the inner nuclear membrane to localize the Y-complex to nascent assembly sites. It is currently unclear whether Nup153 recognizes a distinct feature at the site of the newly forming NPC, and this will be an interesting avenue for future research.

EXPERIMENTAL PROCEDURES

Nuclear assemblies, immunofluorescence, electron microscopy, generation of affinity resins, sperm heads, and floated unlabeled or DiIC18-labeled

membranes were carried out as described (Eisenhardt et al., 2014). Interphasic NPC assembly using dextran influx was performed as in Vollmer et al. (2012). Nuclear import assays using EGFP-NPM2 (importin α/β-dependent cargo), EGFP-Nplc-M9-M10 (transportin-dependent cargo), and EGFP-LBR (aa 146–258), re-isolation of nuclei for western blotting, as well as NPC counting are described in Theerthagiri et al. (2010). Liposome generation and flotations were done as in Eisenhardt et al. (2014) and Vollmer et al. (2012). Pure lipid and EGFP-ycBD-BC08/EGFP-RanBD-BC08-containing GUVs were generated as described (Lorenz et al., 2015); see also Supplemental Experimental Procedures in the Supplemental Information.

To visualize the Y-complex on newly assembling NPCs, the purified complex was labeled with Alexa 488. 50 min after initiation of the nuclear assembly reaction, 10 μl of the sample was supplemented with 0.25 μl Alexa-488-labeled Y-complex (approximately 0.05 μg/μl). Where indicated, interphasic NPC assembly was inhibited by addition of 2 μM importin β at this time point. After an additional 60 min, 0.15 μl 0.25 μg/μl Alexa-594-labeled WGA (Life Technologies) was added. Samples were fixed after additional 10 min in 2% paraformaldehyde in 80 mM Pipes (pH 6.8), 1 mM $MgCl_2$, and 150 mM sucrose and spun through a sucrose cushion on poly-L-lysine coated coverslips. Samples were imaged with a confocal microscope LSM780 (Zeiss) equipped with an Apochromat 63×/1.40 Oil DIC M27 objective with the following acquisition settings: 24-μm pinhole for track 488 nm and 16-μm pinhole for track 561 nm; scaling X = 0.082 μm, Y = 0.082 μm, Z = 0.236 μm; zoom = 5.0–7.5× and 19 to 45 slices per nucleus. 5 μm square of the best in focus slice at the bottom surface of the nucleus was selected, and the two channels were merged.

For quantifying nucleoporin levels on assembling nuclei, chromatin was isolated following a slightly modified version of the protocol described in (Baur et al., 2007). 20 μl of a nuclear assembly reaction was diluted in 1 ml sperm isolation buffer (20 mM Tris-HCl [pH 7.4], 70 mM KCl, 10 mM EDTA, 2 mM DTT, and 2% polyvinylpyrolidone), and chromatin was recovered by centrifugation through 0.5 ml of a 1.3 M sucrose cushion at 5000 × *g* for 10 min in an Eppendorf cooling centrifuge. After carefully removing the supernatant, the nuclei were re-suspended in 20 μl SDS sample buffer and analyzed by western blotting using α-Nup107, α-Nup53, and mAB414 antibodies (to detect Nup62). To block interphasic NPC assembly, we added 2 μM importin β 30 min after initiation of the assembly reaction (i.e., 20 min after addition of membranes) as postmitotic NPC assembly is usually completed at this time point (i.e., chromatin is by then enclosed by an nuclear envelope).

AL were assembled in 15 μl *Xenopus* egg extract cytosol supplemented with 1.5 μl floated membranes, glycogen, and an energy regenerating system (Eisenhardt et al., 2014). After 4 hr at 20°C, samples were processed for electron microscopy or diluted in 1 ml sucrose buffer. Membranes were pelleted by centrifugation (10 min at 15,000 × *g*), washed, and analyzed by western blotting.

Antibodies, protein expression, and purification as well as the transfection experiments are described in detail in the Supplemental Information.

SUPPLEMENTAL INFORMATION

Supplemental Information includes Supplemental Experimental Procedures, five figures, and one movie and can be found with this article online at http://dx.doi.org/10.1016/j.devcel.2015.04.027.

AUTHOR CONTRIBUTIONS

B.V. and W.A. designed the experiments. B.V. performed liposome floatation experiments, B.V. and M.B. purified proteins, M.L. determined NPC numbers, M.L. and D.M.-A. performed live-cell imaging and WGA-based NPC labeling experiments, P.D.M., S.A.A., and A.S. performed nuclear assembly and related experiments, M.F. performed electron microscopy, S.L. performed light scattering of liposomes, and W.A. wrote the manuscript.

ACKNOWLEDGMENTS

This work was supported by core funding of the Max Planck Society and the European Research Council (grant agreement 309528 CHROMDECON to W.A.) and by a PhD Fellowship of the IMPRS "From Molecules to Organisms" to P.D.M.

Received: November 10, 2014
Revised: February 27, 2015
Accepted: April 28, 2015
Published: June 4, 2015

REFERENCES

Ball, J.R., and Ullman, K.S. (2005). Versatility at the nuclear pore complex: lessons learned from the nucleoporin Nup153. Chromosoma *114*, 319–330.

Bastos, R., Lin, A., Enarson, M., and Burke, B. (1996). Targeting and function in mRNA export of nuclear pore complex protein Nup153. J. Cell Biol. *134*, 1141–1156.

Baur, T., Ramadan, K., Schlundt, A., Kartenbeck, J., and Meyer, H.H. (2007). NSF- and SNARE-mediated membrane fusion is required for nuclear envelope formation and completion of nuclear pore complex assembly in Xenopus laevis egg extracts. J. Cell Sci. *120*, 2895–2903.

Brohawn, S.G., Leksa, N.C., Spear, E.D., Rajashankar, K.R., and Schwartz, T.U. (2008). Structural evidence for common ancestry of the nuclear pore complex and vesicle coats. Science *322*, 1369–1373.

Bui, K.H., von Appen, A., DiGuilio, A.L., Ori, A., Sparks, L., Mackmull, M.T., Bock, T., Hagen, W., Andrés-Pons, A., Glavy, J.S., and Beck, M. (2013). Integrated structural analysis of the human nuclear pore complex scaffold. Cell *155*, 1233–1243.

Cordes, V.C., Reidenbach, S., Rackwitz, H.R., and Franke, W.W. (1997). Identification of protein p270/Tpr as a constitutive component of the nuclear pore complex-attached intranuclear filaments. J. Cell Biol. *136*, 515–529.

Cronshaw, J.M., Krutchinsky, A.N., Zhang, W., Chait, B.T., and Matunis, M.J. (2002). Proteomic analysis of the mammalian nuclear pore complex. J. Cell Biol. *158*, 915–927.

D'Angelo, M.A., Anderson, D.J., Richard, E., and Hetzer, M.W. (2006). Nuclear pores form de novo from both sides of the nuclear envelope. Science *312*, 440–443.

Daigle, N., Beaudouin, J., Hartnell, L., Imreh, G., Hallberg, E., Lippincott-Schwartz, J., and Ellenberg, J. (2001). Nuclear pore complexes form immobile networks and have a very low turnover in live mammalian cells. J. Cell Biol. *154*, 71–84.

Dawson, T.R., Lazarus, M.D., Hetzer, M.W., and Wente, S.R. (2009). ER membrane-bending proteins are necessary for de novo nuclear pore formation. J. Cell Biol. *184*, 659–675.

Doucet, C.M., Talamas, J.A., and Hetzer, M.W. (2010). Cell cycle-dependent differences in nuclear pore complex assembly in metazoa. Cell *141*, 1030–1041.

Drin, G., Casella, J.F., Gautier, R., Boehmer, T., Schwartz, T.U., and Antonny, B. (2007). A general amphipathic α-helical motif for sensing membrane curvature. Nat. Struct. Mol. Biol. *14*, 138–146.

Dultz, E., and Ellenberg, J. (2010). Live imaging of single nuclear pores reveals unique assembly kinetics and mechanism in interphase. J. Cell Biol. *191*, 15–22.

Eisenhardt, N., Schooley, A., and Antonin, W. (2014). Xenopus in vitro assays to analyze the function of transmembrane nucleoporins and targeting of inner nuclear membrane proteins. Methods Cell Biol. *122*, 193–218.

Enarson, P., Enarson, M., Bastos, R., and Burke, B. (1998). Amino-terminal sequences that direct nucleoporin nup153 to the inner surface of the nuclear envelope. Chromosoma *107*, 228–236.

Floch, A.G., Tareste, D., Fuchs, P.F., Chadrin, A., Naciri, I., Léger, T., Schlenstedt, G., Palancade, B., and Doye, V. (2015). Nuclear pore targeting of the yeast Pom33 nucleoporin depends on karyopherin and lipid binding. J. Cell Sci. *128*, 305–316.

Franz, C., Walczak, R., Yavuz, S., Santarella, R., Gentzel, M., Askjaer, P., Galy, V., Hetzer, M., Mattaj, I.W., and Antonin, W. (2007). MEL-28/ELYS is required for the recruitment of nucleoporins to chromatin and postmitotic nuclear pore complex assembly. EMBO Rep. *8*, 165–172.

Galy, V., Mattaj, I.W., and Askjaer, P. (2003). Caenorhabditis elegans nucleoporins Nup93 and Nup205 determine the limit of nuclear pore complex size exclusion in vivo. Mol. Biol. Cell *14*, 5104–5115.

Gant, T.M., and Wilson, K.L. (1997). Nuclear assembly. Annu. Rev. Cell Dev. Biol. *13*, 669–695.

Gautier, R., Douguet, D., Antonny, B., and Drin, G. (2008). HELIQUEST: a web server to screen sequences with specific α-helical properties. Bioinformatics *24*, 2101–2102.

Gillespie, P.J., Khoudoli, G.A., Stewart, G., Swedlow, J.R., and Blow, J.J. (2007). ELYS/MEL-28 chromatin association coordinates nuclear pore complex assembly and replication licensing. Curr. Biol. *17*, 1657–1662.

Guan, T., Kehlenbach, R.H., Schirmer, E.C., Kehlenbach, A., Fan, F., Clurman, B.E., Arnheim, N., and Gerace, L. (2000). Nup50, a nucleoplasmically oriented nucleoporin with a role in nuclear protein export. Mol. Cell. Biol. *20*, 5619–5630.

Harborth, J., Elbashir, S.M., Bechert, K., Tuschl, T., and Weber, K. (2001). Identification of essential genes in cultured mammalian cells using small interfering RNAs. J. Cell Sci. *114*, 4557–4565.

Harel, A., Orjalo, A.V., Vincent, T., Lachish-Zalait, A., Vasu, S., Shah, S., Zimmerman, E., Elbaum, M., and Forbes, D.J. (2003). Removal of a single pore subcomplex results in vertebrate nuclei devoid of nuclear pores. Mol. Cell *11*, 853–864.

Hase, M.E., and Cordes, V.C. (2003). Direct interaction with nup153 mediates binding of Tpr to the periphery of the nuclear pore complex. Mol. Biol. Cell *14*, 1923–1940.

Kim, S.J., Fernandez-Martinez, J., Sampathkumar, P., Martel, A., Matsui, T., Tsuruta, H., Weiss, T.M., Shi, Y., Markina-Inarrairaegui, A., Bonanno, J.B., et al. (2014). Integrative structure-function mapping of the nucleoporin Nup133 suggests a conserved mechanism for membrane anchoring of the nuclear pore complex. Mol. Cell. Proteomics *13*, 2911–2926.

Kupke, T., Di Cecco, L., Müller, H.M., Neuner, A., Adolf, F., Wieland, F., Nickel, W., and Schiebel, E. (2011). Targeting of Nbp1 to the inner nuclear membrane is essential for spindle pole body duplication. EMBO J. *30*, 3337–3352.

Lorenz, M., Vollmer, B., Unsay, J.D., Klupp, B.G., García-Sáez, A.J., Mettenleiter, T.C., and Antonin, W. (2015). A single herpesvirus protein can mediate vesicle formation in the nuclear envelope. J. Biol. Chem. *290*, 6962–6974.

Lutzmann, M., Kunze, R., Buerer, A., Aebi, U., and Hurt, E. (2002). Modular self-assembly of a Y-shaped multiprotein complex from seven nucleoporins. EMBO J. *21*, 387–397.

Mitchell, J.M., Mansfeld, J., Capitanio, J., Kutay, U., and Wozniak, R.W. (2010). Pom121 links two essential subcomplexes of the nuclear pore complex core to the membrane. J. Cell Biol. *191*, 505–521.

Moroianu, J., Blobel, G., and Radu, A. (1997). RanGTP-mediated nuclear export of karyopherin alpha involves its interaction with the nucleoporin Nup153. Proc. Natl. Acad. Sci. USA *94*, 9699–9704.

Nakielny, S., Shaikh, S., Burke, B., and Dreyfuss, G. (1999). Nup153 is an M9-containing mobile nucleoporin with a novel Ran-binding domain. EMBO J. *18*, 1982–1995.

Ogawa, Y., Miyamoto, Y., Oka, M., and Yoneda, Y. (2012). The interaction between importin-α and Nup153 promotes importin-α/β-mediated nuclear import. Traffic *13*, 934–946.

Ralle, T., Grund, C., Franke, W.W., and Stick, R. (2004). Intranuclear membrane structure formations by CaaX-containing nuclear proteins. J. Cell Sci. *117*, 6095–6104.

Rasala, B.A., Orjalo, A.V., Shen, Z., Briggs, S., and Forbes, D.J. (2006). ELYS is a dual nucleoporin/kinetochore protein required for nuclear pore assembly and proper cell division. Proc. Natl. Acad. Sci. USA *103*, 17801–17806.

Rasala, B.A., Ramos, C., Harel, A., and Forbes, D.J. (2008). Capture of AT-rich chromatin by ELYS recruits POM121 and NDC1 to initiate nuclear pore assembly. Mol. Biol. Cell *19*, 3982–3996.

Rotem, A., Gruber, R., Shorer, H., Shaulov, L., Klein, E., and Harel, A. (2009). Importin beta regulates the seeding of chromatin with initiation sites for nuclear pore assembly. Mol. Biol. Cell *20*, 4031–4042.

Schooley, A., Vollmer, B., and Antonin, W. (2012). Building a nuclear envelope at the end of mitosis: coordinating membrane reorganization, nuclear pore complex assembly, and chromatin de-condensation. Chromosoma *121*, 539–554.

Shah, S., and Forbes, D.J. (1998). Separate nuclear import pathways converge on the nucleoporin Nup153 and can be dissected with dominant-negative inhibitors. Curr. Biol. *8*, 1376–1386.

Shah, S., Tugendreich, S., and Forbes, D. (1998). Major binding sites for the nuclear import receptor are the internal nucleoporin Nup153 and the adjacent nuclear filament protein Tpr. J. Cell Biol. *141*, 31–49.

Sukegawa, J., and Blobel, G. (1993). A nuclear pore complex protein that contains zinc finger motifs, binds DNA, and faces the nucleoplasm. Cell *72*, 29–38.

Theerthagiri, G., Eisenhardt, N., Schwarz, H., and Antonin, W. (2010). The nucleoporin Nup188 controls passage of membrane proteins across the nuclear pore complex. J. Cell Biol. *189*, 1129–1142.

Ullman, K.S., Shah, S., Powers, M.A., and Forbes, D.J. (1999). The nucleoporin nup153 plays a critical role in multiple types of nuclear export. Mol. Biol. Cell *10*, 649–664.

Varadarajan, P., Mahalingam, S., Liu, P., Ng, S.B., Gandotra, S., Dorairajoo, D.S., and Balasundaram, D. (2005). The functionally conserved nucleoporins Nup124p from fission yeast and the human Nup153 mediate nuclear import and activity of the Tf1 retrotransposon and HIV-1 Vpr. Mol. Biol. Cell *16*, 1823–1838.

Vasu, S., Shah, S., Orjalo, A., Park, M., Fischer, W.H., and Forbes, D.J. (2001). Novel vertebrate nucleoporins Nup133 and Nup160 play a role in mRNA export. J. Cell Biol. *155*, 339–354.

Vollmer, B., and Antonin, W. (2014). The diverse roles of the Nup93/Nic96 complex proteins - structural scaffolds of the nuclear pore complex with additional cellular functions. Biol. Chem. *395*, 515–528.

Vollmer, B., Schooley, A., Sachdev, R., Eisenhardt, N., Schneider, A.M., Sieverding, C., Madlung, J., Gerken, U., Macek, B., and Antonin, W. (2012). Dimerization and direct membrane interaction of Nup53 contribute to nuclear pore complex assembly. EMBO J. *31*, 4072–4084.

Walther, T.C., Fornerod, M., Pickersgill, H., Goldberg, M., Allen, T.D., and Mattaj, I.W. (2001). The nucleoporin Nup153 is required for nuclear pore basket formation, nuclear pore complex anchoring and import of a subset of nuclear proteins. EMBO J. *20*, 5703–5714.

Walther, T.C., Alves, A., Pickersgill, H., Loïodice, I., Hetzer, M., Galy, V., Hülsmann, B.B., Köcher, T., Wilm, M., Allen, T., et al. (2003a). The conserved Nup107-160 complex is critical for nuclear pore complex assembly. Cell *113*, 195–206.

Walther, T.C., Askjaer, P., Gentzel, M., Habermann, A., Griffiths, G., Wilm, M., Mattaj, I.W., and Hetzer, M. (2003b). RanGTP mediates nuclear pore complex assembly. Nature *424*, 689–694.

Wente, S.R., and Rout, M.P. (2010). The nuclear pore complex and nuclear transport. Cold Spring Harb. Perspect. Biol. *2*, a000562.

Yavuz, S., Santarella-Mellwig, R., Koch, B., Jaedicke, A., Mattaj, I.W., and Antonin, W. (2010). NLS-mediated NPC functions of the nucleoporin Pom121. FEBS Lett. *584*, 3292–3298.

Developmental Cell

Supplemental Information

Nup153 Recruits the Nup107-160 Complex to the Inner Nuclear Membrane for Interphasic Nuclear Pore Complex Assembly

Benjamin Vollmer, Michael Lorenz, Daniel Moreno-Andrés, Mona Bodenhöfer, Paola De Magistris, Susanne Adina Astrinidis, Allana Schooley, Matthias Flötenmeyer, Sebastian Leptihn, and Wolfram Antonin

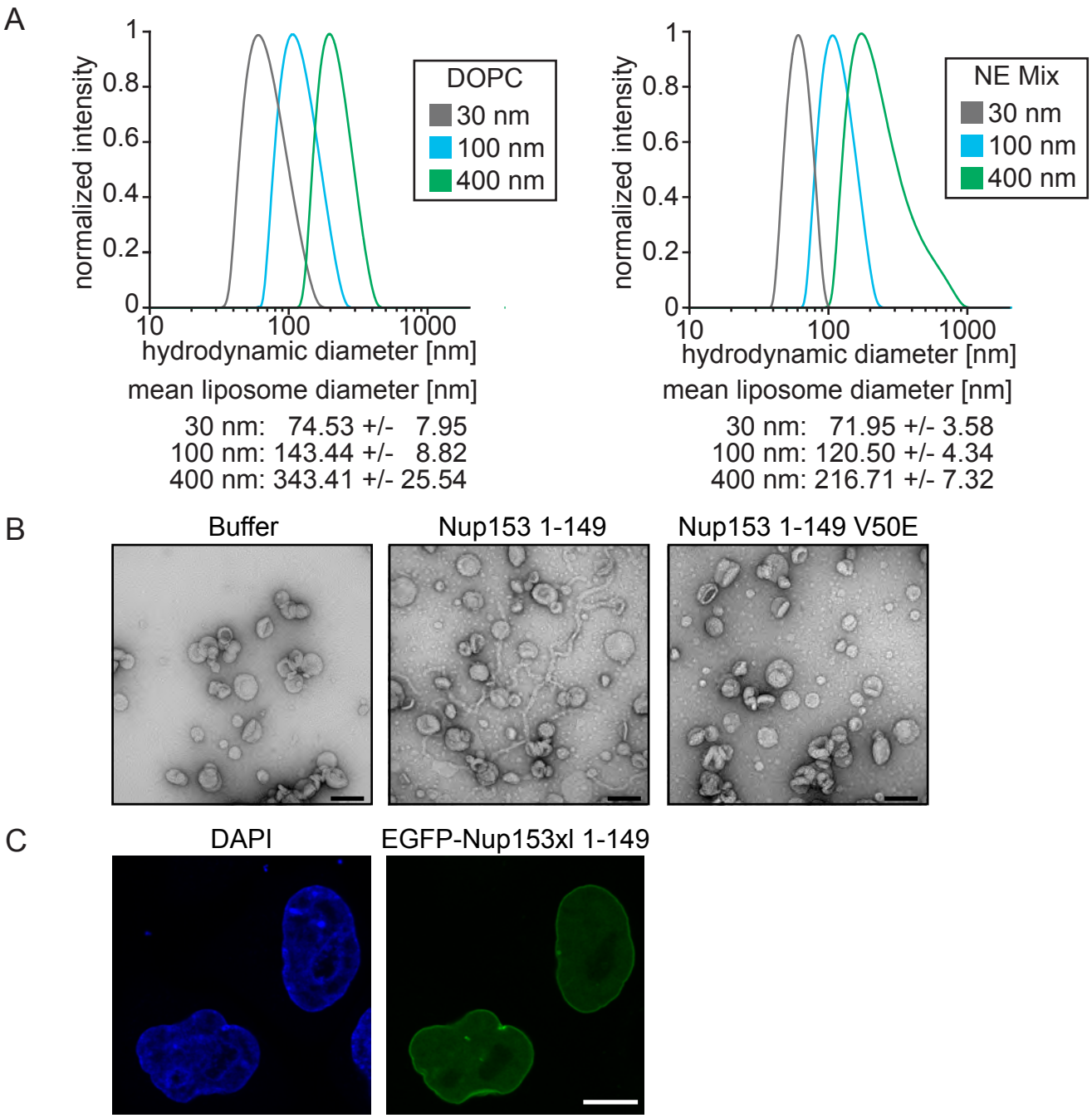

Figure S1, related to Figure 1

(A) Exemplary measurement of the size distribution of DOPC and NE liposomes used in Figure 1A and B as determined by light scattering. The mean diameters of the different sized liposome preparations are indicated below.

(B) The N-terminus of Nup153 can deform membranes: 3 µM *Xenopus* Nup153 N-terminus (aa 1-149) or the corresponding V50E mutant was incubated with 1 mg/ml Folch Fraction I liposomes (average diameter approx. 70 nm). The samples were analyzed on copper grids by transmission electron microscopy on a FEI Technai spirit 120 kV microscope as in (Vollmer et al., 2012). Please note the liposome tubulation in the presence of Nup153 N-terminus, which is not induced by the membrane binding defective V50E mutant or the buffer control. Bar: 100 nm.

(C) EGFP-tagged Nup153 N-terminus localizes to the NE: Images show HeLa cells with lower expression levels of EGFP-tagged Nup153 N-terminus as compared to Figure 1F. DNA was stained with DAPI (blue). Bar: 10 µm.

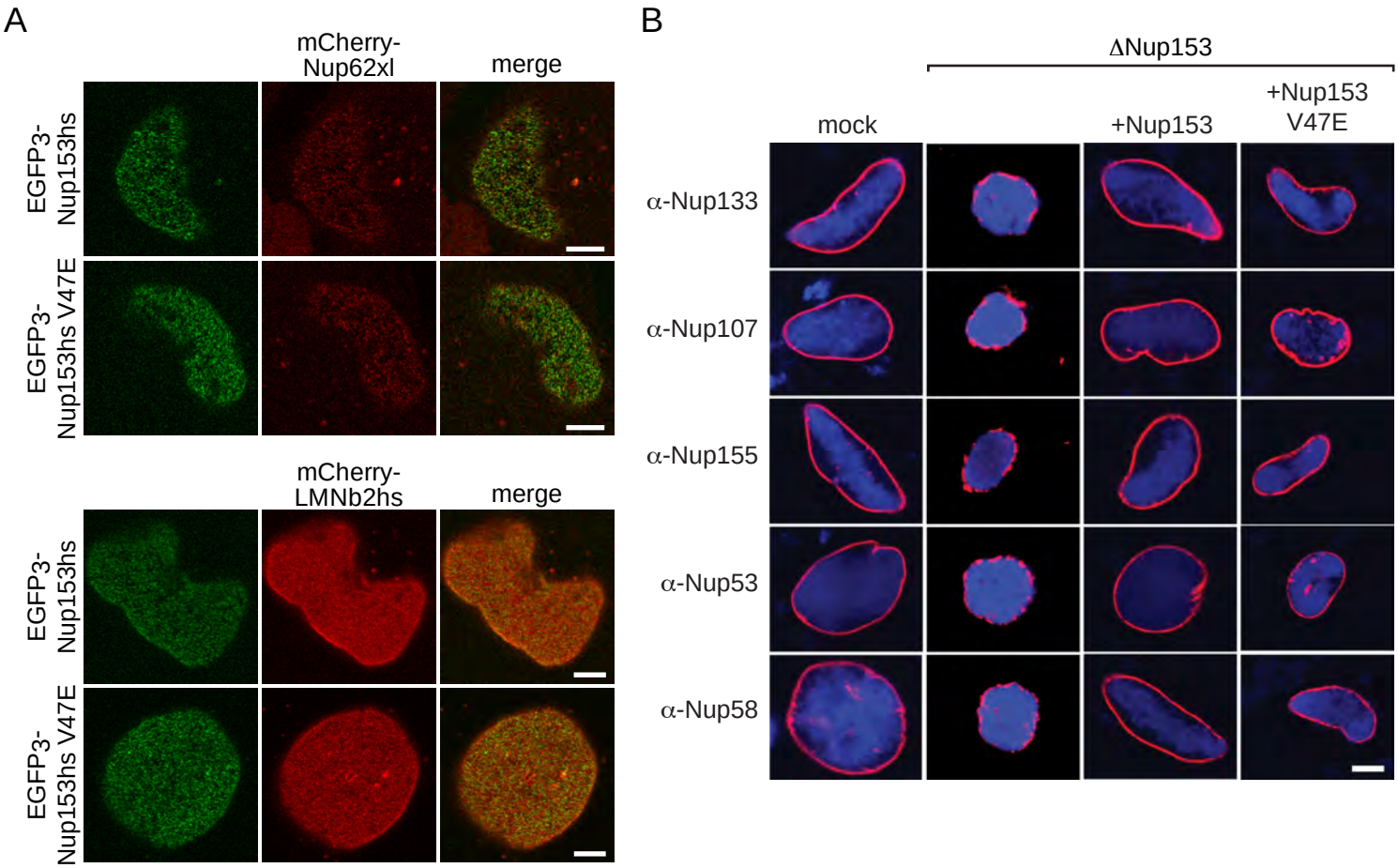

Figure S2, related to Figure 2

(A) Complete images of the nuclear surface of HeLa cells co-transfected with triple-EGFP-tagged human Nup153 or the corresponding V47E mutant and mCherry-Nup62 or mCherry-lamin B which are shown as insets in Figure 2A. Bars: 5 µm.

(B) Nuclei were assembled for 120 min in mock, Nup153 depleted (ΔNup153) or Nup153 depleted extracts supplemented with recombinant wild type protein (Nup153) or the membrane-binding mutant (Nup153 V47E). Samples were analyzed by immunofluorescence for the presence of Nup107 and Nup133 (nucleoporins of the Y-complex), Nup155 and Nup53 (nucleoporins of the Nup93-complex) and Nup58 (a central channel nucleoporin). DNA was stained with DAPI (blue). Bar 10 µm.

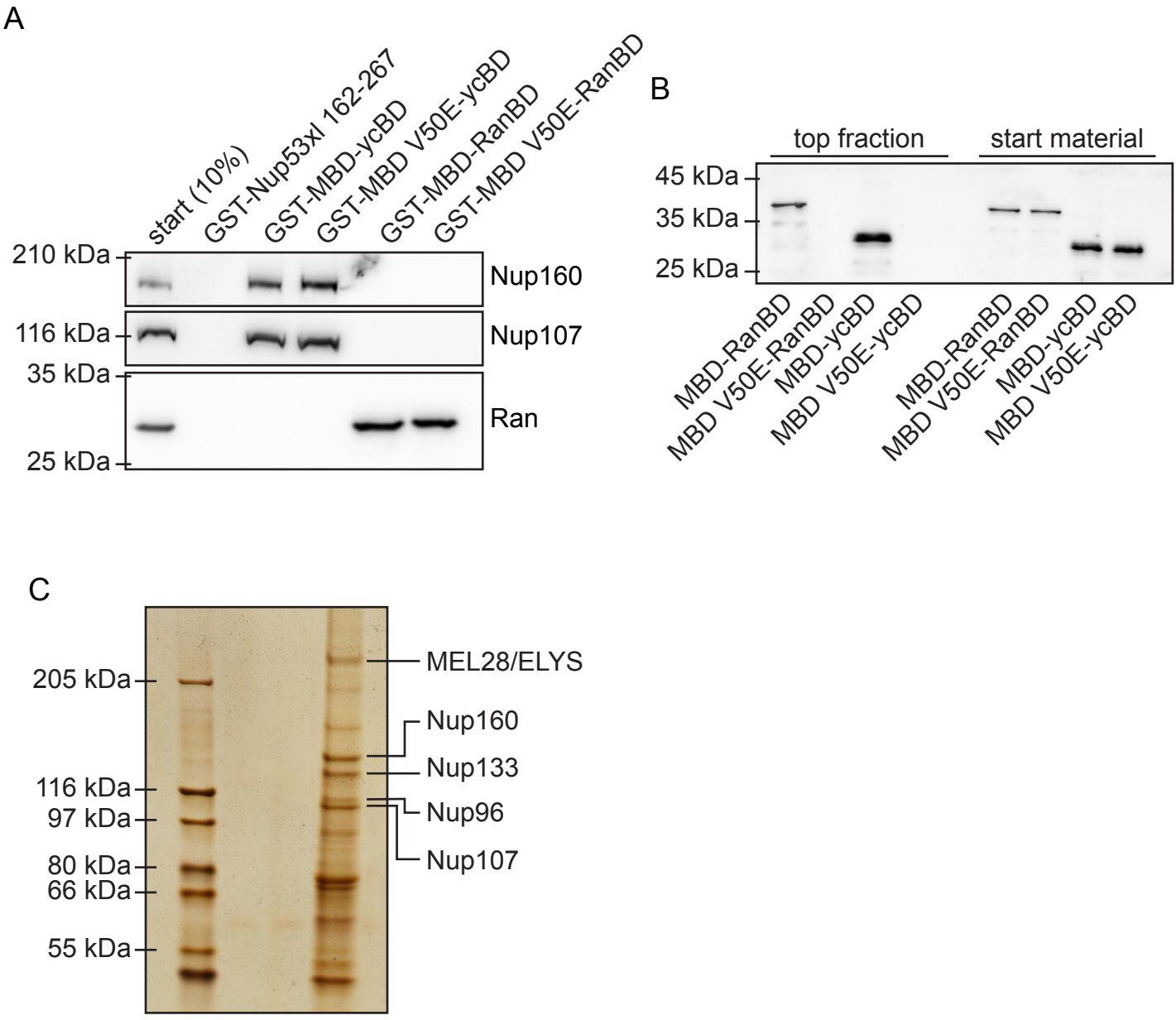

Figure S3, related to Figure 4

(A) GST-fusions of the RRM domain of *Xenopus* Nup53 (aa 162-267) (Vollmer et al., 2012) as a control and GST-fusions of the MBD-ycBD and MBD-RanBD constructs as well as the corresponding membrane binding mutants (V50E), were incubated with cytosol from *Xenopus* egg extracts. Eluates were analyzed by western blotting with antibodies against Nup160, Nup107 and Ran.

(B) 3 µM of the MBD-ycBD and MBD-RanBD fusion proteins as well as the corresponding membrane binding mutants (V50E) were incubated with fluorescently labeled 70 nm NE liposomes and floated through a sucrose gradient. Top gradient fractions and input materials were analyzed by western blot with the α-Nup153 antibody which is directed against the MBD.

(C) Silverstaining of the purified Y-complex. The Y-complex was purified from *Xenopus* egg extracts using TAP-tagged Nup98 (Walther et al., 2003). After TEV protease elution the complex was separated on a 5%-12% SDS-PAGE.

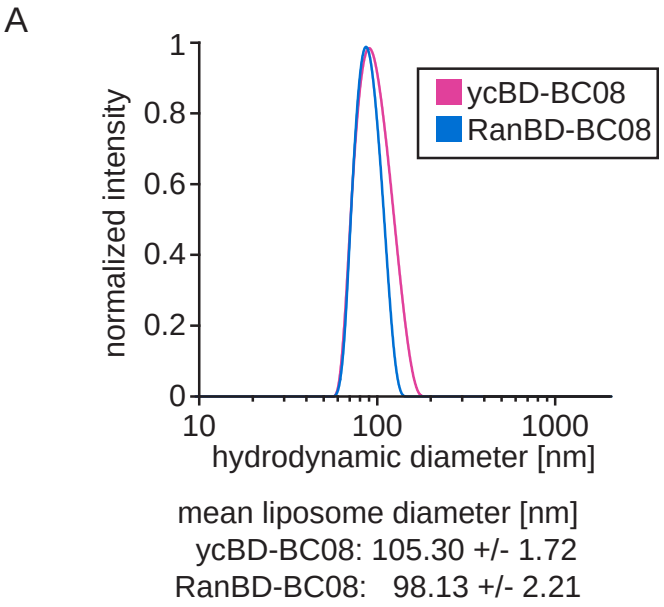

mean liposome diameter [nm]
ycBD-BC08: 105.30 +/- 1.72
RanBD-BC08: 98.13 +/- 2.21

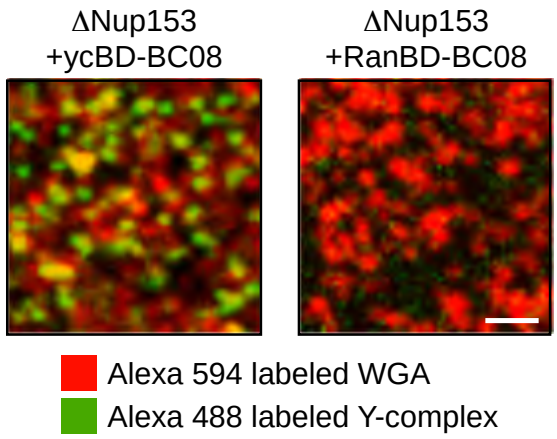

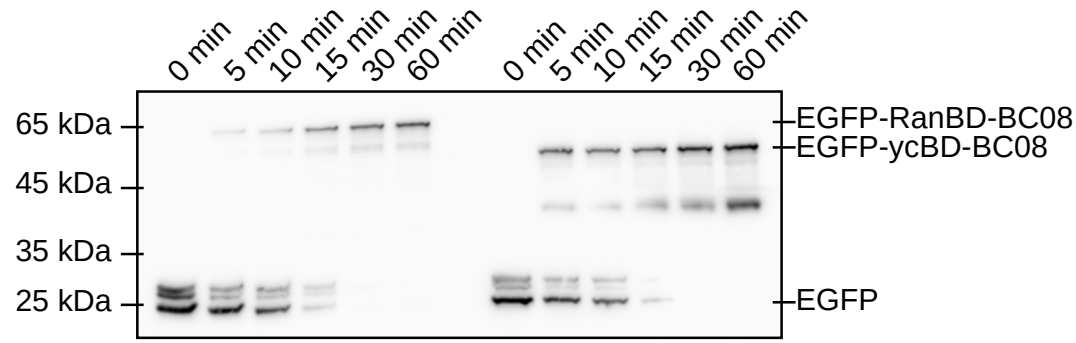

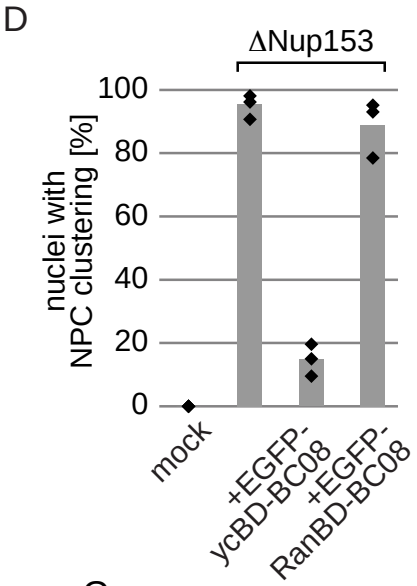

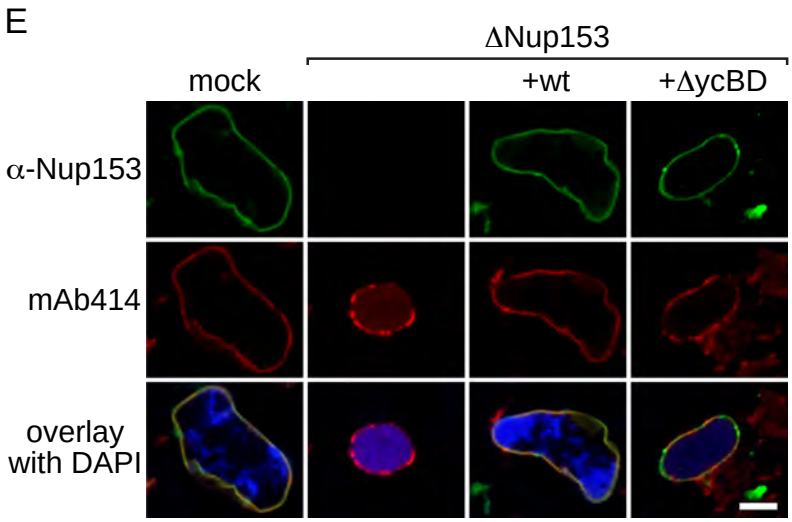

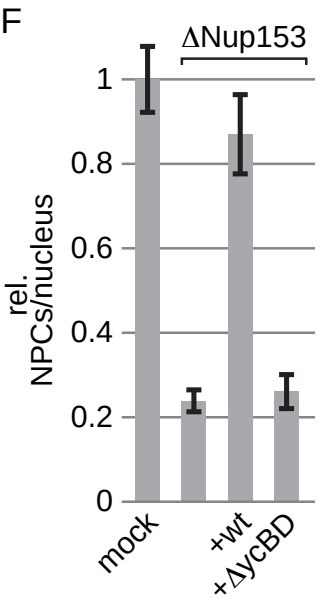

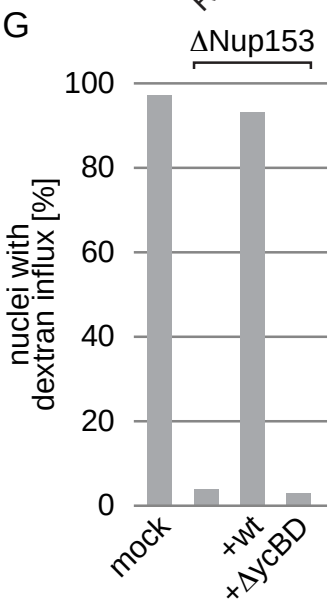

Figure S4, related to Figure 5

(A) Size distribution of EGFP-ycBD-BC08 and EGFP-RanBD-BC08 proteo-liposomes used in Figure 5B and D as determined by light scattering. The mean liposome diameter of the two preparations is indicated.

(B) The ycBD-BC08 fusion recruits the Y-complex to NPC assembly sites. Nuclei were assembled in Nup153 depleted extracts supplemented with ycBD-BC08 or RanBD-BC08 containing liposomes (the EGFP tag was cleaved before liposome reconstitution to avoid interference with the Alexa-488 labeled Y-complex signal). NPCs are visualized with Alexa-594 labeled WGA (red in overlay) and, the purified labeled Y-complex is shown in green. Bar: 1 µm.

(C) The EGFP-RanBD-BC08 and EGFP-ycBD-BC08 fusions translocate to the inner nuclear membrane as determined by a protease protection assay described in (Theerthagiri et al., 2010). Nuclei were assembled in 60 µl *Xenopus* egg extracts. After 50 min, i.e. when a closed NE has formed, proteo-liposomes containing the EGFP-RanBD-BC08 or EGFP-ycBD-BC08 fusions were added. At indicated time points after liposome addition, a 10 µl sample was taken, NusA fused TEV protease was added, and protease cleavage was stopped by addition of SDS sample buffer and boiling. Protease protection of the reporter was analyzed by Western blotting. The position of the un-cleaved (EGFP-RanBD-BC08 and EGFP-ycBD-BC08) and the cleaved EGFP reporter are indicated. Quantification of the EGFP signal reveals a half time of inner nuclear membrane transport of 6.7 min and 7.3 min for EGFP-RanBD-BC08 or EGFP-ycBD-BC08, respectively.

(D) Quantification of nuclei assembled as in Figure 5D with NPC clustering identified by mAB414 staining (three independent experiments with 100 chromatin substrates each). Please note the rescue of the NPC clustering phenotype by the EGFP-ycBD-BC08 construct probably because in this situation newly formed NPCs are inserted in all areas of the nuclear envelope.

(E) Nuclei were assembled for 120 min in mock, Nup153 depleted (ΔNup153) or Nup153 depleted extracts supplemented with recombinant wild type protein (wt) or a Nup153 deletion mutant lacking the Y-complex interaction site (ΔycBD, human Nup153 lacking aa 211-337, see extended experimental procedure section). Samples were analyzed by immunofluorescence with α-Nup153 and mAB414 antibodies. DNA was stained with DAPI (blue). Bar 10 µm

(F) NPC numbers in nuclei assembled as in (B) were determined using mAB414 staining (average from 10 nuclei, normalized to the mock control, error bars are SEM).

(G) Nuclei were assembled as in (B) and interphasic NPC assembly on more than 100 nuclei was analyzed by dextran influx.

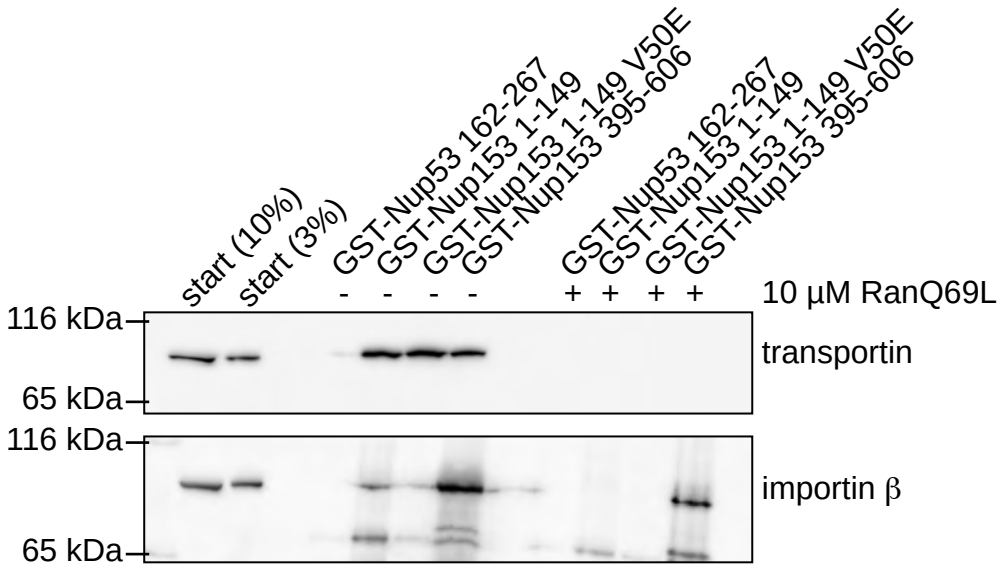

Figure S5, related to Figure 7

GST-fusions of the RRM domain of *Xenopus* Nup53 (aa 162-267) (Vollmer et al., 2012) as a control, of *Xenopus* Nup153 (aa-149), the corresponding membrane binding mutant (V50E), or of a *Xenopus* Nup153 fragment (aa 395-608) that is known to bind Nup50 (Makise et al., 2012), were incubated with cytosol from *Xenopus* egg extracts. Where indicated, 10 µM RanQ69L was added to the incubation. Eluates were analyzed by western blotting with antibodies against transportin and importin β. Please note that transportin binding to the Nup153 N-terminal fragment is not affected by the V50E mutation. The Nup153 aa 395-608 fragment binds transportin, consistent with a previous report that mapped a transportin binding site to a partially overlapping Nup153 fragment (aa 440-720) (Shah and Forbes, 1998)

Supplemental Movie 1

3D reconstruction (generated with IMARIS) of confocal stacked images of a representative HeLa cell transfected with EGFP-Nup153xl 1-149, as shown in Figure 1F.

Supplemental Experimental Procedures

DiIC18 (1,1'-Dioctadecyl-3,3,3',3'-Tetramethylindocarbocyanine Perchlorate), DiDC18 (1,1'-Dioctadecyl-3,3,3',3'-Tetramethylindodicarbocyanine Perchlorate), fluorescently labeled dextrans, Alexa dyes and secondary antibodies were obtained from Life Technologies, detergents from EMD, and lipids from Avanti Polar Lipids.

Antibodies

Antibodies against Nup107 (Walther et al., 2003), GP210 (Antonin et al., 2005), NDC1 (Mansfeld et al., 2006), Nup160 (Franz et al, 2007), Nup53 and LBR (Theerthagiri et al., 2010) and Nup58 (Sachdev et al., 2012) have been described. mAB414 (Babco), transportin and Ran (558660 and 610341, BD Bioscience), EGFP (11814460001, Roche), as well as TPR, human lamin A and B2 antibodies (ab58344, ab26300, ab151735 abcam) were purchased. Antibodies for POM121, RTN4, Nup153 and Nup133, were generated against recombinant fragments of the respective proteins (*Xenopus* POM121 aa 1-314, RTN4 aa 763-1043 and Nup153 aa 1-149, human Nup133 aa 67-514). Antibodies for Nup155, Nup50, importin β, lamin B (expressed as GFP-laminB3, kind gift from Rebecca Heald) are against the *Xenopus* full-length proteins, *Xenopus* importin α and BC08 antibodies are a kind gift from Iain Mattaj.

Protein expression and purification

Constructs for the *Xenopus* Nup153 N-terminus (aa 1-149) were generated from synthetic DNA optimized for codon usage in *E. coli* (Geneart), human full-length constructs from EGFP3-hNup153 (Rabut et al., 2004) and the corresponding V50E or V47E mutants by mutagenesis using QuikChange site-directed mutagenesis kit (Agilent). The Nup153 N-terminus (wildtype and V50E mutant) was cloned into a modified pET28a vector with a yeast SUMO solubility tag followed by a TEV site or into a modified pET28a vector with EGFP upstream of Nup153. MBD-ycBD and MBD-RanBD fusions as well as the corresponding membrane binding mutants were generated by insertion of human Nup153 fragments (aa 210-338 or aa 658-890) into the above mentioned constructs of the *Xenopus* Nup153 N-terminus (wildtype and V50E mutant) in the SUMO containing pET28a vector.

The Nup153 mutant lacking the Y-complex binding domain (Nup153 ΔycBD, Figure S3) was generated by cloning sequentially the N-terminal 210 aa of human Nup153 and the C-terminal Nup153 portion starting from aa 338 into the SUMO containing pET28a vector. Both fragments are joined by a GGSKLGGS linker.

Proteins were expressed in *E. coli* and purified using Ni-agarose. His_6- and SUMO-tags were cleaved using TEV protease and proteins were concentrated using VIVASPIN columns (Sartorius) and separated by gelfiltration (Superdex200 10/300 GL or Superdex200 PC 3.2/30, GE Healthcare) in HEPES buffer (20 mM HEPES pH 7.5, 150 mM NaCl, 1mM DTT). SUMO and EGFP were expressed and purified from the corresponding empty vectors. Human Nup133 (aa 67-514) was generated as described (Vollmer et al., 2012).

Y-complex was purified from *Xenopus* egg extracts using TAP-tagged Nup98 (Walther et al., 2003) and labelled using Alexa Fluor 546 carboxylic acid succinimidyl ester in 200 mM $NaHCO_3$ pH 8.4. Human RanQ69L was expressed from a modified pET28a vector with a His_6-GST tag, which was cleaved of using TEV protease. The protein was separated from the tag after dialysis using Ni-agarose and further purified by gelfiltration (Superdex200 10/300 GL). Purified ranQ69L was labelled using Alexa Fluor 546 C5 maleimide in HEPES buffer. Excess dye was removed by gelfiltration (Superdex200 PC 3.2/30).

EGFP-ycBD-BC08 or EGFP-RanBD-BC08 where generated by insertion of human Nup153 fragments (aa 210-338 or aa 658-890) into an BC08 reporter construct (Theerthagiri et al., 2010) between EGFP and BC08. The corresponding constructs were expressed, purified and reconstituted into small unilamellar liposomes (see below).

Transfection experiments

Plasmids encoding the *Xenopus* Nup153 N-terminus and the corresponding V50E mutant (cloned into a modified pEGFP-C3 vector) were transfected into HeLa cells using Fugene 6 (Roche) following the manufacturer's instructions. After 24 h cells were fixed and analyzed by confocal microscopy. For immunoprecipitations, EGFP3-hNup153 constructs were transfected into HEK293 cells. 24 h post-transfection cells were harvested and lysed in lysis buffer (50 mM TRIS-HCl pH 7.5, 150 mM NaCl, 1 mM EDTA, 10% glycerol, 0.1% Triton X-100 supplemented with protease inhibitors (2 µg/ml leupeptin, 1 µg/ml pepstatin, 2 µg/ml aprotinin, 0.1 mg/ml AEBSF final concentration) for 30 min at 4°C. After centrifugation for 15 min at 15.000 x g the supernatant was immunoprecipitated with GFP-Trap beads (Chromotek) for 2 h, washed 5x with lysis buffer, 2x with lysis buffer supplemented with 500 mM NaCl, 2x with lysis buffer, and 1x with lysis buffer without Triton X-100 and finally eluted with SDS-sample buffer. Eluates and lysed cells (corresponding to 5% of the eluates) were analyzed. For colocalization experiments (Figure 2A), pEGFP3-Nup153hs or pEGFP3-Nup153hsV47E were co-transfected with mCherry-hLMNB2 (kind gift of Martin Hetzer) or mCherry-Nup62xl using jetPRIME (Polyplus transfection). 24 h after transfection live cells were imaged at 37°C with a confocal microscope LSM780 (Zeiss) equipped with incubation chamber and using an Apochromat 63x/1.40 Oil DIC M27 objective.

GST Pulldown experiments

Fragments used for the GST pulldown experiments were cloned into a modified pET28a vector with GST tag followed by a recognition site for TEV protease and purified via the N-terminal His_6 tag. 60 µl GSH–Sepharose (GE Healthcare) was incubated with 300 µg of the indicated proteins, washed and blocked with 5% BSA in PBS. Beads were incubated with cytosol from *Xenopus* egg extracts (diluted 1:1 with PBS, and cleared by centrifugation for 30 min at 100,000 rpm in a TLA110 rotor (Beckman Coulter) for 2 h and washed six times with PBS. Bound proteins were eluted by cleavage with TEV protease (0.5 mg/ml) for 1 h at RT and analyzed by SDS-PAGE and Western blotting.

Liposome generation and flotation

NE lipid mixture - 60 mol% L-α-phosphatidylcholine, 19.8 mol% L-α-phosphatidylethanolamine, 10 mol% L-α-phosphatidylinositol, 5 mol% Cholesterol, 2.5 mol% Sphingomyelin, 2.5 mol% L-α-phosphatidylserine, 0.2 mol% 18:1-12:0 NBD-PE (1-oleoyl-2-{12-[(7-nitro-2-1,3-benzoxadiazol-4-yl)amino]dodecanoyl}-sn-glycero-3-phosphoethanolamine) or DOPC mixture - 99.8 mol% 1,2-dioleoyl-sn-glycero-3-ethylphosphocholine (DOPC), 0.2 mol% 18:1-12:0 NBD-PE - were dissolved in chloroform to a final concentration of 1 mg/ml. Chloroform was evaporated in a glass vial under a low stream of Argon until an even lipid film formed followed by incubation under vacuum for 1-2 h. Liposomes were formed by gentle addition of HEPES buffer to a final concentration of 5 mg/ml. After 1 h of incubation at 45°C, flask was shaken to dissolve residual lipids. After ten cycles of freeze/thawing liposomes were either snap frozen in liquid nitrogen and stored at -80°C or directly

used. Different sized liposomes were formed by passing liposomes sequentially through Nuclepore Track-Etched Membranes (Whatman) with defined pore sizes (400, 100, 30 nm) at 45°C using the Avanti Mini-Extruder until desired size was reached. For 30 nm, liposomes were incubated in a sonication bath for 5 min before final extrusion. To ensure equal concentrations of different sized liposomes, fluorescence intensity was determined after extrusion using a Molecular Imager VersaDoc MP 4000 Imaging System and ImageJ. Concentrations were adjusted by dilution. Liposome sizes were determined by light scattering using the AvidNano W130i with 10 measurements per sample each for 10 sec and analyzed using the iSize software.
For liposome flotations proteins (6 µM) were mixed 1:1 with liposomes (5 mg/ml) and incubated for 30 min at 25°C. 75 µl of the protein/liposome mixture was brought to 37% sucrose concentration in a total volume of 150 µl. 1.7 ml 12% sucrose cushion in HEPES buffer was overlaid, followed by 300 µl HEPES buffer on top. Samples were spun for 2 h at 55 000 rpm in a TLS-55 rotor (Beckman) at 25°C. Liposomes containing top layers were collected (450 µ l). Fluorescence intensities of the start protein/liposome mixture and the top fraction were determined. Usual liposome recovery rates are 60%. Collected fractions were precipitated by the method described by Wessel & Flügge (Wessel and Flugge, 1984). To compare different samples, pellets were resuspended in normalized volumes of sample buffer according to the determined fluorescence signal. Binding efficiency was determined by Western Blot analysis using the Fusion Capt advance software, comparing band intensities of start materials with collected fractions.

Generation of GUVs and analysis

Detergent solubilized EGFP-ycBD-BC08 and EGFP-RanBD-BC08 were reconstituted in proteo-liposomes via gelfiltration (Eisenhardt et al., 2014). For this, 20 µl of the NE lipid mix without NBD-PE (30 mg/ml in 10% octylglucopyranoside) was mixed with 20 µl of 2 µM protein and 100 µl PBS. The sample was applied to a Sephadex G50 fine filled Econo chromatography column (0.5 × 20 cm, Biorad) to remove the detergent. The formed proteo-liposomes were collected and pelleted for 30 min at 100.000 rpm in a TLA120.2 (Beckman Coulter) rotor at 4°C. The pellet was resuspended in 120 µl 20 mM HEPES pH 7.4, 100 mM KCl, 1 mM DTT. 5 µl of resuspended proteo-liposomes were dried onto two 5 mm x 5 mm platinum gauzes (ALS) under vacuum for at least 1 h at room temperature. The gauzes were placed in parallel (5 mm distance) into a cuvette (UVette, Eppendorf) and submerged in 259 mM sucrose solution and for 140 min an AC electric field with 10 Hz, 2.2 V was applied followed by 20 min 2 Hz at 42°C.
Lipid GUVs were generated from chloroform dissolved NE lipid mix (10 mg/ml) and 0.8 nM DiDC18 by electroformation as described (Angelova and Dimitrov, 1986). Equal amounts of the lipid-chloroform solution (25 µg total lipids) were distributed onto two 5 mm x 5 mm platinum gauzes (ALS) and processed as described before. Electroformation time at 10 Hz was reduced to 70 min.
GUVs were visualized in an 8 well glass observation chamber (Chambered #1.0 Borosilicate Coverglass System, Lab-Tek) that was blocked with 5 % (wt/vol) BSA in PBS and washed with PBS. For each reaction 50 µl of freshly prepared GUVs were mixed with 150 µl PBS and placed into a well. Soluble proteins were added to a final concentration of 500 nM. Proteins (25 nM for the purified labelled y-complex) and buffers used for GUV preparation matched the osmotic pressure of the sucrose solution using an osmometer. The mixture was incubated for 5 min and imaged immediately at room temperature on an inverted Olympus Fluoview 1000 confocal

laser scanning system utilizing an UPlanSApo 60x/1.35 oil objective. EGFP and Alexa-546 were excited by an argon ion laser at 488 nm and 515 nm. Emission for EGFP was collected between 500 to 545 nm and between 570 to 625 nm for Alexa-546. DiD was excited by a 635 nm DPSS laser and emission was collected between 655 to 755 nm. The pinhole was set to one airy unit.

Dextran exclusion assay to monitor interphasic NPC formation

Nuclei were assembled by incubating 0.3 µl demembranted sperm heads (10.000/µl)(Gurdon, 1976) with 10 µl mock or depleted cytosol and, where indicated, recombinant proteins or proteo-liposomes. After 10 min, which allows for decondensation of sperm DNA, 0.2 µl floatation purified membranes from egg extracts, 0.2 µl 200 µg/µl glycogen, and 0.2 µl energy mix (50 mM ATP, 50 mM GTP, 500 mM creatine phosphate and 10 mg/ml creatine kinase in sucrose buffer [10 mM HEPES, 250 mM sucrose, 50 mM KCl, 2.5 mM $MgCl_2$, pH 7.4]) was added. After additional 40 min, 20 µl of mock or Nup153 depleted extracts, which had been incubated for 20 min with 30 µl WGA-Agarose (Sigma) to remove the permeability barrier forming nucleoporins, were added. Where indicated 2 µM importin β was added to inhibit further interphasic NPC assembly together with the WGA-treated extracts. After additional 50 min, 0.6 µl of a solution containing 5 µg/µl streptavidin and 5 µg/µl biotinylated WGA (both from Life Technologies) was added in order to reduce the diffusion of 70kDa dextrans through intact pores (Dawson). After 10 min, 2.5 µl of a mixture containing 0.25 µg/µl Alexa-488 labelled WGA (Life Technologies) and 0.25 µg/µl Hoechst in sucrose buffer was added. Samples were directly mounted on microscope slides and analysed by fluorescence microscopy. Nuclei, identified by Hoechst staining, that excluded the fluorescent dextran were counted as negative for interphasic NPC assembly.

NPC counting using mAB414 labeling

Nuclei were assembled by incubating 0.3 µl demembranted sperm heads (10.000/µl) with 10 µl mock or depleted cytosol and, where indicated, recombinant proteins or proteo-liposomes. After 10 min, which allows for decondensation of sperm DNA, 0.2 µl floatation purified membranes from egg extracts, 0.2 µl 200 µg/µl glycogen, and 0.2 µl energy mix (50 mM ATP, 50 mM GTP, 500 mM creatine phosphate and 10 mg/ml creatine kinase in sucrose buffer) was added. After assembly for 120 min, samples were fixed with 4 % paraformaldehyde and 0,5% glutaraldehyde in 80 mM Pipes pH 6.8, 1 mM $MgCl_2$, 150 mM sucrose, spun through a sucrose cushion on Poly-L-Lysine coated coverslips and stained with mAB414 and Alexa-488 labelled α-mouse antibodies and DAPI. Where indicated, further interphasic NPC assembly was inhibited by addition of 2 µM importin β 50 min after initiating the assembly reaction. Although postmitotic NPC assembly is in the assembly reaction usually completed after 30 min (i.e. the time when a closed nuclear envelope has formed, 20 min after addition of membranes) we add also in this assay importin β at the 50 min time point to ensure that only interphasic NPC assembly is affected. The NPCs from 30 - 50 nuclei in each independent experiment were imaged by acquiring stacked images of the envelope surface as well as through entire nuclei. Image recording was performed using an inverted Olympus Fluoview 1000 confocal laser scanning system utilizing an UPlanSApo 60x/1.35 oil objective. DAPI was excited by a 405 nm DPSS laser and emission was collected between 425 to 475 nm. Alexa-488 was excited by an argon ion laser at 488 nm and emission was collected between 500 to 545 nm. The pinhole size was set to 80 µm.

NPCs were counted using Imaris 7.7.1 software (Bitplane Scientific solutions). Individual pores were detected using the semi-automatic spot detection function in surpass mode with the spot detection diameter set to 0.25 µm. The threshold was manually adjusted on the intensity max filter setting in each condition to ensure detection of individual spots. In the same samples, surface area was calculated with the surface function of Imaris based on the absolute intensity of the DAPI signal. NPCs per µm² were calculated, extrapolated to the total surface area of the individual nuclei and plotted as the total number of NPCs per nucleus relative to the mock control. We use this normalization as overall NPCs numbers vary between different experiments due to variability of the egg extract quality.

Supplemental References

Angelova, M.I., and Dimitrov, D.S. (1986). Liposome Electroformation. Faraday Discuss *81*, 303-311.

Antonin, W., Franz, C., Haselmann, U., Antony, C., and Mattaj, I.W. (2005). The integral membrane nucleoporin pom121 functionally links nuclear pore complex assembly and nuclear envelope formation. Molecular cell *17*, 83-92.

Eisenhardt, N., Redolfi, J., and Antonin, W. (2014). Interaction of Nup53 with Ndc1 and Nup155 is required for nuclear pore complex assembly. J Cell Sci *127*, 908-921.

Gurdon, J.B. (1976). Injected nuclei in frog oocytes: fate, enlargement, and chromatin dispersal. J Embryol Exp Morphol *36*, 523-540.

Makise, M., Mackay, D.R., Elgort, S., Shankaran, S.S., Adam, S.A., and Ullman, K.S. (2012). The Nup153-Nup50 protein interface and its role in nuclear import. J Biol Chem *287*, 38515-38522.

Mansfeld, J., Guttinger, S., Hawryluk-Gara, L.A., Pante, N., Mall, M., Galy, V., Haselmann, U., Muhlhausser, P., Wozniak, R.W., Mattaj, I.W.*, et al.* (2006). The conserved transmembrane nucleoporin NDC1 is required for nuclear pore complex assembly in vertebrate cells. Molecular cell *22*, 93-103.

Rabut, G., Doye, V., and Ellenberg, J. (2004). Mapping the dynamic organization of the nuclear pore complex inside single living cells. Nat Cell Biol, 1114-1121.

Sachdev, R., Sieverding, C., Flotenmeyer, M., and Antonin, W. (2012). The C-terminal domain of Nup93 is essential for assembly of the structural backbone of nuclear pore complexes. Mol Biol Cell *23*, 740-749.

Shah, S., and Forbes, D.J. (1998). Separate nuclear import pathways converge on the nucleoporin Nup153 and can be dissected with dominant-negative inhibitors. Curr Biol *8*, 1376-1386.

Theerthagiri, G., Eisenhardt, N., Schwarz, H., and Antonin, W. (2010). The nucleoporin Nup188 controls passage of membrane proteins across the nuclear pore complex. J Cell Biol *189*, 1129-1142.

Vollmer, B., Schooley, A., Sachdev, R., Eisenhardt, N., Schneider, A.M., Sieverding, C., Madlung, J., Gerken, U., Macek, B., and Antonin, W. (2012). Dimerization and direct membrane interaction of Nup53 contribute to nuclear pore complex assembly. EMBO J *31*, 4072-4084.

Walther, T.C., Alves, A., Pickersgill, H., Loiodice, I., Hetzer, M., Galy, V., Hulsmann, B.B., Kocher, T., Wilm, M., Allen, T.*, et al.* (2003). The conserved Nup107-160 complex is critical for nuclear pore complex assembly. Cell *113*, 195-206.

Wessel, D., and Flugge, U.I. (1984). A method for the quantitative recovery of protein in dilute solution in the presence of detergents and lipids. Anal Biochem *138*, 141-143.

Title:
A cell free assay to study chromatin decondensation at the end of mitosis

Authors:
Anna Katharina Schellhaus
Friedrich Miescher Laboratory of the Max Planck Society
Spemannstrasse 39
72076 Tübingen
Germany
katharina.schellhaus@tuebingen.mpg.de

Adriana Magalska
Nencki Institute of Experimental Biology of Polish Academy of Sciences
3 Pasteur Street
02-093 Warsaw
Poland
a.magalska@nencki.gov.pl

Allana Schooley
Friedrich Miescher Laboratory of the Max Planck Society
Spemannstrasse 39
72076 Tübingen
Germany
allana.schooley@tuebingen.mpg.de

Wolfram Antonin
Friedrich Miescher Laboratory of the Max Planck Society
Spemannstrasse 39
72076 Tübingen
Germany
wolfram.antonin@tuebingen.mpg.de

*Anna Katharina Schellhaus and Adriana Magalska contributed equally to this work.

CORRESPONDING AUTHOR:
Wolfram Antonin
Friedrich Miescher Laboratory of the Max Planck Society
Spemannstrasse 39
72076 Tübingen
Germany
wolfram.antonin@tuebingen.mpg.de

KEYWORDS
Cell-free assay, mitotic exit, chromatin isolation, *Xenopus* egg extract, chromatin

decondensation, nuclear reformation, chromatin condensation

SHORT ABSTRACT
The molecular mechanisms of the decondensation of highly compacted mitotic chromatin are ill-defined. We present a cell-free assay based on mitotic chromatin clusters isolated from HeLa cells and *Xenopus laevis* egg extract that faithfully reconstitutes the decondensation process *in vitro*.

LONG ABSTRACT
During the vertebrate cell cycle chromatin undergoes extensive structural and functional changes. Upon mitotic entry, it massively condenses into rod shaped chromosomes which are moved individually by the mitotic spindle apparatus. Mitotic chromatin condensation yields chromosomes compacted fifty-fold denser as in interphase. During exit from mitosis, chromosomes have to re-establish their functional interphase state, which is enclosed by a nuclear envelope and is competent for replication and transcription. The decondensation process is morphologically well described, but in molecular terms poorly understood: We lack knowledge about the underlying molecular events and to a large extent the factors involved as well as their regulation. We describe here a cell-free system that faithfully recapitulates chromatin decondensation *in vitro*, based on mitotic chromatin clusters purified from synchronized HeLa cells and *X. laevis* egg extract. Our cell-free system provides an important tool for further molecular characterization of chromatin decondensation and its co-ordination with processes simultaneously occurring during mitotic exit such as nuclear envelope and pore complex re-assembly.

INTRODUCTION
Xenopus laevis egg extract is a powerful and widely applied tool to study complicated cellular events in the simplicity of a cell-free assay. Since their first description by Lohka & Masui [1] they have been extensively used to study mitotic processes such as chromatin condensation [2], spindle assembly [3], nuclear envelope breakdown [4], but also nucleocytoplasmic transport [5] or DNA replication [6]. The events taking place at the end of mitosis, necessary for reformation of the interphasic nucleus such as nuclear envelope reformation and nuclear pore complex reassembly are much less understood compared to the early mitotic events but can be similarly studied using *Xenopus* egg extract [7]. We have recently established an assay based on *Xenopus* egg extract to study chromatin decondensation at the end of mitosis [8], an under-investigated process that awaits its detailed characterization.

In metazoans, chromatin is highly condensed at mitotic entry in order to perform faithfully segregation of the genetic material. To ensure that the chromatin is accessible for gene expression and DNA replication during interphase, it needs to be de-compacted at the end of mitosis. In vertebrates, chromatin is up to fifty-fold more compacted during mitosis compared to interphase [9], in contrast to yeasts where the mitotic compaction is usually much lower, e.g. only two-fold in *S. cerevisiae* [10]. Vertebrate chromatin decondensation has been mostly studied in the context of sperm DNA reorganization after egg fertilization. A molecular mechanism, in which nucleoplasmin, an abundant oocyte protein, exchanges sperm-specific protamines to

histones H2A and H2B stored in the egg. This process was also elucidated using *Xenopus* egg extract [11,12]. However, the expression of nucleoplasmin is limited to oocytes [13] and mitotic chromatin does not contain these sperm-specific protamines. Therefore chromatin decondensation at the end of mitosis is nucleoplasmin independent [8].

For the *in vitro* decondensation reaction we employ extract generated from activated *X. laevis* eggs and chromatin clusters isolated from synchronized HeLa cells. Treatment of eggs with a calcium ionophore mimics the calcium release into the oocyte generated by sperm entry during fertilization. The calcium wave triggers the cell cycle resumption and the egg, arrested in the second metaphase of meiosis, progresses to the first interphase [14]. Therefore, egg extracts prepared form activated eggs represent the mitotic exit/interphase state and are competent to induce events specific for mitotic exit like chromatin decondensation, nuclear envelope and pore complex reformation. For the isolation of mitotic chromatin clusters we used a slightly modified version of the protocol published by Gasser & Laemmli [15], where chromosome clusters are released by lysis from HeLa cells synchronized in mitosis and isolated in polyamine containing buffers by gradient centrifugations.

PROTOCOL:

Mitotic chromatin cluster isolation from HeLa cells

1. Preparations

1.1) Cell culture solutions:

1.1.1) Prepare complete Dulbecco's modified Eagle's medium (DMEM) by adding 10 % fetal calf serum, 100 units/ml penicillin, 100 µg/ml streptomycin and 2 mM glutamine to the DMEM. Prepare Phosphate buffer saline (PBS) containing 2.7 mM KCl, 137 mM NaCl, 10 mM $Na_2HPO_4 \cdot 2H_2O$ and 2 mM KH_2PO_4 in deionized water, and adjust pH to 7.4 with 10 N NaOH.

Note: PBS can be kept as 10x stock solution over time at room temperature. Dilute it with deionized water to 1x before use. Filter the 1x solution again if it will be used in cell culture.

1.1.2) Prepare a 40 mM stock of thymidine solution (cell culture suitable) in DMEM medium. Dissolve 0.97 g thymidine in 90 ml of DMEM medium. Adjust final volume to 100 ml. Store stock solution at -20 °C. Dissolve (**CAUTION!** work under chemical hood, wear gloves and mouth protection) nocodazole to a 5 mg/ml stock solution in DMSO.

1.2) Mitotic clusters isolation solutions

NOTE: All solutions described in 1.2 need to be kept on ice after preparation/thawing throughout the whole experiment.

1.2.1) Autoclave deionized water for 105 minutes at 121 °C. Dissolve spermine tetrahydrochloride in autoclaved, deionized water to a final concentration of 200 mM (69.6 mg/ml). Store stock solution at -20 °C. Dissolve spermidine trihydrochloride in autoclaved, deionized water to a final concentration of 200 mM (50.8 mg/ml). Store stock solution at -20 °C.

1.2.2) Prepare 5 % (w/v) digitonin (**CAUTION!** work under chemical hood, wear gloves and

mouth protection) in hot, deionized water. Filter and store aliquots at -20 °C. Dissolve phenylmethylsulfonyl fluoride (PMSF) (**CAUTION!** work under chemical hood, wear gloves and mouth protection) to a final concentration of 200 mM (35 mg/ml) in 100 % ethanol. Store stock solution at -20 °C.

1.2.3) Dissolve dithiothreitol (DTT) with deionized water to a final concentration of 1 M (154 mg/ml) (**CAUTION!** work under chemical hood, wear gloves). Filter and store stock solution at -20 °C.

1.2.4) Prepare a 100-fold protease inhibitor mix (**CAUTION!** work under chemical hood, wear gloves) by dissolving 10 mg/ml AEBSF (4-(2-Aminoethly-)-benzensulfonylfluoride), 0.2 mg/ml leupeptin, 0.1 mg/ml pepstatin and 0.2 mg/ml aprotinin in deionized water. Store stock solution at -20 °C.

1.2.5) Prepare a 10x stock solution of buffer A containing 150 mM Tris-Cl (pH 7.4), 800 mM KCl, 20 mM EDTA-KOH (pH 7.4), 2 mM spermine tetrahydrochloride and 5 mM spermidine trihydrochloride. Store buffer A at 4 °C without spermine tetrahydrochloride and spermidine trihydrochloride, which should be added freshly just before use.

NOTE:EDTA only dissolves at pHs higher than 8, therefore, to prepare a high concentrated EDTA-KOH stock solution (0.5 M recommended), add 5 N KOH to pH just above 8 to dissolve it. Afterwards titrate down to pH 7.4.

1.2.6) Prepare a 20 x stock solution of buffer As containing 100 mM Tris-HCl (pH 7.4), 400 mM KCl, 400 mM EDTA-KOH (pH 7.4) and 5 mM spermidine trihydrochloride. Buffer As can be stored under same conditions as buffer A.

NOTE:Prepare the working solutions I to IV (see in the following steps), the glycerol gradient and the colloidal silica particles solutions containing silica particles (15 to 30 nm diameter) coated with non-dialyzable polyvinylpyrrolidone (PVP) freshly just before the isolation procedure (PMSF and digitonin should be added directly before use as PMSF is labile in aqueous solutions and digitonin tends to precipitate upon long term storage on ice).

1.2.7) Prepare 100 ml of solution I by adding 0.5 x buffer A, 1mM DTT, 1:100 of the protease inhibitor mix and 0.1 mM PMSF into autoclaved, deionized water. Prepare 50 ml of solution II (for cell lysis) by adding 1x buffer A, 1 mM DTT, 1:100 of the protease inhibitor mix, 0.1 mM PMSF, 0.1 % digitonin and 10 % glycerol into autoclaved, deionized water.

1.2.8) Prepare 200 ml of solution III containing 0.25x buffer A, 1 mM DTT, 1:100 of the protease inhibitor mix, 0.1 mM PMSF and 0.05 % digitonin in autoclaved, deionized water. Prepare 40 ml of solution IV containing 1x buffer As, 1 mM DTT, 1:100 of the protease inhibitor mix, 0.1 mM PMSF and 0.1 % digitonin in autoclaved, deionized water.

1.2.9) Prepare 120 ml of glycerol gradient solution by adding 25 % glycerol and 0.1 % digitonin

to solution I.

1.2.10) Prepare 150 ml of colloidal silica particles solution containing 60 % v/v (volume per volume) of a suspension containing silica particles (15 to 30 nm diameter) coated with non-dialyzable polyvinylpyrrolidone (PVP), 15 % glycerol, 2 mM spermidine trihydrochloride and 0.8 mM spermine tetrahydrochloride in solution IV.

1.2.11) Prepare cluster storage buffer containing 250 mM sucrose, 15 mM Hepes (pH 7.4), 0.5 mM spermidine trihydrochloride, 0.2 mM spermine tetrahydrochloride, 1:100 of the protease inhibitor mix, 0.3 % BSA and 30 % glycerol. The cluster storage buffer can be kept at -20 °C.

1.2.12) Prepare squash fix solution containing 10 % formaldehyde (**CAUTION!** work under chemical hood, wear gloves), 50 % glycerol, twofold Mark's Modified Ringers buffer (MMR see 4.5.) and 0.2 µg/ml DAPI (**CAUTION!** wear gloves). Store at 4 °C in light protected reaction tubes. It is not crucial for the experiment to use this squash fix recipe, alternative recipes will also work.

2. Synchronization of cells

2.1) On Day 1. Seed HeLa cells in five 75 cm^2 (250 ml) flasks with media and incubate it at 37 ^oC in 5% CO_2. Note: This will yield in approximately 18 x 10^6 cells at the day of chromatin cluster isolation.

2.2) On Day 2. When cells are at least 50 % confluent (roughly half of the surface is covered by cells and there is still room for cells to grow), add thymidine to a final concentration of 2 mM (thymidine block) and culture cells for 24 hours at 37 ^oC in 5% CO_2. Note: This will arrest the cells at the G1/S phase border.

2.3) On Day 3. Aspirate medium containing thymidine and add sterile PBS. Wash cells by delicate rinsing with sterile PBS. Aspirate PBS and gently add 15-20 ml of fresh, warm complete DMEM medium and culture cells for 3 to 4 hours at 37 ^oC in 5% CO_2 to release them from the G1/S-phase block.

2.4) On day 3 (continuation). After releasing the cells from the G1/S-phase block, add nocodazole to a final concentration of 100 ng/ml. Dilute nocodazole by adding 2 µl of stock solution (5mg/ml) to 98 µl of fresh DMEM medium, and add 1µl of diluted nocodazole per each ml of cell culture. Culture cells for approximately 12 hrs at 37 °C in 5 % CO_2. This will block the cells in mitosis.

3. Mitotic clusters isolation

3.1) On day 4 isolate mitotic clusters. Using a bright field microscopy, check if the majority of cells are mitotic. If less than 50 % of the cells are mitotic wait until more cells reach mitosis. Collect mitotic cells by tapping vigorously at the side of the flask (or by gently spraying with the pipette), this will detach remaining mitotic cells. Transfer the cell suspension to 50 ml conical centrifuge tubes.

NOTE:Mitotic cells become round and can be easily detached from the flask bottom (just like cells after trypsinization), unlike cells in other cell cycle stages, which are flat and firmly attached to the flask.

3.2) Harvest mitotic cells by spinning the tubes at 1500 x g for 10 min (4 °C or room temperature) and removing the supernatant afterwards. Resuspend the cell pellet in 8 ml PBS, pool into one 50 ml conical centrifuge tube, fill the tube completely with PBS and spin again for 10 min at 1500 x g. Repeat this washing procedure three times in total.

3.3) From now on perform all steps on ice with cold solutions. Vigorously resuspend the pellet in 37 ml of cold solution II. Transfer the suspension to a cold 40 ml glass-glass homogenizer using a 25 ml pipette and lyse cells on ice by douncing with a tight pestle until mitotic clusters are free of cytoplasmic material. The number of strokes is highly dependent on the digitonin stock and can vary from 3 to 20 times.

NOTE:Homogenization can be fairly vigorous, but should be considered complete when nearly all mitotic cells are lysed and the clusters are seen to be free of cytoplasmic material (see 3.4).

3.4) After a couple of strokes mix 5-10 µl of the cell suspension 1:2 with Trypan blue and check by microscopy in a Neubauer chamber. When the cells are lysed chromatin is stained blue and free of cell membranes (NOTE: possible cytoplasmic remnants will be accumulate around the blue stained chromatin and will be easy to distinguish).

NOTE:Mitotic cells will lyse before interphasic cells but nevertheless be careful not to overdo homogenization in order to avoid contamination with interphasic nuclei and mangled chromatin.

3.5) Immediately layer the whole cell lysate over cold step gradients (with 5 ml of 60 % colloidal silica particles solution at the bottom, overlaid with 19.5 ml of glycerol gradient solution each) in five polycarbonate centrifugation tubes (28.8 x 107.0 mm, it is recommended to place the tubes on ice before to cool them down) using a 10 ml pipette. Do not keep cells in solution II for a long time, thus it is recommended to prepare the tubes and the gradient beforehand (e.g. during the washing steps).

3.6) Centrifuge the gradients for 30 min at 1000 x g at 4 °C in a fixed angle rotor.

NOTE:Nuclei, unlysed cells and clusters are recovered together at the interface of the glycerol and the colloidal silica particles layers.

3.7) Remove the liquid above the interphase using a pipette and transfer the rest to the cold homogenizer. Re-homogenize mixture by 3-15 strokes (again depending on the digitonin stock) with the tight pestle to eliminate aggregates and to remove cytoskeletal fibers from the clusters. After every couple of strokes check the efficiency of homogenization. Mix 1 µl of the

sample with 1 µl of squash fix supplemented with DAPI and examine under the fluorescent microscope.

NOTE:The number of strokes is crucial, the presence of cluster aggregates means, that the number of strokes is insufficient, while mangled chromatin and nuclei debris indicate that the homogenization was too strong.

3.8) Distribute the solution among four new polycarbonate centrifugation tubes (28.8 x 107.0 mm) (approx. 10 ml solution per tube) and fill them completely up with 60 % colloidal silica particles solution (approx. 30 ml colloidal silica particles solution per tube).

NOTE:Avoid overloading the colloidal silica particles gradient since clusters can easily be trapped if there is too much cytoplasmic debris in the gradient.

3.9) Spin for 5 min at 3000 x g, followed by 30 min at 45440 x g at 4 °C in a fixed angle rotor.
Note: As before, interphasic nuclei will be kept from entering the gradient (if homogenization was not done too heavily which releases nuclei from cytoplasmic debris) but the clusters will accumulate around 1.5 cm from the bottom of the tube, often as a loose ball.

3.10) Remove the liquid above the clusters using a pipette, pool the rest into one tube, resuspend well and redistribute to two polycarbonate centrifugation tubes (28.8 x 107.0 mm). Dilute the cluster suspension 1:4 with solution III in each tube and mix well. Mark the site were the pellet will be and spin 1000 x g for 15 min at 4 °C in a fixed angle rotor.

3.11) Resuspend the pellets in Solution III, pool into one 50 ml conical centrifuge tube and fill up with Solution III. Centrifuge at only 300 x g for approximately 10 min. Do not centrifuge at higher velocity - it might cause irreversible aggregation of clusters.

3.12) Wash again with Solution III in 1.5 or 2 ml reaction tubes (resuspend the pellets and fill the tubes completely up) and centrifuge at 300 x g. Remove the supernatant carefully with a pipette. Resuspend pellet carefully in 250 µl cluster storage buffer (if you have several pellets use 250 µl for all together and pool them). Dilute 5-10 µl of the sample 1:2 with Trypan blue and count in the Neubauer chamber. If applicable dilute more to obtain an approximate concentration of 500 clusters/µl.

3.13) Push the suspension through a 100 µm cell strainer to make sure to remove cluster aggregations resulting from improper resuspension. The clusters can be stored for months in -80 °C. To avoid multiple refreezing make appropriate aliquots and snap freeze in liquid nitrogen.

4. Preparations of buffer for interphasic *Xenopus laevis* egg extract

NOTE: *Xenopus laevis* frogs are maintained and treated in accordance with the guidelines and regulations set forth by the Convention of the council of Europe on the protection of vertebrate animals used for experimental and other purposes (EU ratified in 1998) and the German law

pertaining to the use of vertebrate animals in research.

4.1) Prepare DTT and a 100-fold protease inhibitor mix according to 1.2.3 and 1.2.4. Dissolve cytochalasin B to a final concentration of 10 mg/ml in DMSO, aliquot (10 or 20 µl recommended) and store at -20 °C.

4.2) Dissolve cycloheximide to a final concentration of 20 mg/ml in ethanol, aliquot (500 µl recommended) and store at -20 °C. Dissolve the calcium ionophore A23187 to a final concentration of 2 mg/ml in ethanol, aliquot and store at -20 °C.

Note: PI, DTT, cytochalasin B, cycloheximide and A23187 can be repeatedly frozen and thawed.

4.3) Prepare 20x Mark's Modified Ringers buffer (MMR) containing 2 M NaCl, 40 mM KCl, 20 mM $MgCl_2$, 40 mM $CaCl_2$, 2mM EDTA and 100 mM Hepes, adjust pH to 8.0 with 5 N KOH.

NOTE:The 20 x MMR can be kept over long time at room temperature. Depending on the amounts of eggs, for one preparation of interphasic egg extract 1 liter of 1x MMR per injected frog and an additional 5-10 liters for the washing steps are necessary. Re-adjust the pH of 1x MMR to 8.0 with 5 N KOH. 1x MMR prepared to keep the frogs in overnight should be at room temperature. 1x MMR prepared for the extract preparation should be kept cold until it is used, however it is not crucial for the experiment that the 1x MMR is really cold.

4.4) Prepare 1 liter of sucrose buffer containing 250 mM sucrose, 50 mM KCl, 2.5 mM $MgCl_2$ and 10 mM Hepes pH 7.5. Sucrose buffer should be prepared the day before using sterile water and should be kept at 4 °C.

4.5) Prepare the dejellying solution freshly on the morning of the experiment by dissolving 2 % L-cystein in 0.25x MMR. Adjust pH to 7.8 with 5 N KOH. Keep at 4 °C until it is used.

5. Protocol for interphasic *Xenopus laevis* egg extract

5.1) Inject 120 I.E. pregnant mare's serum gonadotropin (PMSG) into the dorsal lymph sac of each frog 3-10 days before the experiment (5 ml syringes, 27G ¾'' needles).

NOTE: This injection will induce ovulation. The amount of eggs one frog lays varies a lot. A well laying frog might produce eggs occupying a volume of up to 7 ml after being de-jellynated which corresponds to up to 3.5 ml of crude extract. However, consider that some frogs might not lay or will lay bad eggs.

5.2) Inject 500 I.E. human chorionic gonadotropin (hCG) per frog the evening before the experiment (5 ml syringes, 27G ¾'' needles). This will induce the release of the eggs. Keep the frogs for 13-17 h at 18 °C in individual tanks containing 1.2 l 1x MMR (pH 8).

5.3) Collect the eggs by pouring them into 600-1000 ml glass beakers.

NOTE:Take only the good batches of eggs that are individually laid, similar in size and clearly pigmented with a dark and a light colored half. Do not take eggs that form strings or that look puffy and white. These should be sorted out throughout the whole procedure using a plastic Pasteur pipette. For a detailed description of good versus bad eggs see Gillespie *et al*[6].

5.4) Wash eggs intensively, approximately 4 times, with 1x MMR by decanting the supernatant when the eggs have settled down and refilling the beaker with fresh buffer afterwards. NOTE: The eggs are stable before they are dejellynated and the washing buffer can be directly applied on the eggs.

5.5) Dejellynate the eggs by incubation in the 2 % cystein solution. Change buffer once after 2-4 min by decanting the buffer and carefully filling the beaker with fresh buffer. Consider dejellying complete when the volume of the eggs drastically decreases and the eggs become more densely packed. NOTE: The dejellying needs approximately 5-7 min and should be stopped when visible but latest after 10 min.

5.6) Wash eggs approximately 4 times with 1x MMR by decanting and refilling the buffer supernatant. NOTE: The eggs are more fragile after being dejellynated and, hence, the washing steps need to be done more carefully. The MMR should be rather rinsed on the wall of the beaker instead of directly onto the eggs.

5.7) Activate eggs in 100 ml 1x MMR by adding 8 µl of the calcium ionophore (2 mg/ml in ethanol). Stop activation when animal cap contraction becomes visible or after 10 min.

NOTE: The animal cap contraction can be identified by the compaction of the black half of the egg.

5.8) Wash carefully 4 times with 1x MMR by decanting and refilling the buffer supernatant.

5.9) Incubate eggs for 20 min in 1x MMR at room temperature.

5.10) Prepare the centrifugation tubes during the incubation time: Place 50 µl sucrose buffer, 50 µl 100-fold protease inhibitor mix, 5 µl 1 M DTT , 12.5 µl cycloheximide (to prevent translation, especially of cyclin B) and 2.5 µl cytochalasin B (to prevent actin polymerization) in 5 ml centrifugation tubes (13 x 51 mm). Alternatively, for more than 30 ml of eggs, 14 ml tubes (14 x 95 mm) can be used, in this case increase volumes by 2.4 times.

5.11) Wash the eggs twice with cold sucrose buffer (decant and refill buffer in the glass beaker) and transfer them into centrifugation tubes using a plastic Pasteur pipette with wide opening (cut off the narrow end).

5.12) Pack eggs by spinning for 1 minute at 130 x g. Put the tubes in 15 ml conical centrifuge tubes for this purpose (put the 14 ml tubes in 50 ml conical centrifuge tubes, respectively). The goal is to remove as much buffer as possible to prevent dilution of the extract. After

centrifugation, remove excess of buffer using a plastic Pasteur pipette and eventually fill more eggs on top.

5.13) Spin in a 6 x 5 ml swing rotor for 20 min at 21,000 x g at 4 °C.

5.14) Remove low speed extract using a 5 ml syringe with a 16 G 1 ½'' needle, between yellow yolk on top and dark broken egg debris in the bottom. For this purpose, push the syringe needle through the wall of the centrifuge tube just above the layer of broken egg debris in the bottom. Hold the tube against a resistance when pushing with the needle.

NOTE: A filled 5 ml centrifugation tube gives between 1.8-2.5 ml of extract.

5.15) Per 1 ml of extract add 10 µl 100-fold protease inhibitor mix, 1 µl of 1M DTT, 2.5 µl cycloheximide (20 mg/ml) and 0.5 µl cytochalasin B (10 mg/ml). Keep the extract on ice.

NOTE: The extract can be either used directly for the experiment or aliquoted, snap frozen and stored in liquid nitrogen for several months. Freezing the extract will decrease its activity. For delicate experiments like immunodepletion it is highly recommended to use fresh extract immediately.

6. Preparation of buffers for *in vitro* reconstitution of chromatin decondensation

6.1) Prepare the energy mix stock solution containing 25 mM ATP, 25 mM GTP, 127.5 mg/ml creatine phosphate and 2.5 mg/ml creatine kinase in buffer containing 250 mM sucrose, 1.2 mM Hepes, 5.9 mM KCl and 0.3 mM $MgCl_2$. Aliquot and store at -80 °C. Use freshly after thawing, do not refreeze.

6.2) Dissolve 0.2 g/ml glycogen in deionized water. Store at -20 °C. Dissolve 6-dimethyl aminopurine (DMAP) to a final concentration of 0.25 M in DMSO. Aliquot and store at -20 °C. Use freshly after thawing, do not refreeze.

6.3) Prepare 30 % (w/v) sucrose in PBS, filter and store at 4 °C. Prepare 4 % VikiFix solution containing 80 mM PIPES pH 6.8, 1 mM $MgCl_2$, 150 mM sucrose and 4 % paraformaldehyde (PFA) (**CAUTION!** work under chemical hood, wear gloves and mouth protection).

NOTE: The PFA is difficult to dissolve therefore it is recommended to do it as following: For 1 l Viki-Fix dissolve 24.2 g PIPES and 40 g PFA in separate beakers, both in hot (almost boiling) deionized water. Both will dissolve through addition of 10 N NaOH but be careful to not add too much. Add 51.4 g sucrose and 1 ml 1 M $MgCl_2$ to the PFA solution. Add the PIPES solution to the other mix. Fill up to 1 l final volume and adjust pH to neutral by adding NaOH.

6.4) Dissolve 10 mg/ml 4',6-diamidino-2-phenylindole (DAPI) in water (**CAUTION!** wear gloves). Store in the dark at – 20 °C.

7. Protocol for *in vitro* reconstitution of chromatin decondensation

7.1) Spin low speed interphasic extract for 12 min at 386,000 x g in a fixed angle 20 x 0.2 ml or at 355 000 x g in a 10 x 2.0 ml rotor.

7.2) Gently remove the lipid layer on top using a vacuum pump or pipette and take the supernatant (thereafter called high speed extract) avoiding membrane contamination from the bottom layer and discard the pellet.

NOTE: To reduce possible membrane contamination it is advisable to spin the extract twice or to dilute the extract with 20 % of the volume with sucrose buffer before the centrifugation. However, dilution and additional centrifugation steps can reduce the extract activity.

7.3) Pipet 18 µl of high speed extract into a 1.5 mL reaction tube, add 0.7 µl mitotic cluster (amount can be slightly varied according to chromatin stock concentration), 0.5 µl glycogen, 0.5 µl energy mix and 0.3 µl DMAP. Use tips with wide opening to mix the reaction as soon as the chromatin is added to prevent shearing of the decondensing chromatin.

NOTE: The reaction can be performed in the presence or absence of membranes (see figure 3). To decondense chromatin in the presence of membranes, add 2 µl of floated membranes prepared according to the protocol described by Eisenhardt *et al*. [16].

7.4) Incubate the reaction mixture for up to 2 hrs (or less to study earlier time points of the decondensation process) at 20 °C.

7.5) Fix the sample by adding ice cold 0.5 ml Viki-Fix containing 0.5 % glutaraldehyde and 0.1 mg/ml DAPI and incubation for 20-30 min on ice.

Note: If the samples will be further processed for immunofluorescence, the fixation should be done without glutaraldehyde as this often interferes with the antibody staining. However if only the DAPI staining will be analyzed, the addition of glutaraldehyde will preserve a nicer chromatin structure.

7.6) Incubate round coverslips (diameter 12 mm) for 5 min with poly-L-lysine solution to increase the affinity of the coverslips to chromatin. Dry the coverslips on filter paper afterwards.

7.7) Assemble flat-bottom centrifugation tubes (6 ml, 16/55 mm) by putting the coverslips with the coated site to the top on the bottom of the centrifugation tube. Add 800 µl of the 30 % sucrose cushion and layer the fixed sample on top.

7.8) Spin for 15 min at 2500 x g at 4 °C.

NOTE:The flat-bottom centrifugation tubes fit to rotors that adopt 15 ml conical centrifuge tubes.

7.9) Decant the supernatant, then remove the coverslips from the tubes by poking carefully the bottom of the centrifugation tube with a 16 G 1 ½'' syringe needle. For this purpose tape the lid of the needle and the needle itself together at their bottoms and cut the front end of the lid so that the needle sticks about 3 mm out. When the coverslip is lifted by the needle on one site, use tweezers to remove the coverslip.

7.10) Wash the coverslip quickly by dipping it in deionized water, dry it gently by touching its side to a filter paper and place it on the microscope slide on a drop of mounting media. Seal it with nail polish, dry and keep in dark.

NOTE:Samples fixed without glutaraldehyde can be stored in PBS in a 24-well plate and used further for immunofluorescence staining. If stored for several days, add 0.05 % sodium azide (**CAUTION!** wear gloves) to the PBS to avoid contamination with bacteria.

7.11) Analyze the samples by fluorescence microscopy of the DAPI signal (using e.g. a confocal microscope with a 405 nm laser).

8. Preparation of buffer for immunofluorescence staining of *in vitro* reconstituted chromatin decondensation samples

8.1) Prepare PBS according to 1.1.1. Dissolve NH_4Cl to a final concentration of 50 mM in PBS. Keep this solution at 4 °C. Dissolve 5 µg/ml DAPI in PBS (prepare freshly). Add 0.1 % Triton X-100 to PBS. Keep at 4 °C. Prepare blocking buffer freshly before use by diluting 3 % bovine serum albumin (BSA) in PBS + 0.1 % Triton X-100.

9. Protocol for immunofluorescence staining of *in vitro* reconstituted chromatin decondensation samples

NOTE:All following incubations of the coverslips are made in a 24-well plate with at least 250 µl solution per well, if not stated otherwise. *In vitro* decondensed chromatin samples are more sensitive than fixed cells therefore be careful when adding or removing solutions. It is recommended to use plastic Pasteur pipettes cut angular. For washing steps and secondary antibody incubation place the plate at room temperature on rocking or rotating platform, moving not faster than 100 rpm.

9.1) Quench samples by incubating coverslips with 1ml NH_4Cl in PBS for 5 minutes. Block samples by incubating them with 1ml blocking buffer for at least 30 minutes.

9.2) Assemble a humidity chamber for the incubation with the primary antibody: Put a wet tissue on the bottom of a closable box and the lid of the 24-well plate upside down on top of the wet tissue. Place parafilm into the lid and add 70 µl of the antibody solution per sample on the parafilm. For the antibody solution, dilute antiserum or affinity purified antibodies 1:100 in blocking buffer.

9.3) Place the coverslips upside down on top of the antibody solution and incubate them for one to two hours. Place the coverslips back to the 24-well plate with the sample side facing up

and wash samples three times for 10 min with 1ml 0.1 % Triton X-100 in PBS.

9.4) Incubate coverslips for 1 h at room temperature in 250 µl secondary fluorescent-tagged antibody diluted in blocking buffer to a concentration recommended by the manufacturer. Protect from light. Wash three times for 10 min with 1ml 0.1 % Triton X-100 in PBS.

9.5) Incubate the samples for 10 minutes with 1ml of 5 µg/ml DAPI in PBS. Wash three times for 5 min with 1ml 0.1 % Triton X-100 in PBS.

9.6) Wash the coverslip quickly by dipping it in deionized water, dry it gently by touching its side to a filter paper and place it on the microscope slide on top of a drop of mounting media. Seal it with nail polish, dry and keep at 4 °C in the dark until used. Analyze the samples by fluorescence microscopy.

REPRESENTATIVE RESULTS:

Time dependence of the decondensation reaction

Figure 1 shows a typical time course of the decondensation assay. The cluster of chromosomes visible at the beginning of the reaction decondenses and merges into a single, round and smooth nucleus. When the egg extract is replaced by sucrose buffer the chromosome cluster remains condensed, which suggest that decondensation activity is present in the egg extract.

Chromatin decondensation is an energy dependent process

The *in vitro* decondensation reaction can be conveniently manipulated e.g. by addition of inhibitors. In the experiment shown on figure 2, the non-hydrolyzable ATP or GTP analogs, ATPγS or GTPγS, were added to the reaction. Both inhibit the decondensation showing, that it is an ATP and GTP dependent, active process (figure 2).

Chromatin decondensation and nuclear envelope reformation can be separated

The decondensation assay was performed in the presence or absence of membranes (figure 3). Please note that in both conditions chromatin undergoes decondensation, however addition of membranes results in bigger nuclei. Most probably, reformation of the nuclear envelope induces a secondary decondensation step by yet another mechanism dependent on nuclear transport.

FIGURE LEGENDS

Figure 1: Time course of the *in vitro* decondensation reaction

Mitotic chromatin clusters from HeLa cells were incubated with interphasic *Xenopus* egg extract. Samples were fixed at indicated time points with 4 % PFA and 0.5 % glutaraldehyde, stained with DAPI and analyzed by confocal microscopy. Re-printed from Magalska *et al*. [8]. Scale bar is 5 µm.

Figure 2: Chromatin decondensation requires ATP and GTP hydrolysis

Chromatin decondensation was performed in the presence of 10 mM ATPγS, 10 mM GTPγS or control buffer. Samples were fixed with 4 % PFA and 0.5 % glutaraldehyde at indicated time

points and analyzed by confocal microscopy. Re-printed from Magalska *et al*. [8]. Scale bar is 5 µm.

Figure 3: Chromatin decondensation in the presence and absence of membranes
Chromatin decondensation was performed in the absence (A) or presence (B) of floatation purified membranes for 120 min. Samples were fixed with 4 % PFA and 0.5 % glutaraldehyde and analyzed by confocal microscopy. Chromatin is stained with DAPI, membranes with $DiIC_{18}$ (1,1'-Dioctadecyl-3,3,3',3'-tetramethylindocarbocyanine perchlorate). Scale bar is 5 µm.

DISCUSSION
Xenopus laevis egg extracts are a very useful tool to faithfully reproduce cellular processes *in vitro*, and this system was successfully used in the characterization of cell cycle and cell division events [2,3,5,6,17]. Due to large stores of nuclear components sequestered in the egg during oogenesis, egg extracts are an excellent source of cellular components. Compared to other approaches like RNAi on mammalian tissue cell lines or genetic manipulation, it offers several advantages: The cell-free system allows studying cellular processes in which cellular viability would be otherwise a limitation. Moreover single steps of complex processes can be analyzed in simple assays. The here presented decondensation assay allows studying molecular mechanisms of postmitotic decondensation with no interference from other mitotic events, respectively. *Xenopus* egg extracts are easy to manipulate by depletion of specific proteins and addition of inhibitors or mutated proteins [8]. For example, figure 2 shows the result of adding the non-hydrolyzable ATP or GTP analogs, ATPγS and GTPγS to the decondensation assay. By dilution and differential centrifugation of *Xenopus* eggs components like membranes and cytosol can be separated [16]. Figure 3 shows the decondensation assay performed in the presence or absence of membranes. Finally, the cell-free assay can also be used to identify novel factors e.g. by a fractionation approach. Using such a strategy we have identified the AAA^+-ATPases RubBL1/RuvBL2 as crucial decondensation factors [8].

In vitro systems based on *X. laevis* eggs have been employed with different DNA templates: Forbes *et al.* showed that injection of phage λ DNA into unfertilized *X. laevis* eggs induced the assembly of chromatin on naked phage λ DNA. As injection of viral DNA activated the egg, the assembly of chromatin was followed by formation of a nucleus-like structure [18] and similarly λ-phage DNA can be used in combination with egg extracts to generate nucleus like structures *in vitro* [19]. Magnetic beads coated with DNA have been used to study chromatinization of DNA [20] and recruitment of nuclear membranes [21] as well as assembly of a nuclear envelope and pore complexes [22], although it remains open to which extent this resembled a bona fide nuclear re-assembly process. The protocol presented here allows decondensation of isolated mitotic chromatin clusters from HeLa cells using extract generated from activated *Xenopus* eggs. It thoroughly reconstructs events leading to a reformation of an interphasic nucleus [8]. Compared to the widely applied nuclear assembly reaction used to study the formation of the nuclear envelope and the nuclear pore complexes at the end of mitosis, in the decondensation assay HeLa mitotic chromatin clusters instead of sperm DNA are used. Sperm DNA can be assembled into mitotic chromatin or even individual chromosomes upon incubation with extract prepared from unfertilized and non-activated eggs [3]. We decided to use mitotic clusters as chromatin

source to simplify the procedure and avoid interference from chromatin condensation. In addition, the preparation of the egg extract is slightly modified: For the chromatin decondensation low speed extract cleared by two high speed centrifugation steps in fixed angle rotors are used. Low speed extract can be stored for up to 6 month in liquid nitrogen without losing its activity. In contrast, in the nuclear assembly reactions, cytosol and floated membranes are generated from low speed extracts by dilution and differential high-speed centrifugation before possible freezing (see Eisenhardt *et al.* [16] for a detailed protocol). In our assay system, addition of membranes allows the formation of a closed nuclear envelope including nuclear pore complexes. The resulting nuclei are competent for nuclear import and export [8]. Thus, this system supports both chromatin decondensation and nuclear envelope reformation. Interestingly, chromatin decondensation is also possible in the absence of membranes (figure 3). However addition of membranes results in slightly bigger nuclei. Most likely, the reformation of the nuclear envelope induces a secondary decondensation step by yet undefined mechanisms, which depends on nuclear import.

For the isolation of mitotic chromatin clusters from HeLa cells, a modified version of the protocol established by Gasser and Laemmli [15] was used. Synchronized mitotic cells are lysed in a buffer containing the non-ionic detergent digitonin and by mechanic forces. The chromatin is isolated as clusters that contain all chromosomes from one nucleus. The crucial difference compared to single chromosome isolation protocols is the fact that the cells are not hypotonically swollen but cooled down to 4°C before lysis. This prevents the disconnection of the individual chromosomes [15,23]. Compared to the protocol published by J.R. Paulson [23] who recognized the advantage of the isolation of whole chromatin clusters, Gasser & Laemmli used EDTA-containing polyamine buffers instead of Mg^{2+} based buffers to reduce the activity of kinases, nucleases, proteases and phosphatases and by this decrease the amount of protein and DNA modifications occurring during the isolation process [15]. Additionally, using a colloidal silica particles gradient during differential centrifugation highly reduces cytoplasmic contamination. The protocol can also be used to isolate mitotic chromatin clusters from Chinese hamster ovary and mouse cells [15].

Altogether, our protocol faithfully reconstitutes chromatin decondensation as it happens at the end of mitosis. The ATP dependence of the *in vitro* chromatin decondensation can be at least in part explained by the involvement of RuvBL1/2 but also another AAA^{+}-ATPase, p97, which removes the mitotic kinase Aurora B from the chromatin during mitotic exit [24]. Why the process requires GTP hydrolysis is one of the open questions that we intend to answer using this setup.

ACKNOWLEDGMENTS

This work was supported by the German Research Foundation and the ERC (AN377/3-2 and 309528 CHROMDECON to W.A.) and a PhD Fellowship of the Boehringer Ingelheim Fonds to A.K.S. Figure 1 & 2 are reprinted from Developmental Cell **31**(3), Magalska *et al.*, RuvB-like ATPases function in chromatin decondensation at the end of mitosis, 305-318, 2014, with kind permission from Elsevier.

DISCLOSURES

The authors have nothing to disclose.

REFERENCES

1 Lohka, M. J. & Masui, Y. Formation in vitro of sperm pronuclei and mitotic chromosomes induced by amphibian ooplasmic components. *Science* **220**, 719-721. (1983).

2 de la Barre, A. E., Robert-Nicoud, M. & Dimitrov, S. Assembly of mitotic chromosomes in Xenopus egg extract. *Methods Mol Biol* **119**, 219-229, doi:10.1385/1-59259-681-9:219 (1999).

3 Maresca, T. J. & Heald, R. Methods for studying spindle assembly and chromosome condensation in Xenopus egg extracts. *Methods Mol Biol* **322**, 459-474, doi:10.1007/978-1-59745-000-3_33 (2006).

4 Galy, V. *et al.* A role for gp210 in mitotic nuclear-envelope breakdown. *J Cell Sci* **121**, 317-328, doi: 10.1242/jcs.022525 (2008).

5 Chan, R. C. & Forbes, D. I. In vitro study of nuclear assembly and nuclear import using Xenopus egg extracts. *Methods Mol Biol* **322**, 289-300 (2006).

6 Gillespie, P. J., Gambus, A. & Blow, J. J. Preparation and use of Xenopus egg extracts to study DNA replication and chromatin associated proteins. *Methods* **57**, 203-213, doi:10.1016/j.ymeth.2012.03.029 (2012).

7 Gant, T. M. & Wilson, K. L. Nuclear assembly. *Annu Rev Cell Dev Biol* **13**, 669-695, doi: 10.1146/annurev.cellbio.13.1.669 (1997).

8 Magalska, A. *et al.* RuvB-like ATPases function in chromatin decondensation at the end of mitosis. *Developmental Cell* **31**, 305-318, doi: 10.1016/j.devcel.2014.09.001 (2014).

9 Belmont, A. S. Mitotic chromosome structure and condensation. *Curr Opin Cell Biol* **18**, 632-638,doi: 10.1016/j.ceb.2006.09.007 (2006).

10 Lavoie, B. D., Tuffo, K. M., Oh, S., Koshland, D. & Holm, C. Mitotic chromosome condensation requires Brn1p, the yeast homologue of Barren. *Mol Biol Cell* **11**, 1293-1304, doi: 10.1091/mbc.11.4.1293 (2000).

11 Philpott, A. & Leno, G. H. Nucleoplasmin remodels sperm chromatin in Xenopus egg extracts. *Cell* **69**, 759-767, doi: 10.1016/0092-8674(92)90288-N (1992).

12 Philpott, A., Leno, G. H. & Laskey, R. A. Sperm decondensation in Xenopus egg cytoplasm is mediated by nucleoplasmin. *Cell* **65**, 569-578, doi:10.1016/0092-8674(91)90089-H (1991).

13 Burglin, T. R., Mattaj, I. W., Newmeyer, D. D., Zeller, R. & De Robertis, E. M. Cloning of nucleoplasmin from Xenopus laevis oocytes and analysis of its developmental expression. *Genes Dev* **1**, 97-107, 10.1101/gad.1.1.97 (1987).

14 Whitaker, M. Calcium at fertilization and in early development. *Physiological reviews* **86**, 25-88, doi:10.1152/physrev.00023.2005 (2006).

15 Gasser, S. M. & Laemmli, U. K. Improved methods for the isolation of individual and clustered mitotic chromosomes. *Exp Cell Res* **173**, 85-98, doi:10.1016/0014-4827(87)90334-X (1987).

16 Eisenhardt, N., Schooley, A. & Antonin, W. Xenopus in vitro assays to analyze the function of transmembrane nucleoporins and targeting of inner nuclear membrane proteins. *Methods Cell Biol* **122**, 193-218, doi:10.1016/B978-0-12-417160-2.00009-6

(2014).
17 Wignall, S. M., Deehan, R., Maresca, T. J. & Heald, R. The condensin complex is required for proper spindle assembly and chromosome segregation in Xenopus egg extracts. *J Cell Biol* **161**, 1041-1051, doi:10.1083/jcb.200303185 (2003).
18 Forbes, D. J., Kirschner, M. W. & Newport, J. W. Spontaneous formation of nucleus-like structures around bacteriophage DNA microinjected into Xenopus eggs. *Cell* **34**, 13-23, doi:10.1016/0092-8674(83)90132-0 (1983).
19 Hartl, P., Olson, E., Dang, T. & Forbes, D. J. Nuclear assembly with lambda DNA in fractionated Xenopus egg extracts: an unexpected role for glycogen in formation of a higher order chromatin intermediate. *J Cell Biol* **124**, 235-248 (1994).
20 Sandaltzopoulos, R., Blank, T. & Becker, P. B. Transcriptional repression by nucleosomes but not H1 in reconstituted preblastoderm Drosophila chromatin. *EMBO J* **13**, 373-379 (1994).
21 Ulbert, S., Platani, M., Boue, S. & Mattaj, I. W. Direct membrane protein-DNA interactions required early in nuclear envelope assembly. *J Cell Biol* **173**, 469-476, doi: 10.1083/jcb.200512078(2006).
22 Zhang, C. & Clarke, P. R. Chromatin-independent nuclear envelope assembly induced by Ran GTPase in Xenopus egg extracts. *Science* **288**, 1429-1432, doi: 10.1126/science.288.5470.1429 (2000).
23 Paulson, J. R. Isolation of chromosome clusters from metaphase-arrested HeLa cells. *Chromosoma* **85**, 571-581, doi:10.1007/BF00327351 (1982).
24 Ramadan, K. *et al.* Cdc48/p97 promotes reformation of the nucleus by extracting the kinase Aurora B from chromatin. *Nature* **450**, 1258-1262, doi:10.1038/nature06388 (2007).

Figure 1

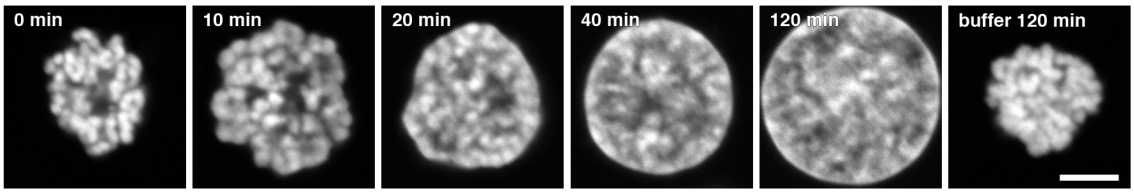

Figure 2

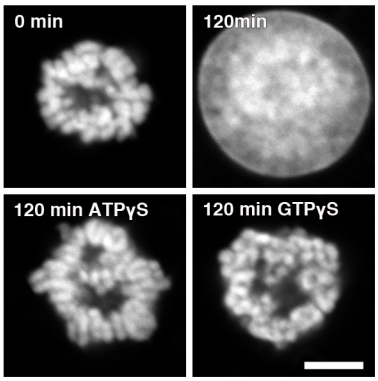

Figure 3

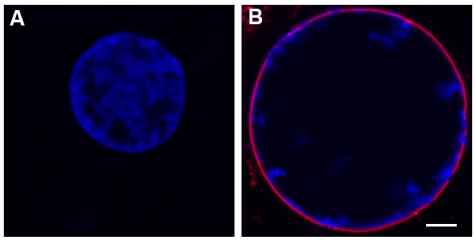

The lysine demethylase LSD1 is required for nuclear envelope formation at the end of mitosis

Allana Schooley, Daniel Moreno-Andrés, Paola De Magistris, Benjamin Vollmer [1], Wolfram Antonin [2]

Friedrich Miescher Laboratory of the Max Planck Society, Spemannstraße 39, 72076 Tübingen, Germany

[1] present address: Oxford Particle Imaging Centre, Division of Structural Biology, Wellcome Trust Centre for Human Genetics, University of Oxford, Oxford OX3 7BN, UK

[2] author for correspondence: wolfram.antonin@tuebingen.mpg.de

Abbreviations List:

aa	amino acid
NPC	nuclear pore complex
Nup	nucleoporin
LSD1	Lysine Specific Demethylase 1
DiIC18	1,1'-Dioctadecyl-3,3,3',3'-Tetramethylindocarbocyanine Perchlorate
DAPI	4′,6-Diamidin-2-phenylindol

Keywords: nuclear envelope formation, nuclear pore complex, mitotic exit, lysine (K)-specific demethylase 1A, KDM1A, histone modification, MEL28, ELYS, POM121, NDC1

JCS Advance Online Article. Posted on 29 July 2015

Abstract

The metazoan nucleus breaks down and reassembles during each cell division. Upon mitotic exit, the successful reestablishment of an interphase nucleus requires the coordinated reorganization of chromatin and formation of a functional nuclear envelope. Here we report that the histone demethylase LSD1 plays a crucial role in nuclear assembly at the end of mitosis. Downregulation of LSD1 in cells extends telophase and impairs nuclear pore complex assembly. *In vitro,* LSD1 demethylase activity is required for the recruitment of MEL28/ELYS and nuclear envelope precursor vesicles to chromatin, crucial steps in nuclear reassembly. Accordingly, the formation of a closed nuclear envelope and nuclear pore complex assembly are impaired upon depletion of LSD1 or inhibition of its activity. Our results identify histone demethylation by LSD1 as a novel regulatory mechanism linking the chromatin state and nuclear envelope formation at the end of mitosis.

Introduction

The nuclear genome is organized and maintained within the two membranes of the nuclear envelope. The envelope itself is a compartment of the endoplasmic reticulum (ER) and the outer nuclear membrane is continuous with the ER network. The inner nuclear membrane contains unique set of integral membrane proteins that connect to chromatin and the nuclear lamina. The exchange of molecules between the cytoplasm and the nucleoplasm is mediated by nuclear pore complexes (NPCs), macromolecular protein assemblies that are found at points of fusion between the inner and outer membranes of the nuclear envelope. In metazoa, the nuclear envelope breaks down during mitosis in order to facilitate the capture of highly condensed chromosomes and their segregation by the spindle apparatus. The complex architecture of the interphasic nucleus must therefore be reestablished upon mitotic exit when the nuclear envelope and pore complexes reassemble on the decondensing chromatin (for review see (Guttinger et al., 2009; Schooley et al., 2012).

Phosphorylation cascades regulate the structural changes to nuclear organization that occur during mitosis, including massive chromatin condensation and nuclear envelope disassembly. At the onset of mitosis, the phosphorylation of lamins (Heald and McKeon, 1990; Peter et al., 1990) and inner nuclear membrane proteins (Foisner and Gerace, 1993; Pyrpasopoulou et al., 1996) initiates the disassembly of the nuclear envelope. The reestablishment of the interphase nucleus at the end of mitosis is coordinated by the reversal of mitotic phosphorylation events

due to the inactivation of mitotic kinases and the activation of phosphatases (Wurzenberger and Gerlich, 2011). Dephosphorylation of lamins enables the reassembly of the nuclear lamina (Thompson et al., 1997). Meanwhile dephosphorylation of inner nuclear membrane proteins increases their affinity for chromatin and initiates nuclear membrane recruitment (Pfaller et al., 1991; Ito et al., 2007) and nuclear envelope formation.

Upon nuclear disassembly, the nuclear membranes are absorbed in the mitotic ER and it is currently unclear whether they maintain their identity as a distinct subcompartment within the network during mitosis. Experiments in *Xenopus laevis* egg extracts, which have been used extensively to study nuclear envelope and NPC assembly in cell free systems (Gant and Wilson, 1997), suggest that indeed they do. The ER derived from egg extract preparations gives rise to distinct vesicle populations that possess different capacities to support nuclear envelope formation. One such population is enriched for the transmembrane nucleoporins POM121 and NDC1, has a high affinity for chromatin, and is part of the initial wave of nuclear membrane recruitment to chromatin during cell-free nuclear assembly (Antonin et al., 2005; Mansfeld et al., 2006). A second vesicle population has a lower affinity for chromatin, is recruited relatively late during nuclear assembly, and is enriched for a third transmembrane nucleoporin, GP210. These distinct vesicle types can also be biochemically separated from a third vesicle pool enriched for typical ER-membrane proteins, which are not strictly essential for nuclear assembly. The physical and functional separation of nuclear membrane vesicle populations implies the existence of microscale partitioning of different membrane domains in the mitotic ER. At the end of mitosis, nuclear membranes segregate from the bulk ER and enclose the decondensing chromatin to form a new nuclear envelope. Chromatin binding by integral inner nuclear membrane proteins is thought to be a crucial determinant in this process (Ulbert et al., 2006; Anderson et al., 2009).

Concomitant with the formation of the nuclear envelope and thus the establishment of a diffusion barrier between the cytoplasm and the nuclear interior, NPCs re-assemble to ensure its transport competence (Bodoor et al., 1999; Daigle et al., 2001). Post-mitotic NPC assembly is initiated by the recruitment of a subset of nucleoporins to chromatin and is particularly well characterized due to the faithful reconstitution of these events in *Xenopus* egg extracts. The chromatin binding nucleoporin MEL28/ELYS initiates NPC assembly by recruiting the Nup107-160 complex, a major structural component of the NPC (Harel et al., 2003; Walther et al., 2003b; Rasala et al., 2006; Franz et al., 2007; Gillespie et al., 2007; Rasala et al., 2008; Rotem et al., 2009). Membranes are next connected to the assembling

NPC due to interactions between the transmembrane nucleoporin POM121 and the Nup107-160 complex (Antonin et al., 2005; Mitchell et al., 2010; Yavuz et al., 2010). NDC1 is also likely to be involved at this step (Mansfeld et al., 2006; Stavru et al., 2006) but its function is less defined. Components of the second major structural subunit of the NPC, the Nup93 complex, subsequently assemble stepwise from the membrane building laterally towards the center of the NPC (Dultz et al., 2008; Sachdev et al., 2012; Vollmer et al., 2012), which allows for the recruitment of the central channel components, the FG-nucleoporins. The final steps of NPC assembly are the addition of peripheral nucleoporins, which form extensions to the cytoplasmic and nucleoplasmic sides of the pore (Bodoor et al., 1999; Hase and Cordes, 2003; Dultz et al., 2008). The small GTPase ran spatially regulates NPC reassembly by promoting the release of transport receptor bound proteins, such as MEL28/ELYS (Franz et al., 2007; Rotem et al., 2009), at post-mitotic chromatin (Walther et al., 2003a). Several nucleoporins are also hyper-phosphorylated during mitosis (Laurell et al., 2011) but the extent to which their dephosphorylation regulates post-mitotic NPC formation is currently not clear.

Although the crucial events of post-mitotic nuclear envelope assembly occur on decondensing chromatin, the regulatory mechanisms that coordinate envelope assembly and the chromatin state at that time are not well understood. Here we identify dynamic demethylation of histone H3 by the Lysine (K) Specific Demethylase, LSD1 (also known as KDM1A), as a novel mechanism coordinating the recruitment and assembly of nuclear envelope and NPC components on post-mitotic chromatin. We report that the loss of LSD1 demethylase activity blocks nuclear envelope and pore complex formation *in vitro*, via impaired recruitment of MEL28/ELYS and POM121/NDC1-containing membrane vesicles. We find that downregulation of LSD1 in human cells elongates telophase and results in ectopic NPC assembly outside of the nuclear envelope. Our data implicate LSD1-dependent demethylation of histones as a requirement for proper nuclear assembly at the end of mitosis.

Results

LSD1 demethylase activity is required for cell-free nuclear assembly

In an effort to identify regulatory landmarks of nuclear envelope reassembly at the end of mitosis we screened various classes of chemical inhibitors for their ability to block nuclear assembly *in vitro*. Cell-free nuclear formation can be faithfully recapitulated on a sperm chromatin template using the cytosolic and membrane fractions of *Xenopus laevis* egg

extracts induced to mimic the late mitotic state (for review see (Gant and Wilson, 1997)). After initial DNA decondensation, a nuclear envelope forms around the chromatin, which continues to decondense and reorganize, giving rise to a functionally competent nucleus. A closed nuclear envelope can be visualized by the smooth nuclear rim incorporation of a fluorescent lipophilic membrane dye, DiIC18 (1,1'-Dioctadecyl-3,3,3',3'-Tetramethylindocarbocyanine Perchlorate) (Fig. 1, untreated). NPCs are integrated in the newly formed envelope and can be observed by immuno-labelling with mAB414, an antibody that recognizes a subset of FG-containing nucleoporins (Davis and Blobel, 1986). We identified a group of inhibitors (*N*-Methyl-*N*-propargylbenzylamine (pargyline), *trans*-2-Phenylcyclopropylamine (2-PCPA), and the 2-PCPA derivative trans-2-(2-benzyloxy-3,5-difluorophenyl)cyclopropylamine hydrochloride (S2101)) targeting the histone lysine demethylase LSD1 that severely impairs nuclear envelope and NPC assembly (Fig. 1).

In order to determine whether LSD1 specifically plays a role in nuclear assembly it was immuno-depleted from *Xenopus* egg extract cytosol using a polyclonal antibody generated against full-length *Xenopus* LSD1 that recognizes both the *Xenopus* and human protein (Fig. S1). LSD1 was efficiently removed from the egg cytosol while the levels of other proteins including the nucleoporins Nup107, Nup62 and MEL28/ELYS, the nuclear GTPase ran, which is important for nuclear transport, and CoREST, which functions as an LSD1 cofactor in H3K4 demethylation (Shi et al., 2005), were unaffected (Fig. 2A). LSD1 depletion rendered the extracts incompetent for nuclear envelope and NPC assembly (Fig. 2B,C). Addition of purified recombinant *Xenopus* LSD1 rescued the formation of a closed nuclear envelope and integrated NPCs, validating the specificity of the depletion phenotype and confirming the requirement for LSD1 in nuclear assembly. We designed a demethylase-deficient version of LSD1 by mutating a lysine residue in the FAD binding pocket, based on structural and functional studies of the human homolog (Stavropoulos et al., 2006). This catalytically inactive LSD1 mutant (a lysine to alanine exchanged in position 643, LSD1 K643A) failed to rescue the nuclear assembly defect (Fig. 2B,C), indicating that the demethylase activity of LSD1 is crucial for nuclear envelope and NPC assembly.

Loss of LSD1 in human cells extends telophase and promotes the formation of annulate lamellae

We performed immunofluorescence experiments in HeLa cells and found that LSD1 localized to the nucleus during interphase but was largely excluded from chromatin during mitosis (Fig. S2). It could first be seen re-associating with chromatin early in telophase coincident with NPC formation, which was detected by mAB414 staining (Fig. S2A, B) and prior to abscission, which was visualized by the loss of midbody-associated α-tubulin between the segregated chromatin masses (Fig. S2C) (Guizetti et al., 2011). To assay the importance of LSD1 during mitotic exit in cells we employed RNAi and followed mitotic events by live cell imaging. LSD1 was efficiently depleted by siRNA for up to 72h in HeLa cells stably expressing histone H2B fused to a mCherry reporter (Fig. 3A, S3A). Cells were imaged over approximately 20h by time-lapse fluorescence microscopy and chromatin features annotated and tracked during mitotic events using the image analysis software CellCognition (Schmitz and Gerlich, 2009; Held et al., 2010). Based on the morphological annotation of chromatin, LSD1-depleted cells displayed a robust extension in the length of telophase (Fig. 3B). In the absence of LSD1, cells maintained condensed telophasic chromatin 10-15 minutes beyond control cells, which spent an average of 18 minutes in telophase. Accordingly, the progressive decrease in chromatin density that occurs upon mitotic exit, based on the average fluorescence intensity of the H2B-mCherry signal, was delayed and incomplete in LSD1-depleted cells compared to controls (Fig. 3C). This extended duration of chromatin compaction following chromosome segregation could be clearly visualized in individual mitotic tracks (Fig. 3D). Although one LSD1-targeting siRNA significantly extended the duration of metaphase, the timing of other cell cycle stages was not affected by LSD1 depletion (Fig. S3B, S3G) and a longer metaphase was not a prerequisite for extended chromatin compaction after anaphase (For example, Fig. 3D). In order to confirm that mitotic exit is delayed in the absence of LSD1, mitotic spindle dynamics were tracked in live cells stably expressing EGFP-tagged α-tubulin and mCherry-H2B. In addition to prolonged telophasic chromatin features (Fig. S3E, F), LSD1-depleted cells maintained midbody-associated tubulin on average 15-30 minutes longer than controls, indicating that abscission, the final step in cytokinesis, was delayed (Fig. S3I). Taken together, these data suggest that the role of LSD1 during mitosis is specific to the events occurring in telophase. Consistent with this, addition of the LSD1-targeting inhibitors 2-PCPA and S2101 to HeLa cells similarly prolonged telophase (Fig. S4A, B).

In addition to extended telophase, the average nuclear volume in unsynchronized populations of LSD1-knockdown cells was significantly reduced compared to control populations (Fig. 4A, S3C). This observation suggests that LSD1 depletion has a lasting effect on chromatin compaction during interphase. In order to further investigate the impact of LSD1 knockdown on nuclear architecture in interphasic cells we employed immunofluorescent labeling of various nuclear envelope and NPC proteins. Labeling with mAB414 revealed that in addition to NPCs in the nuclear envelope, LSD1-depleted cells (Fig. 4B) or cells treated with chemical inhibitors of LSD1 (Fig. S4C) possessed significant cytoplasmic staining for NPCs indicative of annulate lamellae. These arrays of NPCs inserted into membrane stacks of the endoplasmic reticulum (Kessel, 1992) have been found to form when post-mitotic NPC assembly is impaired (Franz et al., 2007). We counted NPCs, based on the mAB414 signal, and found a reduction in their total number at the nuclear envelope when LSD1 was depleted, although NPC density was unaffected (Fig. 4C, D).

Despite the reduction in nuclear volume and the number of NPCs at the nuclear envelope, LSD1 depleted cells were not defective in nuclear lamina assembly, evidenced by the smooth rim staining of lamins A and B (Fig. 4E). Similarly, the inner nuclear envelope proteins lamin B receptor (LBR) and emerin did not seem to be affected by LSD1 knockdown and were found at the nuclear envelope. The nucleoporins Nup62, of the central channel; Nup153, from the nucleoplasmic NPC face; and Nup88, from the cytoplasmic face of the NPC, were all found at the nuclear rim in LSD1 depleted cells. Furthermore, MEL28/ELYS, required for the initial seeding of NPC assembly on post-mitotic chromatin, and POM121, a transmembrane nucleoporin, could also be detected at the nuclear envelopes of LSD1 depleted nuclei.

Taken together, these data suggest that at the end of mitosis LSD1 is required to reestablish interphasic nuclear architecture that is conducive to nuclear expansion and NPC assembly.

LSD1 is not essential for chromatin decondensation

Nuclear reformation at the end of mitosis involves the almost simultaneous decondensation of highly compacted mitotic chromatin and assembly of a closed NPC-containing nuclear envelope (Schooley et al., 2012). Although difficult to functionally discern in a cellular context, these two integral mitotic exit processes can be biochemically separated *in vitro*. Given the apparent compaction of chromatin in both cell-free nuclear assemblies (Fig. 1A,

2B) and in HeLa cells (Fig. 3C, D) when its function was impaired, we wondered whether LSD1 had a direct role in chromatin decondensation.

The initial decondensation of sperm chromatin, the DNA template employed in our cell-free nuclear assembly assays (Fig. 1,2), in *Xenopus* egg extracts occurs due to the exchange of sperm specific protamines by the maternal histones H3 and H4 (Philpott and Leno, 1992). We tested whether this specialized decondensation event requires LSD1 by incubating sperm chromatin in egg extracts lacking membranes and an energy regenerating system for 10 minutes. Under these conditions, histone exchange occurs and results in sperm chromatin decondensation (Fig. 5A, compare buffer to untreated extract) but nuclear assembly cannot proceed. Depletion of LSD1 did not affect sperm chromatin decondensation (Fig. 5A). Thus, the block in cell-free nuclear assembly in the absence of LSD1 activity (Fig. 1,2) is not due to a defect in sperm DNA de-compaction.

Sperm DNA decondensation is mechanistically distinct from the decondensation of highly compacted chromatin at the end of mitosis and we have recently established a cell-free assay to specifically analyze the latter process (Magalska et al., 2014). To this end, we examined changes to the topology of mitotic chromatin clusters isolated from HeLa cells when incubated with *Xenopus* egg extracts. In this modified version of the nuclear assembly assay, the highly condensed mitotic chromatin has been found to progressively decondense in a way that is morphologically analogous to the chromatin of cells exiting mitosis. These structural changes can be quantified based on the smoothness of the chromatin boundary and the homogeneity of DAPI staining, both increasing over time as chromatin decondenses. In the absence of membranes, depletion of LSD1 from the egg extracts had an apparently modest effect on chromatin decondensation, which was not quantifiably different based of the parameters described (Fig. 5B).

In the presence of membranes, mitotic chromatin clusters not only decondense but also support the formation of a closed nuclear envelope containing NPCs, which are competent for nuclear import (Magalska et al., 2014). Accordingly, the addition of membranes to the extracts results in larger nuclei that accommodate further chromatin decondensation (Philpott et al., 1991; Wright, 1999) also known as secondary decondensation or nuclear swelling (Fig. 5C and S4D, mock and untreated). However, when LSD1 activity was blocked by the addition of chemical inhibitors or its specific immuno-depletion, minimal membrane recruitment occurred and chromatin did not undergo any additional decondensation. Consistent with the nuclear assembly assay on sperm chromatin (Fig. 1,2), blocking LSD1 activity impaired

nuclear envelope formation on the HeLa chromatin substrate. These data suggest that LSD1 is not required for chromatin decondensation, at least the steps that occur *in vitro* in the absence of a closed nuclear envelope, but rather to render post-mitotic chromatin competent for the recruitment and assembly of nuclear envelope components.

LSD1 demethylase activity mediates the recruitment of nuclear envelope membranes and MEL28/ELYS to chromatin *in vitro*

To confirm that LSD1 plays a role in the recruitment of nuclear envelope membranes to chromatin we employed DNA-coated magnetic beads (Heald et al., 1996). DNA was chromatinized by incubation with *Xenopus* egg extract cytosol and incubated with the same floated membrane fractions used in cell-free nuclear assembly reactions. Chromatinization resulted in the appearance of chromatin binding proteins, including Ku70 and LSD1 (Fig. 6A), on the DNA beads. The membranes isolated from egg extracts are a mixture of different nuclear envelope precursor and ER vesicles. These include the early chromatin-binding fraction containing POM121 and NDC1, the late chromatin-binding fraction containing GP210, and a bulk ER vesicle population containing, among many other proteins, reticulon 4 (RTN4) and Calnexin. Each of these membrane proteins was recruited to DNA beads chromatinized in mock-treated cytosol. However, when DNA was chromatinized in LSD1-depleted cytosol, we observed a significant reduction in the recruitment of POM121/NDC1-containing vesicles (to 26% or 41%, respectively, Fig. 6B). The recruitment of both GP210 and ER marker-containing vesicles (RTN4 and Calnexin) was unaffected by LSD1 depletion, suggesting that membrane recruitment was not generally affected. Addition of recombinant wildtype LSD1 but not the demethylase deficient K643A mutant to LSD1-depleted extracts rescued the recruitment of POM121 and NDC1. Importantly, binding of MEL28/ELYS, which is required for initiation of NPC assembly on the decondensing chromatin, was also reduced upon LSD1 depletion (to 50%) and rescued by the recombinant wild type protein. The levels of dimethylated H3K4 were elevated by more than two-fold upon LSD1 depletion or addback of the catalytically dead K643A mutant, validating H3K4me2 as an LSD1 substrate in *Xenopus* egg extracts and on chromatinized DNA beads. Consistent with reduced recruitment to DNA beads, nuclei assembled *in vitro* on sperm chromatin in the absence of functional LSD1 lack MEL28/ELYS, POM121 and NDC1 (Fig. 6C). These data indicate that the efficient recruitment of both MEL28/ELYS and POM121/NDC1-containing nuclear envelope precursor vesicles to chromatin is dependent on LSD1 activity and suggest that

LSD1 may function in nuclear assembly by regulating the chromatin dependent recruitment of nuclear envelope and pore complex proteins at the end of mitosis.

Discussion

The restoration of interphasic nuclear architecture at the end of mitosis requires massive reorganization of the condensed mitotic chromatin and the coordinated reassembly of a functional nuclear envelope. We have found that the catalytic activity of LSD1 plays a crucial role in nuclear formation on post-mitotic chromatin. Interfering with the function of LSD1 either by inhibition or by depletion inhibits cell-free nuclear assembly by blocking chromatin recruitment of MEL28/ELYS and POM121/NDC1-containing membranes. In human cells, reduction of LSD1 by RNAi-mediated depletion severely extends telophase and results in significantly smaller nuclei as well as ectopic NPC formation in the cytoplasm. Our data suggest that in addition to dephosphorylation events and the action of the small GTPase ran (Hetzer et al., 2002), histone demethylation plays a crucial role in post-mitotic nuclear envelope and pore complex formation.

Mitotic histone modifications are critical both for memorizing the interphasic transcriptional state of the chromatin (for review see (Moazed, 2011; Wang and Higgins, 2013) and for chromosome segregation during anaphase (Kawashima et al., 2010; Yamagishi et al., 2010). The most prominent of these modifications is the phosphorylation of Histone H3 at T3, T11, S10, and S28 by the kinases Aurora B and Haspin. These marks are removed during mitotic exit by the phosphatase PP1, which is recruited to anaphase chromatin by its targeting cofactor RepoMan/CDCA2 (Trinkle-Mulcahy et al., 2006) and mKI67 (Booth et al., 2014; Takagi et al., 2014). Although it was recently proposed to be upstream of a histone modification cascade that promotes mitotic chromosome condensation (Wilkins et al., 2014), phosphorylation of histone H3 at S10 is dispensable for chromosome condensation (Hsu et al., 2000; MacCallum et al., 2002) and to date there is no evidence to suggest that the reversal of histone phosphorylation events are specifically required for chromatin decondensation at the end of mitosis (Magalska et al., 2014). Instead, chromatin remodeling downstream of histone dephosphorylation has been linked to nuclear envelope assembly by promoting the recruitment of LBR via heterochromatin protein 1β (HP1β) (Ye et al., 1997; Haraguchi et al., 2000; Fischle et al., 2005) and importin β-bound nucleoporins via RepoMan (Vagnarelli et al.,

2011). The results presented here indicate that demethylation of histone H3 plays a comparable role in the regulation of nuclear reassembly.

Our data suggest that LSD1-mediated demethylation is required for the recruitment of MEL28/ELYS and nuclear envelope precursor vesicles, enriched for POM121 and NDC1, to chromatin *in vitro*. In the absence of LSD1, MEL28/ELYS and POM121/NDC1-containing vesicles were not efficiently recruited to chromatinized DNA beads nor were they found on sperm chromatin in 2h nuclear assembly reactions. These defects were rescued by the addition of recombinant catalytically active LSD1 (Fig. 6). Both MEL28/ELYS and POM121/NDC1 vesicles are crucial for NPC assembly (Antonin et al., 2005; Mansfeld et al., 2006; Franz et al., 2007). During mitosis, MEL28/ELYS is localized to kinetochores (Rasala et al., 2006). Although it is considered the seeding point for NPC assembly on chromatin (Franz et al., 2007; Gillespie et al., 2007), the precise mechanism governing the redistribution of MEL28/ELYS on post-mitotic chromatin is currently unknown. Our data suggest that the proper localization of MEL28/ELYS at the end of mitosis depends on changes to chromatin that occur downstream of LSD1 activity. As the recruitment of POM121/NDC1-containing vesicles to chromatin during nuclear assembly relies on the presence of MEL28/ELYS (Rasala et al., 2008), it is likely that the block in nuclear envelope precursor vesicle recruitment we observe occurs, at least partially, upstream of MEL28/ELYS. However, nuclear envelope precursor vesicles crucial to *in vitro* nuclear assembly, including POM121-containing vesicles, have been found to bind DNA in the absence of MEL28/ELYS (Ulbert et al., 2006). Furthermore, a soluble fragment of POM121 can competitively block nuclear assembly *in vitro* without disrupting the recruitment of MEL28/ELYS, and in turn the Nup107-160 complex, due to distinct binding sites on chromatin (Shaulov et al., 2011). Finally, nuclei assembled in the absence of MEL28/ELYS form pore-free albeit closed nuclear envelopes (Franz et al., 2007), which we did not observe upon LSD1 depletion. Taken together, the nuclear assembly defect we observe in the absence of LSD1 activity is most likely the result of a block in the recruitment of multiple factors that interact independently with chromatin in the early stages of mitotic exit.

Reduction of LSD1 by RNAi significantly extended telophase in HeLa cells. The interphasic nuclei were significantly smaller and we observed a reduction in the total number of NPCs assembled at the nuclear envelope. Because NPC density was not affected by the loss of LSD1 (Fig. 4D), we cannot be certain whether the smaller LSD1-depleted nuclei are specifically defective for NPC formation or rather for nuclear envelope membrane expansion.

However, substantial annulate lamellae formation, ectopic NPC assembly in the cytoplasm, was also found in LSD1 knockdown cells. Annulate lamellae are typically observed when interfering with NPC re-assembly at the end of mitosis, for example upon MEL28/ELYS depletion (Walther et al., 2003b; Franz et al., 2007), suggesting that LSD1 activity may be upstream of NPC assembly on chromatin. The relatively modest effect on nuclear envelope assembly in cells could be explained by a lower efficiency of LSD1 depletion compared to the *in vitro* experiments. Although we observed a similar phenotype upon chemical blockade of LSD1 activity (Fig S4A-C), these experiments are difficult to interpret because of predominant cell mortality at the effective concentrations. Alternatively, the role of LSD1-mediated demethylation in post-mitotic nuclear assembly might be partially redundant in HeLa cells. Chemical blockade of LSD1 activity has been found to preferentially inhibit the growth of pluripotent cell types in culture while having very little impact on the growth rate of HeLa cells (Wang et al., 2011).

The *in vitro* assays employed in our study allowed us to separately query the role of LSD1 in chromatin decondensation and nuclear envelope assembly, events that occur simultaneously in cells. Sperm chromatin-specific decondensation, an event that occurs immediately after fertilization due to the nucleoplasmin dependent exchange of sperm protamines for maternal histones (Philpott et al., 1991), was not hindered in LSD1 depleted extracts (Fig. 5A). In uninhibited extracts, decondensed sperm chromatin is the substrate for the assembly of a closed nuclear envelope containing NPCs. Once a functional envelope has formed, the import of nuclear proteins leads to an increase in nuclear volume, a process that is also referred to as nuclear swelling/expansion or secondary decondensation (Philpott et al., 1991; Wright, 1999). A loss of LSD1 activity, either by immuno-depletion or chemical inhibition, blocked nuclear envelope and pore complex formation on the sperm chromatin. In the absence of nuclear envelope formation and the establishment of nuclear import, secondary decondensation could not occur and thus the nuclei assembled appeared small and condensed (Fig. 1,2). Nevertheless, this should be not misinterpreted as defect in chromatin decondensation. Similarly, blocking LSD1 activity did not significantly impair the decondensation of mitotic chromatin clusters from HeLa cells in the absence of membranes (Fig. 5B, S4D top panel). Upon addition of membranes, extracts in which LSD1 activity was removed or blocked gave rise to strikingly smaller nuclei compared to relevant controls (Fig. 5C, S4D bottom panels). This size discrepancy can be attributed to a loss of secondary decondensation in the absence of a closed and functional nuclear envelope when LSD1 activity is blocked. Our data therefore indicate that chromatin decondensation *per se* is not dependent on LSD1.

Nonetheless, loss of LSD1 activity resulted in smaller nuclei in both our membrane-free decondensation assay (Fig. 5B, S4D) and in HeLa cells (Fig. 4A, S3C, S4C), suggesting that LSD1 may play a role in reestablishing interphasic chromatin organization at the end of mitosis. Considering its impact on nuclear envelope formation, we postulate that LSD1 is required to generate post-mitotic chromatin that is competent for proper nuclear envelope and NPC assembly.

LSD1 is a nuclear amine oxidase that catalyzes the FAD-dependent demethylation of histone H3 at lysines 4 and 9 (Shi et al., 2004; Forneris et al., 2005; Shi et al., 2005). It acts mainly as a transcriptional repressor (Shi et al., 2004; Lee et al., 2005; Shi et al., 2005) by demethylating H3K4me2, a mark of active transcription (reviewed in (Black et al., 2012)). However, it has also been found to demethylate repressive H3K9me2 marks and activate the ligand dependent transcription of androgen receptor-responsive genes (Metzger et al., 2005; Wissmann et al., 2007). Importantly, demethylation of histone H3 by LSD1 is locus specific, although the mechanistic details governing this specificity are currently unknown. Consistent with its repressive role, LSD1 has been implicated in heterochromatin formation and maintenance in *drosophila* and *S. pombe* (Lan et al., 2007; Rudolph et al., 2007).

In the context of mitotic exit, it is not clear how LSD1 dependent demethylation primes chromatin for nuclear envelope assembly and this will be an interesting avenue for future research. Because the catalytic activity of LSD1 and not simply its presence on the chromatin was required for cell-free nuclear assembly (Fig. 2), it is unlikely that LSD1 itself acts as a scaffold for the recruitment of nuclear envelope proteins at the end of mitosis. Instead, LSD1-mediated demethylation might result in an accumulation of specific histone marks that facilitate the recruitment and assembly of envelope components. Indeed, we observed a two-fold increase in dimethylated H3K4 upon LSD1 depletion or re-addition of the catalytically inactive mutant on chromatin beads (Fig. 6A, B). However, the contribution of other histone modifications such as methylated H3K9, another LSD1 target, should not be excluded. It is equally possible that in modulating chromatin organization downstream of histone H3 demethylation, either globally or at the chromatin surface, LSD1 promotes a state of chromatin that is competent for nuclear envelope assembly. Finally, LSD1 has been found to demethylate other chromatin-associated proteins including p53 and DNMT1 (Huang et al., 2007; Wang et al., 2009) and it is certainly possible that its role in nuclear envelope assembly is due to demethylation of non-histone substrates.

LSD1 was previously found to localize to the mitotic spindle and to function in chromosome segregation in dividing HeLa cells (Lv et al., 2010). In our live cell imaging experiments, we observed a tendency towards extended metaphase in LSD1-depleted cells (Fig. S3B, S3G), which could be indicative of spindle-related defects in chromosome alignment. However we did not observe a significant increase in the number of lagging chromosomes or chromosome bridges in the siRNA treated cells (data not shown). We found that LSD1 was excluded from chromatin starting at prometaphase and re-associated with chromatin during telophase, concomitant with mAB414 staining and, presumably, nuclear envelope formation but prior to abscission (Fig. S2). A similar dissociation of LSD1 from mitotic chromatin has also been observed in mouse embryonic stem cells (Nair et al., 2012). LSD1 is phosphorylated during mitosis (Lv et al., 2010), and it is possible that this phosphorylation controls its association with chromatin. Alternatively, dynamic histone modifications could be responsible for the cell-cycle dependent localization of LSD1. For example, phosphorylation of histone H3 at serine 10, blocks the binding of LSD1 to a synthetic H3 peptide *in vitro* (Forneris et al., 2005).

The mitotic dependent dissociation of LSD1 from chromatin modulates rapid gene expression changes in embryonic stem cells (Nair et al., 2012). LSD1 has also been found to maintain both the undifferentiated state and proliferative capacity of pluripotent cells, which express relatively high levels of LSD1 (Sun et al., 2010; Adamo et al., 2011; Yang et al., 2011; Nair et al., 2012). Here we have identified a new transcription-independent role for LSD1 in the reestablishment of nuclear architecture following mitotic cell division. Whether the capacity for LSD1 to support nuclear envelope formation on post-mitotic chromatin plays a role in cancer, particularly in cancer stem cells where its expression is frequently mis-regulated (reviewed in (Amente et al., 2013), remains a question for future research.

Materials and Methods

Antibodies and chemicals

The following commercial antibodies were used for immunofluorescence in HeLa cells: LSD1 (abcam, ab17721), α-tubulin (Sigma, T6199), Nup62 (BD Biosciences, 610498), Nup153 (abcam, SA1, ab96462), Nup88 (BD Biosciences, 611896), Lamin A (abcam, ab26300), Lamin B2 (EPR9701(B), abcam, ab151735), Lamin B receptor (Epitomics, 1398-1), and Emerin (Sigma, HPA000609). The human MEL28/ELYS (Franz et al., 2007) and

POM121 (Mansfeld et al., 2006) antibodies were kind gifts from Iain Mattaj and Ulrike Kutay, respectively. mAB414 (Covance, MMS-120R) was used for immunofluorescence in HeLa cells and on *in vitro* assembled nuclei. With the exception of the mAB414 (used to detect Nup62), Ku70 (H3H10, abcam, ab3114) and CoREST (Millipore, 07-455) antibodies, which were employed for western blotting, antibodies raised against *Xenopus* proteins were employed in immunoblotting and immunofluorescence in *Xenopus* egg extract-based assays. Antibodies against *Xenopus laevis* GP210 (Antonin et al., 2005), NDC1 (Mansfeld et al., 2006), POM121 and RTN4 (Vollmer et al., 2015) have been described previously. For the MEL28/ELYS antibody, a construct comprising aa2290-2408 was expressed from a pET28a vector and used for antibody production in rabbits. The same was done for Calnexin, using a construct comprising aa 516-606. The *Xenopus* LSD1 antibody was generated in rabbits using full-length LSD1 expressed from a pET28a vector and used 1:1000 as serum for Western blotting both in Xenopus egg and HeLa cell extracts and 1:100 for immunofluorescence on *in vitro* assembled nuclei. For affinity purification of the antiserum in order to generate affinity resins for depletion experiments (see below) recombinant LSD1 was coupled to Affigel 10 (Biorad).

The LSD1 inhibitors Pargyline-HCL (Sigma), 2PCPA-H_2SO_4 (BPS Bioscience), and S2101 (Calbiochem) were diluted in water and stored at -20°C prior to use. DiIC18 and secondary antibodies (Alexa Fluor 488 goat α-rabbit IgG and Cy3 goat α-mouse IgG) were obtained from Invitrogen.

Protein expression and purification

The construct for *Xenopus laevis* LSD1 (gene bank accession number KR078281) was generated from synthetic DNA optimized for codon usage in *E. coli* (Geneart). The K643A mutant was generated by mutagenesis using the QuikChange site-directed mutagenesis kit (Agilent). Sequences were cloned into a modified pET28a vector containing a N-terminal yeast SUMO solubility tag followed by a TEV cleavage site. Proteins were expressed in *E. coli* and purified by Ni-affinity chromatography. His6- and SUMO-tags were cleaved using tabacco etch virus (TEV) protease and proteins were concentrated using VIVASPIN columns (Sartorius) prior to further purification by size exclusion chromatography (Superdex 200 10/300, GE healthcare) in sucrose buffer (250 mM sucrose, 50 mM KCl, 10 mM Hepes-KOH, 2.5 mM $MgCl_2$).

Cell-free nuclear assembly

Nuclear assemblies and immunofluorescence, including the preparation of high speed interphasic extracts from *Xenopus laevis* eggs, generation of sperm heads, and production of floated labeled and unlabeled membranes are described in detail in (Eisenhardt et al., 2014). Affinity resins used in depletion experiments were generated by crosslinking either purified unspecific rabbit IgG or affinity purified LSD1 IgG to protein-A sepharose using 10 mM Dimethyl Pimelimidate (Thermo Scientific). LSD1 was immunodepleted by incubating the resin with egg cytosol in a ratio of 1:1 and rotating at 4°C for 25 minutes. Unbound cytosol was used immediately. Fluorescence images were acquired using a confocal microscope (FV1000; Olympus; equipped with a photomultiplier [model R7862; Hamamatsu]) using 405-, 488-, and 559-nm laser lines and a 60× NA 1.35 oil immersion objective lens.

Cell-free chromatin decondensation

Isolation of mitotic clusters from HeLa, preparation of low speed interphasic egg extracts and chromatin decondensation reactions are described in detail in (Magalska et al., 2014). Immunodepletion of LSD1 for chromatin decondensation was performed as for nuclear assembly reactions (above). Chromatin decondensation was quantified from confocal images of DAPI-stained nuclei based on two key parameters described in (Magalska et al., 2014): Roughness of the chromatin boundary ($Perimeter^2/Area$) and chromatin heterogeneity (the relative internal area occupied by prominent structures, which were recognized using Fiji's StructureJ plugin http://www.imagescience.org/meijering/). Smoothness and homogeneity were defined as the differences from the maximal roughness and maximal relative area, respectively. A maximum of 20% was adopted for the fully decondensed state in both analyses. The fully condensed state was set to zero.

For sperm DNA decondensation 20 µl of *Xenopus laevis* egg extracts were incubated with 0.3 µl sperm heads (3000 sperm heads per µl) for 10 min. Samples were fixed with 4% paraformaldehyde and 0.5% glutaraldehyde on ice, stained with DAPI and analyzed on a Axiovert 200 M fluorescence wide field microscope (Zeiss). Images for both decondensation assays were acquired using a confocal microscope (FV1000; Olympus; equipped with a photomultiplier [model R7862; Hamamatsu]) using 405- and 559-nm laser lines and a 60× NA 1.35 oil immersion objective lens.

Cell culture experiments

HeLa cells were maintained in DMEM supplemented with 2 mM L-glutamine, 10% FBS, and 500 units/ml penicillin-streptomycin (all from Gibco). HeLa cells stably expressing H2B-mCherry (generated as in (Schmitz et al., 2010) were maintained in DMEM additionally supplemented with 0.5 µg/ml puromycin (Gibco). The H2B-mCherry/tubulin-EGFP cell line (Held et al. 2010) was a kind gift from Daniel Gerlich (IMBA, Vienna) and was maintained in DMEM additionally supplemented with 0.5 µg/ml puromycin (Gibco) and 500 µg/ml G-418/Geneticin (Life Technologies). The following siRNA oligonucleotides were employed in knockdown experiments: siLSD1-1 (AOF2_2) ACATCTTACCTTAGTCATCAA, siLSD1-2 (AOF2-6) AGGCCTAGACATTAAACTGAA, and AllStars negative control siRNA (all from Qiagen). Additionally the following PP2A oligos were routinely used as a pool mixed 1:1:1 (Schmitz et al., 2010): GACCAGGATGTGGACGTCAAA, CCAGGAUGUGGACGUCAAATT, and UUUGACGUCCACAUCCUGGTC (Qiagen) (Schmitz et al., 2010). Reverse transfections of 20 nM siRNA were carried out in HeLa cell suspensions using lipofectamine RNAiMAX (Invitrogen) according to the manufacturer's instructions.

HeLa cells were processed for immunofluorescence by fixation with 4% paraformaldehyde (Sigma) in phosphate buffered saline (PBS) on ice for 10 minutes prior to permeabilization with 2% Triton X-100 in blocking buffer (3% bovine serum albumine + 0.1% Triton X-100 in PBS). Where indicated, cells were permeabilized prior to fixation with 0.1% Trition-X 100 in a 60 mM PIPES, 20 mM HEPES, 10 mM EGTA, 4mM $MgSO_4$ buffer (pH 7). Immunofluorescence staining is described in (Eisenhardt et al., 2014). Images were acquired using a confocal microscope (FV1000; Olympus), 405-, 488- and 559-nm laser lines, and a 60× NA 1.35 oil immersion objective lens. For Nup localization, the photomultiplier [model R7862; Hamamatsu] was employed. The 488 laser line and a GaAsP detector were employed to image NPCs for quantification. NPCs labeled with mAB414 were counted for a given surface area from maximum intensity projections comprising five 0.25 µm-spaced optical Z-sections of the nuclear surface using the Fiji's 3D Object Counter (http://fiji.sc/3D_Objects_Counter). The total nuclear volume was measured from the DAPI signal of 0.5 µm optical Z-sections traversing the entire nucleus using the surpass volume function in IMARIS X64 7.6.3.

For live imaging experiments, H2B-mCherry and H2B-mCherry/α-tubulin-EGFP expressing HeLa cells were transfected with siRNA oligonucleotides and seeded in 8 well µ-slide

chambers (Ibidi). Starting approximately 30 hours post-transfection, cells were imaged using a Plan-Apochromat 10x NA 0.45 objective and a 561 nm diode laser on a LSM 5 live confocal microscope (Zeiss) equipped with a heating and CO_2 incubation system (Ibidi). ZEN software (Zeiss) was used to acquire images from five 7.5 µm-spaced optical Z-sections at various XY positions every three minutes. Single position *.ome files were generated from the maximum intensity projections in ZEN and converted to image sequences in Fiji. Segmentation, annotation, classification, and tracking of cells progressing through mitosis were performed using Cecog analyzer (http://www.cellcognition.org/software/cecoganalyzer) based on the CellCognition platform (Held et al., 2010).

Chromatin recruitment assay

Coupling of genomic DNA in a linearized plasmid to magnetic M-280 Streptavidin beads (Invitrogen) is described in (Ulbert et al., 2006). Once coupled, DNA beads were blocked with 1% lipid free bovine serum albumine in coupling buffer (2.5% polyvinylalcohol, 1M NaCl, 50 mM Tris pH 8.0, 2 mM EDTA pH 8.0), rotating overnight at 4°C. DNA was chromatinized by incubation with high-speed interphasic *Xenopus* egg cytosol (DNA beads:cytosol = 1:2.5), shaking at 350 rpm for 3 hours at 20°C. Beads were washed once with sucrose buffer and tested for protein recruitment by further incubation with egg cytosol and 10x floated membranes (i.e. 10 fold more concentrated than described in (Eisenhardt et al., 2014) purified from *Xenopus* eggs (DNA beads:cytosol:membranes = 1:0.5:1), shaking at 350 rpm for 1 hour at 20°C. After 3 washes with sucrose buffer, DNA beads were resuspended in Laemmli sample buffer and boiled. Supernatants were subjected to SDS-PAGE and transferred to nitrocellulose for immunoblotting. Signal intensities were quantified using the using the Fusion Capt advance software.

Acknowledgments

This work was supported by core funding of the Max Planck Society and the ERC (309528 CHROMDECON to W.A.). We thank C. Liebig (Light Microscopy Facility of the MPI for Developmental Biology) for supporting image acquisition and analysis, Alexander Blässle for help with the generation and maintenance of scripts used to automate the analysis of chromatin decondensation in various assay systems, and Adriana Magalska for helpful discussions.

Author contributions

A.S. and W.A. designed and performed experiments and wrote the manuscript. D. M.-A. performed the live cell experiments in H2B-mCherry/α-tubulin-EGFP cells and generally supported live cell experiments and their analysis. B.V. expressed and purified recombinant LSD1. P.D. supported the preparation of *Xenopus* egg extracts.

Conflict of interest

The authors declare that they have no conflict of interest.

References

Adamo, A., Sese, B., Boue, S., Castano, J., Paramonov, I., Barrero, M. J. and Izpisua Belmonte, J. C. (2011). LSD1 regulates the balance between self-renewal and differentiation in human embryonic stem cells. *Nat Cell Biol* **13**, 652-659.

Amente, S., Lania, L. and Majello, B. (2013). The histone LSD1 demethylase in stemness and cancer transcription programs. *Biochim Biophys Acta* **1829**, 981-986.

Anderson, D. J., Vargas, J. D., Hsiao, J. P. and Hetzer, M. W. (2009). Recruitment of functionally distinct membrane proteins to chromatin mediates nuclear envelope formation in vivo. *The Journal of cell biology* **186**, 183-191.

Antonin, W., Franz, C., Haselmann, U., Antony, C. and Mattaj, I. W. (2005). The integral membrane nucleoporin pom121 functionally links nuclear pore complex assembly and nuclear envelope formation. *Mol Cell* **17**, 83-92.

Black, J. C., Van Rechem, C. and Whetstine, J. R. (2012). Histone lysine methylation dynamics: establishment, regulation, and biological impact. *Mol Cell* **48**, 491-507.

Bodoor, K., Shaikh, S., Salina, D., Raharjo, W. H., Bastos, R., Lohka, M. and Burke, B. (1999). Sequential recruitment of NPC proteins to the nuclear periphery at the end of mitosis. *J Cell Sci* **112**, 2253-2264.

Booth, D. G., Takagi, M., Sanchez-Pulido, L., Petfalski, E., Vargiu, G., Samejima, K., Imamoto, N., Ponting, C. P., Tollervey, D., Earnshaw, W. C. et al. (2014). Ki-67 is a PP1-interacting protein that organises the mitotic chromosome periphery. *eLife* **3**, e01641.

Daigle, N., Beaudouin, J., Hartnell, L., Imreh, G., Hallberg, E., Lippincott-Schwartz, J. and Ellenberg, J. (2001). Nuclear pore complexes form immobile networks and have a very low turnover in live mammalian cells. *J Cell Biol* **154**, 71-84.

Davis, L. I. and Blobel, G. (1986). Identification and characterization of a nuclear pore complex protein. *Cell* **45**, 699-709.

Dultz, E., Zanin, E., Wurzenberger, C., Braun, M., Rabut, G., Sironi, L. and Ellenberg, J. (2008). Systematic kinetic analysis of mitotic dis- and reassembly of the nuclear pore in living cells. *J Cell Biol* **180**, 857-865.

Eisenhardt, N., Schooley, A. and Antonin, W. (2014). Xenopus in vitro assays to analyze the function of transmembrane nucleoporins and targeting of inner nuclear membrane proteins. *Methods Cell Biol* **122**, 193-218.

Fischle, W., Tseng, B. S., Dormann, H. L., Ueberheide, B. M., Garcia, B. A., Shabanowitz, J., Hunt, D. F., Funabiki, H. and Allis, C. D. (2005). Regulation of HP1-chromatin binding by histone H3 methylation and phosphorylation. *Nature* **438**, 1116-1122.

Foisner, R. and Gerace, L. (1993). Integral membrane proteins of the nuclear envelope interact with lamins and chromosomes, and binding is modulated by mitotic phosphorylation. *Cell* **73**, 1267-1279.

Forneris, F., Binda, C., Vanoni, M. A., Mattevi, A. and Battaglioli, E. (2005). Histone demethylation catalysed by LSD1 is a flavin-dependent oxidative process. *FEBS Lett* **579**, 2203-2207.

Franz, C., Walczak, R., Yavuz, S., Santarella, R., Gentzel, M., Askjaer, P., Galy, V., Hetzer, M., Mattaj, I. W. and Antonin, W. (2007). MEL-28/ELYS is required for the recruitment of nucleoporins to chromatin and postmitotic nuclear pore complex assembly. *EMBO Rep* **8**, 165-172.

Gant, T. M. and Wilson, K. L. (1997). Nuclear assembly. *Annu Rev Cell Dev Biol* **13**, 669-695.

Gillespie, P. J., Khoudoli, G. A., Stewart, G., Swedlow, J. R. and Blow, J. J. (2007). ELYS/MEL-28 chromatin association coordinates nuclear pore complex assembly and replication licensing. *Curr Biol* **17**, 1657-1662.

Guizetti, J., Schermelleh, L., Mantler, J., Maar, S., Poser, I., Leonhardt, H., Muller-Reichert, T. and Gerlich, D. W. (2011). Cortical constriction during abscission involves helices of ESCRT-III-dependent filaments. *Science* **331**, 1616-1620.

Guttinger, S., Laurell, E. and Kutay, U. (2009). Orchestrating nuclear envelope disassembly and reassembly during mitosis. *Nat Rev Mol Cell Biol* **10**, 178-191.

Haraguchi, T., Koujin, T., Hayakawa, T., Kaneda, T., Tsutsumi, C., Imamoto, N., Akazawa, C., Sukegawa, J., Yoneda, Y. and Hiraoka, Y. (2000). Live fluorescence imaging reveals early recruitment of emerin, LBR, RanBP2, and Nup153 to reforming functional nuclear envelopes. *J Cell Sci* **113 (Pt 5)**, 779-794.

Harel, A., Orjalo, A. V., Vincent, T., Lachish-Zalait, A., Vasu, S., Shah, S., Zimmerman, E., Elbaum, M. and Forbes, D. J. (2003). Removal of a single pore subcomplex results in vertebrate nuclei devoid of nuclear pores. *Mol Cell* **11**, 853-864.

Hase, M. E. and Cordes, V. C. (2003). Direct interaction with nup153 mediates binding of Tpr to the periphery of the nuclear pore complex. *Mol Biol Cell* **14**, 1923-1940.

Heald, R. and McKeon, F. (1990). Mutations of phosphorylation sites in lamin A that prevent nuclear lamina disassembly in mitosis. *Cell* **61**, 579-589.

Heald, R., Tournebize, R., Blank, T., Sandaltzopoulos, R., Becker, P., Hyman, A. and Karsenti, E. (1996). Self-organization of microtubules into bipolar spindles around artificial chromosomes in Xenopus egg extracts. *Nature* **382**, 420-425.

Held, M., Schmitz, M. H., Fischer, B., Walter, T., Neumann, B., Olma, M. H., Peter, M., Ellenberg, J. and Gerlich, D. W. (2010). CellCognition: time-resolved phenotype annotation in high-throughput live cell imaging. *Nat Methods* **7**, 747-754.

Hetzer, M., Gruss, O. J. and Mattaj, I. W. (2002). The Ran GTPase as a marker of chromosome position in spindle formation and nuclear envelope assembly. *Nat Cell Biol* **4**, E177-184.

Hsu, J. Y., Sun, Z. W., Li, X., Reuben, M., Tatchell, K., Bishop, D. K., Grushcow, J. M., Brame, C. J., Caldwell, J. A., Hunt, D. F. et al. (2000). Mitotic phosphorylation of histone H3 is governed by Ipl1/aurora kinase and Glc7/PP1 phosphatase in budding yeast and nematodes. *Cell* **102**, 279-291.

Huang, J., Sengupta, R., Espejo, A. B., Lee, M. G., Dorsey, J. A., Richter, M., Opravil, S., Shiekhattar, R., Bedford, M. T., Jenuwein, T. et al. (2007). p53 is regulated by the lysine demethylase LSD1. *Nature* **449**, 105-108.

Ito, H., Koyama, Y., Takano, M., Ishii, K., Maeno, M., Furukawa, K. and Horigome, T. (2007). Nuclear envelope precursor vesicle targeting to chromatin is stimulated by protein phosphatase 1 in Xenopus egg extracts. *Exp Cell Res* **313**, 1897-1910.

Kawashima, S. A., Yamagishi, Y., Honda, T., Ishiguro, K. and Watanabe, Y. (2010). Phosphorylation of H2A by Bub1 prevents chromosomal instability through localizing shugoshin. *Science* **327**, 172-177.

Kessel, R. G. (1992). Annulate lamellae: a last frontier in cellular organelles. *International review of cytology* **133**, 43-120.

Lan, F., Zaratiegui, M., Villen, J., Vaughn, M. W., Verdel, A., Huarte, M., Shi, Y., Gygi, S. P., Moazed, D. and Martienssen, R. A. (2007). S. pombe LSD1 homologs regulate heterochromatin propagation and euchromatic gene transcription. *Mol Cell* **26**, 89-101.

Laurell, E., Beck, K., Krupina, K., Theerthagiri, G., Bodenmiller, B., Horvath, P., Aebersold, R., Antonin, W. and Kutay, U. (2011). Phosphorylation of Nup98 by multiple kinases is crucial for NPC disassembly during mitotic entry. *Cell* **144**, 539-550.

Lee, M. G., Wynder, C., Cooch, N. and Shiekhattar, R. (2005). An essential role for CoREST in nucleosomal histone 3 lysine 4 demethylation. *Nature* **437**, 432-435.

Lv, S., Bu, W., Jiao, H., Liu, B., Zhu, L., Zhao, H., Liao, J., Li, J. and Xu, X. (2010). LSD1 is required for chromosome segregation during mitosis. *Eur J Cell Biol* **89**, 557-563.

MacCallum, D. E., Losada, A., Kobayashi, R. and Hirano, T. (2002). ISWI remodeling complexes in Xenopus egg extracts: identification as major chromosomal components that are regulated by INCENP-aurora B. *Mol Biol Cell* **13**, 25-39.

Magalska, A., Schellhaus, A. K., Moreno-Andres, D., Zanini, F., Schooley, A., Sachdev, R., Schwarz, H., Madlung, J. and Antonin, W. (2014). RuvB-like ATPases function in chromatin decondensation at the end of mitosis. *Developmental Cell* **31**, 305-318.

Mansfeld, J., Guttinger, S., Hawryluk-Gara, L. A., Pante, N., Mall, M., Galy, V., Haselmann, U., Muhlhausser, P., Wozniak, R. W., Mattaj, I. W. et al. (2006). The conserved transmembrane nucleoporin NDC1 is required for nuclear pore complex assembly in vertebrate cells. *Mol Cell* **22**, 93-103.

Metzger, E., Wissmann, M., Yin, N., Muller, J. M., Schneider, R., Peters, A. H., Gunther, T., Buettner, R. and Schule, R. (2005). LSD1 demethylates repressive histone marks to promote androgen-receptor-dependent transcription. *Nature* **437**, 436-439.

Mitchell, J. M., Mansfeld, J., Capitanio, J., Kutay, U. and Wozniak, R. W. (2010). Pom121 links two essential subcomplexes of the nuclear pore complex core to the membrane. *J Cell Biol* **191**, 505-521.

Moazed, D. (2011). Mechanisms for the inheritance of chromatin states. *Cell* **146**, 510-518.

Nair, V. D., Ge, Y., Balasubramaniyan, N., Kim, J., Okawa, Y., Chikina, M., Troyanskaya, O. and Sealfon, S. C. (2012). Involvement of histone demethylase LSD1 in short-time-scale gene expression changes during cell cycle progression in embryonic stem cells. *Mol Cell Biol* **32**, 4861-4876.

Peter, M., Nakagawa, J., Doree, M., Labbe, J. C. and Nigg, E. A. (1990). In vitro disassembly of the nuclear lamina and M phase-specific phosphorylation of lamins by cdc2 kinase. *Cell* **61**, 591-602.

Pfaller, R., Smythe, C. and Newport, J. W. (1991). Assembly/disassembly of the nuclear envelope membrane: cell cycle-dependent binding of nuclear membrane vesicles to chromatin in vitro. *Cell* **65**, 209-217.

Philpott, A. and Leno, G. H. (1992). Nucleoplasmin remodels sperm chromatin in Xenopus egg extracts. *Cell* **69**, 759-767.

Philpott, A., Leno, G. H. and Laskey, R. A. (1991). Sperm decondensation in Xenopus egg cytoplasm is mediated by nucleoplasmin. *Cell* **65**, 569-578.

Pyrpasopoulou, A., Meier, J., Maison, C., Simos, G. and Georgatos, S. D. (1996). The lamin B receptor (LBR) provides essential chromatin docking sites at the nuclear envelope. *Embo J* **15**, 7108-7119.

Rasala, B. A., Ramos, C., Harel, A. and Forbes, D. J. (2008). Capture of AT-rich chromatin by ELYS recruits POM121 and NDC1 to initiate nuclear pore assembly. *Mol Biol Cell* **19**, 3982-3996.

Rasala, B. A., Orjalo, A. V., Shen, Z., Briggs, S. and Forbes, D. J. (2006). ELYS is a dual nucleoporin/kinetochore protein required for nuclear pore assembly and proper cell division. *Proc Natl Acad Sci U S A* **103**, 17801-17806.

Rotem, A., Gruber, R., Shorer, H., Shaulov, L., Klein, E. and Harel, A. (2009). Importin beta regulates the seeding of chromatin with initiation sites for nuclear pore assembly. *Mol Biol Cell* **20**, 4031-4042.

Rudolph, T., Yonezawa, M., Lein, S., Heidrich, K., Kubicek, S., Schafer, C., Phalke, S., Walther, M., Schmidt, A., Jenuwein, T. et al. (2007). Heterochromatin formation in Drosophila is initiated through active removal of H3K4 methylation by the LSD1 homolog SU(VAR)3-3. *Mol Cell* **26**, 103-115.

Sachdev, R., Sieverding, C., Flotenmeyer, M. and Antonin, W. (2012). The C-terminal domain of Nup93 is essential for assembly of the structural backbone of nuclear pore complexes. *Mol Biol Cell* **23**, 740-749.

Schmitz, M. H. and Gerlich, D. W. (2009). Automated live microscopy to study mitotic gene function in fluorescent reporter cell lines. *Methods Mol Biol* **545**, 113-134.

Schmitz, M. H., Held, M., Janssens, V., Hutchins, J. R., Hudecz, O., Ivanova, E., Goris, J., Trinkle-Mulcahy, L., Lamond, A. I., Poser, I. et al. (2010). Live-cell imaging RNAi screen identifies PP2A-B55alpha and importin-beta1 as key mitotic exit regulators in human cells. *Nat Cell Biol* **12**, 886-893.

Schooley, A., Vollmer, B. and Antonin, W. (2012). Building a nuclear envelope at the end of mitosis: coordinating membrane reorganization, nuclear pore complex assembly, and chromatin de-condensation. *Chromosoma* **121**, 539-554.

Shaulov, L., Gruber, R., Cohen, I. and Harel, A. (2011). A dominant-negative form of POM121 binds chromatin and disrupts the two separate modes of nuclear pore assembly. *Journal of cell science* **124**, 3822-3834.

Shi, Y., Lan, F., Matson, C., Mulligan, P., Whetstine, J. R., Cole, P. A. and Casero, R. A. (2004). Histone demethylation mediated by the nuclear amine oxidase homolog LSD1. *Cell* **119**, 941-953.

Shi, Y. J., Matson, C., Lan, F., Iwase, S., Baba, T. and Shi, Y. (2005). Regulation of LSD1 histone demethylase activity by its associated factors. *Mol Cell* **19**, 857-864.

Stavropoulos, P., Blobel, G. and Hoelz, A. (2006). Crystal structure and mechanism of human lysine-specific demethylase-1. *Nat Struct Mol Biol* **13**, 626-632.

Stavru, F., Hulsmann, B. B., Spang, A., Hartmann, E., Cordes, V. C. and Gorlich, D. (2006). NDC1: a crucial membrane-integral nucleoporin of metazoan nuclear pore complexes. *J Cell Biol* **173**, 509-519.

Sun, G., Alzayady, K., Stewart, R., Ye, P., Yang, S., Li, W. and Shi, Y. (2010). Histone demethylase LSD1 regulates neural stem cell proliferation. *Mol Cell Biol* **30**, 1997-2005.

Takagi, M., Nishiyama, Y., Taguchi, A. and Imamoto, N. (2014). Ki67 antigen contributes to the timely accumulation of protein phosphatase 1gamma on anaphase chromosomes. *J Biol Chem* **289**, 22877-22887.

Thompson, L. J., Bollen, M. and Fields, A. P. (1997). Identification of protein phosphatase 1 as a mitotic lamin phosphatase. *J Biol Chem* **272**, 29693-29697.

Trinkle-Mulcahy, L., Andersen, J., Lam, Y. W., Moorhead, G., Mann, M. and Lamond, A. I. (2006). Repo-Man recruits PP1 gamma to chromatin and is essential for cell viability. *J Cell Biol* **172**, 679-692.

Ulbert, S., Platani, M., Boue, S. and Mattaj, I. W. (2006). Direct membrane protein-DNA interactions required early in nuclear envelope assembly. *J Cell Biol* **173**, 469-476.

Vagnarelli, P., Ribeiro, S., Sennels, L., Sanchez-Pulido, L., de Lima Alves, F., Verheyen, T., Kelly, D. A., Ponting, C. P., Rappsilber, J. and Earnshaw, W. C. (2011). Repo-Man coordinates chromosomal reorganization with nuclear envelope reassembly during mitotic exit. *Developmental cell* **21**, 328-342.

Vollmer, B., Schooley, A., Sachdev, R., Eisenhardt, N., Schneider, A. M., Sieverding, C., Madlung, J., Gerken, U., Macek, B. and Antonin, W. (2012). Dimerization and direct membrane interaction of Nup53 contribute to nuclear pore complex assembly. *EMBO J* **31**, 4072-4084.

Vollmer, B., Lorenz, M., Moreno-Andres, D., Bodenhofer, M., De Magistris, P., Astrinidis, S. A., Schooley, A., Flotenmeyer, M., Leptihn, S. and Antonin, W. (2015). Nup153 Recruits the Nup107-160 Complex to the Inner Nuclear Membrane for Interphasic Nuclear Pore Complex Assembly. *Dev Cell* **33**, 717-728.

Walther, T. C., Askjaer, P., Gentzel, M., Habermann, A., Griffiths, G., Wilm, M., Mattaj, I. W. and Hetzer, M. (2003a). RanGTP mediates nuclear pore complex assembly. *Nature* **424**, 689-694.

Walther, T. C., Alves, A., Pickersgill, H., Loiodice, I., Hetzer, M., Galy, V., Hulsmann, B. B., Kocher, T., Wilm, M., Allen, T. et al. (2003b). The conserved Nup107-160 complex is critical for nuclear pore complex assembly. *Cell* **113**, 195-206.

Wang, F. and Higgins, J. M. (2013). Histone modifications and mitosis: countermarks, landmarks, and bookmarks. *Trends Cell Biol* **23**, 175-184.

Wang, J., Lu, F., Ren, Q., Sun, H., Xu, Z., Lan, R., Liu, Y., Ward, D., Quan, J., Ye, T. et al. (2011). Novel histone demethylase LSD1 inhibitors selectively target cancer cells with pluripotent stem cell properties. *Cancer Res* **71**, 7238-7249.

Wang, J., Hevi, S., Kurash, J. K., Lei, H., Gay, F., Bajko, J., Su, H., Sun, W., Chang, H., Xu, G. et al. (2009). The lysine demethylase LSD1 (KDM1) is required for maintenance of global DNA methylation. *Nat Genet* **41**, 125-129.

Wilkins, B. J., Rall, N. A., Ostwal, Y., Kruitwagen, T., Hiragami-Hamada, K., Winkler, M., Barral, Y., Fischle, W. and Neumann, H. (2014). A cascade of histone modifications induces chromatin condensation in mitosis. *Science* **343**, 77-80.

Wissmann, M., Yin, N., Muller, J. M., Greschik, H., Fodor, B. D., Jenuwein, T., Vogler, C., Schneider, R., Gunther, T., Buettner, R. et al. (2007). Cooperative demethylation by JMJD2C and LSD1 promotes androgen receptor-dependent gene expression. *Nat Cell Biol* **9**, 347-353.

Wright, S. J. (1999). Sperm nuclear activation during fertilization. *Current topics in developmental biology* **46**, 133-178.

Wurzenberger, C. and Gerlich, D. W. (2011). Phosphatases: providing safe passage through mitotic exit. *Nature reviews. Molecular cell biology* **12**, 469-482.

Yamagishi, Y., Honda, T., Tanno, Y. and Watanabe, Y. (2010). Two histone marks establish the inner centromere and chromosome bi-orientation. *Science* **330**, 239-243.

Yang, P., Wang, Y., Chen, J., Li, H., Kang, L., Zhang, Y., Chen, S., Zhu, B. and Gao, S. (2011). RCOR2 is a subunit of the LSD1 complex that regulates ESC property and substitutes for SOX2 in reprogramming somatic cells to pluripotency. *Stem Cells* **29**, 791-801.

Yavuz, S., Santarella-Mellwig, R., Koch, B., Jaedicke, A., Mattaj, I. W. and Antonin, W. (2010). NLS-mediated NPC functions of the nucleoporin Pom121. *FEBS Lett* **584**, 3292-3298.

Ye, Q., Callebaut, I., Pezhman, A., Courvalin, J. C. and Worman, H. J. (1997). Domain-specific interactions of human HP1-type chromodomain proteins and inner nuclear membrane protein LBR. *J Biol Chem* **272**, 14983-14989.

Figures

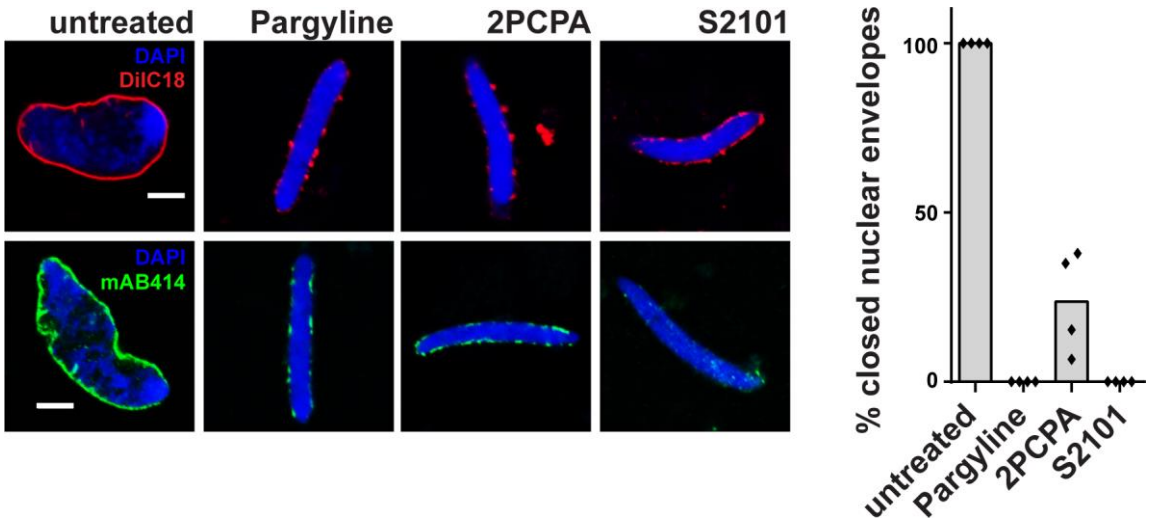

Fig. 1. LSD1 inhibitors block cell-free nuclear assembly

Nuclei assembled on sperm chromatin in *Xenopus* egg extracts for 120 min were fixed and analyzed by confocal microscopy. Where indicated 5 mM pargyline, 2.5 mM 2PCPA or 0.25 mM S2101 was added to assembly reactions at t = 0. Membranes were pre-labelled with DiIC18 (upper panel, red in overlay), NPCs were immuno-labeled following fixation using mAB414 (lower panel, green), and chromatin was stained with DAPI (blue in overlays). In each experiment, 100 randomly chosen chromatin substrates were scored. The average percentage of nuclei with closed nuclear envelopes from four independent experiments is shown. Data points from individual experiments are indicated. Scale bar: 5 µm.

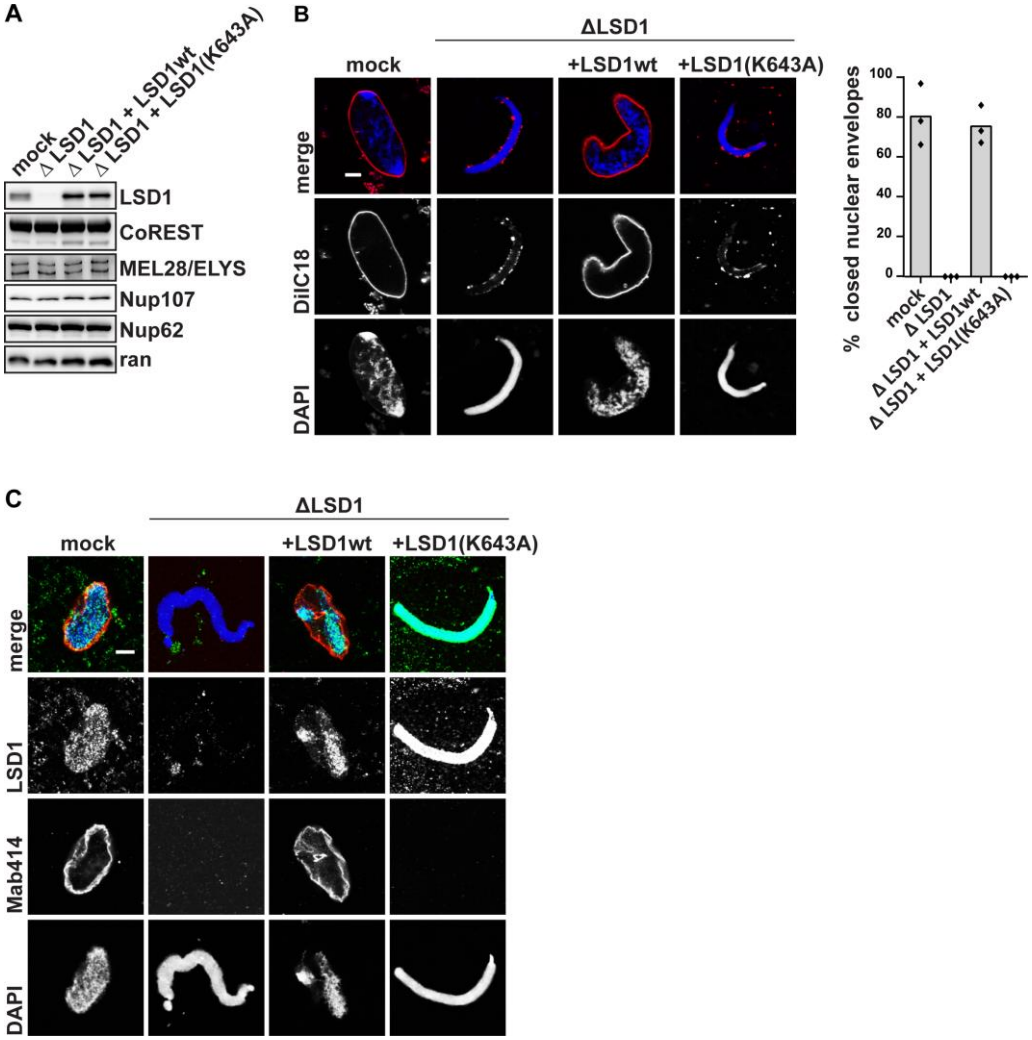

Fig. 2. Cell-free nuclear assembly requires the demethylase activity of LSD1

(A) Western blot analysis of mock depleted, LSD1 depleted (ΔLSD1), and LSD1 depleted *Xenopus* egg extracts supplemented with either recombinant wild type LSD1 or the catalytically inactive LSD1 K643A mutant.

(B) Confocal microscopy images of fixed nuclei assembled for 120 min in the indicated extract conditions. Membranes were pre-labelled with DiIC18 (red in overlay) and chromatin was stained with DAPI (blue in overlay). The average percentage of closed nuclear envelopes for 100 randomly chosen chromatin substrates in each of three independent experiments is shown. Data points from individual experiments are indicated.

(C) Nuclei assembled for 120 min in the indicated extract conditions were fixed and analyzed for the presence of immunolabeled LSD1 (green in overlay) and NPCs (mAB414, red in overlay) on the chromatin (DAPI, blue in overlay) by confocal microscopy.

Scale bars: 5 µm.

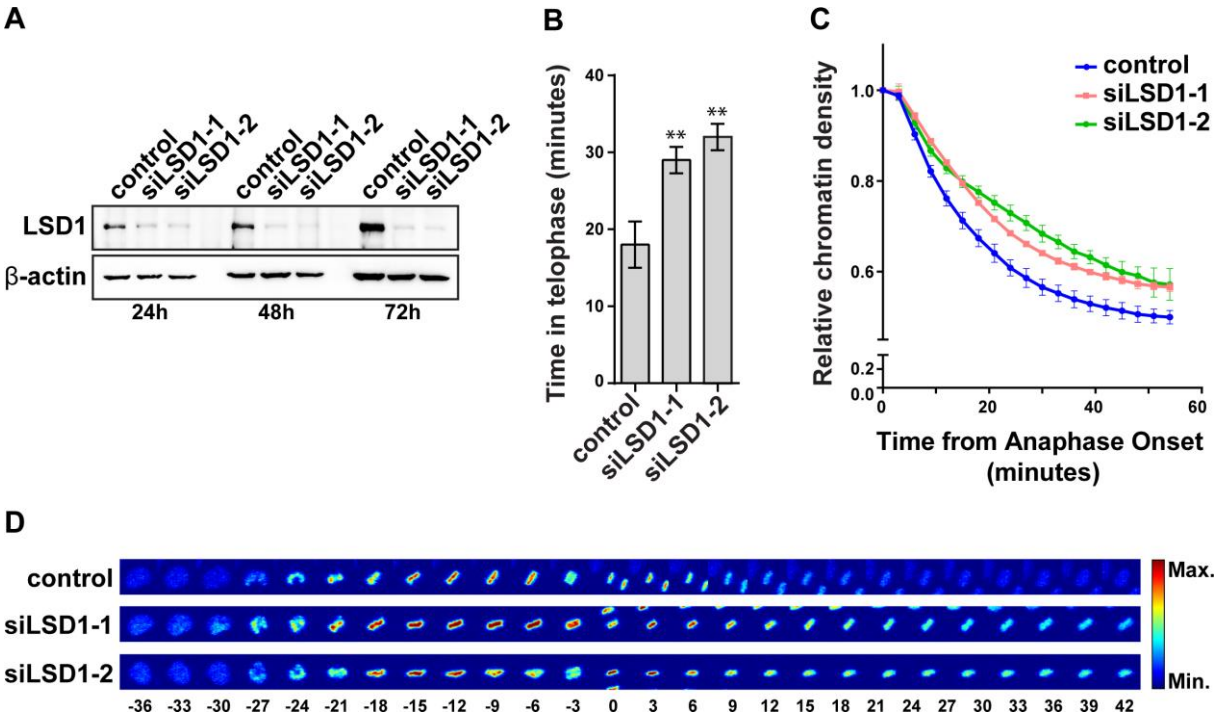

Fig. 3. LSD1 is required for the timely establishment of interphasic chromatin after mitosis in human cells

(A) Western blot analysis of whole cell lysates from HeLa cells stably expressing H2B-mCherry and transfected with 20 nM control, LSD1-1 or LSD1-2 siRNA oligos as indicated. Lysates were harvested 24, 48, and 72h post-transfection.

(B) HeLa cells stably expressing H2B-mCherry and transfected with 20 nM siRNA as indicated were subjected to time-lapse microscopy starting 30h after transfection. Mitotic events were analyzed with CellCognition. The mean of the median time spent in telophase is plotted for more than 100 mitotic events per condition in 3 independent experiments. Error bars represent s.d. **P<0.01, Student's t-test.

(C) The average fluorescence intensity of the H2B-mCherry signal was extracted from the CellCognition data acquired in (B) as an indication of chromatin density. The density was normalized to the first anaphase frame in individual mitotic tracks and the mean relative density for more than 100 mitotic events per condition from three independent experiments is plotted over time. Error bars represent s.d.

(D) HeLa cells stably expressing H2B-mCherry and transfected with 20 nM siRNA were subjected to time-lapse microscopy starting 30h after transfection. Maximum intensity projections of the mCherry signal from five optical z sections are represented as a heat maps. Mitotic tracks are normalized to the first anaphase frame.

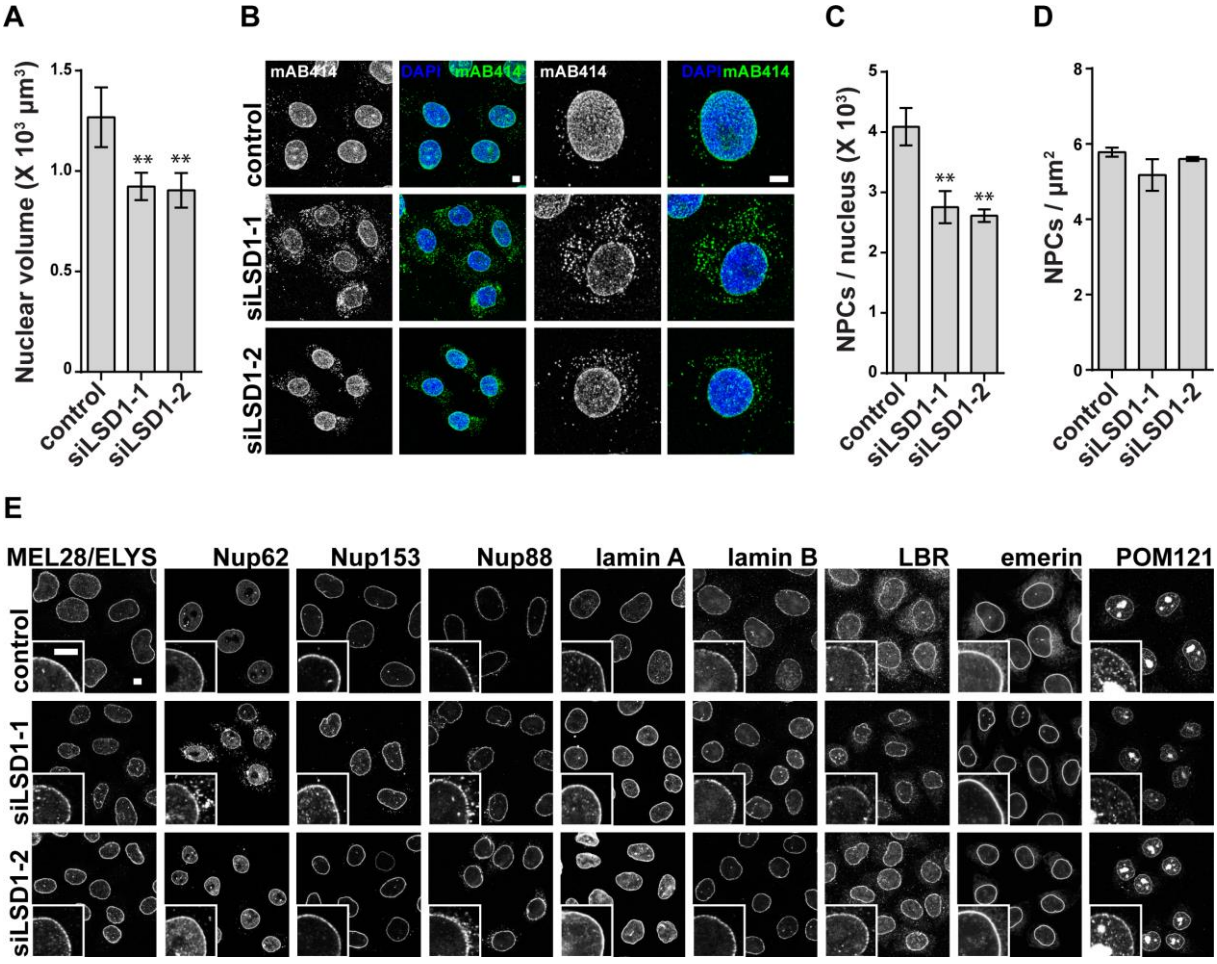

Fig. 4. Loss of LSD1 in human cells affects nuclear volume and NPC assembly

(A) Quantification of nuclear volume based on DAPI staining in HeLa cells transfected with 20 nM control, LSD1-1 or LSD1-2 siRNA oligos and fixed 48h post-transfection. The average nuclear volume from more than 80 nuclei per condition in three independent experiments is plotted. Error bars represent s.d. *P<0.05, Student's t-test.

(B) HeLa cells transfected with 20 nM control, LSD1-1 or LSD1-2 siRNA oligos were fixed 48h post-transfection and processed for immunofluorescence. NPCs were immuno-labelled using mAB414 (green in overlay) and DNA was stained with DAPI (blue). Maximum intensity projections are shown.

(C) Quantification of mAB414-labelled NPCs in HeLa cells transfected with 20 nM control, LSD1-1 or LSD1-2 siRNA oligos and fixed 48h post-transfection. The number of NPCs over a specified surface area was counted and was used to calculate the total number per nucleus

based the nuclear volume. The average number of NPCs per nucleus for 10 nuclei per condition in 3 independent experiments is plotted. Error bars represent s.d. **P<0.01, Student's t-test.

(D) Quantification of NPC density in HeLa cells transfected with 20 nM control, LSD1-1 or LSD1-2 siRNA oligos and fixed 48h post-transfection. The average number of mAB414-labelled NPCs over a specified surface area was counted and the mean NPC density for 10 nuclei per condition in 3 independent experiments is plotted. Error bars represent s.d.

(E) HeLa cells transfected with 20 nM control, LSD1-1 or LSD1-2 siRNA oligos were fixed 48h post-transfection and processed for immunofluorescence. Nuclear envelope proteins were immunolabelled as indicated and representative images are shown. Insets provide a higher magnification view.

Scale bars: 5 μm.

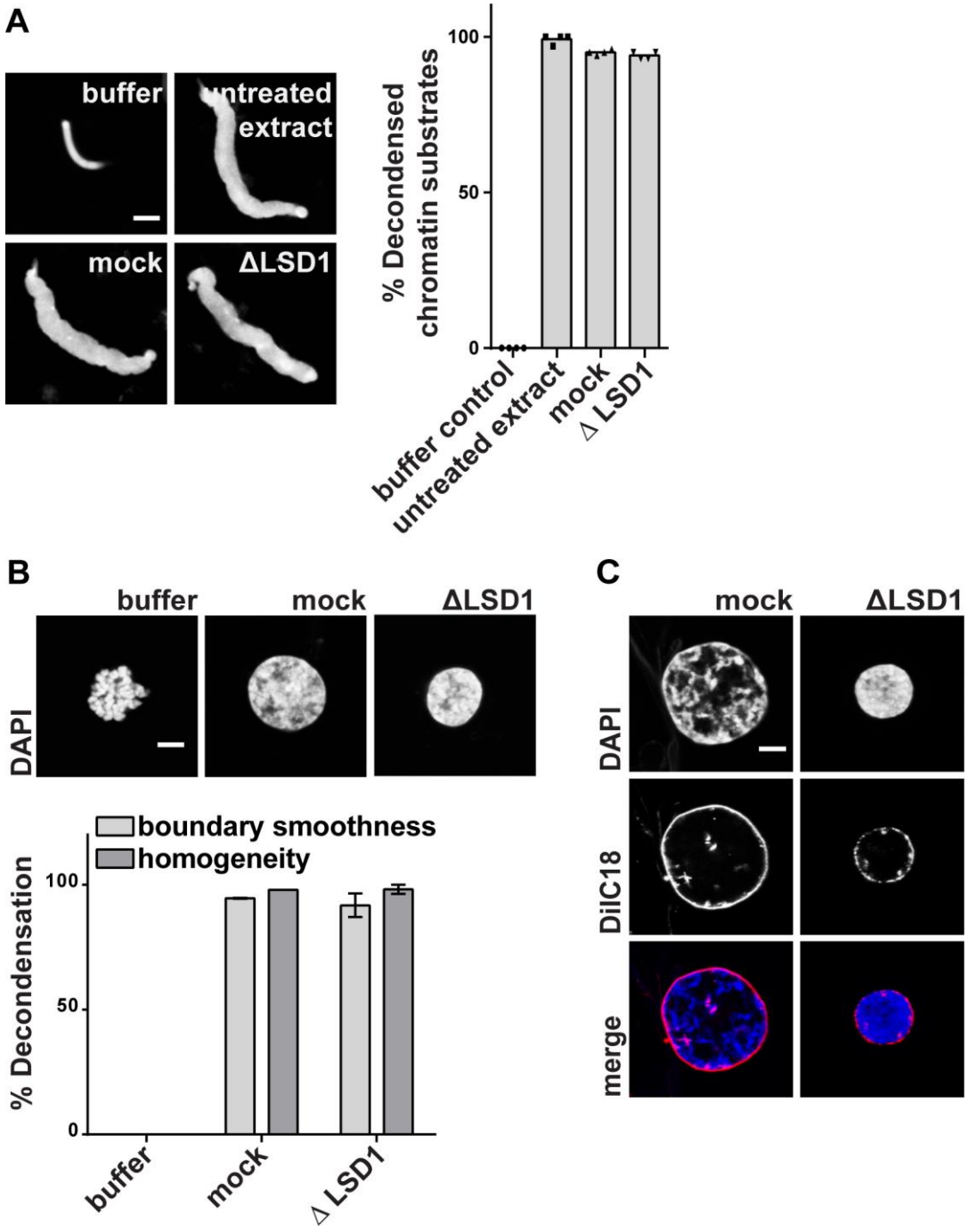

Fig. 5. LSD1 is not required for the membrane-independent decondensation of chromatin *in vitro*

(A) *Xenopus laevis* sperm chromatin heads were incubated in *Xenopus* egg extracts for 10 min, fixed, and analyzed by confocal microscopy. Chromatin was stained with DAPI. The average percentage of decondensed chromatin substrates for 100 randomly chosen templates in each of four independent experiments is shown. Data points from individual experiments are indicated.

(B) Mitotic chromatin clusters from HeLa cells were incubated with buffer, mock or LSD1 depleted *Xenopus* egg extracts in the absence of added membranes. After 120 min sample were fixed, stained with DAPI and analyzed by confocal microscopy. The smoothness of the chromatin boundary (light grey) and the homogeneity of DAPI staining (dark grey) were analyzed as described (Magalska et al., 2014). The mean percent decondensation is plotted for 10 chromatin substrates per condition in each of three independent experiments. Error bars represent s.d.

(C) Mitotic chromatin clusters from HeLa cells were incubated in mock or LSD1 depleted egg extracts in the presence of DiIC18-labelled membranes (red in overlay). Samples were fixed after 120 min, stained with DAPI (blue in overlay), and analyzed by confocal microscopy.

Scale bars: 5 µm.

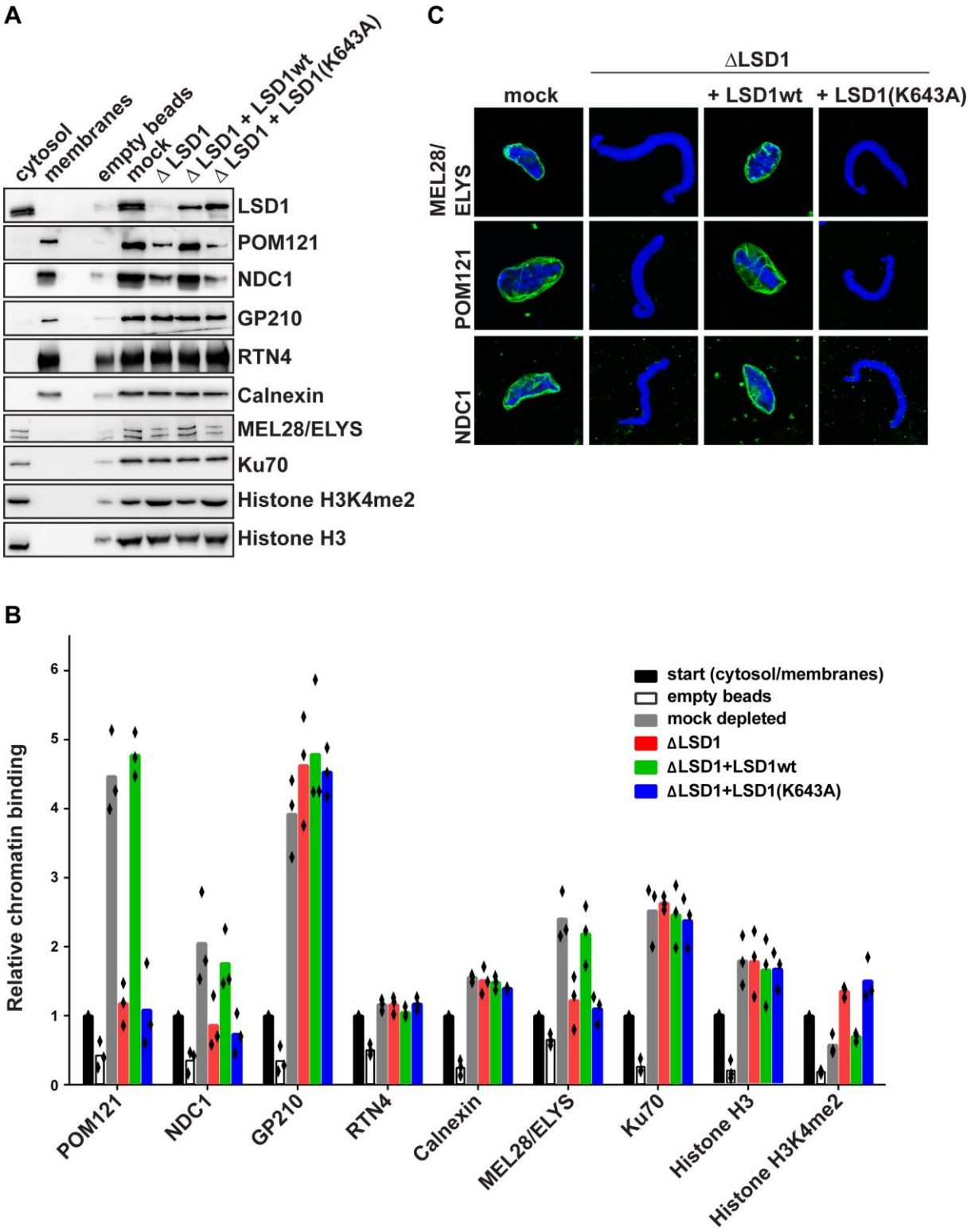

Fig. 6. The recruitment of MEL28/ELYS and POM121/NDC1-membrane vesicles to chromatin *in vitro* depends on LSD1

(A) Linearized plasmid DNA immobilized on magnetic beads was chromatinized for 3h in mock, LSD1 depleted or LSD1 depleted *Xenopus* egg extract cytosol supplemented with

either wildtype LSD1 or the catalytically inactive K643A mutant, as indicated. After re-isolation, beads were washed and incubated a second time with cytosol treated as before and floatation-purified egg extract membranes. Bead bound material was re-isolated after 1h, washed and analyzed by western blotting. For comparison, equal amounts (corresponding to the second incubation) of mock treated extracts and membranes were analyzed. Magnetic beads without DNA (empty beads) were used to estimate the background level of binding of extract components to the beads.

B) Quantification of proteins re-isolated with chromatinized DNA beads performed as in (A). The average intensity from three independent experiments normalized to the start material (cytosol or membranes) is plotted. Individual data points are indicated.

(C) Nuclei assembled for 120 min in the indicated extracts conditions were fixed and analyzed for the presence of MEL28/ELYS, POM121 and NDC1 (green in overlay) by immunofluorescence and confocal microscopy. Chromatin is stained with DAPI (blue). Scale bar: 5 µm.

Supplementary figure legends

Fig. S1. Characterisation of a new *Xenopus laevis* LSD1 antibody

Antiserum generated in rabbits against the full length *Xenopus laevis* LSD1 protein was tested for specificity in immunoblots of lysates from *Xenopus* egg extracts (A) or HeLa cells (B) subjected to SDS-PAGE. Note the strong reduction of the human LSD1 signal upon RNAi mediated LSD1 downregulation.

Fig. S2. LSD1 localisation in HeLa cells

(A) The cell cycle-dependent localization of LSD1 in unsynchronised HeLa cells was analyzed by immunofluorescence and confocal microscopy. LSD1 (green in overlay) and NPCs (mAB414, red) were immunolabeled and chromatin was stained with DAPI (blue).

(B) LSD1 (green) and NPCs (mAB414, red) immunolabeled in cells permeabilized with 0.1% Triton-X 100 prior to fixation. Chromatin was stained with DAPI (blue). Maximum intensity projections are shown.

(C) LSD1 (green) and α-tubulin (red) were immunolabeled in cells permeabilized with 0.1% Triton-X 100 prior to fixation. Chromatin was stained with DAPI (blue). Maximum intensity projections are shown.

Scale bars: 5 µm

Fig. S3. Further characterization of unsynchronized HeLa cell populations depleted of LSD1 by siRNA

(A) HeLa cells transfected with 20 nM control, LSD1-1 or LSD1-2 siRNA oligos were fixed 48h post-transfection and processed for immunofluorescence. LSD1 (top panel, green in overlay) and NPCs (mAB414, red in overlay) were immuno-labeled and chromatin was stained with DAPI (blue in overlay). Scale bar: 10 µm

(B) HeLa cells stably expressing H2B-mCherry and transfected with 20 nM siRNA as indicated were subjected to time-lapse microscopy starting 30h post-transfection. Mitotic events were analyzed with CellCognition. The mean of the median time spent in each cell

cycle stage indicated is plotted for more than 100 mitotic events per condition in 3 independent experiments. Error bars represent s.d. *P<0.05, Student's t-test.

(C) Quantification of nuclear volume based on DAPI staining in HeLa cells transfected with 20 nM control, LSD1-1 or LSD1-2 siRNA oligos and fixed 48h post-transfection. Nuclear volume measurements from 383 nuclei in 3 independent experiments were pooled for each condition and assigned to 200 μm^3 bins. The nuclear volume frequency for each bin is plotted and the center of each bin is indicated on the x-axis.

(D) Western blot analysis of whole cell lysates from HeLa cells stably expressing H2B-mCherry/α-tubulin-EGFP and transfected with 20 nM control, LSD1-1, LSD1-2, or PP2A siRNA oligos as indicated. Lysates were harvested 48h post-transfection.

(E) HeLa cells stably expressing H2B-mCherry/ α-tubulin-EGFP and transfected with 20 nM siRNA were subjected to time-lapse microscopy starting 30h after transfection. Mitotic events were analyzed with CellCognition. The mean of the median time spent in telophase based on chromatin features is plotted for more than 100 mitotic events per condition in 3 independent experiments. Error bars represent s.d. *P<0.05, **P<0.01, Student's t-test.

(F) The average fluorescence intensity of the H2B-mCherry signal was extracted from the CellCognition data acquired in (B) as an indication of chromatin density. The density was normalized to the first anaphase frame in individual mitotic tracks and the mean relative density for more than 100 mitotic events from three independent experiments is plotted over time. Error bars represent s.d.

(G) HeLa cells stably expressing H2B-mCherry/ α-tubulin-EGFP and transfected with 20 nM siRNA were subjected to time-lapse microscopy starting 30h post-transfection. Mitotic events were analyzed with CellCognition. The mean of the median time spent in each cell cycle stage based on chromatin features is plotted for more than 100 mitotic events per condition in 3 independent experiments. Error bars represent s.d. *P<0.05, **P<0.01, Student's t-test.

(H) HeLa cells stably expressing H2B-mCherry/ α-tubulin-EGFP and transfected with 20 nM siRNA were subjected to time-lapse microscopy starting 30h post-transfection. Mitotic events were analyzed with CellCognition. The mean of the median duration of the anaphase spindle, based on the α-tubulin signal, is plotted for more than 100 mitotic events per condition in 3 independent experiments. Error bars represent s.d.

(I) HeLa cells stably expressing H2B-mCherry/ α-tubulin-EGFP and transfected with 20 nM siRNA were subjected to time-lapse microscopy starting 30h post-transfection. Mitotic events were analyzed with CellCognition. The mean of the median duration of detectable midbody-associated α-tubulin is plotted for more than 100 mitotic events per condition in 3 independent experiments. Error bars represent s.d. *P<0.05, Student's t-test.

(J) HeLa cells stably expressing H2B-mCherry/ α-tubulin-EGFP and transfected with 20 nM siRNA were subjected to time-lapse microscopy starting 30h after transfection. Maximum intensity projections of the mCherry and EGFP signals from five optical z sections are shown. Mitotic tracks are normalized to the first anaphase frame.

Fig. S4. Chemical inhibition of LSD1 promotes extended telophase and annulate lamellae formation in HeLa cells but does not block membrane-independent chromatin decondensation *in vitro*

(A) HeLa cells stably expressing H2B-mCherry were treated with different concentrations of the LSD1 inhibitors 2-PCPA and S2101 as indicated and immediately subjected to time-lapse microscopy. Mitotic events were analyzed with CellCognition (control: 73 events, 300 µM 2-PCPA: 35 events, 1mM 2-PCPA: 10 events, 15 µM S2101: 62 events, and 50 µM S2101: 22 events). The number of mitotic events analysed was drastically reduced in the presence of LSD1 inhibitors due to cell lethality at the effective concentrations. The median time spent in telophase is plotted and individual data are shown.

(B) HeLa cells stably expressing H2B-mCherry were treated with different concentrations of the LSD1 inhibitors 2-PCPA and S2101 as indicated and immediately subjected to time-lapse microscopy. Representative maximum intensity projections of the mCherry signal from five optical z sections are represented as a heat maps. Mitotic tracks are normalized to the first anaphase frame.

(C) HeLa cells treated with 300 µM 2-PCPA or 15 µM S2101 as indicated for 24h, fixed, and processed for immunofluorescence. NPCs were immuno-labelled using mAB414 (green in overlay) and DNA was stained with DAPI (blue). Maximum intensity projections are shown. Scale bar: 5 µm.

(D) Mitotic chromatin clusters from HeLa cells were incubated with Xenopus egg extracts in the presence or absence of added membranes. Where indicated 5 mM pargyline, 2.5 mM

2PCPA or 0.25 mM S2101 was added to decondensation reactions at t = 0. After 120 min samples were fixed and analyzed by confocal microscopy. Added membranes were pre-labeled with DiIC18 (red in overlay) and chromatin was stained with DAPI (blue in overlay). Scale bar: 5 µm.

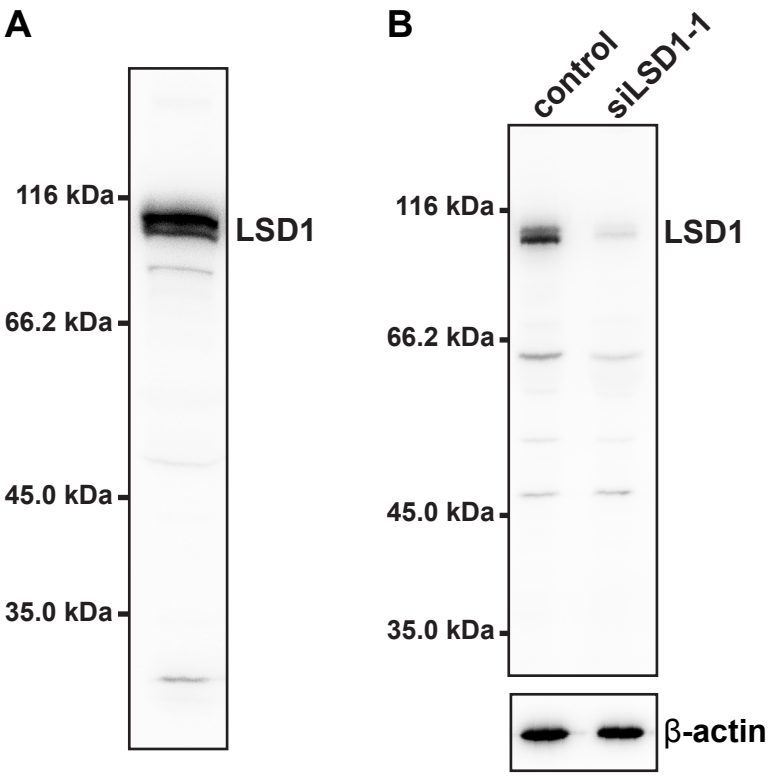
A
116 kDa
LSD1
66.2 kDa
45.0 kDa
35.0 kDa
B
control
siLSD1-1
116 kDa
LSD1
66.2 kDa
45.0 kDa
35.0 kDa
β-actin

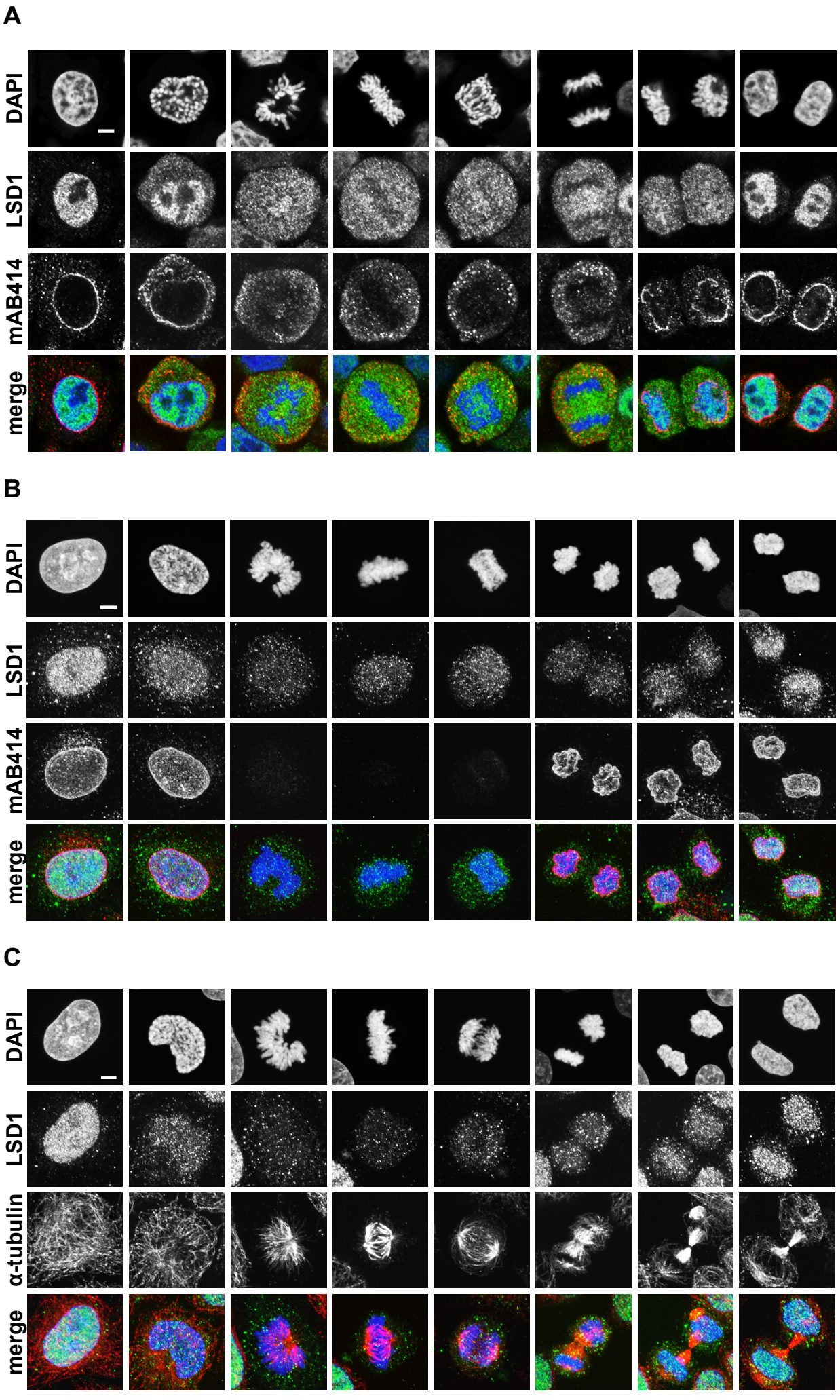
A
DAPI
LSD1
mAB414
merge
B
DAPI
LSD1
mAB414
merge
C
DAPI
LSD1
α-tubulin
merge

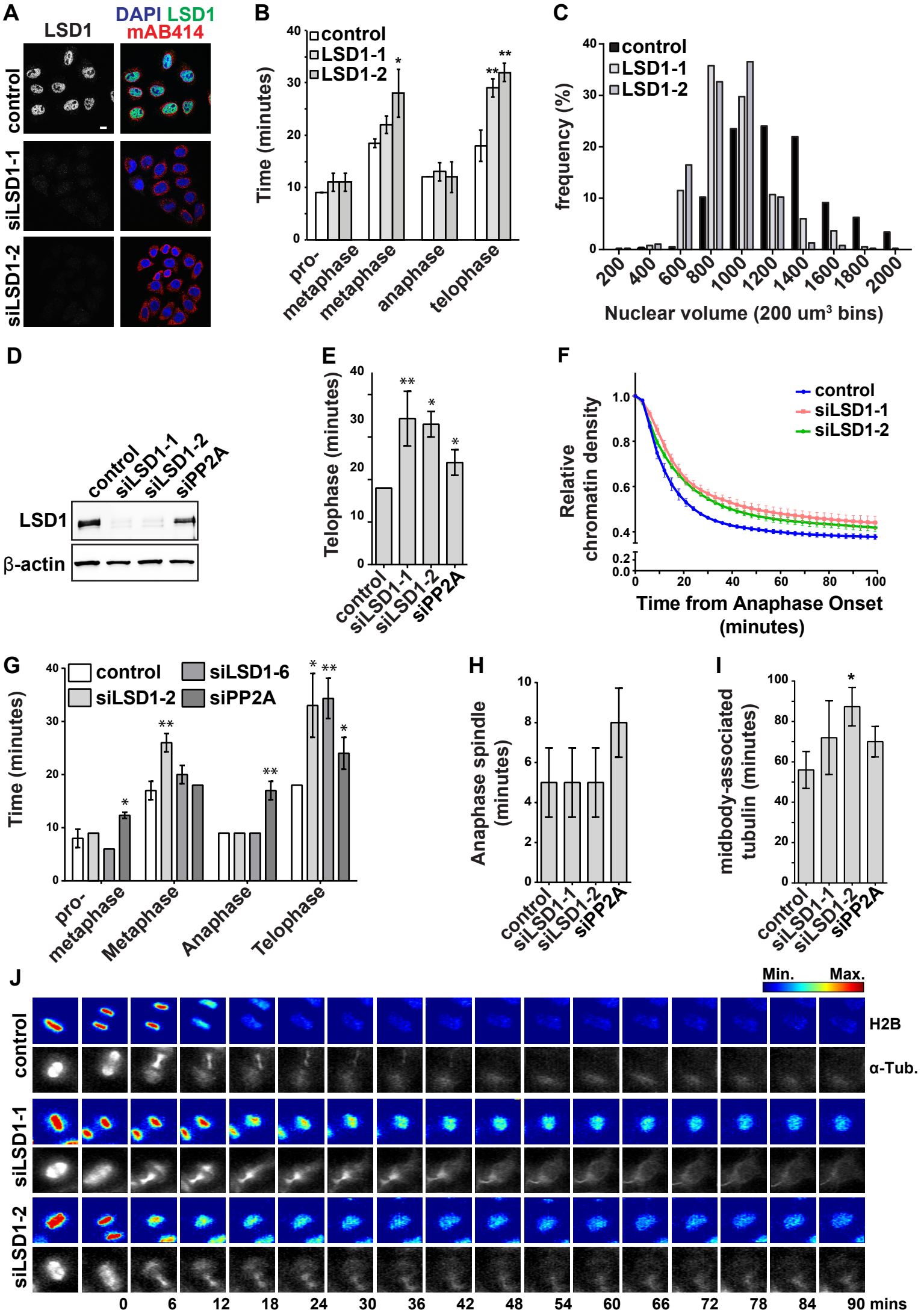
A
LSD1
DAPI LSD1 mAB414
control
siLSD1-1
siLSD1-2
B
control
LSD1-1
LSD1-2
Time (minutes)
pro-metaphase
metaphase
anaphase
telophase
C
control
LSD1-1
LSD1-2
frequency (%)
Nuclear volume (200 um³ bins)
D
control
siLSD1-1
siLSD1-2
siPP2A
LSD1
β-actin
E
Telophase (minutes)
F
control
siLSD1-1
siLSD1-2
Relative chromatin density
Time from Anaphase Onset (minutes)
G
control
siLSD1-6
siLSD1-2
siPP2A
Time (minutes)
pro-metaphase
Metaphase
Anaphase
Telophase
H
Anaphase spindle (minutes)
I
midbody-associated tubulin (minutes)
J
Min.
Max.
control
siLSD1-1
siLSD1-2
H2B
α-Tub.
0 6 12 18 24 30 36 42 48 54 60 66 72 78 84 90 mins

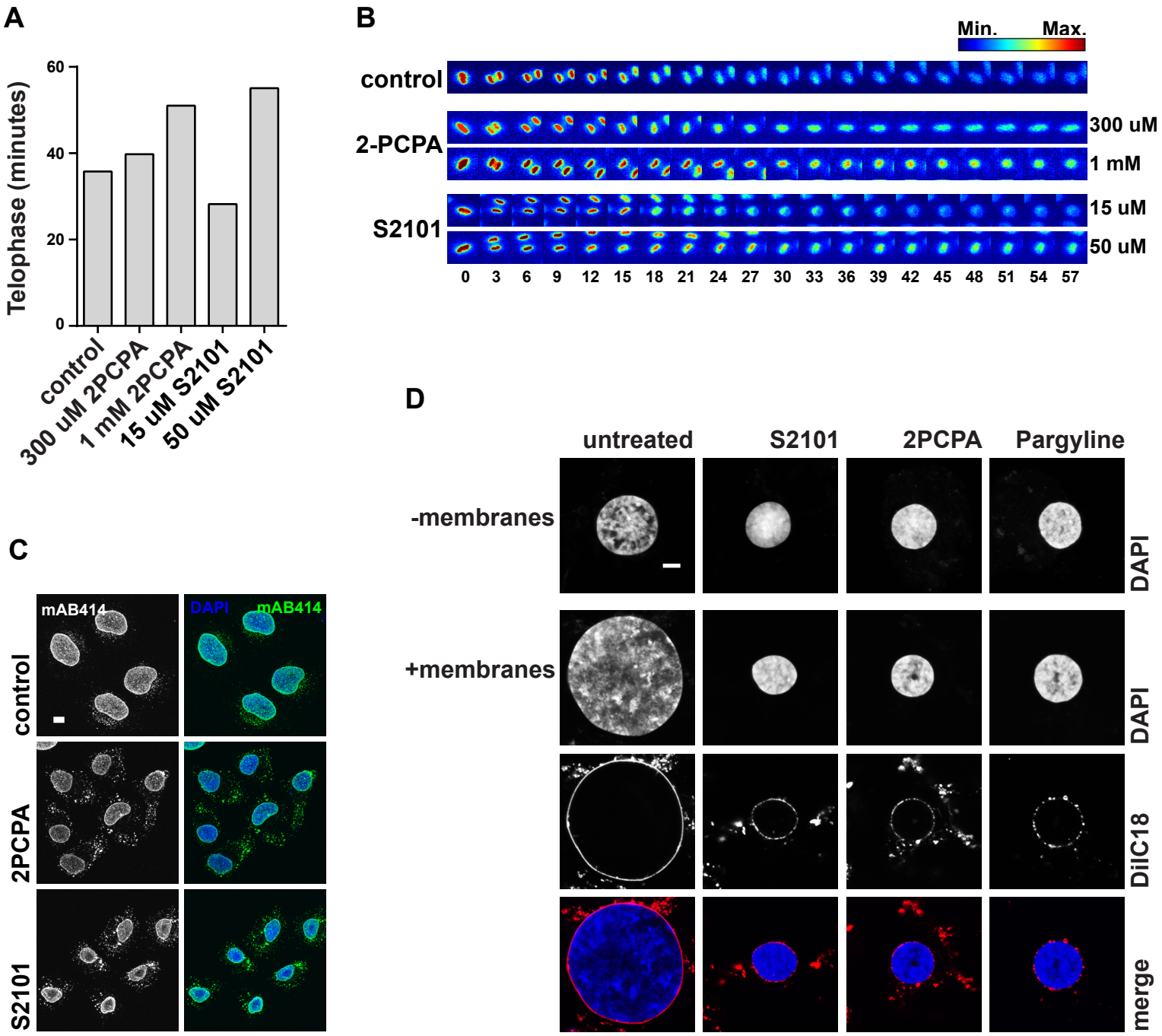
A
Telophase (minutes)
60
40
20
0
control
300 uM 2PCPA
1 mM 2PCPA
15 uM S2101
50 uM S2101
B
Min.
Max.
control
2-PCPA
S2101
300 uM
1 mM
15 uM
50 uM
0 3 6 9 12 15 18 21 24 27 30 33 36 39 42 45 48 51 54 57
C
mAB414
DAPI
mAB414
control
2PCPA
S2101
D
untreated
S2101
2PCPA
Pargyline
-membranes
+membranes
DAPI
DAPI
DilC18
merge